

Biodegradable polymers for biomedical applications, volume III

Edited by

Liqun Yang, Jianshe Hu, Shuai Jiang, Yeh-Hsing Lao
and Yang Yao

Published in

Frontiers in Bioengineering and Biotechnology
Frontiers in Materials



FRONTIERS EBOOK COPYRIGHT STATEMENT

The copyright in the text of individual articles in this ebook is the property of their respective authors or their respective institutions or funders. The copyright in graphics and images within each article may be subject to copyright of other parties. In both cases this is subject to a license granted to Frontiers.

The compilation of articles constituting this ebook is the property of Frontiers.

Each article within this ebook, and the ebook itself, are published under the most recent version of the Creative Commons CC-BY licence. The version current at the date of publication of this ebook is CC-BY 4.0. If the CC-BY licence is updated, the licence granted by Frontiers is automatically updated to the new version.

When exercising any right under the CC-BY licence, Frontiers must be attributed as the original publisher of the article or ebook, as applicable.

Authors have the responsibility of ensuring that any graphics or other materials which are the property of others may be included in the CC-BY licence, but this should be checked before relying on the CC-BY licence to reproduce those materials. Any copyright notices relating to those materials must be complied with.

Copyright and source acknowledgement notices may not be removed and must be displayed in any copy, derivative work or partial copy which includes the elements in question.

All copyright, and all rights therein, are protected by national and international copyright laws. The above represents a summary only. For further information please read Frontiers' Conditions for Website Use and Copyright Statement, and the applicable CC-BY licence.

ISSN 1664-8714
ISBN 978-2-8325-5963-5
DOI 10.3389/978-2-8325-5963-5

About Frontiers

Frontiers is more than just an open access publisher of scholarly articles: it is a pioneering approach to the world of academia, radically improving the way scholarly research is managed. The grand vision of Frontiers is a world where all people have an equal opportunity to seek, share and generate knowledge. Frontiers provides immediate and permanent online open access to all its publications, but this alone is not enough to realize our grand goals.

Frontiers journal series

The Frontiers journal series is a multi-tier and interdisciplinary set of open-access, online journals, promising a paradigm shift from the current review, selection and dissemination processes in academic publishing. All Frontiers journals are driven by researchers for researchers; therefore, they constitute a service to the scholarly community. At the same time, the *Frontiers journal series* operates on a revolutionary invention, the tiered publishing system, initially addressing specific communities of scholars, and gradually climbing up to broader public understanding, thus serving the interests of the lay society, too.

Dedication to quality

Each Frontiers article is a landmark of the highest quality, thanks to genuinely collaborative interactions between authors and review editors, who include some of the world's best academicians. Research must be certified by peers before entering a stream of knowledge that may eventually reach the public - and shape society; therefore, Frontiers only applies the most rigorous and unbiased reviews. Frontiers revolutionizes research publishing by freely delivering the most outstanding research, evaluated with no bias from both the academic and social point of view. By applying the most advanced information technologies, Frontiers is catapulting scholarly publishing into a new generation.

What are Frontiers Research Topics?

Frontiers Research Topics are very popular trademarks of the *Frontiers journals series*: they are collections of at least ten articles, all centered on a particular subject. With their unique mix of varied contributions from Original Research to Review Articles, Frontiers Research Topics unify the most influential researchers, the latest key findings and historical advances in a hot research area.

Find out more on how to host your own Frontiers Research Topic or contribute to one as an author by contacting the Frontiers editorial office: frontiersin.org/about/contact

Biodegradable polymers for biomedical applications, volume III

Topic editors

Liqun Yang — Shengjing Hospital of China Medical University, China

Jianshe Hu — Northeastern University, China

Shuai Jiang — Ocean University of China, China

Yeh-Hsing Lao — University at Buffalo, United States

Yang Yao — ETH Zürich, Switzerland

Citation

Yang, L., Hu, J., Jiang, S., Lao, Y.-H., Yao, Y., eds. (2025). *Biodegradable polymers for biomedical applications, volume III*. Lausanne: Frontiers Media SA.
doi: 10.3389/978-2-8325-5963-5

Table of contents

| | |
|-----|---|
| 05 | Editorial: Biodegradable polymers for biomedical applications - volume III Liqun Yang, Jianshe Hu and Shuai Jiang |
| 08 | PLGA-based drug delivery systems in treating bone tumors Enduo Qiu and Fei Liu |
| 24 | <i>In vitro</i> enzymatic degradation of the PTMC/cross-linked PEGDA blends Wei Li, Meina Lin, Chenchao Wang, Yongping Lu, Yu Sui, Xiang Ni, Jing Guo, Miao Jiang, Liqun Yang and Hong Cui |
| 35 | Biomimetic electrospun nanofibrous scaffold for tissue engineering: preparation, optimization by design of experiments (DOE), <i>in-vitro</i> and <i>in-vivo</i> characterization Shabnam Anjum, Ting Li, Dilip Kumar Arya, Daoud Ali, Saud Alarifi, Wang Yulin, Zhang Hengtong, P. S. Rajinikanth and Qiang Ao |
| 54 | Biodegradable polyester-based nano drug delivery system in cancer chemotherapy: a review of recent progress (2021–2023) Zongheng Wang, Miaomiao Xiao, Fangliang Guo, Yue Yan, Hong Tian, Qianshi Zhang, Shuangyi Ren and Liqun Yang |
| 70 | Multifunctional electrospun nanofibrous scaffold enriched with alendronate and hydroxyapatite for balancing osteogenic and osteoclast activity to promote bone regeneration Shabnam Anjum, Dilip Kumar Arya, Mohammad Saeed, Daoud Ali, Mohammad Saud Athar, Wang Yulin, Saud Alarifi, Xixi Wu, P.S. Rajinikanth and Qiang Ao |
| 88 | Functionalized TMC and ϵ-CL elastomers with shape memory and self-healing properties Siwen Chen, Miaomiao Xiao, Zhipeng Hou, Zhongcun Li, Jianshe Hu, Jing Guo, Jing Chen, Liqun Yang and Quan Na |
| 98 | Comprehensive review of materials, applications, and future innovations in biodegradable esophageal stents Yaochen Yang, Yuanyuan Yang, Zhipeng Hou, Tingting Wang, Peng Wu, Lufan Shen, Peng Li, Kai Zhang, Liqun Yang and Siyu Sun |
| 120 | Recent advances in polymeric microparticle-based drug delivery systems for knee osteoarthritis treatment Guangxin Wang, Xin-an Zhang, Leonid Kapilevich and Mingjie Hu |
| 134 | Application of modified sodium alginate hydrogel for interventional embolization of hemorrhagic diseases Shengchao Wei, Tang Deng, Caixia Wu, Jianshan Shi, Yong Liao, Lin Huang, Yongjie Liu, Shijie Zhong, Xueying Ji and Guiyun Jin |

- 144 **Integration of BMP-2/PLGA microspheres with the 3D printed PLGA/CaSO₄ scaffold enhances bone regeneration**
Li Zhao, Xiaoliang Zhao, Fengpiao Deng, Xiangling Ye, Zhen Shen, Yuanjun Xia and Ying Zhang
- 154 **Materials based on biodegradable polymers chitosan/gelatin: a review of potential applications**
Aref Yarahmadi, Behrooz Dousti, Mahdi Karami-Khorramabadi and Hamed Afkhami
- 176 **Cutting-edge developments in the application of hydrogels for treating skin photoaging**
Lili Cao, Xiaoying Qian, Jie Min, Zhongfeng Zhang, Meiping Yu and Dan Yuan



OPEN ACCESS

EDITED AND REVIEWED BY

Hafiz M. N. Iqbal,
Monterrey Institute of Technology and Higher
Education (ITESM), Mexico

*CORRESPONDENCE

Liqun Yang,
✉ yangliqun@sj-hospital.org

RECEIVED 26 December 2024

ACCEPTED 07 January 2025

PUBLISHED 21 January 2025

CITATION

Yang L, Hu J and Jiang S (2025) Editorial:
Biodegradable polymers for biomedical
applications - volume III.
Front. Mater. 12:1551590.
doi: 10.3389/fmats.2025.1551590

COPYRIGHT

© 2025 Yang, Hu and Jiang. This is an
open-access article distributed under the
terms of the [Creative Commons Attribution
License \(CC BY\)](#). The use, distribution or
reproduction in other forums is permitted,
provided the original author(s) and the
copyright owner(s) are credited and that the
original publication in this journal is cited, in
accordance with accepted academic practice.
No use, distribution or reproduction is
permitted which does not comply with
these terms.

Editorial: Biodegradable polymers for biomedical applications - volume III

Liqun Yang^{1*}, Jianshe Hu² and Shuai Jiang³

¹Research Center for Biomedical Materials, Shenyang Key Laboratory of Biomedical Polymers, Engineering Research Center of Ministry of Education for Minimally Invasive Gastrointestinal Endoscopic Techniques, Shengjing Hospital of China Medical University, Shenyang, China, ²Center for Molecular Science and Engineering, College of Science, Northeastern University, Shenyang, China, ³School of Medicine and Pharmacy, Ocean University of China, Qingdao, China

KEYWORDS

biodegradable polymers, drug delivery, tissue engineering, regenerative medicine, nanoparaticles, scaffold

Editorial on the Research Topic

Biodegradable polymers for biomedical applications -volume III

Biodegradable polymers have emerged as cornerstones in developing advanced biomedical applications, offering solutions for drug delivery (Soppimath et al., 2001), tissue engineering (Iqbal et al., 2019), and regenerative medicine (Arun et al., 2021). With their biocompatibility, tunable properties, and ability to degrade into non-toxic byproducts, biodegradable polymers present ideal solutions for modern medical challenges. This Research Topic, “*Biodegradable Polymers for Biomedical Applications - Volume III*,” brings together cutting-edge research and reviews, highlighting recent advances, innovative strategies, and future directions in this dynamic field.

This volume includes 12 articles, each contributing to the understanding and advancement of biodegradable polymers for biomedical applications. Among them, three articles focus on drug delivery systems (DDS), demonstrating their potential for enhanced therapeutic efficacy and reduced side effects. For instance, Qiu et al. delved into poly (lactic-co-glycolic acid) (PLGA)-based nanoparticles for bone tumor treatment, emphasizing their capability for sustained release and targeted drug delivery. Similarly, Wang et al. discussed PLGA nanoparticles, highlighting their versatility in cancer treatment and ability to improve drug bioavailability while reducing systemic toxicity. Wang et al. focused on recent advances in natural and synthetic polymer-based microsphere delivery systems for treating knee osteoarthritis.

Biodegradable polymers also play a crucial role in tissue engineering and regenerative medicine. Cao et al. summarized recent progress in addressing skin photoaging using hydrogels, exploring the challenges of utilizing hydrogels as therapeutic agents and outlining potential future developments. Similarly, Yang et al. provided a comprehensive overview of current biodegradable esophageal stent materials and their applications, highlighting current research limitations and innovations while offering insights into future development priorities and directions. Zhao et al. prepared a 3D printed composite scaffold of BMP-2/PLGA microspheres with polylactic acid glycolic acid copolymer/CaSO₄, which was used to improve the osteogenic properties of the scaffold. This 3D printed scaffold was able to accelerate the repair of complex bone defects by promoting new bone formation,

suggesting that it may prove to be a potential bone tissue engineering substitute. Anjum et al. demonstrated the promise of HA and ALN-loaded PVP/PVA-ALN-HA nanofiber composite scaffolds for bone regeneration applications. Wei et al. evaluated the potential of MSAH, prepared using OSA and CMC mixtures, for targeted vessel embolization in an internal iliac artery hemorrhage model. MSAH achieved aortic embolization without affecting peripheral arterial blood supply, enabling rapid short-term hemostasis and long-term degradation without target organ necrosis.

Furthermore, biodegradable polymers find extensive applications in other industries. Yarahmadi et al. outlined recent research on applying chitosan and gelatin polymers across various fields, including food packaging, antioxidant and antimicrobial properties, encapsulation of bioactive substances, tissue engineering, microencapsulation technology, water treatment, and drug delivery, showcasing the multiple uses of gelatin and chitosan polymers in addressing environmental issues and advancing different industries.

The development of novel biodegradable materials is a recurring theme in this volume. Anjum et al. prepared PVP/PVA nanofiber scaffolds through novel electrospinning techniques. Results showed that these porous PVP/PVA nanofibers demonstrate excellent biocompatibility with great potential in biomedical applications. Chen et al. introduced a novel smart elastomer, mPEG43-b-(PMBC-co-PCL)n, developed from polyester and polycarbonate blends with excellent shape memory and self-healing capabilities through physical crosslinking systems. This innovative elastomer provides a solid foundation and broad prospects for developing self-shrinking smart surgical sutures in the biomedical field. Additionally, Li et al. proposed a simple and effective strategy for adjusting PTMC degradation rates by blending photoactive PEGDA with PTMC, followed by UV photopolymerization of the mixture to prepare poly (trimethylene carbonate) (PTMC) and crosslinked poly (ethylene glycol) diacrylate (PEGDA) blends. The introduction of UV-crosslinked PEGDA significantly improved PTMC's resistance to lipase erosion, expanding its applications in the medical field.

This volume of “*Biodegradable Polymers for Biomedical Applications - Volume III*” showcases significant progress in utilizing biodegradable polymers for drug delivery, tissue engineering, and other applications. In addition to the insightful contributions, this volume reflects remarkable geographic diversity among the authors, emphasizing the global collaboration within the field of biodegradable polymers for biomedical applications. The articles included in this volume are authored by researchers from a wide range of regions, including China, India, Russia, Saudi Arabi and Iran. This geographic diversity not only underscores the universal relevance of the topic but also highlights the collective effort of the global scientific community to address biomedical challenges. By uniting perspectives from various parts of the world, this volume serves as a bridge for cross-regional innovation and knowledge sharing, setting the foundation for future interdisciplinary collaborations. The authors' contributions provide valuable insights into the design, application, and future potential of these materials. We extend our gratitude to all authors, reviewers, and editors who contributed to this Research Topic. Their efforts have greatly advanced our understanding of biodegradable polymers and their transformative impact on biomedicine.

As we conclude this volume on biodegradable polymers for biomedical applications, several crucial insights emerge that warrant careful consideration. The collected works demonstrate significant

progress in developing biocompatible materials with controlled degradation profiles and enhanced functionality. However, we must acknowledge certain limitations and challenges that persist in this field. While biodegradable polymers show promising results in laboratory settings, concerns about their long-term stability, batch-to-batch consistency, and scalability in industrial production remain valid counterarguments to their immediate widespread adoption. Critics rightfully point out that the cost-effectiveness of these materials compared to traditional alternatives needs further evaluation, and the complete understanding of their degradation products' long-term effects requires additional investigation. Nevertheless, these challenges should not overshadow the tremendous potential of biodegradable polymers in revolutionizing biomedical applications. The key take-home message for readers is that the field is rapidly evolving, with innovative solutions emerging to address current limitations. Future research directions should focus on developing standardized testing protocols, improving manufacturing processes for better consistency, and conducting more comprehensive *in vivo* studies. Additionally, the integration of artificial intelligence and machine learning approaches could accelerate material design and optimization, while enhanced collaboration between academic institutions and industry partners could bridge the gap between laboratory success and clinical application. We encourage readers to approach these developments with both enthusiasm and critical thinking. The challenges identified in this volume should serve as catalysts for innovation rather than barriers to progress. As we move forward, the focus should be on addressing unresolved questions about degradation mechanisms, biocompatibility, and scale-up processes while maintaining an open dialogue about both the possibilities and limitations of these materials. The future of biodegradable polymers in biomedical applications lies in our ability to balance optimism with pragmatic solutions to these remaining challenges.

Author contributions

LY: Conceptualization, Data curation, Supervision, Writing—original draft, Writing—review and editing. JH: Supervision, Writing—review and editing. SJ: Supervision, Writing—review and editing.

Funding

The author(s) declare that no financial support was received for the research, authorship, and/or publication of this article.

Conflict of interest

The authors declare that the research was conducted in the absence of any commercial or financial relationships that could be construed as a potential conflict of interest.

Generative AI statement

The author(s) declare that no Generative AI was used in the creation of this manuscript.

Publisher's note

All claims expressed in this article are solely those of the authors and do not necessarily represent those of their affiliated

organizations, or those of the publisher, the editors and the reviewers. Any product that may be evaluated in this article, or claim that may be made by its manufacturer, is not guaranteed or endorsed by the publisher.

References

- Arun, Y., Ghosh, R., and Domb, A. J. (2021). Biodegradable hydrophobic injectable polymers for drug delivery and regenerative medicine. *Adv. Funct. Mater.* 31 (44), 2010284. doi:10.1002/adfm.202010284
- Iqbal, N., Khan, A. S., Asif, A., Yar, M., Haycock, J. W., and Rehman, I. U. (2019). Recent concepts in biodegradable polymers for tissue engineering paradigms: a critical review. *Int. Mater. Rev.* 64 (2), 91–126. doi:10.1080/09506608.2018.1460943
- Soppimath, K. S., Aminabhavi, T. M., Kulkarni, A. R., and Rudzinski, W. E. (2001). Biodegradable polymeric nanoparticles as drug delivery devices. *J. Control. release* 70 (1-2), 1–20. doi:10.1016/s0168-3659(00)00339-4



OPEN ACCESS

EDITED BY

Shuai Jiang,
Ocean University of China, China

REVIEWED BY

Changfeng Fu,
The First Hospital of Jilin University, China
Yixiu Liu,
Central Hospital Affiliated to Shenyang
Medical College, China

*CORRESPONDENCE

Enduo Qiu,
✉ 46304739@qq.com

RECEIVED 03 April 2023

ACCEPTED 15 May 2023

PUBLISHED 01 June 2023

CITATION

Qiu E and Liu F (2023), PLGA-based drug delivery systems in treating bone tumors. *Front. Bioeng. Biotechnol.* 11:1199343. doi: 10.3389/fbioe.2023.1199343

COPYRIGHT

© 2023 Qiu and Liu. This is an open-access article distributed under the terms of the [Creative Commons Attribution License \(CC BY\)](https://creativecommons.org/licenses/by/4.0/). The use, distribution or reproduction in other forums is permitted, provided the original author(s) and the copyright owner(s) are credited and that the original publication in this journal is cited, in accordance with accepted academic practice. No use, distribution or reproduction is permitted which does not comply with these terms.

PLGA-based drug delivery systems in treating bone tumors

Enduo Qiu* and Fei Liu

Department of Bone and Soft Tissue Tumor Surgery, Cancer Hospital of China Medical University, Liaoning Cancer Hospital & Institute, Shenyang, China

Bone tumor has become a common disease that endangers human health. Surgical resection of bone tumors not only causes biomechanical defects of bone but also destroys the continuity and integrity of bone and cannot completely remove the local tumor cells. The remaining tumor cells in the lesion bring a hidden danger of local recurrence. To improve the chemotherapeutic effect and effectively clear tumor cells, traditional systemic chemotherapy often requires higher doses, and high doses of chemotherapeutic drugs inevitably cause a series of systemic toxic side effects, often intolerable to patients. PLGA-based drug delivery systems, such as nano delivery systems and scaffold-based local delivery systems, can help eliminate tumors and promote bone regeneration and therefore have more significant potential for application in bone tumor treatment. In this review, we summarize the research progress of PLGA nano drug delivery systems and PLGA scaffold-based local delivery systems in bone tumor treatment applications, expecting to provide a theoretical basis for developing novel bone tumor treatment strategies.

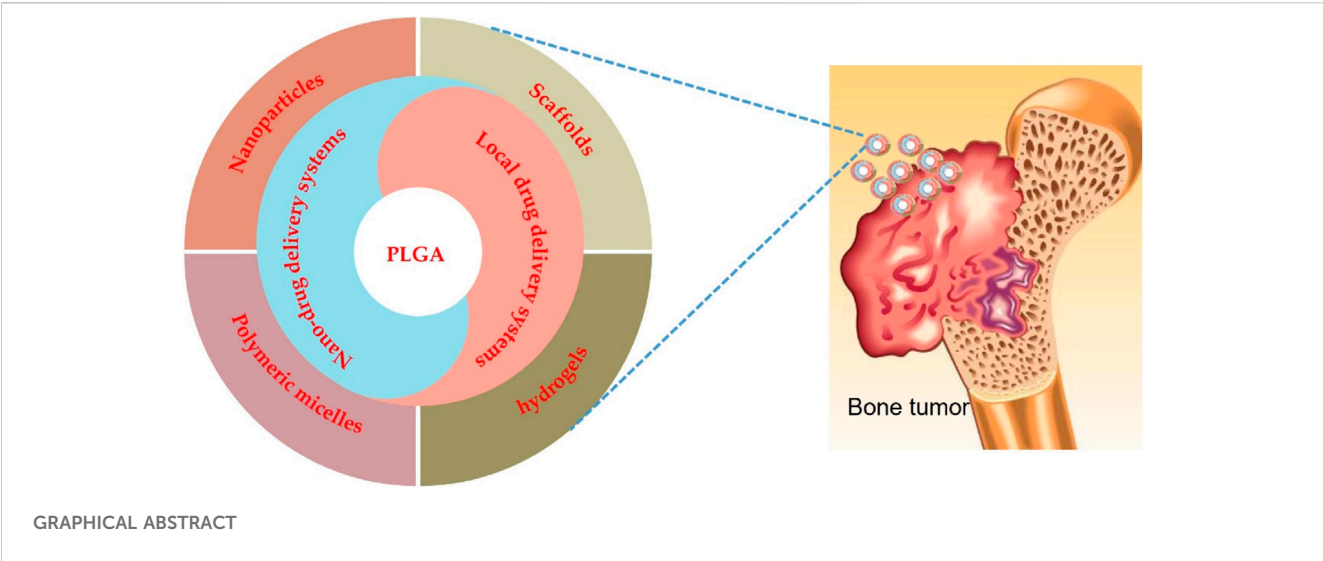
KEYWORDS

bone tumors, PLGA, delivery systems, nanoparticles, scaffolds

1 Introduction

Bone tumors occur in the bones or their attached tissues (Figure 1), classified as benign or malignant (Choi and Ro, 2021), with the latter being more common in adults. Bone and joint pain, masses, and movement disorders are the main symptoms of bone tumors, especially malignant bone tumors, along with deformities, pathological fractures, and systemic symptoms such as insomnia, irritability, loss of appetite, depression, anemia, and cachexia (Bone Tumors, 2021). In line with WHO classifications, bone cancers can be categorized as primarily or secondarily malignant (Choi and Ro, 2021). Primary bone tumors are rare and originate from bone tissue, while secondary malignant bone tumors are those that metastasize to the bone from other tissues or organs in the body (Chowdhry et al., 2009). Despite the relatively low incidence, mortality from primary malignant bone tumors is very high. It has been reported that there were an estimated 24,000 cases and 17,200 deaths from primary bone cancer in China in 2014 (Xia et al., 2019), and 24,200 new cases and 17,900 deaths in 2015 (Xi et al., 2015).

Currently, the main treatments for bone tumors are surgery, chemotherapy (Table 1), and radiotherapy (Bădilă et al., 2021), among which the combination of preoperative and postoperative chemotherapy for limb-preserving surgery is the primary strategy (Ferguson and Turner, 2018). However, these treatments are associated with significant side effects and may not be effective in all cases; for example, surgical resection not only leads to large bone defects (Lu et al., 2019; Zhao et al., 2020a; Hayashi and Tsuchiya, 2022) but also fails to eradicate micrometastases, and the presence of residual tumor cells may increase the risk of disease metastasis and recurrence (Pantel et al., 2009; Massagué and Obenauf, 2016). Therefore, bone reconstruction and recurrence inhibition should be considered in the postoperative management



of bone tumors. Administration of systemic chemotherapy/radiotherapy to patients is commonly used to suppress tumor recurrence; however, the liver, kidney, and digestive systems are stressed by high chemotherapy doses, which may lead to intense side effects (Oun et al., 2018; Schirmacher, 2019). In addition, certain bone tumors, for example, osteosarcoma, are insensitive to radiation therapy and prone to chemoresistance (He et al., 2014; Kim and Kim, 2018). Hence, there is an urgent requirement to develop strategies to reduce systemic side effects and improve therapeutic efficacy, and there is a need for new and more effective treatments for bone tumors.

The elimination of tumor cells and the promotion of bone regeneration are the two critical issues in the treatment of bone tumors. Therefore, to address the clinical challenge of treating bone tumors and the demand for innovative approaches, researchers have focused on developing innovative strategies for bone tumor treatment, where biodegradable polymer-based targeted nano-drug delivery systems and local drug delivery systems have shown strong potential in terms of bone tumor therapeutic efficacy.

2 PLGA targeted nano-drug delivery systems

Much attention has been given to the potential of nanotechnology in drug delivery research, resulting in nanomedicine. The increasing interest in nanomedicine is due

to the ability to improve cancer treatment by minimizing systemic toxicity and more efficacious targeted delivery of drugs (Shi et al., 2017; van der Meel et al., 2019; Wolfram and Ferrari, 2019; Zhang et al., 2020b; Germain et al., 2020; Irvine and Dane, 2020; de Lázaro and Mooney, 2021; Bhatia et al., 2022). The success of nanomedicine research will offer novel approaches for the ideal treatment of bone tumors (Figure 2). Targeting anti-cancer agents to the bone, either passively or actively, via nanocarriers is an attractive therapeutic approach for treating bone tumors, where the design of nanocarriers is vital to improve treatment efficacy and reduce the risk of adverse events (Ambrosio et al., 2021; Prasad et al., 2021).

2.1 PLGA nanoparticles

Among the biodegradable polymers developed for the formulation of polymeric nanoparticles, PLGA has attracted considerable attention and is widely used for its appealing characteristics, such as outstanding biocompatibility, favorable biodegradation, and FDA and EMA approval. PLGA-based delivery systems have demonstrated significant promise in treating bone tumors (Table 2).

Studies have shown that these systems provide controlled drug release, which can enhance their therapeutic efficacy while reducing the side effects associated with traditional chemotherapy. Additionally, PLGA-based systems have demonstrated high

TABLE 1 The First-line therapy agents for osteosarcoma.

| Chemotherapy agent | References |
|--|---|
| Cisplatin and doxorubicin | Kaneko et al. (2016), Zhang et al. (2018) |
| MAP (high-dose methotrexate, cisplatin, and doxorubicin) | Yu et al. (2019a), Zhang et al. (2020a) |
| Doxorubicin, cisplatin, ifosfamide, and high-dose methotrexate | Sampson et al. (2013) |
| Ifosfamide, cisplatin, and epirubicin | Huang et al. (2015) |

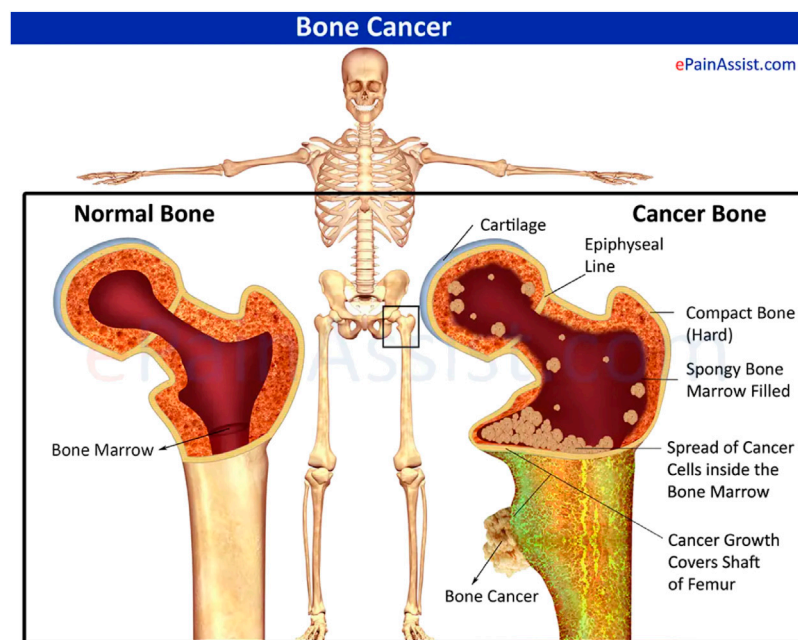


FIGURE 1

Schematic diagram of normal bone with cancerous bone. Reproduced with permission from [www.epainassist.com/bones/bone-cancer].

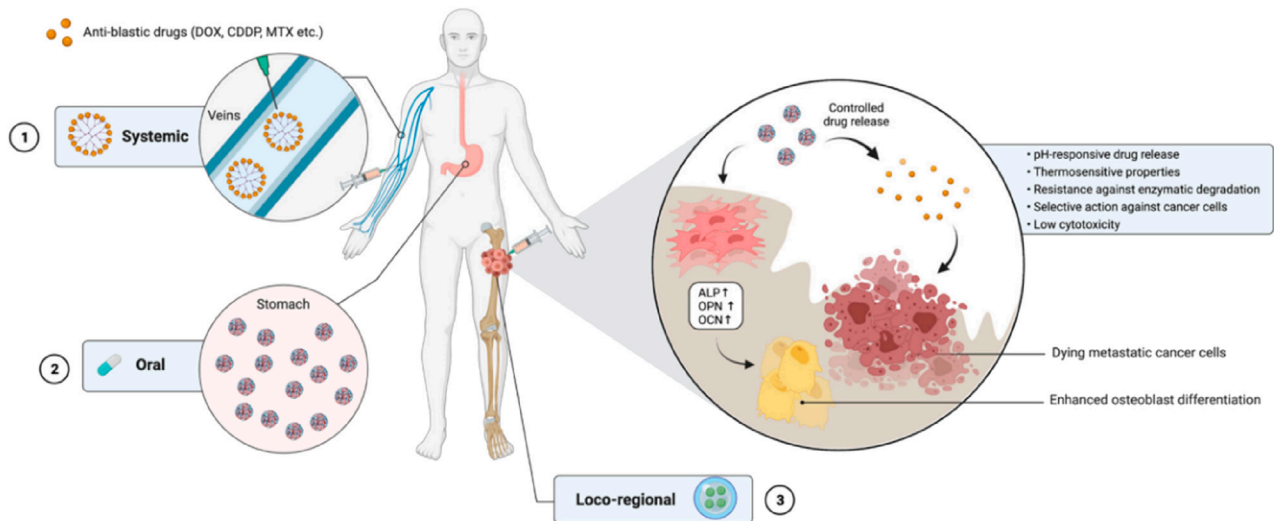


FIGURE 2

The use of nanocarrier-based drug delivery systems for the treatment of bone cancer. Reproduced with permission from Ambrosio L et al., © 2021 by the authors.

biocompatibility and biodegradability, which makes them ideal for long-term use for bone tissue engineering applications. Salerno et al. developed alendronate (ALN)-conjugated PLGA nanoparticles loaded with doxorubicin (DOX) for treating bone metastases from breast cancer (Salerno et al., 2010), and the obtained ALN-PLGA-DOX nanoparticles had good biocompatibility and the ability

to target tumor-induced osteolytic sites (Cenni et al., 2008; Pignatello et al., 2009; Pignatello, 2011; Cenni et al., 2012; Thamake et al., 2012; Yin et al., 2016). *In vivo* studies showed that the ALN-PLGA-DOX nanoparticles could reduce the incidence of tumor metastasis and decrease the number of osteoclasts at tumor sites in mice. Gdowski et al. prepared ALN-conjugated PLGA

TABLE 2 PLGA-based delivery systems investigated for treating bone tumors.

| Anti-cancer drugs | Preparation methods | Particle size (nm) | Encapsulation efficiency (%) | Drug loading (%) | Treatment outcomes | Ref |
|--------------------------------------|--|--------------------|------------------------------|------------------|---|------------------------------------|
| Dox | solvent-displacement | 245.400 ± 4.917 | 60.400 ± 0.600 | — | Both DOX-loaded NP and free DXR reduced the Incidence of metastases in mice | Salerno et al. (2010) |
| Cabazitaxel | water-in-oil-in-water emulsion solvent evaporation | 236.8 ± 1.19 | 55.87% | 3.74% | Showed a significant reduction in tumor burden, reducing pain in the mouse tumor limb | Gdowski et al. (2017) |
| Bortezomib | solvent dispersion | 195 | 24 | 0.74 | Significantly enhanced survival and Decreased tumor burden in mice | Swami et al. (2014) |
| Dox | solvent diffusion | 132 ± 9.5 | 73.53 ± 3.43 | 5.51 | Showed prolonged blood circulation half-life, reduced liver uptake, and significantly higher retention of ZOL-tagged nps at the bone site with enhanced tumor retention | Chaudhari et al. (2012) |
| Gemcitabine and epirubicin | Solvent diffusion or nano-precipitation | 197 ± 7 (pH = 7.0) | 89.8 ± 4.5 | 33.2 ± 4.4 | Significant tumor (250%) regression was seen upon treatment with multiple drug-loaded zoledronic acid conjugated nanoparticle | Yuan et al. (2020) |
| Bisphosphonates | reverse microemulsion | 178.1 ± 1.2 | — | ~32% | Significantly inhibited tumor growth | Li et al. (2019a) |
| Ifosfamide | precipitation | 124 ± 3.45 | 89 ± 1.95 | 20.15 ± 3.5 | Exhibited remarkable <i>in vitro</i> anti-cancer activity | Chen et al. (2015) |
| Paclitaxel (PTX) and etoposide (ETP) | solvent evaporation | 100 ± 3.68 | 92.5 ± 5.6 | 13.6 ± 2.8 | Resulted in Enhanced cell cycle arrest and cell apoptosis | Wang et al. (2015) |
| Melatonin | emulsion–diffusion–evaporation | 212.9 ± 65.6 | 17.3 ± 3.4 | 34.0 ± 4.3 | Caused a toxic effect on the MG-63 cells | Altındal and Gümüşdereioğlu (2016) |
| Salinomycin | Emulsion diffusion evaporation | ~187 nm | 60 | — | Induced caspase-3 expression while Suppressing β -catenin (wnt/ β -catenin pathway) and c-myc gene expressions in Osteosarcoma cancer cells | Irmak et al. (2020) |
| Ptx | nano-precipitation | 132.73 ± 0.61 | 64.86 ± 0.17 | 4.24% ± 0.02 | Suppressed tumor growth in tumor-bearing mice with minimal damage to normal tissues | Cai et al. (2022) |
| Ir780 | water-in-oil-in-water (W/O/W) double-emulsion | 236.8 | 67.8 | 3.25 | Significantly induce HOS cells apoptosis and ferroptosis via excessive accumulation of reactive oxygen species | Wang et al. (2022a) |

nanoparticles loaded with cabazitaxel for enhanced drug delivery to the bone microenvironment (Figure 3). These bone-targeted PLGA-ALN nanoparticles significantly reduced tumor burden and pain in

the tumor-bearing limbs of mice (Gdowski et al., 2017), representing a promising strategy for treating metastatic bone cancer. These results suggest that ALN-conjugated PLGA nanoparticles deserve

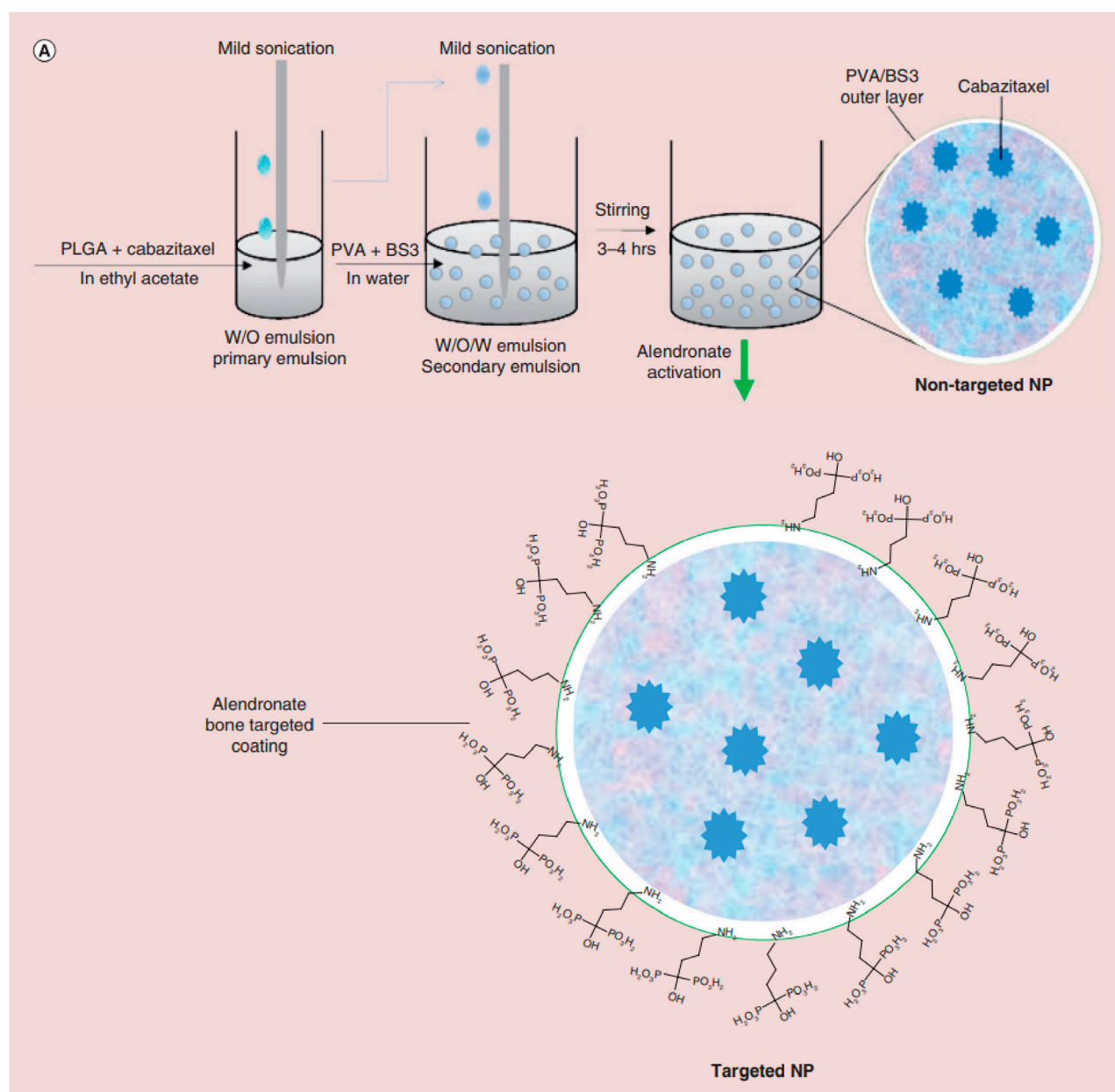


FIGURE 3

Schematic illustrating nanoparticle (NP) synthesis through water-in-oil-in-water double emulsion solvent evaporation technique followed by activation of nanoparticle with alendronate for bone targeting. Reproduced with permission from Gdowski A S et al., © 2017 by the authors.

further evaluation as practical for delivering anti-cancer drugs to bone tumors.

Bortezomib shows significant anti-tumor activity in multiple myeloma. Swami et al. (Swami et al., 2014) found that bortezomib/PLGA nanoparticles inhibited myeloma growth in mice (Figure 4). Modifications of nanoparticle surface with PEG prevent clearance by the reticuloendothelial system. The Bortezomib-loaded ALN-PLGA-PEG nanoparticles exhibited good retentive, accumulative, and bone-homing properties. The zoledronate (ZOL)-conjugated PLGA-PEG-DOX nanoparticles also showed prolonged circulation half-life, reduced hepatic uptake, significantly longer tumor retention, and more effective prevention of multiple myeloma

growth (Chaudhari et al., 2012). Similar observations of enhanced cellular uptake and increased tumor regression in mice (Li et al., 2019a; Yuan et al., 2020) were found for multiple drug-loaded PLGA-ZOL nanoparticles (Figure 5), demonstrating the conjugation of PLGA with a bisphosphonate with anti-tumor agents can be served as a potential treatment for osteosarcoma.

Intravenous administration of ifosfamide (IFS) is indicated as the mainstay of treatment for osteosarcoma. Chen et al. enclosed ifosfamide in a conjugate of dextran and PLGA to evaluate its anti-cancer activity towards osteosarcoma tumor cells (Figure 6). The resulting particles showed a more significant promotion of cell death and apoptosis and superior *in vitro* anti-cancer activity compared to

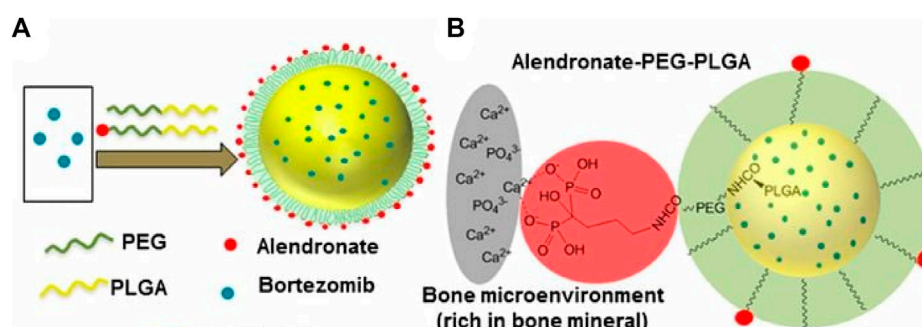


FIGURE 4

(A) Schematic illustration of alendronate-conjugated PEG-PLGA (Ald-PP) NPs synthesized by blending polymers (PLGA-b-PEG-Ald and PLGA-b-PEG) in varying ratios and encapsulating the drug bortezomib. (B) Schematic representation of the mechanism of affinity of Ald-PP NPs with bone mineral (gray, bone mineral; red, Ald; green, PEG; yellow, PLGA). Reproduced with permission from Swami A, S et al. Freely available online through the PNAS open access option.

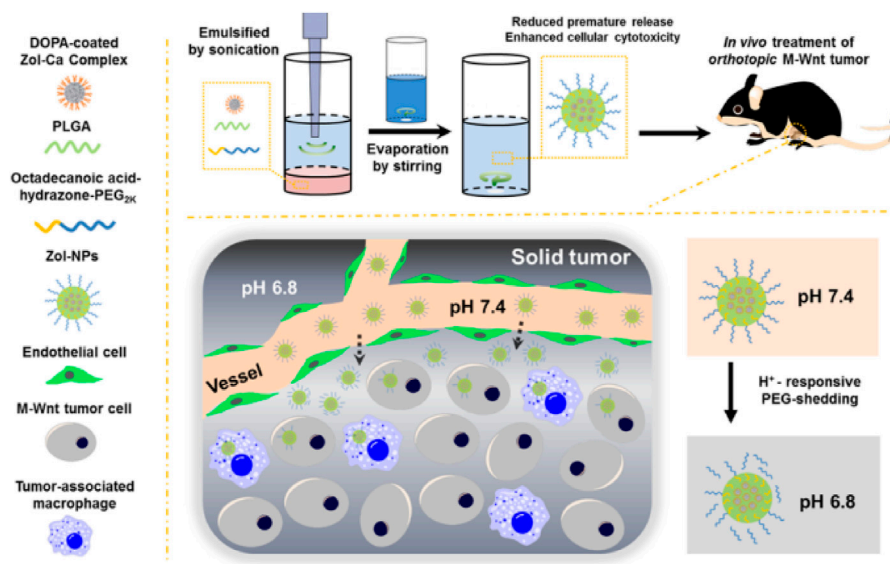


FIGURE 5

Schematic illustrations of zoledronic acid-containing nanoparticles with minimum premature release show enhanced activity against extraskeletal tumors. Reproduced with permission from Li X, S et al. Copyright © 2019, American Chemical Society.

the free ifosfamide (Chen et al., 2015), suggesting that the PLGA nanoparticles obtained could be a possible therapeutic approach for treating osteosarcoma. Due to the complex microenvironment and drug resistance mechanisms of cancer, single-agent cancer therapy remains unsatisfactory (Liu, 2009; Bar-Zeev et al., 2017). Combination therapies are promising strategies to improve treatment efficacy and decrease adverse events (Xiao et al., 2017). The combined administration of more than one chemotherapeutic agent can produce synergistic suppression of cancer cells. Wang et al. encapsulated etoposide (ETP) and paclitaxel (PTX) into PLGA nanoparticles to investigate the synergistic effect of the combination regimen to promote apoptosis as a treatment for osteosarcoma (Wang et al., 2015). The resulting PLGA-PTX-ETP nanoparticles exhibited potent anti-cancer effects in MG63 and Saos-2 cancer cells

in a time- and concentration-dependent manner. Co-administration of PTX and ETP led to the arrest of the cell cycle and enhanced cell apoptosis. The findings revealed that the combination significantly improved the treatment efficacy of the anti-cancer drugs. The combination of nanoparticles has a more significant inhibition effect, which will be beneficial for systemic cancer treatment. In conclusion, multi-drug PLGA nanoparticles will be a highly anticipated anti-cancer delivery system for treating osteosarcoma.

Melatonin has potent antioxidant, immunomodulatory, anti-proliferative, and tumor-suppressive properties (Moradkhani et al., 2020). Studies have shown that melatonin significantly inhibits tumor cell growth and can reduce chemotherapy drugs' side effects (Bondy and Campbell, 2018; Gurunathan et al., 2021). Melatonin has a short half-life, which prolongs its

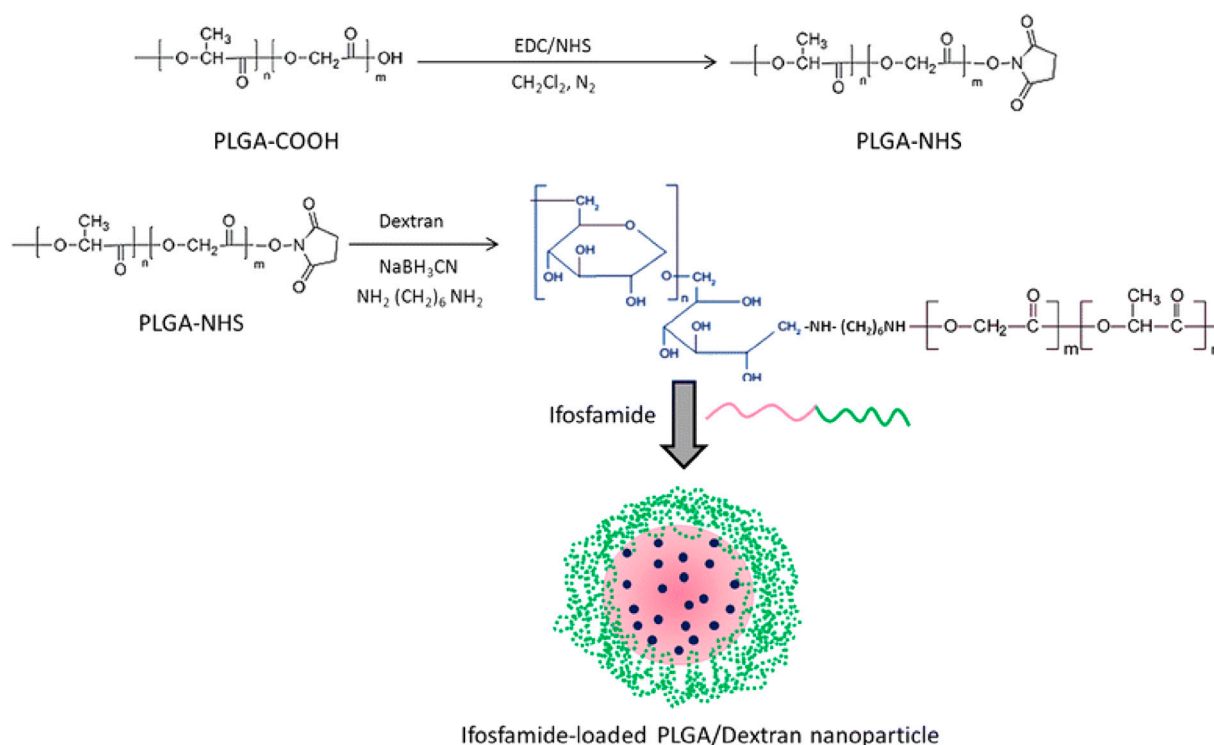


FIGURE 6

Schematic illustration of conjugation of PLGA polymer with the dextran block. Reproduced with permission from Chen B et al. Copyright © 2015, the authors.

pharmacological effect. Altındal et al. used an emulsion-diffusion-evaporation method to encapsulate melatonin in PLGA nanoparticles, and MG-63 cells were significantly inhibited by melatonin/PLGA nanoparticles (Altındal and Gümüşderelioglu, 2016). The results laid the foundation for studying melatonin/PLGA as an adjunct to conventional chemotherapy for osteosarcoma.

Salinomycin (SAL) has a highly selective anti-cancer activity. However, its low solubility in water reduces its therapeutic effect. To overcome this limitation, Irmak et al. encapsulated SAL in PLGA nanoparticles and evaluated the anti-cancer effect of the resulting delivery system. The results showed that PLGA/SAL nanoparticles could reduce proliferation and promote apoptosis of MG-63 cells more than SAL. The nanoparticles were also able to induce caspase-3 expression and inhibit that of β -catenin (Wnt/ β -catenin pathway) and c-myc genes in osteosarcoma cancer cells, thus achieving a synergistic anti-cancer effect (Irmak et al., 2020). The findings showed that PLGA/SAL nanoparticles were faster and more effective than free SAL in eliminating osteosarcoma cells.

PLGA-carbon nanotube (CNT) conjugates provide binding targets for the caspase-3 (CP3) to form a CNT-PLGA-CP3 coupling that can effectively transduce cells and inhibit cell proliferation for up to 1 week at doses down to 0.05 $\mu\text{g}/\text{mL}$. These results are critical in demonstrating the ability of gene delivery using PLGA-functionalized CNTs for cell fate regulation (Cheng et al., 2013). The PLGA nanoparticles loaded with other anti-cancer agents, such as sclareol (Cosco et al., 2019), castalin (Zhang et al., 2022), and simvastatin

(Venkatesan et al., 2019; Jin et al., 2021a), also present potent anti-cancer activity, indicating that PLGA nanoparticle delivery systems have promising potential for treating bone cancers.

Although PLGA-based nanoparticles have been intensively explored for targeted cancer therapeutics because they promise to improve and prolong the efficacy of conventional anti-cancer drugs with fewer adverse effects, they suffer from limitations, including clearance by the reticuloendothelial system and insufficient penetration capacity to tumor cells (Zhang et al., 2016; Wang et al., 2020a). Membrane extracted from tumor cells could be employed for coating nanoparticles to achieve homologous targeting (Sun et al., 2016). Furthermore, nanoparticles coated with tumor membranes exhibited high conjugative capacity and specific uptake into homologous tumor cells, leading to lower levels of immune-clearance after routine administration (Harris et al., 2019). To take advantage of homologous targeting and minimized immunological clearance, Cai et al. prepared paclitaxel (PTX) loaded PLGA nanoparticles encapsulated in osteosarcoma cell membranes and macrophage membranes for the targeted delivery of chemotherapeutic agents to osteosarcoma (Cai et al., 2022). *In vitro* studies demonstrated that PTX-PLGA nanoparticles enhanced the PTX uptake by the tumor cells and caused apoptosis in the osteosarcomas. They showed excellent tumor-targeted activity and significant tumor growth inhibition and were less toxic than free PTX. The research offers a targeted delivery approach for osteosarcoma therapy. The human osteosarcoma cell membrane-coated PLGA nanoparticles loaded with IR780 significantly improved endocytosis *in vitro* and tumor

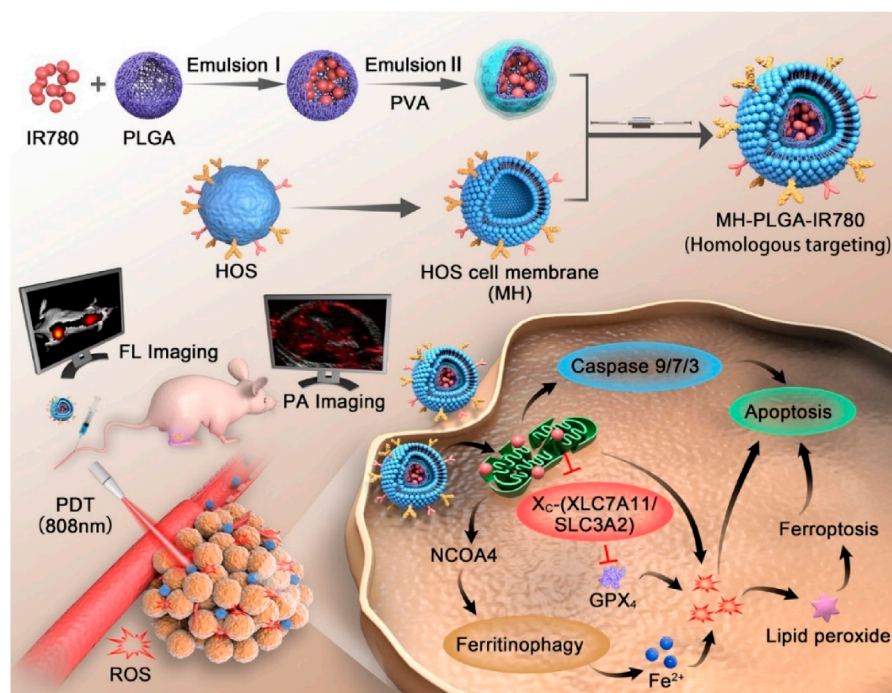


FIGURE 7

Schematic illustration of the construction of the MH-PLGA-IR780 NPs and the specific killing mechanism of the targeted theranostic nanoplateforms-mediated PDT approach. Reproduced with permission from Wang Y et al. Copyright © 2022, The Author(s).

accumulation *in vivo* and induced considerably apoptosis and iron phagocytosis in HOS cells by excessive accumulation of ROS (Figure 7). At the same time, the PLGA-IR780-loaded nanoparticles-guided PDT also significantly inhibited tumor growth *in vivo* (Wang et al., 2022a).

2.2 PLGA-based polymeric micelles

Polymeric micelles are nanometer-sized (5–100 nm) colloidal particles that readily self-assemble from amphiphilic polymers (Jones and Leroux, 1999; Movassaghian et al., 2015). Over the past 20 years, polymeric micelles have received considerable research focus in drug delivery, with particular emphasis on their possible uses in the main areas of delivering drugs, including drug solubilization, controlled drug release, and drug targeting (Croy and Kwon, 2006; Miyata et al., 2011; Ahmad et al., 2014). Polymer micelles have gained attention as a novel approach to treating and diagnosing cancer due to various advances compared to conventional drug delivery. These include the following key advantages, 1) improved drug solubility: many anti-cancer drugs have poor solubility, which can limit their effectiveness. Polymeric micelles can enhance drug solubility, allowing for improved drug delivery and efficacy; 2) selective targeting: polymeric micelles can be engineered to target specific cells or tissues, including cancer cells. This allows for more precise drug delivery and reduces the risk of off-target effects; 3) reduced toxicity: Polymeric micelles can help reduce the toxicity by minimizing their exposure to

healthy cells and tissues, reducing the risk of side effects and improving patient outcomes; 4) enhanced circulation time: polymeric micelles can increase the circulation time of drugs in the body, allowing for sustained drug release and improved therapeutic efficacy; 5) enhanced accumulation of anti-cancer drugs in the tumor: Their enhanced permeability and retention (EPR) effects allow them to accumulate in the tumor microenvironment. Overall, the advantages of polymeric micelles make them promising for treating cancers (Biswas et al., 2016; Yu et al., 2019b; Majumder et al., 2020; Ghosh and Biswas, 2021; Hari et al., 2023). One clinically successful micelle formulation is Genexol, which is paclitaxel encapsulated in a polylactic acid polymer micelle and was approved in Korea in 2007 for treating breast, lung, and ovarian cancer (Egusquiguirre et al., 2012; Cabral and Kataoka, 2014; Deshmukh et al., 2017; Kar et al., 2020; Norouzi and Hardy, 2021).

PLGA-based polymer micelles have demonstrated significant promise in treating bone cancers (Table 3). Research studies have shown that these micelles can effectively deliver anti-cancer drugs to tumor locations and increase the effectiveness of the drugs. In addition, PLGA-based polymeric micelles have also been found to enhance drug solubility and bioavailability, thereby reducing the side effects associated with chemotherapy. For example, PEG–PLGA micelles were used to encapsulate the gallium (III)-difluoride complex for treating osteosarcoma, and the results showed that the resulting nanoparticle formulations were 5,645 times more potent against osteosarcoma than doxorubicin and cisplatin. The nanoparticle formulation also induced nuclear damage to DNA,

TABLE 3 PLGA-based polymer micelles investigated for treating bone tumors.

| Anti-cancer drugs | Preparation method | Particle size (nm) | Encapsulation efficiency (%) | Drug loading (%) | Treatment outcomes | Ref |
|------------------------------------|------------------------------|--------------------|------------------------------|------------------|--|----------------------------------|
| Gallium (III)-difluoride complex 1 | Nanoprecipitation | 95.5 | 24.1 ± 0.7 | 4.8 ± 0.1 | Exhibits up to 5645-fold greater potency towards oses than doxorubicin and cisplatin | Passeri et al. (2023) |
| DOX and ALN | Solvent diffusion | 202 ± 4.2 | 83.7 ± 1.23 | 71.89 | Displayed superior cytotoxicity in MG-63 cells | Liu et al. (2016) |
| Dextran | W/O/W Double emulsion | ~180 | >90 | 28.5 | Exhibited significant apoptosis of mg63 cancer cells, significantly higher g2/m phase arrest in mg63 cells, showed a most significant anti-tumor activity with maximum tumor growth inhibition | Liu et al. (2015) |
| Mithramycin | Emulsion Solvent evaporation | 210–267 | 87 | — | Efficiently inhibits the signaling mediated by the pro-oncogenic factor SP1 | EstupiñánRendueles et al. (2021) |

downregulation of cyclooxygenase-2, and caspase-driven apoptosis (Passeri et al., 2023).

Liu developed chitosan (CS)-conjugated PLGA micelles loaded with docetaxel (DOC) and alendronate (ALN) to increase the therapeutic efficiency in osteosarcoma cells. CS-conjugated PLGA with dual-drug-loaded (DTX and ALN) micelles exhibited typical time-dependent cellular uptake and also showed higher cytotoxicity in MG-63 cells in comparison to blank micelles, which were found to be safe and biocompatible. The findings suggested that the combined loading of DTX and ALN into micelles enhances the therapeutic efficacy of the formulation for osteosarcoma therapy (Liu et al., 2016).

Cisplatin (CDDP) is a potent anti-cancer drug commonly used in the treatment of osteosarcoma, but the efficacy of CDDP is limited by severe undesirable side effects such as renal toxicity and neurotoxicity. The formulation of CDDP in polymer micelles is anticipated to reduce the adverse related impact while improving efficacy. Liu et al. encapsulated CDDP in ALN-PLGA micelles (PLD) conjugated with dextran (DX) to enhance the specificity of the delivered system for bone tumor cells and improve the efficacy of osteosarcoma treatment. *In vitro* cellular cytotoxicity tests showed that PLD/CDDP micelles had outstanding anti-cancer activity and exhibited substantial cellular uptake via an endocytic-mediated mechanism. In comparison with free CDDP, PLD/CDDP had a marked apoptosis effect on MG63 cancer cells. The most important thing, PLD/CDDP demonstrated the most pronounced anti-tumor efficacy and the highest tumor inhibition, suggesting excellent anti-cancer potential in osteosarcoma. Taken together, the PLD/CDDP micelles significantly improve the anti-cancer activity of CDDP in osteosarcoma cells, and PLD-containing CDDP formulations may represent a most promising and efficacious therapeutic approach for the control of osteosarcoma (Liu et al., 2015).

Miller et al. developed PEG-PLGA micelles for the co-delivery of PTX and ALN, which synergistically target bone metastases from breast cancer. *In vitro* results have shown that the PTX-PLGA-ALN micelles have almost identical cytotoxic as well as anti-angiogenic features to those of the free drugs. Furthermore, in a model of mCherry-infected tibia cancer, PTX-PLGA-ALN micelles achieved superior efficacy and safety compared to free PTX. The results

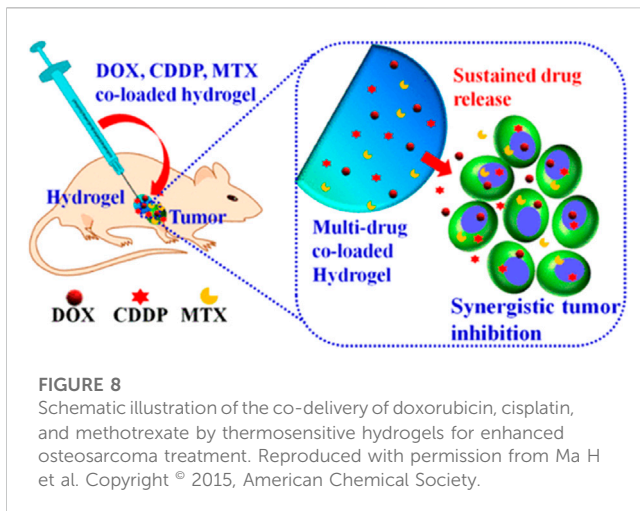
showed that the selective accumulation of the PTX-PLGA-ALN micelles in the tumors resulted in a higher inhibition of tumor growth than the controls (Miller et al., 2013).

Mithramycin A (MTM), a natural chrysophanol polyketide, has been used to treat several types of cancer. Despite its efficacy, serious adverse effects have hindered its use in clinical practice at the concentrations necessary to achieve a beneficial therapeutic outcome. Estupiñán et al. provided MTM-loaded PLGA micelles for efficient nano-delivery of MTM. These MTM nano delivery systems mimic the potent anti-tumor efficacy of free MTM in both liposarcoma and chondrosarcoma models. As with free MTM, nanocarrier-delivered MTM also effectively suppressed SP1-mediated signaling. This suggests they may provide a safer delivery option for MTM that could be investigated for clinical use in the future (EstupiñánRendueles et al., 2021).

These studies suggest that PLGA-based polymeric micelles have great potential for treating bone cancers and could provide a promising alternative to traditional chemotherapy. At the same time, further exploration is necessary to fully understand the potential of these micelles in the treatment of bone cancer. The initial results are promising and suggest they may be a viable treatment option.

3 PLGA-based local drug delivery systems

Local drug delivery systems offer the opportunity to advance the efficiency and acceptability of cancer therapy by maximizing drug delivery to the target site. Polymeric hydrogels loaded with anti-cancer agents can be delivered close to the tumor of interest and generate adequate concentrations of the drug locally (Cirillo et al., 2019; Fan et al., 2019; Kesharwani et al., 2021; Xiao et al., 2021; Yu et al., 2021). Because the drug is administrated locally rather than intravenously, serious side effects due to high drug levels would be minimized (Wei et al., 2017; Zheng et al., 2017; Darge et al., 2019; Zhou et al., 2019; Rafael et al., 2021). Injectable and biodegradable hydrogels have attracted substantial attention in the biomedicine field because they allow for more precise



implantation into hard-to-reach tissue sites and site-specific delivery, as well as their injectability and biodegradability (Li et al., 2012; Lee et al., 2019; Mallick et al., 2020; An et al., 2021; Zhou et al., 2021). Among them, The FDA-approved amphiphilic triblock copolymers PLGA-PEG-PLGA have been employed to prepare thermosensitive hydrogel formulations and received much interest for their medical application potential due to their excellent biological compatibility and biodegradation (Gao et al., 2011; López-Cano et al., 2021; Ghandforoushan et al., 2022; Heine et al., 2022; Lin et al., 2022; Yuan et al., 2022).

3.1 PLGA-based hydrogels for local drug delivery

PLGA-based hydrogels have shown great promise in the therapy of bone tumors. These hydrogels can be loaded with drugs or other therapeutic agents and implanted into the bone, where they slowly release the medicine over time. This approach allows accurate and selective drug delivery directly to the cancer cells with minimal adverse effects on surrounding normal tissues (Jin et al., 2021b; Liao et al., 2021). The FDA-approved PLGA-PEG-PLGA triblock copolymer is a candidate for the local delivery vehicle to bone tumors (Marques and Kumar, 2022). Ma et al. developed a novel strategy for osteosarcoma therapy using PLGA-PEG-PLGA hydrogel to release a combination of drugs, such as MTX, CDDP, and DOX (Figure 8). The results showed that the hydrogels co-loaded with multiple drugs displayed cytotoxicity that was synergistic towards the tumor cells *in vitro*. Following injection into Saos-2 osteosarcoma xenografts, drug-loaded hydrogels provided the most potent tumor suppression *in vivo* for 16 days (Ma et al., 2015). Furthermore, systemic toxicity was reduced, and no significant injury. Thus, local co-administration via a PLGA-PEG-PLGA hydrogel may be a viable therapy to enhance the treatment efficacy of osteosarcoma. The authors also used PLGA-PEG-PLGA hydrogel for local delivery of PLK1shRNA/polyether-modified polyethylene glycol (PEI-Lys) complex and DOX for osteosarcoma therapy. The resulting drug delivery system showed significant and synergistic effects in inducing

osteosarcoma cell apoptosis when cultured with Saos-2 and MG63 osteosarcoma cells. Following subcutaneous injection of the drug delivery system adjacent to Saos-2 osteosarcoma in nude mice, the hydrogels demonstrated more excellent anti-tumor activity *in vivo* (Ma et al., 2014). In particular, the combined *in vivo* therapy resulted in almost total inhibition of tumor proliferation for 16 days without significant organ damage, suggesting that co-delivery of PLK1 shRNA and DOX by PLGA-PEG-PLGA hydrogels might offer the opportunity for effective therapy of osteosarcoma in the clinic.

To develop a more effective combination therapy for treating osteosarcoma, Yang et al. used PLGA-PEG-PLGA as a vehicle to deliver DOX and β -cyclodextrin-curcumin (CD-CUR) to the target tumor in a controlled manner. The co-delivery system demonstrated superior anti-tumor efficacy and a greater capacity to induce apoptosis. Similarly, local PLGA-PEG-PLGA combination treatments exhibited a greater anti-tumor efficiency *in vivo* as compared to free DOX + CD-CUR or single-agent strategies (Yang et al., 2020). In another research, a PLGA-PEG-PLGA hydrogel loaded with DOX and CDDP was utilized for local combination chemotherapy of osteosarcoma. The resulting hydrogel was degradable and biocompatible. *In vitro* cell viability assays showed that the hydrogels co-loaded with DOX and CDDP exhibited synergistic anti-proliferative effects as well as high tumor growth inhibition efficiency. The *in vivo* experimental results indicated that the PLGA-PEG-PLGA hydrogel for local combination chemotherapy promoted increased tumor necrosis and enhanced the modulation of the expression of apoptosis-related genes (Si et al., 2022), indicating synergistic anti-tumor effectiveness *in vivo* with low systemic toxicity. These results indicated that persistent local co-delivery of DOX and CDDP via PLGA-PEG-PLGA hydrogels could be a promising approach to effectively treating osteosarcoma in the clinic.

Although PLGA-PEG-PLGA hydrogels have shown considerable therapeutic promise in local cancer treatment, the maximum tolerated dose (MTD) of these strategies is still unclear. To address this issue, Yang et al. employed PLGA-PEG-PLGA hydrogels loaded with DOX to evaluate the MTD of DOX in the local treatment of osteosarcoma (Yang et al., 2018). The hydrogels exhibited favorable injectable and biodegradable properties *in vivo*, with significantly prolonged drug residence time at the tumor location. The results showed that the local administration of DOX at 5.0 mg/kg could not suppress tumor-sustained growth or extend the survival duration, while the local administration of DOX at 30 mg/kg showed intense activity in suppressing tumor growth but also caused severe weight loss. At the same time, the local administration of DOX at 15 mg/kg showed markedly higher anti-tumor potency and extended average survival time as compared to free DOX (15 mg/kg). The improved MTD and reduced systemic toxicity of DOX administered with hydrogels will offer a potential therapy for osteosarcoma.

3.2 PLGA-based scaffolds for local drug delivery

Recently, local DDS based on bone scaffolds has attracted increasing interest. Drug-loaded scaffolds can generate high local

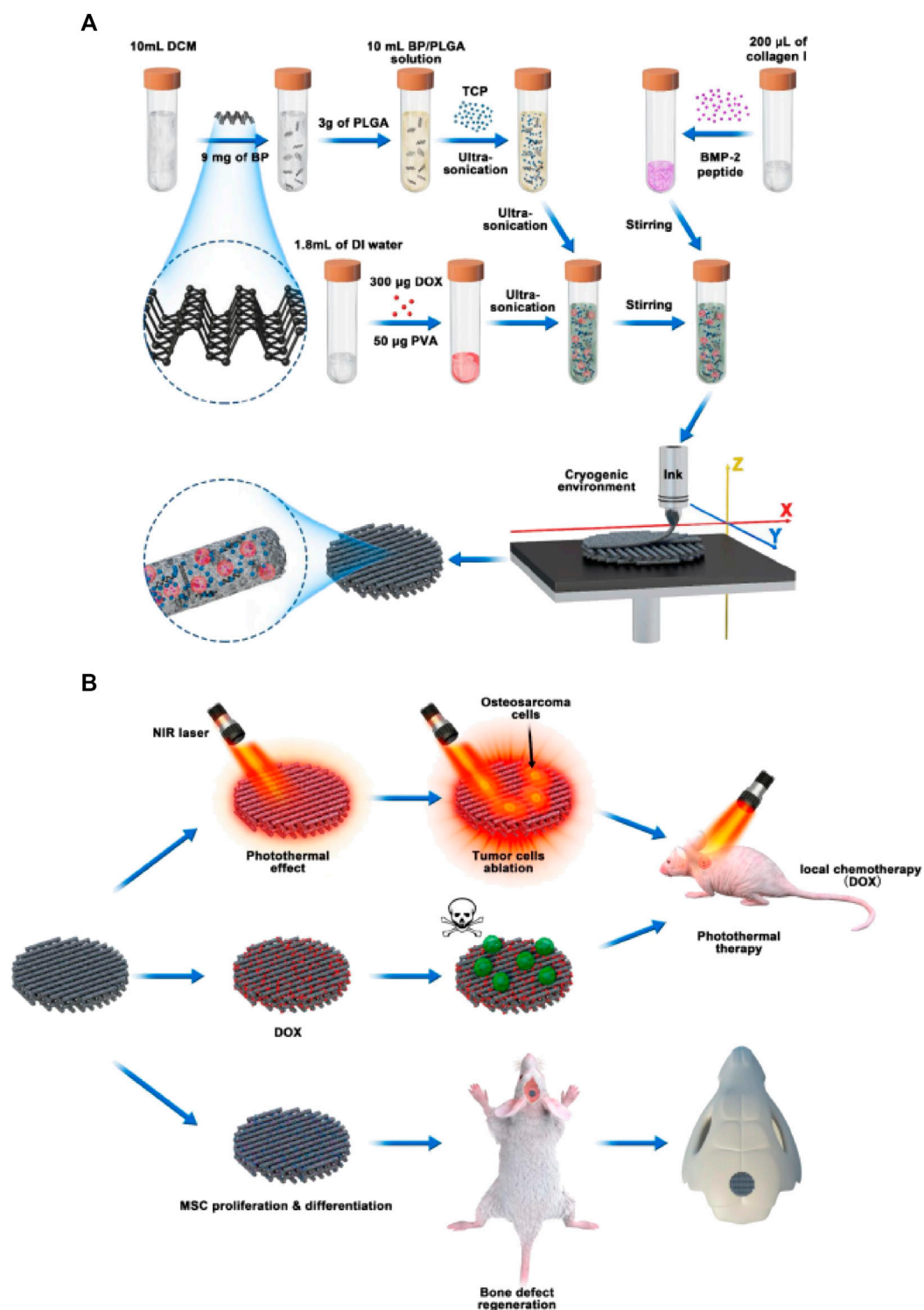


FIGURE 9

Schematic illustration of cryogenic 3D printing of multi-functional scaffolds and their multi-functions. (A) formulation of multi-delivery inks and 3D printing of multi-functional scaffolds; (B) tumor tissue ablation in nude mice through photo-thermal therapy and localized chemotherapy and regeneration of cranial bone defects of rats implanted with multi-functional scaffolds. Reproduced with permission from Wang C et al.

drug concentrations to eradicate residual tumor cells. This approach promises to prevent tumor recurrence and reduce systemic adverse events more effectively than intravenous drug

delivery. The right biomaterial can both treat tumors and promote bone regeneration. Compared to natural polymers, synthetic polymers offer adjustable properties for bone

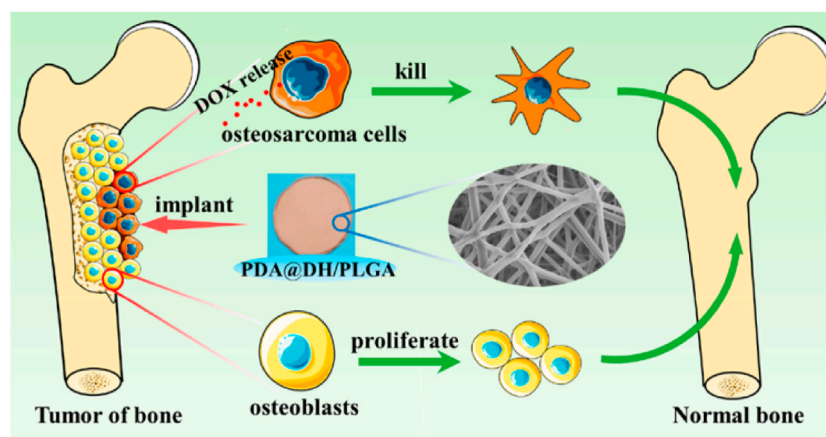


FIGURE 10

Schematic illustration of polydopamine on doxorubicin-loaded lamellar hydroxyapatite/PLGA composite fibers for inhibiting bone tumor recurrence and enhancing bone regeneration. Reproduced with permission from Lu Y et al. Copyright © 2021, American Chemical Society.

scaffolds, allowing the control of molecular weight or functional group ratios to modulate mechanical strength, degradation, and other properties. Among synthetic polymers, PLGA is the most commonly used to fabricate porous scaffolds due to its controlled biodegradability, limited toxicity, and potential capabilities. PLGA-based scaffolds have been developed for the localized delivery system to treat bone tumors and regenerate bone (Sarigol-Calamak and Hascicek, 2018; Wang et al., 2022b).

Using a 3D printing technique at low temperatures, Li et al. fabricated a scaffold composed of PLGA/ β -TCP incorporating salvianolic acid B. Their results indicated that incorporating SB could promote the osseointegration of the obtained scaffolds by enhancing the effect of salvianolic acid B on angiogenesis and osteogenesis (Lin et al., 2019). However, the acidic product produced by the degradation of PLGA may cause an inflammation, which the incorporation of CaP materials can eliminate (Zhao et al., 2020b; Liang et al., 2020; Sokolova et al., 2020). In comparison to conventional chemotherapy, magnetic hyperthermia and photo-thermal therapy are attracting more attention because of their low invasive potential and high specificity. Li et al. fabricated a magnetic scaffold of PLGA, Fe_3O_4 , and HA nanoparticles (Li et al., 2019b). It was found that the resulting scaffolds could raise the internal temperature to 47°C and induce substantial tumor cell apoptosis *in vitro*. In addition, the scaffolds showed an excellent osteogenic capacity to allow new bone to be regenerated in the defect site, with the result that bone volume/total was significantly higher than the untreated group (Li et al., 2019b). Wang et al. (Wang et al., 2020b) used black phosphorus nanosheets, DOX, and hydrophilic osteogenic peptides as photo-thermal agents, chemotherapeutic agents, and osteogenic factors, respectively, blended with β -TCP nanoparticle and PLGA for 3D printing to obtain drug delivery scaffolds for the treatment of bone tumor resection-induced defects (Figure 9). BDPTP scaffolds can cause tumor cell death *in vitro* and tumor clearance *in vivo*. The scaffold has a photo-thermal effect, and laser radiation with a wavelength of 808 nm can raise the BDPTP scaffold temperature

to 60°C within 10 min. The MG63 cells attached to the scaffold were nearly eliminated after 1 day of culturing, the tumor disappeared after 4 days, and the tumor recurrence rate *in vivo* was low by combining chemotherapy and photo-thermal treatment. The *in vivo* experiments showed that the scaffold promoted new bone growth through its osteoinductive and osteogenic inductive effects (Wang et al., 2020b). Therefore, as a multi-functional platform, BDP-PT scaffolds can promote apoptosis and bone tissue regeneration in bone cancer, thereby meeting the clinical need of treating bone cancer.

Bone regeneration after resection of tumor tissue still faces a vast clinical obstacle in the therapy of bone defects, the therapeutic approaches that promote bone regeneration while being antimetastatic are of great interest. s. Hu et al. prepared drug delivery scaffolds by encapsulating BPQDs in PLGA nanoparticles and mixing them with wood/silk hydrogels to achieve adequate mechanical strength, bone formation, and tumor treatment (Hu et al., 2022). The drug delivery scaffolds further potentially enhanced osteogenesis *in vivo* by efficiently enhancing bone mesenchymal stem cells' growth, differentiation, and migration (Hu et al., 2022). More important, the BPQDs in the drug delivery scaffolds could suppress osteoclast differentiation and exert photo-thermal activity on spinal tumor metastasis (Hu et al., 2022). Significant inhibition of the growth of human osteosarcoma cells *in vitro* and reduction of tumor progression *in vivo* was also observed with the nanohydroxyapatite/collagen scaffolds filled with DOX-PLGA nanoparticles (Rong et al., 2016). These researches offer potential evidence for the possible treatment application in clinics for bone regeneration and bone metastasis ablation.

To overcome the difficulties of tumor reoccurrence and extensive bone defect, Long et al. designed an innovative multi-functional PLGA/Mg scaffold for the comprehensive postoperative management of osteosarcoma (Long et al., 2021), which resulted in the total inhibition of tumor reoccurrence when exposed to near-infrared laser radiation as well as the successful repair of bone

defects *in vivo* (Long et al., 2021). In addition, the PLGA/Mg scaffold loaded with β -tricalcium phosphate (β -TCP) also exhibited both osteogenic and angiogenic capabilities, which had a synergetic effect in promoting the new bone generation and strengthening the quality of newly regenerated bone (Lai et al., 2019). The innovative PLGA/Mg scaffolds exhibited superior performance in suppressing postoperative osteosarcoma recurrence and regenerating bone, offering a potential clinically relevant approach for treating osteosarcoma. Lu (Lu et al., 2021) developed a composite scaffold coated with polydopamine, consisting of lamellar hydroxyapatite loaded with DOX and PLGA, to inhibit tumors and repair bones (Figure 10). The scaffold significantly inhibited tumor cell growth, followed by enhanced osteoblast adhesion and proliferation. Improved bone growth around the scaffold was also demonstrated *in vivo* (Lu et al., 2021). The dual-function scaffold holds significant potential for the therapy of bone tumors.

4 Conclusion

Overall, with several studies demonstrating their efficacy in improving survival in animal models, the progress of PLGA-based drug delivery systems in effectively inhibiting bone tumors and promoting bone tissue regeneration is very promising. However, there are still challenges associated with this technology. Most PLGA-based drug delivery systems do not achieve zero-level release, resulting in uneven local drug levels during treatment, and the accurately controlled distribution of the drug in time and space continues to be a significant challenge, making long-term tumor suppression difficult. An increase in drug load may benefit tumor treatment, while high concentrations of chemotherapeutic agents may cause local tissue toxicity that may be detrimental to bone reconstruction. Optimizing these systems and improving their targeting and delivery efficiency will be the subject of further studies. To overcome this significant hurdle, more detailed studies and extensive research are needed to develop new

strategies to optimize drug release kinetics through interdisciplinary collaboration among experts in clinical medicine, materials science, and nanotechnology. Clinical trials will also be needed to evaluate the safety and effectiveness of these systems on human patients with bone tumors.

Author contributions

FL wrote the manuscript, EQ checked and revised the manuscript. All authors contributed to the article and approved the submitted version.

Funding

This work was supported by the Medical-Industrial Crossover Research Fund of Liaoning Cancer Hospital and Dalian University of Technology (YG2022ZD006).

Conflict of interest

The authors declare that the research was conducted in the absence of any commercial or financial relationships that could be construed as a potential conflict of interest.

Publisher's note

All claims expressed in this article are solely those of the authors and do not necessarily represent those of their affiliated organizations, or those of the publisher, the editors and the reviewers. Any product that may be evaluated in this article, or claim that may be made by its manufacturer, is not guaranteed or endorsed by the publisher.

References

- Ahmad, Z., Shah, A., Siddiq, M., and Kraatz, H. B. (2014). Polymeric micelles as drug delivery vehicles. *Rsc Adv.* 4 (33), 17028–17038. doi:10.1039/c3ra47370h
- Altundal, D. Ç., and Gümüşderelioglu, M. (2016). Melatonin releasing PLGA micro/nanoparticles and their effect on osteosarcoma cells. *J. Microencapsul.* 33 (1), 53–63. doi:10.3109/02652048.2015.1115901
- Ambrosio, L., Raucci, M. G., Vadalà, G., Papalia, R., and Denaro, V. (2021). Innovative biomaterials for the treatment of bone cancer. *Int. J. Mol. Sci.* 22 (15), 8214. doi:10.3390/ijms22158214
- An, H., Yang, Y., Zhou, Z., Bo, Y., Wang, Y., He, Y., et al. (2021). Pectin-based injectable and biodegradable self-healing hydrogels for enhanced synergistic anti-cancer therapy. *Acta Biomater.* 131, 149–161. doi:10.1016/j.actbio.2021.06.029
- Bădilă, A. E., Rădulescu, D. M., Niculescu, A. G., Grumezescu, A. M., Rădulescu, M., and Rădulescu, A. R. (2021). Recent advances in the treatment of bone metastases and primary bone tumors: An up-to-date review. *Cancers* 13 (16), 4229. doi:10.3390/cancers13164229
- Bar-Zeev, M., Livney, Y. D., and Assaraf, Y. G. (2017). Targeted nanomedicine for cancer therapeutics: Towards precision medicine overcoming drug resistance. *Drug Resist. Updat.* 31, 15–30. doi:10.1016/j.drug.2017.05.002
- Bhatia, S. N., Chen, X., Dobrovolskaia, M. A., and Lammers, T. (2022). Cancer nanomedicine. *Nat. Rev. Cancer* 22 (10), 550–556. doi:10.1038/s41568-022-00496-9
- Biswas, S., Kumari, P., Lakhani, P. M., and Ghosh, B. (2016). Recent advances in polymeric micelles for anti-cancer drug delivery. *Eur. J. Pharm. Sci.* 83, 184–202. doi:10.1016/j.ejps.2015.12.031
- Bondy, S. C., and Campbell, A. (2018). Mechanisms underlying tumor suppressive properties of melatonin. *Int. J. Mol. Sci.* 19 (8), 2205. doi:10.3390/ijms19082205
- Bone Tumors (2021). *Diagnosis and therapy today[M]*. Berlin, Germany: Springer Nature.
- Cabral, H., and Kataoka, K. (2014). Progress of drug-loaded polymeric micelles into clinical studies. *J. Control. Release* 190, 465–476. doi:10.1016/j.jconrel.2014.06.042
- Cai, J. X., Liu, J. H., Wu, J. Y., Li, Y. J., Qiu, X. H., Xu, W. J., et al. (2022). Hybrid cell membrane-functionalized biomimetic nanoparticles for targeted therapy of osteosarcoma. *Int. J. Nanomedicine* 17, 837–854. doi:10.2147/ijn.s346685
- Cenni, E., Avnet, S., Granchi, D., Fotia, C., Salerno, M., Miceli, D., et al. (2012). The effect of poly (D, L-lactide-co-glycolide)-alendronate conjugate nanoparticles on human osteoclast precursors. *J. Biomaterials Sci. Polym. Ed.* 23 (10), 1285–1300. doi:10.1163/092050611x580373
- Cenni, E., Granchi, D., Avnet, S., Fotia, C., Salerno, M., Miceli, D., et al. (2008). Biocompatibility of poly (D, L-lactide-co-glycolide) nanoparticles conjugated with alendronate. *Biomaterials* 29 (10), 1400–1411. doi:10.1016/j.biomaterials.2007.12.022
- Chaudhari, K. R., Kumar, A., Khandelwal, V. K. M., Ukawala, M., Manjappa, A. S., Mishra, A. K., et al. (2012). Bone metastasis targeting: A novel approach to reach bone

using zoledronate anchored PLGA nanoparticle as carrier system loaded with docetaxel. *J. Control. release* 158 (3), 470–478. doi:10.1016/j.jconrel.2011.11.020

Chen, B., Yang, J. Z., Wang, L. F., Zhang, Y. J., and Lin, X. J. (2015). Ifosfamide-loaded poly (lactic-co-glycolic acid) PLGA-dextran polymeric nanoparticles to improve the anti-tumor efficacy in osteosarcoma. *BMC cancer* 15, 752–759. doi:10.1186/s12885-015-1735-6

Cheng, Q., Blais, M. O., Harris, G., and Jabbarzadeh, E. (2013). PLGA-carbon nanotube conjugates for intercellular delivery of caspase-3 into osteosarcoma cells. *PLoS One* 8 (12), e81947. doi:10.1371/journal.pone.0081947

Choi, J. H., and Ro, J. Y. (2021). The 2020 WHO classification of tumors of bone: An updated review. *Adv. anatomic pathology* 28 (3), 119–138. doi:10.1097/pap.0000000000000293

Chowdhry, M., Cockshott, S., and Jeys, L. (2009). Secondary malignant tumours of bone. *Surg. Oxf.* 27 (2), 86–89. doi:10.1016/j.mpsur.2008.12.008

Cirillo, G., Spizzirri, U. G., Curcio, M., and Iemma (2019). Injectable hydrogels for cancer therapy over the last decade. *Pharmaceutics* 11 (9), 486. doi:10.3390/pharmaceutics11090486

Cosco, D., Mare, R., Paolino, D., Salvatici, M. C., Cilurzo, F., and Fresta, M. (2019). Scleroel-loaded hyaluronan-coated PLGA nanoparticles: Physico-chemical properties and *in vitro* anti-cancer features. *Int. J. Biol. Macromol.* 132, 550–557. doi:10.1016/j.ijbiomac.2019.03.241

Croy, S. R., and Kwon, G. S. (2006). Polymeric micelles for drug delivery. *Curr. Pharm. Des.* 12 (36), 4669–4684. doi:10.2174/138161206779026245

Darge, H. F., Andrigue, A. T., Tsai, H. C., and Lai, J. Y. (2019). Polysaccharide and polypeptide based injectable thermo-sensitive hydrogels for local biomedical applications. *Int. J. Biol. Macromol.* 133, 545–563. doi:10.1016/j.ijbiomac.2019.04.131

de Lázaro, I., and Mooney, D. J. (2021). Obstacles and opportunities in a forward vision for cancer nanomedicine. *Nat. Mater.* 20 (11), 1469–1479. doi:10.1038/s41563-021-01047-7

Deshmukh, A. S., Chauhan, P. N., Noolvi, M. N., Chaturvedi, K., Ganguly, K., Shukla, S. S., et al. (2017). Polymeric micelles: Basic research to clinical practice. *Int. J. Pharm.* 532 (1), 249–268. doi:10.1016/j.ijpharm.2017.09.005

Egusquiguirre, S. P., Igartua, M., Hernández, R. M., and Pedraz, J. L. (2012). Nanoparticle delivery systems for cancer therapy: Advances in clinical and preclinical research. *Clin. Transl. Oncol.* 14, 83–93. doi:10.1007/s12094-012-0766-6

Estupiñán, Ó., Rendueles, C., Suárez, P., Rey, V., Murillo, D., Moris, F., et al. (2021). Nano-encapsulation of mithramycin in transfectosomes and polymeric micelles for the treatment of sarcomas. *J. Clin. Med.* 10 (7), 1358. doi:10.3390/jcm10071358

Fan, D., Tian, Y., and Liu, Z. (2019). Injectable hydrogels for localized cancer therapy. *Front. Chem.* 7, 675. doi:10.3389/fchem.2019.00675

Ferguson, J. L., and Turner, S. P. (2018). Bone cancer: Diagnosis and treatment principles. *Am. Fam. physician* 98 (4), 205–213.

Gao, Y., Ren, F., Ding, B., Sun, N., Liu, X., Ding, X., et al. (2011). A thermo-sensitive PLGA-PEG-PLGA hydrogel for sustained release of docetaxel. *J. drug Target.* 19 (7), 516–527. doi:10.3109/1061186x.2010.519031

Gdowski, A. S., Ranjan, A., Sarker, M. R., and Vishwanatha, J. K. (2017). Bone-targeted cabazitaxel nanoparticles for metastatic prostate cancer skeletal lesions and pain. *Nanomedicine* 12 (17), 2083–2095. doi:10.2217/nnm-2017-0190

Germain, M., Caputo, F., Metcalfe, S., Tosi, G., Spring, K., Åslund, A. K., et al. (2020). Delivering the power of nanomedicine to patients today. *J. Control. Release* 326, 164–171. doi:10.1016/j.jconrel.2020.07.007

Ghandforoushan, P., Hanaee, J., Aghazadeh, Z., Samiei, M., Navali, A. M., Khatibi, A., et al. (2022). Novel nanocomposite scaffold based on gelatin/PLGA-PEG-PLGA hydrogels embedded with TGF-β1 for chondrogenic differentiation of human dental pulp stem cells *in vitro*. *Int. J. Biol. Macromol.* 201, 270–287. doi:10.1016/j.ijbiomac.2021.12.097

Ghosh, B., and Biswas, S. (2021). Polymeric micelles in cancer therapy: State of the art. *J. Control. Release* 332, 127–147. doi:10.1016/j.jconrel.2021.02.016

Gurunathan, S., Qasim, M., Kang, M. H., and Kim, J. H. (2021). Role and therapeutic potential of melatonin in various type of cancers. *OncoTargets Ther.* 14, 2019–2052. doi:10.2147/ott.s298512

Hari, S. K., Gauba, A., Shrivastava, N., Tripathi, R. M., Jain, S. K., and Pandey, A. K. (2023). Polymeric micelles and cancer therapy: An ingenious multimodal tumor-targeted drug delivery system. *Drug Deliv. Transl. Res.* 13 (1), 135–163. doi:10.1007/s13346-022-01197-4

Harris, J. C., Scully, M. A., and Day, E. S. (2019). Cancer cell membrane-coated nanoparticles for cancer management. *Cancers* 11 (12), 1836. doi:10.3390/cancers11121836

Hayashi, K., and Tsuchiya, H. (2022). The role of surgery in the treatment of metastatic bone tumor. *Int. J. Clin. Oncol.* 27 (8), 1238–1246. doi:10.1007/s10147-022-02144-6

He, H., Ni, J., and Huang, J. U. N. (2014). Molecular mechanisms of chemoresistance in osteosarcoma (Review). *Oncol. Lett.* 7 (5), 1352–1362. doi:10.3892/ol.2014.1935

Heine, S., Aguilar-Pimentel, A., Russkamp, D., Alessandrini, F., Gailus-Durner, V., Fuchs, H., et al. (2022). Thermosensitive PLGA-PEG-PLGA hydrogel as depot matrix for allergen-specific immunotherapy. *Pharmaceutics* 14 (8), 1527. doi:10.3390/pharmaceutics14081527

Hu, Z., Lu, J., Hu, A., Dou, Y., Wang, S., Su, D., et al. (2022). Engineering BPQDs/PLGA nanospheres-integrated wood hydrogel bionic scaffold for combinatory bone repair and osteolytic tumor therapy. *Chem. Eng. J.* 446, 137269. doi:10.1016/j.cej.2022.137269

Huang, Y. J., He, A. N., Sun, Y. J., Shen, Z., Min, D. L., and Yao, Y. (2015). Continuous-infusion ifosfamide and doxorubicin combination as second-line chemotherapy for recurrent or refractory osteosarcoma patients in China: A retrospective study. *Asian Pac. J. Cancer Prev.* 16 (6), 2391–2395. doi:10.7314/apjcp.2015.16.6.2391

Irmak, G., Öztürk, M. G., and Gümüşderelioglu, M. (2020). Salinomycin encapsulated PLGA nanoparticles eliminate osteosarcoma cells via inducing/inhibiting multiple signaling pathways: Comparison with free salinomycin. *J. Drug Deliv. Sci. Technol.* 58, 101834. doi:10.1016/j.jddst.2020.101834

Irvine, D. J., and Dane, E. L. (2020). Enhancing cancer immunotherapy with nanomedicine. *Nat. Rev. Immunol.* 20 (5), 321–334. doi:10.1038/s41577-019-0269-6

Jin, H., Ji, Y., Cui, Y., Xu, L., Liu, H., and Wang, J. (2021). Simvastatin-incorporated drug delivery systems for bone regeneration. *ACS Biomaterials Sci. Eng.* 7 (6), 2177–2191. doi:10.1021/acsbmaterials.1c00462

Jin, S., Xia, X., Huang, J., Yuan, C., Zuo, Y., Li, Y., et al. (2021). Recent advances in PLGA-based biomaterials for bone tissue regeneration. *Acta biomater.* 127, 56–79. doi:10.1016/j.actbio.2021.03.067

Jones, M. C., and Leroux, J. C. (1999). Polymeric micelles—a new generation of colloidal drug carriers. *Eur. J. Pharm. Biopharm.* 48 (2), 101–111. doi:10.1016/s0939-6411(99)00039-9

Kaneko, T., Fujioka, T., Suzuki, Y., Sato, Y., and Itoh, H. (2016). Performance characteristics between TDx® FLx and TBA™-25FR for the therapeutic drug monitoring of methotrexate. *J. Pharm. Health Care Sci.* 2 (1), 7–5. doi:10.1186/s40780-016-0042-y

Kar, S., Vignesh, K., and Kolhe, U. D. (2020). “An overview of paclitaxel delivery systems,” in *Sustainable agriculture reviews* (Berlin Germany: Springer), 161–215.

Kesharwani, P., Bisht, A., Alexander, A., Dave, V., and Sharma, S. (2021). Biomedical applications of hydrogels in drug delivery system: An update. *J. Drug Deliv. Sci. Technol.* 66, 102914. doi:10.1016/j.jddst.2021.102914

Kim, M., and Kim, D. J. (2018). GFRA1: A novel molecular target for the prevention of osteosarcoma chemoresistance. *Int. J. Mol. Sci.* 19 (4), 1078. doi:10.3390/ijms19041078

Lai, Y., Li, Y., Cao, H., Long, J., Wang, X., Li, L., et al. (2019). Osteogenic magnesium incorporated into PLGA/TCP porous scaffold by 3D printing for repairing challenging bone defect. *Biomaterials* 197, 207–219. doi:10.1016/j.biomaterials.2019.01.013

Lee, A. L. Z., Yang, C., Gao, S., Hedrick, J. L., and Yang, Y. Y. (2019). Subcutaneous vaccination using injectable biodegradable hydrogels for long-term immune response. *Nanomedicine Nanotechnol. Biol. Med.* 21, 102056. doi:10.1016/j.nano.2019.102056

Li, M., Liu, J., Cui, X., Sun, G., Hu, J., Xu, S., et al. (2019). Osteogenesis effects of magnetic nanoparticles modified-porous scaffolds for the reconstruction of bone defect after bone tumor resection. *Regen. Biomater.* 6 (6), 373–381. doi:10.1093/rb/rbz019

Li, X., Valdes, S. A., Alzhrani, R. F., Hufnagel, S., Hursting, S. D., and Cui, Z. (2019). Zoledronic acid-containing nanoparticles with minimum premature release show enhanced activity against extraskeletal tumor. *ACS Appl. Mater. interfaces* 11 (7), 7311–7319. doi:10.1021/acsami.8b16588

Li, Y., Rodrigues, J., and Tomas, H. (2012). Injectable and biodegradable hydrogels: Gelation, biodegradation and biomedical applications. *Chem. Soc. Rev.* 41 (6), 2193–2221. doi:10.1039/c1cs15203c

Liang, W., Gao, M., Lou, J., Bai, Y., Zhang, J., Lu, T., et al. (2020). Integrating silicon/zinc dual elements with PLGA microspheres in calcium phosphate cement scaffolds synergistically enhances bone regeneration. *J. Mater. Chem. B* 8 (15), 3038–3049. doi:10.1039/c9tb02901j

Liao, J., Han, R., Wu, Y., and Qian, Z. (2021). Review of a new bone tumor therapy strategy based on bifunctional biomaterials. *Bone Res.* 9 (1), 18. doi:10.1038/s41413-021-00139-z

Lin, S., Cui, L., Chen, G., Huang, J., Yang, Y., Zou, K., et al. (2019). PLGA/β-TCP composite scaffold incorporating salvianolic acid B promotes bone fusion by angiogenesis and osteogenesis in a rat spinal fusion model. *Biomaterials* 196, 109–121. doi:10.1016/j.biomaterials.2018.04.004

Lin, Y. W., Fang, C. H., Yang, C. Y., Liang, Y. J., and Lin, F. H. (2022). Investigating a curcumin-Loaded PLGA-PEG-PLGA thermo-sensitive hydrogel for the prevention of Alzheimer's disease. *Antioxidants* 11 (4), 727. doi:10.3390/antiox11040727

Liu, F. S. (2009). Mechanisms of chemotherapeutic drug resistance in cancer therapy—A quick review. *Taiwan. J. Obstetrics Gynecol.* 48 (3), 239–244. doi:10.1016/s1028-4559(09)60296-5

- Liu, P., Sun, L., Zhou, D., Zhang, P., Wang, Y. h., Li, D., et al. (2015). Development of alendronate-conjugated poly (lactic-co-glycolic acid)-dextran nanoparticles for active targeting of cisplatin in osteosarcoma. *Sci. Rep.* 5 (1), 17387. doi:10.1038/srep17387
- Liu, Y. F., Liu, R., Li, X. Y., Song, Z., and Zhao, X. H. (2016). Development of docetaxel and alendronate-loaded chitosan-conjugated polylactide-co-glycolide nanoparticles: *in vitro* characterization in osteosarcoma cells. *Trop. J. Pharm. Res.* 15 (7), 1353–1360. doi:10.4314/tjpr.v15i7.1
- Long, J., Zhang, W., Chen, Y., Teng, B., Liu, B., Li, H., et al. (2021). Multi-functional magnesium incorporated scaffolds by 3D-Printing for comprehensive postsurgical management of osteosarcoma. *Biomaterials* 275, 120950. doi:10.1016/j.biomaterials.2021.120950
- López-Cano, J. J., Sigen, A., Andrés-Guerrero, V., Tai, H., Bravo-Osuna, I., Molina-Martínez, I. T., et al. (2021). Thermo-responsive PLGA-PEG-PLGA hydrogels as novel injectable platforms for neuroprotective combined therapies in the treatment of retinal degenerative diseases. *Pharmaceutics* 13 (2), 234. doi:10.3390/pharmaceutics13020234
- Lu, Y., Chen, G., Long, Z., Ji, C., Wang, F., et al. (2019). Novel 3D-printed prosthetic composite for reconstruction of massive bone defects in lower extremities after malignant tumor resection. *J. bone Oncol.* 16, 100220. doi:10.1016/j.jbo.2019.100220
- Lu, Y., Wan, Y., Gan, D., Zhang, Q., Luo, H., and Deng, X. (2021). Enwrapping polydopamine on doxorubicin-loaded lamellar hydroxyapatite/poly (lactic-co-glycolic acid) composite fibers for inhibiting bone tumor recurrence and enhancing bone regeneration. *ACS Appl. Bio Mater.* 4 (8), 6036–6045. doi:10.1021/acsabm.1c00297
- Ma, H., He, C., Cheng, Y., Li, D., Gong, Y., Liu, J., et al. (2014). PLK1shRNA and doxorubicin co-loaded thermosensitive PLGA-PEG-PLGA hydrogels for osteosarcoma treatment. *Biomaterials* 35 (30), 8723–8734. doi:10.1016/j.biomaterials.2014.06.045
- Ma, H., He, C., Cheng, Y., Yang, Z., Zang, J., Liu, J., et al. (2015). Localized co-delivery of doxorubicin, cisplatin, and methotrexate by thermosensitive hydrogels for enhanced osteosarcoma treatment. *ACS Appl. Mater. interfaces* 7 (49), 27040–27048. doi:10.1021/acsami.5b09112
- Majumder, N., Das, G. N., and Das, S. K. (2020). Polymeric micelles for anti-cancer drug delivery. *Ther. Deliv.* 11 (10), 613–635. doi:10.4155/tde-2020-0008
- Mallick, S. P., Suman, D. K., Singh, B. N., Srivastava, P., Siddiqui, N., Yella, V. R., et al. (2020). Strategies toward development of biodegradable hydrogels for biomedical applications. *Polymer-Plastics Technol. Mater.* 59 (9), 911–927. doi:10.1080/25740881.2020.1719135
- Marques, S. M., and Kumar, L. (2022). PKPD of PLGA-PEG-PLGA copolymeric micelles[M]/Pharmacokinetics and pharmacodynamics of nanoparticulate drug delivery systems. Cham: Springer International Publishing, 273–292.
- Massagué, J., and Obenauf, A. C. (2016). Metastatic colonization by circulating tumour cells. *Nature* 529 (7586), 298–306. doi:10.1038/nature17038
- Miller, K., Clementi, C., Polyak, D., Eldar-Boock, A., Benayoun, L., Barshack, I., et al. (2013). Poly (ethylene glycol)-paclitaxel-alendronate self-assembled micelles for the targeted treatment of breast cancer bone metastases. *Biomaterials* 34 (15), 3795–3806. doi:10.1016/j.biomaterials.2013.01.052
- Miyata, K., Christie, R. J., and Kataoka, K. (2011). Polymeric micelles for nano-scale drug delivery. *React. Funct. Polym.* 71 (3), 227–234. doi:10.1016/j.reactfunctpolym.2010.10.009
- Moradkhani, F., Moloudizargari, M., Fallah, M., Asghari, N., Heidari Khoei, H., and Asghari, M. H. (2020). Immunoregulatory role of melatonin in cancer. *J. Cell. Physiology* 235 (2), 745–757. doi:10.1002/jcp.29036
- Movassaghian, S., Merkel, O. M., and Torchilin, V. P. (2015). Applications of polymer micelles for imaging and drug delivery. *Wiley Interdiscip. Rev. Nanomedicine Nanobiotechnology* 7 (5), 691–707. doi:10.1002/wnan.1332
- Norouzi, M., and Hardy, P. (2021). Clinical applications of nanomedicines in lung cancer treatment. *Acta Biomater.* 121, 134–142. doi:10.1016/j.actbio.2020.12.009
- Oun, R., Moussa, Y. E., and Wheate, N. J. (2018). The side effects of platinum-based chemotherapy drugs: A review for chemists. *Dalton Trans.* 47 (19), 6645–6653. doi:10.1039/c8dt00838h
- Pantel, K., Alix-Panabières, C., and Riethdorf, S. (2009). Cancer micrometastases. *Nat. Rev. Clin. Oncol.* 6 (6), 339–351. doi:10.1038/nrclinonc.2009.44
- Passeri, G., Vincent, R., Xiao, Z., Northcote-Smith, J., and Suntharalingam, K. (2023). Encapsulation and delivery of an osteosarcoma stem cell active gallium (III)-Difluoride complex using polymeric micelles. *ChemMedChem* 18, e202200599. doi:10.1002/cmdc.202200599
- Pignatello, R., Cenni, E., Miceli, D., Fotia, C., Salerno, M., Granchi, D., et al. (2009). A novel biomaterial for osteotropic drug nanocarriers: Synthesis and biocompatibility evaluation of a PLGA-ALE conjugate. *Nanomedicine* 4 (2), 161–175. doi:10.2217/17435889.4.2.161
- Pignatello, R. (2011). “PLGA-alendronate conjugate as a new biomaterial to produce osteotropic drug nanocarriers,” in *Biomaterials applications for nanomedicine* (London, England: IntechOpen), 165–184.
- Prasad, S. R., Kumar, T. S. S., and Jayakrishnan, A. (2021). Nanocarrier-based drug delivery systems for bone cancer therapy: A review. *Biomed. Mater.* 16 (4), 044107. doi:10.1088/1748-605x/abf7d5
- Rafael, D., Melendres, M. M. R., Andrade, F., Montero, S., Martínez-Trucharte, F., Vilar-Hernandez, M., et al. (2021). Thermo-responsive hydrogels for cancer local therapy: Challenges and state-of-art. *Int. J. Pharm.* 606, 120954. doi:10.1016/j.jipharm.2021.120954
- Rong, Z. J., Yang, L. J., Cai, B. T., Zhu, L. X., Cao, Y. L., Wu, G. F., et al. (2016). Porous nano-hydroxyapatite/collagen scaffold containing drug-loaded ADM-PLGA microspheres for bone cancer treatment. *J. Mater. Sci. Mater. Med.* 27, 89–12. doi:10.1007/s10856-016-5699-0
- Salerno, M., Cenni, E., Fotia, C., Avnet, S., Granchi, D., Castelli, F., et al. (2010). Bone-targeted doxorubicin-loaded nanoparticles as a tool for the treatment of skeletal metastases. *Curr. cancer drug targets* 10 (7), 649–659. doi:10.2174/156800910793605767
- Sampson, V. B., Gorlick, R., Kamara, D., and Anders Kolb, E. (2013). A review of targeted therapies evaluated by the pediatric preclinical testing program for osteosarcoma. *Front. Oncol.* 3, 132. doi:10.3389/fonc.2013.00132
- Sarigol-Calamak, E., and Hascicek, C. (2018). Tissue scaffolds as a local drug delivery system for bone regeneration. *Cutting-edge enabling Technol. Regen. Med.* 2018, 475–493.
- Schirmacher, V. (2019). From chemotherapy to biological therapy: A review of novel concepts to reduce the side effects of systemic cancer treatment (review). *Int. J. Oncol.* 54 (2), 407–419. doi:10.3892/ijo.2018.4661
- Shi, J., Kantoff, P. W., Wooster, R., and Farokhzad, O. C. (2017). Cancer nanomedicine: Progress, challenges and opportunities. *Nat. Rev. cancer* 17 (1), 20–37. doi:10.1038/nrc.2016.108
- Si, M., Xia, Y., Cong, M., Wang, D., Hou, Y., and Ma, H. (2022). *In situ* Co-delivery of doxorubicin and cisplatin by injectable thermosensitive hydrogels for enhanced osteosarcoma treatment. *Int. J. Nanomedicine* 17, 1309–1322. doi:10.2147/ijn.s356453
- Sokolova, V., Kostka, K., Shalumon, K. T., Prymak, O., Chen, J. P., and Epple, M. (2020). Synthesis and characterization of PLGA/HAP scaffolds with DNA-functionalised calcium phosphate nanoparticles for bone tissue engineering. *J. Mater. Sci. Mater. Med.* 31, 102–112. doi:10.1007/s10856-020-06442-1
- Sun, H., Su, J., Meng, Q., Yin, Q., Chen, L., Gu, W., et al. (2016). Cancer-cell-biomimetic nanoparticles for targeted therapy of homotypic tumors. *Adv. Mater.* 28 (43), 9581–9588. doi:10.1002/adma.201602173
- Swami, A., Reagan, M. R., Basto, P., Mishima, Y., Kamaly, N., Glavey, S., et al. (2014). Engineered nanomedicine for myeloma and bone microenvironment targeting. *Proc. Natl. Acad. Sci.* 111 (28), 10287–10292. doi:10.1073/pnas.1401337111
- Thamake, S. I., Raut, S. L., Gryczynski, Z., Ranjan, A. P., and Vishwanatha, J. K. (2012). Alendronate coated poly-lactic-co-glycolic acid (PLGA) nanoparticles for active targeting of metastatic breast cancer. *Biomaterials* 33 (29), 7164–7173. doi:10.1016/j.biomaterials.2012.06.026
- van der Meel, R., Sulheim, E., Shi, Y., Kiessling, F., Mulder, W. J. M., and Lammers, T. (2019). Smart cancer nanomedicine. *Nat. Nanotechnol.* 14 (11), 1007–1017. doi:10.1038/s41565-019-0567-y
- Venkatesan, N., Liyanage, A. D. T., Castro-Núñez, J., Asafo-Adjei, T., Cunningham, L. L., Dziubla, T. D., et al. (2019). Biodegradable polymerized simvastatin stimulates bone formation. *Acta biomater.* 93, 192–199. doi:10.1016/j.actbio.2019.04.059
- Wang, B., Yu, X. C., Xu, S. F., and Xu, M. (2015). Paclitaxel and etoposide co-loaded polymeric nanoparticles for the effective combination therapy against human osteosarcoma. *J. nanobiotechnology* 13 (1), 22–11. doi:10.1186/s12951-015-0086-4
- Wang, C., Ma, Z., Yuan, K., and Ji, T. (2022). Using scaffolds as drug delivery systems to treat bone tumor. *Nanotechnology* 33 (21), 212002. doi:10.1088/1361-6528/ac5017
- Wang, C., Ye, X., Zhao, Y., Bai, L., He, Z., Tong, Q., et al. (2020). Cryogenic 3D printing of porous scaffolds for *in situ* delivery of 2D black phosphorus nanosheets, doxorubicin hydrochloride and osteogenic peptide for treating tumor resection-induced bone defects. *Biofabrication* 12 (3), 035004. doi:10.1088/1758-5090/ab6d35
- Wang, S. Y., Hu, H. Z., Qing, X. C., Zhang, Z. C., and Shao, Z. W. (2020). Recent advances of drug delivery nanocarriers in osteosarcoma treatment. *J. Cancer* 11 (1), 69–82. doi:10.7150/jca.36588
- Wang, Y., Zhang, L., Zhao, G., Zhan, F., and Chen, Z. (2022). Homologous targeting nanoparticles for enhanced PDT against osteosarcoma HOS cells and the related molecular mechanisms. *J. nanobiotechnology* 20 (1), 83–28. doi:10.1186/s12951-021-01201-y
- Wei, L., Chen, J., Zhao, S., Ding, J., and Chen, X. (2017). Thermo-sensitive polypeptide hydrogel for locally sequential delivery of two-pronged anti-tumor drugs. *Acta biomater.* 58, 44–53. doi:10.1016/j.actbio.2017.05.053
- Wolfram, J., and Ferrari, M. (2019). Clinical cancer nanomedicine. *Nano today* 25, 85–98. doi:10.1016/j.nantod.2019.02.005
- Xi, Y., Qiao, L., and Na, B. (2015). Primary malignant bone tumors incidence, mortality, and trends in China from 2000 to 2015. *Chin. Med. J.* 10, 1097.
- Xia, L., Zheng, R., Xu, Y., Xu, X., Zhang, S., Zeng, H., et al. (2019). Incidence and mortality of primary bone cancers in China, 2014. *Chin. J. Cancer Res.* 31 (1), 135–143. doi:10.21147/j.issn.1000-9604.2019.01.08

- Xiao, B., Ma, L., and Merlin, D. (2017). Nanoparticle-mediated co-delivery of chemotherapeutic agent and siRNA for combination cancer therapy. *Expert Opin. Drug Deliv.* 14 (1), 65–73. doi:10.1080/17425247.2016.1205583
- Xiao, Y., Gu, Y., Qin, L., Chen, L., Chen, X., Cui, W., et al. (2021). Injectable thermosensitive hydrogel-based drug delivery system for local cancer therapy. *Colloids Surfaces B Biointerfaces* 200, 111581. doi:10.1016/j.colsurfb.2021.111581
- Yang, Z., Liu, J., and Lu, Y. (2020). Doxorubicin and CD-CUR inclusion complex co-loaded in thermosensitive hydrogel PLGA-PEG-PLGA localized administration for osteosarcoma. *Int. J. Oncol.* 57 (2), 433–444. doi:10.3892/ijo.2020.5067
- Yang, Z., Yu, S., Li, D., Gong, Y., Zang, J., Liu, J., et al. (2018). The effect of PLGA-based hydrogel scaffold for improving the drug maximum-tolerated dose for *in situ* osteosarcoma treatment. *Colloids Surfaces B Biointerfaces* 172, 387–394. doi:10.1016/j.colsurfb.2018.08.048
- Yin, Q., Tang, L., Cai, K., Tong, R., Sternberg, R., Yang, X., et al. (2016). Pamidronate functionalized nanoconjugates for targeted therapy of focal skeletal malignant osteolysis. *Proc. Natl. Acad. Sci.* 113 (32), E4601–E4609. doi:10.1073/pnas.1603316113
- Yu, D., Zhang, S., Feng, A., Xu, D., Zhu, Q., Mao, Y., et al. (2019). Methotrexate, doxorubicin, and cisplatin regimen is still the preferred option for osteosarcoma chemotherapy: A meta-analysis and clinical observation. *Medicine* 98 (19), e15582. doi:10.1097/md.00000000000015582
- Yu, G., Ning, Q., Mo, Z., and Tang, S. (2019). Intelligent polymeric micelles for multi-drug co-delivery and cancer therapy. *Artif. cells, nanomedicine, Biotechnol.* 47 (1), 1476–1487. doi:10.1080/21691401.2019.1601104
- Yu, Y., Cheng, Y., Tong, J., Zhang, L., Wei, Y., and Tian, M. (2021). Recent advances in thermo-sensitive hydrogels for drug delivery. *J. Mater. Chem. B* 9 (13), 2979–2992. doi:10.1039/d0tb02877k
- Yuan, B., Zhang, Y., Wang, Q., Ren, G., and Zhou, S. (2022). Thermosensitive vancomycin@ PLGA-PEG-PLGA/HA hydrogel as an all-in-one treatment for osteomyelitis. *Int. J. Pharm.* 627, 122225. doi:10.1016/j.ijpharm.2022.122225
- Yuan, Y., Song, J. X., Zhang, M. N., and Yuan, B. S. (2020). A multiple drug loaded, functionalized pH-sensitive nanocarrier as therapeutic and epigenetic modulator for osteosarcoma. *Sci. Rep.* 10 (1), 15497–15511. doi:10.1038/s41598-020-72552-z
- Zhang, B., Zhang, Y., Li, R., Li, J., and Lu, X. (2020). The efficacy and safety comparison of first-line chemotherapeutic agents (high-dose methotrexate, doxorubicin, cisplatin, and ifosfamide) for osteosarcoma: A network meta-analysis. *J. Orthop. Surg. Res.* 15, 51–10. doi:10.1186/s13018-020-1576-0
- Zhang, C., Yan, L., Wang, X., Zhu, S., Chen, C., Gu, Z., et al. (2020). Progress, challenges, and future of nanomedicine. *Nano Today* 35, 101008. doi:10.1016/j.nantod.2020.101008
- Zhang, S., Ren, H., Sun, H. T., and Cao, S. (2022). Cytotoxic effects of castalin nanoparticles against osteosarcoma. *Appl. Biochem. Biotechnol.* 2022, 1–10. doi:10.1007/s12010-022-03846-3
- Zhang, Y. N., Poon, W., Tavares, A. J., McGilvray, I. D., and Chan, W. C. (2016). Nanoparticle–liver interactions: Cellular uptake and hepatobiliary elimination. *J. Control. release* 240, 332–348. doi:10.1016/j.jconrel.2016.01.020
- Zhang, Y., Yang, J., Zhao, N., Wang, C., Kamar, S., Zhou, Y., et al. (2018). Progress in the chemotherapeutic treatment of osteosarcoma. *Oncol. Lett.* 16 (5), 6228–6237. doi:10.3892/ol.2018.9434
- Zhao, D., Tang, F., Min, L., Lu, M., Wang, J., Zhang, Y., et al. (2020). <p>Intercalary reconstruction of the “ultra-critical sized bone defect” by 3D-printed porous prosthesis after resection of tibial malignant tumor</p>. *Cancer Manag. Res.* 12, 2503–2512. doi:10.2147/cmar.s245949
- Zhao, G., Cui, R., Chen, Y., Zhou, S., Wang, C., Hu, Z., et al. (2020). 3D printing of well dispersed electrospun PLGA fiber toughened calcium phosphate scaffolds for osteoanagenesis. *J. Bionic Eng.* 17, 652–668. doi:10.1007/s42235-020-0051-2
- Zheng, Y., Cheng, Y., Chen, J., Ding, J., Li, M., Li, C., et al. (2017). Injectable hydrogel–microsphere construct with sequential degradation for locally synergistic chemotherapy. *ACS Appl. Mater. interfaces* 9 (4), 3487–3496. doi:10.1021/acsami.6b15245
- Zhou, H., Liang, C., Wei, Z., Bai, Y., Bhaduri, S. B., Webster, T. J., et al. (2019). Injectable biomaterials for translational medicine. *Mater. Today* 28, 81–97. doi:10.1016/j.mattod.2019.04.020
- Zhou, L., Pi, W., Hao, M., Li, Y., Li, Q., et al. (2021). An injectable and biodegradable nano-photothermal DNA hydrogel enhances penetration and efficacy of tumor therapy. *Biomaterials Sci.* 9 (14), 4904–4921. doi:10.1039/d1bm00568e



OPEN ACCESS

EDITED BY

Huihua Yuan,
Nantong University, China

REVIEWED BY

Jing Han,
Chinese Academy of Sciences (CAS),
China

Ajay Devidas Padsalgikar,
Bioling Inc., United States

*CORRESPONDENCE

Miao Jiang,
✉ jiangmiaocpt@aliyun.com
Liqun Yang,
✉ yanglq@lnszjk.com.cn
Hong Cui,
✉ cuih@sj-hospital.org

[†]These authors have contributed equally
to this work

RECEIVED 05 July 2023

ACCEPTED 22 August 2023

PUBLISHED 01 September 2023

CITATION

Li W, Lin M, Wang C, Lu Y, Sui Y, Ni X,
Guo J, Jiang M, Yang L and Cui H (2023),
In vitro enzymatic degradation of the
PTMC/cross-linked PEGDA blends.
Front. Bioeng. Biotechnol. 11:1253221.
doi: 10.3389/fbioe.2023.1253221

COPYRIGHT

© 2023 Li, Lin, Wang, Lu, Sui, Ni, Guo,
Jiang, Yang and Cui. This is an open-
access article distributed under the terms
of the [Creative Commons Attribution
License \(CC BY\)](#). The use, distribution or
reproduction in other forums is
permitted, provided the original author(s)
and the copyright owner(s) are credited
and that the original publication in this
journal is cited, in accordance with
accepted academic practice. No use,
distribution or reproduction is permitted
which does not comply with these terms.

In vitro enzymatic degradation of the PTMC/cross-linked PEGDA blends

Wei Li^{1†}, Meina Lin^{1†}, Chenchao Wang^{2†}, Yongping Lu¹, Yu Sui¹,
Xiang Ni¹, Jing Guo¹, Miao Jiang^{1*}, Liqun Yang^{1*} and Hong Cui^{3*}

¹Liaoning Research Institute of Family Planning, The Affiliated Reproductive Hospital of China Medical University, Shenyang, China, ²Department of Plastic Surgery, First Hospital of China Medical University, Shenyang, China, ³Department of Obstetrics and Gynecology, Shengjing Hospital of China Medical University, Shenyang, China

Introduction: Poly(1,3-trimethylene carbonate) (PTMC) is a flexible amorphous polymer with good degradability and biocompatibility. The degradation of PTMC is critical for its application as a degradable polymer, more convenient and easy-to-control cross-linking strategies for preparing PTMC are required.

Methods: The blends of poly(trimethylene carbonate) (PTMC) and cross-linked poly(ethylene glycol) diacrylate (PEGDA) were prepared by mixing photoactive PEGDA and PTMC and subsequently photopolymerizing the mixture with uv light. The physical properties and *in vitro* enzymatic degradation of the resultant PTMC/cross-linked PEGDA blends were investigated.

Results: The results showed that the gel fraction of PTMC/cross-linked PEGDA blends increased while the swelling degree decreased with the content of PEGDA dosage. The results of *in vitro* enzymatic degradation confirmed that the degradation of PTMC/cross-linked PEGDA blends in the lipase solution occurred under the surface erosion mechanism, and the introduction of the uv cross-linked PEGDA significantly improved the resistance to lipase erosion of PTMC; the higher the cross-linking degree, the lower the mass loss.

Discussion: The results indicated that the blends/cross-linking via PEGDA is a simple and effective strategy to tailor the degradation rate of PTMC.

KEYWORDS

poly(trimethylene carbonate), PEGDA, UV cross-linking, enzymatic degradation, lipase

1 Introduction

Poly(1,3-trimethylene carbonate) (PTMC) is a flexible amorphous polymer with good degradability and biocompatibility (Hou et al., 2021; Hou et al., 2022) while without acidic degradation substances, thus avoiding severe inflammatory reactions (Yang et al., 2014a; Yang et al., 2015). Therefore, PTMC has a wide range of applications in biomedicine, such as drug delivery systems (Fukushima, 2016; Mohajeri et al., 2020; Hou et al., 2023) and tissue engineering (Li et al., 2020; Brossier et al., 2021; He et al., 2021).

The degradation of PTMC is critical for its application as a degradable polymer. Studies have shown that the high molecular weight PTMC has good morphological stability, but the degradation is too fast. On the contrary, low molecular weight PTMC degrades slowly (Yang et al., 2015). However, it has poor morphological stability and creeps quickly at room temperature (Yang et al., 2015). Therefore, suitable methods for modifying PTMC must be

found to obtain polymers with controllable degradation time and stable morphologies. Numerous studies have shown that copolymerization can modulate the physical properties and control the degradation rate of PTMC. As Yang (Yang et al., 2014a) and Hou (Hou et al., 2019) reported, the appropriate introduction of hydrophobic or semi-crystalline segments into the structure reduces the degradation rate of PTMC. Although it is an effective strategy to adjust the degradation rate of PTMC, the degradation rate of copolymers is also affected by several factors, such as the molar ratio (Hou et al., 2022), molecular weight (Hou et al., 2020) of copolymers, etc., resulting in the controlled regulation of the degradation rate of PTMC still faces challenges.

The construction of biodegradable cross-linked networks (BCNs) is one of the efficient ways to retard polymer degradation and maintain morphological stability. Chemical cross-linking is a promising strategy to prevent the degradation of PTMC, and for example, Yang et al. prepared bis-TMC with a structure similar to TMC as a chemical cross-linker to obtain PTMC-BCNs (Yang et al., 2013; Yang et al., 2014b). The resulting PTMC-BCNs showed improved morphological stability and lower degradation rate *in vitro* (Hou et al., 2017) and *in vivo* (Yang et al., 2016). However, the difficulty of forming BCNs after chemical cross-linking severely limits their wide application.

Compared with chemical cross-linking, irradiation cross-linking allows PTMC to be molded before cross-linking. In particular, gamma- and electron beam irradiation enables rapid cross-linking of the molded PTMC (Liu et al., 2021a; Liu et al., 2021b; Jozwiakowska et al., 2011), and the cross-linked PTMC also has a slow degradation rate due to the formation of the cross-linked network (Bat et al., 2009; Bat et al., 2010a; Liu et al., 2021c), which can significantly improve the erosion resistance of PTMC. Grijpma et al. reported that biodegradable elastomeric PTMC-BCNs could be efficiently formed by gamma irradiation of the linear polymer in the presence of pentaerythritol triacrylate (PETA), and the enzymatic erosion rates of the networks could be decreased from 12.0 ± 2.9 to 3.0 ± 1.6 $\mu\text{m/day}$ (Bat et al., 2010b). However, the way of irradiation cross-linking also has specific problems, for example, chain scission that simultaneously occurs with cross-linking, which can make the molecular weight of PTMC decrease (Yang et al., 2014b; Liu et al., 2021b), and the resulting low-molecular weight segments will form defects in the three-dimensional network, and reduce the performance of PTMC-BCNs.

UV photo-cross-linking is a promising solution to the problems of the above strategies. Flexible, elastomeric, and biodegradable networks could be readily prepared by UV irradiating PTMC films (Rongen et al., 2016; Zant and Grijpma, 2016; Wang et al., 2020). The design and preparation of prepolymers functionalized with double bonds are essential for UV photo-crosslinking of PTMC, such as the molecular weight of the prepolymer, the copolymerization ratio, and the number of double bonds can affect the degradation rate of the cross-linked PTMC. This will undoubtedly increase the factors affecting the degradation rate of UV-crosslinked PTMCs. Hence, more convenient and easy-to-control cross-linking strategies for preparing PTMC-BCNs are required.

Currently, poly (ethylene glycol) diacrylate (PEGDA) has been widely used as cross-linking agent (Kedzierska et al., 2022). PEGDA

is a derivative of polyethylene glycol (PEG) with double-bonded acrylate groups at both ends, which can form various cross-linked networks through photo-polymerization in the presence of a photoinitiator. PEGDA is a hydrophilic material with low cytotoxicity and good biocompatibility (Warr et al., 2020). Therefore, multiple combinations of PEGDA-based materials have been developed for biomedical applications (Qin et al., 2021; Soriente et al., 2021).

In this study, PTMC/cross-linked PEGDA blends were prepared directly by UV cross-linking strategy using PEGDA as a cross-linking agent without preparing prepolymers. The thermal properties of the resulting PTMC/cross-linked PEGDA blend with different degrees of cross-linking were investigated. The *in vitro* enzymatic degradation behavior of PTMC/cross-linked PEGDA blends was also performed in lipase solutions to investigate the effect of cross-linked PEGDA on the degradation rate of PTMC.

2 Materials and methods

2.1 Materials

Trimethylene carbonate (TMC) was purchased from Daigang Biomaterial Co., Ltd (Jinan, Shandong, China), recrystallized twice with ethyl acetate, and dried to constant weight before polymerization. Stannous octoate [$\text{Sn}(\text{Oct})_2$] (95%) and lipase from *Aspergillus oryzae* ($\geq 10,000$ U/g) were obtained from Sigma-Aldrich and used as received. PEGDA (average Mw = 400Da) and 2-hydroxy-4-(2-hydroxyethoxy)-2-methylpropiophenone (I2959) were purchased from Innocem (Beijing, China). All other solvents and reagents were analytical grade and used without further purification.

2.2 Measurements

A Thermo Scientific Nicolet iS50 Fourier transforms infrared spectrometer (Madison, WI, USA) with an ATR accessory was used to analyze the chemical structure of the samples. The film sample was placed on the ATR accessory's crystal face, and the samples' infrared spectrum was collected. The testing range was $400\text{--}4,000$ cm^{-1} , the number of scans was 32, and the resolution was 4cm^{-1} . The hydrophilicity of the PTMC/cross-linked PEGDA blend films was tested using a DSA25 drop-shape analyzer (Kruss, Hamburg, Germany). The test temperature was room temperature, and the test time was 3 s. A camera recorded the shape of ultrapure water droplets (5 μL) on the films, and the data were read by the computer. At least three positions were measured for each sample, and the average was taken. The glass transition temperature (T_g) of the PTMC/cross-linked PEGDA blends was determined using a Netzsch DSC 200 F3 (Netzsch, Selb, Germany) equipped with a liquid nitrogen cooling system. The measured temperature range was from -50°C to 100°C , and the heating rate was 10°C/min under a nitrogen atmosphere. The thermal stability of the PTMC/cross-linked PEGDA blends was performed using a Netzsch TGA 209 F3 (Netzsch, Selb,

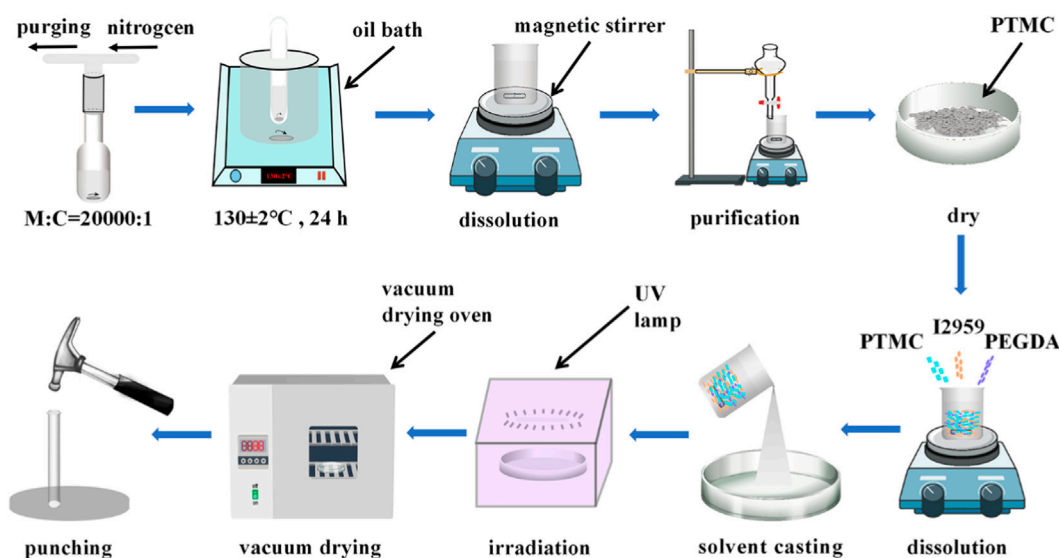


FIGURE 1
Schematic representation of the preparation of PTMC/cross-linked PEGDA blends.

Germany) at a heating rate of 10°C/min from room temperature to 700°C under a nitrogen atmosphere. The temperature was set at T_d when the mass loss was 5%. Before and after degradation, the films were photographed with a camera to obtain the macroscopic morphology of the material. The microscopic morphology of the films was obtained using a TESCAN MIRA LMS scanning electron microscope (SEM) (Brno, South Moravia, Czech Republic). Gold was sprayed on the surface of the materials to increase their electrical conductivity before testing.

2.3 PTMC synthesis

PTMC was synthesized by bulk ring-opening polymerization of TMC using Sn(Oct)₂ as a catalyst (Li et al., 2020). In brief, dried TMC (30 g, 0.29 mol) and an anhydrous toluene solution of Sn(Oct)₂ (0.2 M; 1/20000 eq, 2.9 μL) were added to the ampoule. After purging with dry nitrogen, the ampoule was heat-sealed under a vacuum (5 mmHg) and put in an oil bath at 130°C ± 2°C for 24 h. After the reaction, the ampoule was cooled to room temperature and smashed to obtain the crude polymer, which was dissolved in dichloromethane, followed by purification in ice methanol. The purified PTMC was vacuum dried to constant weight.

2.4 Preparation of PTMC/cross-linked PEGDA blends

Briefly, PTMC, PEGDA, and I2959 (photoinitiator) are dissolved in appropriate dichloromethane according to a predetermined weight ratio and poured into a glass plate (diameter: 9 cm, height: 1.5 cm). The glass plate was placed in a fume hood to allow the solvent to evaporate naturally. After evaporation, the films were irradiated under a UV lamp (365 nm) for 3 min. The photo-crosslinked blends were vacuum dried to

constant weight, and then fixed-size circular films were punched (diameter: 7 mm) for subsequent experiments. The preparation process of PTMC/cross-linked PEGDA blends is shown in Figure 1.

2.5 Gel fraction and swelling degree

Samples were weighed and stored in a glass vial containing dichloromethane for 5 days to determine the gel fraction and swelling degree (SR) of PTMC/cross-linked PEGDA blends. The solvent was changed once a day to remove the soluble fraction altogether. After 5 days, the swollen gel was taken out, and the wet weight of the sample was weighed. Then, the piece was dried to a constant weight using a vacuum-drying oven. The gel fraction and swelling degree were calculated using Eqs 1, 2.

$$\text{Gel fraction (\%)} = \frac{m}{M} \times 100 \quad (1)$$

$$\text{SR (\%)} = \frac{M_t - M}{M} \times 100 \quad (2)$$

M denotes the initial weight of PTMC/cross-linked PEGDA blends before swelling, M_t is the wet weight of PTMC/cross-linked PEGDA blends after 5 days of swelling, and m represents the dry weight of PTMC/cross-linked PEGDA blends after swelling. Three replicate samples were set to measure gel fraction and swelling ratio, and the results were averaged.

2.6 *In vitro* enzymatic degradation

Before degradation, the initial weight (W_i) of the circular films of PTMC/cross-linked PEGDA blends were weighed using an electronic balance (Sartorius, German). The initial thickness (T_i) of the film was recorded by electronic digital calipers (Guanglu, China). Then, the circular films were placed in a glass tube containing 500 μL lipase

TABLE 1 PTMC/cross-linked PEGDA blends with different PEGDA contents.

| | PTMC(g) | PEGDA(g) | I2959(g) |
|----------------|---------|----------|----------|
| N ₁ | 1.5 | 0 | 0 |
| N ₂ | 1.5 | 0.3 | 0.0075 |
| N ₃ | 1.5 | 0.6 | 0.0075 |
| N ₄ | 1.5 | 0.9 | 0.0075 |
| N ₅ | 0 | 0.6 | 0.0075 |

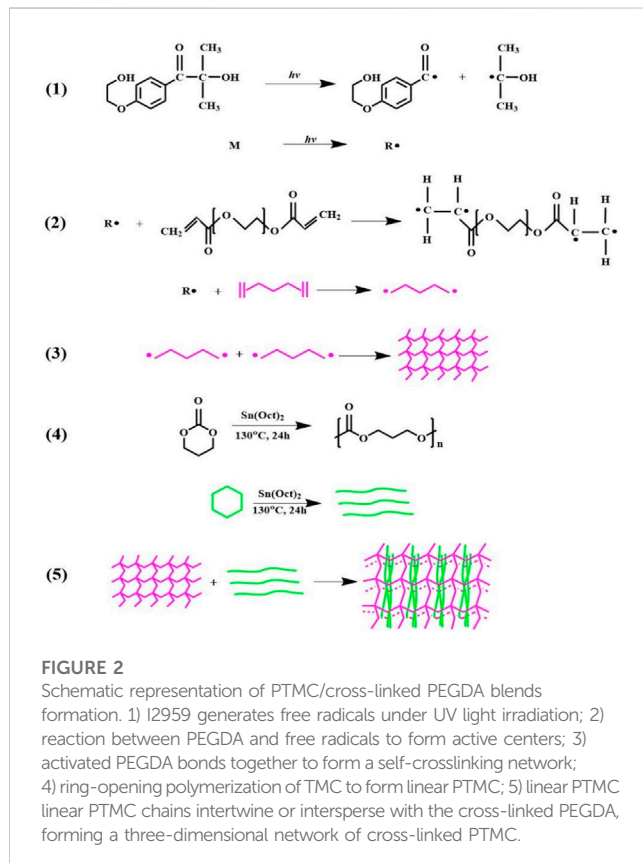


FIGURE 2

Schematic representation of PTMC/cross-linked PEGDA blends formation. 1) I2959 generates free radicals under UV light irradiation; 2) reaction between PEGDA and free radicals to form active centers; 3) activated PEGDA bonds together to form a self-crosslinking network; 4) ring-opening polymerization of TMC to form linear PTMC; 5) linear PTMC chains intertwine or intersperse with the cross-linked PEGDA, forming a three-dimensional network of cross-linked PTMC.

solution that was changed every 4 days. The glass tubes were placed in a constant temperature oscillator at 37°C and gently shaken daily for 8 h. Every 4 days, three parallel samples were taken from the lipase solutions in each group and washed with deionized water. Water from the surface of the samples was absorbed with absorbent paper, and the films were weighed and thickness measured, then dried under vacuum at 37°C to a constant weight for further analysis. Before and after degradation, the pH of the lipase solutions was monitored using a Toledo-Mettler InLabMicro™ pH meter equipped with a three-in-one microelectrode (Toledo-Mettler, Zurich, Switzerland). The mass loss, thickness loss, and water uptake of the samples were calculated according to Eqs 3–5, respectively. The degradation rate constant k was used to quantify the mass loss for each sample set and calculated according to Eq. 6 (Yang et al., 2015; Hou et al., 2021).

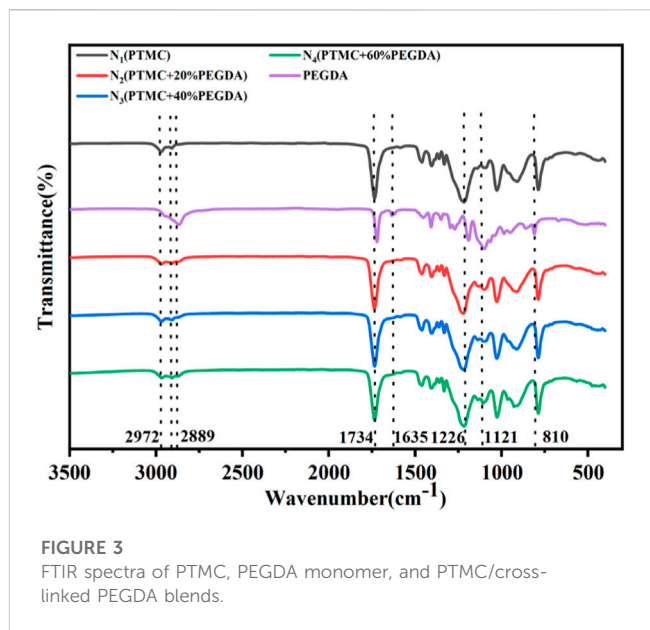


FIGURE 3

FTIR spectra of PTMC, PEGDA monomer, and PTMC/cross-linked PEGDA blends.

$$\text{Mass loss (\%)} = \frac{W_i - W_d}{W_i} \times 100 \quad (3)$$

$$\text{Loss in thickness (\%)} = \frac{T_i - T_d}{T_i} \times 100 \quad (4)$$

$$\text{water uptake (\%)} = \frac{W_w - W_d}{W_d} \times 100 \quad (5)$$

$$M_t = M_i - k(t - t_i) \quad (6)$$

W_i is the initial weight of the sample before degradation, W_w is the wet weight of the sample, and W_d is the dry weight after degradation. T_i is the initial thickness of the sample before degradation, and T_d is the thickness of the dried film after degradation. M_t is the mass loss at degradation time t .

3 Results and discussion

3.1 Preparation of PTMC/cross-linked PEGDA blends

PTMC/cross-linked PEGDA blends with different degrees of cross-linking were prepared by increasing the amount of PEGDA with a given content of PTMC and I2959, as shown in Table 1.

During the cross-linking process, I2959 generates free radicals in the presence of UV light. The radicals attack the $-C=C-$ of PEGDA, creating a reactive center and initiating the self-crosslinking of PEGDA to form a three-dimensional cross-linked structure. The cross-linked PEGDA acts as a physical cross-linking point for the linear PTMC, prompting the linear PTMC chains to intertwine or intersperse with the cross-linked PEGDA, thus forming a three-dimensional network of cross-linked PTMC. The formation of PTMC/cross-linked PEGDA blends is shown in Figure 2.

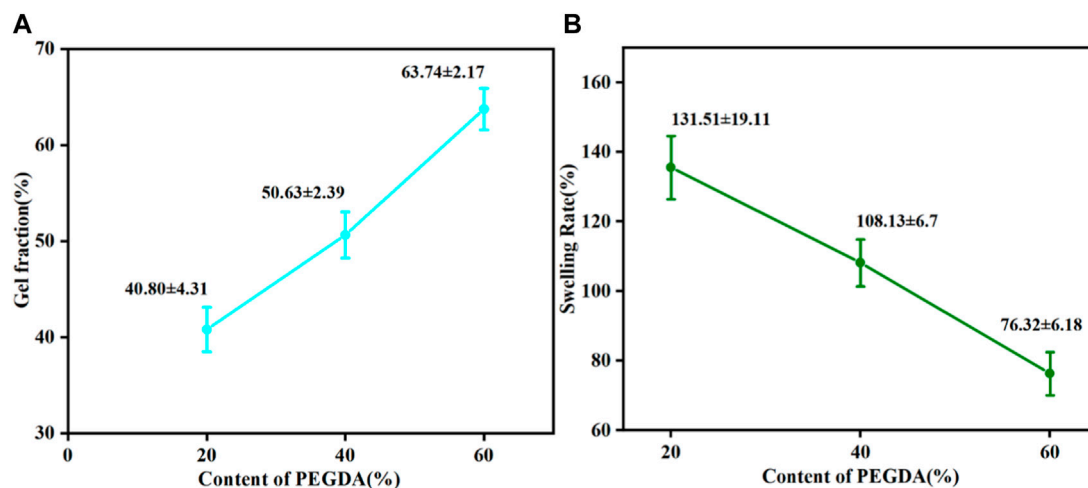


FIGURE 4
Gel fraction (A) and swelling degree (B) of PTMC/cross-linked PEGDA blends.

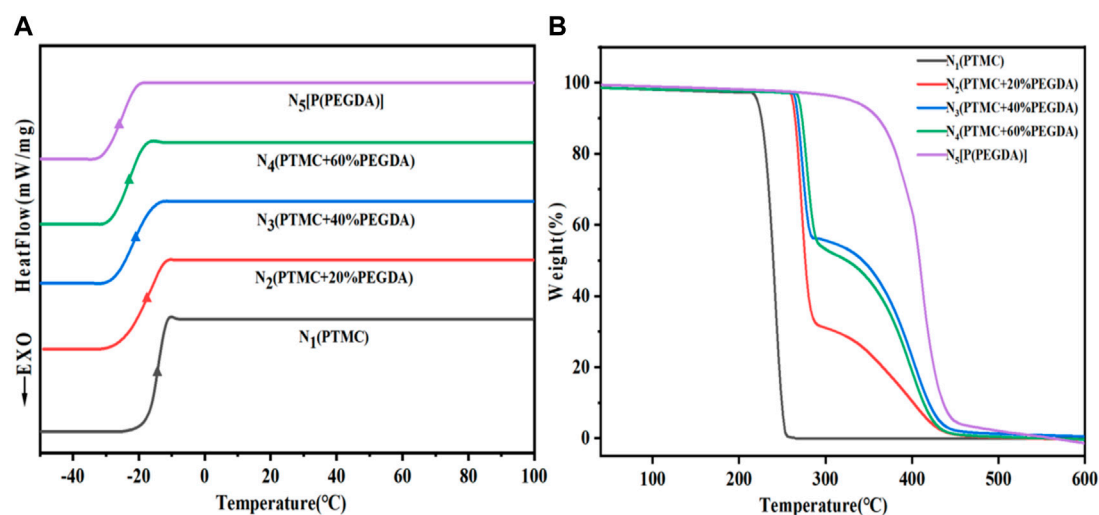


FIGURE 5
DSC (A) and TGA (B) curves of obtained PTMC/cross-linked PEGDA blends.

3.2 Structural characterization

As shown in Figure 3, the FTIR spectra of the pure PTMC, pure PEGDA, and PTMC/cross-linked PEGDA blends were compared to identify the chemical alteration. In PEGDA, the peak at $1,121\text{ cm}^{-1}$ is the symmetric stretching vibration of C-O-C, and the peak at $2,889\text{ cm}^{-1}$ is the symmetric stretching vibration absorption peaks of C-H in $-\text{CH}_2-\text{CH}_2-$ segments. As for the spectrum of PEGDA, it should be noted that the peaks at $1,635$ and 810 cm^{-1} confirmed the presence of alkene moieties. The disappearance of these peaks indicates the curing of acrylates, and PEGDA is successfully self-crosslinked under UV light. The C=O stretching vibration absorption peaks of PEGDA and PTMC is at $1,720\text{ cm}^{-1}$ and $1,734\text{ cm}^{-1}$,

TABLE 2 Thermal properties of PTMC/cross-linked PEGDA blends.

| | N ₁ | N ₂ | N ₃ | N ₄ | N ₅ |
|---------------------|----------------|----------------|----------------|----------------|----------------|
| T _g (°C) | -16.6 | -19.9 | -21.6 | -23.6 | -27.2 |
| T _d (°C) | 239.5 | 263.6 | 264.4 | 265.4 | 329.9 |

respectively, which overlaps in the PTMC/cross-linked PEGDA blends. In PTMC, the absorption peaks caused by the asymmetric and symmetric stretching vibrations of $-\text{CH}_2-$ at $2,972\text{ cm}^{-1}$ and $2,910\text{ cm}^{-1}$ can also be detected. Compared with the PTMC and PEGDA spectra, the PTMC/cross-linked PEGDA blends did not show any apparent new absorption peak, indicating no chemical reaction between the two polymers.

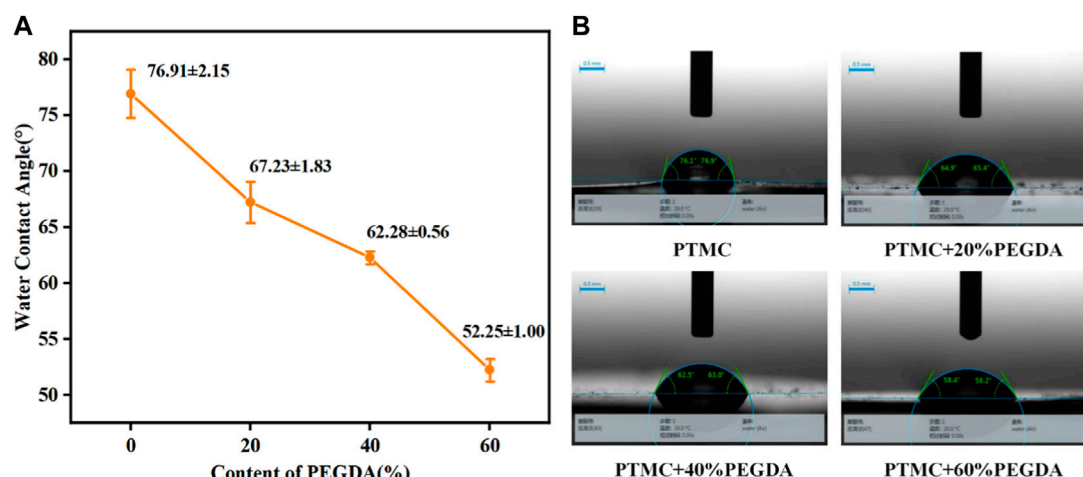


FIGURE 6
The water contact angle of PTMC/cross-linked PEGDA blends.

3.3 Gel fraction and swelling degree

The gel fraction can be used to indicate the degree of cross-linking. Obviously, the gel fraction gradually became more prominent while the swelling degree decreased with the increase of PEGDA, as shown in Figure 4, indicating that the degree of cross-linking of the PTMC/cross-linked PEGDA blends gradually increased. This result suggests that the increase in PEGDA content can lead to the formation of a denser network.

3.4 Thermal properties

As shown in Figure 5A and Table 2, the T_g of PTMC is -16.6°C and the T_g of UV cross-linked P(PEGDA) is -27.2°C . With increased PEGDA content in the feeding ratio, the T_g of PTMC/cross-linked PEGDA blends showed a decreasing trend. It is attributed to the plasticization effect of P(PEGDA) in the blends (Fang et al., 2014; Yang et al., 2019). With the increase of the number of flexible $[-\text{O}-\text{CH}_2-\text{CH}_2-]$ chains from P(PEGDA) in PTMC/cross-linked PEGDA blends, the motion of molecular chains is relatively active, resulting in lower T_g .

As shown in Figure 5B and Table 2, The thermal decomposition temperature of PTMC is about 240°C . The thermal decomposition temperature of P(PEGDA) is higher than that of PTMC, about 330°C . With the increase of PEGDA, the thermal stability of PTMC/cross-linked PEGDA blends gradually increases due to the formation of a cross-linked network.

3.5 Hydrophilicity of PTMC/cross-linked PEGDA blends

Hydrophilicity is an essential factor in determining material properties. The water contact angle is an important parameter to measure the wettability of liquid to materials. A static water contact angle measurement was used to investigate the hydrophilicity of

PTMC/cross-linked PEGDA blends, as shown in Figure 6. It can be seen from Figure 6A that the water contact angle of PTMC is $76.91^\circ \pm 2.15^\circ$, which shows the hydrophobic nature. With the increase of PEGDA dosage, the water contact angle gradually becomes smaller, indicating the hydrophilicity of the material is improved. It suggests that the introduction of hydrophilicity of PEGDA improves the PTMC blends.

3.6 *In vitro* enzymatic degradation of PTMC/cross-linked PEGDA blends films

3.6.1 Mass loss and thickness loss

Mass loss is one of the most critical parameters in studying the degradation properties of biodegradable polymers. The degradation behavior of PTMC/cross-linked PEGDA blends is shown in Figure 7. Figure 7 (a) shows an excellent linear relationship between mass loss and degradation time for each group. The mass loss of PTMC was nearly 100% after 20 days, while the mass loss of the N_4 group (PTMC +60% PEGDA) was only 30% of the initial weight. The results showed that the degradation rate of PTMC/cross-linked PEGDA blends decreased with the increase of PEGDA, which significantly prolonged the degradation period of the materials. As shown in Figure 7B, the degradation rate constant k of PTMC is 49.75%. With the increase of PEGDA, the k value showed a downward trend, indicating that the degradation period of the films became longer. Blending with UV cross-linked PEGDA can effectively slow down the degradation of PTMC. We also investigated the thickness loss of the films as a function of the degradation time, as shown in Figure 7C. The thickness of the films gradually decreases with time. It can be seen from Figure 7D that the mass loss of the film is linearly related to the thickness loss, and both occur simultaneously. This confirms that the degradation of PTMC/cross-linked PEGDA occurred via surface erosion mechanisms.

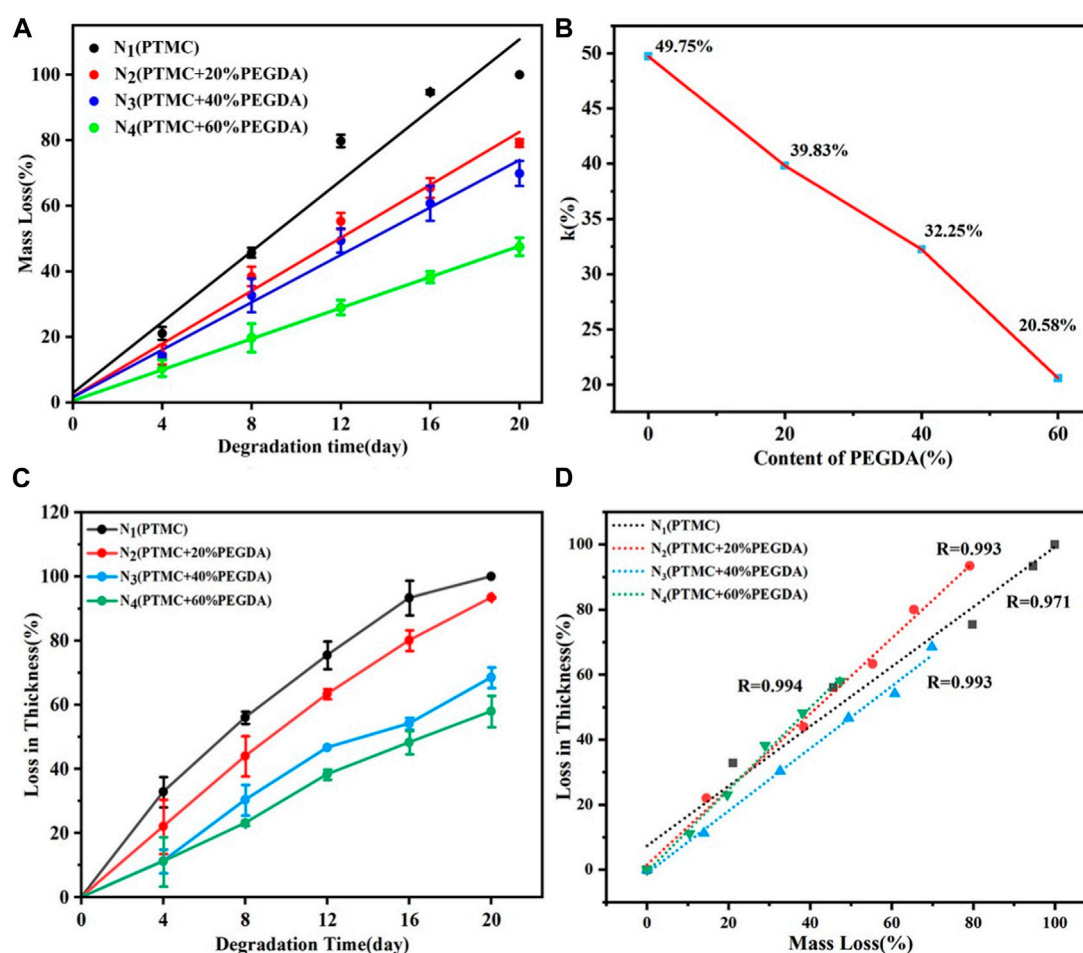


FIGURE 7

Mass loss (A), degradation rate constant k (B) and thickness loss (C) of PTMC/cross-linked PEGDA as a function of degradation time, and thickness loss as function of mass loss (D) of PTMC/cross-linked PEGDA.

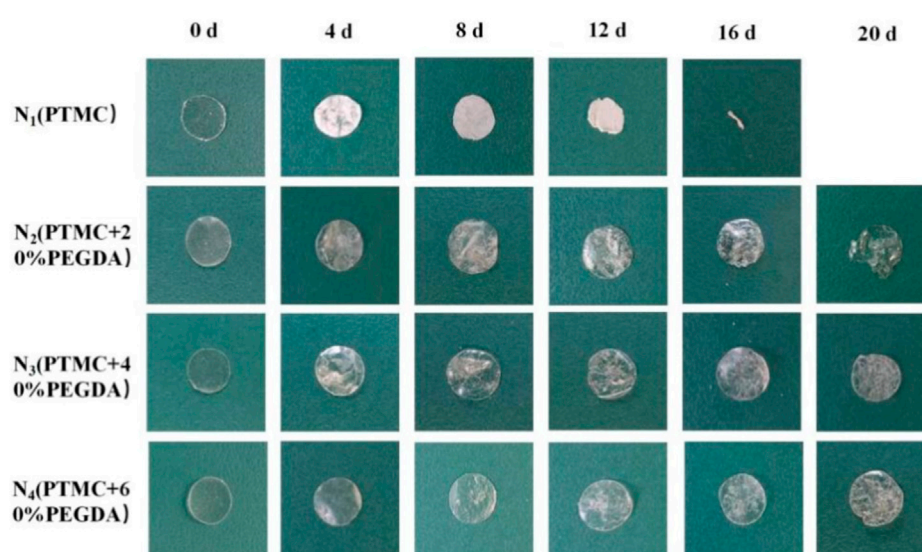


FIGURE 8

The macroscopic morphology of films before and after enzymatic degradation.

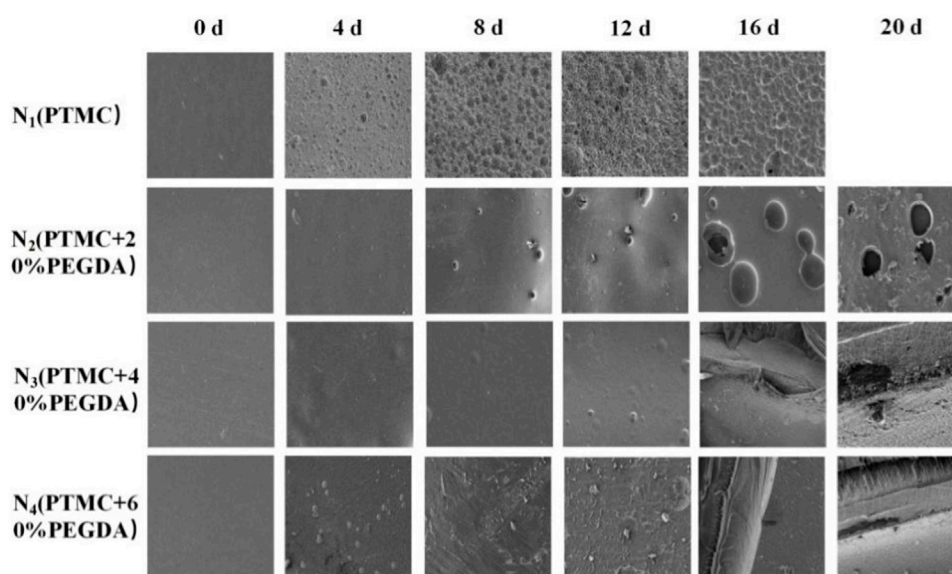


FIGURE 9
The surface morphology of films before and after enzymatic degradation.

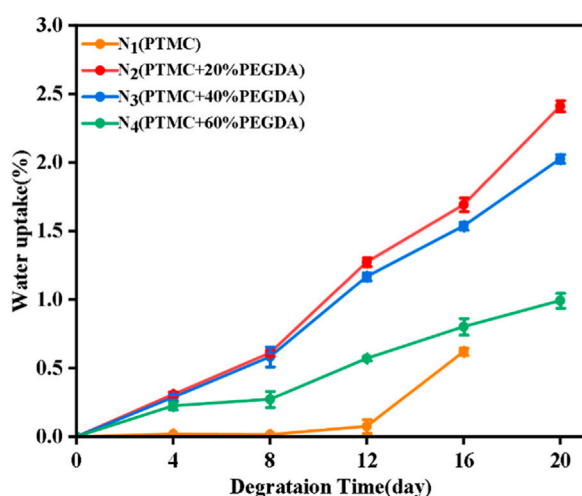


FIGURE 10
The water uptake of films during enzymatic degradation.

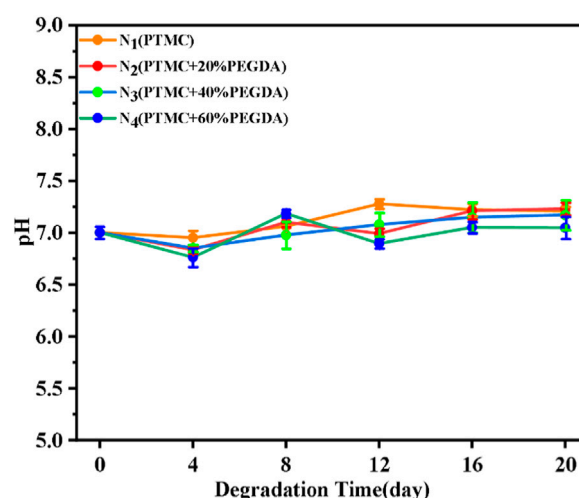


FIGURE 11
The changing trend in the pH value of films during enzymatic degradation.

3.6.2 Macroscopic and microscopic morphology

Photographing samples at different degradation times obtained the macroscopic morphology of the material to determine the stability of the PTMC/cross-linked PEGDA blends. As shown in Figure 8, for the N₁(PTMC) group, the original morphology could not be maintained after degradation of 16 days, and it was degraded entirely at day 20. The N₂ group samples remained in their original shape on day 16. Films were still present on day 20, but the integrity of the films was lost. On day 20, the films of groups N₃ and N₄ retained their integrity and original morphology without curls. However, the films of both groups developed cracks during degradation, which appeared earlier and more severe in the N₃ group than in the N₄ group. It can be seen that the network structure

formed after cross-linking increases the stability of the films, reduces the deformation of the materials, and slows down the degradation.

Figure 9 shows the microscopic surface morphology of the films during degradation. Before degradation, the surfaces of the films are all flat and smooth. A large number of holes appear on the surface of PTMC after degradation. As the degradation time increases, the number of pores and holes and their size gradually increases. Holes also appeared on the surface of the N₂ group films, but the number and size of the holes were smaller than those of PTMC. Fewer holes appear in the N₃ group, and many cracks appear in the later stages of degradation. In the early stage

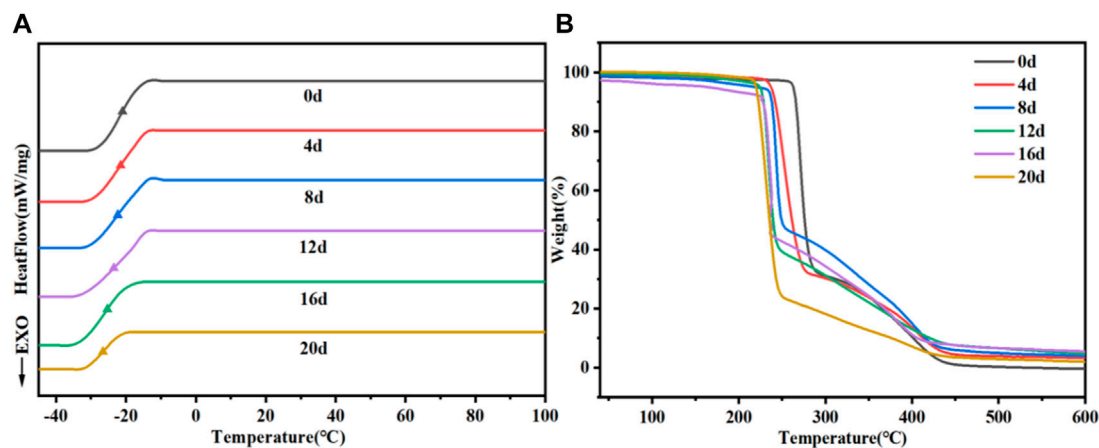


FIGURE 12 Changes in DSC (A) and TGA (B) of PTMC/cross-linked PEGDA blends N_3 during degradation.

TABLE 3 The change of T_g and T_d during degradation.

| | 0d | 4d | 8d | 12d | 16d | 20d |
|------------|-------|-------|-------|-------|-------|-------|
| T_g (°C) | -21.6 | -21.8 | -23.1 | -24.9 | -26.5 | -27.6 |
| T_d (°C) | 263.6 | 237.3 | 224.6 | 220.5 | 219.2 | 163 |

of degradation, no holes appeared in the N_4 group. As the degradation progressed, cracks also appeared in the films of the N_4 group, but the distribution and size were not as large as those of the N_3 group. The results indicate that the formation of cross-linked networks effectively prevents degradation.

3.6.3 Water uptake of films

As shown in Figure 10, the water uptake of the PTMC/cross-linked PEGDA blends gradually increased with the degradation time. As a surfactant, lipase disperses the degradation products into solution, thus accelerating the degradation of the PTMC/cross-linked PEGDA blend (Yang et al., 2015), leading to pores and holes on the material's surface. In the later stages of degradation, the pores and holes became larger. The appearance of pores promotes the storage of water. Although PTMC degrades the fastest and has many pores on its surface, the PEGDA chain segments significantly increase the hydrophilicity of the PTMC/cross-linked PEGDA mixture. The higher the PEGDA content, the more hydrophilic the PTMC/cross-linked PEGDA mixture becomes, which gradually increases its water absorption during degradation.

3.6.4 pH value

During the degradation process, we monitored the lipase solution's pH variation as a function of the degradation time. It has been shown that PTMC does not produce acidic degradation products during enzymatic degradation and is independent of its relative molecular weight (Yang et al., 2015). As shown in Figure 11, the pH of the PTMC/cross-linked PEGDA blends remained stable during the degradation process. This result indicates that the degradation of the PTMC/

cross-linked PEGDA blends did not produce acidic degradation products, thus avoiding the development of local inflammation and having a more significant potential for biomedical applications.

3.6.5 The change in thermal properties

We also examined the changes in the thermal properties of PTMC/cross-linked PEGDA blends during degradation and illustrated with the N_3 group as a typical representative, as shown in Figure 12 and Table 3. As shown in Table 3, the T_g tends to decrease as the degradation proceeds. The breakage of molecular chains leads to a higher degree of motion, and T_g decreases accordingly. The destruction of the cross-linked structure due to degradation causes the polymer to lose thermal stability, which leads to a decrease in the T_d . Furthermore, the accumulation of degradation products on the material's surface also decreases its thermal stability and enhances a lower T_g due to the plastic effect of the degradation products.

4 Conclusion

In this study, PTMC/crosslinked PEGDA blends were prepared directly using UV crosslinking strategy with PEGDA as crosslinking agent. The degradation behavior of the PTMC/cross-linked PEGDA blends was characterized to assess their potential as biomaterials. The gel fraction of the PTMC/cross-linked PEGDA blends became more prominent with increasing PEGDA. The degradation mechanism of the PTMC/cross-linked PEGDA blends was surface erosion. The degradation rate of the PTMC/cross-linked PEGDA blends decreased significantly with increasing cross-linkage. The pH of the enzyme solution confirmed that the PTMC/cross-linked PEGDA blend degraded without acid production. Hence, the introduction of cross-linked PEGDA to fabricate the PTMC/cross-linked PEGDA blend is a simple and effective strategy to tailor the degradation rate of PTMC. This strategy eliminates the preparation of prepolymers, which reduces the influencing

factors affecting the degradation of the blends and avoids defects such as scission of molecular chain due to irradiation. More importantly, this strategy can meet the practical needs of more convenient and easy-to-control cross-linking for PTMC, which can help to enrich the in-depth study of cross-linked PTMC.

Data availability statement

The original contributions presented in the study are included in the article/Supplementary Material, further inquiries can be directed to the corresponding authors.

Author contributions

WL, ML, and CW: Conceptualization, Methodology, Software, Writing—original draft. YL: Methodology, Software. XN and YS: Formal analysis. JG: Methodology, Supervision. LY: Methodology, Resources, Supervision, Validation. MJ: Resources, Supervision. HC: Resources, Supervision. All authors contributed to the article and approved the submitted version.

References

- Bat, E., Feijen, J., and Grijpma, D. W. (2010b). Biodegradable elastomeric networks: highly efficient cross-linking of poly(trimethylene carbonate) by gamma irradiation in the presence of pentaerythritol triacrylate. *Biomacromolecules* 11 (10), 2692–2699. doi:10.1021/bm1007234
- Bat, E., Plantinga, J. A., Harmsen, M. C., van Luyn, M. J. A., Feijen, J., and Grijpma, D. W. (2010a). *In vivo* behavior of trimethylene carbonate and ϵ -caprolactone-based (co) polymer networks: degradation and tissue response. *J. Biomed. Mater. Res. Part A* 95 (3), 940–949. doi:10.1002/jbm.a.32921
- Bat, E., Van Kooten, T. G., Feijen, J., and Grijpma, D. W. (2009). Macrophage-mediated erosion of gamma irradiated poly(trimethylene carbonate) films. *Biomaterials* 30 (22), 3652–3661. doi:10.1016/j.biomaterials.2009.03.033
- Brossier, T., Volpi, G., Vasquez-Villegas, J., Petitjean, N., Guillaume, O., Lapinte, V., et al. (2021). Photoprintable gelatin-*graft*-poly(trimethylene carbonate) by stereolithography for tissue engineering applications. *Biomacromolecules* 22 (9), 3873–3883. doi:10.1021/acs.biomac.1c00687
- Fang, H., Jiang, F., Wu, Q., Ding, Y., and Wang, Z. (2014). Supertough polylactide materials prepared through *in situ* reactive blending with PEG-based diacrylate monomer. *ACS Appl. Mater. Interfaces* 6 (16), 13552–13563. doi:10.1021/am502735q
- Fukushima, K. (2016). Poly(trimethylene carbonate)-based polymers engineered for biodegradable functional biomaterials. *Biomater. Sci.* 4 (1), 9–24. doi:10.1039/c5bm00123d
- He, J., Lin, Z., Hu, X., Xing, L., Liang, G., Chen, D., et al. (2021). Biocompatible and biodegradable scaffold based on poly(trimethylene carbonate)-tricalcium phosphate microspheres for tissue engineering. *Colloids Surfaces B Biointerfaces* 204, 111808. doi:10.1016/j.colsurfb.2021.111808
- Hou, Z., Chen, S., Hu, W., Guo, J., Li, P., Hu, J., et al. (2022). Long-term *in vivo* degradation behavior of poly(trimethylene carbonate-co-2, 2'-dimethyltrimethylene carbonate). *Eur. Polym. J.* 177, 111442. doi:10.1016/j.eurpolymj.2022.111442
- Hou, Z., Chen, S., Li, Z., Chen, Z., Hu, J., Guo, J., et al. (2021). Controllable degradation of poly(trimethylene carbonate) via self-blending with different molecular weights. *Polym. Degrad. Stab.* 189, 109596. doi:10.1016/j.polymdegradstab.2021.109596
- Hou, Z., Hu, J., Li, J., Zhang, W., Li, M., Guo, J., et al. (2017). The *in vitro* enzymatic degradation of cross-linked poly(trimethylene carbonate) networks. *Polymers* 9 (11), 605. doi:10.3390/polym9110605
- Hou, Z., Li, P., Guo, J., Wang, J., Hu, J., and Yang, L., (2020). The effect of molecular weight on thermal properties and degradation behavior of copolymers based on TMC and DTC[J]. *Polym. Degrad. Stab.* 175. doi:10.1016/j.polymdegradstab.2020.109128
- Hou, Z., Xu, W., Chen, S., Guo, J., Li, P., Hu, J., et al. (2023). Biodegradable implants based on photo-cross-linked aliphatic polycarbonates for long-acting contraception. *J. Mater. Sci. Technol.* 156, 129–141. doi:10.1016/j.jmst.2023.01.040
- Hou, Z., Zhang, W., Guo, J., Chen, Z., Hu, J., and Yang, L. (2019). The *in vitro* enzymatic degradation of poly(trimethylene carbonate-co-2, 2'-dimethyltrimethylene carbonate). *Eur. Polym. J.* 112, 51–59. doi:10.1016/j.eurpolymj.2018.12.027
- Jozwiakowska, J., Wach, R. A., Rokita, B., Ulanski, P., Nalawade, S. P., Grijpma, D. W., et al. (2011). Influence of electron beam irradiation on physicochemical properties of poly(trimethylene carbonate). *Polym. Degrad. Stab.* 96 (8), 1430–1437. doi:10.1016/j.polymdegradstab.2011.05.010
- Kedzierska, M., Jamroz, M., Drabczyk, A., Kudlak-Kramarczyk, S., Bańkoš, M., Gruca, M., et al. (2022). Analysis of the influence of both the average molecular weight and the content of crosslinking agent on physicochemical properties of PVP-based hydrogels developed as innovative dressings. *Int. J. Mol. Sci.* 23 (19), 11618. doi:10.3390/ijms231911618
- Li, X., Chen, H., Xie, S., Wang, N., Wu, S., Duan, Y., et al. (2020). Fabrication of photo-crosslinkable poly(trimethylene carbonate)/polycaprolactone nanofibrous scaffolds for tendon regeneration. *Int. J. Nanomedicine* 15, 6373–6383. doi:10.2147/ijn.s246966
- Liu, X., Liu, S., Feng, S., Li, K., Fan, Y., Wang, X., et al. (2021a). Biodegradable cross-linked poly(1,3-trimethylene carbonate) networks formed by gamma irradiation under vacuum. *Polym. Adv. Technol.* 32 (11), 4373–4385. doi:10.1002/pat.5439
- Liu, X., Liu, S., Li, K., Fan, Y., Feng, S., Peng, L., et al. (2021c). Preparation and property evaluation of biodegradable elastomeric PTMC/PLCL networks used as ureteral stents. *Colloids Surfaces A Physicochem. Eng. Aspects* 630, 127550. doi:10.1016/j.colsurfa.2021.127550
- Liu, X., Liu, S., Li, K., Feng, S., Fan, Y., Peng, L., et al. (2021b). Preparation and degradation characteristics of biodegradable elastic poly(1,3-trimethylene carbonate) network. *Polym. Degrad. Stab.* 193, 109718. doi:10.1016/j.polymdegradstab.2021.109718
- Mohajeri, S., Chen, F., de Prinse, M., Phung, T., Burke-Kleinman, J., Maurice, D. H., et al. (2020). Liquid degradable poly(trimethylene carbonate-co-5-hydroxytrimethylene carbonate): an injectable drug delivery vehicle for acid-sensitive drugs. *Mol. Pharm.* 17 (4), 1363–1376. doi:10.1021/acs.molpharmaceut.0c00064
- Qin, X., He, R., Chen, H., Fu, D., Peng, Y., Meng, S., et al. (2021). Methacrylated pullulan/polyethylene glycol diacrylate composite hydrogel for cartilage tissue engineering. *J. Biomater. Sci. Polym. Ed.* 32 (8), 1057–1071. doi:10.1080/09205063.2021.1899888

Funding

This research work was supported by the Natural Science Foundation of Liaoning Province (2022-YGJC-69) and the support program for excellent young scholars of China Medical University.

Conflict of interest

The authors declare that the research was conducted in the absence of any commercial or financial relationships that could be construed as a potential conflict of interest.

Publisher's note

All claims expressed in this article are solely those of the authors and do not necessarily represent those of their affiliated organizations, or those of the publisher, the editors and the reviewers. Any product that may be evaluated in this article, or claim that may be made by its manufacturer, is not guaranteed or endorsed by the publisher.

- Rongen, J. J., van Bochove, B., Hannink, G., Grijpma, D. W., and Buma, P. (2016). Degradation behavior of, and tissue response to photo-crosslinked poly(trimethylene carbonate) networks: tissue response to photo-crosslinked poly(trimethylene carbonate) networks. *J. Biomed. Mater. Res. Part A* 104 (11), 2823–2832. doi:10.1002/jbm.a.35826
- Soriente, A., Amodio, S. P., Fasolino, I., Raucci, M. G., Demitri, C., Engel, E., et al. (2021). Chitosan/PEGDA based scaffolds as bioinspired materials to control *in vitro* angiogenesis. *Mater. Sci. Eng. C* 118, 111420. doi:10.1016/j.msec.2020.111420
- Wang, Y., Xi, L., Zhang, B., Zhu, Q., Su, F., Jelonek, K., et al. (2020). Bioresorbable hydrogels prepared by photo-initiated crosslinking of diacrylated PTMC-PEG-PTMC triblock copolymers as potential carrier of antitumor drugs. *Saudi Pharm. J.* 28 (3), 290–299. doi:10.1016/j.jsps.2020.01.008
- Warr, C., Valdoz, J. C., Bickham, B. P., Knight, C. J., Franks, N. A., Chartrand, N., et al. (2020). Biocompatible PEGDA resin for 3D printing. *ACS Appl. bio Mater.* 3 (4), 2239–2244. doi:10.1021/acsabm.0c00055
- Yang, C., Zhou, M., Lin, Y., Cheng, C., Cheng, F., Liu, W., et al. (2019). Super-tough poly (l-lactide) materials: reactive blending with maleic anhydride grafted starch and poly (ethylene glycol) diacrylate. *Int. J. Biol. Macromol.* 136, 1069–1075. doi:10.1016/j.ijbiomac.2019.06.141
- Yang, L., Li, J., Jin, Y., Zhang, J., Li, M., and Gu, Z. (2014b). Highly efficient cross-linking of poly(trimethylene carbonate) via bis(trimethylene carbonate) or bis(ϵ -caprolactone). *Polymer* 55 (26), 6686–6695. doi:10.1016/j.polymer.2014.10.072
- Yang, L., Li, J., Li, M., and Gu, Z. (2016). The *in vitro* and *in vivo* degradation of cross-linked poly(trimethylene carbonate)-based networks. *Polymers* 8 (4), 151. doi:10.3390/polym8040151
- Yang, L., Li, J., Meng, S., Jin, Y., Zhang, J., Li, M., et al. (2014a). The *in vitro* and *in vivo* degradation behavior of poly (trimethylene carbonate-co- ϵ -caprolactone) implants. *Polymer* 55 (20), 5111–5124. doi:10.1016/j.polymer.2014.08.027
- Yang, L., Li, J., Zhang, W., Jin, Y., Zhang, J., Liu, Y., et al. (2015). The degradation of poly(trimethylene carbonate) implants: the role of molecular weight and enzymes. *Polym. Degrad. Stab.* 122, 77–87. doi:10.1016/j.polymdegradstab.2015.10.016
- Yang, L-Q., He, B., Meng, S., Zhang, J. Z., Li, M., Guo, J., et al. (2013). Biodegradable cross-linked poly(trimethylene carbonate) networks for implant applications: synthesis and properties. *Polymer* 54 (11), 2668–2675. doi:10.1016/j.polymer.2013.03.059
- Zant, E., and Grijpma, D. W. (2016). Tough biodegradable mixed-macromer networks and hydrogels by photo-crosslinking in solution. *Acta biomater.* 31, 80–88. doi:10.1016/j.actbio.2015.12.014



OPEN ACCESS

EDITED BY

Jianshe Hu,
Northeastern University, China

REVIEWED BY

Rishi Paliwal,
Indira Gandhi National Tribal University,
India
Chandra Srivastava,
Amity University Gurgaon, India
Xuehui Zhang,
Peking University Hospital of
Stomatology, China

*CORRESPONDENCE

P. S. Rajinikanth,
✉ psrajinikanth222@gmail.com
Qiang Ao,
✉ aoqiang@scu.edu.cn

[†]These authors have contributed equally
to this work

RECEIVED 06 September 2023

ACCEPTED 16 October 2023

PUBLISHED 31 October 2023

CITATION

Anjum S, Li T, Arya DK, Ali D, Alarifi S,
Yulin W, Hengtong Z, Rajinikanth PS and
Ao Q (2023), Biomimetic electrospun
nanofibrous scaffold for tissue
engineering: preparation, optimization by
design of experiments (DOE), *in-vitro* and
in-vivo characterization.
Front. Bioeng. Biotechnol. 11:1288539.
doi: 10.3389/fbioe.2023.1288539

COPYRIGHT

© 2023 Anjum, Li, Arya, Ali, Alarifi, Yulin,
Hengtong, Rajinikanth and Ao. This is an
open-access article distributed under the
terms of the [Creative Commons
Attribution License \(CC BY\)](#). The use,
distribution or reproduction in other
forums is permitted, provided the original
author(s) and the copyright owner(s) are
credited and that the original publication
in this journal is cited, in accordance with
accepted academic practice. No use,
distribution or reproduction is permitted
which does not comply with these terms.

Biomimetic electrospun nanofibrous scaffold for tissue engineering: preparation, optimization by design of experiments (DOE), *in-vitro* and *in-vivo* characterization

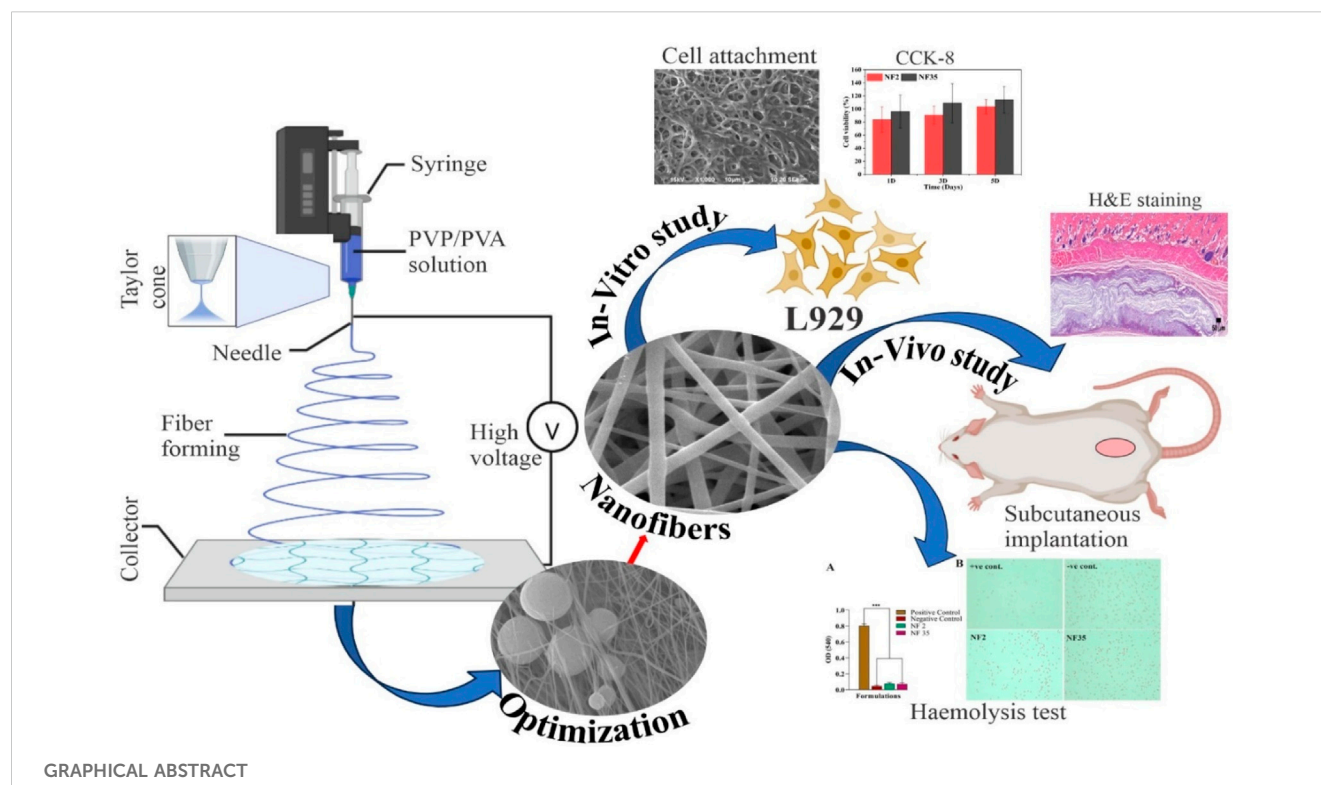
Shabnam Anjum^{1,2†}, Ting Li^{3†}, Dilip Kumar Arya⁴, Daoud Ali⁵,
Saud Alarifi⁵, Wang Yulin², Zhang Hengtong², P. S. Rajinikanth^{4*}
and Qiang Ao^{1,2*}

¹Department of Tissue Engineering, School of Intelligent Medicine, China Medical University, Shenyang, Liaoning, China, ²NMPA Key Laboratory for Quality Research and Control of Tissue Regenerative Biomaterial, National Engineering Research Centre for Biomaterials, Institute of Regulatory Science for Medical Device, Sichuan University, Chengdu, Sichuan, China, ³Department of Laboratory Medicine, Shengjing Hospital of China Medical University, Shenyang, Liaoning, China, ⁴Department of Pharmaceutical Sciences, Babasaheb Bhimrao Ambedkar University, Vidya Vihar, Lucknow, India, ⁵Department of Zoology, College of Science, King Saud University, Riyadh, Saudi Arabia

Electrospinning is a versatile method for fabrication of precise nanofibrous materials for various biomedical application including tissue engineering and drug delivery. This research is aimed to fabricate the PVP/PVA nanofiber scaffold by novel electrospinning technique and to investigate the impact of process parameters (flow rate, voltage and distance) and polymer concentration/solvent combinations influence on properties of electrospun nanofibers. The *in-vitro* and *in-vivo* degradation studies were performed to evaluate the potential of electrospun PVP/PVA as a tissue engineering scaffold. The solvents used for electrospinning of PVP/PVA nanofibers were ethanol and 90% acetic acid, optimized with central composite design via Design Expert software. NF-2 and NF-35 were selected as optimized nanofiber formulation in acetic acid and ethanol, and their characterization showed diameter of 150–400 nm, tensile strength of 18.3 and 13.1 MPa, respectively. XRD data revealed the amorphous nature, and exhibited hydrophilicity (contact angles: 67.89° and 58.31° for NF-2 and NF-35). Swelling and *in-vitro* degradability studies displayed extended water retention as well as delayed degradation. FTIR analysis confirmed solvent-independent interactions. Additionally, hemolysis and *in-vitro* cytotoxicity studies revealed the non-toxic nature of fabricated scaffolds on RBCs and L929 fibroblast cells. Subcutaneous rat implantation assessed tissue response, month-long biodegradation, and biocompatibility through histological analysis of surrounding tissue. Due to its excellent biocompatibility, this porous PVP/PVA nanofiber has great potential for biomedical applications.

KEYWORDS

electrospinning, PVP, PVA, subcutaneous implant, tissue engineering



1 Introduction

In tissue engineering and regenerative medicine (TERM) research, selecting and optimizing a biomaterial that physiochemically replicates the extracellular matrix (ECM) is important (Mao et al., 2023). To mimic the ECM structure of the original tissues, materials must be biocompatible, biodegradable and possess the required physiochemical properties (Qiu et al., 2023; Xin et al., 2023). Tissue engineering offers crucial and viable tissue structures for the purpose of tissue replacement (Zhu et al., 2008; Pezeshki-Modaress et al., 2015; Quan et al., 2022).

Electrospun nanofibers play a key role in tissue regeneration owing to their multiple functionalities, such as high surface area, mechanical stability (stiffness and tensile strength), nanoscale architecture, interfibrillar porous microstructure, sustained drug delivery and high scale-up potential. There is growing evidence that nanofibrous scaffolds are suitable for TERM because they can recapitulate ECM components, modulate cellular responses, and promote mineralization and osseointegration (Anand et al., 2022a; Yu et al., 2023). Electrospinning represents an innovative and effective method for creating biomimetic non-woven nanofibrous scaffolds (Anand et al., 2023). The electrostatic voltage is used as the driving force for the formation of nano-sized fibers from different materials, such as polymers, metals and ceramics. When exposed to a very high electrical potential, the charged polymer is captivated by the collector and forms fiber strands with porous structures.

The dimensions and morphological configuration of nanofibers produced through electrospinning are influenced by a range of factors. These factors can be categorized into three groups: attributes of the polymer solution (such as molecular weight,

concentration, solvent, viscosity, conductivity, and surface tension), operational parameters (including applied voltage, flow rate, collector configuration, and tip-to-collector distance), and environmental conditions (encompassing temperature, atmospheric pressure, and humidity). These factors collectively impact the capability to spin and the morphology of electrospun nanofibers (Anjum et al., 2022). Hence, achieving the intended fiber structure necessitates the optimization and modeling of electrospinning variables. The influence of these variables on fiber shape has been extensively explored in various investigations carried out by numerous researchers.

Polyvinylpyrrolidone (PVP) stands as a significant amorphous polymer, characterized by its notable biocompatibility, high tensile strength, exceptional solubility in various organic solvents, minimal chemical toxicity, proficient spinnability, and non-hazardous nature. The process of electrospinning has found extensive application in transforming diverse materials into fibers, leveraging PVP's spinnability and fiber extraction capabilities. Another synthetic polymer that exhibits a commendable aptitude for forming membranes, along with low toxicity in physiological environments and excellent biocompatibility, is polyvinyl alcohol (PVA) (Agarwal et al., 2021; Thakur et al., 2023). However, a notable drawback of semi-crystalline PVA is its susceptibility to suspension under physiological conditions. By amalgamating PVA and PVP, the constraints posed by this drawback can be surmounted, owing to the presence of inter-chain hydrogen bonds that bolster their stability (Mohammed et al., 2021; Pandey et al., 2023).

Response Surface Methodology (RSM) emerges as a significant approach in modeling the electrospinning procedure due to its capacity to account for the interplay among diverse parameters.

RSM is an amalgamation of mathematical and statistical techniques employed in the experimental modeling and analysis of diverse input data that can impact specific outcomes or the quality aspects of a process. Notably, Gu et al., in their research, explored the quantitative correlation between electrospinning process variables and the distribution of average fiber sizes for gelatin and PVA nanofibers, utilizing RSM (Carvalho et al., 2009). In a separate study, Amiri et al. utilized RSM to fabricate chitosan-collagen nanofibers with minimized diameters through the utilization of electrospinning technology (Amiri et al., 2018). The significance of electric field strength was further explored by Jacobs et al. Through the utilization of a Box-Behnken design within the framework of RSM, they examined the influence of the solvent ratio (trifluoroacetic acid/dichloromethane) as well as interaction effects on the diameter of chitosan nanofibers (Jacobs et al., 2011). The aforementioned exploratory literature has demonstrated that a number of electrospinning parameters affect the fiber's diameters and shape. However, further research is required to fully understand the connection between these variables and fiber structure. There has not been any publicized thorough study that closely examines the impact of numerous parameters. So far, there is limited or no data available in the literature that elucidates the connection between electrospinning parameters and fiber diameter for information and explanations. Additionally, there is an absence of preceding documentation concerning PVP/PVA electrospun nanofibers within varying solvents.

The primary objective of this study is to comprehensively investigate the impact of distinct solvents and process parameters on the diameter of PVP/PVA nanofibers utilizing the electrospinning technique. The research endeavors to optimize various system parameters including concentration, applied voltage (kV), nozzle-collector distance (cm), and flow rate (ml/h) concerning PVP/PVA nanofibers generated in both acetic acid and ethanol solvents. This optimization was conducted using DOE, version 13. RSM with central composite design (CCD) was used to model and optimize the electrospinning process to minimize the nanofiber diameter. The comparison of *in vitro* with *in vivo* degradation was also carried out. There are different sources of lipases in the human body such as leukocytes, present in the wound healing process, with the lipase concentration of healthy adults in the range of 30–190 U/L. Thus, the degradation of the PVP/PVA nanofibers were monitored both in phosphate buffered saline (PBS) and *in-vivo* subcutaneous rat implantation. The *in-vitro* degradation kinetics were evaluated through the quantification of weight loss, swelling degree and thermal behavior whereas *in-vivo* degradation was assessed by using histopathology. Biocompatibility study was investigated using L929 cell lines and hemolysis study.

2 Materials and methods

PVA (Mw: 80,000) and PVP (Mw: 90,000) were purchased from Macklin Biochemical Co. Ltd. (P.R. China). Cell Counting Kit-8 purchased from KeyGEN BioTECH (China). L929 cell lines were gift sample from professor Huang Zhongbing (Biomedical engineering collage; Sichuan university). All additional chemicals and reagents employed in the study were of analytical grade.

2.1 Design and optimization of PVP/PVA nanofiber

2.1.1 Optimization of polymer concentration

DOE software version 13 was used to optimize the polymer concentration as well as their nanofibers producibility. In this study, we applied the RSM technique using a CCD to evaluate the influence of polymers solution concentration on nanofiber producibility in ethanol. Face centered central composite design (FCCD) with four center points was used to investigate the relationship between independent variables and responses. Accordingly, the percentage of polymers (%w/v) was considered as the process parameter in the DOE. Two levels, low (−1) and high (+1), were defined for each polymer with different concentrations. As shown in Table 1, 12 runs were performed and the nanofiber producibility scale range from 1 to 5 was measured as the response.

2.1.2 Optimization of electrospinning process parameters in different solvents

To analyze the effect of process parameters in different electrospinning solvents on the producibility and diameter of nanofibers, the selected batches were used for further studies. In this study, a CCD design was used to prepare and optimize the electrospun nanofibers. The main parameters including voltage (kV), flow rate (ml/hr) and distance (cm) with two levels, low (−1) and high (+1), were evaluated for optimizing the nanofibers. As shown in Table 2 and Table 3, 18 runs were performed and the nanofiber diameter was measured as the response transferred to the software. The main aim of the DOE was to determine the optimal conditions for fabricating nanofibers.

- 1) PVP/PVA in acetic acid solvent.
- 2) PVP/PVA in ethanol solvent.

2.1.3 Preparation of nanofibers by electrospinning

Polymer solutions were prepared in different solvents by mixing 12% PVP and 8% PVA in 90% acetic acid and distilled water under continuous stirring for 8 h to obtain a uniform solution. A mixture consisting of 12% PVP and 8% PVA solutions was meticulously combined in a 50/50 ratio through rigorous stirring to achieve well-blended compounds suitable for electrospinning. The same procedure was replicated using ethanol. These prepared solutions were introduced into a 10 ml syringe fitted with a stainless-steel needle possessing an inner diameter of 0.4 mm. By connecting a positive electrode to the needle, a high-voltage power source was employed. For the collection of nanofibers, a collector enveloped in aluminum foil was employed, positioned at a distance of 8–12 cm from the spinning electrode. To ensure controlled extrusion, the syringe pump's flow rate was fine-tuned to 1.5–2.5 ml/h, while the solutions were pumped using a high electric voltage ranging from 18–26 kV.

2.2 Physio-chemical characterization

2.2.1 Scanning electron microscopy (SEM) analysis

The morphology of the electrospun nanofiber batches was analyzed using a SEM model S4800 from Hitachi, Japan. In this investigation, nanofiber samples were affixed to SEM specimen stubs utilizing double-sided carbon tape. Subsequently, a sputter-coating process with Au-Pd

TABLE 1 DOE table for the optimization of polymer (PVP and PVA) concentration.

| Nanofiber batches | Run | Factor 1 | Factor 2 | Response 1 NF producibility |
|-------------------|-----|---------------|---------------|-----------------------------|
| | | A: PVP (%w/v) | B: PVA (%w/v) | |
| NF1 | 1 | 12.00 | 5.00 | 4 |
| NF2 | 2 | 8.00 | 2.00 | 2 |
| NF3 | 3 | 8.00 | 5.00 | 2 |
| NF4 | 4 | 4.00 | 2.00 | 1 |
| NF5 | 5 | 8.00 | 5.00 | 2 |
| NF6 | 6 | 4.00 | 8.00 | 1 |
| NF7 | 7 | 12.00 | 2.00 | 3 |
| NF8 | 8 | 4.00 | 5.00 | 1 |
| NF9 | 9 | 8.00 | 5.00 | 2 |
| NF10 | 10 | 8.00 | 8.00 | 3 |
| NF11 | 11 | 12.00 | 8.00 | 5 |
| NF12 | 12 | 8.00 | 5.00 | 2 |

The bold values represent has optimized batches.

TABLE 2 CCD design for the optimization of electrospinning process parameters in acetic acid.

| Nanofiber batches | Run | Factor 1 | Factor 2 | Factor 3 | Response 1 |
|-------------------|-----|----------------------|-----------------|------------------|----------------|
| | | A: Flow rate (ml/hr) | B: Voltage (kV) | C: Distance (cm) | Diameter (nm) |
| NF1 | 1 | 1.50 | 26.00 | 12.00 | 232.11 |
| NF2 | 2 | 2.50 | 26.00 | 8.00 | 179.224 |
| NF3 | 3 | 2.00 | 18.00 | 10.00 | 235.502 |
| NF4 | 4 | 2.00 | 26.00 | 10.00 | 272.6 |
| NF5 | 5 | 2.00 | 22.00 | 10.00 | 192.093 |
| NF6 | 6 | 2.00 | 22.00 | 8.00 | 121.91 |
| NF7 | 7 | 2.50 | 18.00 | 12.00 | 96.379 |
| NF8 | 8 | 2.00 | 22.00 | 12.00 | 136.3 |
| NF9 | 9 | 2.00 | 22.00 | 10.00 | 192.093 |
| NF10 | 10 | 1.50 | 22.00 | 10.00 | 258.611 |
| NF11 | 11 | 1.50 | 18.00 | 12.00 | 237.92 |
| NF12 | 12 | 2.50 | 26.00 | 12.00 | 207.983 |
| NF13 | 13 | 2.50 | 22.00 | 10.00 | 177.731 |
| NF14 | 14 | 1.50 | 26.00 | 8.00 | 189.144 |
| NF15 | 15 | 1.50 | 18.00 | 8.00 | 262.178 |
| NF16 | 16 | 2.50 | 18.00 | 8.00 | 129.306 |
| NF17 | 17 | 2.00 | 22.00 | 10.00 | 192.093 |
| NF18 | 18 | 2.00 | 22.00 | 10.00 | 192.093 |

The bold values represent has optimized batches.

TABLE 3 CCD design for the optimization of electrospinning process parameters in ethanol.

| Nanofiber batches | Run | Factor 1 | Factor 2 | Factor 3 | Response 1 |
|-------------------|-----------|----------------------|-----------------|------------------|----------------|
| | | A: Flow rate (ml/hr) | B: Voltage (kV) | C: Distance (cm) | Diameter (nm) |
| NF19 | 1 | 2.00 | 22.00 | 12.00 | 182.845 |
| NF20 | 2 | 1.50 | 18.00 | 12.00 | 309.61 |
| NF21 | 3 | 2.00 | 22.00 | 10.00 | 183.681 |
| NF22 | 4 | 1.50 | 22.00 | 10.00 | 336.599 |
| NF23 | 5 | 2.00 | 22.00 | 10.00 | 183.681 |
| NF24 | 6 | 2.00 | 22.00 | 10.00 | 183.681 |
| NF25 | 7 | 2.50 | 26.00 | 12.00 | 388.681 |
| NF26 | 8 | 2.50 | 18.00 | 8.00 | 272.57 |
| NF27 | 9 | 2.50 | 22.00 | 10.00 | 406.577 |
| NF28 | 10 | 2.00 | 22.00 | 8.00 | 84.346 |
| NF29 | 11 | 2.00 | 22.00 | 10.00 | 183.736 |
| NF30 | 12 | 2.00 | 18.00 | 10.00 | 198.105 |
| NF31 | 13 | 1.50 | 26.00 | 8.00 | 121.897 |
| NF32 | 14 | 1.50 | 18.00 | 8.00 | 328.217 |
| NF33 | 15 | 2.50 | 18.00 | 12.00 | 275.956 |
| NF34 | 16 | 2.00 | 26.00 | 10.00 | 192.736 |
| NF35 | 17 | 2.50 | 26.00 | 8.00 | 271.065 |
| NF36 | 18 | 1.50 | 26.00 | 12.00 | 155.389 |

The bold values represent has optimized batches.

was conducted for a duration of 70 s. The analysis was carried out under varying magnifications at an accelerating voltage. The software employed for assessing the nanofiber scaffold diameter was ImageJ. Measurements of fiber diameters were taken at multiple locations for accuracy (Anand et al., 2022b).

2.2.2 Mechanical testing

The mechanical characteristics of the nanofibrous mats were assessed using a Universal Testing Machine (UTM) (YG005A; Baien Instrument China) with a load cell of 5 cN capacity and the standard followed was American Society for Testing and Materials (ASTM, D882). The nanofibrous samples ($n = 3$) were cut into 1 mm width and 20 mm length, placed between the two clasps, and subjected to tensile displacement a crosshead speed of 8 mm/min. The stress-strain curve was utilized to calculate the Young's modulus, tensile strength, and elongation at the point of fracture for the samples.

2.2.3 Hydrophilicity characterization by contact angle

The angle formed between the solid surface and the interface of the liquid/vapor is known as the contact angle. To assess the surface wettability, whether it is hydrophilic or hydrophobic, of the nanofibers, a water contact angle instrument (model JC 2000C1; POWEREACH China) was employed. In this process, the sample was initially positioned on a level surface, following which a water

droplet was carefully dispensed onto it using a moving needle. The spherical image of the droplet was captured by a digital camera and projected onto a monitor. Subsequently, the contact angle formed between the droplet and the surface of the nanofibers was measured. To ensure accuracy, at least three measurements were taken at different locations on the film and then averaged for comprehensive data analysis.

2.2.4 Fourier transform infrared spectroscopy (FTIR)

FTIR (NEXUS 670; NICOLET USA) spectrometer was used to determine the constituting functional groups of different nanofibers. The structural changes occurring during electrospinning, blending, coating etc. was scanned by FTIR, using standard KBr crystal at room temperature. The spectra were obtained in transmission mode over a wavenumber ranged from 4,000 to 400 cm^{-1} with a resolution of 4 cm^{-1} (Gupta et al., 2018).

2.2.5 X-ray diffraction (XRD)

The crystalline arrangement of the nanofiber scaffolds were assessed using an X-ray diffractometer (model DX-1000; PHILIPS USA). The samples were positioned on quartz zero background holders and subjected to examination with a commercially available XRD system. For detection, a solid-state Germanium detector cooled with liquid nitrogen was utilized, operating with Cu k-alpha radiation at a current of 45 kV and

40 mA. XRD patterns were gathered within a 2θ range spanning from 5 to 60°, with a scanning rate set at 2° per minute (Pandey et al., 2022; Deepak et al., 2023).

2.2.6 Thermo-gravimetric analysis (TGA)

TGA (TGA/DSC 2/1600-ThermoStar; METTLER TOLEDO Switzerland) was used to employed thermal stability of different nanofibers. In a nitrogen atmosphere, all samples were subjected to heating at a rate of 10°C per minute across a temperature range spanning from 25°C to 800°C.

2.2.7 In-vitro degradation

The degradation characteristics of the nanofibers were assessed by monitoring the weight loss at various time intervals. Scaffolds measuring $1 \times 1 \text{ cm}^2$ were precisely weighed (W_i) and then placed into 5 ml plastic tubes containing 4 ml of PBS solution with a pH of 7.4. These tubes were subsequently positioned within a shaking incubator set at 100 rpm and 37°C. The incubation medium was renewed on a weekly basis. At each predetermined time interval, the samples were dried until a constant weight was achieved (W_f) (Li et al., 2023). The weight loss percentage (%) was calculated using the formula:

$$\text{Weight loss (\%)} = \frac{W_i - W_f}{W_i} \times 100$$

Where W_i and W_f represents the initial weight of the sample and the final weight after degradation, respectively.

2.2.8 Water uptake capacity

The water retention capacity of the scaffolds was assessed by calculating the swelling ratio. Initially, the samples were sectioned into $1 \times 1 \text{ cm}^2$ pieces, and their dry weight (W_d) was determined using an electronic weighing balance and recorded. Subsequently, the samples were immersed in a PBS (pH 7.4) at room temperature. At specified time intervals, the samples were retrieved from the solution and positioned on tissue paper to eliminate excess water adhering to the nanofiber surface (Singh et al., 2023). The weight of the moist nanofiber (W_w) was then promptly measured. All measurements were executed in triplicate, and the water uptake capacity was computed using the subsequent equation:

$$\% \text{Water uptake capacity} = \frac{W_w - W_d}{W_d} \times 100$$

Where W_w represents the weight of the wet nanofiber scaffold and W_d corresponds to the dried weight. A triplicate analysis was conducted, and the average value was adopted as the percentage of water uptake.

2.3 In-vitro compatibility test

2.3.1 In-vitro hemocompatibility test

The assessment of scaffolds' hemocompatibility involved the use of freshly collected blood samples from healthy rats. Blood samples (5 ml) were gathered into tubes coated with heparin and then subjected to centrifugation at 3,000 rpm, leading to the separation of plasma from red blood cell (RBC) pellets settled at the tube's bottom. With careful removal of the supernatant, the introduction of PBS into the tube ensued. A subsequent centrifugation step was applied to resuspended

RBCs for cell isolation. The subsequently purified blood cells were diluted to achieve a 25 ml volume, thus creating an RBC suspension. Following this, 0.5 ml of the RBC suspension was aliquoted into four 1.5 ml tubes. Among these, two tubes were designated as negative and positive controls, wherein 1 ml of PBS and water was added, respectively. The remaining two tubes were subjected to treatment with nanofibers (NF2 and NF35) sized $1 \times 1 \text{ cm}^2$. All tubes, including controls and treated samples, were then incubated at 37°C for a duration of 3 h. Upon the conclusion of this incubation period, all tubes underwent centrifugation at 3,000 rpm for 10 min. After incubation and centrifugation, 200 μL of the supernatant from all the samples was transferred to a 96-well plate, followed by the measurement of haemoglobin absorption at a wavelength of 540 nm (Ghorai et al., 2022). The following formula was employed to determine the percentage hemolysis of the samples.

$$\text{Hemolysis (\%)} = \frac{OD_{\text{Sample}} - OD_{\text{Negative control}}}{OD_{\text{Positive control}} - OD_{\text{Negative control}}} \times 100$$

Where OD_{Sample} , $OD_{\text{Negative Control}}$, $OD_{\text{Positive Control}}$ represents the optical density (OD) of the samples, negative control and positive control.

Microscopic images of the RBC condition were also captured.

2.3.2 In-vitro cell line study on L929

2.3.2.1 Cell viability study

L929 fibroblast cells will be seeded into 96-well culture plates at a predetermined cell density of 1×10^5 cells/well. The cells will be cultured under standard conditions using appropriate DMEM media, supplemented with 10% foetal bovine serum and 1% penicillin-streptomycin, at a temperature of 37°C and under an atmospheric condition of 5% CO_2 . Prior to conducting the cell experiments, nanofibers with a standard size of $6 \text{ cm}^2/\text{ml}$ will be sterilized using UV light and 70% alcohol.

To generate extract solutions, sterile nanofibers will be placed in culture medium (DMEM containing 10% FBS and 1% penicillin-streptomycin). These mixtures will be incubated in a constant temperature shaker at 37°C for 24 h. At the conclusion of the extraction period, samples will be retrieved and the resulting extract solutions will be maintained at 37°C during the subsequent cytotoxicity testing. L929 cells will be exposed to the nanofiber extract solution, and cell proliferation on various nanofibers will be quantitatively assessed using Cell Counting Kit-8 (CCK-8; KeyGEN BioTECH; China) assay at specified time points. The OD value will be measured at 450 nm using a spectrophotometric microplate reader. The experiment will be conducted in triplicate to ensure statistical validity. The acquired data will be analysed to ascertain the impact of nanofibers on L929 fibroblast cell viability on days 1, 3, and 5. Cell viability was calculated using the following formula:

$$\text{Cell viability (\%)} = \frac{OD_{\text{Scaffold}}}{OD_{\text{Control}}} \times 100\%$$

2.3.2.2 Cytocompatibility and cell adhesion test on L929 cell lines

The L929 cells (murine fibroblast) were cultivated in DMEM culture media supplemented with 10% fetal bovine serum and 1% penicillin-streptomycin. The cells were then incubated at 37°C in an

environment with 5% CO₂. The nanofibers were trimmed to dimensions of 2 × 2 cm², after which they underwent a sterilization process involving exposure to UV light for 30 min and treatment with 70% alcohol. Following this, nanofiber-coated 12-well plates were utilized to seed 1 × 10⁴ cells per well, and subsequent incubation took place. On the third and fifth days, the cell culture media was removed, and the cells were rinsed with PBS (7.4), fixed using a 4% w/v paraformaldehyde solution for 30 min, and subjected to a dehydration process using ethanol (ranging from 10% to 100%). To enable microscopic mineralization analysis, the samples were coated with a layer of platinum using sputter coating and studied using SEM.

2.4 In-vivo study

2.4.1 Subcutaneous implantation

All surgical procedures involving animals received approval from the Animal Use and Care Committee of Sichuan University. The nanofibers underwent sterilization through exposure to both 70% ethanol and UV light. Wistar rats, each with a weight ranging from 200 to 250 g, were selected for the animal experiments. These rats were divided randomly into three groups: the first group underwent surgery alone, the second group received PVP/PVA in ethanol (NF35), and the third group received PVP/PVA in acetic acid (NF2); each group comprised six rats. Before the surgical procedures, all experimental animals were anesthetized using chloral hydrate. The dorsal region of the animals was shaved and then sterilized using a solution of 70% ethanol. A sterile surgical blade was employed to create an incision on the dorsum of each animal. Subsequently, a subcutaneous pouch was formed, and an implant measuring 1 × 1 cm² was inserted into this pouch. Following the polymer implantation, the incision was sutured using a non-absorbable surgical black braided silk thread.

2.4.2 In-vivo biocompatibility study

At the end of 1 and 3 weeks, the rats were humanely euthanized. The regions where the implants were positioned were carefully collected; this encompassed both the complete PVP/PVA nanofiber and the adjacent tissue. The collected samples were then immersed in a 4% (w/v) paraformaldehyde solution for fixation, allowing them to be preserved overnight. To prepare the samples for further analysis, they underwent a dehydration process by passing through a series of alcohol baths with varying concentrations, followed by treatment with xylene. Subsequently, the samples were embedded in paraffin and sliced into sections that were 5 μm thick. These sections were mounted onto slides, facilitating histological staining and subsequent imaging.

2.5 Statistical analysis

The data from all experiments were presented in the form of mean values accompanied by standard deviations (S.D.). Analysis of the data was performed using OriginPro 2019b software. One-way ANOVA was utilized to assess the data across all experiments, and this was followed by the application of the Tukey test for *post hoc* analysis. Statistical significance was indicated by * for a *p*-value less

than 0.05, ** for a *p*-value less than 0.01, and *** *p*-value less than 0.001.

3 Results

3.1 Effect of polymer concentration on nanofiber producibility

During optimization, it was found that the polymer concentration plays a very important role in the formation of nanofibers; otherwise, nanofibers will form with numerous beads having no uniformity. The relationship between solution viscosity and polymer concentration is highly dependent on the concentration of polymer/solvent system. Each set of PVP/PVA was optimized by DOE for their concentration as mentioned earlier (Table 1), on the basis of their nanofiber producibility scale ranging from 1 to 5, which was measured as the response (Table 2; Table 3). SEM images for nanofiber producibility were represented in Figure 1.

As depicted in Figure 2A, the coordination between predicted and experimental values is commendable, encompassing a majority of the responses. This is further supported by the fact that all models possess AP (adequate precision) values surpassing 4, signifying a high level of precision. The NF11 batch was selected from (Table 1) which showed good nanofiber production whereas in other concentrations, polymers were failed to produce nanofibers due to high or low viscosity and lack of sufficient surface tension.

3.2 Effect of electrospinning process parameters

In this study, the primary objective was to achieve the production of uniform and smooth nanofibers by optimizing the electrospinning process parameters, namely distance, voltage, and flow rate, utilizing both acetic acid and ethanol solvents. To gain a deeper understanding of the process parameters and to establish a quantifiable relationship between the electrospinning process parameters and the resulting fiber diameter, the RSM was employed (Gu et al., 2005). By employing the DOE software, quadratic equations were generated to depict the governing relationships between the electrospinning parameters and the designated responses. The influences of diverse processing parameters such as applied voltage, flow rate, and distance, employed in distinct solvents, on all the generated nanofiber batches are presented in Figure 5. The contour and 3D plots, showcased in Figures 3, 4, aptly illustrate the high dependency of fiber diameter on the applied voltage, flow rate, and distance.

3.2.1 Effect of voltage

The influence of voltage on fiber diameter remains a subject of debate and is markedly influenced by the specific characteristics of the polymer and solution employed. Elevated voltage levels can yield disparate outcomes in terms of fiber diameter alteration, as depicted in Figures 3, 4. The impact of heightened voltage on fiber diameter has prompted varying findings, with certain reports suggesting an augmentation in

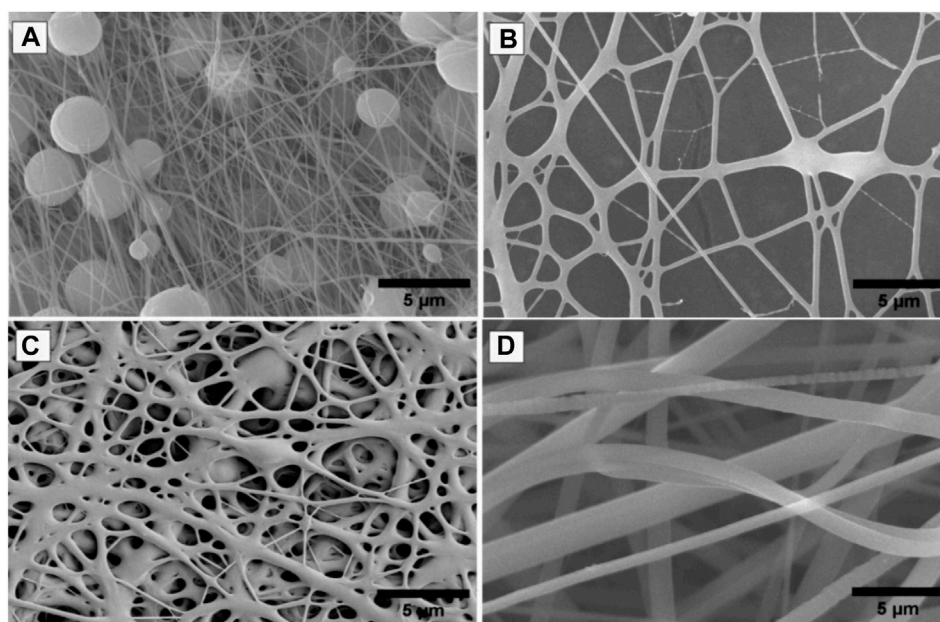


FIGURE 1

SEM images for nanofiber producibility to optimize the concentration of polymers, (A) Non-uniform nanofibers formed with beads, (B) Nanofiber formed but not smooth, (C) Non-uniform nanofibers formed with fewer beads, (D) Beads free uniform nanofibers formed.

correlation with increased voltage for solutions involving PVA polymer (Zhang et al., 2005). Conversely, several studies focusing on the electrospinning of PVP have indicated a decrease in fiber diameter as voltage increases, attributed to the heightened repulsion force. Subsequently intensifying the electric field strength can lead to an expansion in diameter, likely due to the amplified electrostatic forces at play (Chuangchote et al., 2009). Elevated voltage levels facilitate a greater transport of fluid from the polymer solution. Moreover, they serve to expedite the exit of the polymer jet from the Taylor cone, thereby reducing the duration of the jet's flight time (Miri et al., 2016). Enabling a greater polymer carriage and diminishing flight duration can contribute to the production of more substantial fibers at increased voltages. Nevertheless, heightened voltages concurrently amplify the electrostatic repulsion along the jet's surface, potentially leading to a reduction in fiber diameter. Furthermore, exceedingly elevated voltage levels can induce the emergence of branched structures within the jets and fibers, ultimately yielding thinner fibers characterized by a broader diameter distribution (Garg and Bowlin, 2011). The impact of applied voltage and the distance between the nozzle and collector on the diameter of electrospun PVP/PVA nanofibers is twofold. In the case of an acetic acid solvent system, employing a shorter nozzle-collector distance and higher applied voltage leads to a reduced duration for both jet elongation and acetic acid solvent evaporation. Consequently, this combination encourages the production of smaller diameter PVP/PVA nanofibers. Conversely, within an ethanol solvent system, a higher applied voltage grants more time for the jet to elongate in the electric field and for the volatile ethanol solvent to evaporate. As a result, this configuration favours the formation of larger diameter nanofibers.

When examining the acetic acid solvent system at a constant nozzle-collector distance, augmenting the applied voltage leads to a decrease in the average diameter of PVP/PVA nanofibers. However, with a fixed applied voltage, elevating the nozzle-collector distance leads to a reduction in the average diameter (AD) of the nanofibers. This discrepancy can be elucidated by considering the relatively higher boiling point of acetic acid (118°C). In contrast, when using an ethanol solvent, decreasing the applied voltage or increasing the nozzle-collector distance diminishes the strength of the electric field, resulting in less acceleration and stretching of the jet. Consequently, this leads to the generation of larger PVP/PVA nanofibers during the electrospinning process. Subsequent to the dispersion and division of an unstable jet, solvents with lower boiling points, such as ethanol (78.37°C), swiftly undergo evaporation (Nasouri et al., 2015).

3.2.2 Effect of flow rate

The rate at which the polymer solution flows within a given timeframe constitutes an additional element impacting the quality of nanofibers. As evidenced by the findings and outcomes presented in Table 2 and Table 3, employing lower flow rates yields nanofibers characterized by diminished and consistent diameters, attributed to the heightened charge density inherent in such conditions. It has been documented that elevating the flow velocity gives rise to the creation of nanofibers with larger diameters. The conjecture that nanofiber diameter decreases owing to amplified charge density at lower rates has also been put forth (Beachley et al., 2009). Furthermore, there are reports indicating that raising the flow rate leads to an augmentation in fiber diameter (Reneker and Chun, 1996). Furthermore, it is noteworthy that when the flow rate was decreased at 10 kV, the reduction in fibre diameters was more pronounced compared to the situation at 18 kV. This

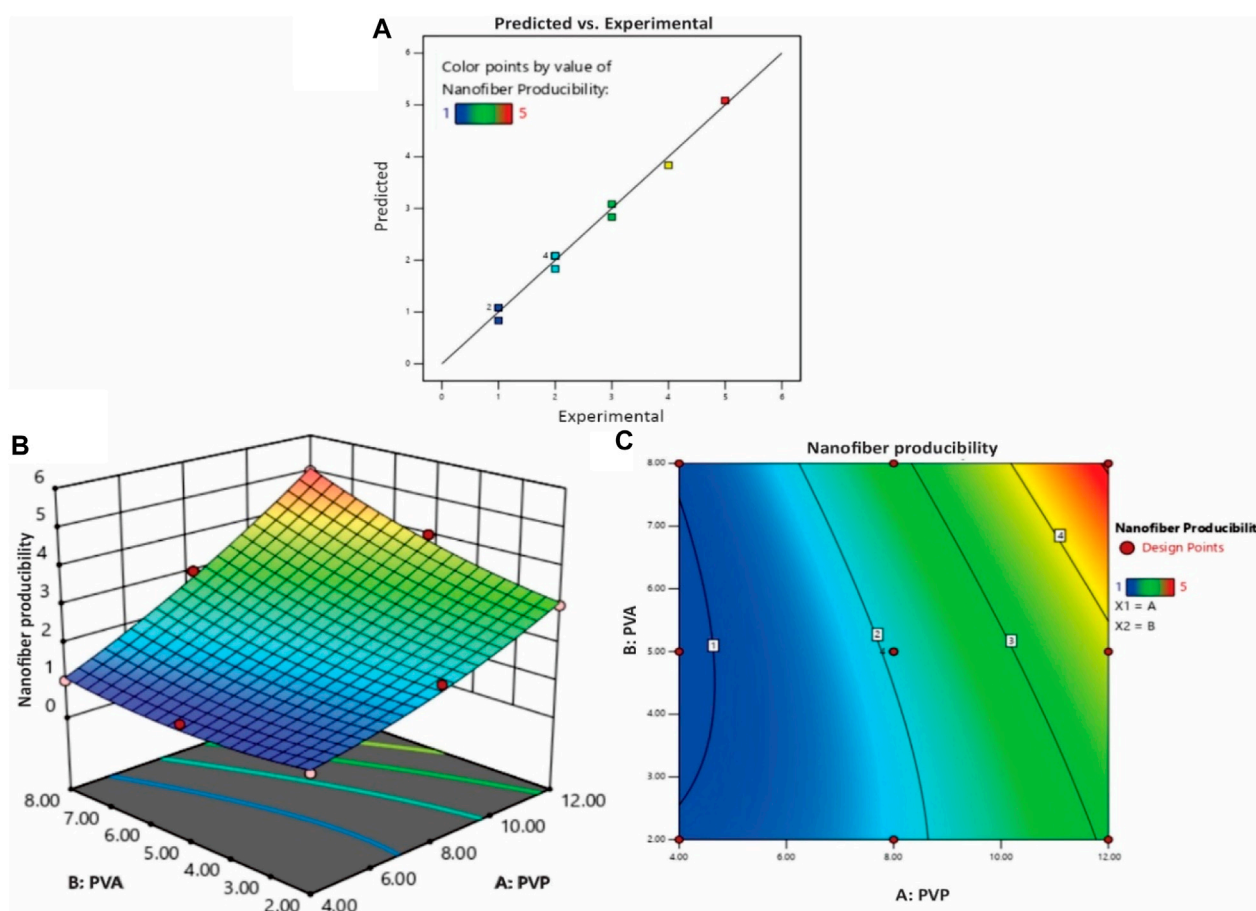


FIGURE 2

(A) The experimental versus predicted plot for optimizing polymer concentration (%) of PVP/PVA nanofibers and the effect of polymer concentration (%) PVP/PVA on the nanofiber production; (B) three-dimensional (3D) RSM plot and (C) Contour-plot.

observation suggests that the impact of flow rate on fibre diameter is more conspicuous at lower voltages. Multiple studies have documented an upsurge in fibre diameter when flow rates are elevated. This correlation is rooted in the fact that increasing the flow rate enhances the solution volume available for electrospinning and the initial radius of the ejected jet. The resultant enlargement of the initial jet radius curtails bending instability and jet stretching, consequently leading to an increase in fibre diameter.

However, it is essential to note that an excessive flow rate not only augments nanofiber agglomeration but also gives rise to bead formation within the fibre structure due to insufficient time for solvent evaporation.

3.2.3 Effect of distance

The distance between the nozzle and the collector constitutes an additional parameter influencing the regulation of nanofiber morphology and diameter. Achieving precise control over polymer solution evaporation before the fiber reaches the collector necessitates the optimization of this distance. Drawing insights from the outcomes and findings presented in Table 2 and Table 3, it becomes evident that the distance parameter is more closely tied to the applied voltage and flow

rate. Extended distances have been associated with the generation of thinner nanofibers in accordance with reported results (Doshi and Reneker, 1995). Furthermore, the occurrence of beads becomes apparent when the distance between the nozzle and the collector is either excessively short or overly long (Yang et al., 2004). It has also been documented that reducing the distance to the collector can enhance the probability of fiber fusion. However, extending the distance beyond a certain threshold leads to a decrease in the strength of the electric field. At a specific point, this attenuation of field strength becomes notably significant (Ding et al., 2010).

3.3 Nanofiber morphology and diameter

Figure 5 illustrates SEM images of typical PVP/PVA electrospun nanofibers, offering insight into the diameter distribution of nanofiber samples. The average fibre diameter spanned from 100 to 400 nm. The SEM depictions of PVP/PVA nanofibers underscored the substantial influence of high voltage (18–26 kV), flow rate (1.5–2.5 ml/h), distance (8–12 cm), and solvent on fibre diameter. For instance, within an ethanol solvent using a flow rate of 2 ml/h, a voltage of 18 kV, and a distance of 10 cm, the resulting fibre

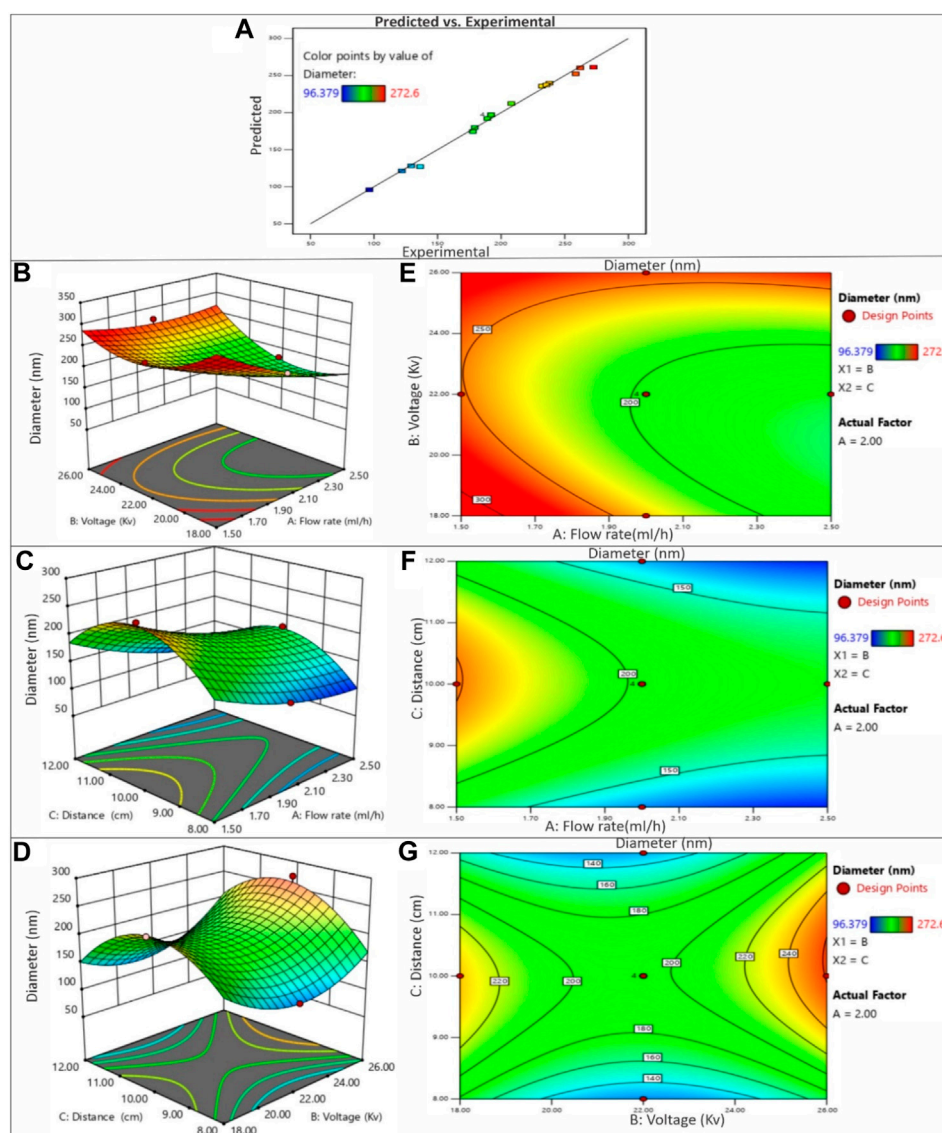


FIGURE 3

(A) The predicted versus experimental plot for average diameter of PVP/PVA nanofibers in acetic acid. Effect of process parameters on diameter of PVP/PVA nanofiber in acetic acid; (B) Effect of voltage and flow rate, (C) Effect of distance and flow rate, (D) Effect of voltage and distance - 3D RSM and (E) Contour plot showing the effect of voltage and flow rate, (F) distance and flow rate and (G) voltage and distance on nanofiber diameter.

exhibited an uneven surface. In contrast, under identical parameters but with an acetic acid solvent, a smooth and homogeneous nanofiber formation was observed.

A noteworthy observation entailed a minimal fibre diameter of 179.224 nm, achieved at a voltage of 26 kV, flow rate of 2.5 ml/h, and distance of 8 cm in the acetic acid solvent. Correspondingly, the average diameter of electrospun PVP/PVA nanofibers, measuring 271.065 nm, was attained using a voltage of 26 kV, flow rate of 2.5 ml/h, and distance of 8 cm in an ethanol solvent. Ethanol exhibited promise as a suitable solvent for PVP/PVA, yielding electrospun fibres with a broad range of diameter distribution conducive to microfiber production. Comprehensive analysis substantiated that polymer concentration, solvent selection, and process parameters all exerted noteworthy impacts on the resulting diameter values.

3.4 Physiochemical properties

3.4.1 Tensile strength

Mechanical properties hold paramount importance for nanofibers, as the underlying matrix must possess robust mechanical strength to effectively facilitate tissue repair. Evaluating the scaffolds' tensile strength (TS) measured in MPa was accomplished through the assessment of strain-stress curves. Figures 6A–C illustrate stress-versus-strain curves and the corresponding variations in TS and elongation at break (EB) for selected scaffolds. In the case of PVP/PVA produced using an acetic acid solvent (designated as NF2), the recorded TS and EB values were 18.3 MPa and 228.06%, respectively. Similarly, for PVP/PVA synthesized with an ethanol solvent (NF35), the TS and EB values were 13.1 MPa and 224.6%, respectively (Figures

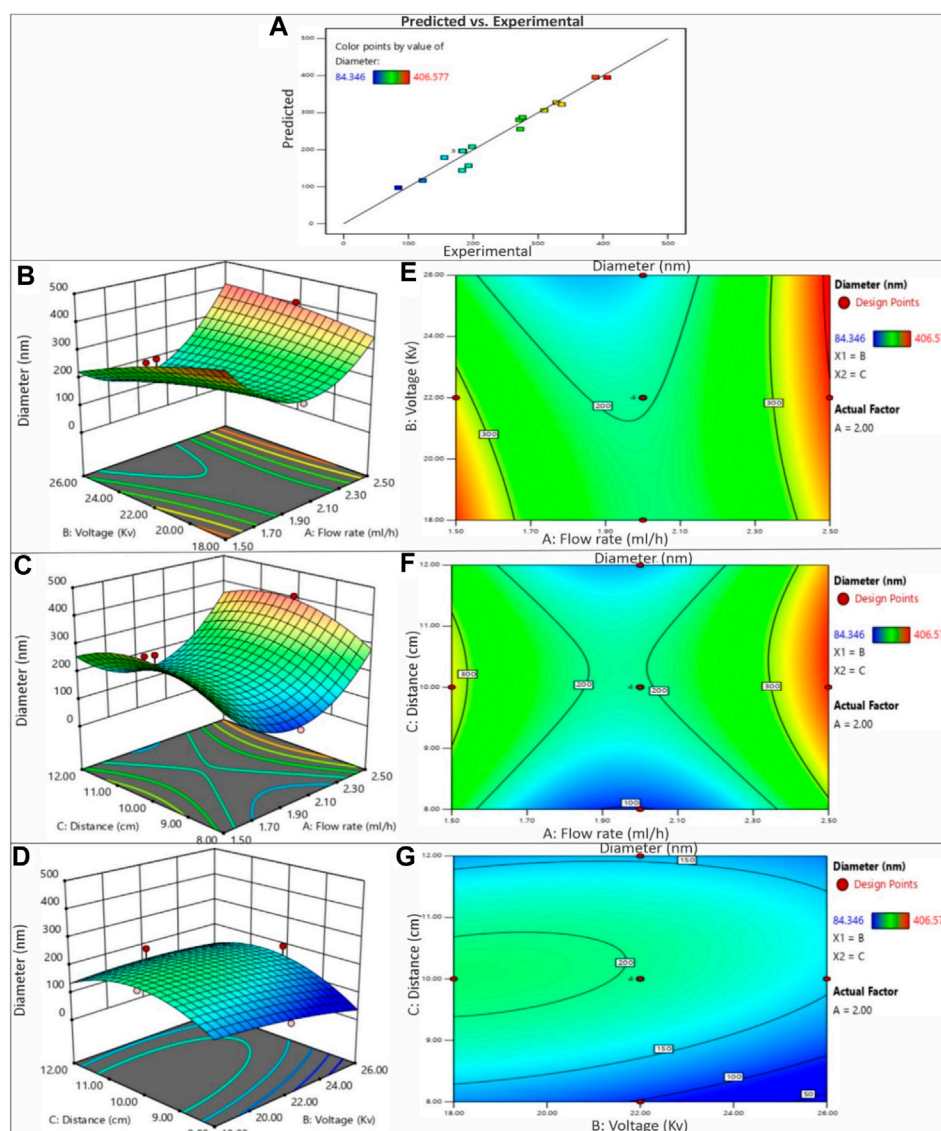


FIGURE 4

(A) The predicted versus experimental plot for average diameter of PVP/PVA nanofibers in ethanol solvent. Effect of process parameters on diameter of PVP/PVA nanofiber in ethanol; (B) Effect of voltage and flow rate, (C) Effect of distance and flow rate, (D) Effect of voltage and distance - 3D RSM and (E) Contour plot showing the effect of voltage and flow rate, (F) distance and flow rate, (G) voltage and distance on nanofiber diameter.

6B, C). It has been substantiated that a heightened porosity tends to adversely impact mechanical behaviour (Maheshwari et al., 2017). Considering the nanofiber diameters, a reduction in diameter correspondingly amplified the mechanical response, encompassing Young's modulus and tensile strength. This augmentation in mechanical attributes was attributed to the constrained distribution of stress within the fibres due to the surface confinement of polymer chains. An intriguing hypothesis emerges: nanofibers characterized by uniform diameter distributions yield a consistent structure that bolsters resistance against axial tensile forces. However, the mechanical strength must strike an optimal balance, neither being excessively high nor overly low. Excessively high TS might lead to prolonged scaffold presence post-regeneration, while insufficient TS could

hinder adequate cell growth and support during the critical regeneration phase.

3.4.2 Contact angle

The determination of hydrophilicity and wettability of the NF2 and NF35 scaffolds involved employing the static water contact angle method through (JC 2000C1; POWEREACH China) instrument. This methodology facilitated the measurement of the contact angle for the optimized nanofiber formulations. Wettability holds pivotal importance as it significantly impacts a scaffold's mechanical stability and its interactions with adhering cells. In the course of contact angle analysis, the shape of the liquid droplet was contingent upon variables such as liquid surface tension, gravity, and the density difference between the liquid and the nanofibers. The

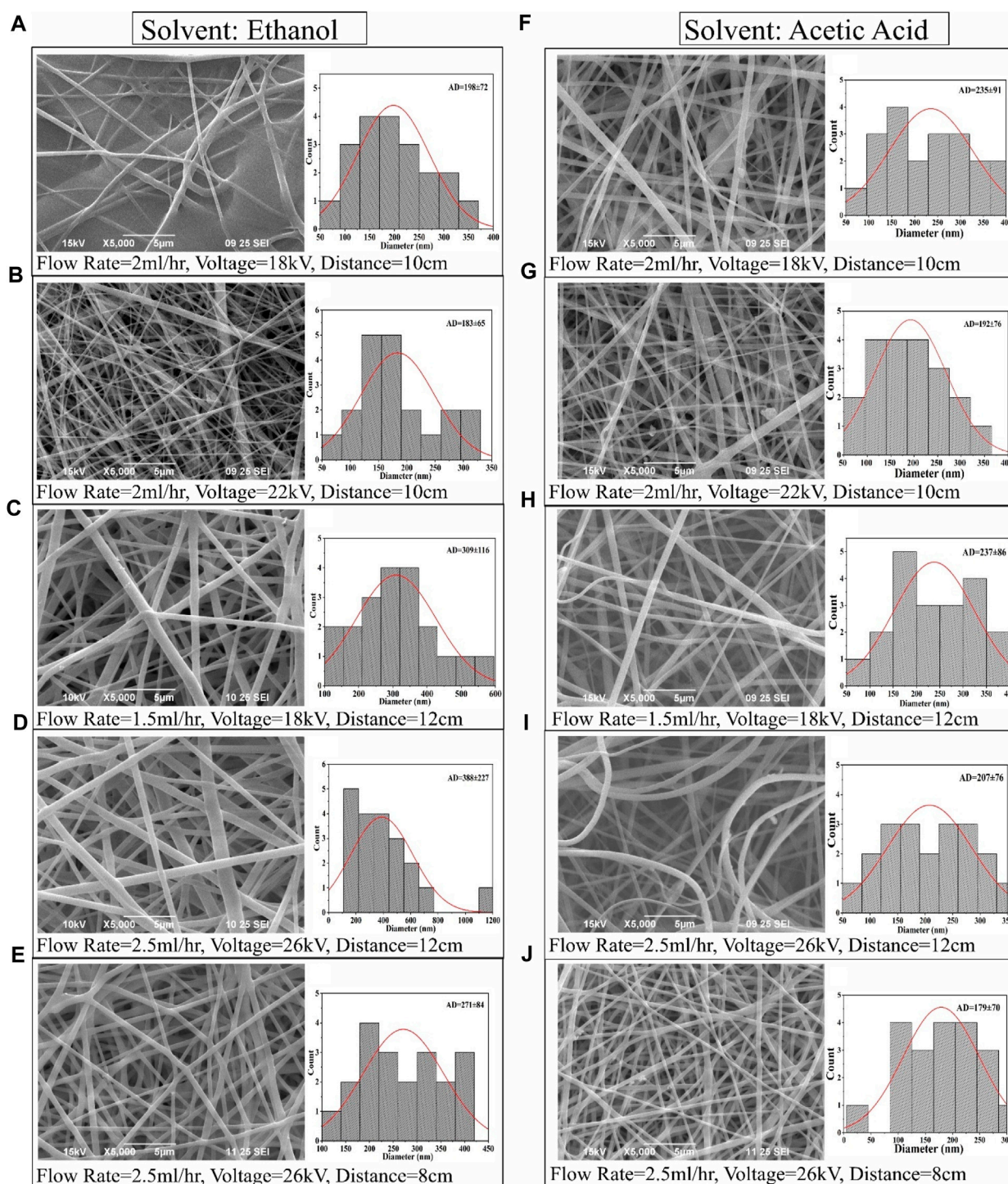
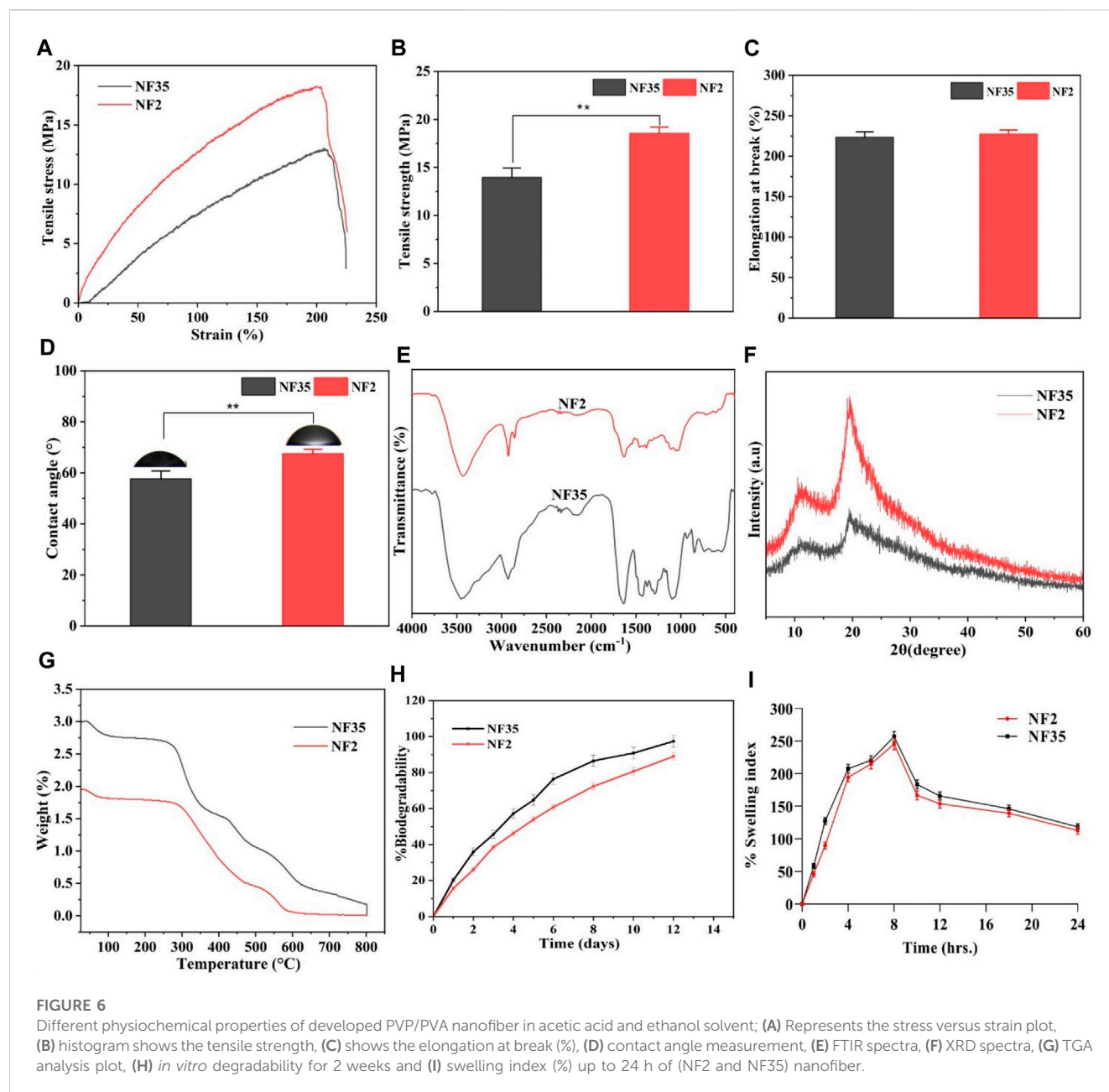


FIGURE 5

SEM images and corresponding fiber diameter distribution of PVP/PVA electrospun fibers in ethanol solvent (A–E) and acetic acid (F–J) at various electrospinning process parameter.

outcomes of the contact angle measurements, visualized in Figure 6D, showcased water droplet behaviour on the nanofiber surfaces. Notably, the abundant water content characteristic of natural polymers engenders a hydrated environment conducive to nutrient and metabolite diffusion, thus favourably influencing cellular regulatory processes.

Hydrophilicity is a key determinant of bioactivity, rendering hydrophilic scaffolds preferable for tissue engineering applications. Specifically, a surface is considered hydrophilic if the contact angle measures below 90° and hydrophobic if the angle exceeds 90° . For NF2 and NF35, the contact angles were 67.89° and 58.31° , respectively. This divergence in contact angles between NF2 and



NF35 might be attributed to the influence of solvent effects and nanofiber diameter.

3.4.3 FTIR analysis

Different absorption bands within $4,000\text{--}500\text{ cm}^{-1}$ were recorded in FTIR spectra of PVA/PVP nanofibers. Figure 6E shows FTIR spectra of the two selected nanofiber scaffolds (NF2 and NF35) obtained from acetic acid and ethanol. The FTIR spectrum of both the nanofiber showed a broad peak at $3,468\text{ cm}^{-1}$ along with strong intensity due to the stretching vibrations of hydroxyl group in both the nanofiber. But the intensity of peak of hydroxyl group in NF35 was more, it may be due to the presence of more hydrogen bonding in the presence of ethanol. The C-H bending at 842 cm^{-1} in PVA polymer, the band at $1,077\text{ cm}^{-1}$ confirm the presence of C-O vibration of PVA-PVP. In

addition, the presence of a $1,631\text{ cm}^{-1}$ peak was due to stretching vibrations of the carbonyl group present in PVA. The band at about $1,279\text{ cm}^{-1}$ corresponds to C-O stretching of acetyl groups present on the PVA backbone. The appearance of C-O stretching is due to the semi-crystalline nature of the blends. A band at $1,373\text{ cm}^{-1}$ is attributed to C-N bond, mainly from the functional group of PVP. The vibration band at about $1,636\text{ cm}^{-1}$ corresponds to C-O symmetric bending of PVA and PVP. The band corresponding to CH₂ asymmetric stretching vibration appeared around $2,928\text{ cm}^{-1}$ in PVP.

3.4.4 XRD study

An XRD study was conducted to investigate electrospinning-induced crystalline changes and provide details regarding the occurrence of complex formation between different polymers.

The XRD patterns of the PVP/PVA blends with different solvents are shown in [Figure 6F](#), and data interpretation was performed using the intensities of the peaks obtained from the spectra. The sharp peaks in the pattern confirmed the crystalline nature of the polymers. The diffraction patterns of the spectra with broad halos confirmed the amorphous nature of the polymers. NF2 fabricated using acetic acid and NF35 produced with ethanol exhibited notably similar significant peaks in the PVP-PVA blend nanofibers, specifically at $2\theta = 19.61^\circ$ for PVP and 11.52° for PVA. Within NF2, the peak intensity experienced an augmentation compared to NF35, while the peak position remained constant. These peaks, observed for both NF2 and NF35, were characterized by short and broad profiles, indicative of the substantially amorphous nature inherent to the blend nanofibers. The observed shift in peak position in the blended samples was attributed to hydrogen bonding interactions between PVA and PVP. This phenomenon likely arises due to hydrogen bonding between the hydroxyl (OH) groups present in PVA and the carbonyl group in PVP ([Yadav et al., 2022](#)).

3.4.5 TGA analysis

The thermal stabilities of the selected NF2 and NF35 nanofibers in different solvents were examined by TGA, as shown in [Figure 6G](#). From the figure it can be seen that both the materials are thermally stable as the materials get completely decomposed at 800°C . NF35 constrains slightly better stability than the NF2 at different temperature as $\sim 320^\circ\text{C}$, 440°C and 590°C . This increase in temperature declares the decomposition of materials because of the degradation of polymeric side chain. Hence, both the materials were thermally stable.

3.4.6 *In-vitro* degradation studies

The degree of degradation of NF 2 and NF 35 scaffold was also determined by observing the mass change of the samples after immersion in PBS. The degradation behavior of the scaffold's during incubation is depicted in [Figure 6H](#). Changes in electrospinning parameters cause variations in nanofiber density and diameter. Scaffolds NF2 and NF35 showed 88% and 97% degradation, after 12 days of incubation in PBS with similar patterns. Scaffolds NF2 and NF35 exhibited low and high rates of deterioration, respectively. The deterioration behavior can be influenced by several factors. The changes in the parameters of electrospinning led to differences in the density and diameter of the nanofibers.

3.4.7 Swelling studies

The swelling behaviour exhibited by the scaffolds (NF2 and NF35) underscores their capacity to facilitate nutrient and waste exchange between the cellular environment and the cells embedded within the scaffold, a crucial aspect in the creation of artificial tissues. Swelling, in this context, signifies the ability to imbibe moisture and establish stability within biological systems. It offers potential as a carrier material for cell proliferation and differentiation, consequently playing a vital role in tissue engineering. Upon implantation, biomaterials interact with the surrounding fluids, initially by uptaking them, thus promoting the degradation process. The water uptake makes the materials more flexible and promotes changes in the dimensions of the implant material.

As portrayed in [Figure 6I](#), the swelling behaviour of the selected electrospun scaffolds is depicted. Notably, hydrophilicity holds significance for tissue engineering scaffolds, as it enhances cell viability and proliferation. Despite all the scaffolds being composed of a PVP/PVA compound, variations exist in their operating parameters. Nanofiber diameter emerges as a pivotal parameter in electrospun scaffolds, influenced by factors such as surface tension, solution viscosity, working distance, flow rate, crystallization characteristics, and applied voltage. Furthermore, the nanofiber diameter's influence extends to scaffold porosity. In light of these factors, it can be inferred that alterations in operating conditions can exert a measurable impact on the scaffold's level of porosity ([Shimko et al., 2005](#)).

3.5 *In-vitro* hemocompatibility test

The hemolysis test is valuable in assessing blood compatibility as it reflects cytotoxicity. RBCs can lyse and release biomolecules like hemoglobin when they encounter water or foreign substances, due to osmotic stress. Damaged RBCs can attract platelets, accelerating coagulation and hindering tissue regeneration ([Balaji et al., 2016](#)). An optimal nanofiber dressing should preserve RBC integrity and avoid triggering coagulation while supporting tissue healing. The central focus of our study was to evaluate material compatibility with RBCs. Typically, for implanted materials, hemolysis levels below 5% are recommended. Microscopic images ([Figure 7B](#)) reaffirmed intact RBCs and nanofiber compatibility. As depicted in [Figure 7A](#), the positive control exhibited notably higher hemolysis (few intact RBCs) compared to the negative control, NF2, and NF35. Notably, NF2 and NF35 displayed hemolysis similar to the negative control, evident by numerous intact RBCs in microscopic images. Consequently, NF2 and NF35 can be deemed highly biocompatible and non-toxic, positioning them favorably for biomedical and tissue regeneration applications.

3.6 *In-vitro* cell line study

3.6.1 Cell viability

The impact of PVP/PVA nanofibers, specifically NF2 and NF5, on L929 fibroblast cell viability was assessed through a CCK-8 assay. The cell viability results from day 1 displayed more than 80% cell viability for NF2 and 90% for NF35 ([Figure 7C](#)). Remarkably, on days 3 and 5 of the viability assay, both nanofiber types exhibited a notable augmentation in cell viability compared to day 1. This observed trend of enhanced cell viability suggests a potential positive influence of these nanofibers on the proliferation of L929 cells over time. So, it may be concluded from above results that these nanofibers are non-toxic as well as biocompatible and significantly enhanced the cell proliferation and ascertained the potential applications of these nanofibers in promoting cell growth and viability.

3.6.2 Cytocompatibility and cell adhesion test on L929 cell lines

[Figure 7D](#) show L929 cells adhesion and proliferation after treatment with prepared nanofibers on different time intervals of 3 and 5 days. The SEM photomicrographs indicate that the seeded

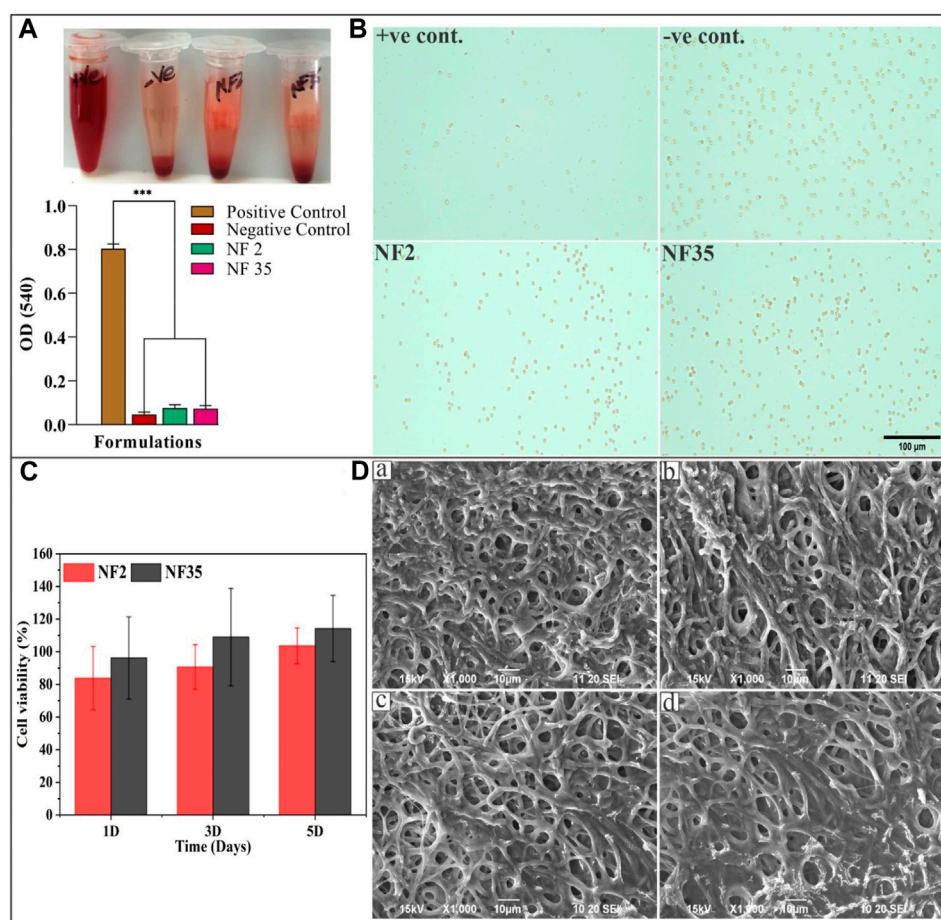


FIGURE 7

The study of hemolysis and the effect of scaffold on RBCs as well as cell viability and cytocompatibility of nanofiber; (A) The histogram demonstrated the absorbance value of +Ve control, -Ve control, NF2 and NF35 at 540 nm; (B) The microscopic image of intact RBCs status after 3 h of incubation with the control groups and nanofiber group (NF2 and NF35); (C) Effects of NF2 and NF35 nanofibers on cell viability of L929 cells for 1, 3 and 5 days. (D) SEM images of L929 cells seeded on NF2 and NF35 nanofibers after 3 days (A,B) and (C,D) presents the adhered cells after 5 days of seeding.

cells are well adhered onto the surface of the scaffolds, which signifies the good biocompatibility of the scaffolds. Our results showed that nanofiber provided a good cell adhesion and proliferation property.

3.7 Subcutaneous implantation

The subcutaneous implantation of PVP/PVA nanofiber was performed in rat (Figures 8A, B), followed by careful suturing and housing the animals in a controlled environment, represented a pivotal experimental approach to investigate the *in vivo* biocompatibility and potential therapeutic applications of these nanofibers. This procedure facilitated the exploration of nanofiber-host tissue interactions, cellular responses, and overall biodegradation processes within a controlled condition. The chosen subcutaneous implantation technique, along with precise suturing and controlled animal housing, ensured a more realistic representation of the nanofibers' interaction with the surrounding tissue. After 3 weeks of subcutaneous implantation, the nanofibers' macroscopic appearance was similar to that of pre-implant hydrated fibre (Figures 8C, D). These studies significantly contributed to our

understanding of the materials' viability for applications in tissue engineering, wound healing, and other biomedical fields.

3.8 *In-vivo* biocompatibility study by (H&E) staining

The *in vivo* degradation of the NF2 and NF35 electrospun nanofiber was evaluated by implant tests. One week after subcutaneous implantation, the nanofibers' macroscopic appearance was similar to that of pre-implant hydrated fibre (Figure 9). After the implantation and retrieval of the electrospun nanofiber, the specimens were routinely processed for histology, and transversal sections were analyzed by standard H&E staining.

The H&E-stained tissue samples collected after one and 3 weeks revealed the absence of any significant adverse reactions, inflammatory responses, or cellular infiltrations in the surrounding tissue (Figures 9, 10). This positive outcome can be attributed to the favourable interaction between the nanofibers and various cells present within the tissue. Specifically, fibroblasts play a crucial role in tissue repair and extracellular matrix formation, contributing to the nanofibers'

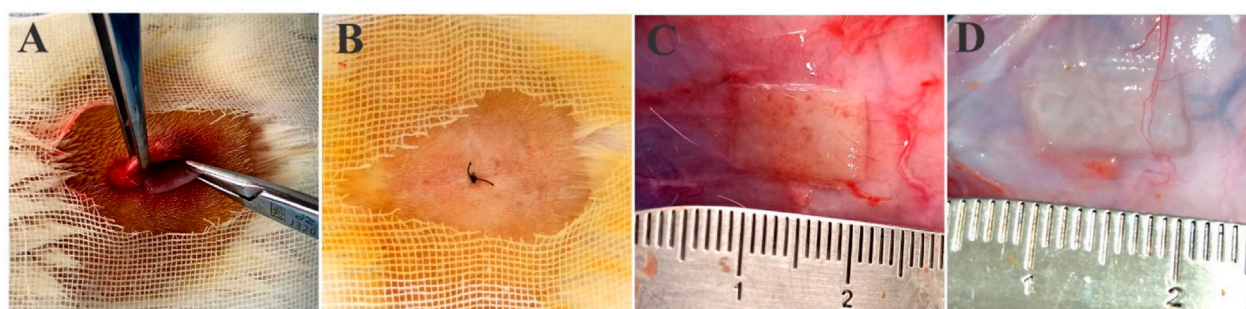


FIGURE 8

(A) Surgical scheme of scaffold's subcutaneous implantation, (B) post-implantation suturing, (C) postoperative images of the scaffold NF2 and (D) NF35 nanofibers scaffolds remained 3 weeks after implantation.

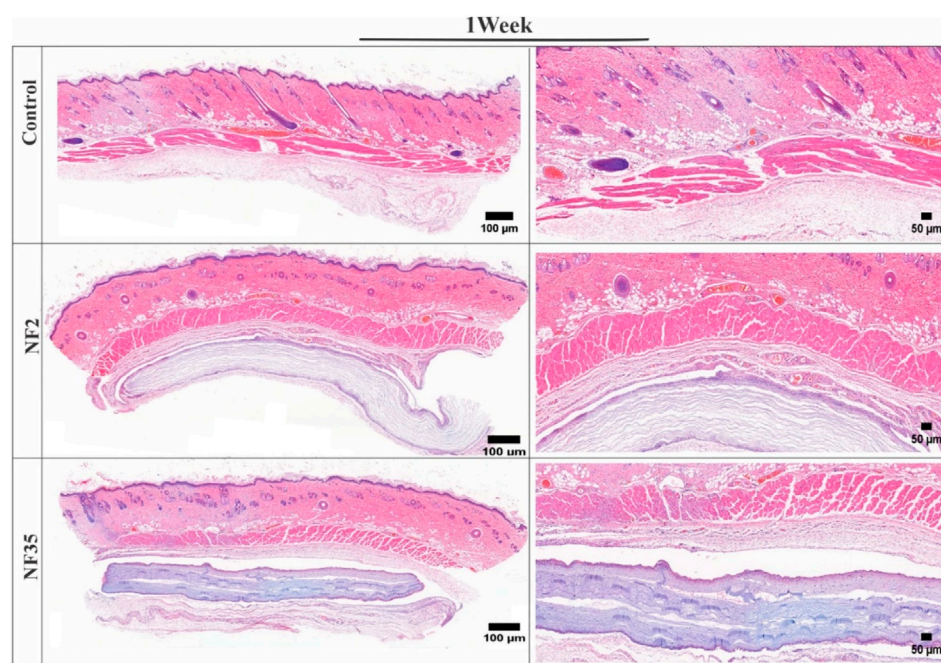


FIGURE 9

H&E-stained images of surrounding tissue of subcutaneously implanted PVP/PVA nanofiber for control, NF2 and NF35. Reconstruction of the full and interior membrane sections after 1 week of implantation.

integration into the tissue. Additionally, the presence of macrophages and neutrophils indicates the absence of a robust immune response, further affirming the biocompatibility of NF2 and NF5. These findings suggest that the nanofibers have the potential to support tissue regeneration and therapeutic interventions, making them promising candidates for various biomedical applications.

4 Discussion

Accordingly, the *in vitro* and *in vivo* studies described previously regarding the non-conformable results, it is important to highlight that PVP/PVA were used with different molecular weights, different

types of solvents with different concentrations, and the degradation was monitored over different periods of time. Each parameter or all together directly influence the results, compromising a correlation between the studies.

This comprehensive study successfully explored the influence of process parameters such as concentration, voltage, nozzle-to-collector distance, flow rate and solvent selections on the properties of electrospun PVP/PVA nanofibers. The CCD analysis confirmed that polymer concentration, solvent type and operating parameters were the main significant variables affecting the PVP/PVA nanofiber surface morphology. The quadratic equations derived from the DOE software were subjected to ANOVA and goodness-of-fit statistics, the summarized results of

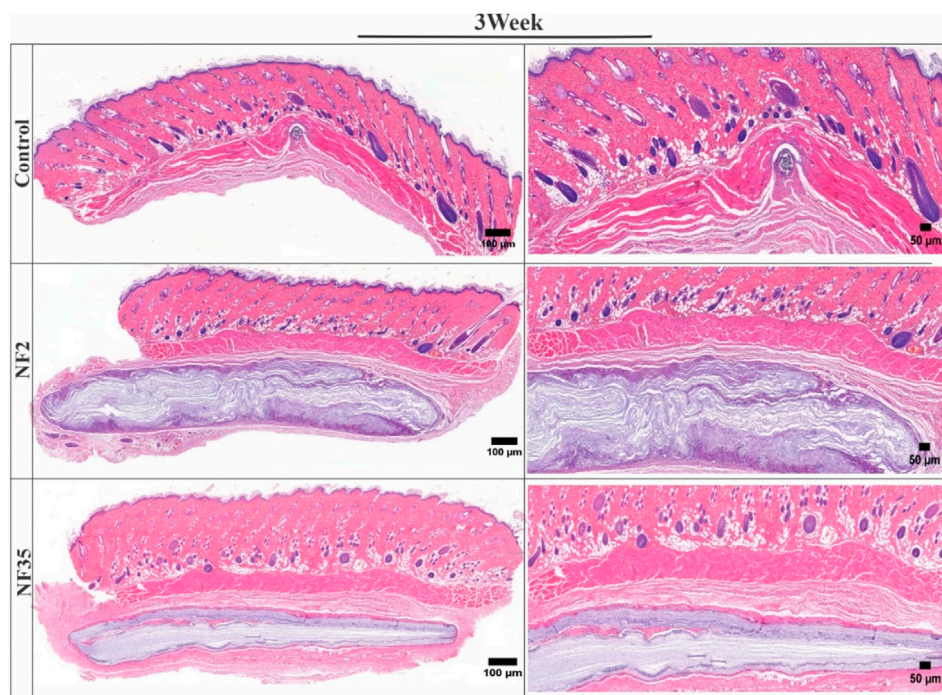


FIGURE 10

H&E-stained images of surrounding tissue of subcutaneous implanted PVP/PVA nanofiber for control, NF2 and NF35. Reconstruction of the full and interior membrane sections after 3 weeks of implantation.

which are presented in (Supplementary Table S1). The reliability of a model is substantiated by examining the p -value, which, across all designs, is consistently below 0.05. This implies that the generated models are both valid and significant. Evaluating the influence of polymer concentration on nanofiber producibility, the reliability of the fitted model is assessed through the R-squared (R^2) value, along with its adjusted counterpart (adjusted R^2). In this context, a model is considered valid if its R^2 value is equal to or greater than 0.60, as affirmed by the model under consideration. The predictive capability of the model for new observations is reflected in the Predictive R-squared (Pred- R^2), while the regular R^2 and adjusted R^2 values reflect the model's alignment with empirical outcomes. The Pred- R^2 and Adj- R^2 values stand at 0.9323 and 0.9817, respectively for nanofiber producibility (Supplementary Table S1).

A preliminary series of experiments were conducted to ascertain the optimal electrospinning parameters for the PVP/PVA solution. Voltages below 8 kV led to the formation of droplets at the tip of the capillary, with no subsequent jet formation. By increasing the applied voltage to the range of 8–10 kV, the size of the hanging droplet decreased until the emergence of the Taylor cone and the stabilization of a jet between 8–10 kV. At voltages exceeding 26 kV, the jet became unstable and exhibited splitting. It was evident that a delicate equilibrium had to be maintained between the rate of solution insertion and removal at the needle's tip.

For the electrospinning process, an appropriate flow rate within the range of 1–2.6 ml/h was determined. Higher flow rates caused an accumulation of excessive solution at the nozzle's tip, resulting in solution dripping and the formation of wet fibers on the collector. Conversely, lower flow rates were insufficient to sustain equilibrium, leading to the disappearance of the Taylor cone and the initiation of jet

formation from within the needle, ultimately interrupting the jet stream. Consequently, flow rates between 1.5–2.5 ml/h and distances of 8–12 cm were chosen as the optimal lower and upper limits, respectively. An array of 18 experiments was systematically conducted, covering the specified ranges for voltage, flow rate, and distance. The outcomes of these experiments were subsequently evaluated using RSM.

These process parameters were subsequently evaluated using ANOVA, with the summarized outcomes presented in Supplementary Tables S2, S3. The obtained p -values, all below 0.05, signify the reliability of all models. Another crucial indicator for assessing the models is the coefficient of determination (R-squared or R^2). This value signifies the proportion of the total variability that the regression model is able to explain. The R^2 values obtained in this study confirmed the models' validity, as they exceeded the threshold of 0.60. Exploration of the comprehensive impact of these parameters on all produced nanofiber batches is elaborated upon in the subsequent discussion.

SEM was utilized for the morphological analysis of nanofibers, encompassing characteristics such as fiber shape, diameter, and surface structure. This inspection exposed the vital role of nanofiber topography in early cellular processes, such as adhesion and proliferation (Teixeira et al., 2004). Upon attaining optimal process parameters, the resultant non-woven fiber mats exhibited a composition of uniform, porous, and randomly aligned fibers devoid of beads.

The obtained nanofibers exhibited a consistent and controlled diameter range of 150–400 nm, indicative of a precise electrospinning process. Mechanical testing revealed notable tensile strength values ranged from 13.81 to 18.3 MPa for PVP/PVA nanofibers, highlighting their structural integrity and suitability for regenerative medicine and drug delivery applications. XRD analysis

underscored the amorphous nature of the PVP/PVA nanofibers, suggesting their potential for enhanced drug loading and release kinetics. The FTIR results provided evidence of consistent and solvent-independent interactions, reinforcing the reliability and reproducibility of the fabrication process. The significant hydrophilicity exhibited by the PVP/PVA nanofibers, as evidenced by contact angle measurements, bodes well for their interactions with biological systems. This property was further corroborated by the extended water retention observed in swelling studies, aligning with the requirements of sustained and controlled drug release applications. Moreover, the 2-week biodegradation timeframe revealed through *in-vitro* degradation studies indicates that these nanofibers possess the necessary characteristics for tissue regeneration. The *in-vivo* evaluation, including subcutaneous rat implantation and histological analysis, underscored the exceptional tissue biocompatibility of the PVP/PVA nanofibers over a month-long period. Furthermore, the *in-vitro* cell lines studies indicated nanofibrous material promoted cell growth/proliferation.

5 Conclusion

PVP/PVA nanofiber scaffold was successfully prepared by using electrospinning method and explored the influence of process parameters such as concentration, voltage, nozzle-to-collector distance, flow rate and solvent selections on the properties of these nanofibers. Through a meticulous investigation using CCD and DOE, the optimal conditions for electrospinning of PVP/PVA nanofibers using ethanol and acetic acid were determined, leading to remarkable insights into their potential application in biomedical field. The physiochemical property of obtained nanofibers exhibited hydrophilic nature with porous structure similar to that found in native ECM. The *in-vivo* biocompatibility of the PVP/PVA nanofibers was assessed by histological analysis of surrounding tissue, which underline the exceptional tissue biocompatibility and appropriate *in-vivo* biodegradation. This outcome holds great promise for their application in tissue engineering, where biocompatibility and biodegradability are paramount.

Data availability statement

The original contributions presented in the study are included in the article/**Supplementary Material**, further inquiries can be directed to the corresponding authors.

Ethics statement

The animal study was approved by the National Engineering Research Centre for Biomaterials, Sichuan University, Chengdu,

Sichuan, 610064, China. The study was conducted in accordance with the local legislation and institutional requirements.

Author contributions

ShA: Data curation, Methodology, Writing–original draft. TL: Formal Analysis, Writing–review and editing. DiA: Data curation, Software, Writing–review and editing. DaA: Funding acquisition, Validation, Writing–review and editing. SaA: Formal Analysis, Resources, Writing–review and editing. WY: Data curation, Validation, Writing–review and editing. ZH: Conceptualization, Resources, Writing–review and editing. PR: Project administration, Supervision, Writing–original draft. QA: Project administration, Supervision, Writing–original draft.

Funding

The author(s) declare financial support was received for the research, authorship, and/or publication of this article. This work was funded by National Key R&D Program of China (2023YFC2410403); Liaoning Provincial Natural Science Foundation of China (No. 2022-MS-194); Shengjing Hospital 345 Talent Project. This research was supported by Researchers Supporting Project number (RSP2023R27), King Saud University, Riyadh, Saudi Arabia.

Conflict of interest

The authors declare that the research was conducted in the absence of any commercial or financial relationships that could be construed as a potential conflict of interest.

Publisher's note

All claims expressed in this article are solely those of the authors and do not necessarily represent those of their affiliated organizations, or those of the publisher, the editors and the reviewers. Any product that may be evaluated in this article, or claim that may be made by its manufacturer, is not guaranteed or endorsed by the publisher.

Supplementary material

The Supplementary Material for this article can be found online at: <https://www.frontiersin.org/articles/10.3389/fbioe.2023.1288539/full#supplementary-material>

References

- Agarwal, Y., Rajinikanth, P., Ranjan, S., Tiwari, U., Balasubramniam, J., Pandey, P., et al. (2021). Curcumin loaded polycaprolactone-/polyvinyl alcohol-silk fibroin based electrospun nanofibrous mat for rapid healing of diabetic wound: an *in-vitro* and *in-vivo* studies. *in-vitro in-vivo Stud.* 176, 376–386. doi:10.1016/j.ijbiomac.2021.02.025
- Amiri, N., Moradi, A., Tabasi, S. a.S., and Movaffagh, J. J. M. R. E. (2018). Modeling and process optimization of electrospinning of chitosan-collagen nanofiber by response surface methodology. *Mater. Res. Express* 5, 045404. doi:10.1088/2053-1591/aaba1d

- Anand, S., Pandey, P., Begum, M. Y., Chidambaram, K., Arya, D. K., Gupta, R. K., et al. (2022a). Electrospun biomimetic multifunctional nanofibers loaded with ferulic acid for enhanced antimicrobial and wound-healing activities in STZ-Induced diabetic rats. *Pharm. (Basel)* 15, 302. doi:10.3390/ph15030302
- Anand, S., Rajinikanth, P., Pandey, P., Deepak, P., Thakur, S., Arya, D. K., et al. (2023). *Biomaterial-based nanofibers for drug delivery applications*, 531–546.
- Anand, S., Rajinikanth, P. S., Arya, D. K., Pandey, P., Gupta, R. K., Sankhwar, R., et al. (2022b). Multifunctional biomimetic nanofibrous scaffold loaded with asiaticoside for rapid diabetic wound healing. *Pharmaceutics* 14, 273. doi:10.3390/pharmaceutics14020273
- Anjum, S., Rahman, F., Pandey, P., Arya, D. K., Alam, M., Rajinikanth, P. S., et al. (2022). Electrospun biomimetic nanofibrous scaffolds: a promising prospect for bone tissue engineering and regenerative medicine. *Int. J. Mol. Sci.* 23, 9206. doi:10.3390/ijms23169206
- Balaji, A., Jaganathan, S. K., Ismail, A. F., and Rajasekar, R. J. I. J. O. N. (2016). Fabrication and hemocompatibility assessment of novel polyurethane-based bio-nanofibrous dressing loaded with honey and Carica papaya extract for the management of burn injuries. *Int. J. Nanomedicine* Vol. 11, 4339–4355. doi:10.2147/ijn.s112265
- Beachley, V., Wen, X. J. M. S., and C, E. (2009). Effect of electrospinning parameters on the nanofiber diameter and length. *Mater Sci. Eng. C Mater Biol. Appl.* 29, 663–668. doi:10.1016/j.msec.2008.10.037
- Carvalho, R. A. D., Maria, T., Moraes, I., Bergo, P. V. A., Kamimura, E. S., Habitante, A., et al. (2009). Study of some physical properties of biodegradable films based on blends of gelatin and poly (vinyl alcohol) using a response-surface methodology. *Mater. Sci. Eng. C* 29, 485–491. doi:10.1016/j.msec.2008.08.030
- Chuangchote, S., Sagawa, T., and Yoshikawa, S. J. J. O. A. P. S. (2009). Electrospinning of poly (vinyl pyrrolidone): effects of solvents on electrospinnability for the fabrication of poly (p-phenylene vinylene) and TiO₂ nanofibers. *J. Appl. Polym. Sci.* 114, 2777–2791. doi:10.1002/app.30637
- Deepak, P., Kumar, P., Arya, D. K., Pandey, P., Kumar, S., Parida, B. P., et al. (2023). c (RGDfK) anchored surface manipulated liposome for tumor-targeted Tyrosine Kinase Inhibitor (TKI) delivery to potentiate liver anticancer activity. *Int. J. Pharm.* 642, 123160. doi:10.1016/j.ijpharm.2023.123160
- Ding, W., Wei, S., Zhu, J., Chen, X., Rutman, D., Guo, Z., et al. (2010). Manipulated electrospun PVA nanofibers with inexpensive salts. *Macromol. Mater. Eng.* 295, 958–965. doi:10.1002/mame.201000188
- Doshi, J., and Reneker, D. H. J. J. O. E. (1995). Electrospinning process and applications of electrospun fibers. *J. Electrostat.* 35, 151–160. doi:10.1016/0304-3886(95)00041-8
- Garg, K., and Bowlin, G. L. J. B. (2011). Electrospinning jets and nanofibrous structures. *Biomicrofluidics* 5, 13403. doi:10.1063/1.3567097
- Ghorai, S. K., Roy, T., Maji, S., Ray, P. G., Sarkar, K., Dutta, A., et al. (2022). A judicious approach of exploiting polyurethane-urea based electrospun nanofibrous scaffold for stimulated bone tissue regeneration through functionally nobbled nanohydroxyapatite. *Chem. Eng. J.* 429, 132179. doi:10.1016/j.cej.2021.132179
- Gu, S., Ren, J., and Vancso, G. J. E. P. J. (2005). Process optimization and empirical modeling for electrospun polyacrylonitrile (PAN) nanofiber precursor of carbon nanofibers. *Eur. Polym. J.* 41, 2559–2568. doi:10.1016/j.eurpolymj.2005.05.008
- Gupta, P. C., Kapoor, A., Pandey, P. J., and Research, M. (2018). *Designing and characterization of econazole nitrate nanostructured lipid carriers gel for topical delivery*, 5, 559–567. doi:10.13140/RG.2.2.20751.07842
- Jacobs, V., Patanaik, A., D Anandjiwala, R., and Maaza, M. J. C. N. (2011). Optimization of electrospinning parameters for chitosan nanofibers. *Curr. Nanosci.* 7, 396–401. doi:10.2174/157341311795542570
- Li, W., Lin, M., Wang, C., Lu, Y., Sui, Y., Ni, X., et al. (2023). *In vitro* enzymatic degradation of the PTMC/cross-linked PEGDA blends. *Front. Bioeng. Biotechnol.* 11, 1253221. doi:10.3389/fbioe.2023.1253221
- Maheshwari, S. U., Govindan, K., Raja, M., Raja, A., Pravin, M., and Kumar, S. V. J. B.-M. M. E. (2017). Preliminary studies of PVA/PVP blends incorporated with HAp and β -TCP bone ceramic as template for hard tissue engineering. *Biomed. Mater. Eng.* 28, 401–415. doi:10.3233/bme-171682
- Mao, X., Li, T., Cheng, J., Tao, M., Li, Z., Ma, Y., et al. (2023). Nerve ECM and PLA-PCL based electrospun bilayer nerve conduit for nerve regeneration. *Front. Bioeng. Biotechnol.* 11, 1103435. doi:10.3389/fbioe.2023.1103435
- Miri, M. A., Movaffagh, J., Najafi, M. B. H., Najafi, M. N., Ghorani, B., Koocheki, A., et al. (2016). Optimization of electrospinning process of zein using central composite design. *Fibers Polym.* 17, 769–777. doi:10.1007/s12221-016-6064-0
- Mohammed, R., Jawad, H., and Al-Zubiedy, A. (2021). Blended PVA/PVP electro spun nanofibers for coating application. *J. Phys. Conf. Ser.* 2114, 012031. doi:10.1088/1742-6596/2114/1/012031
- Nasouri, K., Shoushtari, A. M., and Mojtahedi, M. R. M. J. P. S. S. A. (2015). Effects of polymer/solvent systems on electrospun polyvinylpyrrolidone nanofiber morphology and diameter. *Polym. Sci. Ser. A* 57, 747–755. doi:10.1134/s0965545x15060164
- Pandey, G., Pandey, P., Arya, D. K., Kanaujiya, S., Kapoor, D. D., Gupta, R. K., et al. (2023). Multilayered nanofibrous scaffold of Polyvinyl alcohol/gelatin/poly (lactic-co-glycolic acid) enriched with hemostatic/antibacterial agents for rapid acute hemostatic wound healing. *Int. J. Pharm. X.* 638, 122918. doi:10.1016/j.ijpharm.2023.122918
- Pandey, P., Arya, D. K., Ramar, M. K., Chidambaram, K., and Rajinikanth, P. J. D. D. T. (2022). Engineered nanomaterials as an effective tool for HER2+ breast cancer therapy. *Drug Discov. Today* 27, 2526–2540. doi:10.1016/j.drudis.2022.06.007
- Pezeshki-Modaress, M., Mirzadeh, H., Zandi, M. J. M. S., and C, E. (2015). Gelatin–GAG electrospun nanofibrous scaffold for skin tissue engineering: fabrication and modeling of process parameters. *Mater Sci. Eng. C Mater Biol. Appl.* 48, 704–712. doi:10.1016/j.msec.2014.12.023
- Qiu, E., and Liu, F. (2023). PLGA-based drug delivery systems in treating bone tumors. *Front. Bioeng. Biotechnol.* 11, 1199343. doi:10.3389/fbioe.2023.1199343
- Quan, L., Xin, Y., Wu, X., and Ao, Q. J. P. (2022). Mechanism of self-healing hydrogels and application in tissue engineering. *Polym. (Basel)* 14, 2184. doi:10.3390/polym14112184
- Reneker, D. H., and Chun, I. J. N. (1996). Nanometre diameter fibres of polymer, produced by electrospinning. *Prod. by electrospinning* 7, 216–223. doi:10.1088/0957-4484/7/3/009
- Shimko, D. A., Shimko, V. F., Sander, E. A., Dickson, K. F., and Nauman, E. (2005). Effect of porosity on the fluid flow characteristics and mechanical properties of tantalum scaffolds. *J. Biomed. Mater. Res. B Appl. Biomater.* 73, 315–324. doi:10.1002/jbm.b.30229
- Singh, P., Pandey, P., Arya, D. K., Anjum, M. M., Poonguzhali, S., Kumar, A., et al. (2023). Biomimicking dual drug eluting twisted electrospun nanofiber yarns for post-operative wound healing. *Biomed. Mater.* 18, 035006. doi:10.1088/1748-605x/acc4a1
- Teixeira, A. L., Nealey, P. F., and Murphy, C. J. (2004). Responses of human keratocytes to micro- and nanostructured substrates. *J. Biomed. Mater. Res. A* 71, 369–376. doi:10.1002/jbm.a.30089
- Thakur, S., Anjum, M. M., Jaiswal, S., Kumar, A., Deepak, P., Anand, S., et al. (2023). Novel synergistic approach: tazarotene-calcipotriol-loaded-PVA/PVP-nanofibers incorporated in hydrogel film for management and treatment of psoriasis. *Mol. Pharm.* 20, 997–1014. doi:10.1021/acs.molpharmaceut.2c00713
- Xin, Y., Quan, L., Zhang, H., and Ao, Q. (2023). Emerging polymer-based nanosystems strategies in delivery of antifungal drugs. *Pharmaceutics* 15 (7), 1866. doi:10.3390/pharmaceutics15071866
- Yadav, S., Arya, D. K., Pandey, P., Anand, S., Gautam, A. K., Ranjan, S., et al. (2022). ECM mimicking biodegradable nanofibrous scaffold enriched with curcumin/ZnO to accelerate diabetic wound healing via multifunctional bioactivity. *Int. J. Nanomedicine*, 6843–6859. doi:10.2147/IJN.S388264
- Yang, Q., Li, Z., Hong, Y., Zhao, Y., Qiu, S., Wang, C., et al. (2004). Influence of solvents on the formation of ultrathin uniform poly (vinyl pyrrolidone) nanofibers with electrospinning. *J. Polym. Sci. B. Polym. Phys.* 42, 3721–3726. doi:10.1002/polb.20222
- Yu, H., Liu, H., Shen, Y., and Ao, Q. (2023). Synthetic biodegradable polymer materials in the repair of tumor-associated bone defects. *Front. Bioeng. Biotechnol.* 11, 1096525. doi:10.3389/fbioe.2023.1096525
- Zhang, C., Yuan, X., Wu, L., Han, Y., and Sheng, J. J. E. P. J. (2005). Study on morphology of electrospun poly (vinyl alcohol) mats. *Eur. Polym. J.* 41, 423–432. doi:10.1016/j.eurpolymj.2004.10.027
- Zhu, X., Cui, W., Li, X., and Jin, Y. J. B. (2008). Electrospun fibrous mats with high porosity as potential scaffolds for skin tissue engineering. *Biomacromolecules* 9, 1795–1801. doi:10.1021/bm800476u



OPEN ACCESS

EDITED BY

Junjie Li,
Kyushu University, Japan

REVIEWED BY

Panyue Wen,
University of Science and Technology of
China, China
Jianxun Ding,
Chinese Academy of Sciences (CAS),
China
Yao Chenchi,
Anhui Normal University, China

*CORRESPONDENCE

Qianshi Zhang,
✉ zhangqianshi1987@qq.com
Shuangyi Ren,
✉ renshuangyid@163.com
Liqun Yang,
✉ yanglq@lnszjk.com.cn

[†]These authors have contributed equally
to this work and share first authorship

RECEIVED 16 September 2023

ACCEPTED 16 October 2023

PUBLISHED 01 November 2023

CITATION

Wang Z, Xiao M, Guo F, Yan Y, Tian H,
Zhang Q, Ren S and Yang L (2023),
Biodegradable polyester-based nano
drug delivery system in cancer
chemotherapy: a review of recent
progress (2021–2023).
Front. Bioeng. Biotechnol. 11:1295323.
doi: 10.3389/fbioe.2023.1295323

COPYRIGHT

© 2023 Wang, Xiao, Guo, Yan, Tian,
Zhang, Ren and Yang. This is an open-
access article distributed under the terms
of the [Creative Commons Attribution
License \(CC BY\)](#). The use, distribution or
reproduction in other forums is
permitted, provided the original author(s)
and the copyright owner(s) are credited
and that the original publication in this
journal is cited, in accordance with
accepted academic practice. No use,
distribution or reproduction is permitted
which does not comply with these terms.

Biodegradable polyester-based nano drug delivery system in cancer chemotherapy: a review of recent progress (2021–2023)

Zongheng Wang^{1,2†}, Miaomiao Xiao^{2,3†}, Fangliang Guo^{1†}, Yue Yan⁴,
Hong Tian⁵, Qianshi Zhang^{1*}, Shuangyi Ren^{1*} and Liqun Yang^{6,2*}

¹Department of Gastrointestinal Surgery, The Second Affiliated Hospital of Dalian Medical University, Dalian, China, ²Liaoning Research Institute of Family Planning (The Reproductive Hospital of China Medical University), Shenyang, China, ³College of Kinesiology, Shenyang Sport University, Shenyang, China, ⁴Department of Emergency, The Second Affiliated Hospital of Dalian Medical University, Dalian, China, ⁵Department of Oncology, The 4th People's Hospital of Shenyang, China Medical University, Shenyang, China, ⁶Research Center for Biomedical Materials, Shengjing Hospital of China Medical University, Shenyang, China

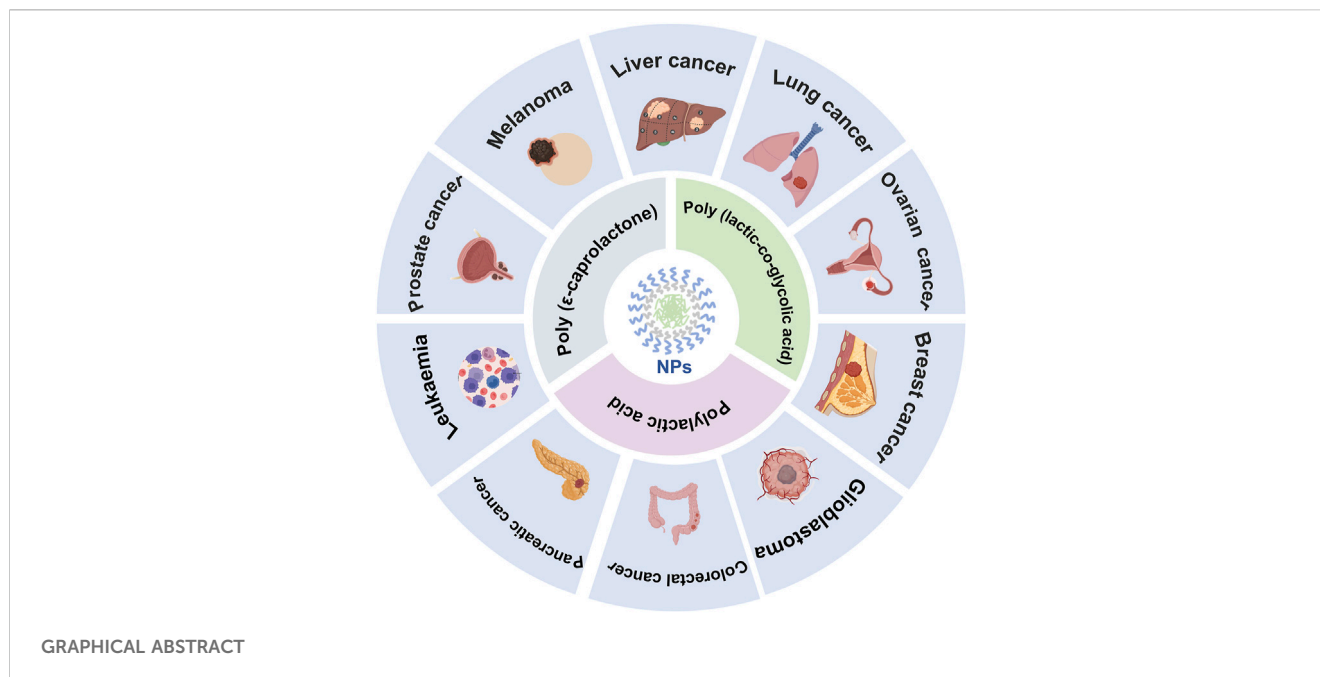
Cancer presents a formidable threat to human health, with the majority of cases currently lacking a complete cure. Frequently, chemotherapy drugs are required to impede its progression. However, these drugs frequently suffer from drawbacks such as poor selectivity, limited water solubility, low bioavailability, and a propensity for causing organ toxicity. Consequently, a concerted effort has been made to seek improved drug delivery systems. Nano-drug delivery systems based on biodegradable polyesters have emerged as a subject of widespread interest in this pursuit. Extensive research has demonstrated their potential for offering high bioavailability, effective encapsulation, controlled release, and minimal toxicity. Notably, poly (ϵ -caprolactone) (PCL), poly (lactic-co-glycolic acid) (PLGA), and polylactic acid (PLA) have gained prominence as the most widely utilized options as carriers of the nano drug delivery system. This paper comprehensively reviews recent research on these materials as nano-carriers for delivering chemotherapeutic drugs, summarizing their latest advancements, acknowledging their limitations, and forecasting future research directions.

KEYWORDS

biodegradable polyester, drug delivery system, nanoparticles, cancer, chemotherapy

1 Introduction

Cancer is the second most prominent contributor to global mortality, trailing only behind cardiovascular diseases (Mattiuzzi and Lippi, 2019). Figure 1 illustrates data from the World Health Organization, revealing that breast cancer claimed the top spot for new cancer cases in 2020, closely followed by lung cancer (W.H. O, 2023). Based on statistics provided by the American Cancer Society, it was projected that the United States would witness 1,958,310 new cancer diagnoses and 609,820 cancer-related fatalities in 2023 (Siegel et al., 2023). Undoubtedly, cancer exerts a substantial financial burden on healthcare systems worldwide, posing significant challenges to their fiscal resources and long-term viability (Qiu et al., 2021).



Current treatment modalities primarily encompass surgical procedures, chemotherapy, and immunotherapy. However, certain advanced-stage patients may not qualify for surgical interventions, and even post-surgery, some may encounter relapses (Almeida et al., 2019). Immunotherapy, while available, remains accessible to only a limited fraction of patients and carries severe side effects, including autoimmune reactions and non-specific inflammation (Riley et al., 2019). Chemotherapy, administered before and after tumor removal, serves the dual purpose of facilitating surgical procedures and preventing the resurgence of residual cancer cells. It enjoys widespread utilization and is indispensable in cancer treatment (Hellmann et al., 2016). Prominent chemotherapy agents such as 5-fluorouracil (5-FU), paclitaxel (PTX), doxorubicin (DOX), and cis-diamminedichloro-platinum (CDDP) find extensive clinical application and yield favorable treatment outcomes (Roth and Ajani, 2003). Nevertheless, these chemotherapy drugs have limitations, including

restricted bioavailability, suboptimal tissue penetration, the absence of specific targeting ligands, and the necessity for frequent administration (Kozovska et al., 2014; Chou et al., 2020). Furthermore, although some patients exhibit an initial positive response to treatment, they may subsequently develop resistance to chemotherapy, culminating in tumor recurrence (Biller and Schrag, 2021; Xiao et al., 2021; Yoon et al., 2021).

Hence, the quest for an improved drug delivery system has piqued the interest of scholars, with nanoparticles based on biodegradable polyesters emerging as a focal point of attention (Cheng and Pun, 2015). Biodegradable polyesters are polymeric materials that boast environmentally friendly attributes (Gross and Kalra, 2002). Additionally, they exhibit commendable biocompatibility and can decompose into small molecule byproducts within the human physiological milieu. Several have secured approval from the U.S. Food and Drug Administration for diverse clinical applications in drug delivery systems, including PCL (Malikmammadov et al., 2018), PLA (Williams, 2007; Pandey et al., 2015) and PLGA (Sonam Dongsar et al., 2023), among others. Their structures are outlined in Table 1 (Washington et al., 2017).

On the one hand, these nanoparticles can traverse the endothelial barriers of the spleen and liver; on the other hand, they leverage the enhanced permeability and retention (EPR) effect to passively accumulate at tumor sites (Zhang et al., 2014; Asadi et al., 2017). They possess robust drug-loading capabilities, facilitate optimal intracellular uptake, and harness the enhanced permeability and retention phenomena (Bae et al., 2011; Yao et al., 2020). In principle, nanomaterials offer a hydrophobic core for encapsulating drugs, enhancing their stability in the bloodstream (Gupta et al., 2021). Moreover, they can be customized by incorporating various functional groups to modulate their functions within the body (Esfandiyari-Manesh et al., 2016).

To enhance the active targeting of the delivery system, researchers usually employed cancer cell-specific ligands as targets. These ligands enable easy entry into cancer cells through

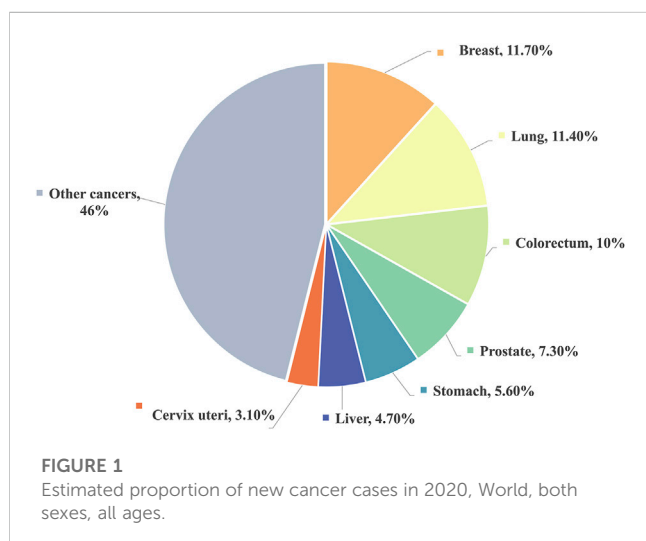
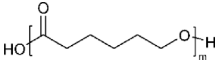
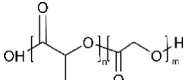
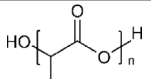


TABLE 1 The structures of the polymers.

| Polymer | Structure | T _g (°C) | T _m (°C) |
|---------|---|---------------------|---------------------|
| PCL |  | -60 | 60 |
| PLGA |  | 35–60 | 120–200 |
| PLA |  | 60–65 | 150–160 |

receptor-mediated transcytosis, circumventing sole reliance on the EPR effect. Such ligands encompass peptides, polysaccharides, antibodies, and more (Sun et al., 2018).

This review presents an overview of the researches conducted over the past 3 years concerning biodegradable polyesters for the delivery of cancer chemotherapeutic drugs. Our focus centers on the extensively studied PCL, PLGA, and PLA, summarizing the latest advancements, recognizing their limitations, and shedding light on future research trends.

2 Biodegradable polyester-based drug delivery systems

2.1 Poly (ε-caprolactone) (PCL)

PCL is a biodegradable and biocompatible semi-crystalline linear aliphatic polyester (Khan et al., 2017). It is non-toxic, biodegradable, and biocompatible attributes, which is used in a wide range of bio-applications (Bhadran et al., 2023; Murab et al., 2023). The details about the applications of PCL in cancer chemotherapy are shown in Table 2.

To harness the advantages of PCL in addressing the short half-life and limited bioavailability associated with intravenous drug administration, Jan et al. (2021) employed a nanoprecipitation method to create PCL nanoparticles loaded with arabinosylcytosine. They investigated the *in vitro* anti-cancer effects of these nanoparticles on KG-1 leukemia cells. The *in vitro* release experiments revealed an initial burst release followed by sustained release over 48 h. Additionally, cytotoxicity experiments demonstrated that the IC₅₀ value of PCL nanoparticles was nearly two orders of magnitude lower than that of the pure drug injection. This underscored the effectiveness of arabinosylcytosine-loaded PCL nanoparticles as a drug carrier, effectively mitigating dose-related toxicity while offering a controlled release mechanism.

In contrast to free drugs, liposomes exhibit improved pharmacokinetics and enhanced biocompatibility. They can accommodate hydrophilic and lipophilic drugs and can be customized as needed. However, liposomes face limitations such as low drug loading, rapid release, leakage, and instability during storage. To address these issues, Khan et al. (2021) employed a nanoprecipitation technique to create 5-fluorouracil-loaded lipid-

polymer hybrid nanoparticles (LPHNPs). The IC₅₀ values of free 5-FU and 5-FU LPHNPs were 60.78 μg/mL and 47.34 μg/mL for HeLa cells and 58.35 μg/mL and 43.33 μg/mL for MCF-7 cells, respectively. The reduced IC₅₀ values of LPHNPs suggest they are more effective at killing cancer cells than free drugs. *In vitro* release studies showed an initial burst release of 40% in the first 9 h, followed by continuous release over 72 h.

Furthermore, Kimiya Hasanbegloo and colleagues conducted similar research. They loaded paclitaxel into liposomes and embedded them within PCL/chitosan nanofibers to enhance sustained paclitaxel delivery. Drug release experiments indicated a sustained release period of up to 30 days, demonstrating the improved delivery capabilities of the nanofibers (Hasanbegloo et al., 2023).

However, nanoparticles composed solely of single-component polymers have limitations, such as poor water solubility and susceptibility to clearance by the reticuloendothelial system. Amphiphilic block copolymers have garnered significant attention to enhance nanoparticle properties and achieve long-term therapeutic effects (Zhan et al., 2022). PEG as a hydrophilic moiety has been widely adopted, and nano-carriers based on the PEG-PCL architecture have become an essential strategy for increasing drug accumulation at specific target sites while minimizing non-specific drug uptake (Grossen et al., 2017). In line with this concept, Hongdan She and colleagues utilized ring-opening polymerization to synthesize methoxy polyethylene glycol-block-poly(ε-caprolactone) (mPEG-b-PCL) copolymers. Subsequently, they derived the polymer mPEG-b-PCL-DOX through orchestrated esterification and amidation reactions. *In vitro* experiments demonstrated that the IC₅₀ of free DOX and mPEG-b-PCL-DOX NPs on HCT116 cells were 3.85 ± 0.16 μg/mL and 2.65 ± 0.29 μg/mL, respectively, highlighting the superior anti-tumor activity of the nanoparticles (Shen et al., 2021).

In contrast to monotherapy, combination therapy harnesses the synergistic effects of multiple drugs to achieve superior anti-tumor effects. Akanksha Behl and colleagues developed a multifunctional nano-carrier delivery system, PEG-PCL, capable of simultaneously delivering the chemotherapeutic drug Gemcitabine (GEM) and a MUC1 inhibitor. MUC1 is a transmembrane MUC found in human breast tumors due to its high overexpression. The MUC1 inhibitor disrupts the nucleus of human breast cancer cells, disrupts redox balance, and triggers DNA damage response. *In vivo* experiments, the average tumor volumes for Gem NPs, MUC1 inhibitor NPs, Gem-MUC1 inhibitor NPs, blank NPs, 5-FU, and sterile saline were approximately 828.75, 747.07, 473.75, 1055.14, 373.92, and 1119 mm³, respectively. Additionally, the NPs demonstrated strong tumor-targeting capabilities in the acidic tumor microenvironment, enhancing the efficacy of anti-cancer drugs both *in vitro* and *in vivo* (Behl et al., 2022). Furthermore, Jin et al. (2023) synthesized mPEG-b-PC, simultaneously loaded with PTX and sorafenib, achieving significant results with a tumor growth inhibition rate of up to 90.44%.

In addition to using PEG, Jiajia Xiang, and colleagues discovered a versatile poly(tertiary amine oxide) (PTAO) as a superior alternative to PEG. PTAO-PCL/DOX exhibited enhanced tumor enrichment compared to PEG-PCL/DOX. Specifically, OPDMA-PCL/DOX and OPDEA-PCL/DOX micelles displayed DOX accumulation in tumors 2.7 and 2.3 times higher than PEG-PCL/

TABLE 2 PCL-based nano drug delivery systems investigated for treating cancers.

| Author | Year | Nanoparticles system | Size (nm) | Encapsulation efficiency (%) | Drug loading (%) | IC50 | The blood circulation time | Type of tumor | Chemotherapy drug | Reference |
|--------------------------|------|--------------------------------------|---------------------------|------------------------------|------------------|--|----------------------------|-----------------------------|-------------------|---------------------------|
| Nasrullah Jan et al | 2021 | Cytarabine-PCL | 120.5 ± 1.18–341.5 ± 3.02 | 41.31 ± 0.49–62.28 ± 0.39% | 6–20 | KG-1 cells, 48 h, 8.80 ± 0.48 µg/mL | — | Leukaemia and breast cancer | Cytarabine | Jan et al. (2021) |
| Safiullah Khan et al | 2021 | 5-FU LPHNPs | 174 ± 4–267 ± 2.65 | 92.87 ± 0.59–94.13 ± 0.77 | 6.25–12.5 | HeLa cells, 47.34 µg/mL | — | Breast cancer | 5-FU | Khan et al. (2021) |
| Hongdan Shen et al | 2021 | mPEG-b-PCL-DOX | 300 | — | 4 | HCT116 cells, 2.65 ± 0.29 µg/mL | — | Colorectal cancer | DOX | Shen et al. (2021) |
| Akanksha Behl et al | 2022 | PEG-PCL | 128.66 ± 23 | 85.4 | — | MCF-7 cells, 22 nM | — | Breast cancer | Gemcitabine | Behl et al. (2022) |
| Wufa Fan et al | 2022 | OPDEA-PCL | 45.4 | — | 7.3 | NCI-H520 cells, 48 h, 2.52/0.62 µg/mL (CDDP/PTX) | >24 h | Liver and lung cancer | CDDP/PTX | Fan et al. (2022) |
| De-Chao Yang et al | 2022 | mPEG-b-PCL | — | — | 4 | HepG2 cells, 1.89 nM | — | Liver and lung cancer | Camptothecin | Yang et al. (2022) |
| Jiajia Xiang et al | 2022 | OPDMA-PCL/OPDEA-PCL | 29/25 | 82.3/80.8 | 15.7/14.9 | HeLa cells, 1.15/1.38 µg/mL | >8 h | Breast cancer | DOX | Xiang et al. (2022) |
| Ziting Zhang et al | 2022 | RSV-NPs@RBCm | 160.91 ± 0.63 | 45.25 | 7.54 | HCT116 cells 23.65 ± 3.21 µg/mL | >48 h | Colorectal cancer | Resveratrol | Zhang et al. (2022a) |
| Qianqian Zhang et al | 2022 | Spm-PEG-PCL-DOX | 69.3 ± 3.4 | 110.91 ± 9.68 | 13.9 ± 0.6 | HCT116 cells 35.42 ± 1.16 µg/mL | — | Lung cancer | DOX | Zhang et al. (2022b) |
| Kimiya Hasanbegloo et al | 2023 | chitosan (core)/PCL-chitosan (shell) | 135 ± 45 | 72.1 ± 2.8 | — | — | — | Breast cancer | PTX | Hasanbegloo et al. (2023) |
| Chae Eun Jin et al | 2023 | mPEG-b-PCL | 33.1 ± 2.15 | 94.4 ± 4.14 | 2.61 ± 0.26 | HeyA8 cells 75.8 nM | 4 h | Ovarian cancer | PTX | Jin et al. (2023) |
| Yihong He et al | 2023 | ARV-DOX/cRGD-PEG-PCL | 59.31 | 94 | 2.5 | — | — | Colorectal cancer | DOX | He et al. (2023) |

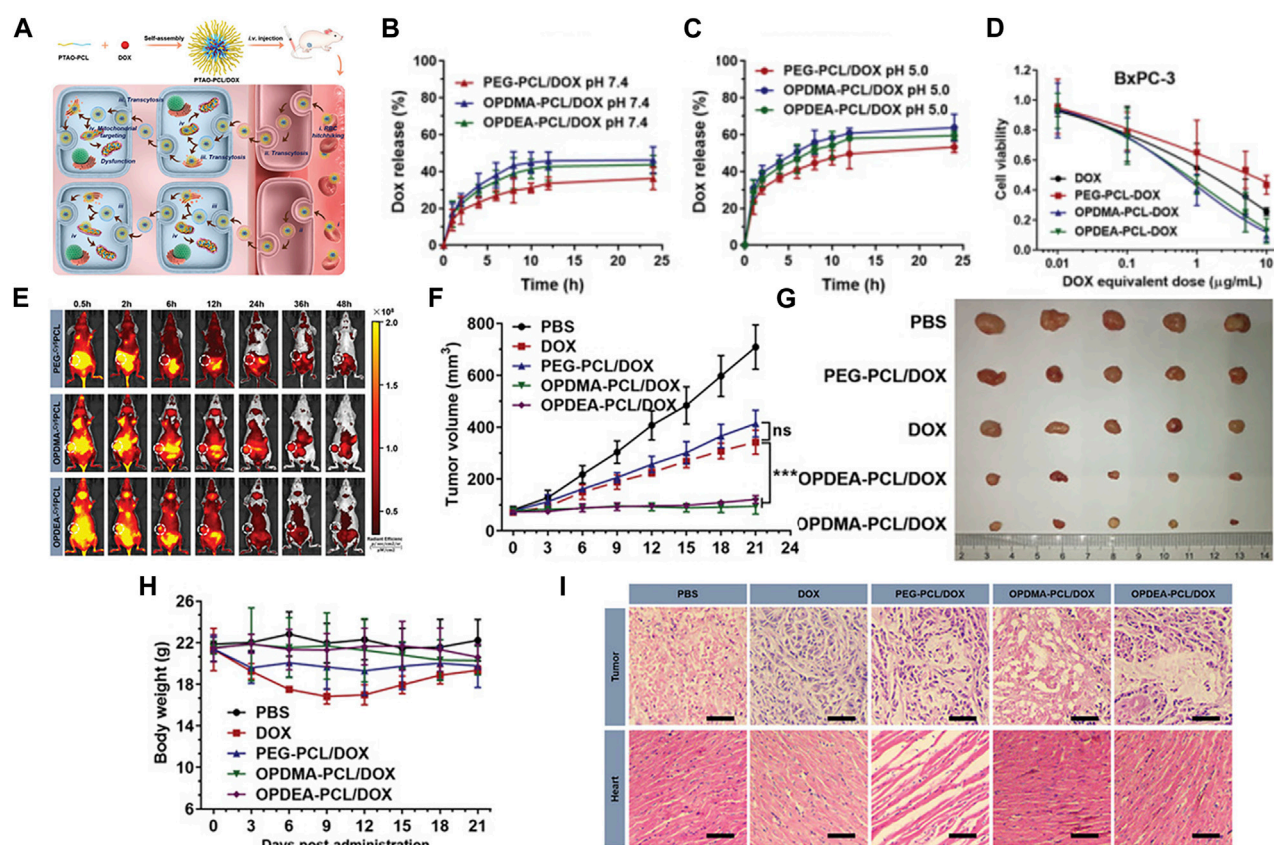


FIGURE 2

(A) Schematic illustration of PTAO-PCL micelles for cancer drug delivery. (a) The encapsulation of DOX into PTAO micelles self-assembled from PTAO-PCL block copolymers. (b) After intravenous injection, PTAO micelles i) circulate long in blood via red blood cell (RBC) hitchhiking and ii) attach on cell membranes to trigger transcytosis-mediated extravasation and iii) subsequent active tumor penetration. Inside tumor cells, a portion of PTAO micelles iv) target mitochondria and induce cell death. (B) The drug release profiles of the DOX-loaded micelles at pH 7.4. (C) The drug release profiles of the DOX-loaded micelles at pH 5.0. (D) The *in vitro* cytotoxicity of DOX-loaded micelles against adherent BxPC-3 and MCF-7/ADR cells determined by the MTT assay (48 h treatment). (E) *In vivo* real-time imaging of tumor-bearing mice after a single intravenous injection of PEG-Cy5PCL, OPDMA-Cy5PCL, or OPDEA-Cy5PCL (Cy5-eq. dose of 0.5 mg kg⁻¹). The tumor regions were circled in white. (F) Antitumor activities of DOX-loaded PTAO-PCL micelles against orthotopic MCF-7/ADR tumors. Tumor growth curves of the mice. (G) Photographs of the tumors resected at the end of the experiment. (H) Body weight variation of the mice during the experiment. (I) Representative histological features of the tumors and hearts. The 10-µm-thick tissue sections were stained with hematoxylin-eosin and observed using light microscopy. Scale bar: 50 µm. Reproduced with permission from ref Xiang et al. (2022). CC BY 4.0. Copyright 2022 The Authors.

DOX. This phenomenon could be attributed to PTAO-PCL micelles inducing extracellular transport, allowing PTAO-PCL/DOX to bypass the enhanced permeability and retention effect. Regarding tumor penetration, it was over 27 times more potent than PEG-PCL micelles. Furthermore, DOX-loaded PTAO micelles could target mitochondria, leading to mitochondrial dysfunction (Xiang et al., 2022) (See Figure 2 for further details).

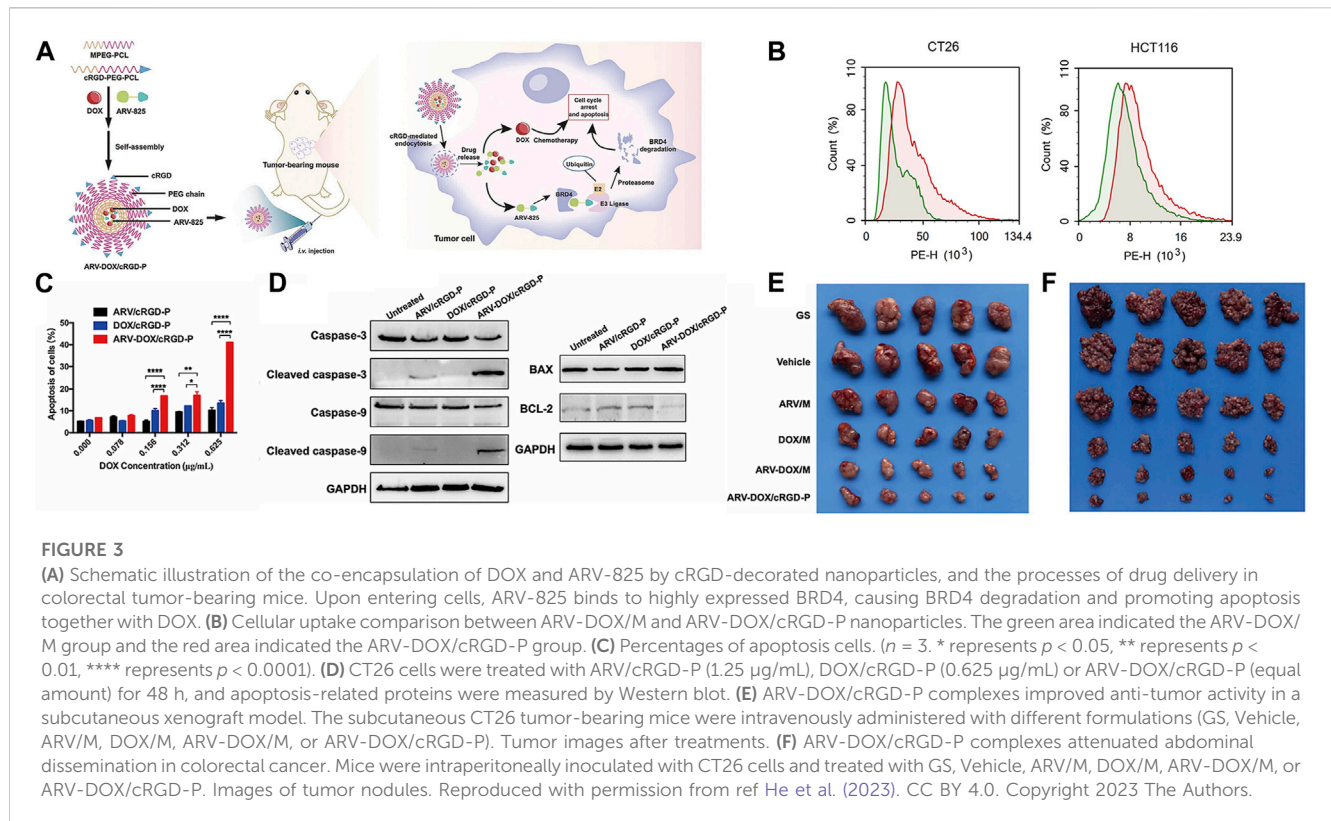
Mitochondria produced ATP for ATP-binding cassette transporters like P-glycoprotein. They may possess mutations in mitochondrial DNA that contribute to multidrug resistance (MDR). So disrupting ATP synthesis and causing DNA damage within mitochondria could be an approach to surmount the multidrug resistance in tumor cells (Choi and Yu, 2014).

Furthermore, Zhang et al. (2022a) ingeniously enveloped PCL-PEG nanoparticles carrying respiratory syncytial virus (RSV) within red blood cell membranes to evade potential interactions with the immune system. This inventive fusion gave rise to a biomimetic nano-carrier named RSV-NPs@RBCm. Notably, this design

exhibited remarkable potential for evading macrophage phagocytosis and demonstrated an extended circulation effect.

Most cancer cells highly express polyamine transport systems, considered promising tumor targeting sites. These sites can significantly enhance cellular uptake efficiency and boost cytotoxicity against cancer cells. Therefore, Zhang et al. (2022b) employed spermine (Spm) to modify PEG-PCL micelles, imparting them with strong targeting properties for carrying DOX. *In vivo*, experimental results demonstrated that micelles attached to the surface of PLGA microspheres greatly improved drug accumulation in the lungs and tumors. The combination of passive and active targeting mechanisms significantly enhanced the efficiency of DOX targeting.

Previous studies have revealed significant expression of αvβ3 integrins in tumor tissues, and cyclo (Arg-Gly-Asp-D-Phe-Lys) (cRGD) has been shown to specifically bind to its receptors (Chou, 2010; Fang et al., 2017). Leveraging this knowledge, Yihong He and colleagues developed cRGD-PEG-PCL nanoparticles loaded with the chemotherapy drug DOX and the bromodomain-



containing protein 4 (BRD4) degrader ARV-825. As depicted in Figure 3, cell uptake studies revealed that the red fluorescence intensity of the ARV-DOX/cRGD-P group was significantly higher than that of the ARV-DOX/M group, indicating superior targeting capabilities of the cRGD-P vector. Cell apoptosis experiments demonstrated that ARV-DOX/cRGD-P promoted cell apoptosis by activating the caspase signaling pathway and the BCL-11/BAX pathway in colorectal cancer cells, with a much more pronounced effect than other treatment groups. In subcutaneous tumor and peritoneal dissemination models, cRGD-PEG-PCL exhibited the most potent therapeutic effect. This underlined the excellent targeting and anti-cancer efficacy of this nanoparticle from various angles (He et al., 2023) (Refer to Figure 3 for further details).

2.2 Poly (lactic-co-glycolic acid) (PLGA)

PLGA stands out as one of the most successful advancements in drug delivery systems, which is known for its biocompatibility and flexibility to control particle polymer systems by changing chemical structure and molecular weight (Molavi et al., 2020). Its capacity to undergo hydrolysis within the body, ultimately breaking down into biodegradable monomers such as lactic acid and glycolic acid. This property not only ensures exceptional biocompatibility but also minimizes systemic toxicity. Consequently, PLGA is highly suitable for use as a carrier in drug delivery and as a crucial material in various biomedical applications (Kumari et al., 2010; Zhu et al., 2018). The details about the applications of PLGA in cancer chemotherapy are shown in Table 3.

Due to its excellent biocompatibility, many researchers have considered utilizing PLGA as a viable option for drug delivery (Shive et al., 1997). Reem M. Gahtani et al. prepared PLGA nanoparticles loaded with 5-FU. *In vitro* experiments revealed a biphasic release pattern of 5-FU from these nanoparticles, with an initial rapid release followed by a slow and steady release. When cells were treated with a 5-FU solution, cell viability decreased by 70%, whereas 5-FU-PLGA-NPs containing the same drug dose induced nearly 100% cell toxicity. This suggested that the delivery system may significantly enhance intracellular drug accumulation and improve therapeutic efficacy (Gahtani et al., 2023).

Nanoparticles possess a drawback in that the reticuloendothelial system recognizes them as foreign particles and are consequently partially cleared by immune cells. However, this limitation can be effectively addressed by employing biomimetic nanoparticles cloaked with natural cell membranes, which remarkably enhance the targeted delivery of drugs to specific cells (Li R. et al., 2019). In light of this, Hongqiao Cai et al. devised an innovative strategy involving macrophage membrane-coated nanoparticles (MPGNPs) that were loaded with gemcitabine and encapsulated within PLGA nanoparticles. This approach aimed to mitigate drug toxicity while simultaneously enhancing drug accumulation within tumors (Cai et al., 2021). Furthermore, building upon the concept of cell membrane coating, Yue Li et al. introduced the incorporation of tumor cell membrane (CCM) onto PLGA nanoparticles to achieve immune evasion. Comparative investigations between PLGANPs and PTX injection disclosed that CCMNPs showcased 1.3- and 2.0-fold tumor suppression rates in xenograft nude mice models, respectively (Li et al., 2023) (Refer to Figure 4 for further details).

TABLE 3 PLGA-based nanoparticle delivery systems investigated for treating cancers.

| Author | Year | Nanoparticles system | Encapsulation efficiency (%) | Size (nm) | Drug loading (%) | IC50 | Type of tumor | Chemotherapy drug | Reference |
|---------------------------|------|----------------------|------------------------------|----------------|------------------|------------------------------|------------------------------|-------------------|--------------------------|
| Hongqiao Cai et al | 2021 | MPGNPs | 74.1 | 192 | 20 | PANC-1 cells, 16.1 nM | Pancreatic cancer | Gemcitabine | Cai et al. (2021) |
| Xiaozheng Zhao et al | 2021 | NS-TAX@Lipo-VAC | — | 200 | 5 | — | Pancreatic cancer | TAX | Zhao et al. (2021) |
| Ru Zhang et al | 2022 | DOX/FA-HASS-PLGA | 83.25 ± 0.45 | 307.47 ± 1.50 | 21.1 ± 0.1 | — | Breast cancer | DOX | Zhang et al. (2022c) |
| Meng Wang et al | 2022 | PG@KMCM | — | 117.8 ± 54.5 | 82.8 | — | Pancreatic cancer | Gemcitabine | Wang et al. (2022) |
| Razan B. Al-Humaidi et al | 2022 | paclitaxel-PLGA-NPs | 59 | 85.54 ± 0.6427 | 41.41 | MCF-7 cells, 39.41 ± 1.33 nM | Breast cancer | PTX | Al-Humaidi et al. (2022) |
| Reem M. Gahtani et al | 2023 | 5-FU-PLGA | ≥90 | 200 | 1 | — | Lung cancer | 5-FU | Gahtani et al. (2023) |
| Fakhrossadat Emami et al | 2023 | DRT-DTX-PLGA | 71.9 ± 1.2 | 124.2 ± 1.1 | 2.5 ± 0.8 | — | Glioblastoma and lung cancer | DTX | Emami et al. (2023) |
| Yue Li et al | 2023 | CCMNPs | 74.42 | 94.13 | 4.16 | NCI-H460 cells, 3.02 µg/mL | Lung cancer | PTX | Li et al. (2023) |
| Huai-An Chen et al | 2023 | HA/PMNPc | — | 300 | 18 | U87 cells, 0.297 µg/mL | Glioblastoma | CDDP | Chen et al. (2023) |
| Dasharath Chaudhari et al | 2023 | PTX- ADN-PEG-PLGA | 79.26 ± 2.52 | 135 ± 12 | 7.5 | 4T1 cells, 3.16 µg/mL | Breast cancer | PTX | Chaudhari et al. (2023) |

Sometimes, the EPR effect is highly variable, and the frequent occurrence of low EPR, especially in clinical tumors, compromises the delivery of EPR-dependent nanoparticles (Tietjen and Saltzman, 2015). The researchers used tumor cell-specific ligands as targets to confer active targeting to the delivery system, aiming to improve the limitations of the EPR effect. In recent years, adenosine (ADN) receptors have emerged as pivotal mediators in tumor growth and progression. Studies conducted by Swami et al. (2015) have revealed that ADN could effectively function as a targeting ligand, directing delivery systems toward specific cancer cells. Chaudhari et al. (2023) harnessed ADN as a targeting ligand while utilizing PEG as a linker to augment hydrophilicity. They made PLGA-PEG-ADN nanoparticles loaded with paclitaxel for anti-cancer therapy. The results indicated that The ADN modification over PLGA NPs rendered higher particle internalization, resulting in a 3.5-fold reduction in IC50 values in TNBC cells. Further, the ADN modification allowed particles to exhibit a higher apoptosis index in TNBC cells when compared to non-modified PLGA NPs and the free PTX group. This demonstrated the superior anti-cancer performance of the nanoparticles containing targeting ligands.

In addition to targeting ligands, it is possible to achieve chemophotothermal combined therapy for cancer by co-loading chemotherapy drugs and photothermal agents. Chen et al. (2018) prepared hyaluronic acid (HA)-modified PLGA nanoparticles,

where HA exhibited targeting by binding to CD44 receptors on the surface of tumor cells. Alongside encapsulating the chemotherapy drug CDDP, they simultaneously loaded oleic acid-coated iron oxide magnetic nanoparticles (IOMNP) with photothermal properties, resulting in HA/PMNPc nanoparticles. The IOMNP served as a photothermal agent for photothermal cancer therapy when exposed to near-infrared light. On the one hand, targeted drug delivery increased the drug's therapeutic effect. On the other hand, the nanoparticles exhibited a hyperthermic effect upon short-term near-infrared light irradiation, further enhancing cell apoptosis through photothermal effects. Results demonstrated that HA/PMNPc nanoparticles increased intracellular uptake through active targeting and improved drug release rates in the acidic intracellular environment. Additionally, their cytotoxicity was enhanced, with an IC50 value only at 46% of the free drugs. In *in vivo* experiments, mice injected with HA/PMNPc nanoparticles exhibited the slowest tumor growth rate and longest survival time. In conclusion, the dual-targeting ability and chemophotothermal treatment capabilities provided by HA/PMNPc hold significant potential for cancer therapy (Chen et al., 2023).

Dual-receptor targeting nanoparticles containing two different targeting agents have garnered widespread attention due to their potential for higher cellular selectivity, cellular uptake, and

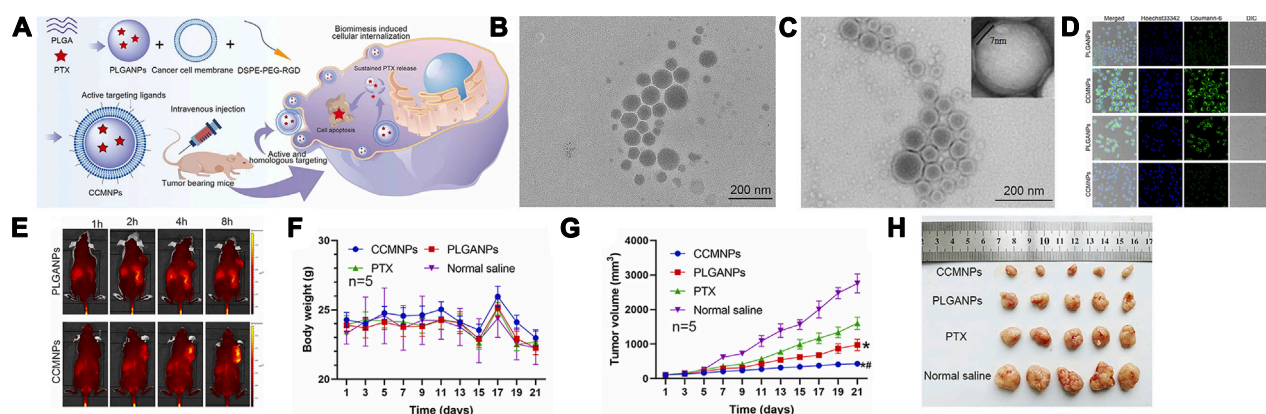


FIGURE 4

(A) Assembly of CCMNPs, injection in mice, and *in vivo* drug release. (B) TEM image of PLGANPs. (C) TEM image of CCMNPs. (D) Laser confocal microscopic images of NCI-H460 human lung cancer cells and mononuclear macrophages of RAW264.7 mice. (E) *In vivo* distribution over time after tail vein injection of PLGANPs and CCMNPs in BALB/C nude mice. (F) Broken line diagram of weight change in nude mice bearing tumor. (G) Broken line diagram of tumor volume changes in nude mice bearing tumor. (H) Experimental results of tumor growth inhibition after administration, $n = 5$. Reproduced with permission from ref Li et al. (2023). CC BY 4.0. Copyright 2023 The Authors.

cytotoxicity against cancer cells. Fakhrossadat Emami and colleagues functionalized PLGA nanoparticles with anti-EGFR antibodies and anti-PDL1 antibodies, encapsulating DTX to create DRT-DTX-PLGA nanoparticles. The results showed that compared to other formulations, treatment with DRT-DTX-PLGA significantly reduced the cell viability of human glioblastoma cells U87-MG and human non-small cell lung cancer cells A549, with survival rates of $25.1\% \pm 5.3\%$ and $20.6\% \pm 7.8\%$, respectively. In both cell lines, the cytotoxic effects of DRT-DTX-PLGA were significantly higher than those of NT-DTX-PLGA and free DTX, indicating a substantial synergistic enhancement of intracellular uptake by the dual ligand nanoparticle system (Emami et al., 2023).

Wang et al. (2022) had also developed dual-targeting nanoparticles known as PG@KMCM. The results showed that these nanoparticles could effectively reprogram the tumor microenvironment, killing pancreatic cancer cells and enhancing the overall therapeutic potential.

However, there was a problem in previous studies: the drug encapsulated in the carrier cannot be released after tumor cells ingest this dual-targeted drug delivery system. Therefore, Zhang et al. (2022c) designed dual-targeting nanoparticles, DOX/FA-HASS-PLGA, where folic acid (FA) can bind to overexpressed folate receptors on cancer cell surfaces, and hyaluronic acid (HA) can bind to overexpressed CD44 receptors on cancer cell surfaces. Moreover, they used disulfide bonds to connect the HA hydrophilic shell to the PLGA hydrophobic core. Because glutathione (GSH) levels in tumor cells were 7–10 times higher than in normal tissues, this highly reducing environment led to rapid breakage of micelles that reached the tumor site via thiol-disulfide bond exchange, which allowed for rapid drug release. In experiments with tumor-bearing mice, the DOX/FA-HA-SS-PLGA group exhibited the highest survival rate, smallest tumor volume, and significantly extended average survival time compared to other control groups. These results further illustrated that DOX/FA-HA-SS-PLGA possessed the

most effective anti-cancer properties, and these dual-targeting reducible drug-loaded micelles had a promising therapeutic effect on tumors (Refer to Figure 5 for further details).

2.3 Polylactic acid (PLA)

PLA is a lactic acid derivative derived from renewable sources such as wheat, straw, corn, and sorghum (Rydz et al., 2014). Recent research has shown that it can also be extracted from agricultural waste materials like sugarcane bagasse and olive pits (Cox et al., 2023; Haokok et al., 2023). Its remarkable biodegradability distinguishes PLA, as it undergoes degradation within the body into lactic acid monomers that participate in the human tricarboxylic acid cycle, ultimately breaking down into CO_2 and water (Kumari et al., 2010). It has been widely used in drug delivery due to its biodegradability and tunable mechanical properties (Lee et al., 2016). The details about the applications of PLA in cancer chemotherapy are shown in Table 4.

Qin et al. (2019) once employed ultrasound emulsification to merge PLA, with chitosan, resulting in nanoparticles loaded with 5-fluorouracil and irinotecan. *In vivo* experiments also unveiled its capacity to suppress the growth of cancers, outperforming intravenous injection.

However, nanoparticles can result in challenges such as poor solubility. To address issues related to dissolution and stability of nanoparticles, researchers have implemented strategies involving the chemical crosslinking of hydrophilic polyethylene glycol (Im et al., 2021).

Therefore, Chen et al. (2021a) employed the emulsion solvent diffusion method to synthesize DTX-mPEG-PLA nanoparticles designed for sarcoma treatment. Incorporating a PEG shell could enable prolonged circulation and facilitate tumor targeting through the EPR effect. The study results showed that due to the nanoparticles' good pharmacokinetic properties, DTX NPS showed a tumor inhibition rate of 94.66% in a hormonal mouse

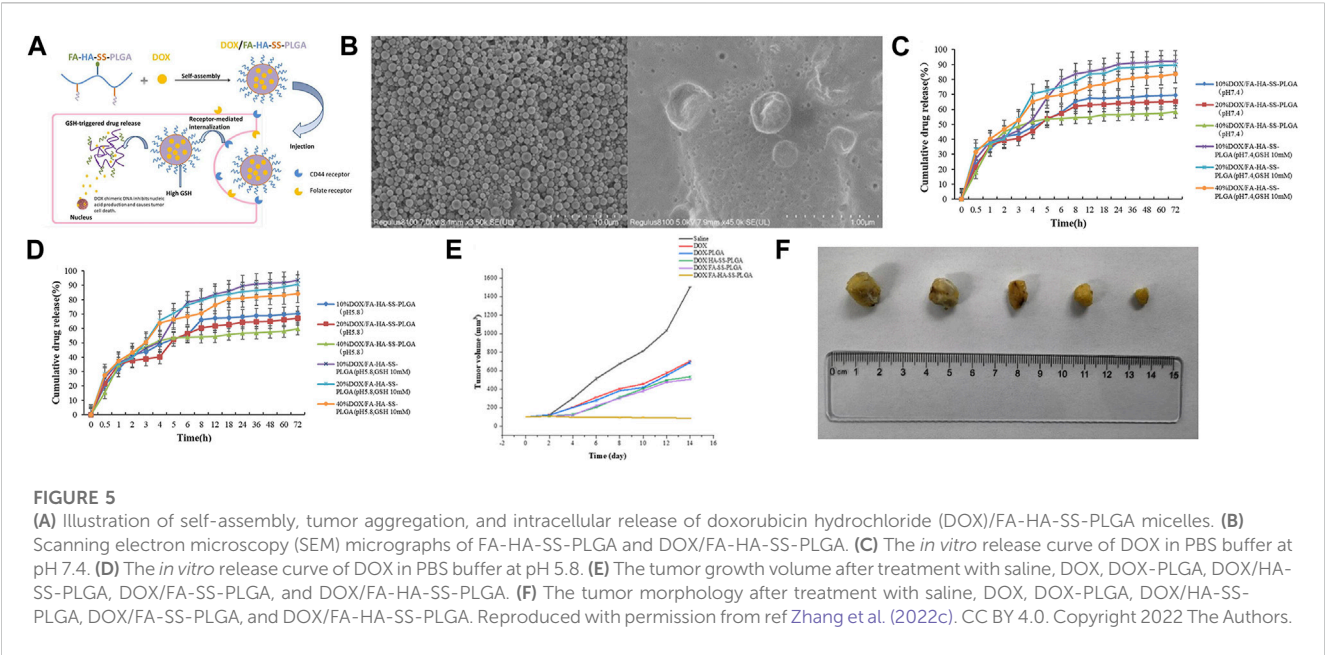


TABLE 4 PLA-based nanoparticle delivery systems investigated for treating cancers.

| Author | Year | Nanoparticles system | Encapsulation efficiency (%) | Size (nm) | Drug loading (%) | IC50 | Type of tumor | Chemotherapy drug | Reference |
|---------------------|------|-----------------------------------|--------------------------------|-------------|----------------------------------|---|---------------|-------------------|------------------------|
| Jianhua Chen et al | 2021 | DTX-mPEG-PLA | — | 100 | — | — | Sarcoma | DTX | Chen et al. (2021a) |
| Sungho Lee et al | 2021 | PTXx@Hap | — | 80 | — | — | Breast cancer | PTX | Lee et al. (2021) |
| Jamie K. Hu et al | 2021 | PLA-HPG | — | 200–300 | — | — | Skin cancer | Camptothecin | Hu et al. (2021) |
| Mohd Anees et al | 2022 | mPEG-PLA and LA-pluronic L-61-PLA | 83.3 ± 4.6/94.7 ± 2.2 DOX/PIRA | 130.5 ± 2.4 | 3.19 ± 0.13/3.61 ± 0.06 DOX/PIRA | MDA-MB 231 cells 1.378 ± 0.336/0.293 ± 0.075 nM DOX/PIRA | Breast cancer | DOX/PIRA | Anees et al. (2022) |
| Neha Mehrotra et al | 2023 | NAV/DCB NPs | 40–70 | 90–145 | — | — | Breast cancer | Decitabine | Mehrotra et al. (2023) |

model, which was 1.24 times higher than that of DTX injection. These findings emphasize the promise of mPEG-PLA nanoparticles in advancing drug delivery.

To enhance the hydrophobicity of the diblock copolymer core and make the nanoparticles denser, Mohd Anees et al. blended a pentablock copolymer PLA-pluronic L-61-PLA with mPEG-PLA as a hybrid system to prepare PIRA encapsulated NPs. *In vivo* experiments, the tumor regression rates for free DOX and free PIRA treatment in mice were 74.74% ± 4.5% and 85.07% ± 1.6%, respectively. However, the tumor regression rates increased to 86.65% ± 2.6% and 94.36% ± 2.3% when using DOX NPs and PIRA NPs, respectively. Significantly, the use of polymers did not induce unnecessary non-targeted cardiac toxicity or myocardial atrophy (Anees et al., 2022) (Refer to Figure 6 for further details).

Mehrotra et al. (2023) also employed a hybrid-block copolymer nanoparticle system, PLA-mPEG/PLA-L61-PLA NPs, to simultaneously deliver the chemotherapy drug navitoclax and decitabine (DCB) for combined cancer therapy. Decitabine is a chemotherapy drug, while navitoclax is one of the first-generation pan-Bcl-2 inhibitors that have demonstrated potent activity in clinical trials against certain solid tumors. In cell experiments, the NAV/DCB dual-drug-loaded NPs significantly reduced the IC50 values compared to NAV/DCB dual-drug-loaded NPs alone, indicating a synergistic mechanism of action. In animal experiments, the NAV/DCB dual-drug-loaded NPs exhibited a significant tumor growth inhibition effect in a xenograft tumor model. Compared to the control group, the treatment group saw a 43.6% reduction in tumor size, once again demonstrating the

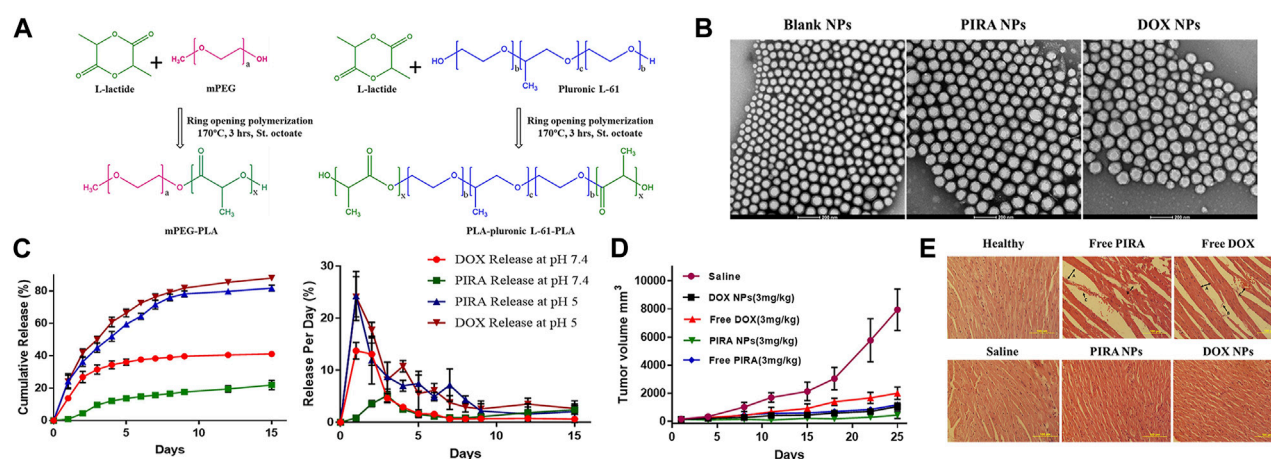


FIGURE 6

(A) Schematic representation of ring opening polymerization of L-lactide using polymerizing initiators mPEG and pluronic L-61. (B) HR-TEM images of PLA-based hybrid block copolymeric NPs. The scale bar represents 200 nm. (C) *In-vitro* release profile of PIRA/DOX from PLA-based hybrid block copolymeric NPs at pH 7.4 and pH 5. (D) Change in tumor volume of mice treated with free drugs, drug-loaded NPs, and saline throughout the study period. (E) Histopathological images of cardiac tissue of all treated/untreated mice. The scale bar represents 100 μ m. Reproduced with permission from ref Anees et al. (2022). CC BY 4.0. Copyright 2022 The Authors.

synergistic effect of dual-drug loading (Refer to Figure 7 for further details).

In addition to using PEG to form hydrophilic shells, research has reported using other polymer molecules as hydrophilic shells. Hu et al. (2021) developed a bioadhesive nanoparticle (BNP) drug delivery system composed of biodegradable polymer, poly(lactic acid)-hyperbranched polyglycerol (PLA-HPG), encapsulating camptothecin (CPT). The surface chemistry of HPG molecules was altered by treatment with sodium periodate, converting adjacent diols into aldehydes. Aldehydes can form strong covalent bonds with amines on the surface of tumor cells and extracellular matrix proteins. In *in vivo* experiments, the results showed that after 10 days of injection of BNP-CPT, approximately 50% of CPT was still retained in the tumor, whereas CPT was undetectable in tumors injected with free CPT. BNP-CPT also significantly reduced tumor burden, with some established tumors (about 20%) showing histological cure following BNPCPT treatment.

Apart from targeting specific receptors, researchers have also capitalized on the distinct pH levels surrounding tumors to enhance drug delivery outcomes. Lee et al. (2021) adopted an approach to fabricate poly lactic acid/hydroxyapatite (PLA/HAp) core-shell nanoparticles loaded with PTX. Hydroxyapatite maintains stability under neutral pH conditions yet dissolves within acidic environments. This pH responsiveness enabled its dissolution in the acidic milieu characteristic of cancer cells, thus facilitating drug release. The outcomes revealed persistent cytotoxic effects on 4T1 cells for a duration of up to 48 h, signifying its potential as a drug carrier for tumor inhibition.

2.4 Other polyester

The design of thermoplastic polyesters (e.g., PLA) often requires the use of toxic initiators, catalysts, or solvents. So, catalyst-free

thermal polyesterification has recently emerged as a potential strategy (Tham et al., 2016). Among them, Poly(Glycerol Sebacate) (PGS) can be formed by a polycondensation reaction of two monomers, glycerol, and sebacic acid, both of which are biocompatible and have been approved by the FDA.

In 2022, Massironi et al. (2022) prepared curcumin-loaded PGS-NPs by nanoprecipitation. The results showed that the PGS-NPs had good biostability over 14 days. The IC₅₀ value of curcumin-loaded PGS-NPs at 72 h (15.95 μ M) was significantly lower than that of free curcumin (21.27 μ M) suggesting a higher cytotoxic effect of curcumin-loaded PGS-NP. It suggested that curcumin-loaded PGS-NPs may represent a possible adjuvant therapy for treating cancer cells.

3 Discussion

3.1 The mechanisms of nanoparticles in cancer treatment

It was first thought that nanoparticles could passively extravasate into solid tumors through the porous vascular system and reside within the tumor to achieve accumulation, a phenomenon known as the enhanced permeability and retention (EPR) effect, a consensus that persisted for many years (Maeda, 2012).

But in recent years different discoveries have been made, Liu et al. (2019) found that nanoparticles could also enter tumors through an active transcellular transport process, and that transcytosis may be an important mechanism for cancer nanodrugs. It included receptor-mediated transcytosis (RMT), absorptive-mediated transcytosis (AMT), and bulk-phase or fluid-phase transcytosis (FPT) (Li and Kataoka, 2021).

Al-Humaidi et al. (2022) produced paclitaxel-PLGA-NPs with a particle size of 85.5 nm using the modified nanoprecipitation

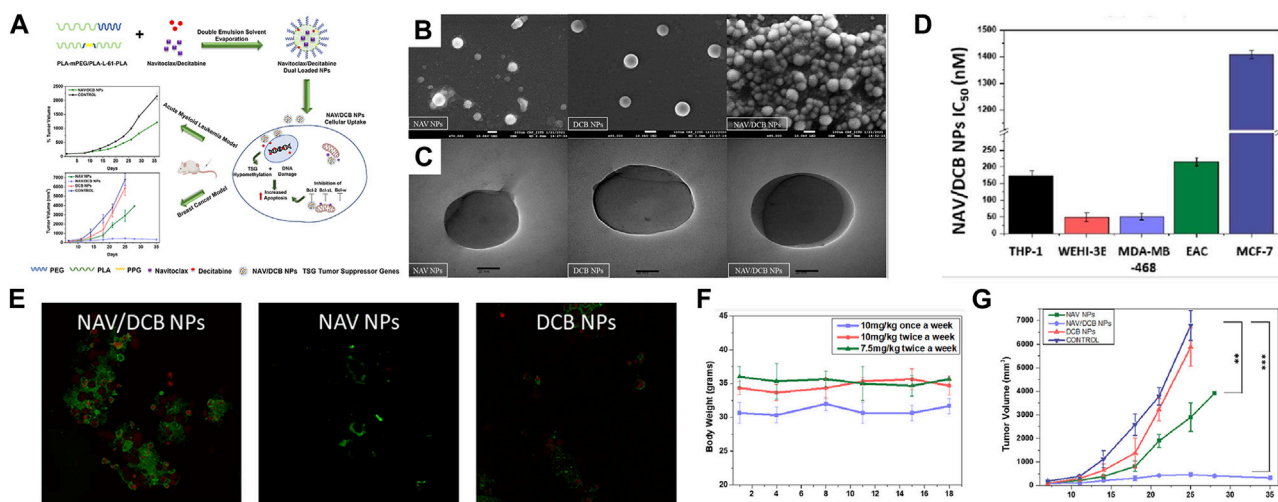


FIGURE 7

(A) Schematic representation of concomitant delivery of BH3 mimetic navitoclax and DNA methyltransferase inhibitor decitabine using poly(lactic acid) hybrid block copolymeric nanoparticles. Upon entry of nanoparticles into cells, navitoclax inhibits BCL expression and decitabine causes DNA damage, which together lead to apoptosis. The results showed potent synergistic cytotoxicity against both acute myeloid leukemia and breast cancer cell lines *in vitro*. (B) FE-SEM images of NAV/DCB single and dual NPs. (C) HR-TEM images of NAV/DCB single and dual NPs. (D) IC₅₀ values for NAV/DCB NPs on various AML and breast cancer cell lines. (E) Confocal microscopy in EAC cells post 48-h exposure to 100 nM NAV/DCB single and dual NPs. (F) *In vivo* dose tolerability study for NAV/DCB dual NPs in healthy BABL/c for three dosing schedules. (G) Tumor inhibition study using NAV/DCB single and dual NPs for syngeneic breast cancer model. Reproduced with permission from ref Mehrotra et al. (2023). CC BY 4.0. Copyright 2023 The Authors.

method. Through the use of different endocytosis inhibitors, they demonstrated that macropinocytosis was the primary endocytosis pathway for the paclitaxel-PLGA-NPs.

Sindhvani et al. (2020) also showed that nanoparticle entry into tumors is an active process rather than passive transport. These findings provide important fundamental theories and research directions for further advancement of nanoparticle-based drug delivery systems.

3.2 Effect of nanoparticle shape on properties

The shapes of nanoparticles can be broadly categorized as spherical and non-spherical, such as filamentous, discoidal, hemispherical, and worm-like, among others. It has been recognized as a key factor influencing cellular uptake, circulation time, biodistribution, and cancer drug delivery (Truong et al., 2015).

Compared to spherical nanoparticles, non-spherical shape hinders the uptake of microparticles by macrophages, with a negative correlation between uptake rate and aspect ratio, which prolongs the residence time of the nanoparticles in the bloodstream and increases their chances of reaching the target site (Florez et al., 2012; Mathaes et al., 2014). Non-spherical nanoparticles are also better than spherical nanoparticles in terms of tumor extravasation, on the one hand, it has a long circulation time in the blood, and on the other hand, it has a higher surface adhesion interaction area than spherical particles (Cooley et al., 2018).

Although non-spherical particles can improve cytotoxicity, alter biodistribution, and improve *in vivo* anti-tumor efficacy. However, the design of non-spherical particles for degradable polymers still faces many difficulties (Jindal, 2017).

In addition to nanoparticles of specific sizes and shapes, size- and shape-transformable nanoparticles have emerged as a promising strategy for tumor theranostics. But it also means their designs are more complex (Chen et al., 2021b).

3.3 The shell materials

As nanoparticles circulate within the body, they encounter challenges in immune system clearance mechanisms (Fu et al., 2021). In order to minimize RES clearance and prolong blood circulation time, various shell materials have been used to shield their surfaces and achieve a stealth effect, which prevents nonspecific protein adsorption and subsequent phagocytosis. Wen et al. (2023) provided a detailed review of invisible nanocarriers and proposed the concept of “pseudo-stealth effect.”

Among the various stealth shell materials, the most frequently employed is PEG (Cho et al., 2016; Liang et al., 2017; Menconi et al., 2021). Research on polyethylene glycol to extend the circulation time of liposomes in the bloodstream dates back to the 1990s (Klibanov et al., 1990). However, polyethylene glycolization prevents interaction with diseased cells, a problem known as the “PEG dilemma” (Hatakeyama et al., 2011). In addition to PEG, researchers have also identified other phospholipid-binding zwitterion that can enhance tumor permeability and prolong blood circulation, such as poly(2-(N-oxide-N, N-diethylamino) ethyl methacrylate) (OPDEA) (Chen S. et al., 2021).

People have also utilized biomimetic methods, such as using cell membrane coatings, which can make nanoparticles look more like their own cells, thus evading removal by the immune system (Chen S. et al., 2021; Guo et al., 2022). Brenner et al. (2018) have also utilized red blood cell (RBC)-hitchhiking (RH) to increase uptake of nanoparticles in organs. Zhang et al. (2020) also produced

albumin-based nanoparticles to increase circulation time and reduce the toxic side effects of free drugs.

3.4 Stimuli-responsive polyester

Nanodrugs are usually released prematurely before the nanocarriers reach the target lesions. Therefore, the application of stimuli-responsive nanomaterials for drug delivery has received increasing attention. Stimuli-responsive nanomaterials can be categorized into three classes, endogenous stimuli-responsive materials, exogenous stimuli-responsive materials, and multi-stimuli-responsive materials (Li L. et al., 2019).

Endogenous stimuli-responsive materials mainly include pH, enzyme, and redox-responsive materials. Tumor tissues exhibit a slightly acidic extracellular pH of around 6.5, while normal tissues typically range from pH 7.2 to 7.4 (Singhvi et al., 2019). Consequently, researchers have harnessed these environmental variations to develop pH-sensitive drug delivery systems (Zheng et al., 2020; Qian et al., 2021). Nanocarriers can also utilize the different pH gradients within cellular components to achieve precise drug release (Zhang et al., 2014).

Enzyme-responsive delivery systems have also received increasing attention. Li et al. (2021) exploited the MMP overactivation in tumor-associated tissues to design enzymatically transformable polymersomes-based nanotherapeutics to guide the co-delivery of colchicine and marimastat. It not only exposes the guanidine moiety for improving tissue/cell targeting to enhance bioavailability but also to differentially release drugs.

Glutathione levels are usually elevated in tumor cells, which leads to a higher reducing environment. Therefore, nanoparticles based on redox-responsive drugs targeting cancer cells have also been extensively studied (Park et al., 2015).

Exogenous stimulus-responsive materials such as light (Chen Y. et al., 2021), ultrasound (Papa et al., 2017; Huang et al., 2023), and magnetic field (Garcia-Garcia et al., 2020) responsive materials can also be applied to achieve accurate drug release at the tumor site. The combined application of multiple stimulus-responsive materials has also received attention. In conclusion, the stimuli-crosslinking strategy shows promising potential for cancer treatments (Xue et al., 2022).

4 Current limitations

Ideally, nano drug delivery systems should be low or even non-toxic, have good drug encapsulation efficiency, be capable of controlled release, and continuous delivery, and be easy to perform clinically. Unfortunately, current technologies cannot simultaneously fulfill all of these requirements (Liu et al., 2023).

Despite significant advances in biodegradable polyesters, many shortcomings remain. PLA suffers from shortcomings (low-ductility and toughness, glass transition and heat distortion temperature, rate of crystallization; high sensitivity to moisture and fast degradation by hydrolysis, etc.) (Murariu and Dubois, 2016). PCL has low mechanical strength, an insufficient number of cellular recognition sites, poor bioactivity, and hydrophobicity (Homaeigohar and Boccacini, 2022). PLGA also faces drawbacks such as low drug loading, high production cost, and difficulty in large-scale production (Lu et al., 2023).

Furthermore, most nanoparticles were still in the cellular and animal experimental stages. Some have entered clinical trials, but the results were often unsatisfactory. People realized that the EPR affected works in rodents, but its role in humans needed to be further verified (Nichols and Bae, 2014; Danhier, 2016). They still have a long way to go before they can be used in clinical applications (Wilhelm et al., 2016; Ouyang et al., 2020).

First, the safety issue is of utmost concern. The entry of nanoparticles into the blood circulation may cause adverse effects, such as inflammation, cell cycle alteration, oxidative stress, DNA damage, etc. (Ciappellano et al., 2016). Whether adequate clearance through the glomerular filtration membrane is possible deserves further investigation. In addition, non-specific accumulation in normal tissues may also occur, resulting in further adverse effects (Rehman et al., 2022).

In addition, acidic products were observed during the degradation of polyester, which can lead to an inflammatory response. Polycarbonate is superior to polyester in this respect, as it does not produce acidic products during degradation (Yu et al., 2021).

Nanoparticles also face low drug loading rates, with most of the nanoparticles currently approved by the FDA having no more than a 20% drug loading rate. This means that excessive carrier material may be required to achieve a therapeutic effect, which needs to be further verified to see if this will further exacerbate its potential toxicity. In addition, to increase stability, coatings such as PEG are added to prevent premature uptake by macrophages, but this can also lead to a decrease in encapsulation rate when new materials are added. Consequently, this leads to difficulties in applying it to clinical (Liu et al., 2020; Et et al., 2021).

In addition, biodegradable polyester nanoparticles face problems such as complicated fabrication and high cost (James et al., 2016). These hinder its mass production and become a hindrance to clinical applications.

5 Conclusion and outlook

As drug delivery carriers, biodegradable polyesters have many good properties, such as increasing the solubility of hydrophobic drugs, improving drug efficacy, prolonging drug action time, and improving drug bioavailability (Janrao et al., 2023). This review summarizes the recent applications of biodegradable polyester-based nano-drug delivery systems over the past 3 years.

In recent years, polyester-based delivery systems have been increasingly studied, ranging from individual nanoparticles to amphiphilic block copolymers. Subsequently, their surfaces are modified to avoid phagocytosis by the immune system. In addition, the drugs carried have evolved from single chemotherapeutic agents to combinations of multiple drugs. Some researchers have also carried nucleic acids (Zhao et al., 2018; Zhao et al., 2023), siRNA (Xu et al., 2018), and immunomodulatory agents (Narmani et al., 2023), yielding desirable results.

A polyester-based polymer micelle known as Genexol-PM has received marketing approval in South Korea. A Phase III clinical trial has revealed that it exhibited non-inferior and even superior clinical efficacy when compared to standard paclitaxel in patients with a

manageable safety profile in patients with metastatic breast cancer. This represented a milestone for polymeric nanomedicines toward clinical translation (Kim et al., 2001; Park et al., 2017; Yi et al., 2018).

However, for the other nanoparticles, there is still a need for further safety and toxicology testing of nanoparticles to ensure their benefits outweigh their harm to the human body. It is also essential to find ways to improve its drug loading rate for more efficient treatment, which will also reduce the impact of nanoparticles themselves on the human body.

The process of making nanoparticles also needs to be further simplified to ensure its robustness. This will further increase the possibility of it being promoted in the clinic treatments.

Author contributions

ZW: Writing—original draft. MX: Writing—original draft. FG: Writing—original draft. YY: Writing—original draft. HT: Writing—review and editing. QZ: Writing—review and editing. SR: Writing—review and editing. LY: Writing—review and editing.

Funding

The authors declare financial support was received for the research, authorship, and/or publication of this article. This work was supported

References

- Al-Humaidi, R. B., Fayed, B., Shakartalla, S. B., Jagal, J., Jayakumar, M. N., Al Shareef, Z. M., et al. (2022). Optimum inhibition of MCF-7 breast cancer cells by efficient targeting of the macropinocytosis using optimized paclitaxel-loaded nanoparticles. *Life Sci.* 305, 120778. doi:10.1016/j.lfs.2022.120778
- Almeida, S. N., Elliott, R., Silva, E. R., and Sales, C. M. D. (2019). Fear of cancer recurrence: a qualitative systematic review and meta-synthesis of patients' experiences. *Clin. Psychol. Rev.* 68, 13–24. doi:10.1016/j.cpr.2018.12.001
- Anees, M., Tiwari, S., Mehrotra, N., Kharbanda, S., and Singh, H. (2022). Development and evaluation of PLA based hybrid block copolymeric nanoparticles for systemic delivery of pirarubicin as an anti-cancer agent. *Int. J. Pharm.* 620, 121761. doi:10.1016/j.ijpharm.2022.121761
- Asadi, N., Davaran, S., Panahi, Y., Hasanazadeh, A., Malakootikhah, J., Fallah Moafi, H., et al. (2017). Application of nanostructured drug delivery systems in immunotherapy of cancer: a review. *Artif. Cells Nanomed Biotechnol.* 45 (1), 18–23. doi:10.1080/21691401.2016.1178136
- Bae, K. H., Chung, H. J., and Park, T. G. (2011). Nanomaterials for cancer therapy and imaging. *Mol. Cells* 31 (4), 295–302. doi:10.1007/s10059-011-0051-5
- Behl, A., Sarwalia, P., Kumar, S., Behera, C., Mintoo, M. J., Datta, T. K., et al. (2022). Codelivery of gemcitabine and MUC1 inhibitor using PEG-PCL nanoparticles for breast cancer therapy. *Mol. Pharm.* 19 (7), 2429–2440. doi:10.1021/acs.molpharmaceut.2c00175
- Bhadran, A., Shah, T., Babanyinah, G. K., Polara, H., Taslimy, S., Biewer, M. C., et al. (2023). Recent advances in polycaprolactones for anticancer drug delivery. *Pharmaceutics* 15 (7), 1977. doi:10.3390/pharmaceutics15071977
- Biller, L. H., and Schrag, D. (2021). Diagnosis and treatment of metastatic colorectal cancer: a review. *JAMA* 325 (7), 669–685. doi:10.1001/jama.2021.0106
- Brenner, J. S., Pan, D. C., Myerson, J. W., Marcos-Contreras, O. A., Villa, C. H., Patel, P., et al. (2018). Red blood cell-hitchhiking boosts delivery of nanocarriers to chosen organs by orders of magnitude. *Nat. Commun.* 9 (1), 2684. doi:10.1038/s41467-018-05079-7
- Cai, H., Wang, R., Guo, X., Song, M., Yan, F., Ji, B., et al. (2021). Combining gemcitabine-loaded macrophage-like nanoparticles and erlotinib for pancreatic cancer therapy. *Mol. Pharm.* 18 (7), 2495–2506. doi:10.1021/acs.molpharmaceut.0c01225
- Chaudhari, D., Kuche, K., Yadav, V., Ghadi, R., Date, T., Bhargavi, N., et al. (2023). Exploring paclitaxel-loaded adenosine-conjugated PEGylated PLGA nanoparticles for targeting triple-negative breast cancer. *Drug Deliv. Transl. Res.* 13 (4), 1074–1087. doi:10.1007/s13346-022-01273-9
- by the Natural Science Foundation of Liaoning Province (2022-YGJC-69 and 2020-MS-327), the support program for excellent young scholars of China Medical University and the Health Commission of Shenyang (2021-wjkt-009).
- Chen, C., Zhao, S., Karnad, A., and Freeman, J. W. (2018). The biology and role of CD44 in cancer progression: therapeutic implications. *J. Hematol. Oncol.* 11 (1), 64. doi:10.1186/s13045-018-0605-5
- Chen, H. A., Lu, Y. J., Dash, B. S., Chao, Y. K., and Chen, J. P. (2023). Hyaluronic acid-modified cisplatin-encapsulated poly(lactic-co-glycolic acid) magnetic nanoparticles for dual-targeted NIR-responsive chemo-photothermal combination cancer therapy. *Pharmaceutics* 15 (1), 290. doi:10.3390/pharmaceutics15010290
- Chen, J., Jiang, Z., Zhang, Y. S., Ding, J., and Chen, X. (2021b). Smart transformable nanoparticles for enhanced tumor theranostics. *Appl. Phys. Rev.* 8 (4), 0061530. doi:10.1063/5.0061530
- Chen, J., Ning, E., Wang, Z., Jing, Z., Wei, G., Wang, X., et al. (2021a). Docetaxel loaded mPEG-PLA nanoparticles for sarcoma therapy: preparation, characterization, pharmacokinetics, and anti-tumor efficacy. *Drug Deliv.* 28 (1), 1389–1396. doi:10.1080/10717544.2021.1945167
- Chen, S., Zhong, Y., Fan, W., Xiang, J., Wang, G., Zhou, Q., et al. (2021c). Enhanced tumour penetration and prolonged circulation in blood of polyzwitterion-drug conjugates with cell-membrane affinity. *Nat. Biomed. Eng.* 5 (9), 1019–1037. doi:10.1038/s41551-021-00701-4
- Chen, Y., Zhang, L., Li, F., Sheng, J., Xu, C., Li, D., et al. (2021d). Combination of chemotherapy and photodynamic therapy with oxygen self-supply in the form of mutual assistance for cancer therapy. *Int. J. Nanomedicine* 16, 3679–3694. doi:10.2147/ijn.s298146
- Cheng, J., and Pun, S. H. (2015). Polymeric biomaterials for cancer nanotechnology. *Biomater. Sci.* 3 (7), 891–893. doi:10.1039/c5bm90025e
- Cho, H., Gao, J., and Kwon, G. S. (2016). PEG-b-PLA micelles and PLGA-b-PEG-b-PLGA sol-gels for drug delivery. *J. Control Release* 240, 191–201. doi:10.1016/j.jconrel.2015.12.015
- Choi, Y. H., and Yu, A.-M. (2014). ABC transporters in multidrug resistance and pharmacokinetics, and strategies for drug development. *Curr. Pharm. Des.* 20 (5), 793–807. doi:10.2174/138161282005140214165212
- Chou, P. L., Huang, Y. P., Cheng, M. H., Rau, K. M., and Fang, Y. P. (2020). <p>Improvement of paclitaxel-associated adverse reactions (ADRs) via the use of nano-based drug delivery systems: a systematic review and network meta-analysis</p>. *Int. J. Nanomedicine* 15, 1731–1743. doi:10.2147/ijn.s231407
- Chou, T.-C. J. C. r. (2010). Drug combination studies and their synergy quantification using the chou-talalay method. *Chou-Talalay method* 70 (2), 440–446. doi:10.1158/0008-5472.can-09-1947

Acknowledgments

Some of the graphics in the graphical abstract are derived from <https://www.BioRender.com>, for which we are deeply grateful.

Conflict of interest

The authors declare that the research was conducted in the absence of any commercial or financial relationships that could be construed as a potential conflict of interest.

Publisher's note

All claims expressed in this article are solely those of the authors and do not necessarily represent those of their affiliated organizations, or those of the publisher, the editors and the reviewers. Any product that may be evaluated in this article, or claim that may be made by its manufacturer, is not guaranteed or endorsed by the publisher.

- Ciappellano, S. G., Tedesco, E., Venturini, M., and Benetti, F. (2016). *In vitro* toxicity assessment of oral nanocarriers. *Adv. Drug Deliv. Rev.* 106, 381–401. doi:10.1016/j.addr.2016.08.007
- Cooley, M., Sarode, A., Hoore, M., Fedosov, D. A., Mitragotri, S., and Sen Gupta, A. (2018). Influence of particle size and shape on their margination and wall-adhesion: implications in drug delivery vehicle design across nano-to-micro scale. *Nanoscale* 10 (32), 15350–15364. doi:10.1039/c8nr04042g
- Cox, R., Narisetty, V., Castro, E., Agrawal, D., Jacob, S., Kumar, G., et al. (2023). Fermentative valorisation of xylose-rich hemicellulosic hydrolysates from agricultural waste residues for lactic acid production under non-sterile conditions. *Waste Manag.* 166, 336–345. doi:10.1016/j.wasman.2023.05.015
- Danhier, F. (2016). To exploit the tumor microenvironment: since the EPR effect fails in the clinic, what is the future of nanomedicine? *J. Control Release* 244, 108–121. doi:10.1016/j.jconrel.2016.11.015
- Emami, F., Duwa, R., Banstola, A., Woo, S. M., Kwon, T. K., and Yook, S. (2023). Dual receptor specific nanoparticles targeting EGFR and PD-L1 for enhanced delivery of docetaxel in cancer therapy. *Biomed. Pharmacother.* 165, 115023. doi:10.1016/j.biopha.2023.115023
- Esfandyari-Manesh, M., Darvishi, B., Ishkuh, F. A., Shahmoradi, E., Mohammadi, A., Javanbakht, M., et al. (2016). Paclitaxel molecularly imprinted polymer-PEG-folate nanoparticles for targeting anticancer delivery: characterization and cellular cytotoxicity. *Mater. Sci. Eng. C Mater. Biol. Appl.* 62, 626–633. doi:10.1016/j.msec.2016.01.059
- Etter, E. L., Mei, K.-C., and Nguyen, J. (2021). Delivering more for less: nanosized, minimal-carrier and pharmacocative drug delivery systems. *Adv. Drug Deliv. Rev.* 179, 113994. doi:10.1016/j.addr.2021.113994
- Fan, W., Wei, Q., Xiang, J., Tang, Y., Zhou, Q., Geng, Y., et al. (2022). Mucus penetrating and cell-binding polyzwitterionic micelles as potent oral nanomedicine for cancer drug delivery. *Adv. Mater.* 34 (16), e2109189. doi:10.1002/adma.202109189
- Fang, Y., Jiang, Y., Zou, Y., Meng, F., Zhang, J., Deng, C., et al. (2017). Targeted glioma chemotherapy by cyclic RGD peptide-functionalized reversibly core-crosslinked multifunctional poly (ethylene glycol)-b-poly (ϵ -caprolactone) micelles. *Acta Biomater.* 50, 396–406. doi:10.1016/j.actbio.2017.01.007
- Florez, L., Herrmann, C., Cramer, J. M., Hauser, C. P., Koynov, K., Landfester, K., et al. (2012). How shape influences uptake: interactions of anisotropic polymer nanoparticles and human mesenchymal stem cells. *Small* 8 (14), 2222–2230. doi:10.1002/smll.201102002
- Fu, D., Wang, Z., Tu, Y., and Peng, F. (2021). Interactions between biomedical micro-/nano-motors and the immune molecules, immune cells, and the immune system: challenges and opportunities. *Adv. Healthc. Mater.* 10 (7), e2001788. doi:10.1002/adhm.202001788
- Gahtani, R. M., Alqahtani, A., Alqahtani, T., Asiri, S. A., Mohamed, J. M. M., Venkatesa Prabhu, S., et al. (2023). 5-Fluorouracil-Loaded PLGA nanoparticles: formulation, physicochemical characterisation, and *in Vitro* Anti-cancer activity. *Bioinorg. Chem. Appl.* 2023, 1–11. doi:10.1155/2023/2334675
- Garcia-Garcia, G., Fernandez-Alvarez, F., Cabeza, L., Delgado, A. V., Melguizo, C., Prados, J. C., et al. (2020). Gemcitabine-loaded magnetically responsive poly(ϵ -caprolactone) nanoparticles against breast cancer. *Polym. (Basel)* 12 (12), 2790. doi:10.3390/polym12122790
- Gross, R. A., and Kalra, B. (2002). Biodegradable polymers for the environment. *Science* 297 (5582), 803–807. doi:10.1126/science.297.5582.803
- Grossen, P., Witzigmann, D., Sieber, S., and Huwyler, J. (2017). PEG-PCL-based nanomedicines: a biodegradable drug delivery system and its application. *J. Control Release* 260, 46–60. doi:10.1016/j.jconrel.2017.05.028
- Guo, Y., Wang, Z., Shi, X., and Shen, M. (2022). Engineered cancer cell membranes: an emerging agent for efficient cancer theranostics. *Exploration* 2 (1), 20210171. doi:10.1002/exp.20210171
- Gupta, P. K., Gahtori, R., Govarthanan, K., Sharma, V., Pappuru, S., Pandit, S., et al. (2021). Recent trends in biodegradable polyester nanomaterials for cancer therapy. *Mater. Sci. Eng. C Mater. Biol. Appl.* 127, 112198. doi:10.1016/j.msec.2021.112198
- Haokok, C., Lunprom, S., Reungsang, A., and Salakkam, A. (2023). Efficient production of lactic acid from cellulose and xylan in sugarcane bagasse by newly isolated *Lactiplantibacillus plantarum* and *Levilactobacillus brevis* through simultaneous saccharification and co-fermentation process. *Heliyon* 9 (7), e17935. doi:10.1016/j.heliyon.2023.e17935
- Hasanbegloo, K., Banihashem, S., Faraji Dizaji, B., Bybordi, S., Farrokhi-Eslamlou, N., Abadi, P. G., et al. (2023). Paclitaxel-loaded liposome-incorporated chitosan (core)/poly(ϵ -caprolactone)/chitosan (shell) nanofibers for the treatment of breast cancer. *Int. J. Biol. Macromol.* 230, 123380. doi:10.1016/j.jbiomac.2023.123380
- Hatakeyama, H., Akita, H., and Harashima, H. (2011). A multifunctional envelope type nano device (MEND) for gene delivery to tumours based on the EPR effect: a strategy for overcoming the PEG dilemma. *Adv. Drug Deliv. Rev.* 63 (3), 152–160. doi:10.1016/j.addr.2010.09.001
- He, Y., Ju, Y., Hu, Y., Wang, B., Che, S., Jian, Y., et al. (2023). Brd4 proteolysis-targeting chimera nanoparticles sensitized colorectal cancer chemotherapy. *J. Control Release* 354, 155–166. doi:10.1016/j.jconrel.2022.12.035
- Hellmann, M. D., Li, B. T., Chaff, J. E., and Kris, M. G. (2016). Chemotherapy remains an essential element of personalized care for persons with lung cancers. *Ann. Oncol.* 27 (10), 1829–1835. doi:10.1093/annonc/mdw271
- Homaeigohar, S., and Boccaccini, A. R. (2022). Nature-derived and synthetic additives to poly(ϵ -Caprolactone) nanofibrous systems for biomedicine; an updated overview. *Front. Chem.* 9, 809676. doi:10.3389/fchem.2021.809676
- Hu, J. K., Suh, H. W., Qureshi, M., Lewis, J. M., Yaqoob, S., Moscato, Z. M., et al. (2021). Nonsurgical treatment of skin cancer with local delivery of bioadhesive nanoparticles. *Proc. Natl. Acad. Sci. U. S. A.* 118 (7), e2020575118. doi:10.1073/pnas.2020575118
- Huang, D., Wang, J., Song, C., and Zhao, Y. (2023). Ultrasound-responsive matters for biomedical applications. *Innovation* 4 (3), 100421. doi:10.1016/j.xinn.2023.100421
- Im, S. H., Im, D. H., Park, S. J., Chung, J. J., Jung, Y., and Kim, S. H. (2021). Stereocomplex polylactide for drug delivery and biomedical applications: a review. *Molecules* 26 (10), 2846. doi:10.3390/molecules26102846
- James, R., Manoukian, O. S., and Kumbar, S. G. (2016). Poly(lactic acid) for delivery of bioactive macromolecules. *Adv. Drug Deliv. Rev.* 107, 277–288. doi:10.1016/j.addr.2016.06.009
- Jan, N., Madni, A., Rahim, M. A., Khan, N. U., Jamshaid, T., Khan, A., et al. (2021). *In vitro* anti-leukemic assessment and sustained release behaviour of cytarabine loaded biodegradable polymer based nanoparticles. *Life Sci.* 267, 118971. doi:10.1016/j.lfs.2020.118971
- Janrao, C., Khopade, S., Bavaskar, A., Gomte, S. S., Agnihotri, T. G., and Jain, A. (2023). Recent advances of polymer based nanosystems in cancer management. *J. Biomater. Sci. Polym. Ed.* 34 (9), 1274–1335. doi:10.1080/09205063.2022.2161780
- Jin, C. E., Yoon, M. S., Jo, M. J., Kim, S. Y., Lee, J. M., Kang, S. J., et al. (2023). Synergistic encapsulation of paclitaxel and sorafenib by methoxy poly(ethylene glycol)-b-poly(caprolactone) polymeric micelles for ovarian cancer therapy. *Pharmaceutics* 15 (4), 1206. doi:10.3390/pharmaceutics15041206
- Jindal, A. B. (2017). The effect of particle shape on cellular interaction and drug delivery applications of micro- and nanoparticles. *Int. J. Pharm.* 532 (1), 450–465. doi:10.1016/j.ijpharm.2017.09.028
- Khan, I., Ray Dutta, J., and Ganesan, R. (2017). Lactobacillus sps. lipase mediated poly (epsilon-caprolactone) degradation. *Int. J. Biol. Macromol.* 95, 126–131. doi:10.1016/j.jbiomac.2016.11.040
- Khan, S., Aamir, M. N., Madni, A., Jan, N., Khan, A., Jabar, A., et al. (2021). Lipid poly (ϵ -caprolactone) hybrid nanoparticles of 5-fluorouracil for sustained release and enhanced anticancer efficacy. *Life Sci.* 284, 119909. doi:10.1016/j.lfs.2021.119909
- Kim, S. C., Kim, D. W., Shim, Y. H., Bang, J. S., Oh, H. S., Wan Kim, S., et al. (2001). *In vivo* evaluation of polymeric micellar paclitaxel formulation: toxicity and efficacy. *J. Control Release* 72 (1–3), 191–202. doi:10.1016/s0168-3659(01)00275-9
- Klibanov, A. L., Maruyama, K., Torchilin, V. P., and Huang, L. (1990). Amphipathic polyethyleneglycols effectively prolong the circulation time of liposomes. *FEBS Lett.* 268 (1), 235–237. doi:10.1016/0014-5793(90)81016-h
- Kozovska, Z., Gabrisova, V., and Kucerova, L. (2014). Colon cancer: cancer stem cells markers, drug resistance and treatment. *Biomed. Pharmacother.* 68 (8), 911–916. doi:10.1016/j.biopha.2014.10.019
- Kumari, A., Yadav, S. K., and Yadav, S. C. (2010). Biodegradable polymeric nanoparticles based drug delivery systems. *Colloids Surf. B Biointerfaces* 75 (1), 1–18. doi:10.1016/j.colsurfb.2009.09.001
- Lee, B. K., Yun, Y., and Park, K. (2016). PLA micro- and nano-particles. *Adv. Drug Deliv. Rev.* 107, 176–191. doi:10.1016/j.addr.2016.05.020
- Lee, S., Miyajima, T., Sugawara-Narutaki, A., Kato, K., and Nagata, F. (2021). Development of paclitaxel-loaded poly(lactic acid)/hydroxyapatite core-shell nanoparticles as a stimuli-responsive drug delivery system. *R. Soc. Open Sci.* 8 (3), 202030. doi:10.1098/rsos.202030
- Li, J., Ge, Z., Toh, K., Liu, X., Dirisala, A., Ke, W., et al. (2021). Enzymatically transformable polymersome-based nanotherapeutics to eliminate minimal relapsable cancer. *Adv. Mater.* 33 (49), e2105254. doi:10.1002/adma.202105254
- Li, J., and Kataoka, K. (2021). Chemo-physical strategies to advance the *in vivo* functionality of targeted nanomedicine: the next generation. *J. Am. Chem. Soc.* 143 (2), 538–559. doi:10.1021/jacs.0c09029
- Li, L., Yang, W. W., and Xu, D. G. (2019b). Stimuli-responsive nanoscale drug delivery systems for cancer therapy. *J. Drug Target* 27 (4), 423–433. doi:10.1080/1061186x.2018.1519029
- Li, R., He, Y., Zhu, Y., Jiang, L., Zhang, S., Qin, J., et al. (2019a). Route to rheumatoid arthritis by macrophage-derived microvesicle-coated nanoparticles. *Nano Lett.* 19 (1), 124–134. doi:10.1021/acs.nanolett.8b03439
- Li, Y., Ke, J., Jia, H., Ren, J., Wang, L., Zhang, Z., et al. (2023). Cancer cell membrane coated PLGA nanoparticles as biomimetic drug delivery system for improved cancer therapy. *Colloids Surf. B Biointerfaces* 222, 113131. doi:10.1016/j.colsurfb.2023.113131
- Liang, H., Friedman, J. M., and Nacharaju, P. (2017). Fabrication of biodegradable PEG-PLA nanospheres for solubility, stabilization, and delivery of curcumin. *Artif. Cells Nanomed. Biotechnol.* 45 (2), 297–304. doi:10.3109/21691401.2016.1146736

- Liu, W., Ma, Z., Wang, Y., and Yang, J. (2023). Multiple nano-drug delivery systems for intervertebral disc degeneration: current status and future perspectives. *Bioact. Mater.* 23, 274–299. doi:10.1016/j.bioactmat.2022.11.006
- Liu, Y., Huo, Y., Yao, L., Xu, Y., Meng, F., Li, H., et al. (2019). Transcytosis of nanomedicine for tumor penetration. *Nano Lett.* 19 (11), 8010–8020. doi:10.1021/acs.nanolett.9b03211
- Liu, Y., Yang, G., Jin, S., Xu, L., and Zhao, C. X. (2020). Development of high-drug-loading nanoparticles. *Chempluschem* 85 (9), 2143–2157. doi:10.1002/cplu.202000496
- Lu, Y., Cheng, D., Niu, B., Wang, X., Wu, X., and Wang, A. (2023). Properties of poly (Lactic-co-Glycolic acid) and progress of poly (Lactic-co-Glycolic acid)-based biodegradable materials in biomedical research. *Pharmaceuticals* 16 (3), 454. doi:10.3390/ph16030454
- Maeda, H. (2012). Macromolecular therapeutics in cancer treatment: the EPR effect and beyond. *J. Control Release* 164 (2), 138–144. doi:10.1016/j.jconrel.2012.04.038
- Malikmammadov, E., Tanir, T. E., Kiziltay, A., Hasirci, V., and Hasirci, N. (2018). PCL and PCL-based materials in biomedical applications. *J. Biomater. Sci. Polym. Ed.* 29 (7–9), 863–893. doi:10.1080/09205063.2017.1394711
- Massironi, A., Marzorati, S., Marinelli, A., Toccaceli, M., Gazzotti, S., Ortenzi, M. A., et al. (2022). Synthesis and characterization of curcumin-loaded nanoparticles of poly(glycerol sebacate): a novel highly stable anticancer system. *Molecules* 27 (20), 6997. doi:10.3390/molecules27206997
- Mathaes, R., Winter, G., Besheer, A., and Engert, J. (2014). Influence of particle geometry and PEGylation on phagocytosis of particulate carriers. *Int. J. Pharm.* 465 (1–2), 159–164. doi:10.1016/j.ijpharm.2014.02.037
- Mattiuzzi, C., and Lippi, G. (2019). Current cancer epidemiology. *J. Epidemiol. Glob. Health* 9 (4), 217–222. doi:10.2991/jegeh.k.191008.001
- Mehrotra, N., Anees, M., Tiwari, S., Kharbanda, S., and Singh, H. (2023). Polylactic acid based polymeric nanoparticle mediated co-delivery of navitoclax and decitabine for cancer therapy. *Nanomedicine* 47, 102627. doi:10.1016/j.nano.2022.102627
- Menconi, A., Marzo, T., Massai, L., Pratesi, A., Severi, M., Petroni, G., et al. (2021). Anticancer effects against colorectal cancer models of chloro(triethylphosphine)gold(I) encapsulated in PLGA-PEG nanoparticles. *Biomaterials* 34 (4), 867–879. doi:10.1007/s10534-021-00313-0
- Molavi, F., Barzegar-Jalali, M., and Hamishehkar, H. (2020). Polyester based polymeric nano and microparticles for pharmaceutical purposes: a review on formulation approaches. *J. Control Release* 320, 265–282. doi:10.1016/j.jconrel.2020.01.028
- Murab, S., Herold, S., Hawk, T., Snyder, A., Espinal, E., and Whitlock, P. (2023). Advances in additive manufacturing of polycaprolactone based scaffolds for bone regeneration. *J. Mater. Chem. B* 11 (31), 7250–7279. doi:10.1039/d2tb02052a
- Murariu, M., and Dubois, P. (2016). PLA composites: from production to properties. *Adv. Drug Deliv. Rev.* 107, 17–46. doi:10.1016/j.addr.2016.04.003
- Narmani, A., Ganji, S., Amirishoar, M., Jahedi, R., Kharazmi, M. S., and Jafari, S. M. (2023). Smart chitosan-PLGA nanocarriers functionalized with surface folic acid ligands against lung cancer cells. *Int. J. Biol. Macromol.* 245, 125554. doi:10.1016/j.ijbiomac.2023.125554
- Nichols, J. W., and Bae, Y. H. (2014). EPR: evidence and fallacy. *J. Control. Release Official J. Control. Release Soc.* 190, 451–464. doi:10.1016/j.jconrel.2014.03.057
- Ouyang, B., Poon, W., Zhang, Y. N., Lin, Z. P., Kingston, B. R., Tavares, A. J., et al. (2020). The dose threshold for nanoparticle tumour delivery. *Nat. Mater* 19 (12), 1362–1371. doi:10.1038/s41563-020-0755-z
- Pandey, S. K., Ghosh, S., Maiti, P., and Haldar, C. (2015). Therapeutic efficacy and toxicity of tamoxifen loaded PLA nanoparticles for breast cancer. *Int. J. Biol. Macromol.* 72, 309–319. doi:10.1016/j.ijbiomac.2014.08.012
- Papa, A. L., Korin, N., Kanapathipillai, M., Mammoto, A., Mammoto, T., Jiang, A., et al. (2017). Ultrasound-sensitive nanoparticle aggregates for targeted drug delivery. *Biomaterials* 139, 187–194. doi:10.1016/j.biomaterials.2017.06.003
- Park, H. K., Lee, S. J., Oh, J. S., Lee, S. G., Jeong, Y. I., and Lee, H. C. (2015). Smart nanoparticles based on hyaluronic acid for redox-responsive and CD44 receptor-mediated targeting of tumor. *Nanoscale Res. Lett.* 10 (1), 288. doi:10.1186/s11671-015-0981-5
- Park, I. H., Sohn, J. H., Kim, S. B., Lee, K. S., Chung, J. S., Lee, S. H., et al. (2017). An open-label, randomized, parallel, phase III trial evaluating the efficacy and safety of polymeric micelle-formulated paclitaxel compared to conventional cremophor EL-based paclitaxel for recurrent or metastatic HER2-negative breast cancer. *Cancer Res. Treat.* 49 (3), 569–577. doi:10.4143/crt.2016.289
- Qian, Y., Zhang, J., Xu, R., Li, Q., Shen, Q., and Zhu, G. (2021). Nanoparticles based on polymers modified with pH-sensitive molecular switch and low molecular weight heparin carrying Celastrol and ferrocene for breast cancer treatment. *Int. J. Biol. Macromol.* 183, 2215–2226. doi:10.1016/j.ijbiomac.2021.05.204
- Qin, C., Shen, Y., Wang, B., Zhao, X., Liu, Y., Yang, S., et al. (2019). An acellular tissue matrix-based drug carriers with dual chemo-agents for colon cancer growth suppression. *Biomed. Pharmacother.* 117, 109048. doi:10.1016/j.biopha.2019.109048
- Qiu, H., Cao, S., and Xu, R. (2021). Cancer incidence, mortality, and burden in China: a time-trend analysis and comparison with the United States and United Kingdom based on the global epidemiological data released in 2020. *Cancer Commun. (Lond)* 41 (10), 1037–1048. doi:10.1002/cac2.12197
- Rehman, M. U., Khan, A., Imtiyaz, Z., Ali, S., Makeen, H. A., Rashid, S., et al. (2022). Current nano-therapeutic approaches ameliorating inflammation in cancer progression. *Semin. Cancer Biol.* 86 (2), 886–908. doi:10.1016/j.semcancer.2022.02.006
- Riley, R. S., June, C. H., Langer, R., and Mitchell, M. J. (2019). Delivery technologies for cancer immunotherapy. *Nat. Rev. Drug Discov.* 18 (3), 175–196. doi:10.1038/s41573-018-0006-z
- Roth, A. D., and Ajani, J. (2003). Docetaxel-based chemotherapy in the treatment of gastric cancer. *Ann. Oncol.* 14 (2), ii41–4. doi:10.1093/annonc/mdg728
- Rydz, J., Sikorska, W., Kyulavska, M., and Christova, D. (2014). Polyester-based (bio) degradable polymers as environmentally friendly materials for sustainable development. *Int. J. Mol. Sci.* 16 (1), 564–596. doi:10.3390/ijms16010564
- Shen, H., Liu, Q., Liu, D., Yu, S., Wang, X., and Yang, M. (2021). Fabrication of doxorubicin conjugated methoxy poly(ethylene glycol)-block-poly(ϵ -caprolactone) nanoparticles and study on their *in vitro* antitumor activities. *J. Biomater. Sci. Polym. Ed.* 32 (13), 1703–1717. doi:10.1080/09205063.2021.1937462
- Shive, M. S., and Anderson, J. M. (1997). Biodegradation and biocompatibility of PLA and PLGA microspheres. *Adv. Drug Deliv. Rev.* 28 (1), 5–24. doi:10.1016/s0169-409x(97)00048-3
- Siegel, R. L., Miller, K. D., Wagle, N. S., and Jemal, A. (2023). Cancer statistics, 2023. *CA Cancer J. Clin.* 73 (1), 17–48. doi:10.3322/caac.21763
- Sindhwani, S., Syed, A. M., Ngai, J., Kingston, B. R., Maiorino, L., Rothschild, J., et al. (2020). The entry of nanoparticles into solid tumours. *Nat. Mater* 19 (5), 566–575. doi:10.1038/s41563-019-0566-2
- Singhvi, M. S., Zinjarde, S. S., and Gokhale, D. V. (2019). Polylactic acid: synthesis and biomedical applications. *J. Appl. Microbiol.* 127 (6), 1612–1626. doi:10.1111/jam.14290
- Sonam Dongsar, T., Tsering Dongsar, T., Molugulu, N., Annadurai, S., Wahab, S., Gupta, N., et al. (2023). Targeted therapy of breast tumor by PLGA-based nanostructures: the versatile function in doxorubicin delivery. *Environ. Res.* 233, 116455. doi:10.1016/j.envres.2023.116455
- Sun, W., Fan, J., Wang, S., Kang, Y., Du, J., and Peng, X. (2018). Biodegradable drug-loaded hydroxyapatite nanotherapeutic agent for targeted drug release in tumors. *ACS Appl. Mater Interfaces* 10 (9), 7832–7840. doi:10.1021/acsami.7b19281
- Swami, R., Singh, I., Jeengar, M. K., Naidu, V. G., Khan, W., and Sistla, R. (2015). Adenosine conjugated lipidic nanoparticles for enhanced tumor targeting. *Int. J. Pharm.* 486 (1–2), 287–296. doi:10.1016/j.ijpharm.2015.03.065
- Tham, W. H., Wahit, M. U., Abdul Kadir, M. R., Wong, T. W., and Hassan, O. (2016). Polyol-based biodegradable polyesters: a short review. *Rev. Chem. Eng.* 32 (2). doi:10.1515/revce-2015-0035
- Tietjen, G. T., and Saltzman, W. M. (2015). Nanomedicine gets personal. *Nanomedicine gets Personal. Sci. Transl. Med.* 7 (314), 314fs47. doi:10.1126/scitranslmed.aad6645
- Truong, N. P., Whittaker, M. R., Mak, C. W., and Davis, T. P. (2015). The importance of nanoparticle shape in cancer drug delivery. *Expert Opin. Drug Deliv.* 12 (1), 129–142. doi:10.1517/17425247.2014.950564
- Wang, M., Hu, Q., Huang, J., Zhao, X., Shao, S., Zhang, F., et al. (2022). Engineered a dual-targeting biomimetic nanomedicine for pancreatic cancer chemimmunotherapy. *J. Nanobiotechnology* 20 (1), 85. doi:10.1186/s12951-022-01282-3
- Washington, K. E., Kularatne, R. N., Karmegam, V., Biewer, M. C., and Stefan, M. C. (2017). Recent advances in aliphatic polyesters for drug delivery applications. *Wiley Interdiscip. Rev. Nanomed Nanobiotechnol* 9 (4). doi:10.1002/wnan.1446
- Wen, P., Ke, W., Dirisala, A., Toh, K., Tanaka, M., and Li, J. (2023). Stealth and pseudo-stealth nanocarriers. *Adv. Drug Deliv. Rev.* 198, 114895. doi:10.1016/j.addr.2023.114895
- W.H. O (2023). Data visualization tools for exploring the global cancer burden in 2020. Available at: <https://gco.iarc.fr/today/home> (Accessed July 8, 2023).
- Wilhelm, S., Tavares, A. J., Dai, Q., Ohta, S., Audet, J., Dvorak, H. F., et al. (2016). *Analysis nanoparticle Deliv. tumours* 1 (5), 1–12. doi:10.1038/natrevmats.2016.14
- Williams, C. K. (2007). Synthesis of functionalized biodegradable polyesters. *Chem. Soc. Rev.* 36 (10), 1573–1580. doi:10.1039/b614342n
- Xiang, J., Shen, Y., Zhang, Y., Liu, X., Zhou, Q., Zhou, Z., et al. (2022). Multipotent poly(tertiary amine-oxide) micelles for efficient cancer drug delivery. *Adv. Sci. (Weinh)* 9 (12), e2200173. doi:10.1002/advs.202200173
- Xiao, H., Zheng, Y., Ma, L., Tian, L., and Sun, Q. (2021). Clinically-relevant ABC transporter for anti-cancer drug resistance. *Front. Pharmacol.* 12, 648407. doi:10.3389/fphar.2021.648407
- Xu, Z., Wang, D., Cheng, Y., Yang, M., and Wu, L. P. (2018). Polyester based nanovehicles for siRNA delivery. *Mater Sci. Eng. C Mater Biol. Appl.* 92, 1006–1015. doi:10.1016/j.msec.2018.05.031
- Xue, X., Qu, H., and Li, Y. (2022). Stimuli-responsive crosslinked nanomedicine for cancer treatment. *Exploration* 2 (6), 20210134. doi:10.1002/exp.20210134
- Yang, D. C., Yang, X. Z., Luo, C. M., Wen, L. F., Liu, J. Y., and Lin, Z. (2022). A promising strategy for synergistic cancer therapy by integrating a photosensitizer into a

- hypoxia-activated prodrug. *Eur. J. Med. Chem.* 243, 114749. doi:10.1016/j.ejmech.2022.114749
- Yao, Y., Zhou, Y., Liu, L., Xu, Y., Chen, Q., Wang, Y., et al. (2020). Nanoparticle-based drug delivery in cancer therapy and its role in overcoming drug resistance. *Front. Mol. Biosci.* 7, 193. doi:10.3389/fmolb.2020.00193
- Yi, Y., Lin, G., Chen, S., Liu, J., Zhang, H., and Mi, P. (2018). Polyester micelles for drug delivery and cancer theranostics: current achievements, progresses and future perspectives. *Mater. Sci. Eng. C Mater. Biol. Appl.* 83, 218–232. doi:10.1016/j.msec.2017.10.004
- Yoon, M. J., Cha, H., Ahn, J., Lee, D., Jeong, H. S., Koo, H. S., et al. (2021). Dysfunctional activity of classical DNA end-joining renders acquired resistance to carboplatin in human ovarian cancer cells. *Cancer Lett.* 520, 267–280. doi:10.1016/j.canlet.2021.08.003
- Yu, W., Maynard, E., Chiaradia, V., Arno, M. C., and Dove, A. P. (2021). Aliphatic polycarbonates from cyclic carbonate monomers and their application as biomaterials. *Chem. Rev.* 121 (18), 10865–10907. doi:10.1021/acs.chemrev.0c00883
- Zhang, B., Wan, S., Peng, X., Zhao, M., Li, S., Pu, Y., et al. (2020). Human serum albumin-based doxorubicin prodrug nanoparticles with tumor pH-responsive aggregation-enhanced retention and reduced cardiotoxicity. *J. Mater. Chem. B* 8 (17), 3939–3948. doi:10.1039/d0tb00327a
- Zhang, D., Liu, L., Wang, J., Zhang, H., Zhang, Z., Xing, G., et al. (2022). Drug-loaded PEG-PLGA nanoparticles for cancer treatment. *Front. Pharmacol.* 13, 990505. doi:10.3389/fphar.2022.990505
- Zhang, L., Li, Y., and Yu, J. C. (2014). Chemical modification of inorganic nanostructures for targeted and controlled drug delivery in cancer treatment. *J. Mater. Chem. B* 2 (5), 452–470. doi:10.1039/c3tb21196g
- Zhang, Q., Bao, J., Duan, T., Hu, M., He, Y., Wang, J., et al. (2022b). Nanomicelle-microsphere composite as a drug carrier to improve lung-targeting specificity for lung cancer. *Pharmaceutics* 14 (3), 510. doi:10.3390/pharmaceutics14030510
- Zhang, R., Jiang, Y., Hao, L., Yang, Y., Gao, Y., Zhang, N., et al. (2022c). CD44/Folate dual targeting receptor reductive response PLGA-based micelles for cancer therapy. *Front. Pharmacol.* 13, 829590. doi:10.3389/fphar.2022.829590
- Zhang, Z., Ji, Y., Hu, N., Yu, Q., Zhang, X., Li, J., et al. (2022a). Ferroptosis-induced anticancer effect of resveratrol with a biomimetic nano-delivery system in colorectal cancer treatment. *Asian J. Pharm. Sci.* 17 (5), 751–766. doi:10.1016/j.ajps.2022.07.006
- Zhao, J., Weng, G., Li, J., Zhu, J., and Zhao, J. (2018). Polyester-based nanoparticles for nucleic acid delivery. *Mater. Sci. Eng. C Mater. Biol. Appl.* 92, 983–994. doi:10.1016/j.msec.2018.07.027
- Zhao, M., Wang, R., Yang, K., Jiang, Y., Peng, Y., Li, Y., et al. (2023). Nucleic acid nanoassembly-enhanced RNA therapeutics and diagnosis. *Acta Pharm. Sin. B* 13 (3), 916–941. doi:10.1016/j.apsb.2022.10.019
- Zhao, X., Yang, X., Wang, X., Zhao, X., Zhang, Y., Liu, S., et al. (2021). Penetration cascade of size switchable nanosystem in desmoplastic stroma for improved pancreatic cancer therapy. *ACS Nano* 15 (9), 14149–14161. doi:10.1021/acsnano.0c08860
- Zheng, P., Liu, Y., Chen, J., Xu, W., Li, G., and Ding, J. (2020). Targeted pH-responsive polyion complex micelle for controlled intracellular drug delivery. *Chin. Chem. Lett.* 31 (5), 1178–1182. doi:10.1016/j.ccllet.2019.12.001
- Zhu, S., Xing, H., Gordiichuk, P., Park, J., and Mirkin, C. A. (2018). PLGA spherical nucleic acids. *Adv. Mater.* 30 (22), e1707113. doi:10.1002/adma.201707113



OPEN ACCESS

EDITED BY

Shuai Jiang,
Ocean University of China, China

REVIEWED BY

Bhupendra Gopalbhai Prajapati,
Ganpat University, India
Mohankumar Ramar,
University of Connecticut, United States
Madawamy Muthu,
Indian Institute of Technology (BHU),
India
Ubaidulla Uthumansha,
B. S. Abdur Rahman Crescent Institute of
Science And Technology, India

*CORRESPONDENCE

P.S. Rajinikanth,
✉ aoqiang@scu.edu.cn
Qiang Ao,
✉ psrajinikanth222@gmail.com

RECEIVED 26 September 2023

ACCEPTED 23 October 2023

PUBLISHED 09 November 2023

CITATION

Anjum S, Arya DK, Saeed M, Ali D,
Athar MS, Yulin W, Alarifi S, Wu X,
Rajinikanth PS and Ao Q (2023),
Multifunctional electrospun nanofibrous
scaffold enriched with alendronate and
hydroxyapatite for balancing osteogenic
and osteoclast activity to promote
bone regeneration.
Front. Bioeng. Biotechnol. 11:1302594.
doi: 10.3389/fbioe.2023.1302594

COPYRIGHT

© 2023 Anjum, Arya, Saeed, Ali, Athar,
Yulin, Alarifi, Wu, Rajinikanth and Ao. This
is an open-access article distributed
under the terms of the [Creative
Commons Attribution License \(CC BY\)](https://creativecommons.org/licenses/by/4.0/).
The use, distribution or reproduction in
other forums is permitted, provided the
original author(s) and the copyright
owner(s) are credited and that the original
publication in this journal is cited, in
accordance with accepted academic
practice. No use, distribution or
reproduction is permitted which does not
comply with these terms.

Multifunctional electrospun nanofibrous scaffold enriched with alendronate and hydroxyapatite for balancing osteogenic and osteoclast activity to promote bone regeneration

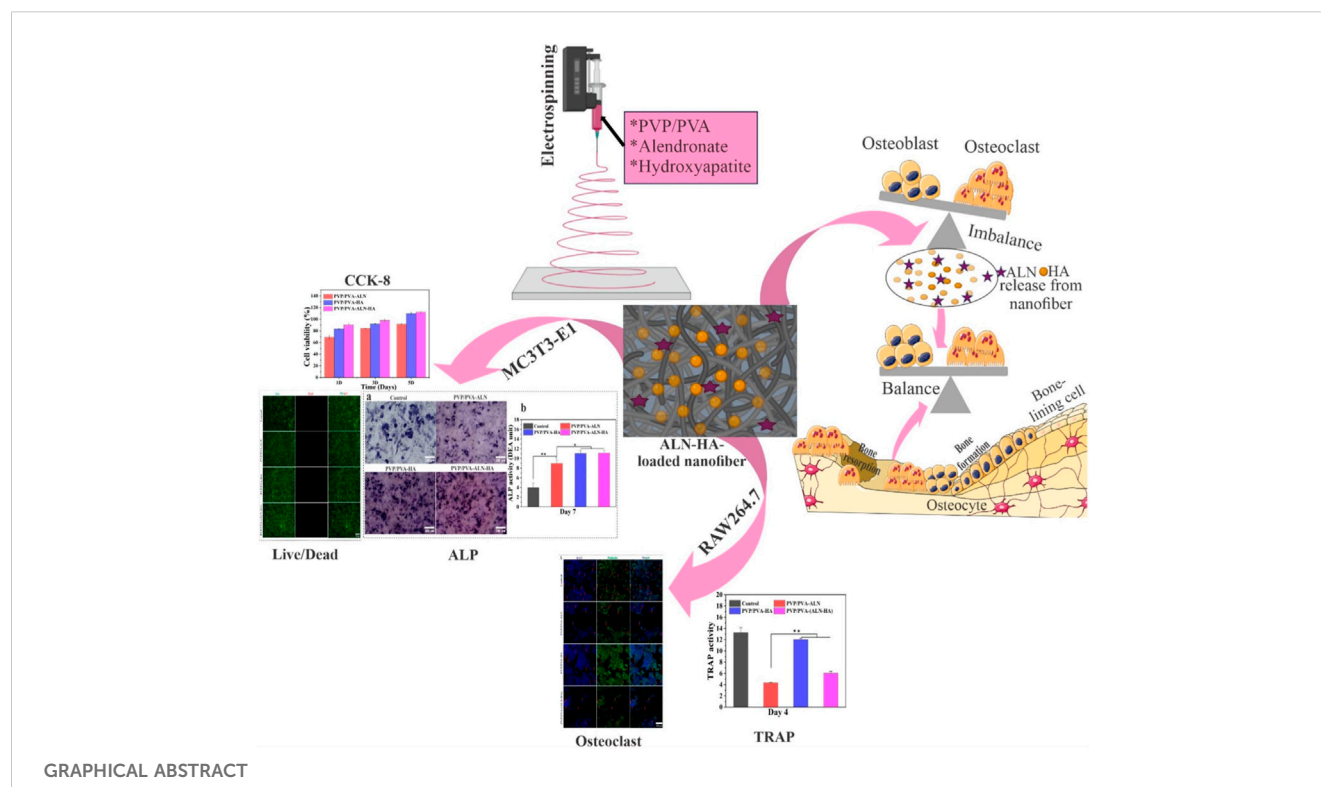
Shabnam Anjum^{1,2}, Dilip Kumar Arya³, Mohammad Saeed⁴,
Daoud Ali⁵, Mohammad Saud Athar⁶, Wang Yulin², Saud Alarifi⁵,
Xixi Wu², P.S. Rajinikanth^{3*} and Qiang Ao^{1,2*}

¹Department of Tissue Engineering, School of Intelligent Medicine, China Medical University, Shenyang, Liaoning, China, ²NMPA Key Laboratory for Quality Research and Control of Tissue Regenerative Biomaterial, Institute of Regulatory Science for Medical Device, National Engineering Research Center for Biomaterials, Sichuan University, Chengdu, Sichuan, China, ³Department of Pharmaceutical Sciences, Babasaheb Bhimrao Ambedkar University, Lucknow, India, ⁴Department of Pharmacology, Dr. A.P.J. Abdul Kalam Technical University, Lucknow, India, ⁵Department of Zoology, College of Science, King Saud University, Riyadh, Saudi Arabia, ⁶Department of Chemistry, Aligarh Muslim University, Aligarh, India

Electrospun composite nanofiber scaffolds are well known for their bone and tissue regeneration applications. This research is focused on the development of PVP and PVA nanofiber composite scaffolds enriched with hydroxyapatite (HA) nanoparticles and alendronate (ALN) using the electrospinning technique. The developed nanofiber scaffolds were investigated for their physicochemical as well as bone regeneration potential. The results obtained from particle size, zeta potential, SEM and EDX analysis of HA nanoparticles confirmed their successful fabrication. Further, SEM analysis verified nanofiber's diameters within 200–250 nm, while EDX analysis confirmed the successful incorporation of HA and ALN into the scaffolds. XRD and TGA analysis revealed the amorphous and thermally stable nature of the nanofiber composite scaffolds. Contact angle, FTIR analysis, Swelling and biodegradability studies revealed the hydrophilicity, chemical compatibility, suitable water uptake capacity and increased *in-vitro* degradation making it appropriate for tissue regeneration. The addition of HA into nanofiber scaffolds enhanced the physiochemical properties. Additionally, hemolysis cell viability, cell adhesion and proliferation by SEM as well as confocal microscopy and live/dead assay results demonstrated the non-toxic and biocompatibility behavior of nanofiber scaffolds. Alkaline phosphatase (ALP) and tartrate-resistant acid phosphatase (TRAP) assays demonstrated osteoblast promotion and osteoclast inhibition, respectively. These findings suggest that developed HA and ALN-loaded PVP/PVA-ALN-HA nanofiber composite scaffolds hold significant promise for bone regeneration applications.

KEYWORDS

electrospinning, alendronate, hydroxyapatite nanoparticle, nanofibrous scaffold, bone regeneration



1 Introduction

The use of biomaterial-based bone grafts as alternatives for natural bone healing is common, and they have several benefits over previous grafting methods. The shattered bone underwent ineffective self-healing and slow auto-regeneration. Maintaining the immunological microenvironment's regulation, balancing the interplay between bone formation and resorption, and establishing a functional neovascularization network are crucial factors. The formidable task lies in creating a remarkably bioactive scaffold for bone tissue engineering, capable of orchestrating the bone remodeling process to effectively enhance bone regeneration (Zhu et al., 2021). Bone remodeling constitutes an intricate biochemical response involving the osteoclast-driven bone resorption and osteoblast-mediated bone formation processes. It is important to highlight that several bone tissue regeneration frameworks have focused solely on stimulating the differentiation of bone stem cells to encourage bone reformation, often overlooking the interdependent interplay between bone resorption (osteoclasts) and bone formation (osteoblasts). Research prior to this has demonstrated that concurrently administering bone morphogenetic proteins (BMPs) and connective tissue growth factor (CTGF) remarkably augments the process of bone remodeling and accelerates the healing process (Cheng et al., 2019). Additionally, this approach predominantly emphasizes bone reformation through the stimulation of bone stem cell differentiation and the facilitation of angiogenesis. However, it tends to overlook the significant impact of osteoclastogenesis on the overall process of bone healing.

Nowadays, biomaterial-based bone grafts have gained extensive utilization as substitutes for bone healing. These grafts offer

numerous advantages compared to alternatives developed using different grafting methodologies (Ahmed et al., 2021). Tissue engineering concepts have introduced fresh possibilities through the combination of suitable scaffolds, cells, and growth factors. These innovative strategies use scaffolds for regenerative purposes in the repair of damaged tissues (Anand et al., 2023). Extensive research has demonstrated that the electrospinning technique is a superb method for producing nanofibers characterized by finely controllable hierarchical structures and desirable constituents (Anand et al., 2022a; Thakur et al., 2023). The electrospun nanofibers possess a distinctive hierarchical micro/nanofiber architecture, which incorporates a highly porous structure. This configuration facilitates exceptional transmission of essential elements such as nutrients, oxygen, growth factors, and waste materials (Pandey et al., 2023; Singh et al., 2023). Their effectiveness in supporting bone regeneration hinges on their pivotal contributions to cell recruitment, cytokine release, and the transport of oxygen, nutrients, and metabolic waste. The absence of these functions would render successful bone regeneration unachievable (Jin et al., 2022; Sadeghi et al., 2022). The remarkable mechanical properties of nanofibers establish them as temporary mechanical barriers, effectively thwarting the undesirable migration of fibroblasts. Simultaneously, they promote the proliferation and differentiation of osteoblasts, crucial for the generation of new bone tissue.

Electrospun composites are crafted to harness the benefits of diverse materials within a single scaffold, aiming to capitalize on their combined advantages. Numerous polymer blends and composites have been successfully electrospun into unified mats through the utilization of both single and twin extrusion systems.

Among these, PVA and PVP have excellent material properties in biomedical applications. PVA has exceptional features such as good biocompatibility, suitable degradability, good chemical resistance properties and hydrophilicity (Chahal et al., 2016). In addition, PVP is biocompatible and nontoxic, and has better blending abilities with other materials, to form composite materials. The Hydroxyl group of PVA and the proton accepting carboxyl groups of PVP intend to interact with each other to form a polymeric scaffold with good mechanical properties and controlled solubility (Chaudhuri et al., 2016). The fabricated composite scaffold consisting of bioactive polymers and ceramics will be further exposed to the differentiation and proliferation of osteoblasts for artificial bone formation.

HA, a predominant constituent of bones, stands as a biomaterial valued for its notable biocompatibility and osteoconductivity. Among ceramic bone grafts, HA is widely employed and serves as a suitable coating for orthopaedic implants but HA exhibits limitations in terms of its slow biodegradability and relatively modest mechanical properties. (Brannigan and Griffin, 2016; Anjum et al., 2022). Notably, combining HA with scaffolds has been shown to create an optimal microenvironment, closely mimicking the natural bone conditions (Balaji Raghavendran et al., 2014). Beyond this, HA particles have been explored as carriers for diverse drugs and proteins, including antibiotics and growth factors (Brannigan and Griffin, 2016).

ALN is a member of nitrogen containing bisphosphonate. It contains two side chains, one (-OH) is responsible for bone affinity and second one $-(CH_2)_3-NH_2$ is responsible for antiresorptive capacity (Gong et al., 2011). It is used as an amino-bisphosphonate medication that may be useful in treating conditions including osteoporosis, Paget's disease, hypercalcemia from malignancies, metastatic bone disease, and hypercalcemia from periodontal disease that are characterized by aberrant bone turnover (Balaji Raghavendran et al., 2014). ALN is found to be more potential and specific due to the presence of a primary amino group in the side chain (Palazzo et al., 2007). Many researchers have documented and substantiated the efficacy of ALN, both *in vitro* and *in vivo*, as a potent inhibitor of bone resorption. This effectiveness stems from its ability to suppress osteoclast activity (Drake, Clarke, and Khosla, 2008; Gong et al., 2011). However, due to its hydrophilic nature and intense polarity, ALN has low bioavailability in aqueous circumstances, which is one of its main drawbacks. An intriguing observation lies in ALN's robust affinity for HA, opening the possibility of hybridizing the two to address the challenge of low bioavailability (Al-Baadani et al., 2022; Klara and Joanna, 2022). Furthermore, the calcium phosphate crystals present in HA exhibit a strong binding capability with ALN molecules, leading to an optimal loading of ALN. For instance, Shen et al. devised ALN-loaded HA titanium dioxide nanotubes, ensuring a controlled drug release that enhanced bone regeneration around implants in an osteoporosis model (Shi et al., 2009; Shen et al., 2016; Wang et al., 2019). In another investigation, Qu et al. successfully incorporated ALN into ultrahigh molecular weight polyethylene, achieving a sustained local release that effectively prevented osteolysis stemming from artificial joint wear (Yang et al., 2012). Assessing the osteogenic effects, Young et al. cultivated adipose-derived stem cells on ALN-loaded PCL nanofibrous scaffolds, revealing promising results with the 10% ALN/PCL scaffolds demonstrating significant alkaline

phosphatase activity. These findings highlight the favourable impact of ALN/PCL nanofibrous scaffolds on bone regeneration (Yun et al., 2014).

In this research, the PVP/PVA nanofiber scaffolds loaded with ALN and HA was fabricated and characterized for its physicochemical properties, haemocompatibility, cytocompatibility (e.g., cell adhesion and proliferation on MC3T3-E1 bone cell line) and osteogenic and osteoclast activity.

2 Materials and methods

2.1 Materials

PVA (Mw: 80,000), PVP (Mw: 90,000), Alendronate sodium (Mw: 325.12), Calcium hydroxide $Ca(OH)_2$ and Ortho-phosphoric acid (H_3PO_4) were purchased from Macklin Biochemical Co. Ltd. (P.R. China). Cell Counting Kit-8 purchased from KeyGEN BioTECH (China). MC3T3-E1 and RAW 264.7 cell lines were gift sample from professor Huang Zhongbing (Biomedical Engineering College; Sichuan University). All additional chemicals and reagents employed in the study were of analytical grade.

2.2 Synthesis of hydroxyapatite nanoparticle

The preparation of HA nanoparticles were carried out by the following procedure outlined in a previous reference (Ganachari et al., 2016). To elaborate briefly, aqueous solutions of 0.3 M H_3PO_4 and 0.5 M $Ca(OH)_2$ were meticulously prepared. The H_3PO_4 solution was meticulously loaded into a burette, while the calcium hydroxide $Ca(OH)_2$ solution was placed within a conical flask, ensuring thorough dissolution of all lime particles in water. The H_3PO_4 solution was then cautiously added drop by drop, maintaining a rate of approximately 2 mL/min, to the $Ca(OH)_2$ solution. Throughout the process, the pH was gauged using a pH meter and upheld within a basic range through the introduction of ammonium hydroxide. The experimental conditions encompassed a temperature between 40°C and 45°C, pH between 8.5 and 10, and the solution was kept in continuous agitation. As the solution turned milky, it was left to undergo a 24 h ageing period, resulting in the formation of a precipitate. This precipitate was subsequently vacuum-dried at 60°C for an overnight duration. The experiment meticulously maintained a stoichiometric Ca/P ratio, while the basic medium was upheld for result comparison purposes.

2.3 Fabrication of PVP/PVA-ALN-HA nanofiber composite scaffold

The optimal concentrations for the electrospinning solutions have been detailed in Table 1. The PVP/PVA-ALN-HA nanofiber scaffold was prepared by the selection of optimum concentration of PVP/PVA nanofiber suitable for electrospinning. Initially, 12% PVP and 8% PVA solutions were made in 90% acetic acid and distilled water, respectively, under continuous stirring for 8 h, in a ratio of 50/

TABLE 1 Optimized concentration of polymers and drug solution for electrospinning.

| Formulation | PVA (%) | PVP (%) | Ratio | HA | ALN |
|----------------|---------|---------|-------|----|-----|
| PVA-PVP-HA | 8 | 12 | 50/50 | 2% | - |
| PVA-PVP-ALN | 8 | 12 | 50/50 | - | 2% |
| PVA-PVP-ALN-HA | 8 | 12 | 50/50 | 2% | 2% |

50 to prepare homogenous blends for electrospinning. The electrospinning solution for PVP-PVA-ALN-HA was generated by dissolving 2% ALN and 2% HA, combined at a 1:1 ratio (ALN 200 mg and HA 200 mg), in 10 mL of 90% acetic acid through ultrasonic dispersion for 30 min. Subsequently, 1.2 g of PVP was introduced to this solution, and after 1.5 h, 10 mL of 8% PVA solution was incorporated into the PVP-ALN-HA mixture. The resultant solution was then vigorously stirred until it achieved transparency.

The formulated solutions were loaded into a 10 mL syringe outfitted with a stainless-steel needle featuring an inner diameter of 0.4 mm. A positive electrode was connected to the needle to administer high-voltage power. A flat collector, enveloped in aluminum foil, was utilized to gather the nanofibers and was placed 10 cm away from the spinning electrode. Regulating the electrospinning procedure, the flow rate of the syringe pump was calibrated to 2 mL/h, and the solutions were propelled using a robust electric voltage of 22 kV.

2.4 Physiochemical characterization

2.4.1 Particle size distribution and zeta potential analysis

The particle size and zeta potential of the nanoparticles were assessed using a Malvern Instrument Zetasizer, nano-series, which employs laser Doppler anemometry and photon correlation spectroscopy. A quantity of 0.01 mg of the sample was introduced into 20 mL of water, and subsequently, 2 mL of the resulting solution underwent sonication. The sample was then moved to a cuvette for the determination of size and zeta potential at room temperature (Rajinikanth, Sankar, and Mishra, 2003; Al-Baadani et al., 2022; Deepak et al., 2023).

2.4.2 Scanning electron microscopy (SEM) and energy dispersive X-ray spectroscopy (EDX) analysis

SEM (S4800; Hitachi Japan) was employed to characterize the morphology of the electrospun nanofiber batches. In this study, nanofiber samples were affixed onto SEM specimen stubs using double-sided carbon tape and subsequently coated with an Au-Pd layer via sputtering for 60 s. The analysis was conducted at varying magnifications and an accelerating voltage. For diameter determination, ImageJ software was employed, measuring the nanofiber scaffolds' diameter at multiple locations. An EDS (S4800; Hitachi Japan) was also employed to analyse the elemental composition and distribution within the nanofiber scaffolds (Pandey et al., 2022; Yadav et al., 2022).

2.4.3 Determination of λ_{\max} of alendronate by UV–visible spectrophotometer

Spectroscopic analysis of alendronate was performed by a UV/Vis-spectrophotometer (U-3010; Hitachi Japan) in the UV range 200–800 nm for determining λ_{\max} . For this analysis, an alendronate sodium standard solution, (1 mg/mL) was prepared in distilled water. Aliquots of stock solution were transferred to a 10 mL of volumetric flask using a micropipette to give final concentration of 5, 10, 15, 20, 25, and 30 $\mu\text{g/mL}$. Since the ALN standard curve was unable to be established directly, the medium needed to be reacted with ninhydrin, as reported in previous literature [25]. 2.5 mL of 0.2% ninhydrin solution, 0.5 mL of 0.05 M sodium bicarbonate (NaHCO_3) and the mixture was mixed well and heated in a water bath at $95^\circ\text{C} \pm 5^\circ\text{C}$ for 35 min, resulting in purple solution. The flasks were cooled and the volume was made up to the mark with distilled water. The absorbance was measured at 568 nm against a reagent blank. Regression equation, correlation coefficient, slope and intercept were calculated from the graph.

2.4.4 FTIR (fourier transform infrared spectroscopy)

FTIR (NEXUS 670; NICOLET, United States) was used to determine the constituting functional groups of different nanofibers. The structural changes occurring during electrospinning, blending, coating, etc. were scanned by FTIR, using standard KBr crystal at room temperature. The spectra were acquired in transmission mode spanning a wavenumber range from 4,000 to 400 cm^{-1} , utilizing a resolution of 4 cm^{-1} (Anand et al., 2022b).

2.4.5 XRD (X-ray diffraction)

The crystalline and amorphous characteristics of the synthesized nanomaterials and scaffolds were ascertained via X-ray diffractometer (DX-1000; PHILIPS United States). Samples were positioned on quartz zero background holders within a standard XRD setup. A solid-state Germanium detector cooled by liquid nitrogen was employed, and Cu K-alpha radiation at 45 kV and 40 mA current was utilized. Patterns were acquired across a 2θ range of 5° – 80° at a scan rate of 2° per minute (Rajinikanth and Jestin, 2016).

2.4.6 TGA (thermo-gravimetric analysis)

TGA (TGA/DSC 2/1600-ThermoStar; METTLER TOLEDO, Switzerland) was used to employed thermal stability of different nanofibers. All samples were heated at a rate of $10^\circ\text{C min}^{-1}$ in a range of 25°C – 800°C under a nitrogen atmosphere (Athar et al., 2023).

2.4.7 Mechanical testing

The mechanical characteristics of the nanofibrous mats were assessed using a universal Testing Machine (UTM) (YG005A; Baier Instrument China) equipped with a 5 cN capacity load cell. Nanofibrous samples ($n = 3$) were cut into dimensions of 1 mm width and 20 mm length. These samples were positioned between two clamps and subjected to tensile displacement at a crosshead speed of 8 mm/min. From the stress-strain curve, the Young's modulus, tensile strength, and elongation at break of the samples were determined.

2.4.8 Hydrophilicity characterization by contact angle

The angle formed between the solid surface and the interface of the liquid or vapour is termed the contact angle (CA). The surface's wetting properties, indicating its hydrophilicity or hydrophobicity, were assessed using a water contact angle instrument (JC 2000C1; POWEREACH China). To perform this evaluation, the sample was positioned on a flat surface, followed by carefully placing a water droplet onto it using a moving needle. The spherical image of the droplet was captured by a digital camera and projected onto a monitor, allowing for the measurement of the contact angle between the droplet and the nanofiber web surface. For data analysis, at least three measurements were taken at different locations on the film, and the values were averaged.

2.4.9 *In vitro* drug release

To investigate drug release from the prepared nanofibers, the mats were cut into $1 \times 1 \text{ cm}^2$ sections and incubated in 10 mL of Phosphate buffer saline (PBS at pH 7.4). The incubation was conducted at 37°C with a shaking rate of 100 rpm in a thermostatic shaking incubator. Subsequently, 2 mL aliquots of the sample were withdrawn at predetermined time intervals (1, 2, 3, 4, 5, 6, 8, 10, 12 and 14 days), and equivalent volumes of fresh PBS were introduced to maintain a sink condition (Wu et al., 2014). The release of alendronate from different nanofiber groups was quantified using UV-visible spectroscopy, following a procedure outlined in another study (Gao et al., 2016). In essence, 1 mL of the release medium was combined with 2.5 mL of a 0.2% ninhydrin solution and 0.5 mL of 0.05 M NaHCO_3 . This mixture was thoroughly mixed and heated in a water bath at $95^\circ\text{C} \pm 5^\circ\text{C}$ for 35 min, resulting in a purple solution of 4 mL. Finally, the purple solution was diluted with deionized water to a final volume of 5 mL, and the absorbance at 568 nm was measured.

2.4.10 *In vitro* degradation

The degradation pattern of the nanofibers was examined by observing the weight loss at various time intervals. Scaffolds measuring $1 \times 1 \text{ cm}^2$ were meticulously weighed (W_i) and then placed within 5 mL plastic tubes, each containing 4 mL of PBS solution with a pH of 7.4. These tubes were subsequently positioned in a shaking incubator at a speed of 100 rpm and a temperature of 37°C . The incubation media were changed on a weekly basis. At predetermined time points, the samples were subjected to drying until a consistent weight was achieved (W_f) (Agarwal et al., 2021). The weight loss percentage (%) was determined using the formula:

$$\text{Weight loss (\%)} = \frac{W_i - W_f}{W_i} \times 100$$

Where W_i = initial weight of the sample and W_f = final weight after degradation.

2.4.11 Water uptake capacity

The water retention ability of the scaffolds was assessed through the calculation of the swelling ratio. Initially, the samples were cut into dimensions of $1 \times 1 \text{ cm}^2$, and their dry weight (W_d) was determined using an electronic weighing balance and duly recorded. Subsequently, these samples were immersed in PBS with a pH of 7.4 at room temperature. At specified intervals, the

samples were taken out of the solution and placed on tissue paper to eliminate any excess water clinging to the nanofiber surface. The wet weight of the nanofibers (W_w) was promptly measured. All measurements were conducted in triplicate, and the water uptake capacity was calculated using the following equation:

$$\% \text{Water uptake capacity} = \frac{W_w - W_d}{W_d} \times 100$$

Where W_w = weight of the wet nanofiber scaffold and W_d = dried weight.

A triplicate study was performed, and the average value was taken as the percentage of water uptake.

2.5 Hemolysis study

To determine the hemocompatibility of a developed PVP/PVA nanofiber scaffold loaded with ALN and HA encompassed the utilization of freshly obtained blood samples from healthy rats. Blood is a gift from professor Huang Zhongbing, (Biomedical Engineering College; Sichuan University). Blood specimens (5 mL each) were collected into heparin-coated tubes and subsequently subjected to centrifugation at 3,000 rpm, resulting in the separation of plasma from the red blood cells (RBCs) pellets settled at the bottom of the tubes. Careful removal of the liquid above the sediment was followed by the introduction of PBS into the tubes. Another round of centrifugation was employed to isolate the re-suspended RBCs. The resultant refined blood cells were diluted to attain a final volume of 25 mL, thus creating an RBCs suspension in PBS. Subsequently, 0.5 mL of this RBC suspension was divided into five 1.5 mL tubes. Within this set, two tubes were marked as negative control (PBS) with a pH of 7.4 and positive controls (water), received 1 mL, respectively. The remaining three tubes underwent treatment with nanofibers (PVP/PVA-ALN, PVP/PVA-HA and PVP/PVA-ALN-HA) sized at $1 \times 1 \text{ cm}^2$. All the tubes, encompassing both control and treated samples, were incubated at 37°C for a duration of 3 h. Following this incubation period, all tubes were centrifuged at 3,000 rpm for 10 min. After the incubation and centrifugation steps, 200 μL of the supernatant from each sample was transferred into a 96-well plate, enabling the measurement of haemoglobin absorption at a wavelength of 540 nm.

2.6 *In vitro* biological evaluation

2.6.1 Scaffold sterilization

Prior to the cell-seeding process, it is crucial to sterilize the nanofibers. The procedure involved submerging the samples in 70% ethanol and subjecting them to ultraviolet (UV) light exposure on both sides for a duration of 30 min. Following this, the ethanol was eliminated, and the samples were rinsed with PBS three times before initiating the cell culture experiments.

2.6.2 Cell culture and seeding

MC3T3-E1 cells were maintained in α -MEM (Gibco; United States) containing 10% foetal bovine serum (Amresco; United States) and 1% penicillin-streptomycin (Gibco; United States), and incubated at 37°C under a 5% CO_2 atmosphere.

2.6.3 *In vitro* cytotoxicity (CCK-8 assay)

Cell proliferation and viability of MC3T3-E1 cells were assessed using the Cell Counting Kit-8 in accordance with the manufacturer's instructions. In triplicate, MC3T3-E1 cells (1×10^4 cells/well) were seeded onto various nanofibers. Following cell culture in 96-well plates for 1, 3, and 5 days, a CCK-8 solution was introduced to each well. After a 2 h incubation at 37°C, the optical density (OD) at 450 nm was measured using a microplate reader (Thermo Fisher). Cell viability was determined using the following formula:

$$\text{Cell viability (\%)} = \frac{OD_{\text{Scaffold}}}{OD_{\text{Control}}} \times 100\%$$

2.6.4 Live/dead staining

To further determine the cytocompatibility of the fabricated scaffolds, MC3T3-E1 cells (1×10^4 cells/well) were cultured for 3 days on the scaffolds. After incubation, the samples were washed thrice with PBS and stained with acetoxymethyl ester of calcein (calcein AM) and propidium iodide (PI) staining solution (Solarbio; China) for 20 min in the dark. Next, images were captured using by Inverted fluorescence microscope (Nikon).

2.6.5 Cell adhesion and morphology

The investigation of cell adhesion was conducted using MC3T3-E1 cells cultured on PVP/PVA nanofiber scaffolds incorporating ALN and HA. Cell adhesion was assessed through the examination of adhered cell morphology. Nanofiber samples measuring 1×1 cm² in diameter were positioned in 48-well culture plates. MC3T3-E1 cells (1×10^4 cells/well) were cultured on fabricated scaffolds for 1 and 3 days. Following the designated incubation period, the culture medium was aspirated, and the cells were gently rinsed 3 times with PBS to remove any non-adherent cells. Subsequently, the adherent cells were fixed with a solution of 4% paraformaldehyde for 15 min at room temperature followed by permeabilization with 0.1% Triton X-100 for 5 min. Finally, the adhered cells were then air-dried, sputter-coated with gold or platinum, and the morphology was analysed by SEM.

The cell adhesion was also analyzed by visualizing the morphology of the adhered cells by staining the actin cytoskeleton structures. After the cell fixation, the scaffolds were stained with DAPI (Solarbio; China) and phalloidin (Solarbio; China) for 10 min and 1 h, respectively, at room temperature. The images were captured using confocal laser scanning microscopy (CLSM) (LSM880 Airyscan with STEDYCON; Carl Zeiss Germany) with 405 nm (blue, DAPI) and 561 nm (green, phalloidin) excitation filters.

2.6.6 Alkaline phosphatase (ALP) activity

To assess the early osteogenic differentiation potential of MC3T3-E1 cells, ALP activity was carried out [16]. In 48-well plates, MC3T3-E1 cells at a density of 1×10^4 cells per well were cultured on various nanofibers for 7 days. After the addition of a 1% Triton X-100 (Solarbio; China) solution, proteins were extracted. The resulting cell lysates underwent centrifugation at 12,000 rpm for 10 min, yielding supernatant for the ALP test. The Alkaline Phosphatase Assay Kit (Beyotime; China) was employed to measure ALP activity. The optical density (OD) values at 520 nm were determined using a spectrophotometric microplate reader.

For ALP staining, the adherent cells were fixed using 4% paraformaldehyde (Solarbio; China) and then subjected to staining using a BICP/NBP ALP Stain Development Kit following the manufacturer's instructions (Beyotime; China). Representative images were captured using an inverted fluorescence microscope (Nikon).

2.6.7 Osteoclast formation

RAW 264.7 cells (3×10^4 cells/cm²) were seeded onto different nanofiber membranes in 48-well plates and cultured in DMEM (high glucose) medium supplemented with 10% foetal bovine serum (FBS). This medium was enriched with 50 ng/mL RANKL and 20 ng/mL MCSF for a period of 4 days. Subsequently, the cytoskeleton and nuclei of the adherent cells were fixed and stained using phalloidin and DAPI, respectively. The stained cells were examined using CLSM.

Additionally, the TRAP activity of the RAW 264.7 cells was evaluated using a TRAP Assay Kit (Beyotime, China) following the manufacturer's instructions. The assessment was conducted using a spectrophotometric microplate reader, measuring the absorbance at 405 nm (Gong et al., 2011).

2.7 Statistical analysis

The experimental data in this study were presented as Mean \pm SD, with a sample size of $n = 3$. Data analysis included the use of a one-way ANOVA followed by the Bonferroni multiple comparison test, conducted using OriginPro 2019b software. Statistical significance was indicated by a p -value of less than 0.05, denoted as *, while p -values less than 0.01 were indicated as **, representing high significance. In cases where the p -value was less than 0.001, the significance was considered very high and denoted as ***.

3 Result and discussion

3.1 Particle size distribution and zeta potential analysis of HA nanoparticle

The particle size distribution and zeta potential analysis of the HA sample is presented in Figure 1. The analysis revealed a wide peak of sizes spanning from 100 to 300 nm, accompanied by a polydispersity index (PDI) of 0.306. The average size of the HA particles was measured at 241.2 nm. The zeta potential of the HA sample was determined to be -0.11 mV.

3.2 Morphology of nanofibers and HA

The morphological assessment of nanofibers, encompassing characteristics such as fibre shape, diameter, and surface structure, was carried out through SEM. This analysis unveiled the topographical features of nanofibers, a crucial factor influencing initial cell interactions like adhesion and proliferation (Teixeira et al., 2004). To explore the morphology of both pure HA and the composite nanofibers, the prepared scaffolds were subjected to SEM analysis (Figure 2). SEM images of PVP/PVA-ALN, PVP/

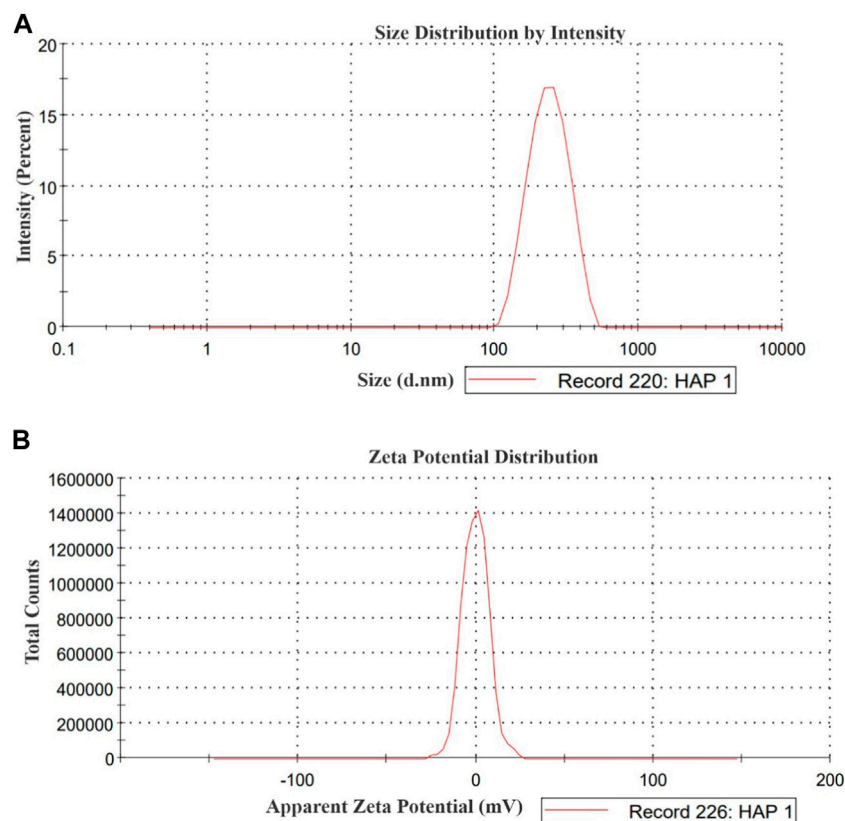


FIGURE 1

(A) Particle size distribution and (B) Zeta potential of HA nanoparticle.

PVA-HA, and PVP/PVA-ALN-HA showcased uniform nanofiber sizes that were randomly distributed, devoid of any bead defects (Figures 2A–C).

ALN and HA nanoparticles were successfully incorporated homogeneously into the nanofibers evidenced by SEM images. Additionally, HA particles were integrated within the structure of blend nanofiber scaffolds and appeared to have a rougher surface compared to PVP/PVA-ALN fibers, indicating the successful incorporation of HA into nanofibers. Visible aggregation of ALN-HA or HA can be observed within the nanofibers, as indicated by the red arrows as shown in Figures 2B, C. The rough surface of HA loaded nanofiber may be beneficial for cell attachment and proliferation.

The average diameters of the PVP/PVA-ALN, PVP/PVA-HA, and PVP/PVA-ALN-HA composite nanofibers were measured to be 208.53, 233.95, and 200.93 nm, respectively (Figures 2D–F). The data indicated that there was no notable distinction in nanofiber size between PVP/PVA-ALN, PVP/PVA-HA and PVP/PVA-ALN-HA. The SEM findings for the synthesized HA nanoparticles indicated grain sizes spanning from 50 to 250 nm, as displayed in Figure 2G. EDX results showed that HA nanoparticles had a Ca/P ratio of 1.55, very close to natural bone (Figure 2H). Further confirmation of the presence of HA and ALN within the PVP/PVA-ALN-HA nanofibers was attained through EDX spectra analysis (Figure 2I). The peaks attributed to sodium (Na) and phosphorus (P) could be attributed to the presence of both ALN and HA, while the calcium (Ca) peak

indicated the integration of HA particles within the PVP/PVA nanofiber. Elemental analysis resulted in a Ca/P ratio of 1.86, closely resembling the stoichiometric ratio found in HA and approaching the ratio of 1.67 observed in natural bone tissue. This finding verifies the successful incorporation of ALN and HA within the nanofiber structure.

The nanofibrous scaffold, produced through the electrospinning process in this study, exhibited uniform orientation, interconnecting pores, and a web-like porous structure. This structural feature was crucial for facilitating oxygen exchange, fluid flow, nutrient transport, fibroblast infiltration, cell adhesion, and attachment. The outcomes demonstrated that the hybrid nanofibers developed possessed the desired physical and structural attributes necessary for bone tissue regeneration (BTR).

3.3 Physiochemical properties

3.3.1 λ_{\max} validation of ALN

Alendronate contains a primary aliphatic amino group which is known to react with ninhydrin reagent. This reagent is used for the determination of primary amines and amino acids. UV-vis absorption spectrum of the purple-colour complex produced by the reaction of ninhydrin with alendronate was recorded in the range from 200 to 800 nm against reagent blank. The maximum absorbance λ_{\max} was found at 568 nm (Figures 3A–C). The

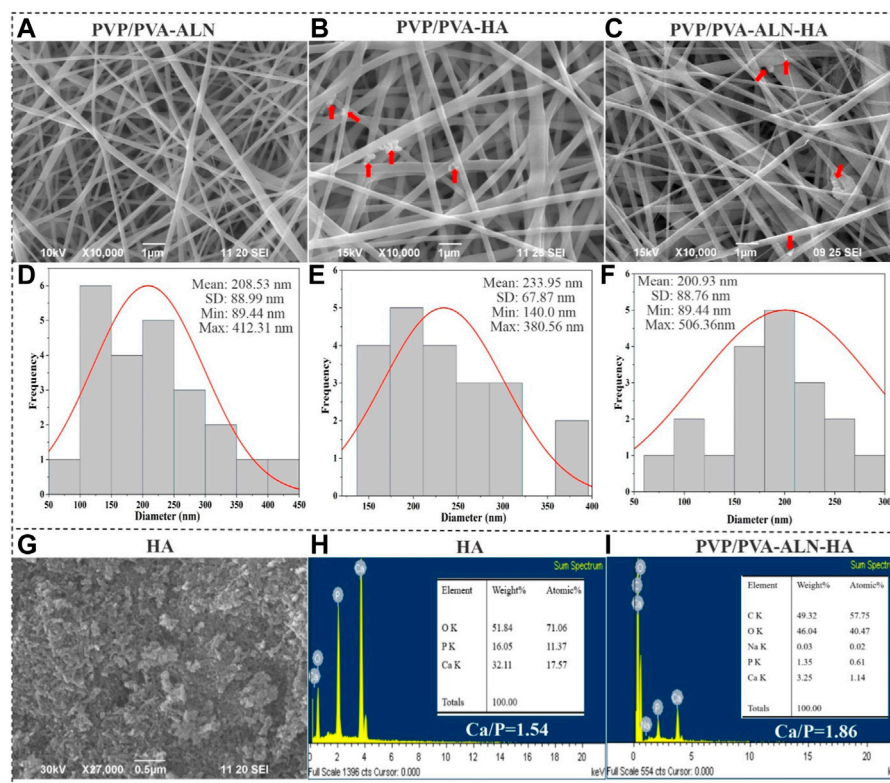


FIGURE 2

SEM images of (A) PVP/PVA-ALN, (B) PVP/PVA-HA and (C) PVP/PVA-ALN-HA nanofibers, and the red arrow in the SEM images indicates the presence of HA into nanofiber scaffolds; (D–F) Represents their corresponding histogram showing average diameters; (G) SEM image of HA nanoparticles; (H) EDX analysis of HA nanoparticles; (I) EDX analysis of PVP/PVA-ALN-HA nanofiber composite scaffold.

reaction between ninhydrin and alendronate is temperature dependent.

3.3.2 FTIR

The FT-IR spectrum shows prominent bands of HA along with the bands of PVP/PVA in the fabricated nanofibers (Figure 4A). The FTIR data of the nanofiber demonstrated a broad peak at $3,748\text{ cm}^{-1}$ along with strong intensity due to the stretching vibrations of hydroxyl group in PVP/PVA-ALN and PVP/PVA-HA nanofibers. But the intensity of peak of hydroxyl group in PVP/PVA-ALN-HA was less around $3,378\text{ cm}^{-1}$, it may be due to the hybridization of ALN and HA. The band at $1,016\text{ cm}^{-1}$ confirm the presence of C-O vibration of PVA-PVP (Salim et al., 2021). In addition, the presence of a $1,530\text{ cm}^{-1}$ peak was due to stretching vibrations of the carbonyl group present in PVA. The band at about $1,256\text{ cm}^{-1}$ corresponds to C-O stretching of acetyl groups present on the PVA backbone. The appearance of C-O stretching is due to the semi-crystalline nature of the blends. A band at $1,396\text{ cm}^{-1}$ is attributed to C-N bond, mainly from the functional group of PVP. The vibration band at about $1,701\text{ cm}^{-1}$ corresponds to C-O symmetric bending of PVA and PVP. The FTIR spectra of the nanofiber blend agreed well with the reported values [30,32]. When ALN was added, no additional peaks of ALN were detected in these scaffolds may be due to the spectra of ALN and HA overlap. The characteristic peaks of crystalline phosphate (PO_4^{3-}) at $1,040$,

920 and 805 cm^{-1} were detected in the FTIR spectra, confirming the presence of HA.

3.3.3 XRD analysis

XRD analysis was conducted to explore the structural and crystalline properties of the prepared nanofibers (Figure 4B). The distinct peaks present in the pattern affirm the crystalline nature of the HA component. Conversely, the diffraction patterns of spectra showing broad halos indicate the amorphous nature of the polymers. The XRD spectrum for pure PVA/PVP demonstrates diffused and broadened peaks within the range of $2\theta = 11.08^\circ$ – 21.26° , indicative of the amorphous nature of the polymers (Maheshwari et al., 2017).

HA features a crystalline structure with multiple diffractive planes, each manifesting its unique diffraction peak at a specific position. Various diffractive planes such as 002, 211, 202, 310, 222, and 213 are identified by sharp peaks at 26.1° , 32.1° , 34.2° , 39.9° , 46.7° , and 49.30° , respectively. This pattern strongly suggests the crystalline nature of the synthesized HA. In the case of composite scaffolds, the HA phase peak is noticeable (marked by *). In the context of polymer composites, the incorporation of ALN and HA results in weakened peak intensities for PVP/PVA-ALN-HA, without altering the peak positions. This phenomenon could be attributed to the enhanced diffraction of ceramic crystals or possibly an overlap of diffraction peaks from HA and ALN.

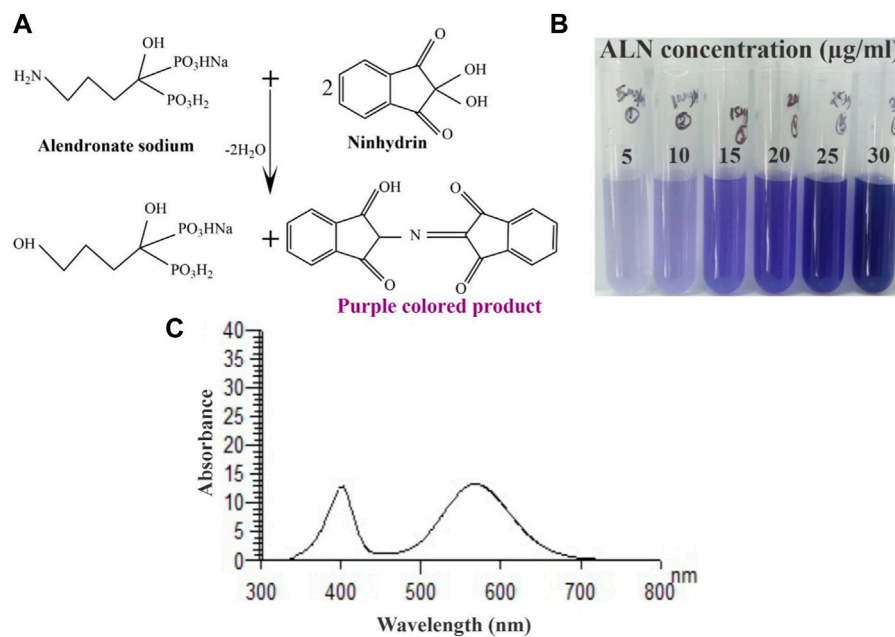


FIGURE 3

(A) Schematic representation of ninhydrin binding to ALN, (B) An image of the final reacted solutions which correspond to different ALN concentrations and (C) Absorption spectrum of the reaction product of alendronate sodium (25 µg/mL) with ninhydrin.

3.3.4 TGA analysis

Thermal stability analysis of PVP/PVA-ALN, PVP/PVA-HA, and PVP/PVA-ALN-HA nanofibers was conducted using TGA, as depicted in Figure 4C. The figure illustrates the improved thermal stability of the polymer composite achieved through the incorporation of nanomaterials (such as HA) within the polymer matrix. The findings indicated that the weight loss occurring within the temperature range of 70°C–130°C was attributed to the evaporation of water content present in the samples. In PVP/PVA-HA, it can be seen from Figure 4C that the weight loss in two states at ~370°C and 480°C, which was due to the loss of polymeric chain in the material and the entire material gets decomposed at 600°C which represents the remarkable thermal stability. PVP/PVA-ALN and PVP/PVA-ALN-HA showed the weight loss observed at ~280°C, 460°C and 360°C, 485°C and total weight loss observed at ~600°C, which might be due to the diminishing labile group and eruption of adhered material. Hence, these results revealed that the material is thermally stable.

3.3.5 Mechanical strength measurement

The response of the developed nanofiber scaffolds to mechanical loads is presented in Figure 4D. The characteristic tensile stress-strain curves and corresponding tensile properties, including Young's modulus, elongation-at-break, and tensile strength, are displayed (Figures 4D–G). The outcomes highlighted that all scaffolds exhibited a certain degree of stiffness and resistance to deformation. Previous research exhibited that the elastic modulus and tensile strength of human cancellous bone ranges from 0.05 to 0.5 GPa and 1–20 MPa, depending on the apparent density (Roeder et al., 2003). Comparing the PVP/PVA-ALN sample, the tensile strength of PVP/PVA-HA and PVP/PVA-ALN-HA displayed substantial enhancements upon the introduction of HA.

Figure 4E revealed that the Young's modulus of PVP/PVA-HA (255.94 MPa) and PVP/PVA-ALN-HA (372.32 MPa) exhibited the highest values compared to PVP/PVA-ALN (137.80 MPa). The maximum tensile strength (TS) of PVP/PVA-ALN-HA is evident in Figure 4F. The incorporation of HA led to improved mechanical properties of the nanofibers.

Furthermore, PVP/PVA-ALN exhibited TS of 9.23 MPa and an elongation at break (EB) value of 84.23% (Figure 4G). In contrast, PVP/PVA-HA and PVP/PVA-ALN-HA demonstrated TS and EB values of 19.90 MPa, 23.47 MPa, and 82.91%, 50.39%, respectively. It is worth noting that high porosity can negatively impact mechanical behaviour [28]. The lower TS of PVP/PVA-ALN compared to PVP/PVA-ALN-HA could be attributed to the limited bioavailability of ALN in aqueous conditions. The incorporation of ALN-HA nanoparticles resulted in an increased TS. Research has indicated that the addition of HA to electrospun blends enhances the mechanical properties of the nanofibers (Wuriantika et al., 2021).

In summary, the homogeneous distribution of ALN-incorporated HA nanoparticles along the fibre axis played a significant role in altering the mechanical properties of the nanofibers, enhancing their stiffness rather than flexibility. These results imply that PVP/PVA-ALN-HA holds promise for BTR. These enhancements in mechanical properties could effectively bolster the nanofiber's ability to withstand external forces during surgical procedures, meeting the demands of functioning as a mechanical barrier.

3.3.6 Contact angle

We conducted CA measurements on the scaffold to assess the influence of HA and ALN (Figure 4H). The average CAs for PVP/PVA-ALN, PVP/PVA-HA, and PVP/PVA-ALN-HA were found to be 31.75°, 51.69°, and 55.85°, respectively. The nanofiber loaded with

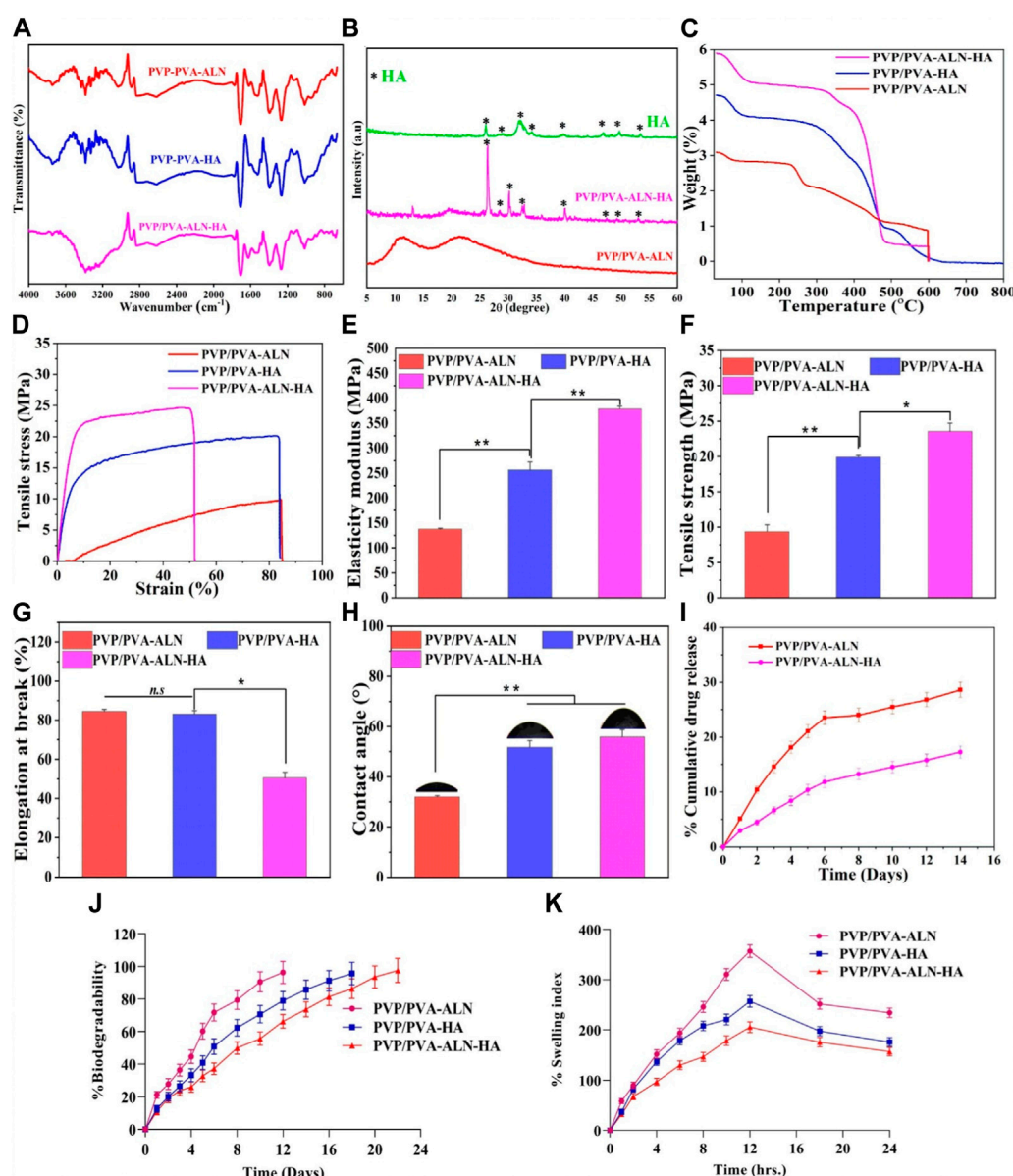


FIGURE 4

Different physicochemical properties of developed PVP/PVA-ALN, PVP/PVA-HA and PVP/PVA-ALN-HA nanofiber composite scaffolds; (A) FTIR spectra, (B) XRD spectra, (C) TGA analysis plot, (D) Stress versus strain plot, (E) histogram representing elasticity modulus in (MPa) (F) histogram showing the tensile strength graph in (MPa), (G) shows the elongation at break (%), (H) contact angle measurement, (I) %Cumulative drug release of Alendronate, (J) *in-vitro* biodegradability for 2 weeks and (K) swelling index (%) up to 24 h for nanofiber scaffolds.

ALN exhibited inherent hydrophilicity, while those loaded with HA displayed slight reduction in hydrophilic characteristics. Wettability stands as a crucial parameter for scaffolds, significantly impacting their mechanical stability, cell adhesion, and proliferation properties. It is noted that nanofiber surfaces serve as excellent platforms for sustained drug delivery, as they slow down degradation and extend the time for cell attachment prior to degradation, enhancing cell adhesion capabilities. This property holds immense importance for the application of nanofibers in BTR. In essence, the prepared nanofiber batches displayed appropriate contact angles, aligning with the requirements for an ideal scaffold in the context of BTR.

3.3.7 Drug release behavior

The cumulative concentration of released ALN from PVP/PVA-ALN and PVP/PVA-ALN-HA is presented in Figure 4I. The results clearly illustrate that ALN was released at a slower rate from PVP/PVA-ALN-HA compared to PVP/PVA-ALN. This suggests that encapsulating ALN within HA nanoparticles can effectively extend the duration of drug release. It is noteworthy that both PVP/PVA-ALN and PVP/PVA-ALN-HA nanofibers exhibited an initial burst release in the first 3 days. However, the ALN from the PVP/PVA-ALN-HA nanofiber exhibited a more prolonged release pattern as compared to PVP/PVA-ALN, specifically observed between day 3 and day 14. Due to the potential for severe side effects

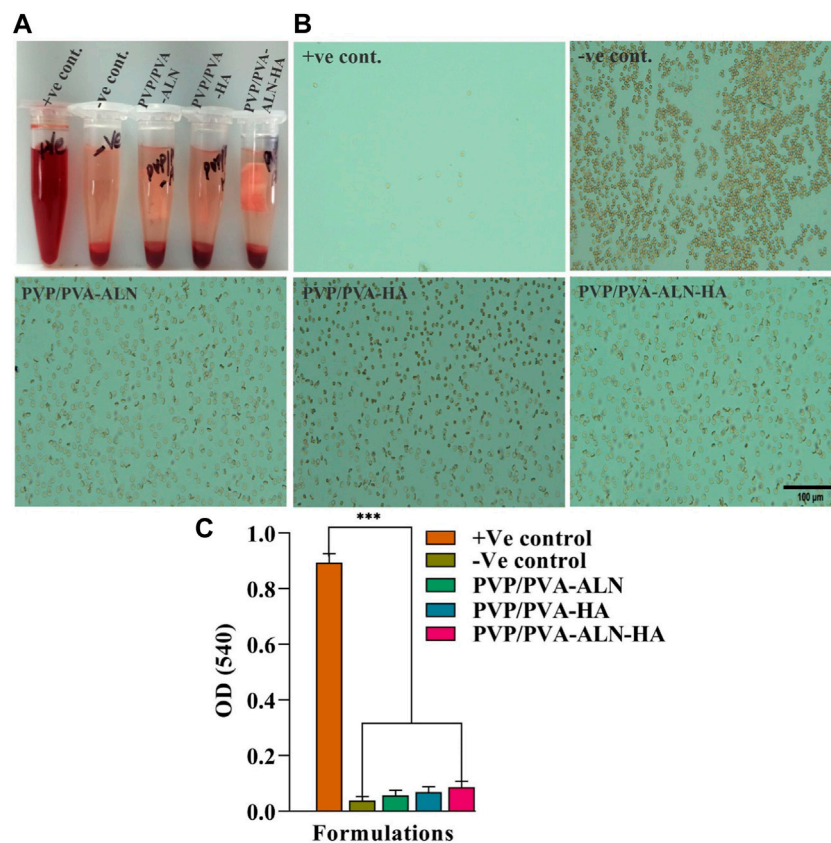


FIGURE 5

The study of hemolysis and the effect of scaffold on the lysis RBCs; (A) The hemolytic behavior of all the groups; (B) The microscopic image of intact RBCs status after 3 h of incubation with the control groups and nanofiber group PVP/PVA-ALN, PVP/PVA-HA and PVP/PVA-ALN-HA; (C) The histogram demonstrated the absorbance value of +Ve control, -Ve control, PVP/PVA-ALN, PVP/PVA-HA and PVP/PVA-ALN-HA at 540 nm. All the significant values are denoted as $*p \leq 0.05$, $**p \leq 0.01$, $***p \leq 0.001$.

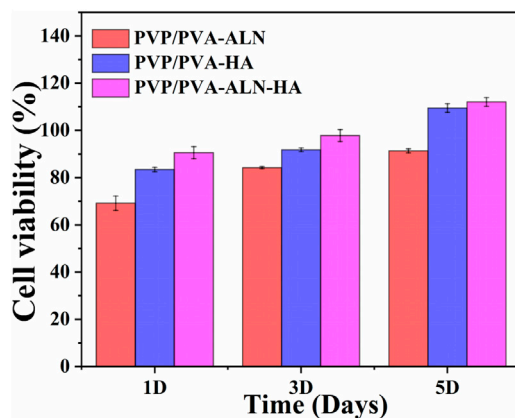


FIGURE 6

Cell viability study of the nanofibrous scaffold (PVP/PVA-ALN, PVP/PVA-HA and PVP/PVA-ALN-HA) for 1, 3 and 5 days on MC3T3-E1 cells.

associated with excessive ALN release, the controlled release of ALN from the nanofibers offers a way to mitigate the toxicity linked to high doses. Consequently, the utilization of PVP/PVA-ALN-HA

nanofibrous scaffolds has the potential to facilitate extended ALN delivery and support the BTR process for targeted size defects.

3.3.8 *In vitro* biodegradation

The degradation behavior of the scaffolds during the incubation period is depicted in Figure 4J. The results showed that nanofibers PVP/PVA-ALN had degraded by almost 96.35% after day 12 while PVP/PVA-HA showed a slower degradation rate 95.62% after 18 days. After addition of HA into nanofiber scaffold, PVP/PVA-ALN-HA nanofiber degraded more slowly and demonstrated 97.53% after 22 days. The variation in nanofiber degradation rates is directly attributed to the hydrophilic nature of the two polymers; higher hydrophilicity leads to faster degradation. This implies that the nanofibers would naturally dissolve within the body without necessitating their removal.

3.3.9 % water uptake capacity

The swelling behaviour of the scaffold demonstrates its capacity to facilitate the exchange of nutrients and waste materials between the environment and the cells encapsulated within the scaffold, creating an environment conducive to artificial tissue production. Swelling refers to the scaffold's ability to hydrate and stabilize within biological systems. It can

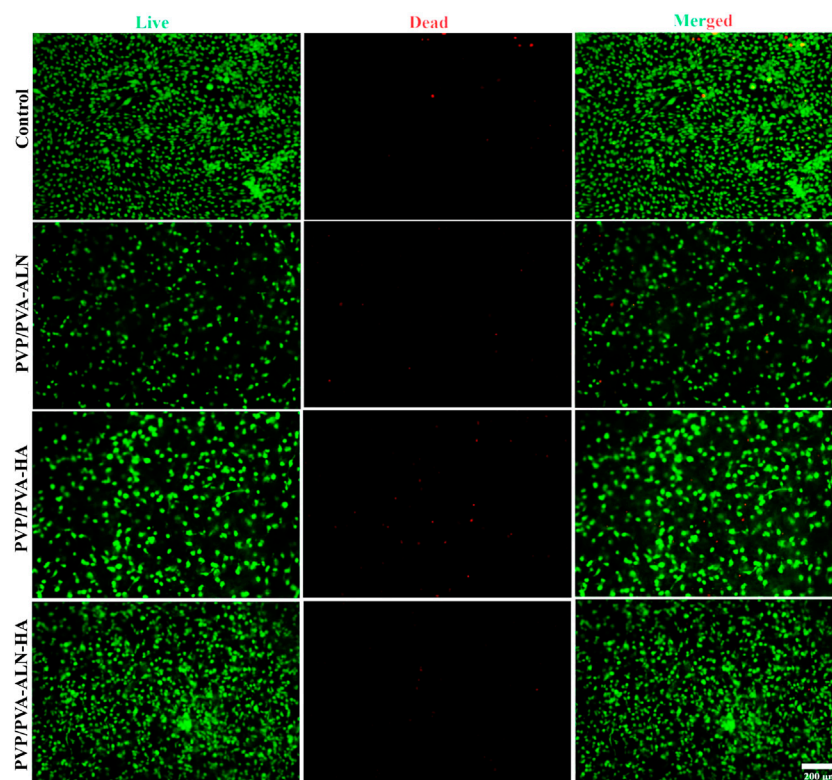


FIGURE 7
Fluorescence microscopic images of live/dead staining assay of MC3T3-E1 cells cultured with PVP/PVA-ALN, PVP/PVA-HA, PVP/PVA-ALN-HA on nanofiber scaffold surfaces for 3 days.

be employed as a carrier material for facilitating cell proliferation and differentiation processes. Hydrophilicity is a crucial characteristic in tissue engineering scaffolds, as it can enhance cell viability and proliferation.

Significant disparities were observed among the three tested scaffold groups (PVP/PVA-ALN, PVP/PVA-HA, PVP/PVA-ALN-HA), as displayed in [Figure 4K](#). Notably, PVP/PVA-ALN exhibited a remarkably high swelling ratio of approximately 356.92% after 12 h, surpassing PVP/PVA-HA at around 256.92% after 12 h of swelling index. This divergence might be attributed to the presence of ALN in PVP/PVA-ALN, which features hydrophilic groups, such as amino groups, enabling the penetration of water molecules within the scaffold's chains. Consequently, this scaffold showcased the highest hydrophilicity and swelling capability when compared to the other scaffolds tested.

Upon incorporating HA nanoparticles into the nanofibers, a notable reduction in swelling capacity was observed. Specifically, PVP/PVA-ALN-HA nanofibers demonstrated a swelling ratio of approximately 205.24% after 12 h of swelling. This reduction implies that the inclusion of HA nanoparticles into the nanofibers significantly curtailed the swelling rate. This outcome can be attributed to the hybridization of ALN and HA nanoparticles, which collectively circumvent low bioavailability, resulting in a reduction in swelling.

3.4 Hemolysis study

The non-haemolytic potential of any developed material is the most important characteristic, required for any type of tissue regeneration applications. The scaffolds developed for such type of applications should possess haemolytic index less than 5%. Achieving a hemolytic index lower than 2% would indicate excellent biocompatibility. The hemolytic outcomes for all the groups are illustrated in [Figure 5A](#). Microscopic examination of the obtained images provided valuable insights into the haemolytic behaviour of the different materials ([Figure 5B](#)). Remarkably, the results clearly demonstrated that PVP/PVA-ALN, PVP/PVA-HA, and PVP/PVA-ALN-HA, exhibited non-haemolytic characteristics that were notably similar to those observed with the -Ve control, as there was no lysis occurred in these groups. This outcome indicates that the interaction between the composite scaffolds and RBCs did not lead to any significant haemolytic effects. However, in +Ve control, intact RBCs were not observed. The haemolytic % of all the groups compared to + Ve control was less than 2%, indicating its high biocompatibility ([Figure 5C](#)). The absence of haemolysis in the nanofiber composite scaffolds suggests their potential suitability for biomedical applications, particularly where blood-contacting materials are concerned. These findings underscore the biocompatible nature of the developed nanofiber scaffolds, enhancing their attractiveness for various regenerative approaches.

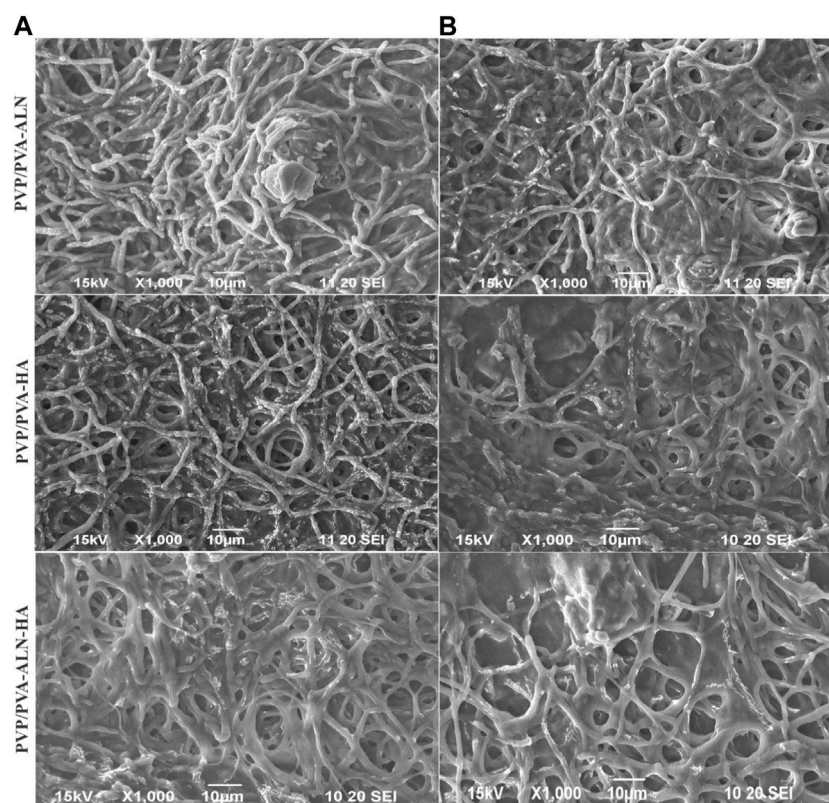


FIGURE 8

SEM images of MC3T3-E1 cells seeded on electrospun nanofiber (A) after 1 day presents the adhered cells; (B) cell adhesion after 3 days of seeding.

3.5 *In vitro* biological characterization

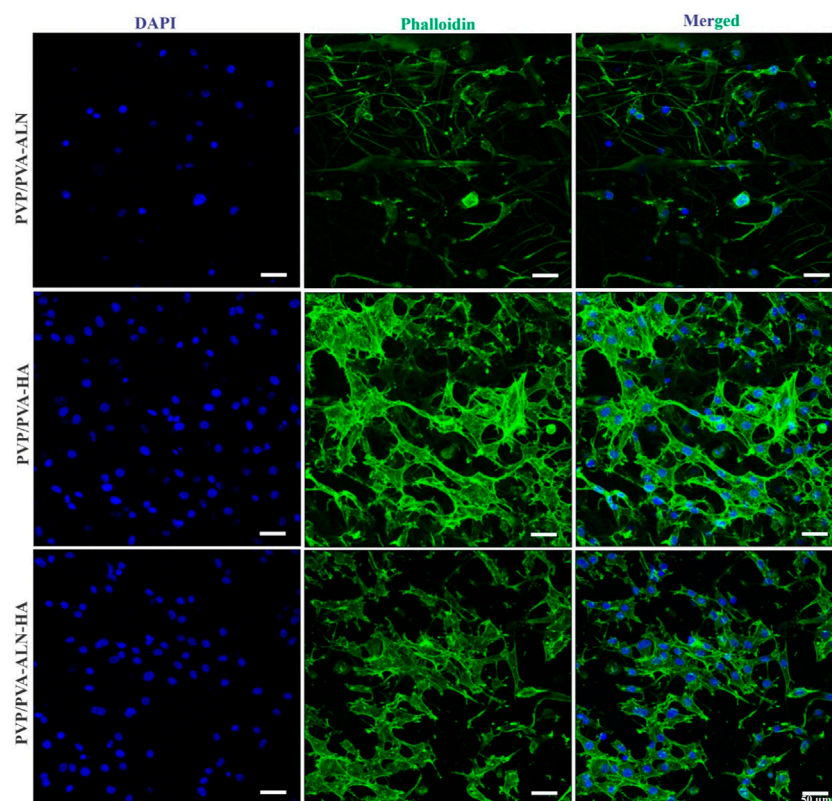
3.5.1 *In vitro* cytotoxicity

Cell viability is intricately linked to the extent of new bone formation, while initial cell adhesion commonly governs cellular function and eventual tissue integration. The presence of greater amounts of bone tissue around the scaffolds can be attributed to the enhanced adhesion and proliferation of stem cells (Wang et al., 2014). To showcase the cell viability of MC3T3-E1 cells on nanofibers *in vitro*, a CCK-8 assay was conducted to determine cell counts after 1, 3, and 5 days. The results reveal that all tested nanofibers (PVP/PVA-ALN, PVP/PVA-HA, and PVP/PVA-ALN-HA) foster the proliferation of MC3T3-E1 cells (Figure 6). Notably, nanofibers containing HA, such as PVP/PVA-HA and PVP/PVA-ALN-HA composite nanofibers, exhibited robust cell viability among MC3T3-E1 cells. This enhanced cell proliferation can be attributed to the synergistic effect of both ALN and HA, which may expedite bone tissue regeneration and wound healing. This notion is grounded in the extensive application of HA in various biotechnological domains, including tissue regeneration, biomedical imaging, bone repair, and drug delivery. Furthermore, HA has demonstrated significant roles in cell proliferation and growth (Januariyasa et al., 2020). The findings indicate that materials with low toxicity can serve as preliminary indicators for the proliferation assessment of MC3T3-E1 cells on these materials. The better biocompatibility of the composite scaffolds,

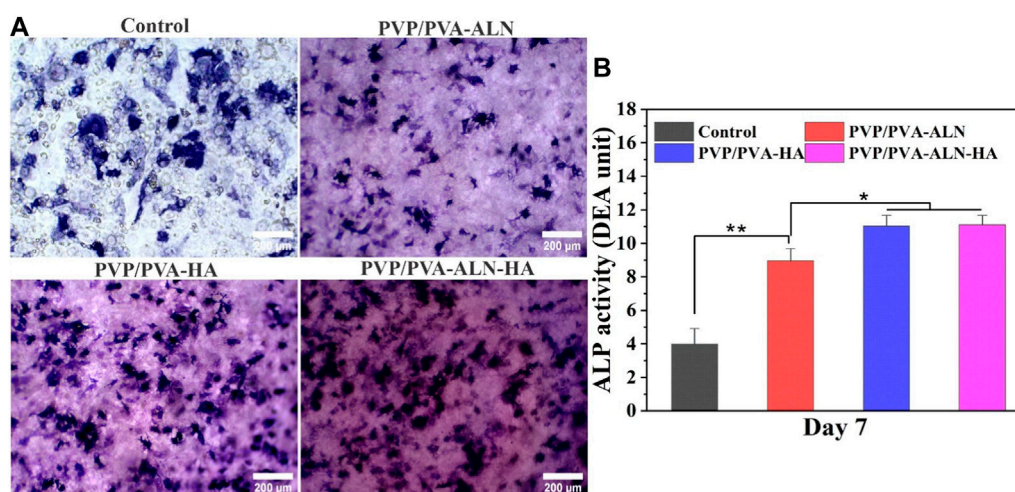
namely, PVP/PVA-ALN, PVP/PVA-HA, and PVP/PVA-ALN-HA scaffolds, is evident from the results. These outcomes signify that the incorporation of an appropriate quantity of ALN and HA nanoparticles into PVP/PVA nanofibers can effectively enhance cell adhesion and proliferation. Figure 6 also showed that embedding HA into electrospun PVP/PVA leads to improved cell viability compared to PVP/PVA-ALN scaffolds. This observation aligns with the established understanding that the addition of HA increases scaffold surface roughness and mechanical strength, while providing functional sites for cell adhesion. Consequently, this study affirms that the fabricated composite nanofiber PVP/PVA-ALN-HA exhibits favorable cytocompatibility with MC3T3-E1 cells.

3.5.2 Live/dead assay

The cytotoxicity of nanofibers was further confirmed by the results of live/dead staining of MC3T3-E1 cells on the scaffold surfaces, in which the live cells were stained green, while the dead cells were stained red (Figure 7). Dead cells were rarely found in live/dead-stained images, and most of the MC3T3-E1 cells were alive and uniformly distributed, suggesting that all scaffolds had excellent cytocompatibility. Fluorescent images revealed that MC3T3-E1 cells were more spread out on PVP/PVA-ALN-HA scaffold compared to other scaffolds after 3 days in culture. This was consistent with reports that ALN and HA effectively improved the bioactivity of PVP/PVA composites.

**FIGURE 9**

CLSM images of PVP/PVA-ALN, PVP/PVA-HA, PVP/PVA-ALN-HA nanofiber composite scaffolds stained with DAPI and Phalloidin dye on MC3T3-E1 cells after 3 days of incubation on scaffolds.

**FIGURE 10**

Osteogenic effect of the different PVP/PVA-ALN, PVP/PVA-HA and PVP/PVA-ALN-HA nanofibers, (A) ALP staining after 7 days of culture; (B) Quantitative analysis of ALP staining showing different groups control, PVP/PVA-ALN, PVP/PVA-HA and PVP/PVA-ALN-HA nanofiber scaffolds. *p*-value < 0.05 and 0.01 were represented by * and **, respectively, considered as significant.

3.5.3 Cell adhesion test onto nanofiber scaffolds

The cellular morphology was visualized using SEM over different time intervals for the respective nanofiber scaffolds.

Figure 8 displays the adhesion and proliferation of MC3T3-E1 cells after treatment with the prepared drug-loaded nanofibers for 1 and 3 days. The SEM images reveal that the seeded cells adhered

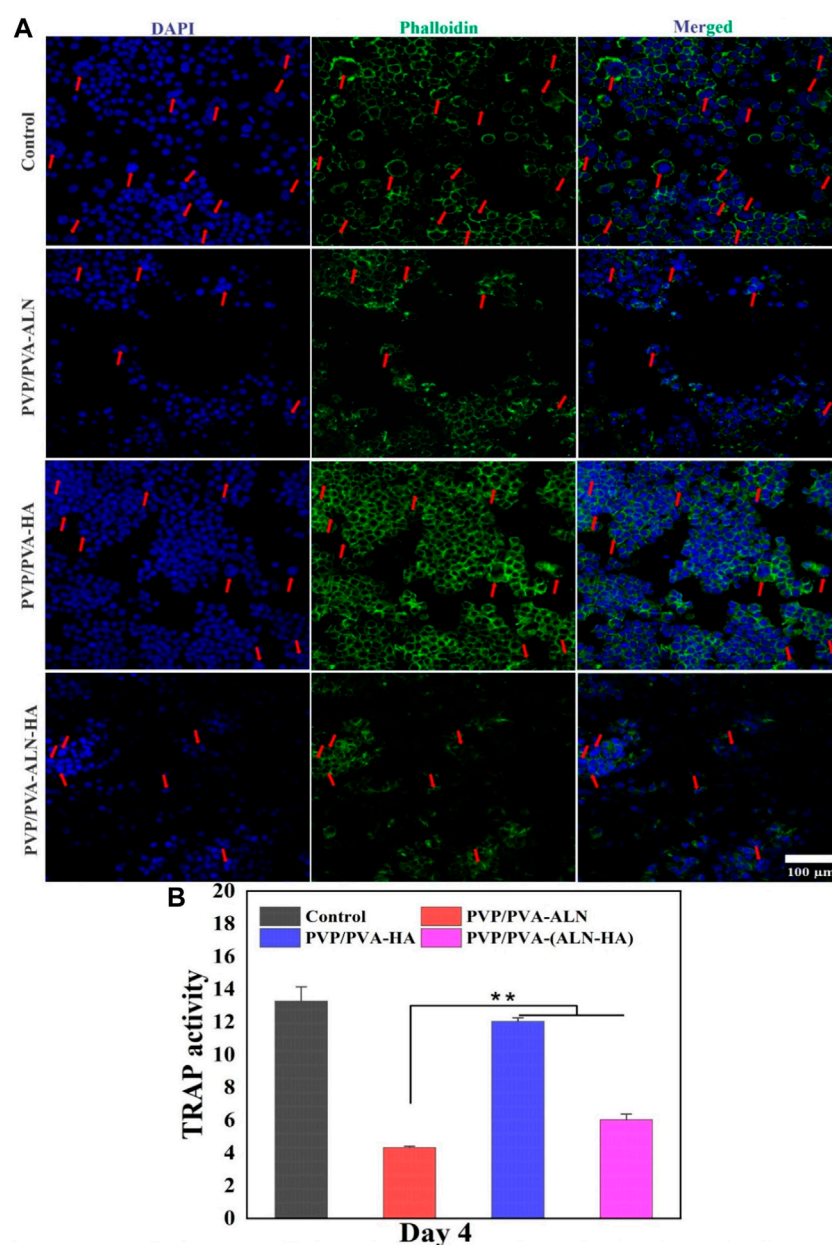


FIGURE 11

(A) Representative nucleus/cytoskeleton staining images of RAW 264.7 cells grown on different PVP/PVA-ALN, PVP/PVA-HA and PVP/PVA-ALN-HA nanofiber composite scaffolds whereas cytoskeleton and cell nuclei were stained by Phalloidin (green) and DAPI (blue), respectively (red arrows represent the formed osteoclasts); (B) Enzyme activity of TRAP from RAW 264.7 cells cultured on different scaffolds. *p*-value < 0.05 and 0.01 were denoted by * and **, respectively.

well to the surface of the scaffolds (Figure 8A), underscoring the favourable biocompatibility of the scaffolds. The results indicate that all tested nanofibers facilitated robust cell adhesion, even after prolonged contact between the nanofibers and MC3T3-E1 cells. Notably, PVP/PVA-ALN-HA exhibited the highest cell adhesion and proliferation behaviour. Over time, cell proliferation increased (Figure 8B), and by the third day, the scaffold appeared to be fully covered with highly spread cells, indicating the excellent biocompatibility of the composite nanofibers. The cells have effectively enveloped the nanofibrous scaffold, highlighting the importance of aligning the scaffold's structure with the

extracellular matrix (ECM). These observations strongly suggest that the developed nanofibrous scaffolds hold significant potential for promoting bone tissue regeneration.

The confocal microscopy images presented in Figure 9, confirmed that PVP/PVA-ALN, PVP/PVA-HA, PVP/PVA-ALN-HA nanofibers composite scaffolds are non-toxic to MC3T3-E1 cells. The use of confocal microscopy provided a powerful tool to capture intricate details of the cell on nanofibers. The high-resolution images acquired showcased the cell nuclei stained with DAPI, providing insight into the distribution and adhesion of the MC3T3-E1 cells on the PVP/PVA nanofiber scaffolds. Furthermore, the visualization of

the actin cytoskeleton, illuminated by phalloidin staining, confirmed the cell adhesion and proliferation of MC3T3-E1 cells on PVP/PVA-ALN, PVP/PVA-HA, PVP/PVA-ALN-HA. The presence of densely proliferated cells displaying an elongated, spindle-like morphology is particularly noteworthy, as this is a characteristic trait of MC3T3-E1 cell lines. It is evident from Figure 9 that PVP/PVA-HA and PVP/PVA-ALN-HA showed higher cell proliferation as compared to PVP/PVA-ALN group. So, it may be concluded that addition of HA in PVP/PVA nanofiber significantly enhanced the cell growth.

3.5.4 ALP activity measurement

The promotion of osteogenic differentiation around the interface between implant materials and bone is of paramount importance for successful bone reconstruction. An ideal bone implant should not only demonstrate favourable cytocompatibility but also encourage osteogenic activity (Wang and Lu, 2020). Building upon the positive results obtained from *in vitro* cell line studies, the early osteogenic differentiation of MC3T3-E1 cells induced by different scaffolds was confirmed through the assessment of ALP activity. ALP activity serves as a biochemical marker for osteoblastic activity, manifesting an increase in the early stages of osteogenesis and signifying differentiation towards osteoblasts (Gouma et al., 2012). The staining density and distribution of ALP in MC3T3-E1 cells cultured on PVP/PVA-ALN, PVP/PVA-HA, and PVP/PVA-ALN-HA were found to be higher than the control group, as illustrated in Figure 10A. Quantitative analysis further corroborated the staining results (Figure 10B). Notably, there was no significant difference observed between PVP/PVA-HA and PVP/PVA-ALN-HA nanofibers. This suggests that the presence of HA in the scaffold promoted osteogenic differentiation, thereby facilitating the development of new bone tissue. The ability of HA to stimulate osteogenic differentiation of stem cells has been supported by numerous studies (Behere et al., 2021; Niu et al., 2021). However, the combination of ALN and HA exhibited additive effects on osteogenesis. By incorporating ALN within a safe range and ensuring controlled release via a dual delivery system, the potential side effects of ALN can be mitigated. This approach aligns with an appropriate strategy to harness the benefits of ALN without undesirable consequences. These findings are consistent with previous research (Park et al., 2015; van Houdt et al., 2018). Overall, the prepared PVP/PVA-ALN-HA nanofiber scaffold demonstrated promising capabilities for osteogenic differentiation, rendering it feasible for application in bone regeneration scenarios.

3.5.5 Osteoclast formation

Bone healing is a multifaceted process that involves not only osteoblasts but also osteoclasts. Effective reduction in osteoclastogenesis can offer advantages for successful bone regeneration. Osteoclasts, responsible for bone mineral resorption, are formed through the fusion of hematopoietic cells of the monocyte-macrophage lineage, induced by specific stimuli like receptor activator of nuclear factor κ B ligand (RANKL) and macrophage colony-stimulating factor (M-CSF) (Lee et al., 2018). The development of multinucleated osteoclasts is governed by the activation of intracellular pathways, including nuclear factor κ B (NF- κ B) and nuclear factor of activated T cells c1 (NFATc1) (Ahmad et al., 2020). Studies have suggested that ALN can

inhibit osteoclast formation by suppressing the activation of the ERK1/2 and Akt pathways (Jiang, Mao, and Gao, 2015).

To assess the impact of the nanofibers on osteoclastic activity, the morphology of osteoclast differentiation was examined. In Figure 11A, numerous large multinucleated osteoclasts were observed on the surface of the PVP/PVA-HA scaffold and the control group. In contrast, significantly fewer multinucleated osteoclasts were present in the PVP/PVA-ALN and PVP/PVA-ALN-HA groups. The development and maturation of functionally active osteoclasts encompass several complex steps, including precursor cell fusion to form multinucleated cells, significant cytoskeletal rearrangements, adhesion, polarization, and actin ring formation.

The effect of ALN-containing scaffolds on osteoclasts was further evaluated through TRAP activity, an enzyme marker of osteoclasts (Huang et al., 2019). As shown in Figure 11B, TRAP activity of RAW 264.7 cells in the ALN-loaded nanofiber groups exhibited a significant reduction ($p < 0.01$) compared to other groups. This suggests that ALN played a role in inhibiting osteoclast maturation. Therefore, the findings highlight that ALN-HA loaded nanofibers have the potential to inhibit osteoclast formation, indicating their potential role in promoting bone formation. This bodes well for their application in bone regeneration scenarios.

4 Conclusion

The objective of this study was to develop nanofiber scaffolds that could effectively balance bone remodelling and regeneration processes. Through the electrospinning technique, we successfully created nanofibers loaded with ALN and HA nanoparticles. These nanoparticles were seamlessly integrated into a PVP/PVA nanofiber scaffolds to enhance its overall properties. The combination of ALN and HA within the electrospun PVP/PVA-ALN-HA nanofibers aimed to synergistically regulate the equilibrium between bone resorption and formation. Our findings demonstrated that the nanofibers possessed a porous and highly hydrophilic network structure, resembling the natural ECM of human bone tissue. Incorporating ALN and HA into the nanofibers led to increased water retention capacity and desired biodegradability for bone regeneration. Furthermore, HA incorporation improved the mechanical strength and thermal stability of PVP/PVA-ALN-HA. EDX analysis confirmed the successful integration of ALN and HA nanoparticles into the PVP/PVA nanofibers. Notably, PVP/PVA-ALN-HA nanofibers exhibited a sustained release of ALN over 2 weeks.

In vitro evaluations further corroborated the biocompatibility of the scaffolds, demonstrating non-toxicity and supporting bone cell adhesion and proliferation on MC3T3-E1 cells, evidenced by SEM images after 1 and 3 days of incubation. The cell adhesion and proliferation of scaffolds was further assessed by CLSM images on MC3T3-E1 cells after 3 days of incubation. The fluorescence microscopy images of Live/dead assay revealed the absence of dead cells. Significantly higher level of ALP in PVP/PVA-HA and PVP/PVA-ALN-HA groups as compared to control, promoted osteogenic differentiation which leads to formation of new bone tissue. Moreover, our studies indicated that the PVP/PVA-ALN-HA

nanofiber scaffold had the potential to enhance osteogenesis and significantly inhibited the multinucleated osteoclast formation. However, the reduction in TRAP level in ALN containing nanofiber scaffolds confirmed the inhibition of osteoclast formation. These collective results indicate that the fabricated PVP/PVA-ALN-HA nanofibrous scaffolds could serve as a promising platform for bone regeneration applications and this suggest the potential consideration of *in-vivo* studies in future.

Data availability statement

The original contributions presented in the study are included in the article/supplementary material, further inquiries can be directed to the corresponding authors.

Ethics statement

This study uses strains obtained from cell lines and blood were gift sample from professor Huang Zhongbing, (Biomedical engineering college; Sichuan University), approved by the Animal Ethics Committee of Sichuan University (Approval No. KS2020039).

Author contributions

SA: Data curation, Methodology, Validation, Writing–original draft. DA: Methodology, Software, Validation, Writing–original draft. MS: Investigation, Resources, Validation, Writing–review and editing. DA: Funding acquisition, Investigation, Resources, Validation, Writing–review and editing. MA: Formal Analysis, Methodology, Validation, Writing–review and editing. WY: Data

curation, Validation, Visualization, Writing–review and editing. SA: Formal Analysis, Funding acquisition, Validation, Writing–review and editing. XW: Formal Analysis, Investigation, Validation, Writing–review and editing. PR: Conceptualization, Supervision, Writing–review and editing. QA: Formal Analysis, Methodology, Resources, Supervision, Writing–review and editing.

Funding

The authors declare financial support was received for the research, authorship, and/or publication of this article. This work was funded by National Key R&D Program of China (2023YFC2410403). This research was supported by Researchers Supporting Project number (RSP2023R27), King Saud University, Riyadh, Saudi Arabia.

Conflict of interest

The authors declare that the research was conducted in the absence of any commercial or financial relationships that could be construed as a potential conflict of interest.

Publisher's note

All claims expressed in this article are solely those of the authors and do not necessarily represent those of their affiliated organizations, or those of the publisher, the editors and the reviewers. Any product that may be evaluated in this article, or claim that may be made by its manufacturer, is not guaranteed or endorsed by the publisher.

References

- Agarwal, Y., Rajinikanth, P. S., Ranjan, S., Tiwari, U., Balasubramniam, J., Pandey, P., et al. (2021). Curcumin loaded polycaprolactone-/polyvinyl alcohol-silk fibroin based electrospun nanofibrous mat for rapid healing of diabetic wound: an *in-vitro* and *in-vivo* studies. *Int. J. Biol. Macromol.* 176, 376–386. doi:10.1016/j.ijbiomac.2021.02.025
- Ahmad, T., Byun, H., Shin, H. J., Lee, J., Sajeesh Kumar Madhurakkat, P., Kim, E. Mi, et al. (2020). Polydopamine-assisted one-step modification of nanofiber surfaces with adenosine to tune the osteogenic differentiation of mesenchymal stem cells and the maturation of osteoclasts. *J. Biomaterials Sci.* 8, 2825–2839. doi:10.1039/c9bm01990a
- Ahmed, M. K., Mansour, S. F., Al-Wafi, R., and Abdel-Fattah, E. (2021). Nanofibers scaffolds of co-doped Bi/Sr-hydroxyapatite encapsulated into polycaprolactone for biomedical applications. *J. Mater. Res. Technol.* 13, 2297–2309. doi:10.1016/j.jmrt.2021.05.074
- Al-Baadani, M. A., Xu, L., Kendrick Hii, R. Y., Sun, A., Gao, X., Cai, K., et al. (2022). *In situ* preparation of alendronate-loaded ZIF-8 nanoparticles on electrospun nanofibers for accelerating early osteogenesis in osteoporosis. *Mater. Des.* 217, 110596. doi:10.1016/j.matdes.2022.110596
- Anand, S., Pandey, P., Mohammed Yasmin, B., Chidambaram, K., Kumar Arya, D., Gupta, R. K., et al. (2022a). Electrospun biomimetic multifunctional nanofibers loaded with ferulic acid for enhanced antimicrobial and wound-healing activities in STZ-Induced diabetic rats. *Pharmaceuticals* 15, 302. doi:10.3390/ph15030302
- Anand, S., Paruvathanahalli Siddalingam, R., Kumar Arya, D., Pandey, P., Gupta, R. K., Sankhwar, R., et al. (2022b). Multifunctional biomimetic nanofibrous scaffold loaded with asiaticoside for rapid diabetic wound healing. *Pharmaceutics* 14, 273. doi:10.3390/pharmaceutics14020273
- Anand, S., Rajinikanth, P. S., Pandey, P., Payal, D., Thakur, S., and Dilip Kumar, A. (2023). Biomaterial-based nanofibers for drug delivery applications. *Biomed. Res. Med. Dis.*, 531–546. doi:10.1201/9781003220404-38
- Anjum, S., Rahman, F., Pandey, P., Kumar Arya, D., Alam, M., Paruvathanahalli Siddalingam, R., et al. (2022). Electrospun biomimetic nanofibrous scaffolds: a promising prospect for bone tissue engineering and regenerative medicine. *Int. J. Mol. Sci.* 23, 9206. doi:10.3390/ijms23169206
- Athar, M. S., Rasool, Z., Muner, M., Altass, H. M., Althagafi, I. I., and Saleh, A. A. (2023). Fabrication of direct Z-scheme CoNiWO₄/Ph-gC₃N₄ heterocomposites: enhanced photodegradation of bisphenol A and anticancer activity. *ACS Omega* 8, 38272–38287. doi:10.1021/acsomega.3c04653
- BalajiRaghavendran, H. R., Puvaneswary, S., Talebian, S., Murali, M. R., Sangeetha Vasudevaraj, N., Krishnamurthy, G., et al. (2014). A comparative study on *in vitro* osteogenic priming potential of electron spun scaffold PLLA/HA/Col, PLLA/HA, and PLLA/Col for tissue engineering application. *PLoS one* 9, e104389. doi:10.1371/journal.pone.0104389
- Behere, I., Pardawala, Z., Vaidya, A., Kale, V., and Ganesh, I. (2021). Osteogenic differentiation of an osteoblast precursor cell line using composite PCL-gelatin-nHAp electrospun nanofiber mesh. *Int. J. Polym. Mater. Polym. Biomaterials* 70, 1281–1295. doi:10.1080/00914037.2020.1767619
- Brannigan, K., and Griffin, M. (2016). An update into the application of nanotechnology in bone healing. *Open Orthop. J.* 10, 808–823. doi:10.2174/1874325001610010808
- Chahal, S., Fathima Shahitha Jahir, H., Kumar, A., Mohammad Syaiful Bahari Abdull, R., and Mashitah, M. Y. (2016). Fabrication, characterization and *in vitro* biocompatibility of electrospun hydroxyethyl cellulose/poly (vinyl) alcohol nanofibrous composite biomaterial for bone tissue engineering. *Chem. Eng. Sci.* 144, 17–29. doi:10.1016/j.ces.2015.12.030
- Chaudhuri, B., Mondal, B., and RaySarkar, SKSC (2016). A novel biocompatible conducting polyvinyl alcohol (PVA)-polyvinylpyrrolidone (PVP)-hydroxyapatite (HAP) composite scaffolds for probable biological application. *Colloids surfaces B Biointerfaces*. 143, 71–80. doi:10.1016/j.colsurfb.2016.03.027

- Cheng, Gu, Yin, C., Hu, Tu, Jiang, S., Wang, Q., Zhou, X., et al. (2019). Controlled co-delivery of growth factors through layer-by-layer assembly of core-shell nanofibers for improving bone regeneration. *ACS Nano* 13, 6372–6382. doi:10.1021/acsnano.8b06032
- Deepak, P., Kumar, P., Kumar Arya, D., Pandey, P., Kumar, S., Prasad Parida, B., et al. (2023). c (RGDfK) anchored surface manipulated liposome for tumor-targeted Tyrosine Kinase Inhibitor (TKI) delivery to potentiate liver anticancer activity. *Int. J. Pharm.* 642, 123160. doi:10.1016/j.jipharm.2023.123160
- Drake, M. T., Clarke, B. L., and Khosla, S. (2008). "Bisphosphonates: mechanism of action and role in clinical practice," in *Mayo clinic proceedings* (Elsevier), 1032–1045.
- Ganachari, S. V., Bevinakatti, A. A., Yaradoddi, J. S., Banapurmath, N. R., Hunashyal, A. M., and Shettar, A. S. (2016). Rapid synthesis, characterization, and studies of hydroxyapatite nanoparticles. *Adv. Mater. Sci. Res.* 10, 9–13.
- Gao, X., Song, J., Ji, P., Zhang, X., Li, X., Xu, X., et al. (2016). Polydopamine-templated hydroxyapatite reinforced polycaprolactone composite nanofibers with enhanced cytocompatibility and osteogenesis for bone tissue engineering. *ACS Appl. Mater. Interfaces* 8, 3499–3515. doi:10.1021/acsmi.5b12413
- Gong, Li, Altman, R. B., and Klein, T. E. (2011). Bisphosphonates pathway. *Pharmacogenetics genomics* 21, 50–53. doi:10.1097/fpc.0b013e328335729c
- Gouma, P., Xue, R., Goldbeck, C. P., Perrotta, P., and Balázsi, C. (2012). Nano-hydroxyapatite—cellulose acetate composites for growing of bone cells. *Mater. Sci. Eng. C* 32, 607–612. doi:10.1016/j.msec.2011.12.019
- Huang, X.-L., Huang, L.-Yu, Cheng, Y.-T., Li, F., Zhou, Q., Wu, C., et al. (2019). Zoledronic acid inhibits osteoclast differentiation and function through the regulation of NF- κ B and JNK signalling pathways. *Int. J. Mol. Med.* 44, 582–592. doi:10.3892/ijmm.2019.4207
- Januariyasa, I. K., Ika Dewi, A., and Yusril, Y. (2020). Nanofibrous poly (vinyl alcohol)/chitosan contained carbonated hydroxyapatite nanoparticles scaffold for bone tissue engineering. *Mater. Sci. Eng. C Mater. Biol. Appl.* 107, 110347. doi:10.1016/j.msec.2019.110347
- Jiang, P., Mao, Z., and Changyou, G. (2015). Combinational effect of matrix elasticity and alendronate density on differentiation of rat mesenchymal stem cells. *Acta biomater.* 19, 76–84. doi:10.1016/j.actbio.2015.03.018
- Jin, S., Gao, J., Yang, R., Yuan, C., Wang, R., Qin, Z., et al. (2022). A baicalin-loaded coaxial nanofiber scaffold regulated inflammation and osteoclast differentiation for vascularized bone regeneration. *Bioact. Mater.* 8, 559–572. doi:10.1016/j.bioactmat.2021.06.028
- Klara, J., and Joanna, L. L. (2022). How efficient are alendronate-nano/biomaterial combinations for anti-osteoporosis therapy? An evidence-based review of the literature. *Int. J. Nanomedicine* Vol. 17, 6065–6094. doi:10.2147/ijn.s388430
- Lee, K., Seo, I., Choi, M. H., and Daewon, J. (2018). Roles of mitogen-activated protein kinases in osteoclast biology. *J. Mol. Sci. Jeong* 19, 3004. doi:10.3390/ijms19103004
- Maheshwari, S. U., Govindan, K., Raja, M., Raja, A., Pravin, M. B. S., and Vasanth Kumar, S. (2017). Preliminary studies of PVA/PVP blends incorporated with HAp and β -TCP bone ceramic as template for hard tissue engineering. *Bio-Med. Mat. Eng.* 28, 401–415. doi:10.3233/bme-171682
- Niu, X., Wang, L., Xu, M., Qin, M., Zhao, L., Yan, W., et al. (2021). Electrospun polyamide-6/chitosan nanofibers reinforced nano-hydroxyapatite/polyamide-6 composite bilayered membranes for guided bone regeneration. *Carbohydr. Polym.* 260, 117769. doi:10.1016/j.carbpol.2021.117769
- Palazzo, B., Iafisco, M., Laforgia, M., Margiotta, N., Natile, G., Bianchi, C. L., et al. (2007). Biomimetic hydroxyapatite-drug nanocrystals as potential bone substitutes with antitumor drug delivery properties. *Adv. Funct. Mater.* 17, 2180–2188. doi:10.1002/adfm.200600361
- Pandey, G., Pandey, P., Kumar Arya, D., Kanaujiya, S., Deshraj Deepak, K., Gupta, R. K., et al. (2023). Multilayered nanofibrous scaffold of Polyvinyl alcohol/gelatin/poly (lactic-co-glycolic acid) enriched with hemostatic/antibacterial agents for rapid acute hemostatic wound healing. *Int. J. Pharm.* 638, 122918. doi:10.1016/j.jipharm.2023.122918
- Pandey, P., Kumar Arya, D., Kumar Ramar, M., Chidambaram, K., and Rajinikanth, P. S. (2022). Engineered nanomaterials as an effective tool for HER2+ breast cancer therapy. *Drug Discov. Today* 27, 2526–2540. doi:10.1016/j.drudis.2022.06.007
- Park, K.-W., Yun, Y.-P., SungKim, E., and Song, H.-R. (2015). The effect of alendronate loaded biphasic calcium phosphate scaffolds on bone regeneration in a rat tibial defect model. *Int. J. Mol. Sci.* 16, 26738–26753. doi:10.3390/ijms161125982
- Rajinikanth, P. S., and Jestin, C. (2016). Development and evaluation of nanostructured lipid carrier-based hydrogel for topical delivery of 5-fluorouracil. *Int. J. nanomedicine* Vol. 11, 5067–5077. doi:10.2147/ijn.s117511
- Rajinikanth, P. S., Sankar, C., and Mishra, B. (2003). Sodium alginate microspheres of metoprolol tartrate for intranasal systemic delivery: development and evaluation. *Drug Deliv.* 10, 21–28. doi:10.1080/713840323
- Roeder, R. K., Sproul, M. M., and Charles, H. (2003). Hydroxyapatite whiskers provide improved mechanical properties in reinforced polymer composites. *J. Biomed. Mater. Res. A* 67, 801–812. The Australian Society for Biomaterials, and the Korean Society for Biomaterials. doi:10.1002/jbm.a.10140
- Sadeghi, E., Seyed Mojtaba, Z., Khademi, F., and Elham, B. (2022). Enhancing structural strength and improving cell survival through Polycaprolactone/(gelatin/hydroxyapatite) Core-Shell nanofibers for tissue engineering. *Polym. Compos.* 43, 7379–7389. doi:10.1002/pc.26819
- Salim, S. A., Loutfy, S. A., EsmailEl-Fakharany, M., Tarek, H. T., Hussien, Y., and Elbadawy, A. K. (2021). Influence of chitosan and hydroxyapatite incorporation on properties of electrospun PVA/HA nanofibrous mats for bone tissue regeneration: nanofibers optimization and *in-vitro* assessment. *J. Drug Deliv. Sci. Technol.* 62, 102417. doi:10.1016/j.jddst.2021.102417
- Shen, X., Ma, P., Hu, Y., Xu, G., Xu, K., Chen, W., et al. (2016). Alendronate-loaded hydroxyapatite-TiO₂ nanotubes for improved bone formation in osteoporotic rabbits. *J. Mater. Chem. B* 4, 1423–1436. doi:10.1039/c5tb01956g
- Shi, X., Wang, Y., Ren, Li, Gong, Y., and Dong-An, W. (2009). Enhancing alendronate release from a novel PLGA/hydroxyapatite microspheric system for bone repairing applications. *Pharm. Res.* 26, 422–430. doi:10.1007/s11095-008-9759-0
- Singh, P., Pandey, P., Kumar Arya, D., Anjum, M. M., Poonguzhali, S., Kumar, A., et al. (2023). Biomimicking dual drug eluting twisted electrospun nanofiber yarns for post-operative wound healing. *Biomed. Mater.* 18, 035006. doi:10.1088/1748-605x/accd41
- Teixeira, A. I., Nealey, P. F., and Christopher, J. M. (2004). Responses of human keratocytes to micro- and nanostructured substrates. *J. Biomed. Mater. Res. Part A* 71, 369–376. doi:10.1002/jbm.a.30089
- Thakur, S., Anjum, Md M., Jaiswal, S., Kumar, A., Payal, D., Anand, S., et al. (2023). Novel synergistic approach: tazarotene-calcipotriol-loaded-PVA/PVP-nanofibers incorporated in hydrogel film for management and treatment of psoriasis. *Mol. Pharm.* 20, 997–1014. doi:10.1021/acs.molpharmaceut.2c00713
- van Houdt, C. I. A., Gabbai-Armelin, P. R., Lopez-Perez, P. M., Dietmar, J. O. U., Jansen, J. A., Ana Claudia, M. R., et al. (2018). Alendronate release from calcium phosphate cement for bone regeneration in osteoporotic conditions. *Sci. Rep.* 8, 15398. doi:10.1038/s41598-018-33692-5
- Wang, C., Lu, W. W., and Min, W. (2020). Multifunctional fibrous scaffolds for bone regeneration with enhanced vascularization. *J. Mater. Chem. B* 8, 636–647. doi:10.1039/c9tb01520e
- Wang, L., He, S., Wu, X., Liang, S., Mu, Z., Wei, J., et al. (2014). Polyetheretherketone/nano-fluorohydroxyapatite composite with antimicrobial activity and osseointegration properties. *Biomaterials* 35, 6758–6775. doi:10.1016/j.biomaterials.2014.04.085
- Wang, Yi, Cui, W., Zhao, X., Wen, S., Sun, Y., Han, J., et al. (2019). Bone remodeling-inspired dual delivery electrospun nanofibers for promoting bone regeneration. *Nanoscale* 11, 60–71. doi:10.1039/c8nr07329e
- Wu, H., Xu, Y., Liu, G., Ling, J., Dash, B. C., Ruan, J., et al. (2014). Emulsion cross-linked chitosan/nanohydroxyapatite microspheres for controlled release of alendronate. *J. Mater. Sci. Mater. Med.* 25, 2649–2658. doi:10.1007/s10856-014-5289-y
- Wuriantika, M. I., Utomo, J., Nurhuda, M., Santjojo, DJDH, and Masrurroh, (2021). Nanostructure, porosity and tensile strength of PVA/Hydroxyapatite composite nanofiber for bone tissue engineering. *Mater. Today Proc.* 44, 3203–3206. doi:10.1016/j.matpr.2020.11.438
- Yadav, S., Kumar Arya, D., Pandey, P., Anand, S., Kumar Gautam, A., Ranjan, S., et al. (2022). ECM mimicking biodegradable nanofibrous scaffold enriched with curcumin/ZnO to accelerate diabetic wound healing via multifunctional bioactivity. *Int. J. Nanomedicine* Vol. 17, 6843–6859. doi:10.2147/ijn.s388264
- Yang, D., Qu, S., Huang, J., Cai, Z., and Zhongrong, Z. (2012). Characterization of alendronate sodium-loaded UHMWPE for anti-osteolysis in orthopedic applications. *Mater. Sci. Eng. C* 32, 83–91. doi:10.1016/j.msec.2011.09.012
- Yun, Y.-P., Kim, S.-Ju, Lim, Y.-M., Park, K., Kim, H.-J., Kim, S. E., et al. (2014). The effect of alendronate-loaded polycaprolactone nanofibrous scaffolds on osteogenic differentiation of adipose-derived stem cells in bone tissue regeneration. *J. Biomed. Nanotechnol.* 10, 1080–1090. doi:10.1166/jbn.2014.1819
- Zhu, G., Zhang, T., Chen, M., Yao, Ke, Huang, X., Zhang, Bo, et al. (2021). Bone physiological microenvironment and healing mechanism: basis for future bone-tissue engineering scaffolds. *Bioact. Mater.* 6, 4110–4140. doi:10.1016/j.bioactmat.2021.03.043



OPEN ACCESS

EDITED BY

Hengchong Shi,
Chinese Academy of Sciences (CAS),
China

REVIEWED BY

Xiaoming Yang,
Soochow University, China
Lidong Zhang,
East China Normal University, China

*CORRESPONDENCE

Quan Na,
✉ naq@sj-hospital.org
Liqun Yang,
✉ yangliqun@cmu.edu.cn,
✉ yanglq@lnsjk.com.cn
Jing Chen,
✉ chenjsj-hospital.org

[†]These authors have contributed equally
to this work and share first authorship

RECEIVED 22 September 2023

ACCEPTED 06 November 2023

PUBLISHED 16 November 2023

CITATION

Chen S, Xiao M, Hou Z, Li Z, Hu J, Guo J,
Chen J, Yang L and Na Q (2023),
Functionalized TMC and ϵ -CL elastomers
with shape memory and self-
healing properties.
Front. Bioeng. Biotechnol. 11:1298723.
doi: 10.3389/fbioe.2023.1298723

COPYRIGHT

© 2023 Chen, Xiao, Hou, Li, Hu, Guo,
Chen, Yang and Na. This is an open-
access article distributed under the terms
of the [Creative Commons Attribution
License \(CC BY\)](#). The use, distribution or
reproduction in other forums is
permitted, provided the original author(s)
and the copyright owner(s) are credited
and that the original publication in this
journal is cited, in accordance with
accepted academic practice. No use,
distribution or reproduction is permitted
which does not comply with these terms.

Functionalized TMC and ϵ -CL elastomers with shape memory and self-healing properties

Siwen Chen^{1,2†}, Miaomiao Xiao^{3†}, Zhipeng Hou^{1†}, Zhongcun Li²,
Jianshe Hu², Jing Guo⁴, Jing Chen^{5*}, Liqun Yang^{1,4*} and
Quan Na^{5*}

¹Research Center for Biomedical Materials, Engineering Research Center of Ministry of Education for Minimally Invasive Gastrointestinal Endoscopic Techniques, Shengjing Hospital of China Medical University, Shenyang, China, ²Center for Molecular Science and Engineering, College of Science, Northeastern University, Shenyang, China, ³College of Kinesiology, Shenyang Sport University, Shenyang, China, ⁴Liaoning Research Institute for Eugenic Birth and Fertility, China Medical University, Shenyang, China, ⁵Department of Obstetrics and Gynecology, Shengjing Hospital of China Medical University, Shenyang, China

Introduction: Smart elastomers, which possess self-healing and shape memory capabilities, have immense potential in the field of biomedical applications. Polycarbonates and polyesters have gained widespread interest due to their remarkable biocompatibility over the last century. Nevertheless, the lack of functional versatility in conventional polyesters and polycarbonates means that they fall short of meeting the ever-evolving demands of the future.

Methods: This paper introduced a new smart elastomer, named mPEG₄₃-b-(PMBC-co-PCL)_n, developed from polyester and polycarbonate blends, that possessed shape memory and self-heal capabilities via a physical crosslinking system.

Results: The material demonstrated a significant tensile strength of 0.38 MPa and a tensile ratio of 1155.6%, highlighting its favorable mechanical properties. In addition, a conspicuous shape retrieval rate of 93% was showcased within 32.5 seconds at 37°C. Remarkably, the affected area could be repaired proficiently with no irritation experienced during 6h at room temperature, which was indicative of an admirable repair percentage of 87.6%. Furthermore, these features could be precisely modified by altering the proportion of MBC and ϵ -CL to suit individual constraints.

Discussion: This innovative elastomer with exceptional shape memory and self-heal capabilities provides a solid basis and promising potential for the development of self-contracting intelligent surgical sutures in the biomedical field.

KEYWORDS

elastomer, polycarbonate, polyester, self-healing, shape recovery

1 Introduction

In practical applications, elastomers are frequently exposed to external factors such as environmental conditions and external stresses. These exposures can result in external damage, fractures, or internal cracking, ultimately leading to material failure (Utrera-Barrios et al., 2022). Most elastomers lack self-healing properties, and once the material is damaged,

it cannot be reshaped, often resulting in significant waste (Wemyss et al., 2020). Self-healing elastomers have the capability to restore their structural integrity under specific conditions following material damage (Wang and Urban, 2020). Self-healing elastomers are typically divided into exogenous and intrinsic types (White et al.; Guo et al., 2020). The self-healing capacity of exogenous self-healing elastomers is restricted by the pre-embedded repair reagents within the material. Once these repair reagents are exhausted, the material loses its self-healing ability (Kanu et al., 2019). Intrinsic self-healing elastomers derive their self-healing ability from the breakage and reorganization of reversible chemical bonds in dynamic cross-linked networks, such as hydrogen bonds, ionic interactions, metal-ligand coordination, disulfide exchange, and Diels–Alder reactions (Jian et al., 2018; Song et al., 2018; Fan et al., 2019; Li et al., 2020; Wang et al., 2020; Yang et al., 2020). Compared to exogenous self-healing elastomers, intrinsic self-healing elastomers possess the advantage of an unlimited number of repair cycles, as the repair reagent does not impose limitations. In addition to their self-healing capabilities, these elastomers generally exhibit a higher Young's modulus and stress, greater elongation at break, and enhanced heat resistance compared to similar non-self-repairing elastomers (Xie et al., 2021).

Shape Memory Elastomers (SMEs) belong to a category of smart materials known for their capability to revert from a temporarily programmed shape to their original permanent shape in response to applied forces and external stimuli, such as temperature, pH, light, water or solvents, as well as electric and magnetic fields, among others (Lapcik et al., 1998; Liu et al., 2009; Han et al., 2012; Qi et al., 2014; Bai and Shi, 2017; Zhao et al., 2017; Kong et al., 2019; Davidson et al., 2020; Ze et al., 2020; Cui et al., 2021). Briefly, SMEs are exposed to an external stimulus, typically by heating them above the glass transition temperature while applying an external force. This is followed by cooling below the glass transition temperature for temporary programming, and finally, returning to their original permanent shape upon heating to an appropriate temperature (Chen et al., 2020). Permanent shapes are typically established through covalent bonding, whereas temporarily programmed shapes are generally achieved through weak interactions such as hydrogen bonding, hydrophobic interactions, π - π superposition, ionic bonding, host-guest interactions, etc (Jiang et al., 2017; Wu et al., 2020; Chen Z. et al., 2021; Gallos et al., 2021). Among them, thermally induced shape memory elastomers have garnered significant attention from researchers in recent years, owing to their high deformation rates and ease of production techniques (Chen et al., 2020; Zhao et al., 2020; Yin et al., 2022).

Surgical sutures are one of the most frequently utilized medical devices in daily practice, aimed at facilitating wound healing and minimizing scarring through the secure joining of body tissues. The ideal surgical suture should have good biocompatibility, appropriate mechanical properties, low inflammatory response, and ease of knotting (Shao et al., 2016; Alshomer et al., 2017). The primary challenge encountered with surgical sutures lies in their limited maneuverability during specific minimally invasive procedures for wound closure, posing difficulties in achieving secure suturing and knotting. Moreover, inadequate suture strength can result in visible scar tissue at the wound site, potentially causing infections and hernias. Conversely, excessive suture strength may escalate patient discomfort and induce tissue necrosis at the wound site (Sheng et al., 2017; Tsukamoto et al., 2018; Chen et al., 2022). The utilization of SMEs as a promising choice for surgical sutures represents an appealing

strategy. SMEs equipped with temperature-sensitive triggers can undergo solidification at lower temperatures, effectively storing internal stresses, and subsequently tightening the suture by releasing these stresses at body temperature (Duarah et al., 2018). Therefore, surgical sutures crafted using temperature-sensitive SMEs hold great potential for enhancing surgical maneuvers.

Trimethylene carbonate (TMC) and ϵ -CL are common polymer monomers within the biomedical field. The copolymerization of these monomers exhibits excellent biocompatibility and has been the subject of extensive research in recent years (Mathot et al., 2007; Danhier et al., 2009; Yang et al., 2014a; Yang et al., 2014b; Pires et al., 2016). The conventional P (TMC-co-CL)_n lacks self-healing and shape memory capabilities, thereby limiting its potential applications. In materials science, functionalized modifications to monomers are a prevalent approach to bestow polymers with superior properties (Xu et al., 2014; Ansari et al., 2021). The copolymer's potential for biomedical applications could be significantly enhanced by incorporating ambient temperature self-healing properties and shape memory functionality into P (TMC-co-CL)_n using this method.

In this investigation, we presented a novel shape memory elastomer with self-healing properties, denoted as mPEG₄₃-b-P (MBC-co-CL)_n, obtained by copolymerization of the TMC-functionalised monomer MBC and ϵ -CL. The elastomer was synthesized using mPEG₄₃ as the macromolecular initiator, MBC and CL as the functional monomers, and Sn(Oct)₂ as the reaction catalyst for the ring-opening polymerization reaction. Due to the introduction of benzyl carbonyl groups in MBC, mPEG₄₃-b-P (MBC-co-CL)_n became insoluble in dichloromethane. Infrared analysis confirmed the formation of an internally structured physical crosslinked network within the elastomer, created by hydroxyl and carbonyl groups interacting to form hydrogen bonds. The elastomer mPEG₄₃-b-P (MBC-co-CL)_n exhibited excellent mechanical properties and stretchability. It automatically healed wounds at room temperature without external stimulation and simultaneously demonstrated impressive shape memory at human body temperature. These functions could be regulated by adjusting the ratio of MBC to ϵ -CL, wherein self-healing capability and shape recovery rate increased with higher MBC content. Compared to P (TMC-co-CL)_n, the elastomer mPEG₄₃-b-P (MBC-co-CL)_n demonstrated enhanced self-healing and shape memory functions, thus broadening the potential applications of P (TMC-co-CL)_n in the biomedical field. Compared to traditional surgical sutures, the mPEG₄₃-b-P (MBC-co-CL)_n elastomer exhibits excellent self-healing and shape memory properties at room temperature, with the potential to create knotless self-tightening surgical sutures. This advancement opens up prospects for its potential use in self-retracting surgical suture applications.

2 Experimental section

2.1 Materials

2,2-Bis(hydroxymethyl) propionic acid (99%) was bought from Tianjin Bodi Chemical Co., Ltd. (Tianjin, China). Toluene (99%), Calcium hydride (CaH₂), and Benzyl chloride (99%) were purchased from Sinopharm Chemical Reagent Co. Ltd. (Shanghai, China). Triethylamine (99%) and tetrahydrofuran were purchased from Tianjin Damao Chemical Reagent Factory.

TABLE 1 Reaction conditions for the elastomer mPEG₄₃-b-P (MBC-co-CL).

| Samples | MBC: ϵ -CL | M: I | M: C | T (°C) | t(h) |
|----------------|---------------------|--------|---------|--------|------|
| M ₁ | 1:1 | 2000:1 | 1,000:1 | 130 | 24 |
| M ₂ | 3:1 | 2000:1 | 1,000:1 | 130 | 24 |
| M ₃ | 5:1 | 2000:1 | 1,000:1 | 130 | 24 |

(Tianjin, China). Methoxy polyethylene glycol (mPEG₄₃, 1.9 kDa) was purchased from InnoChem Technology Co. Ltd. (Beijing, China). ϵ -CL and Stannous octoate [Sn(Oct)₂] (99%) were supplied by Sigma-Aldrich. Ethyl chloroformate (99%) was purchased from Xinyi Huili Fine Chemical Co., Ltd. (Xinyi, China). The MBC is synthesized according to a previously published procedure (Liu et al., 2003). ϵ -CL was stirred with CaH₂ for 2 days to dry and then distilled under reduced pressure. 5-methyl-5-benzyloxycarbonyl-1,3-dioxan-2-one (MBC) was synthesized based on previous work (Chen et al., 2020). Toluene was de-watered by sodium filament azeotropic reflux before use. Standard methods purified all other solvents in this study.

2.2 Synthesis of the elastomer mPEG₄₃-b-P (MBC-co-CL)_n

Utilizing mPEG₄₃ as the initiator for ring-opening polymerization and Sn(Oct)₂ as the catalyst, the ratios of monomer MBC and CL were determined as 1:1, 3:1, and 5:1. The ratio of monomer to the initiator (M:I) was set to 2,000:1 and the ratio of monomer to catalyst (M:C) was given at 1,000:1. These combinations resulted in three distinct ratios of elastomers named M₁, M₂, and M₃, with specific details outlined in Table 1. In summary, the polymerization cross-linking process began by placing the PTFE tube mold (length 30 mm, inner diameter 2 mm) inside an ampoule. Subsequently, a toluene solution (0.2 mol/L) containing the monomer, mPEG₄₃ and Sn(Oct)₂ was added to the ampoule. The system was vacuumed and purged with nitrogen three times before the ampoule was sealed to maintain a vacuum-tight system (<15 Pa). Afterward, the ampoule was positioned in an oil bath container at 130°C for 24 h. The elastomers underwent a 72 h immersion in dichloromethane (DCM) to exclude polymer chain segments not involved in cross-linking, including any unreacted monomers. Afterwards, they were vacuum-dried for 24 h until a stable weight was attained.

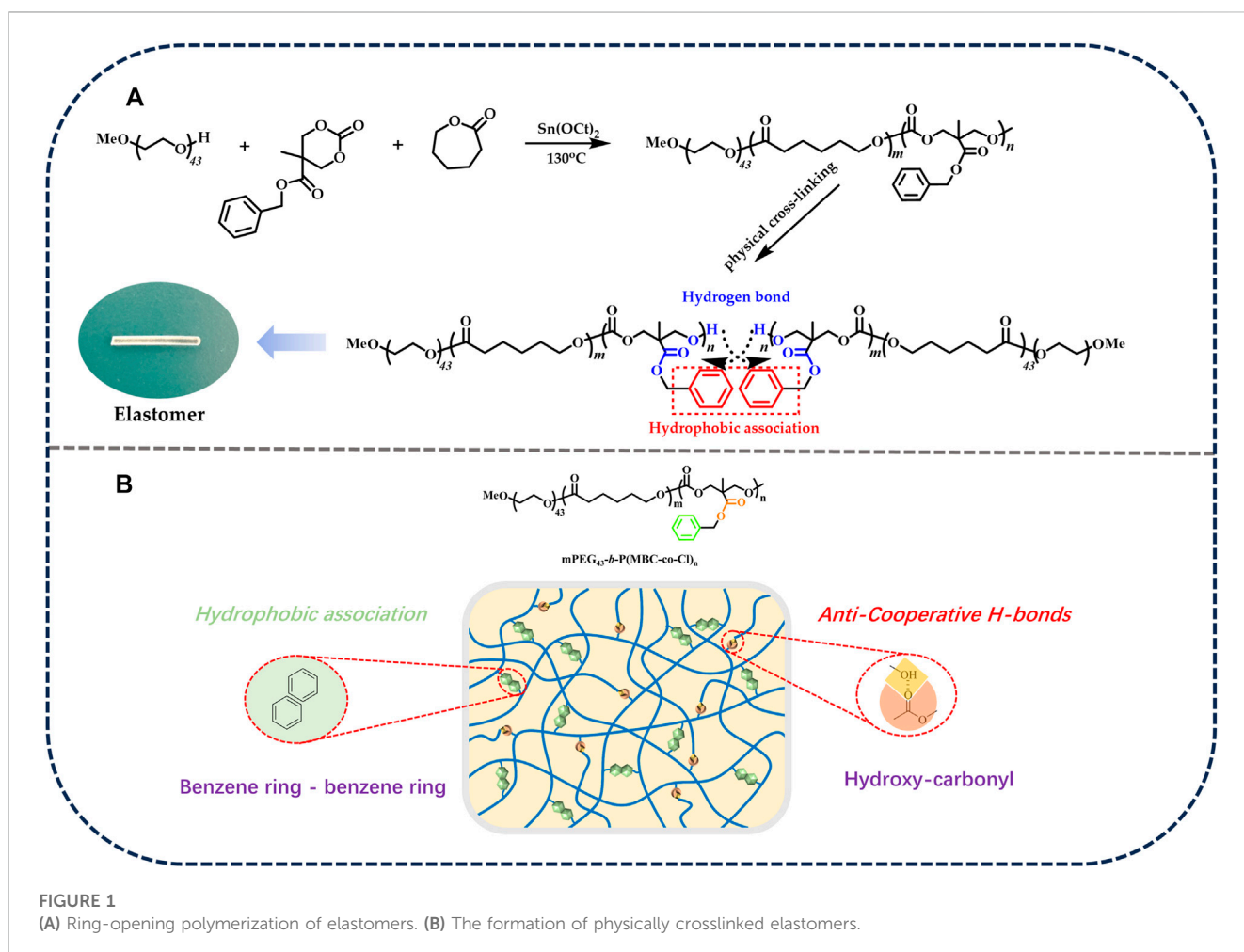
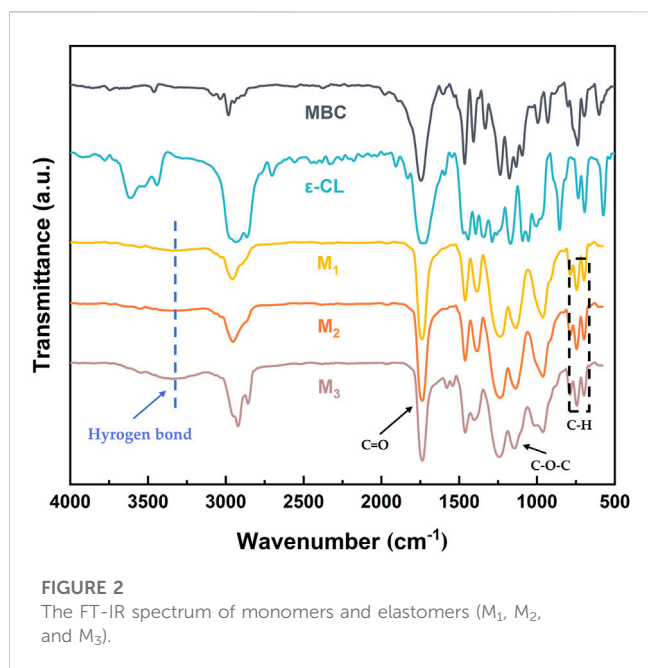


FIGURE 1

(A) Ring-opening polymerization of elastomers. (B) The formation of physically crosslinked elastomers.



2.3 Characterization

Fourier transform infrared spectra (FT-IR) was acquired using a PerkinElmer Spectrum One (B) Spectrometer (PerkinElmer, Foster City, CA, USA) over the range of 4,000–500 cm^{-1} at room temperature.

Thermogravimetric analysis (TGA) was conducted using a Netzsch 209C TGA instrument (Netzsch, Hanau, Germany) over the temperature range of 40°C–800°C with a ramp rate of 20°C/min under nitrogen purging. Differential scanning calorimetry (DSC) was performed utilizing a NETZSCH DSC-204 thermal analyzer (Netzsch, Hanau, Germany). Data was recorded within the temperature range of –50°C–200°C at a rate of 10°C/min under a flowing nitrogen atmosphere.

The swelling experiments were carried out in water and dichloromethane. The weighed samples were immersed in the solvent and changed the solvent every 24 h for a total of 72 h. After removing and drying the surface solvent, the samples were weighed (W_1) and vacuum-dried to constant weight (W_2). The swelling rate (SR) of the elastomer was calculated by Eq. 1, and the gel fraction (GF) was calculated by Eq. 2.

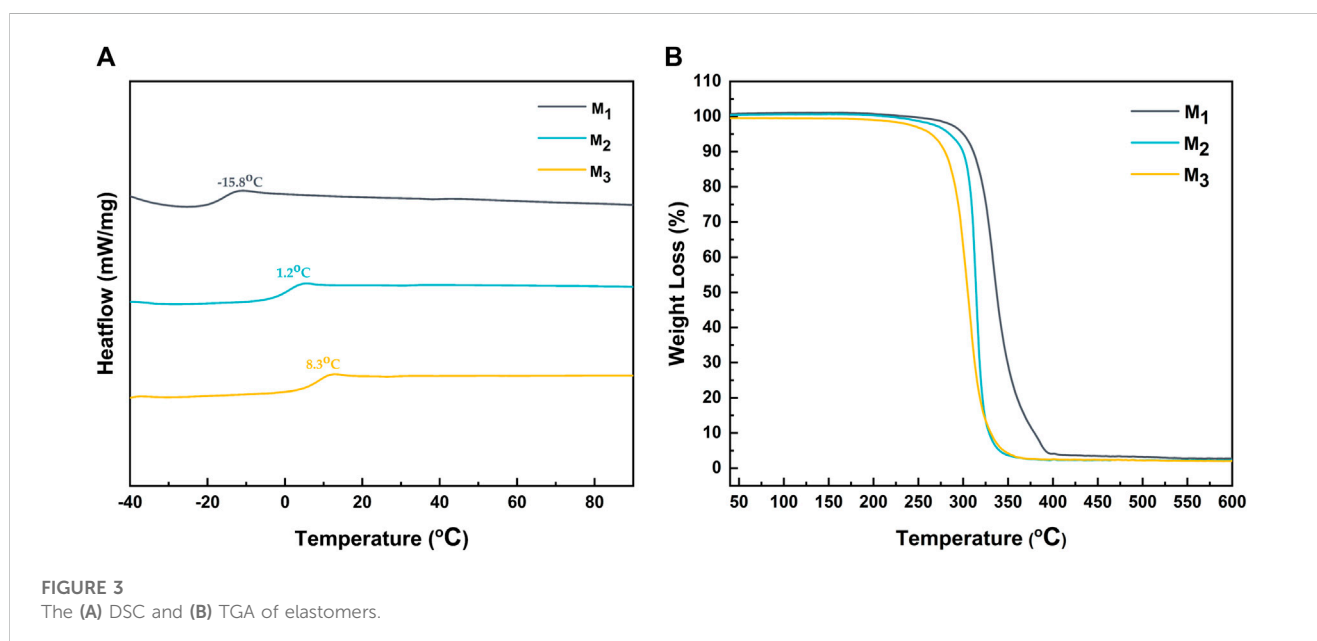
$$SR = \frac{W_1 - W_0}{W_0} \times 100\% \quad (1)$$

$$GF = \frac{W_2}{W_0} \times 100\% \quad (2)$$

W_0 : Initial weight of the elastomer.

A dynamic mechanical analyzer (242E Artemis DMA, Netzsch, Germany) was employed to assess the viscoelastic properties of the polymer. During all tests, measurements were conducted in the tensile mode using cylindrical samples measuring 2 mm in diameter and 20 mm in length. The storage modulus (E') and loss modulus (E'') of the polymers were measured at 25°C over a frequency range of 0.1–100 Hz for frequency testing and at a constant frequency of 1 Hz for various temperatures ranging from 25°C to 70°C. Three replicates were carried out for each sample scale. Tensile mechanical properties of the elastomer were evaluated using the MTS MCT-6103 (Meister, China) universal mechanical testing machine. Elastomeric rods, 20 mm in length and 2 mm in diameter were tested at room temperature with a clamping distance of 10 mm and a stretching rate of 10 mm/min.

The investigation into the self-healing properties of elastomers involved cutting a rod-shaped elastomer in half and rejoining the two cut surfaces, allowing them to contact and self-heal at 25°C for a specified duration. The repaired elastomer was then examined under an optical microscope (Smartzoom 5) to document alterations in the self-healing scratch trajectory. Subsequently, mechanical properties were evaluated using a universal testing machine.



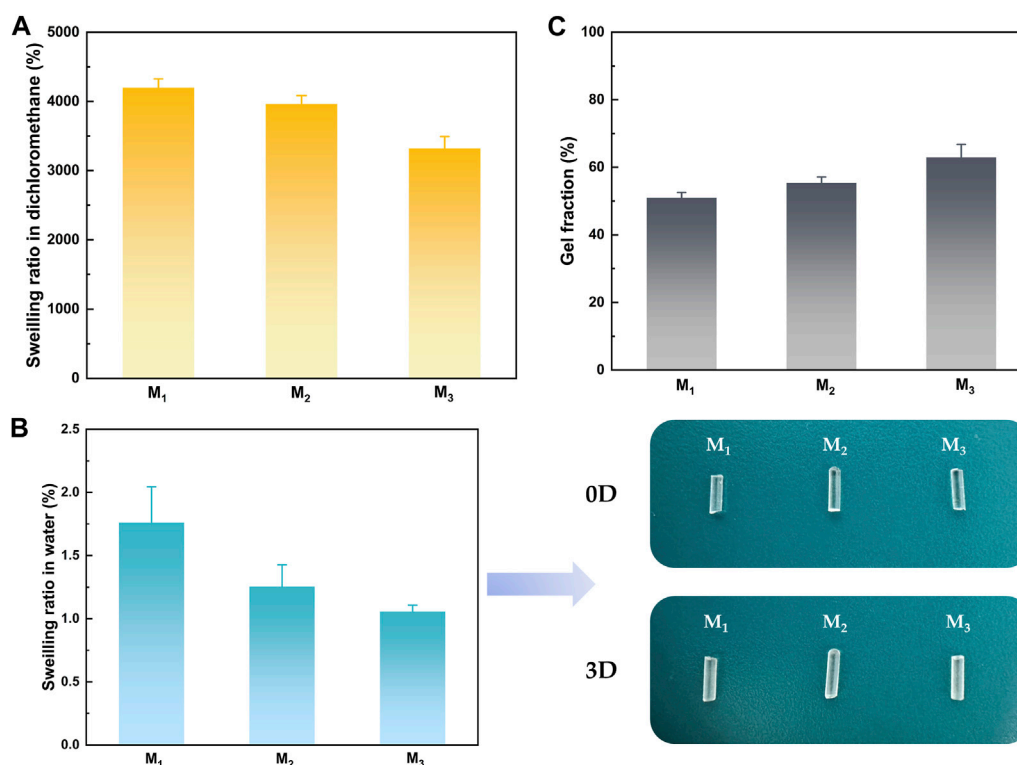


FIGURE 4

Solubilization properties of elastomers in (A) dichloromethane (B) water, and (C) gel fraction.

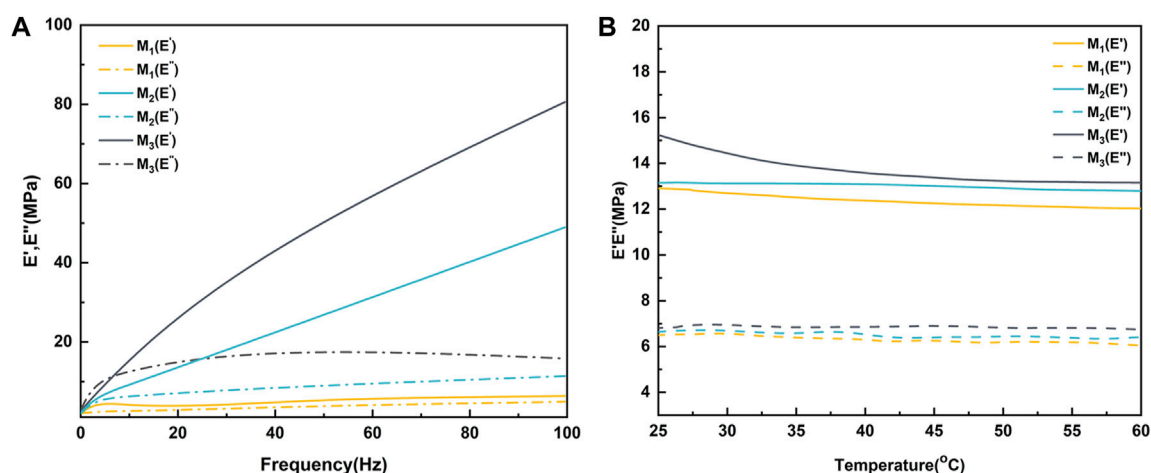


FIGURE 5

Dynamic thermo-mechanical properties of elastomers with (A) variable frequency at room temperature and (B) variable temperature at 1 Hz.

The assessment of the elastomer's shape memory capability proceeded as follows: an external force was applied to the I-shaped rod elastomer at room temperature, causing it to adopt a U-shape (temporary form). Subsequently, the elastomer was solidified in a -20°C environment. Finally, the elastomer was transferred to a 37°C environment, reverting it to its original I-shape (permanent form). The entire process was meticulously recorded using a video camera. Shape

recovery rate (R_f) and shape fixation rate (R_r) were calculated by Eqs 3, 4. The shape memory measurement process is shown in Figure 6A.

$$R_f = \frac{180 - \alpha_0}{180} \times 100\% \quad (3)$$

$$R_r = \frac{180 - \alpha_0 - \alpha_t}{180 - \alpha_0} \times 100\% \quad (4)$$

α_0 : The angle of the elastomer at initial fixation. α_t : The angle of the elastomer at time t .

3 Result and discussion

3.1 Structural characterization of elastomers

The polymerization conditions of the elastomers are shown in Table 1. The process of the ring-opening polymerization reaction and the formation of physically crosslinked elastomers are shown in Figure 1. The structures of the elastomers were analyzed by FT-IR.

The FT-IR of the elastomer is shown in Figure 2. The mPEG-*b*-(PMBC-co-PCL)_n copolymer was synthesized by initiating the ring-opening polymerization of MBC and ϵ -CL by using mPEG₄₃ as initiator and Sn(Oct)₂ as catalyst. The C-H stretching vibrations of 3,100–3,000 cm⁻¹ and the out-of-plane bending vibrations of C-H of 698 and 744 cm⁻¹ proved the existence of the benzene ring. The stretching vibrations at 1,737 and 1,134 cm⁻¹ were the ester carbonyl and aliphatic ether bonds of the copolymer, which demonstrated the successful participation of MBC and ϵ -CL in the ring-opening polymerization reaction. The broad peaks appearing at 3,500–3,150 cm⁻¹ in the FT-IR spectrum of M₁, M₂, and M₃ were due to the hydrogen bonding reaction between the hydroxyl group at the end of the polymer and the ester carbonyl group of the PMBC side chain (Chen C. et al., 2021). The gradual enhancement of the hydrogen bonding peaks of M₁, M₂, and M₃ was attributed to the increase in the MBC content which increased the probability of hydrogen bond formation.

3.2 Thermodynamic properties of elastomers

The glass transition temperature analysis of the elastomer was performed using DSC. As illustrated in Figure 3A, there was a notable increase in the glass transition temperature of the elastomer with the augmentation of MBC content, ranging from -15.8°C for M₁ to 8.3°C for M₃. This phenomenon could be attributed to the increase in the number of benzene rings and side chain ester carbonyls in MBC, elevating the likelihood of π - π conjugation between benzene rings and the formation of both intramolecular and intermolecular hydrogen bonding within the system. Additionally, a decreased ϵ -CL ratio resulted in fewer flexible chain segments in the molecule, consequently enhancing the overall rigidity of the elastomer. Furthermore, TGA characterization was performed to analyze the thermal behavior of the elastomers.

Figure 3B demonstrated the weight loss of the elastomer at various temperatures, and the temperature at which the elastomer experiences a 5% weight loss is defined as its decomposition temperature. Interestingly, the decomposition temperature decreased with an increase in MBC content. This was due to the fact that the decomposition temperature of PMBC is lower than that of PCL. Specifically, the decomposition temperature for M₁, M₂, and M₃ were determined to be 300.1°C, 285°C, and 264.3°C, respectively.

3.3 Swelling properties of elastomers

The impact of MBC content on the crosslinking network was revealed through the analysis of the swelling behavior of elastomers in water and organic solvents with three distinct MBC ratios. Based on the data presented in Figures 4A, B, it was observed that as the MBC content increased, the swelling ratio of the elastomer in both dichloromethane and water decreased. As the MBC content in the crosslinked network rose, there was an increase in π - π conjugation between the benzene rings and an elevated quantity of hydrogen bonds between the hydroxyl groups at the polymer segment termini and the ester carbonyls of the side chains, leading to an increase in the degree of cross-linking. Furthermore, the benzene ring, classified as a lipophilic group, played a role in enhancing the hydrophobicity of the elastomer due to an increased presence of benzene rings within the polymer chain segments. This heightened hydrophobicity was evidenced by the gel fraction of the elastomers depicted in Figure 4C, showcasing an augmentation with the rise in MBC content. The escalation of MBC content facilitated an increase in the number of hydrogen bonds within the crosslinked network. Consequently, intermolecular and intramolecular entanglements were more readily formed, contributing to the heightened gel fraction of the elastomers. Elastomers are virtually insoluble in water, so there was no change in properties in the body due to fluid exchange. Therefore, the elastomers held promising potential for their application in surgical suture direction.

3.4 Dynamic thermo-mechanical properties

The dynamic thermo-mechanical properties of the elastomers are illustrated in Figure 5. In the frequency sweep test at room temperature (Figure 5A), M₁ displayed the highest energy storage modulus (E') at 6.3 MPa and a loss modulus (E'') of 4.9 MPa at 100 Hz. Across all samples, there was a noticeable trend of increasing E' and E'' with higher frequencies. Additionally, both E' and E'' of the elastomers exhibited a significant upward trend with increasing MBC content. Specifically, for M₃, the values were measured at 80.6 MPa (E') and 15.82 MPa (E''), respectively. This phenomenon could be attributed to the increase in MBC content, resulting in a higher number of side-chain hydroxyl groups and benzene rings in the molecular chain segments. This increase enhanced the likelihood of hydrogen bonding, π - π stacking formation, and an overall rise in crosslink density. Beyond the frequency sweep test, a fixed 1 Hz variable temperature test was conducted on the elastomers (Figure 5B). It was observed that regardless of the monomer ratio, the E' and E'' of the elastomers decreased with increasing temperature. This could be explained by heightened molecular thermal motion at high temperatures, causing an increase in distance between the molecules of the chain segments and reducing the effects of hydrogen bonding and π - π stacking. This outcome suggested that elastomers tend to exhibit higher viscosity at elevated temperatures, potentially enhancing their self-healing properties.

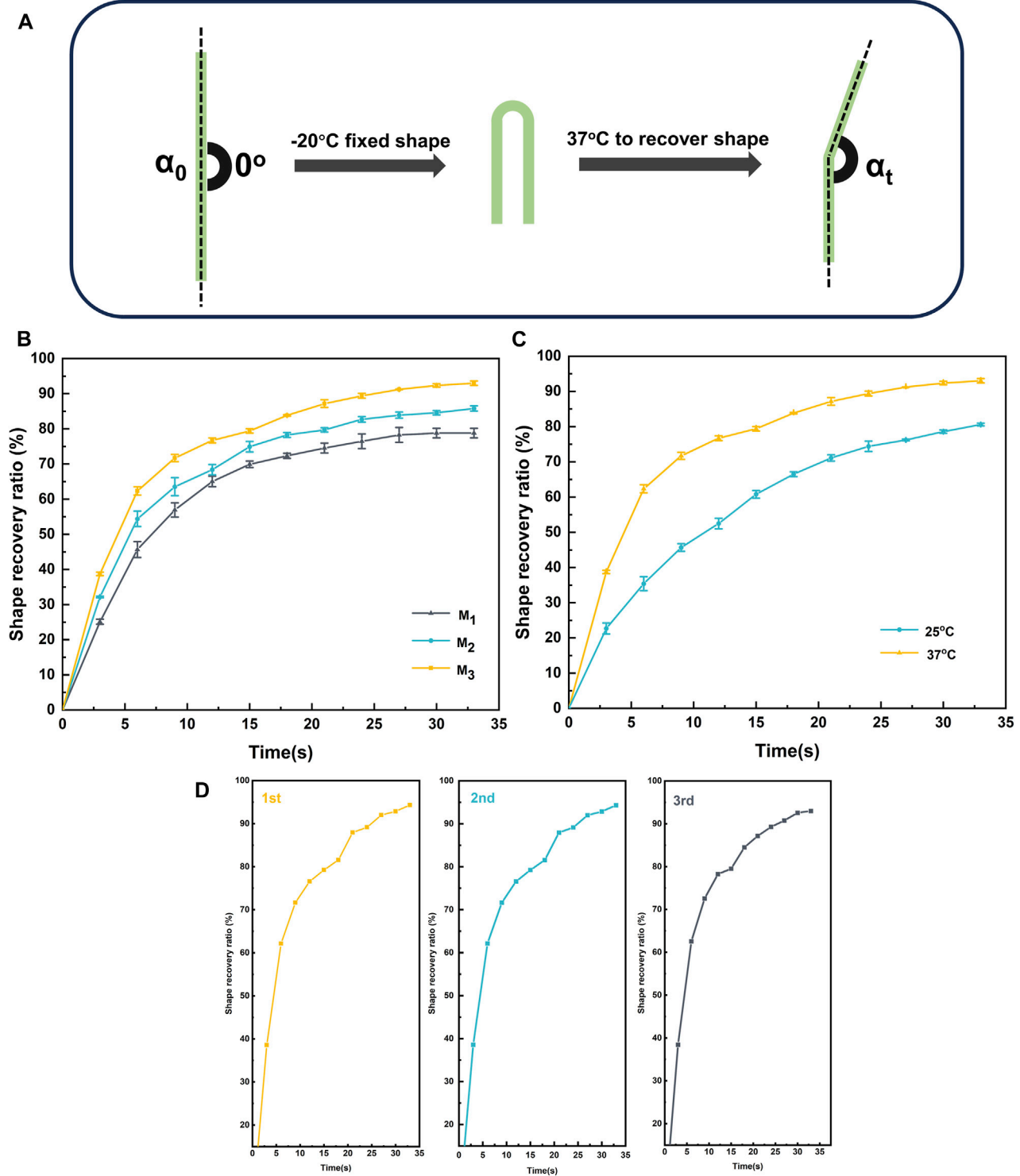


FIGURE 6 Shape memory (A) processes of elastomers with (B) different monomer ratios, (C) different temperatures of M_3 and (D) shape memory repeatability of M_3 .

TABLE 2 Shape memory properties of M_1 , M_2 , and M_3 .

| Samples | R_r (%) | R_f (%) |
|---------|-----------|-----------|
| M_1 | 95.2 | 78.8 |
| M_2 | 92.1 | 85.8 |
| M_3 | 87.2 | 93 |

3.5 Shape memory behaviors and self-healing properties

Elastomers could be endowed with shape memory properties utilizing a dynamic crosslinked network structure and a glass transition temperature (T_g). Initially, the elastomer was shaped into a temporary form at room temperature and subsequently solidified in an environment below T_g . Later, when exposed to a 37°C environment, the molecular motion within the elastomer's

crosslinked network was reactivated, and the rigidity was induced to revert to the initial shape. This transformation was facilitated by the increased rigidity effect resulting from hydrogen bonding and π - π stacking. Figure 6A illustrated the shape memory process of the elastomer. Figure 6B illustrated the deformation recovery at various recovery times for the elastomer samples denoted as M_1 , M_2 , and M_3 . The deformation recovery for M_1 , M_2 , and M_3 was observed to be completed within 32.5 s at 37°C, displaying recovery rates (R_r) of 87.2% and remarkable restoration rates (R_f) of 93% (Table 2). As the MBC content increased in the elastomer, there was a notable decrease in R_f , although R_r exhibited a significant increase. This behavior stemmed from the interplay of MBC content with the elastomer's rigidity and interaction forces within the rigid chain segments. Specifically, at lower MBC content, the interaction force among the rigid chain segments in the elastomer was relatively weak, resulting in a gel with a feeble restoring force. Conversely, higher MBC content intensified hydrogen bonding and π - π stacking in the crosslinked network, enhancing the elastomer's rigidity, inducing

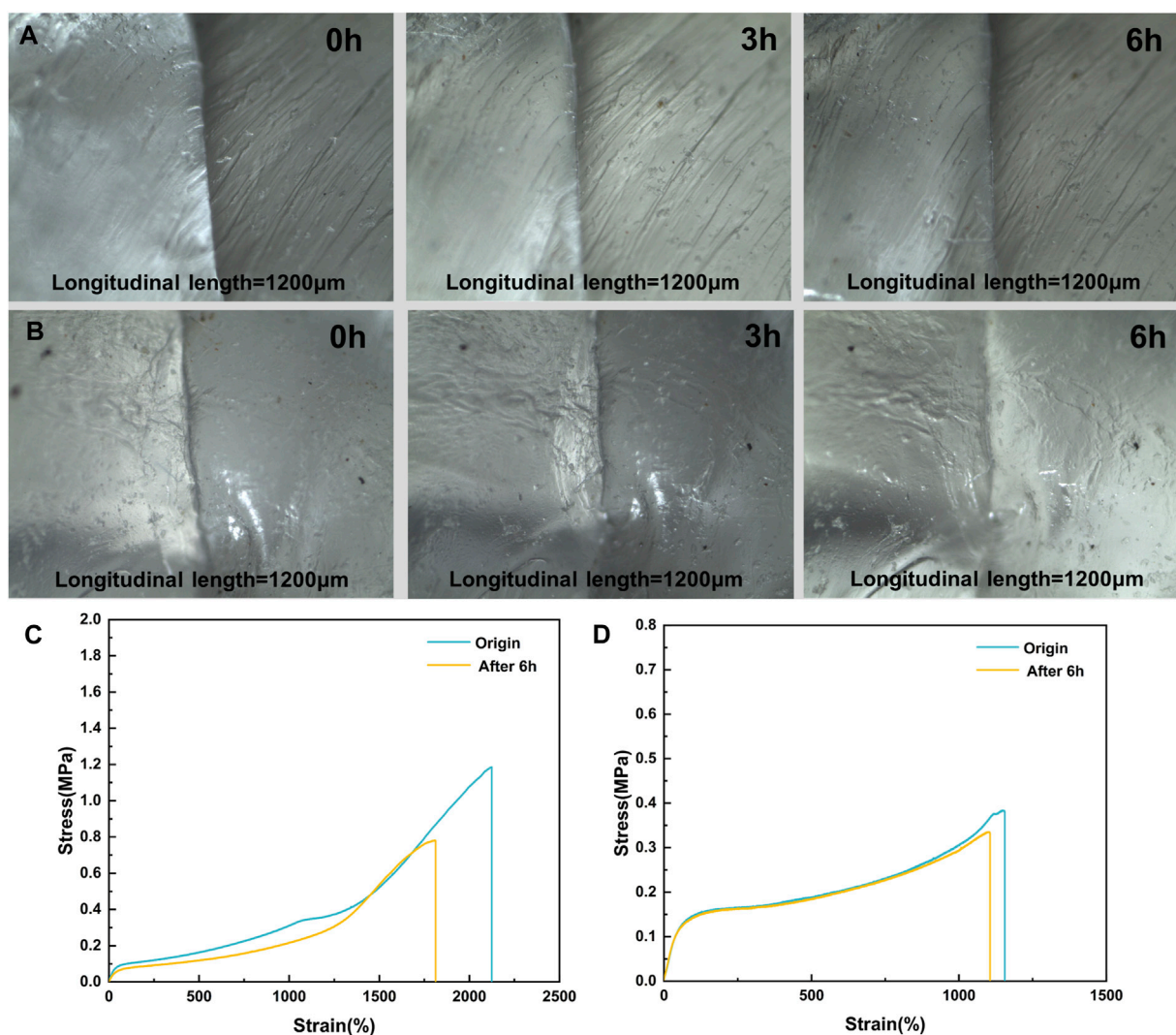


FIGURE 7 (A,B) Optical Images of Scratch Self-healing and (C,D) Tensile Properties Before and After Repair for M_1 and M_3 .

substantial phase separation, and making shape fixation less facile, yet augmenting repulsive forces. Furthermore, we conducted a study on the shape memory functionality of the elastomer at different temperatures. As shown in Figure 6C, at 37°C, the elastomer exhibited a significantly higher R_f (93%) compared to the R_f (80.6%) observed at 25°C. This is attributed to the elevated temperature, which accelerates the motion of polymer chain segments within the elastomer, resulting in a faster shape recovery. In addition to the analysis of R_f and R_r , evaluating the repeatability and fatigue resistance of elastomer shape memory was paramount for assessing its potential in practical applications. Using M_3 as a representative, as depicted in Figure 6D, we examined the shape memory capability of the elastomer over three consecutive cycles. Remarkably, the same sample exhibited no signs of fatigue and maintained a consistently stable shape memory capacity throughout the three consecutive cycles. This observation underscored the elastomer's robust fatigue resistance and its capability to sustain a reliable shape memory performance over subsequent practical applications.

The physical cross-linking network inherent in elastomers not only imparted them with shape memory functionality but also endowed them with self-healing properties. The self-heal capacity of elastomers relies on the reversible dynamics of hydrogen bonding and the predominance of π - π stacking interactions. We have examined the self-heal capability of elastomers through meticulous analysis using optical microscopy and precise tensile testing. The self-healing phenomena depicted in Figures 7A, B vividly showcased the remarkable self-healing attributes of the elastomer. Upon bisecting the elastomer into two segments, optimal self-healing was achieved by carefully aligning and adhering the wounded surfaces without external pressure, followed by a 37°C incubation for 6 h. Leveraging its inherent shape memory function, the elastomer could substantially restore the original configuration of the damaged site through stored strain, maximizing the contact area during the repair process. Upon contact, the fractured hydrogen bonding network underwent a reconstructive phase, enabling the healing of the elastomer wound.

In addition to examining the macroscopic morphology, it was crucial to consider the recovery of elastomer mechanical properties. By analyzing stress-strain curves of the original samples following self-healing, Figures 7C, D illustrated that after 6 h of self-healing at 37°C, the fracture stress of M_3 was restored to 87.6% of its initial value, whereas M_1 only recovered to 65.8% of its initial value. The study demonstrated that the self-healing ability of M_3 surpasses that of M_1 . This was attributable to the higher MBC content found in M_3 than in M_1 . As a result, there was a greater likelihood and number of hydrogen bonding and π - π stacking formation, which enhanced the self-healing process. The excellent room temperature self-repairing properties and shape memory at body temperature of the elastomers gave them the potential to be prepared as self-retracting surgical suture money, which was further investigated in the clinic.

4 Conclusion

Through the copolymerization of MBC and ϵ -CL with mPEG₄₃ as the initiator and Sn(Oct)₂ as the catalyst, novel smart elastomers, denoted as mPEG-*b*-(PMBC-co-PCL)_n, were successfully

synthesized. These elastomers exhibited exceptional mechanical properties, demonstrated by a tensile ratio of 1,155.6% and a tensile strength of 0.38 MPa. Notably, a remarkable shape recovery of 93% was achieved within 32.5 s at 37°C, underscoring their efficient shape memory performance. Moreover, their self-healing capability, primarily driven by hydrogen bonding and π - π stacking interactions, showcased an impressive self-healing efficiency of 87.6% after a 6 h self-healing process at room temperature without external stimuli. The elastomer mPEG-*b*-(PMBC-co-PCL)_n boasted exceptional attributes, including its near insolubility in water, remarkable shape memory capabilities, and outstanding self-heal efficiency. These unique qualities opened up possibilities for its utilization in the realm of self-retracting surgical sutures, potentially revolutionizing the field of clinical surgical procedures.

Data availability statement

The raw data supporting the conclusion of this article will be made available by the authors, without undue reservation.

Author contributions

SC: Data curation, Methodology, Writing—original draft. MX: Writing—original draft, Software. ZH: Writing—review and editing, Supervision. ZL: Writing—review and editing, Data curation. JH: Writing—review and editing, Supervision. JG: Writing—review and editing, Project administration. JC: Formal Analysis, Writing—review and editing. LY: Writing—review and editing, Conceptualization. QN: Writing—review and editing, Visualization, Supervision.

Funding

The author(s) declare financial support was received for the research, authorship, and/or publication of this article. This research work was supported by the Natural Science Foundation of Liaoning Province (2022-YGJC-69) and the support program for excellent young scholars of China Medical University.

Conflict of interest

The authors declare that the research was conducted in the absence of any commercial or financial relationships that could be construed as a potential conflict of interest.

Publisher's note

All claims expressed in this article are solely those of the authors and do not necessarily represent those of their affiliated organizations, or those of the publisher, the editors and the reviewers. Any product that may be evaluated in this article, or claim that may be made by its manufacturer, is not guaranteed or endorsed by the publisher.

References

- Alshomer, F., Madhavan, A., Pathan, O., and Song, W. (2017). Bioactive sutures: a review of advances in surgical suture functionalisation. *Curr. Med. Chem.* 24 (2), 215–223. doi:10.2174/0929867324666161118141724
- Ansari, I., Singh, P., Mittal, A., Mahato, R. I., and Chitkara, D. (2021). 2,2-Bis(hydroxymethyl) propionic acid based cyclic carbonate monomers and their (co) polymers as advanced materials for biomedical applications. *Biomaterials* 275, 120953. doi:10.1016/j.biomaterials.2021.120953
- Bai, J., and Shi, Z. (2017). Dynamically cross-linked elastomer hybrids with light-induced rapid and efficient self-healing ability and reprogrammable shape memory behavior. *ACS Appl. Mater. Interfaces* 9 (32), 27213–27222. doi:10.1021/acsami.7b06407
- Chen, C., Chen, S., Guo, Z., Hu, W., Chen, Z., Wang, J., et al. (2020). Highly efficient self-healing materials with excellent shape memory and unprecedented mechanical properties. *J. Mater. Chem. A* 8 (32), 16203–16211. doi:10.1039/d0ta04933f
- Chen, C., Hou, Z., Chen, S., Guo, J., Chen, Z., Hu, J., et al. (2022). Photothermally responsive smart elastomer composites based on aliphatic polycarbonate backbone for biomedical applications. *Compos. Part B Eng.* 240, 109985. doi:10.1016/j.compositesb.2022.109985
- Chen, C., Li, Z., Chen, S., Kong, L., Guo, Z., Hu, J., et al. (2021b). The preparation of hydrogels with highly efficient self-healing and excellent mechanical properties. *J. Mol. Liq.* 329, 115581. doi:10.1016/j.molliq.2021.115581
- Chen, Z., Li, Y., and Yao, C. (2021a). Biomass shape memory elastomers with rapid self-healing properties and high recyclability. *Biomacromolecules* 22 (6), 2768–2776. doi:10.1021/acs.biomac.1c00465
- Cui, Y., Li, D., Gong, C., and Chang, C. (2021). Bioinspired shape memory hydrogel artificial muscles driven by solvents. *ACS nano* 15 (8), 13712–13720. doi:10.1021/acsnano.1c05019
- Danhier, F., Magotteaux, N., Ucakar, B., Lecouturier, N., Brewster, M., and Préat, V. (2009). Novel self-assembling PEG-p-(CL-co-TMC) polymeric micelles as safe and effective delivery system for paclitaxel. *Eur. J. Pharm. Biopharm.* 73 (2), 230–238. doi:10.1016/j.ejpb.2009.06.015
- Davidson, E. C., Kotikian, A., Li, S., Aizenberg, J., and Lewis, J. A. (2020). 3D printable and reconfigurable liquid crystal elastomers with light-induced shape memory via dynamic bond exchange. *Adv. Mater.* 32 (1), 1905682. doi:10.1002/adma.201905682
- Duarah, R., Singh, Y. P., Gupta, P., Mandal, B. B., and Karak, N. (2018). Smart self-tightening surgical suture from a tough bio-based hyperbranched polyurethane/reduced carbon dot nanocomposite. *Biomed. Mater.* 13 (4), 045004. doi:10.1088/1748-605x/aab93c
- Fan, C.-J., Huang, Z.-C., Li, B., Xiao, W.-X., Zheng, E., Yang, K.-K., et al. (2019). A robust self-healing polyurethane elastomer: from H-bonds and stacking interactions to well-defined microphase morphology. *Sci. China Mater.* 62 (8), 1188–1198. doi:10.1007/s40843-019-9422-7
- Gallois, A., Crowet, J.-M., Michely, L., Raghuvanshi, V. S., Mention, M. M., Langlois, V., et al. (2021). Blending ferulic acid derivatives and polylactic acid into biobased and transparent elastomeric materials with shape memory properties. *Biomacromolecules* 22 (4), 1568–1578. doi:10.1021/acs.biomac.1c00002
- Guo, H., Han, Y., Zhao, W., Yang, J., and Zhang, L. (2020). Universally autonomous self-healing elastomer with high stretchability. *Nat. Commun.* 11 (1), 2037. doi:10.1038/s41467-020-15949-8
- Han, X. J., Dong, Z. Q., Fan, M. M., Liu, Y., Li, J. H., Wang, Y. F., et al. (2012). pH-induced shape-memory polymers. *Macromol. rapid Commun.* 33 (12), 1055–1060. doi:10.1002/marc.201200153
- Jian, X., Hu, Y., Zhou, W., and Xiao, L. (2018). Self-healing polyurethane based on disulfide bond and hydrogen bond. *Polym. Adv. Technol.* 29 (1), 463–469. doi:10.1002/pat.4135
- Jiang, Z.-C., Xiao, Y.-Y., Kang, Y., Pan, M., Li, B.-J., and Zhang, S. (2017). Shape memory polymers based on supramolecular interactions. *ACS Appl. Mater. interfaces* 9 (24), 20276–20293. doi:10.1021/acsami.7b03624
- Kanu, N. J., Gupta, E., Vates, U. K., and Singh, G. K. (2019). Self-healing composites: a state-of-the-art review. *Compos. Part A Appl. Sci. Manuf.* 121, 474–486. doi:10.1016/j.compositesa.2019.04.012
- Kong, D., Li, J., Guo, A., Zhang, X., and Xiao, X. (2019). Self-healing high temperature shape memory polymer. *Eur. Polym. J.* 120, 109279. doi:10.1016/j.eurpolymj.2019.109279
- Lapcik, L., Jr, Lapcik, L., De Smedt, S., Demeester, J., and Chabreck, P. (1998). Hyaluronan: preparation, structure, properties, and applications. *Chem. Rev.* 98 (8), 2663–2684. doi:10.1021/cr941199z
- Li, Z., Shan, Y., Wang, X., Li, H., Yang, K., and Cui, Y. (2020). Self-healing flexible sensor based on metal-ligand coordination. *Chem. Eng. J.* 394, 124932. doi:10.1016/j.cej.2020.124932
- Liu, Y., Lv, H., Lan, X., Leng, J., and Du, S. (2009). Review of electro-active shape-memory polymer composite. *Compos. Sci. Technol.* 69 (13), 2064–2068. doi:10.1016/j.compscitech.2008.08.016
- Liu, Z. L., Zhou, Y., and Zhuo, R. X. (2003). Synthesis and properties of functional aliphatic polycarbonates. *J. Polym. Sci. Part A Polym. Chem.* 41 (24), 4001–4006. doi:10.1002/pola.11001
- Mathot, F., des Rieux, A., Arien, A., Schneider, Y.-J., Brewster, M., and Préat, V. (2007). Transport mechanisms of mmePEG750P (CL-co-TMC) polymeric micelles across the intestinal barrier. *J. Control. release* 124 (3), 134–143. doi:10.1016/j.jconrel.2007.09.001
- Pires, L. R., Guarino, V., Oliveira, M. J., Ribeiro, C. C., Barbosa, M. A., Ambrosio, L., et al. (2016). Ibuprofen-loaded poly (trimethylene carbonate-co-ε-caprolactone) electrospun fibres for nerve regeneration. *J. tissue Eng. Regen. Med.* 10 (3), E154–E166. doi:10.1002/term.1792
- Qi, X., Yao, X., Deng, S., Zhou, T., and Fu, Q. (2014). Water-induced shape memory effect of graphene oxide reinforced polyvinyl alcohol nanocomposites. *J. Mater. Chem. A* 2 (7), 2240–2249. doi:10.1039/c3ta14340f
- Shao, K., Han, B., Gao, J., Jiang, Z., Liu, W., Liu, W., et al. (2016). Fabrication and feasibility study of an absorbable diacetyl chitin surgical suture for wound healing. *J. Biomed. Mater. Res. Part B Appl. Biomaterials* 104 (1), 116–125. doi:10.1002/jbm.b.33307
- Sheng, Z.-Z., Liu, X., Min, L.-L., Wang, H.-L., Liu, W., Wang, M., et al. (2017). Bioinspired approaches for medical devices. *Chin. Chem. Lett.* 28 (6), 1131–1134. doi:10.1016/j.cclet.2017.03.033
- Song, Y., Liu, Y., Qi, T., and Li, G. L. (2018). Towards dynamic but supertough healable polymers through biomimetic hierarchical hydrogen-bonding interactions. *Angew. Chem. Int. Ed.* 57 (42), 13838–13842. doi:10.1002/anie.201807622
- Tsakamoto, Y., Oshima, H., Katsumori, T., Hamaguchi, H., Yamamoto, S., Iwanaga, T., et al. (2018). Endoscopic topical therapy using mesh for refractory suture failure after rectal cancer surgery. *Cancer & Chemother.* 45 (3), 474–476.
- Utrera-Barrios, S., Verdejo, R., López-Manchado, M. Á., and Santana, M. H. (2022). The final frontier of sustainable materials: current developments in self-healing elastomers. *Int. J. Mol. Sci.* 23 (9), 4757. doi:10.3390/ijms23094757
- Wang, S., and Urban, M. W. (2020). Self-healing polymers. *Nat. Rev. Mater.* 5 (8), 562–583. doi:10.1038/s41578-020-0202-4
- Wang, X., Liang, D., and Cheng, B. (2020). Preparation and research of intrinsic self-healing elastomers based on hydrogen and ionic bond. *Compos. Sci. Technol.* 193, 108127. doi:10.1016/j.compscitech.2020.108127
- Wemyss, A. M., Bowen, C., Plesse, C., Vancaeyzeele, C., Nguyen, G. T., Vidal, F., et al. (2020). Dynamic crosslinked rubbers for a green future: a material perspective. *Mater. Sci. Eng. R Rep.* 141, 100561. doi:10.1016/j.mser.2020.100561
- White, S. R., Sottos, N. R., Geubelle, P. H., Moore, J. S., Kessler, M. R., Sriram, S., et al. (2001). Autonomic healing of polymer composites. *Nature* 409 (6822), 794–797. doi:10.1038/35057232
- Wu, W., Zhou, Y., Li, J., and Wan, C. (2020). Shape memory and self-healing behavior of styrene-butadiene-styrene/ethylene-methacrylic acid copolymer (SBS/EMAA) elastomers containing ionic interactions. *J. Appl. Polym. Sci.* 137 (19), 48666. doi:10.1002/app.48666
- Xie, Z., Hu, B.-L., Li, R.-W., and Zhang, Q. (2021). Hydrogen bonding in self-healing elastomers. *ACS omega* 6 (14), 9319–9333. doi:10.1021/acsomega.1c00462
- Xu, J., Feng, E., and Song, J. (2014). Renaissance of aliphatic polycarbonates: new techniques and biomedical applications. *J. Appl. Polym. Sci.* 131 (5), 39822. doi:10.1002/app.39822
- Yang, L., Li, J., Jin, Y., Zhang, J., Li, M., and Gu, Z. (2014b). Highly efficient cross-linking of poly(trimethylene carbonate) via bis(trimethylene carbonate) or bis(ε-caprolactone). *Polymer* 55 (26), 6686–6695. doi:10.1016/j.polymer.2014.10.072
- Yang, L., Li, J., Meng, S., Jin, Y., Zhang, J., Li, M., et al. (2014a). The *in vitro* and *in vivo* degradation behavior of poly (trimethylene carbonate-co-ε-caprolactone) implants. *Polymer* 55 (20), 5111–5124. doi:10.1016/j.polymer.2014.08.027
- Yang, S., Du, X., Deng, S., Qiu, J., Du, Z., Cheng, X., et al. (2020). Recyclable and self-healing polyurethane composites based on Diels-Alder reaction for efficient solar-to-thermal energy storage. *Chem. Eng. J.* 398, 125654. doi:10.1016/j.cej.2020.125654
- Yin, C., Wang, T., Shen, X., Fu, J., Li, T., and Jiang, T. (2022). Body-temperature programmable ultra-soft shape memory elastomers for comfort fitting. *Smart Mater. Struct.* 31 (10), 105029. doi:10.1088/1361-665x/ac9101
- Ze, Q., Kuang, X., Wu, S., Wong, J., Montgomery, S. M., Zhang, R., et al. (2020). Magnetic shape memory polymers with integrated multifunctional shape manipulation. *Adv. Mater.* 32 (4), 1906657. doi:10.1002/adma.201906657
- Zhao, W., Liu, Y., Zhang, Z., Feng, X., Xu, H., Xu, J., et al. (2020). High-strength, fast self-healing, aging-insensitive elastomers with shape memory effect. *ACS Appl. Mater. interfaces* 12 (31), 35445–35452. doi:10.1021/acsami.0c09045
- Zhao, X., Dong, R., Guo, B., and Ma, P. X. (2017). Dopamine-incorporated dual bioactive electroactive shape memory polyurethane elastomers with physiological shape recovery temperature, high stretchability, and enhanced C2C12 myogenic differentiation. *ACS Appl. Mater. interfaces* 9 (35), 29595–29611. doi:10.1021/acsami.7b10583



OPEN ACCESS

EDITED BY

Lin Yu,
Fudan University, China

REVIEWED BY

Daokun Shi,
MicroPort Medical Science Co., Ltd.,
China
Bhupendra Gopalbhai Prajapati,
Ganpat University, India

*CORRESPONDENCE

Kai Zhang,
✉ zhangkaidoctor@163.com
Liqun Yang,
✉ yangliqun@cmu.edu.cn,
✉ yangliqun@inszjk.com.cn
Siyu Sun,
✉ sun-siyu@163.com

[†]These authors have contributed equally
to this work and share first authorship

RECEIVED 25 October 2023

ACCEPTED 27 November 2023

PUBLISHED 06 December 2023

CITATION

Yang Y, Yang Y, Hou Z, Wang T, Wu P,
Shen L, Li P, Zhang K, Yang L and Sun S
(2023), Comprehensive review of
materials, applications, and future
innovations in biodegradable
esophageal stents.
Front. Bioeng. Biotechnol. 11:1327517.
doi: 10.3389/fbioe.2023.1327517

COPYRIGHT

© 2023 Yang, Yang, Hou, Wang, Wu,
Shen, Li, Zhang, Yang and Sun. This is an
open-access article distributed under the
terms of the [Creative Commons
Attribution License \(CC BY\)](https://creativecommons.org/licenses/by/4.0/). The use,
distribution or reproduction in other
forums is permitted, provided the original
author(s) and the copyright owner(s) are
credited and that the original publication
in this journal is cited, in accordance with
accepted academic practice. No use,
distribution or reproduction is permitted
which does not comply with these terms.

Comprehensive review of materials, applications, and future innovations in biodegradable esophageal stents

Yaochen Yang^{1,2†}, Yuanyuan Yang^{1†}, Zhipeng Hou^{2†},
Tingting Wang¹, Peng Wu¹, Lufan Shen¹, Peng Li³, Kai Zhang^{1*},
Liqun Yang^{2,3*} and Siyu Sun^{1*}

¹Department of Gastroenterology, Endoscopic Center, Engineering Research Center of Ministry of Education for Minimally Invasive Gastrointestinal Endoscopic Techniques, Shengjing Hospital of China Medical University, Shenyang, China, ²Research Center for Biomedical Materials, Engineering Research Center of Ministry of Education for Minimally Invasive Gastrointestinal Endoscopic Techniques, Shengjing Hospital of China Medical University, Shenyang, China, ³Liaoning Research Institute for Eugenic Birth and Fertility, China Medical University, Shenyang, China

Esophageal stricture (ES) results from benign and malignant conditions, such as uncontrolled gastroesophageal reflux disease (GERD) and esophageal neoplasms. Upper gastrointestinal endoscopy is the preferred diagnostic approach for ES and its underlying causes. Stent insertion using an endoscope is a prevalent method for alleviating or treating ES. Nevertheless, the widely used self-expandable metal stents (SEMS) and self-expandable plastic stents (SEPS) can result in complications such as migration and restenosis. Furthermore, they necessitate secondary extraction in cases of benign esophageal stricture (BES), rendering them unsatisfactory for clinical requirements. Over the past 3 decades, significant attention has been devoted to biodegradable materials, including synthetic polyester polymers and magnesium-based alloys, owing to their exceptional biocompatibility and biodegradability while addressing the challenges associated with recurring procedures after BES resolves. Novel esophageal stents have been developed and are undergoing experimental and clinical trials. Drug-eluting stents (DES) with drug-loading and drug-releasing capabilities are currently a research focal point, offering more efficient and precise ES treatments. Functional innovations have been investigated to optimize stent performance, including unidirectional drug-release and anti-migration features. Emerging manufacturing technologies such as three-dimensional (3D) printing and new biodegradable materials such as hydrogels have also contributed to the innovation of esophageal stents. The ultimate objective of the research and development of these materials is their clinical application in the treatment of ES and other benign conditions and the palliative treatment of malignant esophageal stricture (MES). This review aimed to offer a

Abbreviations: ES, esophageal stricture; BES, benign esophageal stricture; MES, malignant esophageal stricture; RBES, refractory benign esophageal stricture; GERD, gastroesophageal reflux disease; ESD, endoscopic submucosal dissection; EMR, endoscopic mucosal resection; ESCC, esophageal squamous cell carcinoma; EAC, esophageal adenocarcinoma; SEMS, self-expanding metal stents; SEPS, self-expanding plastic stents; BDS, biodegradable stents; FDA, the US Food and Drug Administration; PLA, polylactic acid; PLLA, poly (L-lactic acid); PLGA, poly (lactic-co-glycolic acid); PDO, polydioxanone; PCL, poly (ε-caprolactone); PTMC, poly (1, 3-trimethylene carbonate); 5-FU, 5-fluorouracil.

comprehensive overview of current biodegradable esophageal stent materials and their applications, highlight current research limitations and innovations, and offer insights into future development priorities and directions.

KEYWORDS

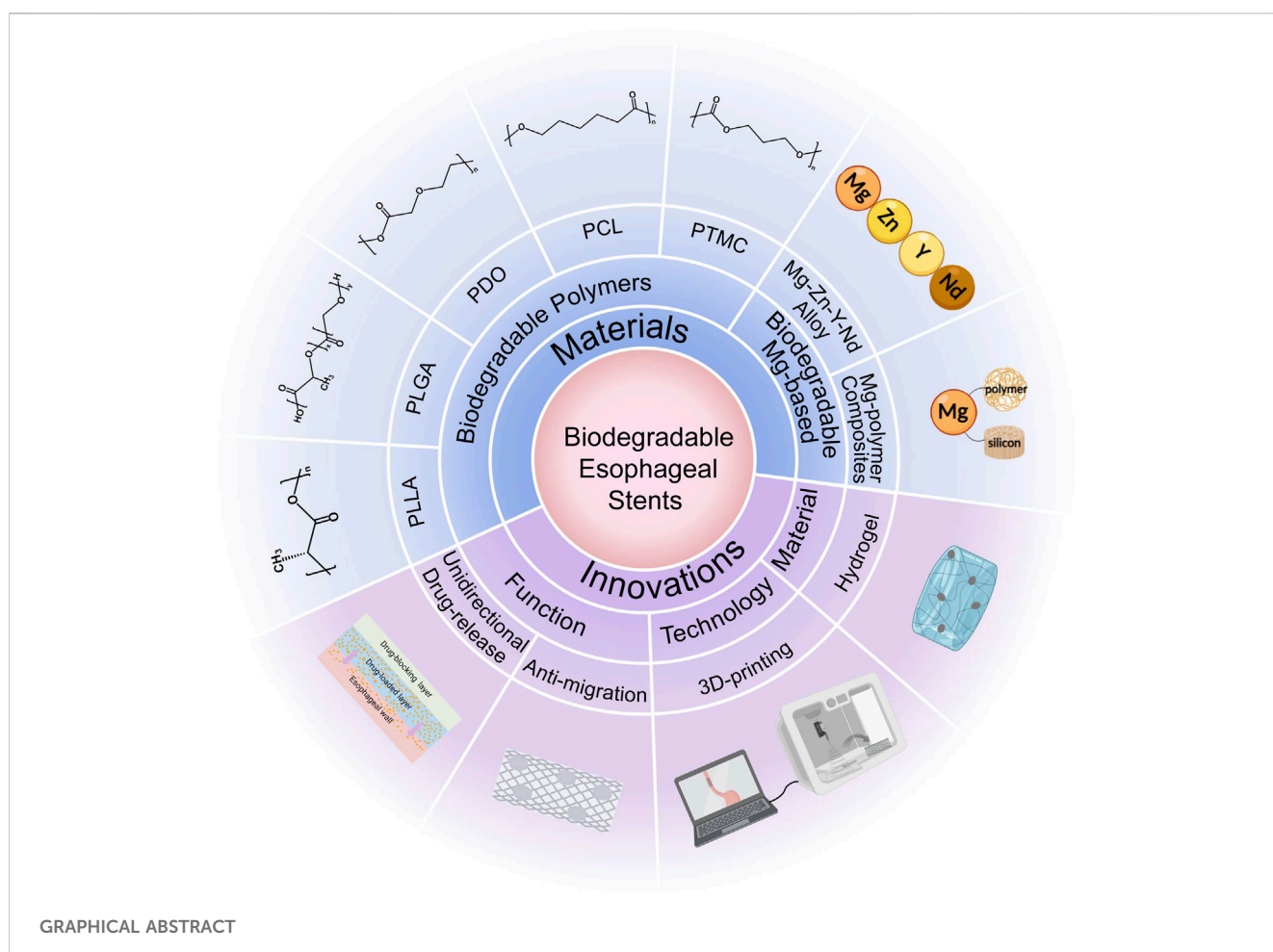
biodegradable esophageal stents, esophageal stricture, esophageal cancer, polydioxanone, poly (L-lactic-acid), magnesium alloy, drug-eluting stents

1 Introduction

Esophageal stricture (ES) results from prevalent clinical conditions and is categorized into two primary types: benign esophageal stricture (BES) and malignant esophageal stricture (MES). The most frequently encountered BES subtype is peptic strictures (Desai et al., 2020), typically stemming from uncontrolled gastroesophageal reflux disease (GERD), radiation-induced strictures, and iatrogenic injuries (De Wijkerslooth et al., 2011; Liu et al., 2022). In contrast, MES is predominantly associated with esophageal neoplasms and extraneous malignancies that compress the esophagus (Siersema, 2008). Upper gastrointestinal endoscopy serves as the preferred diagnostic modality for identifying ES and its root causes (Siersema, 2008). Patients commonly present with dysphagia once the stenosis reduces the esophageal lumen by 50% (Adler and Siddiqui, 2017). ES can trigger

various adverse consequences such as malnutrition, weight loss, acid-base imbalance, and hypoalbuminemia. Consequently, timely intervention is imperative, particularly when these adverse conditions manifest.

Current treatments for ES encompass various modalities, including drug therapy, surgical interventions, endoscopic esophageal dilation, and endoscopic stent placement, among others (Sehgal and Sami, 2021). Pharmacological treatment entails the administration of proton pump inhibitors (PPI) for managing GERD (Peng et al., 2023). Additionally, endoscopy-guided infusion of adrenocorticotrophic and cytotoxic drugs into the stenosis site serves to inhibit fibrosis and scar formation in damaged tissue, thereby alleviating scarring-induced permanent ES (Zein et al., 1995). However, these drugs may prove ineffective, lead to disease recurrence upon discontinuation, and even give rise to significant side effects, limiting their standalone usage in current



clinical practice. Esophagectomy becomes necessary in severe ES unresponsive to conservative measures such as endoscopic treatment.

In contrast to surgery, endoscopy boasts advantages such as reduced trauma, a high cure rate, and rapid recovery (Chen et al., 2022). Esophageal dilation is one of the most practical and effective techniques for managing BES, with a success rate exceeding 80%–90% (Siersema, 2019). Balloon dilation is the preferred method for achieving this outcome. Moreover, endoscopic dilation of the esophagus, whether by employing a Savary (bougie) or a balloon dilator, serves as the initial step in managing refractory benign esophageal stricture (RBES) (Sehgal and Sami, 2021). Balloon dilation in ES yields immediate relief; however, it cannot ensure sustained dilation. Patients with RBES often require repeated dilations, which can be inconvenient and necessitate high compliance rates (Siersema, 2019). Additionally, balloon dilation can serve as a complementary procedure to esophageal stent insertion by performing several balloon dilations before stent placement, which prepares the stricture for the smooth passage of the stent delivery device. Esophageal stent insertion using endoscopy involves the deployment of a stent to support the stricture and maintain radial pressure, facilitating the remodeling of the stenosis and its surrounding tissue.

Indications for esophageal stent placement include BES, primarily resulting from GERD-induced chronic inflammation (Desai et al., 2020), scarred strictures following chemical burns, and stenosis after post-surgical anastomosis or endoscopic resection procedures such as endoscopic submucosal dissection (ESD) and endoscopic mucosal resection (EMR) (Siersema, 2019). Stent placement is also indicated for MES, including unresectable esophageal or gastric cardiac cancer, local recurrence at the anastomosis site following esophagectomy, and strictures arising after radiation therapy for esophageal cancer. Additionally, stents may be employed to address other conditions such as esophagotracheal fistulas and esophageal ruptures, among others. Among these indications, MES is frequently linked to esophageal cancer, which encompasses two distinct pathological and epidemiological subtypes: esophageal squamous cell carcinoma (ESCC) and esophageal adenocarcinoma (EAC) (Smyth et al., 2017). Esophageal cancer is a global health concern, ranking as the sixth most prevalent cause of cancer-related fatalities each year. Over 50% of patients with esophageal cancer experience dysphagia due to malignant obstruction. Treatment for esophageal cancer hinges on patient-specific factors and tumor characteristics, particularly the TNM stage, which is usually identified using imaging methods and histopathologic biopsies (Liu et al., 2023; Matsunami et al., 2023). Early-stage tumors are typically amenable to endoscopic resection, whereas locally advanced cancers necessitate surgical resection, neoadjuvant chemoradiotherapy, chemotherapy, radiotherapy, or a combination thereof (Chen et al., 2023). However, a considerable proportion of patients present with advanced, unresectable tumors at the time of diagnosis. Treatment objectives in such cases primarily constitute restoring oral food intake and enhancing quality of life (Rozanes et al., 2002). Notably, over half of the patients pursuing curative treatment will experience tumor recurrence, necessitating

palliative care for the majority of individuals in the long term (Smyth et al., 2017). Consequently, improved treatment options for esophageal cancer should be explored.

Esophageal stenting has a rich history that dates back over a century. Its origins can be traced back to Symonds' pioneering proposal in 1885 regarding the advantages of esophageal stent placement. In 1977, Arkinson introduced a cylindrical plastic tube to address inoperable esophageal tumors, marking the inception of the clinical use of esophageal stents. Frimberger first treated ES with a spiral metal stent in 1983, and Domschke applied the Wallstent to treat cancer-related ES in 1990. A pivotal moment occurred in 1996 when Goldin et al. (1996) introduced an esophageal stent constructed from poly-L-lactide (PLLA), which was both biodegradable and self-expandable (Sehgal and Sami, 2021). Subsequently, a diverse array of esophageal stents employing various materials and functions emerged thereafter. Currently, several types of esophageal stents exist (Wang et al., 2021b): self-expandable metal stents (SEMS), self-expandable plastic stents (SEPS), biodegradable stents (BDS), and hybrids that combine elements of the aforementioned stents, such as SEMS with an anti-reflux valve, DES, and radioactive SEMS, among others. Among these options, SEMS has emerged as the preferred and efficacious choice for managing BES and MES (Yang et al., 2016). The most commonly employed endoscopic therapeutic approach for palliation involves the placement of esophageal stents (Rabenstein, 2015), particularly in cases involving patients with cancer and limited life expectancy who require rapid relief from dysphagia or those unresponsive to chemoradiotherapy. However, SEMS has certain limitations. The necessity of stent removal after stenosis resolution in certain benign conditions and the potential complications of metal materials such as bleeding, retrosternal pain, esophageal fistula, tissue ingrowth, and restenosis (Song et al., 1997; Ackroyd et al., 2001; Evrard et al., 2004; Yang et al., 2016), has rendered SEMS less than ideal for ES treatment, particularly BES treatment. SEPS offers advantages, such as reduced tissue trauma, minimal tissue proliferation, and ease of removal (Verschuur et al., 2008; Rabenstein, 2015); however, its long-term effectiveness is disappointing. SEPS often requires reintervention and carries a higher complication rate than SEMS, including complications such as stent migration (Conio et al., 2007; Ham and Kim, 2014; Fuccio et al., 2015). Moreover, its infrequent application for the management of malignant dysphagia can be linked to factors such as the wide diameter of the stent deployment catheter, the complex and unwieldy assembly and operation, and its heightened mobility (Adler and Siddiqui, 2017).

Over the past 3 decades, biodegradable materials, including synthetic polyester polymers and magnesium (Mg)-based alloys (Wu et al., 2012; Yuan et al., 2016; Liu et al., 2022), have garnered substantial attention owing to their distinct advantages when compared to SEMS and SEPS. An ideal biodegradable esophageal stent should possess exceptional mechanical properties, compliance, and histocompatibility, ultimately undergoing complete degradation after providing a period of mechanical support. The resulting degradation products should have no adverse effects on human health (Yang et al., 2016). Considering that a stent's degradability is pivotal in mitigating the risk of severe long-term complications, stents crafted from biodegradable materials are highly favorable for managing benign

TABLE 1 Comparison of biodegradable polymer stents currently available for clinical use.

| | PLLA-BD stent (Tanaka-Marui stent; Marui Textile Machinery Co., Ltd., Osaka, Japan) | SX ELLa-BD stent (Ella-CS, Hradec Kralove, Czech Republic) |
|-------------------------------|---|---|
| Materials | Knitted PLLA monofilament | Woven PDO monofilament |
| Initial application time | 2006 | 2008 |
| Length and diameter | Designed according to the esophageal lesion of each individual patient | Size: 18, 20, 23, 25 mm Length: 60, 80, 100, 135 mm |
| Procedure for stent insertion | One end of the PLLA stent is to be tied into a 5 mm diameter by silk sutures and then fitted over an endoscope | Manually load the stent into the delivery system and position it on the basis of the metal stent markers at both ends. The stent can be fully expanded to its designed diameter after 24–48 h in the body |
| Biodegradable time | 3–6 months (acidic environment will accelerate its degradation) | 2–3 months (acidic environment will accelerate its degradation) |
| Advantages | Excellent expansion capacity, high radial force (117 gf, which is comparable to commercially available metallic stents), low incidence of stent-related complications | Superior flexibility and biocompatibility |
| Disadvantages | Low flexibility, early spontaneous migration | Lower mechanical stability compared to PLLA stent, prone to complications |

conditions (Tamai et al., 2000; Saito et al., 2004; Tanaka et al., 2007). The critical factor in developing an outstanding esophageal stent lies in the selection of appropriate biodegradable materials. Consequently, our discussion centered on the materials and applications of biodegradable esophageal stents, highlighted the current research challenges, and offered insights into future development priorities and directions.

2 Materials used in biodegradable esophageal stents

A diverse array of effective stents constructed from biodegradable materials, encompassing synthetic polyester polymers and Mg-based alloys, has found widespread application in the cardiovascular, airway, esophageal, and urinary systems in contemporary medical practice (Li et al., 2023). In 2006, the US Food and Drug Administration (FDA) approved the use of several synthetic polymers in medical devices (Kohn et al., 2007), including poly-L-lactide (PLLA), poly (lactic-co-glycolic acid) (PLGA), polydioxanone (PDO), poly (ϵ -caprolactone) (PCL) and poly (1, 3-trimethylene carbonate) (PTMC). Presently, these materials, their copolymers, and their composites constitute the forefront of ongoing research efforts in this field. Notably, the ultimate products of their degradation within the human body are water and carbon dioxide, posing no harm to human health (Li et al., 2023).

Two notable options among the biodegradable polymer stents currently accessible in clinical practice are the PLLA-BD stent (Marui Textile Machinery Co., Ltd., Osaka, Japan), comprising braided PLLA monofilaments (Tanaka et al., 2007), and the SX ELLa-BD stent (Ella-CS, Hradec Kralove, Czech Republic), composed of PDO, which is a type of surgical suture material (Stivaros et al., 2010) (Table 1).

Metals containing elements naturally present in the human body are deemed biocompatible, rendering them suitable for the fabrication of biodegradable stents. Notably, Mg, iron (Fe), zinc (Zn) and their respective alloys are among this category. These

metals and alloys offer sustained radial support over a defined period of time, while undergoing spontaneous degradation within the body (Bowen et al., 2016; Liu et al., 2022). Therefore, they can help minimize inflammation from local tissue hyperplasia or prolonged physical stimulation (Ragunath, 2008), precluding the need for secondary stent removal (Chen et al., 2019a). Among these biodegradable alloys, Mg holds particular significance as an essential trace element and a structural component of tissues (Moravej and Mantovani, 2011). Furthermore, Mg is recognized as a non-carcinogenic element (Xu et al., 2007). Additionally, Mg-based alloys exhibit superior strength, specific stiffness, corrosion resistance, and processability (Bowen et al., 2016; Liu et al., 2022). The following section presents a comprehensive review of synthetic polyester polymers, Mg-based alloys and their related substances, focusing on materials, applications and innovative developments.

2.1 Biodegradable polymers

2.1.1 PLLA

Poly(lactic acid) (PLA) is an aliphatic polyester that is biodegradable, bio-based, and can be entirely sourced from renewable materials such as corn, potatoes, sugar cane, and similar resources (Yusoff et al., 2021). PLA demonstrates commendable biocompatibility, showcasing notable attributes such as strength, toughness, and plasticity. PLA hydrolysis yields products such as lactic acid, which is absorbed and metabolized by the human body, ultimately generating carbon dioxide and water that can be efficiently expelled from the body without leaving any residues. Lactic acid is a chiral molecule that exists in L and D isomers; therefore, four types of PLA arise, including isotactic PLA (PLLA), isotactic poly-D-lactic acid (PDLA), and atactic and syndiotactic poly-D, L-lactic acid (PDLLA) (Lasprilla et al., 2012; Zhou et al., 2021). Among them, PLLA, which is one of the stereo configurations of PLA (Wu et al., 2023), is a biodegradable material produced through the polymerization of L-lactic acid. Its versatility has led to its application in surgical sutures, bone screws, and tissue engineering scaffolds (Saito et al., 2007; Tanaka et al., 2007; Shuai

TABLE 2 Clinical studies of PLLA-BDS.

| Author | Year | Study design | n | Indication | Follow-up | Migration (%) | Complication | Clinical success (%) | Reference |
|------------------|------|----------------|----|---|---------------------|---|--------------|----------------------|-------------------------|
| Tanaka et al. | 2006 | Clinical trial | 2 | BES (corrosive stenosis and postoperative anastomotic stenosis) | 6 months | 10 days and 2 weeks, respectively | 0 | 2 (100%) | Tanaka et al. (2007) |
| Saito et al. | 2007 | Case report | 13 | BES (corrosive stenosis, stricture after surgical resection of esophageal cancer, preventive placement for post-ESD stenosis) | 7 months to 2 years | 10 (77%): spontaneous migration within 10–21 days | 0 | 13 (100%) | Saito et al. (2007) |
| Saito et al. | 2008 | Case report | 2 | BES following ESD | 6 months | 0 | 0 | 2 (100%) | Saito et al. (2008) |
| Mochizuki et al. | 2012 | Case report | 1 | Recurrent esophageal cancer after chemoradiotherapy | 1 month | 0 | obstruction | 1 (100%) | Mochizuki et al. (2012) |

et al., 2019; Liu et al., 2020; Shuai et al., 2021; Yin et al., 2022), and an array of stents designed for use in coronary arteries, urinary systems, bronchial passages, and biliary tracts (Tamai et al., 2000; Saito et al., 2004; Isotalo et al., 2006; Song et al., 2022).

In 1996, Goldin et al. (1996) documented the groundbreaking experience with a novel stent that possessed the unique features of self-expansion and biodegradability. The stent was constructed as a coil spring using a solitary strand of PLLA (InStent Inc) and was designed to treat BES. Furthermore, Fry and Fleischer (Fry and Fleischer, 1997) pioneered the application of PLLA-BDS (EsophaCoil; InStent, Eden Prairie, MN, United States) in the United States, particularly for BES caused by radiation-induced injury. This marked a significant expansion of the knowledge and experience in the application of biodegradable esophageal stents.

A limited amount of research has been conducted on the clinical application of PLLA stents (Table 2). In 2006, Tanaka et al. (2007) introduced a new biodegradable Ultraflex-type stent, utilizing machine-knitted polylactic acid monofilaments (Marui Textile Machinery Co., Ltd., Osaka, Japan), to treat two patients with benign strictures in the upper gastrointestinal tract. These stents were layered with a water-soluble contrast agent (gastrografin) to enhance visibility during placement and were subsequently guided into position using a combination of fluoroscopy and endoscopy. A thread was used to fasten the stent's tip and diminish its diameter, resulting in easier navigation through narrower sections. In case 1, a 19-year-old woman had engaged in a suicide attempt by consuming caustic potash, resulting in the development of ES 2 weeks later. In case 2, a 75-year-old man developed stenosis at the anastomotic site after undergoing surgical resection for esophageal cancer. Balloon dilatation therapy was attempted multiple times; however, neither patient experienced relief from their dysphagia. Consequently, both individuals received the same treatment approach. After two sessions of balloon dilatation, the stents were meticulously placed under combined fluoroscopic and endoscopic guidance, resulting in immediate improvement of their strictures. Remarkably, the stents naturally migrated and were excreted with feces via bowel movements at 10 and 14 days post implantation for cases 1 and 2, respectively, with no associated complications. In case 1, there was no recurrence at the 6-month follow-up examination. However, mild

restenosis occurred 1 week later in case 2 but did not necessitate further dilatation therapy during the subsequent 6 months of follow-up.

Saito et al. (2007) used PLLA-BDS (Marui Textile Machinery Co., Ltd., Osaka, Japan) to treat BES in 2007. These stents were composed of PLLA monofilaments (molecular mass 183 kD, diameter 0.23 mm), with a machine-knitted design akin to ultra-flex metallic stents. These stents were applied in various cases, including BES resulting from anastomosis following surgical resection for esophageal cancer, corrosive liquid ingestion in suicide attempts, and the preventive insertion of biodegradable stents for post-ESD strictures. Each PLLA-BDS was custom-tailored to the specific characteristics of the patient's esophageal condition and meticulously fitted using an endoscope. Remarkably, spontaneous early migration was observed in 77% (10/13) of these stents, possibly attributed to stent degradation, leading to loss of patency. No signs of restenosis were observed during the follow-up period, which ranged from 7 months to 2 years. This study demonstrated the utility of biodegradable stents in managing BES, with a specific focus on their role in preventing post-ESD stenosis. Presently, a rising number of patients diagnosed with early-stage esophageal cancer are opting for full resection through minimally invasive endoscopic techniques such as ESD. However, strictures tend to develop when the mucosal defect encompasses >75% of the esophageal circumference (Oyama et al., 2005), and endoscopic dilation or stenting may be required in these cases. Saito et al. (2008) also reported two cases of using PLLA stents to successfully improve BES following ESD in patients with early ESCC and repeated failed balloon dilatation.

Additionally, researchers reported a case of a patient with recurrent ESCC following chemoradiotherapy (CRT) (Mochizuki et al., 2012). Biodegradable esophageal stents composed of PLLA monofilaments (Saito et al., 2008) were promptly inserted on the same day of ESD to prevent stenosis resulting from the mucosal defect. This study demonstrated the potential efficacy of combining ESD with biodegradable stents, introducing a viable approach for managing recurrent ESCC following CRT and offering a promising avenue for enhancing the treatment outcomes and prognosis of esophageal malignancies.

Tanaka et al. (2007) substantiated the superior radial force of their biodegradable stent, which was constructed from polylactic

acid monofilaments, with higher radial force measurements than commercially available metal stents. Moreover, this stent exhibited a marked reduction in various complications typically associated with the use of metal stents in BES treatment. Nonetheless, these studies also highlighted a potential drawback of PLLA stents, namely, the occurrence of early migration. PLLA-BDS take months to degrade; therefore, the migration risk arises from the gradual loss of radial force before complete degradation. No complications were observed with the softened stents during defecation; nevertheless, the ideal approach is to prevent these early displacements to ensure the stents effectively treat strictures. The research group speculated on the necessity of securing the stents in place for a minimum of 2 weeks, which represents the required time for healing inflammatory changes in the lesions. No bowel obstruction caused by PLLA stents was reported in the aforementioned cases; however, vigilant attention should be directed towards the potential risk of bowel obstruction from migrated stents.

In summary, PLLA stents exhibit noteworthy attributes, including excellent expansion capacity, high radial force, and the ability to biodegrade within 3–6 months when exposed to an acidic environment (Yang et al., 2016). These qualities contribute to a low incidence of stent-related complications. However, their inherent brittleness limits their flexibility (Han et al., 2018). Furthermore, PLLA stents tend to experience a relatively high rate of early spontaneous migration as they gradually degrade, necessitating vigilant monitoring for potential complications such as intestinal obstruction.

2.1.2 PLGA

PLGA is a biodegradable and biocompatible polyester copolymer constructed by the polymerization of lactic acid and glycolide (Stevanović et al., 2009; Ma et al., 2011) and has emerged as a principal biodegradable polymer over the past few decades. It serves as the primary polymer for drug delivery (Shakya et al., 2023) and plays a pivotal role in diverse clinical applications (Liu et al., 2016). The hydrolytic breakdown of PLGA yields lactic acid and glycolic acid (Ma et al., 2011; Song et al., 2022), which are ultimately converted into carbon dioxide and water and subsequently eliminated through the body's normal metabolic processes. PLGA is renowned for its low toxicity and rapid degradation and is widely used in the treatment of bone defects, tissue engineering, surgical sutures, and drug release systems (Stevanović et al., 2009; Fredenberg et al., 2011; Lanao et al., 2011; Babilotte et al., 2021; Jin et al., 2021).

Liu et al. (2016) designed a novel biodegradable stent comprising three curved segments of covered metal mesh linked together by biodegradable PLGA threads. As these PLGA threads degraded, the stent disintegrated and safely passed into the stomach. This study investigated the novel stent's attributes using *in vitro* assessments, including evaluations of radial forces, pH levels, and morphology, among others. Additionally, they conducted *in vivo* animal studies, involving the insertion of these stents into the narrow middle esophagi of rabbits, which had incurred damage from alkali burns. The braided design of these stents enabled a reduction of the radial force, reaching 0 N (Hirdes et al., 2013), without any associated stent-related complications. This innovative design, namely, combining the strengths of metallic stents in terms of radial force with the biodegradability of biodegradable stents,

holds considerable promise and offers a novel avenue for the future development of biodegradable stent technology.

Prior studies have demonstrated the promise of utilizing PLGA as a surface coating, particularly on Mg or Zn alloys, owing to its commendable attributes including robust biocompatibility, pronounced hydrophobicity, and proficient drug-loading capabilities (Wang et al., 2006; Zhu and Braatz, 2015; Dou et al., 2023). The versatile applications of PLGA coatings have been extensively explored by researchers in various stent domains, including cardiovascular stents (Fang et al., 2021; Dou et al., 2023), ureteral stents (Antonowicz et al., 2021), and gastrointestinal stents (Kwak et al., 2017), among others.

Liu et al. (2022) designed and tested a groundbreaking Mg-based braided stent coated with PLGA infused with paclitaxel (PTX) to avoid secondary removal by endoscopic procedures and inhibit restenosis of the esophagus (Figure 1). This ingeniously engineered stent was designed to undergo self-degradation within the body after ensuring esophageal patency for a specified duration, precluding the necessity for subsequent removal procedures. In addition, the stent's surface was coated with anti-proliferative drugs, which can further inhibit local tissue growth and extend the unobstructed period of esophageal function. The safety and effectiveness of this combined stent have been validated through *in vitro* and *in vivo* testing, whereas its sustained applicability and worthiness await further evaluation in subsequent studies. In conclusion, this stent effectively amalgamated the merits of biodegradable alloys and polymers, thereby compensating for their limitations. This innovation presents a promising and novel avenue for future research and development in biodegradable stent technology.

2.1.3 PDO

PDO is a biodegradable polymer with a semicrystalline structure, belonging to the polyester family. Its degradation occurs through the random hydrolysis of ester bonds within its molecular structure, with glyoxylic acid, a degradation product, primarily serving as a precursor for oxalic acid and playing a role as an intermediate in the transformation of glycolic acid into glycine. All of PDO's degradation products and intermediates are non-toxic (Repici et al., 2010). A significant milestone was achieved when PDO gained FDA approval in 1981 for its use in biodegradable sutures (Bartholomew, 1981). PDO can be knitted into tubes of the desired shapes and dimensions, and stents composed of PDO have been inserted into the bronchus, trachea, intestine, and bile duct, in addition to the esophagus (Lischke et al., 2011; Rejchrt et al., 2011; Siiki et al., 2017). PDO's utility extends even further into domains such as tissue engineering (Boland et al., 2005; Okata et al., 2014; Goonoo et al., 2015), bone regeneration (Saska et al., 2021), and drug delivery systems (Goonoo et al., 2015; Bottino et al., 2019), among others. The SX ELLa-BD stent (Ella-CS, Hradec Kralove, Czech Republic) is a biodegradable esophageal stent constructed using commercially accessible PDO absorbable surgical sutures (Repici et al., 2010). This stent is Conformité Européenne approved and is indicated for use in benign strictures, including digestive, erosive, anastomotic, and post-radiation strictures (van Hooff et al., 2011). The ELLa-BDS comes in various sizes, with stent body diameters ranging from 18 to 25 mm and lengths from 60 to 135 mm when fully deployed. It should be compressed and installed

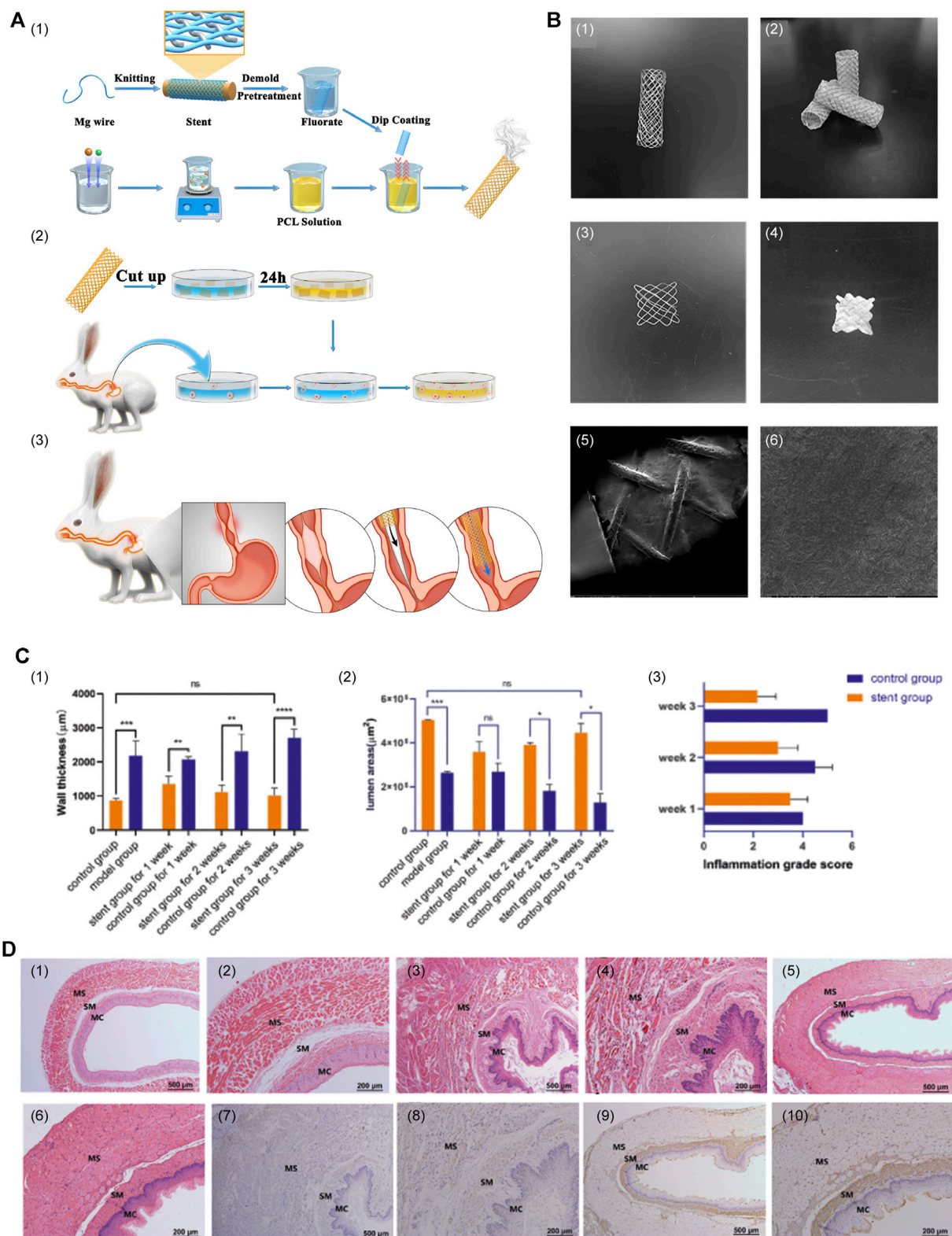
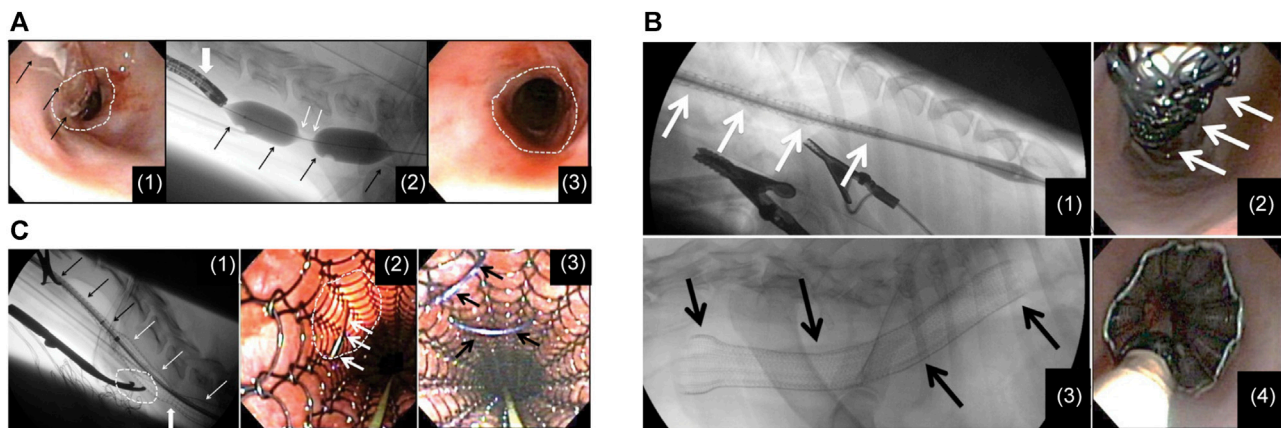


FIGURE 1

(A) Primary procedure and methods. (1) Construction of PLGA-coated drug-eluting Mg stents. (2) Experiments on *in vitro* degradation, drug release, and cytotoxicity. (3) Insertion of the stent. (B) Macrostructure and surface characteristics of the stent. (1) The Mg alloy bare stent. (2) The PTX-PLGA-coated Mg-based stent. (3) The 1 cm x 1 cm stent sheet of bare stent. (4) The 1 cm x 1 cm stent sheet of the coated stent. (5 and 6) SEM images of the surface characteristics. (C) (1–3) Wall thickness of the esophagus, lumen area, and degree of inflammation between the stent group and sham stent group. (D) (1 and 2) Esophageal tissue of normal control rabbits. (3 and 4) Imaging of esophageal tissue over a period (Continued)

FIGURE 1 (Continued)

of 3 weeks after successful modeling, with no stent insertion. (5 and 6) Imaging of esophageal tissue 3 weeks after stent insertion following the successful modeling. (7 and 8) Immunohistochemical staining images of stent group and (9 and 10) the sham stent group. Reproduced with permission from ref [(Liu et al., 2022)]. Copyright 2022 Acta Materialia Inc.

**FIGURE 2**

(A) (I) A flexible endoscope and dilatation balloon were inserted into the esophagus to visualize the stricture. Balloon dilatation was performed to allow the endoscope to pass through. (II) The stent in a restricted state was advanced with the guidance of fluoroscopy. (III) Following the deployment of the stent, the upper thoracic stricture was resolved at the site of stent constriction, revealing a clear and unobstructed esophageal passage. (B) (I) A restricted stent was advanced through an esophageal constriction within the thoracic area. (II) Endoscopic image of the stent while it was constrained before deployment. (III) Lateral fluoroscopic image following the stent insertion. (IV) The endoscopic picture taken right after stent insertion, illustrating effective esophageal wall apposition. (C) (I) Lateral fluoroscopic image showing an esophageal stent in a state of partial deployment and partial constriction. (II) Endoscopic view showing a lumined area where the surgical approach had been performed and the suture needle passing through the esophageal wall and engaging the stent. (III) Endoscopic view after 2 polypropylene sutures had been placed to tack the stent to the esophageal wall. Reproduced with permission from ref [(Lam et al., 2013)]. Copyright 2013 American College of Veterinary Internal Medicine.

onto a 9.4 mm (28F) delivery system prior to clinical use. Regarding performance, this stent exhibits a relatively high axial force and initially low radial force, which gradually decreases to 0 N (Hirdes et al., 2013). Its structural integrity and radial expansion strength remain stable for a period of 6–8 weeks, after which disintegration occurs within 11–12 weeks post implantation. Notably, low pH can accelerate its degradation; therefore, the use of a PPI is advised to extend the integrity of the stent (Yang et al., 2016).

Several preclinical studies on ELLa-BDS have been conducted. For example, Battersby and Doyle (2010) used a biodegradable PDO self-expanding stent to treat BES in a cat in 2010. A fluoroscopic examination revealed the complete disappearance of the stent 4 months after placement, with no signs of obstruction. In 2012, Pauli et al. (2012) reported ELLa-BDS's potential to alleviate the development of severe strictures after performing circumferential endoscopic esophageal mucosectomy (EEM) in a porcine model. The findings indicated that the BDS group exhibited significantly extended survival compared to the control group (9.2 weeks vs. 2.4 weeks). However, the stent was unable to entirely prevent the development of high-grade strictures, and the timing of stenosis formation appeared to be linked to the gradual loss of radial force and stent disintegration. A retrospective review (Lam et al., 2013) of records for six dogs with RBES revealed initial improvements in dysphagia following ELLa-BDS

insertion (Figure 2). Nonetheless, close monitoring is essential owing to the potential complications, including regurgitation, stent migration, and restenosis.

ELLA-BDS is recognized as the first commercially available biodegradable esophageal stent (Vandenplas et al., 2009; Repici et al., 2010; Stivaros et al., 2010) and has been extensively employed in clinical studies to evaluate its effectiveness and safety in the treatment of BES (Table 3). Previous studies have shown that ELLa-BDS offers a practical approach to managing RBES by reducing the need for repetitive endoscopic dilations and cutting treatment costs (Dhar et al., 2009; Repici et al., 2010; van Boeckel et al., 2011; Muñoz et al., 2013). A single BDS placement provides only temporary relief; therefore, the sequential placement of stents emerges as an excellent option to preclude the need for serial dilations (Hirdes et al., 2012a). Moreover, the commendable efficacy and safety of ELLa-BDS in addressing corrosive esophageal strictures and dysphagia from benign anastomotic esophageal strictures have also been demonstrated (Vandenplas et al., 2009; van Hooft et al., 2011). In a noteworthy case (Basha et al., 2013), researchers employed ELLa-BDS to treat a patient with corrosive (sulfuric acid-induced) esophageal and pyloric strictures. The patient underwent transhiatal esophagectomy with colonic transposition 6 months after stent insertion. The examination of the resected esophageal specimen marked the first-ever report of histological evidence in a human case, confirming ELLa-BDS's

TABLE 3 Clinical studies of ELLa-BDS.

| Author | Year | Study design | n | Indication | Follow-up | Migration (%) | Complication | Clinical success (%) | Reference |
|----------------------|------|---------------|----|--|---|---------------|---|----------------------|-------------------------------|
| Orive-Calzada et al. | 2009 | Case report | 1 | BES (postoperative anastomotic stenosis) | 3 months | 0 | Severe epithelial hyperplasia stenosis | 0 | Orive-Calzada et al. (2009) |
| Stivaros et al. | 2010 | Retrospective | 2 | 1 BES (a peptic stricture in the distal esophagus) and 1 MES (a carcinoma at the gastro-esophageal junction) | 3–4 months | 2 (100%) | Transient nausea | 2 (100%) | Stivaros et al. (2010) |
| Hair et al. | 2010 | Case report | 1 | BES (achalasia) | 8 weeks | 0 | Severe hyperplasia stenosis, stent collapse, regurgitation and moderate weight loss | 0 | Hair and Devonshire (2010) |
| Jung et al. | 2010 | Case report | 1 | RBES (stenosis after CRT for a ESCC) | 4 weeks | 0 | Tracheoesophageal fistula | 0 | Jung et al. (2010) |
| van Hooft et al. | 2011 | Prospective | 10 | BES (benign anastomotic esophagogastric strictures) | 6 months | 2 (20%) | Tissue hyperplasia, reobstruction | 6 (60%) | van Hooft et al. (2011) |
| van Boeckel et al. | 2011 | Prospective | 18 | RBES (peptic, anastomotic, post radiation, caustic and other strictures) | 166 days (range 21–559 days) | 4 (22%) | Hemorrhage, severe retrosternal pain | 6 (33%) | van Boeckel et al. (2011) |
| Hirdes et al. | 2012 | Prospective | 28 | RBES (peptic, anastomotic, corrosive, radiotherapy-induced, lichenplanus and other strictures) | 90 days (range 14–618 days) | Not mentioned | Severe retrosternal pain with or without vomiting, hemorrhage, fever and aspiration pneumonia | 7 (25%) | Hirdes et al. (2012a) |
| Griffiths et al. | 2012 | Prospective | 24 | Benign strictures ($n = 7$) and esophageal cancer ($n = 17$) | 20 weeks (range 13–111) in benign group | 0 | Upper gastrointestinal bleed, nausea and vomiting, bronchopleural fistula | 17 (77%) | Griffiths et al. (2012) |
| Hirdes et al. | 2012 | Prospective | 19 | MES (16 EAC and 3 ESCC) | 51–140 days | 1 (5%) | Severe retrosternal pain, nausea and vomiting, hematemesis and recurrent dysphagia | 100% | Hirdes et al. (2012b) |
| Fischer et al. | 2012 | Case report | 2 | BES (restenosis after thoraco-abdominal esophageal resection for cancer and perforation) | 12 months | 0 | Hypergranulation | 1 (50%) | Fischer et al. (2012) |
| Dumoulin et al. | 2012 | Case report | 1 | RBES (high grade peptic stenosis in the distal esophagus) | 4 months | 0 | Tissue hyperplasia | 1 (100%) | Dumoulin and Plassmann (2012) |
| Basha et al. | 2013 | Case report | 1 | BES (corrosive-induced esophageal and pyloric strictures) | 12 months | 0 | 0 | 1 (100%) | Basha et al. (2013) |
| van den Berg et al. | 2014 | Prospective | 10 | MES (9 EAC and 1 ESCC) | 93–166 days | 0 | Retrosternal pain, stent obstruction due to necrotic tissue development | 10 (100%) | van den Berg et al. (2014) |
| McCain et al. | 2016 | Retrospective | 20 | 9 RBES and 11 MES | At least 30 days | 0 | Post-procedural pain and failed deployment | Not mentioned | McCain et al. (2016) |
| Yano et al. | 2017 | Prospective | 18 | RBES (stricture after ESD, esophagectomy, or CRT of esophageal cancer) | 24 weeks | 0 | Reactive hyperplastic nodules, esophageal pain, GERD, vomiting | 12 (66.7%) | Yano et al. (2017) |

(Continued on following page)

TABLE 3 (Continued) Clinical studies of ELLa-BDS.

| Author | Year | Study design | n | Indication | Follow-up | Migration (%) | Complication | Clinical success (%) | Reference |
|------------------------|------|---------------|-----|---|----------------------|---------------|---|----------------------|-------------------------------|
| Walter et al. | 2018 | Prospective | 32 | Recurrent BES (mainly anastomotic strictures) | 12 months | 1 (3.1%) | Stent occlusion, tracheoesophageal fistula, stent migration | Not mentioned | Walter et al. (2018) |
| Maishman et al. | 2021 | Prospective | 12 | MES (10 EAC and 2 ESCC) | 52 weeks/until death | Not mentioned | Pain, vomit, esophageal or upper gastrointestinal hemorrhage | 7 (58.3%) | Maishman et al. (2021) |
| Lopez-Tobaruela et al. | 2021 | Case report | 1 | BES (stricture in the upper esophagus) | 2 weeks | 0 | Hepatic abscess | 1 (100%) | Lopez-Tobaruela et al. (2021) |
| Yano et al. | 2022 | Prospective | 30 | BES (28 post treatment for esophageal cancer, 1 post-gastrectomy for gastric cancer, 1 congenital esophageal stricture) | 6 months | 0 | Mucosal hyperplasia, esophageal pain, minor oropharyngeal pain, minor GERD, brain abscess | 14 (46.7%) | Yano et al. (2022) |
| Kailla et al. | 2023 | Meta-analysis | 246 | BES (post-surgical, radiation, peptic, caustic and other strictures) | Not mentioned | 6.5% | Recurrent dysphagia, severe thoracic pain, food bolus obstruction, tracheoesophageal fistula, esophageal ulceration, etc. | 41.9% | Kailla et al. (2023) |

excellent biocompatibility, minimal tissue response, and complete degradation capabilities. A cohort study conducted in 2016 (McCain et al., 2016) revealed that ELLa-BDS offered a probability of long-term symptom relief that exceeds 50% for patients with benign conditions. Regarding patients that required re-intervention, the duration of symptom-free periods and the time until re-intervention significantly surpassed expectations in comparison to SEMS, SEPS, or dilation procedures. In 2018, Walter et al. (2018) conducted a comparative study between early dilation and ELLa-BDS insertion in the treatment of recurrent BES and concluded that ELLa-BDS insertion reduced the need for repeated dilations and prolonged the time before recurrent dysphagia, in contrast to dilation. In 2022, a non-randomized, single-arm prospective trial (Yano et al., 2022) conducted across eight institutions provided compelling evidence that ELLa-BDS was indeed effective in treating RBES and demonstrated a satisfactory safety profile. Furthermore, a recent systematic review and proportion meta-analysis conducted by Kailla et al. (2023) in 2023 demonstrated that ELLa-BDS's high technical sophistication and moderate clinical efficacy support its use in the management of adult BES. However, further evidence is required to substantiate its advantage over alternative approaches such as endoscopic dilation.

ELLA-BDS has been extensively investigated in the management of MES, in addition to BES. In 2010, Stivaros et al. (2010) implanted two ELLa-BDSs in an octogenarian patient with cancer at the gastro-esophageal junction (GOJ). The study's findings suggested that patients with dysphagia and potentially curable esophageal carcinoma could consider BDS as an alternative to gastrostomy, particularly in the context of neo-adjuvant or radical chemo/radiotherapy. Subsequently, a research group in 2012 treated 16 patients experiencing dysphagia from MES with ELLa-BDS (Griffiths et al., 2012). These patients included those scheduled to

undergo neoadjuvant chemotherapy and planned esophagectomy ($n = 9$), those slated for radical radiotherapy with or without chemotherapy ($n = 6$), and those with metastatic esophageal cancer. This pioneering study represented the first exploration of BDS use in patients with a variety of malignancies. The results indicated that ELLa-BDS significantly alleviated dysphagia and reduced the need for enteral tubes in patients receiving radical chemoradiotherapy or awaiting esophagectomy. McCain et al. (2016) inserted ELLa-BDS in 11 patients with MES in 2016, further confirming the utility of ELLa-BDS in MES. Their study provided compelling evidence that BDS placement was a safe and effective adjunct in the management of MES. Importantly, it enabled the maintenance of enteral nutrition after staging or neo-adjuvant therapy, without adversely affecting subsequent surgical resection.

The insertion of an esophageal stent delivers instant relief in the palliative treatment of MES-induced dysphagia, whereas brachytherapy provides sustained relief (Hirdes et al, 2012b). A study conducted in 2012 assessed the impact of concurrent brachytherapy and ELLa-BDS insertion in 19 patients diagnosed with unresectable esophageal cancer (Hirdes et al, 2012b). This combination approach successfully restored lumen patency; however, it cannot be recommended for palliative esophageal carcinoma treatment owing to the increased likelihood of severe complications associated with the procedure. In 2014, van den Berg et al. (2014) investigated the safety and efficacy of ELLa-BDS as a surgical bridge preceding CRT in patients with dysphagia from locally advanced esophageal cancer. This study marked the first description of BDS insertion prior to neoadjuvant CRT in individuals diagnosed with locally advanced esophageal cancer. Importantly, no significant adverse incidents or mortality within 30 days associated with the procedure were observed, establishing the approach as safe and feasible. Individuals with esophageal cancer

are at risk of developing RBES following ESD or CRT. Yano et al. (2017) confirmed that BDS is an efficient and well-tolerated therapeutic choice for RBES that occurs after esophageal cancer treatment, particularly following ESD or CRT; however, its long-term efficacy remains limited. In 2021, Maishman et al. (2021) employed the SIMON two-stage, single-arm, prospective phase II trial design to assess the efficacy of biodegradable stents in combination with radiotherapy in patients with esophageal cancer-related dysphagia who were not candidates for radical interventions. The observed elevated intervention rates indicate that the proposed alternative treatments may not be sufficiently efficacious to justify their inclusion in larger-scale trial designs. Therefore, additional research is required.

Furthermore, certain complications associated with ELLa-BDS treatment for BES have been documented. These include severe epithelial hyperplasia (Orive-Calzada et al., 2009; Hair and Devonshire, 2010; Dumoulin and Plassmann, 2012; Fischer et al., 2012), tracheoesophageal fistula (Jung et al., 2010), and hepatic abscess (Lopez-Tobaruela et al., 2021). In 2009, researchers inserted ELLa-BDS to address postoperative anastomotic stenosis in a patient (Orive-Calzada et al., 2009). However, the patient developed progressive dysphagia 3 months afterwards. Endoscopic examination showed that the stent had already degraded, and a new severe stenosis had developed, which was attributed to hyperplastic inflammatory tissue. This marked the inaugural report of this particular complication associated with ELLa-BDS, which was effectively managed using balloon dilation. In 2012, Dumoulin and Plassmann (2012) suggested argon plasma coagulation as another potential treatment option for this complication, considering its low risk of complications (Manner, 2008) and the alleviation of tissue hyperplasia once the stent is fully degraded.

In summary, ELLa-BDS demonstrates remarkable flexibility and biocompatibility. As previously mentioned, multiple studies have consistently confirmed the safety and efficacy of ELLa-BDS (van Boeckel et al., 2011; van Hooft et al., 2011; Hirdes et al., 2012a; McCain et al., 2016; Walter et al., 2018; Kailla et al., 2023). ELLa-BDS exhibited more promising results than PLLA-BDS, with a notably low migration rate (Dhar et al., 2009; van Boeckel et al., 2011; van Hooft et al., 2011; Yang et al., 2016). However, it has lower mechanical stability and a faster degradation rate than PLLA, typically undergoing complete degradation within 11–12 weeks. It should be emphasized that this rapid degradation can potentially lead to complications, such as the development of severe epithelial hyperplasia.

Han et al. (2018) designed a groundbreaking PDO and PLLA sheath-core biphasic monofilament to develop a novel BDS with enhanced mechanical characteristics and regulated biodegradability. This monofilament was further enhanced through functionalization with a conjugate of hyaluronic acid (HA) and dopamine (DA) and the addition of BaSO₄ to enhance tissue adhesion and radiopacity. This pioneering stent design effectively harnessed PLLA's relatively high mechanical properties, while mitigating the inherent drawback of PDO's low mechanical stability during degradation. PDO/PLLA sheath-core monofilaments consistently exhibited superior long-term mechanical stability throughout the *in vitro* degradation assessment compared to PDO alone. Simultaneously, the stent combined DA's outstanding binding properties with HA's

enhanced biocompatibility and anti-fouling effects. Furthermore, this design eliminated the need for stent removal and the associated trauma compared to non-degradable stents. Therefore, the performance of the newly developed biodegradable esophageal stent model in this study surpassed that of non-degradable stents and PDO stents. These findings hold significant relevance for future research in this field.

2.1.4 PCL

PCL is an aliphatic polyester that belongs to the category of semi-crystalline polymers. It degrades relatively slowly and generates only minimal acidity during the degradation process (Rai et al., 2016). PCL is distinctive among other biodegradable polyesters owing to its commendable biocompatibility, elastic properties, resistance to fatigue, and cost-effectiveness (Little et al., 2009). PCL has been utilized in a variety of medical domains, including wound dressings, drug delivery devices, tissue engineering scaffolds, artificial blood vessels, and nerve regeneration devices (Sinha et al., 2004; Woodruff and Huttmacher, 2010; Abedalwafa et al., 2013; Mohamed and Yusoh, 2016). Furthermore, PCL is a highly promising candidate for use in drug delivery devices owing to its excellent biodegradability, mechanical characteristics, synthetic adaptability, compatibility with various drugs, and high drug permeability (Guarino et al., 2002; Labet and Thielemans, 2009; Rai et al., 2016; Washington et al., 2017; Thakur et al., 2021; Łukasiewicz et al., 2021).

Lei et al. (2010) employed 5-fluorouracil (5-FU) and PCL to produce multilayered films on esophageal stents. These films comprised a drug-free backing layer and a surface drug layer applied on the primary drug layer, allowing for a unidirectional and controlled drug release while enhancing mechanical characteristics. A series of studies focusing on the release and permeation behavior of the 5-FU-PCL multilayer proved the excellent performance of these multilayer films in the context of drug-controlled release stents. These flexible multilayer films exhibited the capacity to modulate drug release effectively and were regarded as a promising avenue for the development of DES. In 2013, Zhu et al. (2013a) (Zhu et al., 2013b) developed a novel biodegradable PCL-PTX nanofiber-covered metal stent. They evaluated its efficacy in managing benign cardiac stenosis in dogs, demonstrating that this innovative stent delivered ample radial force compared to its bare metal counterpart. Furthermore, PTX was steadily and continuously released through matrix diffusion and degradation, even with prolonged stent placement. This controlled release of PTX reduced inflammation and fibrosis and hindered scar tissue formation, ultimately improving disease prognosis. Notably, PTX exhibited a stable release duration under the acidic condition (pH = 4.0), lasting up to 32 days. *In vitro* studies showed that fibrous membranes containing a higher PTX concentration exhibited a more significant inhibitory impact on the proliferation rate of smooth muscle cells.

2.1.5 PTMC

PTMC is a flexible amorphous polymer and a linear aliphatic polyester compound renowned for its remarkable elasticity and high toughness under room temperature and *in vivo* conditions (Jiang et al., 2022). Its exceptional biocompatibility and biodegradability (Hou et al., 2020), coupled with the absence of acidic degradation

products during breakdown, effectively prevent severe inflammatory reactions (Yang et al., 2014; Yang et al., 2015). This versatility renders PTMC a valuable material in various biomedical applications, including drug delivery systems (Mohajeri et al., 2020; Hou et al., 2023) and tissue engineering (Li et al., 2020; Brossier et al., 2021; He et al., 2021), among others. In recent studies, researchers have explored hybrid polymers that combine PCL and PTMC as biodegradable coatings on Mg alloy stents, with promising results (Yuan et al., 2016). The growing attention on PTMC indicates its substantial potential for further advancements, despite its underutilization in esophageal stents.

2.2 Biodegradable Mg-based materials

Some studies have reported promising clinical trial outcomes for biodegradable polymer stents; however, they present with shortcomings, primarily concerning mechanical strength. Researchers have focused their attention on Mg alloys, a type of biodegradable metal, owing to their remarkable biocompatibility (Chen et al., 2018) and robust support capabilities. Mg alloys provide ample radial support force, particularly in cases of moderate to severe stenosis, effectively mitigating tissue hyperplasia (Gu et al., 2009; Li et al., 2015). Additionally, the degradation products of Mg alloys are alkaline, capable of neutralizing the acidic pH environment found at cancer sites, thus exhibiting the potential to inhibit cancer cells (Wang et al., 2019). Currently, Mg alloys have widespread applications in the biomedical field, including their use in fracture fixation, treatment of tracheal stenosis, and clinical deployment in coronary vascular stents, among others (Zhang et al., 2010; Perkins et al., 2015; Yue et al., 2015; Han et al., 2016). Nevertheless, a significant barrier that hinders the broad acceptance of Mg-based implants is their swift rate of degradation, with approximately 50% degradation occurring *in vitro* within just 1 week. This rapid degradation can result in the swift deterioration of the alloy's mechanical properties, introducing difficulties in maintaining long-term structural support post implantation for effective disease treatment (Wong et al., 2010). Therefore, researchers in the field of biomaterials often focus on enhancing the corrosion resistance of Mg-based alloys, which is a critical advancement for the clinical application of Mg-based stents (Kirkland et al., 2010; Mueller et al., 2010). Some studies have explored methods involving the combination of Mg alloys with other metals or the coating of Mg alloys with non-degradable or degradable materials to address the limitations of pure Mg stents.

2.2.1 Mg-Zn-Y-Nd alloy

Alloying strategies are frequently employed to enhance the properties of Mg alloys. Wang et al. (2020) investigated an Mg-Zn-Y-Nd alloy (Henan Key Laboratory of Advanced Magnesium Alloy, Zhengzhou, China), which has attracted substantial interest in the realm of cardiovascular stents (Chen et al., 2018; Wang et al., 2019). They investigated the viability of using this alloy as a biodegradable material for esophageal stents by conducting a comparative analysis of its mechanical properties against 317L stainless steel (a commercial non-degradable metal) and investigating the function of this alloy in inhibiting esophageal cancer cells. Their findings unveiled the promising potential of

the Mg-Zn-Y-Nd alloy, primarily attributed to its low hardness and capacity to impede the growth of pathological cells associated with esophageal cancer. The integration of Mg alloy with advanced surface modification technologies may enhance the effectiveness of esophageal stents, thereby raising the standard of care for individuals with MES (Wang et al., 2020).

2.2.2 Mg-polymer composites

The application of surface coatings on Mg alloys is essential for improving the performance of Mg-based stents. Currently, a variety of polymer materials have been widely employed to protect the surface of Mg alloys. These polymers include PLA (Chen et al., 2011; Li et al., 2018), PLGA (Liu and Xi, 2016; Chen et al., 2019b) and PCL (Chen et al., 2011; Zhang et al., 2016). Liu et al. (2022) focused on surface coating for esophageal stents and designed and tested a braided Mg-based stent coated with PLGA containing PTX, as previously described. This stent combined the strengths of Mg alloy and biodegradable synthetic polymer, with the additional benefit of PTX to inhibit tissue proliferation and prevent restenosis. This innovative approach has paved the way for further research, providing exciting opportunities to explore synergies between stents, coatings, and drug therapies to achieve functional improvements.

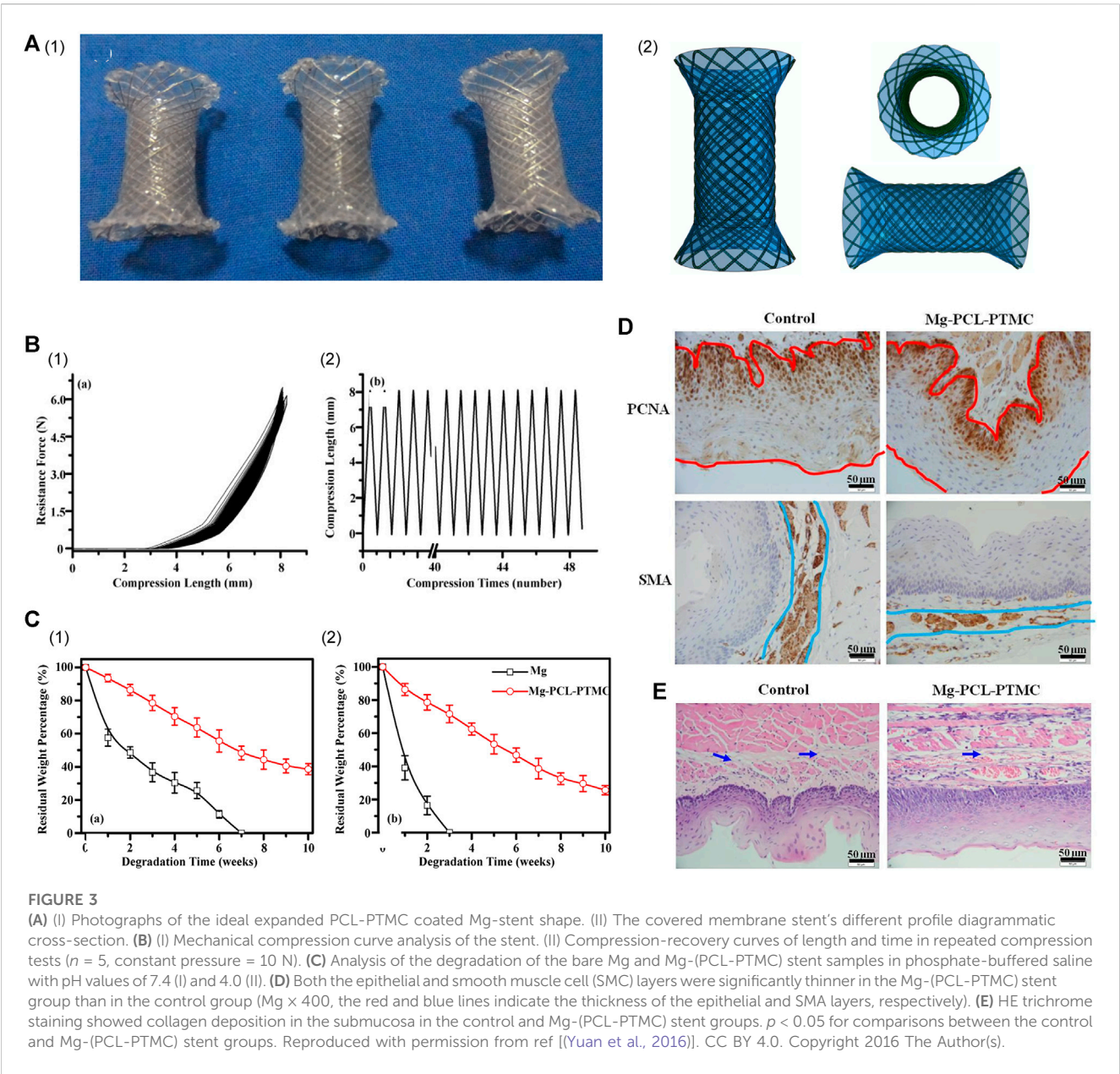
However, the acidic degradation products and general degradation behavior of the aforementioned polymers may potentially compromise the corrosion resistance of Mg alloy, rather than enhance it (Chen et al., 2011). Therefore, PTMC has garnered attention owing to its homogeneous surface-eroding behavior, which occurs uniformly from exterior to interior, and the production of charge-neutral degradation products. Its exceptional protective qualities render it a highly promising material for polymer coatings (Wang et al., 2013; Pan et al., 2020; Pan et al., 2022; Tang et al., 2022). Furthermore, silicon is a commonly utilized non-biodegradable coating that has garnered widespread applications in SEMS and SEPS.

Several studies have applied coatings of the aforementioned polymers or silicon to enhance the performance of esophageal stents constructed from Mg-based alloys (Table 4). In 2016, Yuan et al. (2016) selected a blended polymer composed of PCL and PTMC for use as a biodegradable coating on Mg alloy (AZ31, Mg-3Al-1Zn) stents to develop a fully biodegradable esophageal stent. This innovative approach yielded stents characterized by exceptional flexibility, elasticity, and remarkable resistance to lesion compression, as validated through rigorous mechanical testing. The PCL-PTMC membrane played a pivotal role in significantly slowing the degradation rate of Mg alloys *in vitro*. *In vivo* research further emphasized the potential of these stents, illustrating their capacity to offer substantial support for a minimum of 4 weeks, devoid of any significant harm or excessive collagen accumulation. This breakthrough holds promise for clinical applications and offers a fresh perspective for the future development of biodegradable stents (Figure 3).

Yang et al. (2019) (Zhu et al., 2017) developed an Mg stent coated with silicon, which possessed excellent flexibility and elasticity and exhibited impressive resilience to lesion compression during *in vivo* testing. In their study, the research team inserted the stents into the healthy esophagi of rabbits and observed that they offered sufficient radial force, with the silicon

TABLE 4 Studies of Mg stents coated with membranes.

| Author | Year | Animal model | Coating | Longest follow-up time | Effective support time | Degradation time <i>in vitro</i> | Technical success (%) | Migration (%) | Reference |
|-------------|------|---------------------------------|----------|------------------------|------------------------|----------------------------------|-----------------------|---------------|--------------------|
| Yuan et al. | 2016 | 5 New Zealand rabbits | PCL-PTMC | 4 weeks | 4 weeks | 10 weeks | 5 (100%) | 2 (40%) | Yuan et al. (2016) |
| Zhu et al. | 2017 | 15 healthy rabbits | silicon | 4 weeks | 2 weeks | 10 weeks | 15 (100%) | 6 (40%) | Zhu et al. (2017) |
| Yang et al. | 2019 | 15 New Zealand rabbits with BES | silicon | 3 weeks | 2 weeks | 10 weeks | 15 (100%) | 8 (53.3%) | Yang et al. (2019) |
| Liu et al. | 2022 | 12 New Zealand rabbits with BES | PTX-PLGA | 3 weeks | 3 weeks | 13 weeks | 12 (100%) | 7 (58.3%) | Liu et al. (2022) |



membrane significantly decreasing the rate of Mg biodegradation. Remarkably, the stent facilitated the remodeling of the esophageal wall with minimal tissue damage and elicited a minimal inflammatory response. Importantly, the stent proved capable of meeting crucial clinical requirements, including strength, safety, and reduced complications, with no esophagus injury or stent migration occurring in the rabbit experiments. Therefore, this silicon-coated Mg stent is expected to become a promising strategy for treating BES.

The fusion of Mg alloys with surface modification techniques bestows Mg-based materials with new surface attributes while preserving their intrinsic qualities. The application of suitable coatings onto the surface of Mg-based stents is a potent means to extend the degradation timeline of Mg-based implants, bolster their mechanical properties, and enhance their biological functionalities. Nonetheless, single-layer coatings might fall short of meeting the comprehensive performance requirements, including corrosion resistance and multiple functionalities. Therefore, future endeavors should focus on crafting composite coatings that harness the advantageous properties of each individual layer, thereby elevating the biological activity and adhesion of Mg-based stents (Zhang et al., 2021). In addition, the effective support duration of covered Mg stents remains limited, partly owing to a relatively high migration rate ranging from 40% to 58.3% (Yuan et al., 2016; Zhu et al., 2017; Yang et al., 2019; Liu et al., 2022). Addressing this issue necessitates further research focused on reducing the biodegradation rate and prolonging the duration of support. Extended follow-up studies are also essential for evaluating the efficacy of covered Mg stents, identifying the best time for insertion, and elucidating tissue reactions.

In summary, esophageal stents constructed from synthetic polyester polymers and Mg-based alloy materials have their own individual set of advantages and disadvantages, highlighting the need for further research to explore stents with improved performance. Currently, esophageal stents primarily serve the purpose of enlarging the esophageal lumen, particularly for addressing MES such as tumors. Coated SEMs have shown promise in reducing tumor cell ingrowth (Rozanes et al., 2002); however, they lack inherent anti-tumor or anti-proliferation capabilities. DES has been in development for many years; however, its research and application have been predominantly concentrated in the fields of coronary artery disease and peripheral artery disease, with research on esophageal stents being comparatively underexplored with slow progress. Stent migration is also a common problem with esophageal stents. Further technological innovation and animal and clinical trials are required to address these challenges. Additionally, the existing stent manufacturing technologies and materials are relatively limited, relying mainly on braiding technology, polyester polymers, and alloy materials. Urgent innovation is required to diversify and customize stent types, functions, and manufacturing processes.

3 Innovations and outlook

3.1 Functional innovation

3.1.1 Unidirectional drug-release function

In recent years, DES has garnered increasing attention across various medical disciplines. It typically comprises three primary components: the stent body, the stent coating (generally

composed of polymers), and an anti-proliferative drug (Garg et al., 2013). As previously mentioned, researchers are integrating antiproliferative drugs with stent coatings, applying them to either traditional SEMs or emerging BES. This approach preserves the primary function of the stent and facilitates the localized, sustained release of drugs. This effectively inhibits tissue proliferation in restenosis or tumor growth to attain the required local drug concentration, without necessitating potentially harmful systemic doses. Furthermore, some researchers have pioneered innovative drug-loading techniques to enhance the drug-release performance of DES. They have designed double-layer or multi-layer drug-loaded films that enable the unidirectional release of drug molecules onto the esophageal wall, ultimately achieving more precise and efficient treatment.

Guo et al (2007a) (Guo et al., 2007b) fully blended 5-FU particles and ethylene-vinyl acetate (EVA) in various proportions and compressed them into a film using a heat source to create a 5-FU-loaded layer. The drug-loaded layer was combined with a drug-free EVA protective layer, resulting in the development of an esophageal stent coating capable of unidirectional drug molecule release. Subsequently, they wrapped this coating around a nickel-titanium stent under controlled pressure at 70°C to form a 5-FU-coated stent. The findings indicated that regulating the permeation rate of 5-FU through the porcine esophageal mucosa was possible by adjusting the drug content within the coating. The coating containing 20%–60% 5-FU exhibited the ability to endure repeated binding and release through the stent introducer. In a subsequent study by the same team, they inserted the stent into the esophagi of healthy New Zealand albino rabbits. The results revealed that the 5-FU concentration in the esophageal tissue exposed to the stent, particularly the mucosal layer, consistently exceeded that in the serum or liver. This indicated that the stent had high efficiency and long-term local drug delivery capabilities and held the potential for the treatment of esophageal tumors and other tumors within the digestive and respiratory tracts (Guo et al., 2010). In 2015, Liu et al. (2015) (Wang et al., 2015) utilized the aforementioned approach (Guo et al., 2007b; Guo et al., 2010) to prepare nickel-titanium alloy stents. These stents incorporated a bilayered polymer film that contained either 5-FU or PTX. The researchers subsequently inserted these stents into the esophagi of healthy Bama mini-pigs for *in vivo* evaluation. The 5-FU stent and PTX stent did not induce significant damage to the esophageal wall at their insertion sites and did not exhibit obvious local or systemic toxicity. Furthermore, these stents efficiently suppressed ulceration, inflammation, and the growth of granulation tissue. These two DESs exhibited dual functionality as a stent and a localized drug delivery device, presenting a potential approach characterized by high effectiveness and an absence of systemic toxicity for treating esophageal cancer.

Researchers conducted experiments by incorporating varying concentrations of DTX into PurSil AL 20 (silicone-modified polyurethane polymer, PUS), which serves as a suitable material for covering SEMs, to achieve different loadings (Figure 4) (Shaikh et al., 2015). The solution was mixed evenly by vortex and ultrasonic, resulting in the formation of DTX-loaded films after the solution was dried. Researchers attached a blank film to the DTX-loaded film, creating a bilayer film, to ensure unidirectional drug delivery to the

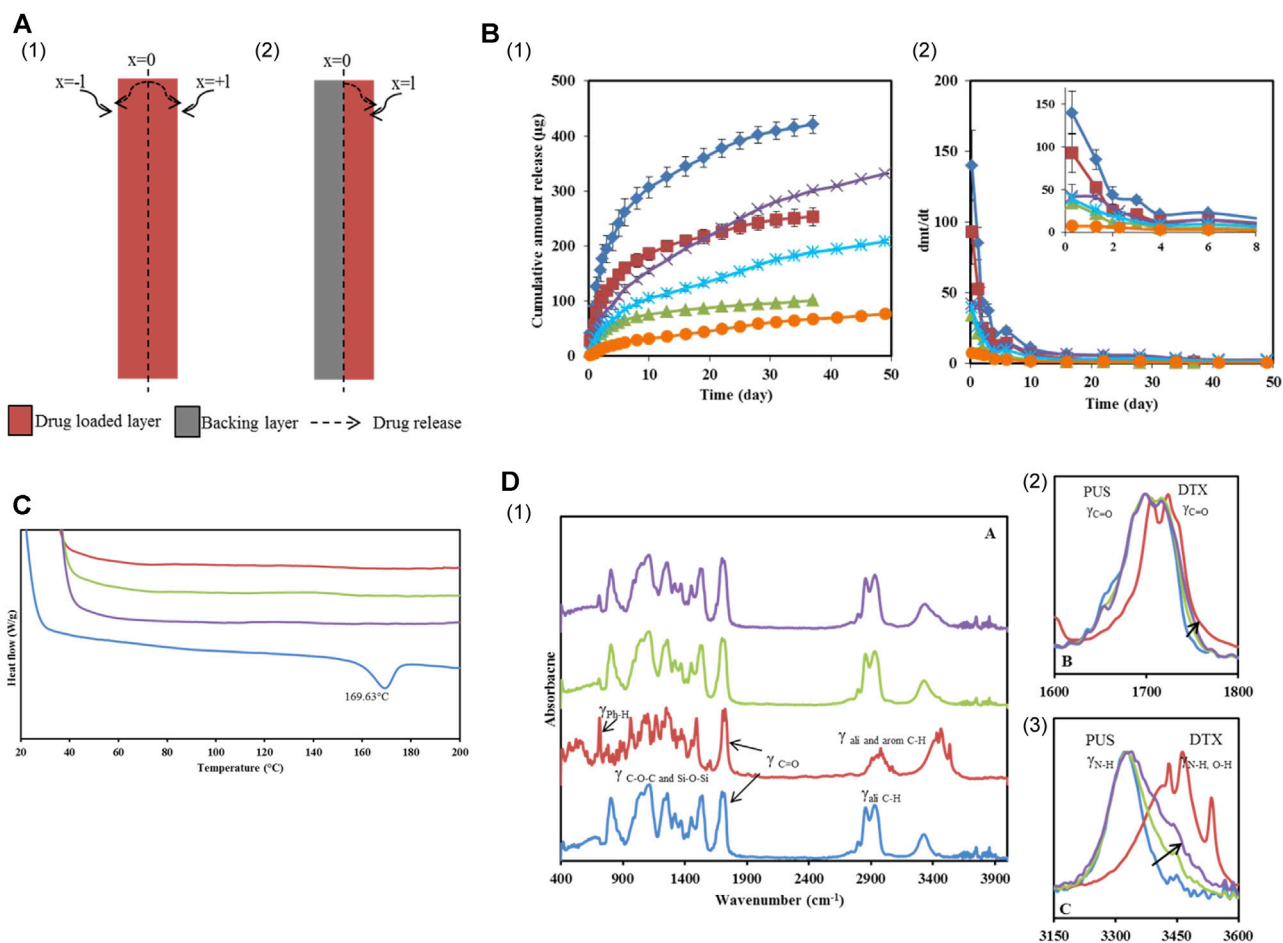


FIGURE 4

(A) Schematic illustration of DTX permeation through the mono and bilayer film. (B) *In vitro* DTX release profiles from Group 2 and 3 films. (I) Cumulative amount released and (II) Release rate from films loaded with different concentrations. (C) DES thermograms of PUS, 10% and 20% w/w DTX loaded PUS films and DTX. (D) (I) PA-FTIR spectra of PUS, DTX, 10% and 20% w/w DTX loaded films. (II and III) were the magnified spectra of the carbonyl and H-bond stretching regions. Reproduced with permission from ref [Shaikh et al., 2015]. Copyright 2015 American Chemical Society.

esophagus. Test outcomes demonstrated the physical and chemical compatibility of DTX and PUS, highlighting the outstanding physical and chemical stability of the DTX-loaded PUS membrane. The bilayer film ingeniously designed by the team exhibited sustained release properties (over 30 days) and held promise as a localized, continuous drug delivery system when combined with a stent.

In addition, Jin et al. (2018) introduced an innovative approach by designing and developing a novel antitumor drug/esophagus stent combination. This combination consisted of a magnetocaloric nitinol stent with a bi-layered film, which included one layer of ethylene-vinyl acetate copolymer (EVA) as a drug-blocking layer and another layer of EVA containing 10% PTX and 30% temperature-sensitive phase-change fatty alcohol (1-tetradecanol, 1-hexadecanol or 1-octadecanol). The stent exhibited excellent compatibility and safe magnetothermal drug release capabilities. The release rate of PTX from the PTX/nitinol complex accelerated upon subjection to an alternating electromagnetic field, resulting in a greater release amount. The penetration of PTX into the esophageal wall or deep esophageal musculature was significantly enhanced

compared to that at 37°C. This experiment essentially combined a stent, an anticancer drug, and a phase-change material to enhance drug release and ease the penetration of drugs into esophageal tissue. This novel approach introduced a fresh stent design concept for managing esophageal cancer.

In conclusion, the introduction of drug-eluting esophageal stents and associated technological innovations has introduced new dimensions to the overall progress in esophageal stent development. Conducting valuable research aimed at improving drug-loaded polymers, refining drug coating manufacturing techniques, and performing associated investigations is crucial to further this advancement. Extensive studies of additional animals and patients are imperative to substantiate the efficacy and safety of these promising implants. Additionally, exploring alternatives such as DNA, siRNA, miRNA, and nanoparticles instead of traditional drugs for stent improvement, which is a field more extensively studied in cardiovascular stents (Zhao et al., 2018; Beshchasna et al., 2020), holds significant reference value for the ongoing development of esophageal stents.

3.1.2 Anti-migration function

Due to the inherent physiological characteristics and peristaltic movements of the esophagus, coupled with the limited mechanical resilience of biodegradable stents, especially, there is a notable susceptibility to migration in biodegradable esophageal stents. Previous studies have indeed reported instances of early migration (Saito et al., 2007; Tanaka et al., 2007). Besides, despite the commendable mechanical properties of SEMS, the issue of stent migration persists, particularly in the case of fully-covered SEMS. Consequently, the innovation in the realm of anti-migration function emerges as a pivotal factor in enhancing stent performance.

In a noteworthy advancement in 2018, Lin et al. (2019) utilized 3D printing technology to fabricate esophageal stents with spirals. These stents exhibited substantial potential in mitigating the risk of migration, which will be elaborated upon later. Furthermore, in a recent patent, Clerc et al. (2022) introduced a novel approach by employing dissolvable or degradable adhesive polymers to fashion an anti-migration stent. This stent comprised both an inner and outer surface, with at least a portion of the outer surface incorporating a dissolvable or degradable adhesive polymer. The dissolvable adhesive polymer gradually dissolved in an aqueous environment over time, and the polymer layer was strategically positioned to come into contact with the inner surface of esophagus. Consequently, the activation of these polymer layers enhanced the adhesion of the self-expanding stent to esophagus, effectively resisting migration.

Moreover, it is crucial to design stents that not only minimize the extent of migration within the body lumen but also allow for easy removal and/or repositioning post-deployment. Hynes et al. (2022) introduced an expandable stent with distinct areas: a covered first section (facilitating removal) and an uncovered second section (reducing migration tendency). A biodegradable gripping material, featuring a roughened outer surface to resist post-implantation migration, was applied to at least one area of the biostable covering's outer surface. The stent was designed to transition from a collapsed to an expanded state, with the second section intended to contact the inner surface of the body cavity in the expanded state.

While the stent designs outlined in the aforementioned patents have not been implemented in animals and clinical patients, their innovative approach to preventing migration has charted a new course for enhancing the performance of esophageal stent in future developments. It is anticipated that, leveraging these designs, multifunctional esophageal stents with enhanced performance can be developed.

3.2 Manufacturing technology innovation

Stent manufacturing technology has undergone continuous breakthroughs and advancements. Five main stent manufacturing methods are currently used: etching, micro-electro discharge machining, electroforming, die-casting, and the most commonly used laser cutting (Kathuria, 2006). Although laser cutting technology has matured, it still presents disadvantages such as high costs and the inability to cater to patients' personalized customization needs (Wang et al., 2021a). Consequently, attention is shifting towards 3D printing technology, which is cost-effective,

allows for personalized customization, and offers a broader range of material options.

3D printing is a digital manufacturing technology that utilizes bondable materials to construct objects layer-by-layer. Various 3D printing technologies, such as inkjet printing, stereolithography, selective laser sintering, and fused deposition modelling (Wang et al., 2021a), provide distinct advantages over traditional methods such as weaving, knitting, laser cutting, and segmentation. This innovative approach overcomes some of the limitations of current stent production and facilitates the customization and personalization of stent designs (Kang, 2019).

In 2018, a group utilized simulated structural parameters to 3D print four types of PLA/polyurethane (TPU) stents that incorporated spirals using a custom-made 3D printer equipped with four sets of PLA/TPU composites (Lin et al., 2019). Their findings indicated that 3D-printed stents with spirals displayed a significant potential for reducing migration risk and exhibited greater expansion force compared to stents lacking spirals. These stents degraded slowly, and their mechanical properties remained relatively stable even after 3 months of insertion, exhibiting the promising potential of 3D-printed esophageal stents in managing malignant esophageal diseases. Notably, this pioneering research marked the initial utilization of 3D printing technology for creating a polymer esophageal stent, showcasing the capability of this technique to produce esophageal stents with varying sizes and shapes. Further research is warranted to fully explore the functionality of 3D-printed esophageal stents (Kang, 2019).

In 2020, Fouladian et al. (2020) fabricated a 3D-printed DES using fused deposition modelling. This innovative stent featured a design where the central segment of the stent was constructed using PU filament loaded with 5-FU, whereas the two ends were constructed with drug-free PU filament. Test results indicated that this stent was capable of consistently releasing 5-FU over an impressive period of 110 days. Additionally, the stent exhibited remarkable stability, even when subjected to sterilization procedures involving gamma and ultraviolet irradiation and during accelerated storage conditions. This research demonstrated the effectiveness of 3D printing as a robust tool for constructing DES, which can be readily personalized to offer patient-specific geometries and precise drug dosages.

3D printing technology has seen limited application in the production of biodegradable esophageal stents; nevertheless, the results from previous experiments and its successful use in manufacturing other stent types are promising. We anticipate ongoing advancements and increased utilization of 3D printing technology to offer more tailored and precise treatments for esophageal stents, including DES with enhanced functionalities.

3.3 Material innovation

Hydrogels arising from the physical or chemical cross-linking of polymer chains represent hydrophilic polymers characterized by a three-dimensional porous structure (Zhang and Khademhosseini, 2017; Liu et al., 2018). They possess a soft and pliable texture, excel in retaining water, and exhibit commendable biocompatibility (Cai et al., 2022). Hydrogels have promising applications across various biomedical fields (Ustürk et al., 2022), including drug delivery

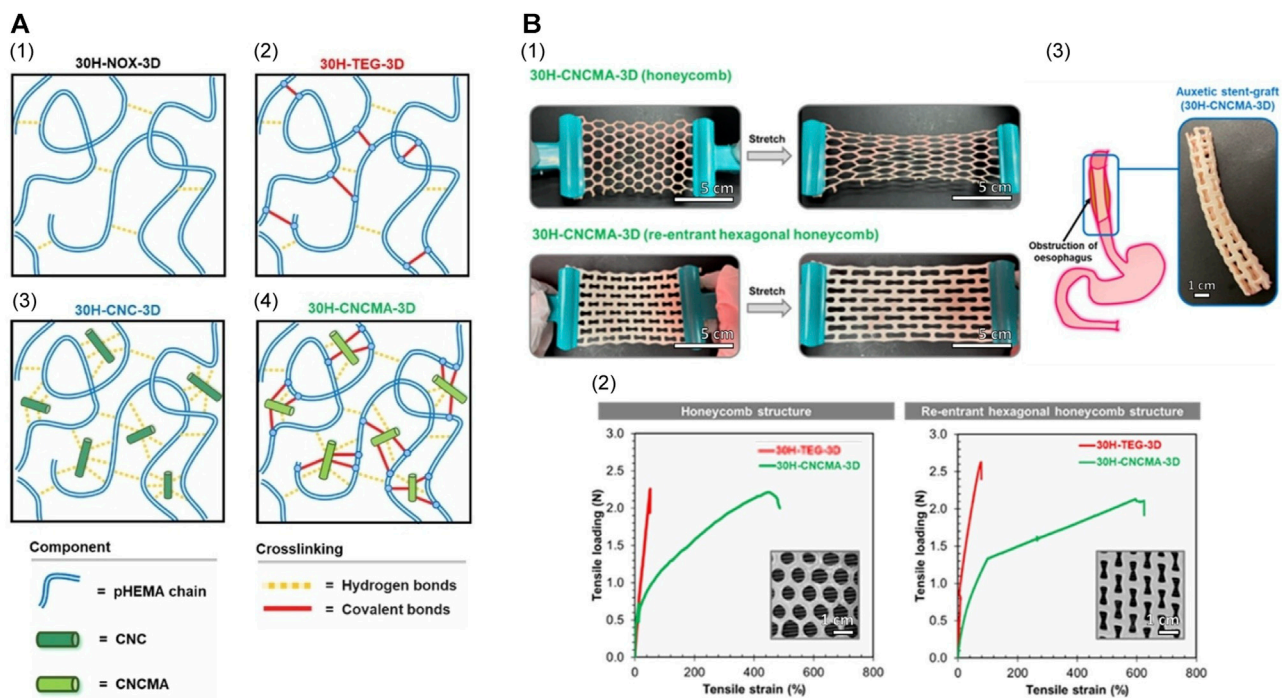


FIGURE 5

(A) Proposed schematic cross-linking networks for each hydrogel system. (B) Mechanical properties of pHEMA hydrogel specimens with conventional honeycomb and auxetic re-entrant hexagonal honeycomb structures. (I) Demonstration of the conventional and auxetic CNCMA-HEMA hydrogel specimens. The auxetic hydrogel specimen was expandable in the lateral direction when stretched while the conventional hydrogel specimen contracted. (II) Tensile load-strain curves of pHEMA hydrogel specimens with conventional and auxetic structures. (III) Esophageal stent made from auxetic CNCMA-HEMA hydrogel. Reproduced with permission from ref [(Pruksawan et al., 2022)]. Copyright 2022 Wiley-VCH GmbH.

systems (Zhang et al., 2019; Kasiński et al., 2020), cell culture substrates (Fukunaga et al., 2019), wound dressings (Mandal et al., 2020), and tissue engineering scaffolds (Neves et al., 2020; Unal and West, 2020).

In 2020, Raman et al. (2020) constructed a tough acrylate ortho-nitrobenzyl (oNB) light-triggered degradable hydrogel with adjustable mechanical characteristics and a modular design that can undergo safe, contact-free degradation at various anatomical sites within the body. The material and its degradation by-products were shown to be biocompatible. This group constructed an oNB esophageal stent using this light-triggerable hydrogel in combination with PCL, envisioning its application for offering structural support and/or localized drug delivery within the esophagus. Results from a series of *in vitro* and *ex vivo* trials suggested that these stents would persist in the esophagus when deployed *in vivo* until they naturally biodegrade. Subsequently, peristaltic waves within the gastrointestinal tract would gently transport the degraded material, eliminating the need for mechanical, thermal, or chemical triggers and minimizing adverse effects on the esophagus. This light-triggering mechanism provided a non-contact approach for the safe extraction of the stent from the lower esophageal sphincter, rendering it suitable for addressing both benign and malignant strictures. In a recent study, researchers developed CNCMA-pHEMA hydrogels using methacrylate cellulose nanocrystals (CNCMA) as a macro-cross-linking agent in poly (2-hydroxyethyl methacrylate) (pHEMA) hydrogels

(Figure 5) (Pruksawan et al., 2022). These hydrogels exhibited significantly enhanced toughness and tensile properties compared to hydrogels cross-linked with conventional agents. The remarkable strength and durability of these hydrogels render them promising candidates for advanced flexible implantable devices, including biodegradable esophageal self-expanding stents. Consequently, biodegradable hydrogels hold tremendous potential for the development of such stents.

3.4 Outlook

Biodegradable esophageal stents have garnered significant attention owing to their favorable biocompatibility and unique advantages, including the avoidance of secondary interventions. These stents have been employed in numerous animal experiments and clinical applications. However, biodegradable stents lag behind metal stents in terms of stiffness and strength. This discrepancy can lead to complications such as early displacement. Additionally, they are susceptible to the acidic environment in the esophagus, hastening the degradation process. The development of a more optimal biodegradable stent remains a challenge, despite the abovementioned ongoing innovative research in functions, technologies, and materials. Future research should delve more deeply into the material's mechanical properties, degradation time, and surface characteristics to address these issues.

4 Conclusion

Biodegradable esophageal stents approved for clinical use, such as PLLA-BDS, ELLA-BDS, and other stents manufactured from synthetic polyester polymers and Mg-based alloys, have shown promising results in performance tests and clinical applications. However, this is only the beginning of the era of biodegradable esophageal stents, and the stents currently available in the market require further improvement regarding mechanical stability and material degradation rate, among others. Another promising characteristic of stents is their exceptional capacity to transport and locally release drugs to inhibit tissue proliferation or exert antitumor effects. These drugs can be eluted as the stent itself or the coating degrades, assisting in the treatment of stenosis or eliminating the cause of stenosis, with minimal systemic side effects. In addition, unidirectional drug-release function, anti-migration function, 3D printing technology and hydrogel materials are currently valuable innovations that deserve further exploration to develop better biodegradable esophageal stents.

In summary, the development of biodegradable esophageal stents remains in its initial exploration stage. It is anticipated that this field will witness the application of more appropriate biodegradable materials, enhanced and personalized stent manufacturing methods, improved stent structure and performance, and more precise drug-release technology.

Author contributions

YaY: Conceptualization, Data curation, Visualization, Writing–original draft. YuY: Conceptualization, Data curation, Visualization, Writing–original draft. ZH: Conceptualization, Methodology, Visualization, Writing–original draft. TW: Formal Analysis, Methodology, Visualization, Writing–original draft. PW: Conceptualization, Formal Analysis, Supervision, Writing–original draft. LS: Data curation, Formal Analysis, Methodology, Writing–original draft. PL: Formal Analysis, Methodology,

Supervision, Writing–original draft. KZ: Funding acquisition, Resources, Supervision, Writing–review and editing. LY: Formal Analysis, Funding acquisition, Methodology, Writing–review and editing. SS: Conceptualization, Project administration, Supervision, Writing–review and editing.

Funding

The author(s) declare financial support was received for the research, authorship, and/or publication of this article. This work was supported by the National Natural Science Foundation of China (Grant No. 82000625), the Natural Science Foundation of Liaoning Province (Grant No. 2022-YGJC-69), the support program for excellent young scholars of China Medical University, Young and middle-aged science and technology innovation talent Program (Grant No. RC220482), the Doctoral Scientific Research Foundation of Liaoning Province (Grant No. 2020-BS-109) and 345 Talent Project.

Conflict of interest

The authors declare that the research was conducted in the absence of any commercial or financial relationships that could be construed as a potential conflict of interest.

Publisher's note

All claims expressed in this article are solely those of the authors and do not necessarily represent those of their affiliated organizations, or those of the publisher, the editors and the reviewers. Any product that may be evaluated in this article, or claim that may be made by its manufacturer, is not guaranteed or endorsed by the publisher.

References

- Abedalwafa, M., Wang, F., Wang, L., and Li, C. (2013). Biodegradable poly-epsilon-caprolactone (PCL) for tissue engineering applications: a review. *Rev. Adv. Mater. Sci.* 34 (2), 123–140.
- Ackroyd, R., Watson, D. I., Devitt, P. G., and Jamieson, G. G. (2001). Expandable metallic stents should not be used in the treatment of benign esophageal strictures. *J. gastroenterology hepatology* 16 (4), 484–487. doi:10.1046/j.1440-1746.2001.02367.x
- Adler, D. G., and Siddiqui, A. A. (2017). Endoscopic management of esophageal strictures. *Gastrointest. Endosc.* 86 (1), 35–43. doi:10.1016/j.gie.2017.03.004
- Antonowicz, M., Szweczenko, J., Jaworska, J., Jelonek, K., Jozsko, K., Gzik-Zroska, B., et al. (2021). Functional properties of polyurethane ureteral stents with PLGA and papaverine hydrochloride coating. *Int. J. Mol. Sci.* 22 (14), 7705. doi:10.3390/ijms22147705
- Babilotte, J., Martin, B., Guduric, V., Bareille, R., Agniel, R., Roques, S., et al. (2021). Development and characterization of a PLGA-HA composite material to fabricate 3D-printed scaffolds for bone tissue engineering. *Mater. Sci. Eng. C* 118, 111334. doi:10.1016/j.msec.2020.111334
- Bartholomew, R. (1981). PDS (polydioxanone suture): a new synthetic absorbable suture in cataract surgery. *Ophthalmologica* 183 (2), 81–85. doi:10.1159/000309144
- Basha, J., Appasani, S., Vaiphei, K., Gupta, V., Singh, K., and Kochhar, R. (2013). Biodegradable stents: truly biodegradable with good tissue harmony. *Endoscopy* 45 (S 02), E116–E117. doi:10.1055/s-0032-1326111
- Battersby, I., and Doyle, R. (2010). Use of a biodegradable self-expanding stent in the management of a benign oesophageal stricture in a cat. *J. Small Animal Pract.* 51 (1), 49–52. doi:10.1111/j.1748-5827.2009.00868.x
- Beshchasna, N., Saqib, M., Kraskiewicz, H., Wasyluk, L., Kuzmin, O., Duta, O. C., et al. (2020). Recent advances in manufacturing innovative stents. *Pharmaceutics* 12 (4), 349. doi:10.3390/pharmaceutics12040349
- Boland, E. D., Coleman, B. D., Barnes, C. P., Simpson, D. G., Wnek, G. E., and Bowlin, G. L. (2005). Electrospinning polydioxanone for biomedical applications. *Acta biomater.* 1 (1), 115–123. doi:10.1016/j.actbio.2004.09.003
- Bottino, M. C., Albuquerque, M. T., Azabi, A., Münchow, E. A., Spolnik, K. J., Nör, J. E., et al. (2019). A novel patient-specific three-dimensional drug delivery construct for regenerative endodontics. *J. Biomed. Mater. Res. Part B Appl. Biomaterials* 107 (5), 1576–1586. doi:10.1002/jbm.b.34250
- Bowen, P. K., Shearier, E. R., Zhao, S., Guillory, R. J., Zhao, F., Goldman, J., et al. (2016). Biodegradable metals for cardiovascular stents: from clinical concerns to recent Zn-Alloys. *Adv. Healthc. Mater.* 5 (10), 1121–1140. doi:10.1002/adhm.201501019
- Brossier, T., Volpi, G., Vasquez-Villegas, J., Petitjean, N., Guillaume, O., Lapinte, V., et al. (2021). Photoprintable gelatin-graft-poly (trimethylene carbonate) by stereolithography for tissue engineering applications. *Biomacromolecules* 22 (9), 3873–3883. doi:10.1021/acs.biomac.1c00687
- Cai, G., Hou, Z., Sun, W., Li, P., Zhang, J., Yang, L., et al. (2022). Recent developments in biomaterial-based hydrogel as the delivery system for repairing endometrial injury. *Front. Bioeng. Biotechnol.* 10, 894252. doi:10.3389/fbioe.2022.894252
- Chen, C., Chen, J., Wu, W., Shi, Y., Jin, L., Petrini, L., et al. (2019a). *In vivo* and *in vitro* evaluation of a biodegradable magnesium vascular stent designed by shape optimization strategy. *Biomaterials* 221, 119414. doi:10.1016/j.biomaterials.2019.119414

- Chen, H., Wang, X., Shao, S., Zhang, J., Tan, X., and Chen, W. (2022). Value of EUS in determining infiltration depth of early carcinoma and associated precancerous lesions in the upper gastrointestinal tract. *Endosc. ultrasound* 11 (6), 503. doi:10.4103/eus-d-21-00218
- Chen, L., Li, J., Chang, J., Jin, S., Wu, D., Yan, H., et al. (2018). Mg-Zn-Y-Nd coated with citric acid and dopamine by layer-by-layer self-assembly to improve surface biocompatibility. *Sci. China Technol. Sci.* 61, 1228–1237. doi:10.1007/s11431-017-9190-2
- Chen, L., Sheng, Y., Zhou, H., Li, Z., Wang, X., and Li, W. (2019b). Influence of a MAO+ PLGA coating on biocorrosion and stress corrosion cracking behavior of a magnesium alloy in a physiological environment. *Corros. Sci.* 148, 134–143. doi:10.1016/j.corsci.2018.12.005
- Chen, X., Chen, X., Bao, Y., Zhang, W., Jiang, L., Zhu, J., et al. (2023). EUS-derived maximum tumor thickness and tumor shrinkage rate as independent prognostic factors in locally advanced esophageal squamous cell carcinoma after neoadjuvant chemoradiotherapy. *Endosc. Ultrasound* 12 (4), 369–376. doi:10.1097/eus.0000000000000008
- Chen, Y., Song, Y., Zhang, S., Li, J., Zhao, C., and Zhang, X. (2011). Interaction between a high purity magnesium surface and PCL and PLA coatings during dynamic degradation. *Biomed. Mater.* 6 (2), 025005. doi:10.1088/1748-6041/6/2/025005
- Clerc, C. O., Fredrickson, G., and Boden, M. (2022). Dissolvable or degradable adhesive polymer to prevent stent migration. *Google Pat.*
- Conio, M., Repici, A., Battaglia, G., De Pretis, G., Ghezzi, L., Bittinger, M., et al. (2007). A randomized prospective comparison of self-expandable plastic stents and partially covered self-expandable metal stents in the palliation of malignant esophageal dysphagia. *Official J. Am. Coll. Gastroenterology| ACG* 102 (12), 2667–2677. doi:10.1111/j.1572-0241.2007.01565.x
- Desai, M., Hamade, N., and Sharma, P. (2020). Management of peptic strictures. *Official J. Am. Coll. Gastroenterology| ACG* 115 (7), 967–970. doi:10.14309/ajg.0000000000000655
- De Wijkerslooth, L. R., Vleggaar, F. P., and Siersema, P. D. (2011). Endoscopic management of difficult or recurrent esophageal strictures. *Official J. Am. Coll. Gastroenterology| ACG* 106 (12), 2080–2091. doi:10.1038/ajg.2011.348
- Dhar, A., Topping, J. H., Johns, E., and O'Neill, D. (2009). Biodegradable stents in refractory benign oesophageal strictures—first report of 4 patients from UK. *Gastrointest. Endosc.* 69 (5), AB254–AB255. doi:10.1016/j.gie.2009.03.655
- Dou, Z., Chen, S., Wang, J., Xia, L., Maitz, M. F., Tu, Q., et al. (2023). A “built-up” composite film with synergistic functionalities on Mg–2Zn–1Mn bioresorbable stents improves corrosion control effects and biocompatibility. *Bioact. Mater.* 25, 223–238. doi:10.1016/j.bioactmat.2023.02.004
- Dumoulin, F., and Plassmann, D. (2012). Tissue hyperplasia following placement of a biodegradable stent for a refractory esophageal stricture: treatment with argon plasma coagulation. *Endoscopy* 44 (S 02), E356–E357. doi:10.1055/s-0032-1310021
- Evrard, S., Le Moine, O., Lazaraki, G., Dormann, A., El Nakadi, I., and Devière, J. (2004). Self-expanding plastic stents for benign esophageal lesions. *Gastrointest. Endosc.* 60 (6), 894–900. doi:10.1016/s0016-5107(04)02278-3
- Fang, H., Qi, X., Zhou, S., Yang, S., Hang, C., Tian, Y., et al. (2021). High-efficient vacuum ultraviolet-ozone assist-deposited polydopamine for poly (lactic-co-glycolic acid)-coated pure Zn toward biodegradable cardiovascular stent applications. *ACS Appl. Mater. Interfaces* 14 (2), 3536–3550. doi:10.1021/acsami.1c21567
- Fischer, A., Bausch, D., Baier, P., Braun, A., and Richter-Schrag, H. (2012). Risk of biodegradable stent-induced hypergranulation causing re-stenosis of a gastric conduit after esophageal resection. *Endoscopy* 44 (S 02), E125–E126. doi:10.1055/s-0031-1291693
- Fouladian, P., Kohlhaagen, J., Arafat, M., Afinjuomo, F., Workman, N., Abuhelwa, A. Y., et al. (2020). Three-dimensional printed 5-fluorouracil eluting polyurethane stents for the treatment of oesophageal cancers. *Biomaterials Sci.* 8 (23), 6625–6636. doi:10.1039/d0bm01355b
- Fredenberg, S., Wahlgren, M., Reslow, M., and Axelsson, A. (2011). The mechanisms of drug release in poly (lactic-co-glycolic acid)-based drug delivery systems—a review. *Int. J. Pharm.* 415 (1–2), 34–52. doi:10.1016/j.ijpharm.2011.05.049
- Fry, S. W., and Fleischer, D. E. (1997). Management of a refractory benign esophageal stricture with a new biodegradable stent. *Gastrointest. Endosc.* 45 (2), 179–182. doi:10.1016/s0016-5107(97)70244-x
- Fuccio, L., Hassan, C., Frazzoni, L., Miglio, R., and Repici, A. (2015). Clinical outcomes following stent placement in refractory benign esophageal stricture: a systematic review and meta-analysis. *Endoscopy* 48, 141–148. doi:10.1055/s-0034-1393331
- Fukunaga, K., Tsutsumi, H., and Mihara, H. (2019). Self-assembling peptides as building blocks of functional materials for biomedical applications. *Bull. Chem. Soc. Jpn.* 92 (2), 391–399. doi:10.1246/bcsj.20180293
- Garg, S., Bourantas, C., and Serruys, P. W. (2013). New concepts in the design of drug-eluting coronary stents. *Nat. Rev. Cardiol.* 10 (5), 248–260. doi:10.1038/nrcardio.2013.13
- Goldin, E., Fiorini, A., Ratan, Y., Keter, D., Loshakove, A., Globerman, O., et al. (1996). A new biodegradable and self-expandable stent for benign esophageal strictures. *Gastrointest. Endosc.* 4 (43), 294. doi:10.1016/s0016-5107(96)80017-4
- Goonoo, N., Jeetah, R., Bhaw-Luximon, A., and Jhurry, D. (2015). Polydioxanone-based bio-materials for tissue engineering and drug/gene delivery applications. *Eur. J. Pharm. Biopharm.* 97, 371–391. doi:10.1016/j.ejpb.2015.05.024
- Griffiths, E. A., Gregory, C. J., Pursnani, K. G., Ward, J. B., and Stockwell, R. C. (2012). The use of biodegradable (SX-ELLA) oesophageal stents to treat dysphagia due to benign and malignant oesophageal disease. *Surg. Endosc.* 26, 2367–2375. doi:10.1007/s00464-012-2192-9
- Gu, X., Zheng, Y., Cheng, Y., Zhong, S., and Xi, T. (2009). *In vitro* corrosion and biocompatibility of binary magnesium alloys. *Biomaterials* 30 (4), 484–498. doi:10.1016/j.biomaterials.2008.10.021
- Guarino, V., Gentile, G., Sorrentino, L., and Ambrosio, L. (2002). Polycaprolactone: synthesis, properties, and applications. *Encycl. Polym. Sci. Technol.*, 1–36. doi:10.1002/0471440264.pst658
- Guo, Q., Guo, S., and Wang, Z. (2007a). A type of esophageal stent coating composed of one 5-fluorouracil-containing EVA layer and one drug-free protective layer: *in vitro* release, permeation and mechanical properties. *J. Control. Release* 118 (3), 318–324. doi:10.1016/j.jconrel.2006.12.030
- Guo, Q.-h., Guo, S.-r., and Wang, Z.-m. (2007b). Estimation of 5-fluorouracil-loaded ethylene-vinyl acetate stent coating based on percolation thresholds. *Int. J. Pharm.* 333 (1–2), 95–102. doi:10.1016/j.ijpharm.2006.10.011
- Guo, S.-R., Wang, Z.-M., Zhang, Y.-Q., Lei, L., Shi, J.-M., Chen, K.-M., et al. (2010). *In vivo* evaluation of 5-fluorouracil-containing self-expandable nitinol stent in rabbits: efficiency in long-term local drug delivery. *J. Pharm. Sci.* 99 (7), 3009–3018. doi:10.1002/jps.22066
- Hair, C., and Devonshire, D. (2010). Severe hyperplastic tissue stenosis of a novel biodegradable esophageal stent and subsequent successful management with high-pressure balloon dilation. *Endoscopy* 42 (S 02), E132–E133. doi:10.1055/s-0029-1244011
- Ham, Y. H., and Kim, G. H. (2014). Plastic and biodegradable stents for complex and refractory benign esophageal strictures. *Clin. Endosc.* 47 (4), 295–300. doi:10.5946/ce.2014.47.4.295
- Han, C.-M., Lih, E., Choi, S.-K., Bedair, T. M., Lee, Y.-J., Park, W., et al. (2018). Biodegradable sheath-core biphasic monofilament braided stent for bio-functional treatment of esophageal strictures. *J. Industrial Eng. Chem.* 67, 396–406. doi:10.1016/j.jiec.2018.07.014
- Han, J., Wan, P., Ge, Y., Fan, X., Tan, L., Li, J., et al. (2016). Tailoring the degradation and biological response of a magnesium–strontium alloy for potential bone substitute application. *Mater. Sci. Eng. C* 58, 799–811. doi:10.1016/j.msec.2015.09.057
- He, J., Lin, Z., Hu, X., Xing, L., Liang, G., Chen, D., et al. (2021). Biocompatible and biodegradable scaffold based on poly(trimethylene carbonate)-tricalcium phosphate microspheres for tissue engineering. *Colloids Surfaces B Biointerfaces* 204, 111808. doi:10.1016/j.colsurfb.2021.111808
- Hirdes, M., Siersema, P. D., Van Boeckel, P., and Vleggaar, F. P. (2012a). Single and sequential biodegradable stent placement for refractory benign esophageal strictures: a prospective follow-up study. *Endoscopy* 44 (07), 649–654. doi:10.1055/s-0032-1309818
- Hirdes, M. M., van Hooff, J. E., Wijdeman, H. K., Hulshof, M. C., Fockens, P., Reerink, O., et al. (2012b). Combination of biodegradable stent placement and single-dose brachytherapy is associated with an unacceptably high complication rate in the treatment of dysphagia from esophageal cancer. *Gastrointest. Endosc.* 76 (2), 267–274. doi:10.1016/j.gie.2012.04.442
- Hirdes, M. M., Vleggaar, F. P., De Beule, M., and Siersema, P. D. (2013). *In vitro* evaluation of the radial and axial force of self-expanding esophageal stents. *Endoscopy* 45 (12), 997–1005. doi:10.1055/s-0033-1344985
- Hou, Z., Li, P., Guo, J., Wang, J., Hu, J., and Yang, L. (2020). The effect of molecular weight on thermal properties and degradation behavior of copolymers based on TMC and DTC. *Polym. Degrad. Stab.* 175, 109128. doi:10.1016/j.polymdegradstab.2020.109128
- Hou, Z., Xu, W., Chen, S., Guo, J., Li, P., Hu, J., et al. (2023). Biodegradable implants based on photo-cross-linked aliphatic polycarbonates for long-acting contraception. *J. Mater. Sci. Technol.* 156, 129–141. doi:10.1016/j.jmst.2023.01.040
- Hynes, M., Folan, M. G., Wulfman, D. R., Keating, T. M., Montague, M., and Nolan, D. V. (2022). Stent including anti-migration capabilities. *Google Pat.*
- Isotalo, T. M., Nuutinen, J. P., Vaajanen, A., Martikainen, P. M., Laurila, M., Törmälä, P., et al. (2006). Biocompatibility properties of a new braided biodegradable urethral stent: a comparison with a biodegradable spiral and a braided metallic stent in the rabbit urethra. *BJU Int.* 97 (4), 856–859. doi:10.1111/j.1464-410x.2006.06000.x
- Jiang, D., Zou, H., Zhang, H., Zhao, W., Lan, Y., and Yuan, M. (2022). Preparation and properties of electrospun PLLA/PTMC scaffolds. *Polymers* 14 (20), 4406. doi:10.3390/polym14204406
- Jin, S., Xia, X., Huang, J., Yuan, C., Zuo, Y., Li, Y., et al. (2021). Recent advances in PLGA-based biomaterials for bone tissue regeneration. *Acta biomater.* 127, 56–79. doi:10.1016/j.actbio.2021.03.067

- Jin, Z., Wu, K., Hou, J., Yu, K., Shen, Y., and Guo, S. (2018). A PTX/nitinol stent combination with temperature-responsive phase-change 1-hexadecanol for magnetocaloric drug delivery: magnetocaloric drug release and esophagus tissue penetration. *Biomaterials* 153, 49–58. doi:10.1016/j.biomaterials.2017.10.040
- Jung, G., Sauer, P., and Schaible, A. (2010). Tracheoesophageal fistula following implantation of a biodegradable stent for a refractory benign esophageal stricture. *Endoscopy* 42 (S 02), E338–E339. doi:10.1055/s-0030-1256005
- Kailla, E., Rezai, F., Kansci, A. K., Akande, O., and Gossage, J. (2023). SX-ELLA biodegradable stent for benign oesophageal strictures: a systematic review and proportion meta-analysis. *Surg. Endosc.* 37 (4), 2476–2484. doi:10.1007/s00464-022-09767-w
- Kang, Y. (2019). A review of self-expanding esophageal stents for the palliation therapy of inoperable esophageal malignancies. *Biomed. Res. Int.* 2019, 1–11. doi:10.1155/2019/9265017
- Kasiński, A., Zielińska-Pisklak, M., Oledzka, E., and Sobczak, M. (2020). Smart hydrogels—synthetic stimuli-responsive antitumor drug release systems. *Int. J. Nanomedicine* 15, 4541–4572. doi:10.2147/ijn.s248987
- Kathuria, Y. (2006). The potential of biocompatible metallic stents and preventing restenosis. *Mater. Sci. Eng. A* 417 (1–2), 40–48. doi:10.1016/j.msea.2005.11.007
- Kirkland, N., Lespagnol, J., Biribilis, N., and Staiger, M. (2010). A survey of bio-corrosion rates of magnesium alloys. *Corros. Sci.* 52 (2), 287–291. doi:10.1016/j.corsci.2009.09.033
- Kohn, J., Welsh, W. J., and Knight, D. (2007). A new approach to the rationale discovery of polymeric biomaterials. *Biomaterials* 28 (29), 4171–4177. doi:10.1016/j.biomaterials.2007.06.022
- Kwak, T. W., Lee, H. L., Song, Y. H., Kim, C., Kim, J., Seo, S.-J., et al. (2017). Vorinostat-eluting poly (DL-lactide-co-glycolide) nanofiber-coated stent for inhibition of cholangiocarcinoma cells. *Int. J. Nanomedicine* 12, 7669–7680. doi:10.2147/ijn.s141920
- Labet, M., and Thielemans, W. (2009). Synthesis of polycaprolactone: a review. *Chem. Soc. Rev.* 38 (12), 3484–3504. doi:10.1039/b820162p
- Lam, N., Weisse, C., Berent, A., Kaae, J., Murphy, S., Radlinsky, M., et al. (2013). Esophageal stenting for treatment of refractory benign esophageal strictures in dogs. *J. Veterinary Intern. Med.* 27 (5), 1064–1070. doi:10.1111/jvim.12132
- Lanao, R. P. F., Leeuwenburgh, S. C., Wolke, J. G., and Jansen, J. A. (2011). Bone response to fast-degrading, injectable calcium phosphate cements containing PLGA microparticles. *Biomaterials* 32 (34), 8839–8847. doi:10.1016/j.biomaterials.2011.08.005
- Lasprilla, A. J., Martinez, G. A., Lunelli, B. H., Jardini, A. L., and Maciel Filho, R. (2012). Poly-lactic acid synthesis for application in biomedical devices—a review. *Biotechnol. Adv.* 30 (1), 321–328. doi:10.1016/j.biotechadv.2011.06.019
- Lei, L., Liu, X., Guo, S., Tang, M., Cheng, L., and Tian, L. (2010). 5-Fluorouracil-loaded multilayered films for drug controlled releasing stent application: drug release, microstructure, and *ex vivo* permeation behaviors. *J. Control. Release* 146 (1), 45–53. doi:10.1016/j.jconrel.2010.05.017
- Li, L., Zhang, X., Shi, J., Chen, Y., Wan, H., Herth, F. J., et al. (2023). Airway stents from now to the future: a narrative review. *Respiration* 102 (6), 439–448. doi:10.1159/000530421
- Li, L.-Y., Cui, L.-Y., Zeng, R.-C., Li, S.-Q., Chen, X.-B., Zheng, Y., et al. (2018). Advances in functionalized polymer coatings on biodegradable magnesium alloys—A review. *Acta biomater.* 79, 23–36. doi:10.1016/j.actbio.2018.08.030
- Li, X., Chen, H., Xie, S., Wang, N., Wu, S., Duan, Y., et al. (2020). Fabrication of photocrosslinkable poly (trimethylene carbonate)/polycaprolactone nanofibrous scaffolds for tendon regeneration. *Int. J. Nanomedicine* 15, 6373–6383. doi:10.2147/ijn.s246966
- Li, X., Chu, C., Liu, L., Liu, X., Bai, J., Guo, C., et al. (2015). Biodegradable poly-lactic acid based-composite reinforced unidirectionally with high-strength magnesium alloy wires. *Biomaterials* 49, 135–144. doi:10.1016/j.biomaterials.2015.01.060
- Lin, M., Firoozi, N., Tsai, C.-T., Wallace, M. B., and Kang, Y. (2019). 3D-printed flexible polymer stents for potential applications in inoperable esophageal malignancies. *Acta biomater.* 83, 119–129. doi:10.1016/j.actbio.2018.10.035
- Lischke, R., Pozniak, J., Vondrys, D., and Elliott, M. J. (2011). Novel biodegradable stents in the treatment of bronchial stenosis after lung transplantation. *Eur. J. cardiothoracic Surg.* 40 (3), 619–624. doi:10.1016/j.ejcts.2010.12.047
- Little, U., Buchanan, F., Harkin-Jones, E., McCaigue, M., Farrar, D., and Dickson, G. (2009). Accelerated degradation behaviour of poly (ϵ -caprolactone) via melt blending with poly (aspartic acid-co-lactide) (PAL). *Polym. Degrad. Stab.* 94 (2), 213–220. doi:10.1016/j.polymdegradstab.2008.11.001
- Liu, G., Fu, M., Li, F., Fu, W., Zhao, Z., Xia, H., et al. (2020). Tissue-engineered PLLA/gelatin nanofibrous scaffold promoting the phenotypic expression of epithelial and smooth muscle cells for urethral reconstruction. *Mater. Sci. Eng. C* 111, 110810. doi:10.1016/j.msec.2020.110810
- Liu, J., Shang, L., Liu, J., and Qin, C. (2016). A novel biodegradable esophageal stent: results from mechanical and animal experiments. *Am. J. Transl. Res.* 8 (2), 1108–1114.
- Liu, J., Wang, Z., Wu, K., Li, J., Chen, W., Shen, Y., et al. (2015). Paclitaxel or 5-fluorouracil/esophageal stent combinations as a novel approach for the treatment of esophageal cancer. *Biomaterials* 53, 592–599. doi:10.1016/j.biomaterials.2015.03.009
- Liu, J., and Xi, T. (2016). Enhanced anti-corrosion ability and biocompatibility of PLGA coatings on MgZnYNd alloy by BTSE-APTES pre-treatment for cardiovascular stent. *J. Mater. Sci. Technol.* 32 (9), 845–857. doi:10.1016/j.jmst.2016.06.021
- Liu, J.-B., Machado, P., Eisenbrey, J. R., Gummadi, S., Forsberg, F., Wessner, C. E., et al. (2023). Identification of sentinel lymph nodes in esophageal cancer patients using contrast-enhanced EUS with peritumoral injections. *Endosc. Ultrasound* 12 (4), 362–368. doi:10.1097/eus.0000000000000001
- Liu, L., Feng, X., Pei, Y., Wang, J., Ding, J., and Chen, L. (2018). α -Cyclodextrin concentration-controlled thermo-sensitive supramolecular hydrogels. *Mater. Sci. Eng. C* 82, 25–28. doi:10.1016/j.msec.2017.08.045
- Liu, L.-L., Qin, J., Zeng, C.-H., Du, R.-J., Pan, T., Ji, J.-J., et al. (2022). Biodegradable PTX-PLGA-coated magnesium stent for benign esophageal stricture: an experimental study. *Acta Biomater.* 146, 495–505. doi:10.1016/j.actbio.2022.04.038
- Lopez-Tobaruela, J. M., Valverde-Lopez, F., de Hierro-Ruiz, M. L., and Redondo-Cerezo, E. (2021). Hepatic abscess after biodegradable esophageal stent placement: a rare complication. *Official J. Am. Coll. Gastroenterology | ACG* 116 (1), 222–223. doi:10.14309/ajg.00000000000000821
- Lukasiewicz, S., Mikolajczyk, A., Błasiak, E., Fic, E., and Dziedzicka-Wasylewska, M. (2021). Polycaprolactone nanoparticles as promising candidates for nanocarriers in novel nanomedicines. *Pharmaceutics* 13 (2), 191. doi:10.3390/pharmaceutics13020191
- Ma, X., Oyamada, S., Wu, T., Robich, M. P., Wu, H., Wang, X., et al. (2011). *In vitro* and *in vivo* degradation of poly (D, L-lactide-co-glycolide)/amorphous calcium phosphate copolymer coated on metal stents. *J. Biomed. Mater. Res. Part A* 96 (4), 632–638. doi:10.1002/jbm.a.33016
- Maishman, T., Sheikh, H., Boger, P., Kelly, J., Cozens, K., Bateman, A., et al. (2021). A phase II study of biodegradable stents plus palliative radiotherapy in oesophageal cancer. *Clin. Oncol.* 33 (5), e225–e231. doi:10.1016/j.clon.2020.12.010
- Mandal, A., Clegg, J. R., Anselmo, A. C., and Mitragotri, S. (2020). Hydrogels in the clinic. *Bioeng. Transl. Med.* 5 (2), e10158. doi:10.1002/btm2.10158
- Manner, H. (2008). Argon plasma coagulation therapy. *Curr. Opin. gastroenterology* 24 (5), 612–616. doi:10.1097/mog.0b013e32830bf825
- Matsunami, Y., Itoi, T., Tsuchiya, T., Ishii, K., Tanaka, R., Tonozuka, R., et al. (2023). Objective evaluation of the resistance forces of 22-gauge EUS-FNA and fine-needle biopsy needles. *Endosc. Ultrasound* 12 (2), 251. doi:10.4103/eus-d-22-00059
- McCain, S., McCain, S., Quinn, B., Gray, R., Morton, J., and Rice, P. (2016). The role of biodegradable stents in the management of benign and malignant oesophageal strictures: a cohort study. *Surg.* 14 (6), 322–326. doi:10.1016/j.surge.2015.01.002
- Mochizuki, Y., Saito, Y., Tanaka, T., Nitta, N., Yamada, H., Tsujikawa, T., et al. (2012). Endoscopic submucosal dissection combined with the placement of biodegradable stents for recurrent esophageal cancer after chemoradiotherapy. *J. Gastrointest. cancer* 43, 324–328. doi:10.1007/s12029-011-9283-z
- Mohajeri, S., Chen, F., de Prinse, M., Phung, T., Burke-Kleinman, J., Maurice, D. H., et al. (2020). Liquid degradable poly (trimethylene-carbonate-co-5-hydroxy-trimethylene carbonate): an injectable drug delivery vehicle for acid-sensitive drugs. *Mol. Pharm.* 17 (4), 1363–1376. doi:10.1021/acs.molpharmaceut.0c00064
- Mohamed, R. M., and Yusoh, K. (2016). A review on the recent research of polycaprolactone (PCL). *Adv. Mater. Res.* 1134, 249–255. doi:10.4028/www.scientific.net/amr.1134.249
- Moravej, M., and Mantovani, D. (2011). Biodegradable metals for cardiovascular stent application: interests and new opportunities. *Int. J. Mol. Sci.* 12 (7), 4250–4270. doi:10.3390/ijms12074250
- Mueller, W.-D., Nascimento, M. L., and De Mele, M. F. L. (2010). Critical discussion of the results from different corrosion studies of Mg and Mg alloys for biomaterial applications. *Acta biomater.* 6 (5), 1749–1755. doi:10.1016/j.actbio.2009.12.048
- Muñoz, D. S., Ortiz-Moyano, C., and Gómez-Rodríguez, B. (2013). Resolution of a refractory anastomotic stricture with a novel biodegradable esophageal stent. *Clin. Gastroenterology Hepatology* 11 (9), e63. doi:10.1016/j.cgh.2012.11.023
- Neves, S. C., Moroni, L., Barrias, C. C., and Granja, P. L. (2020). Leveling up hydrogels: hybrid systems in tissue engineering. *Trends Biotechnol.* 38 (3), 292–315. doi:10.1016/j.tibtech.2019.09.004
- Okata, Y., Hisamatsu, C., Bitoh, Y., Yokoi, A., Nishijima, E., Maeda, K., et al. (2014). Efficacy and histopathological esophageal wall damage of biodegradable esophageal stents for treatment of severe refractory esophageal anastomotic stricture in a child with long gap esophageal atresia. *Clin. J. gastroenterology* 7, 496–501. doi:10.1007/s12328-014-0537-8
- Orive-Calzada, A., Alvarez-Rubio, M., Romero-Izquierdo, S., Martin, M. C., Juanmartínez, J., Ogúeta-Fernández, M., et al. (2009). Severe epithelial hyperplasia as a complication of a novel biodegradable stent. *Endoscopy* 41 (S 02), E137–E138. doi:10.1055/s-0029-1214634
- Oyama, T., Tomori, A., Hotta, K., Morita, S., Kominato, K., Tanaka, M., et al. (2005). Endoscopic submucosal dissection of early esophageal cancer. *Clin. Gastroenterology Hepatology* 3 (7), S67–S70. doi:10.1016/s1542-3565(05)00291-0
- Pan, K., Li, X., Meng, L., Hong, L., Wei, W., and Liu, X. (2020). Photo-cross-linked polycarbonate coating with surface-erosion behavior for corrosion resistance and cytocompatibility enhancement of magnesium alloy. *ACS Appl. Bio Mater.* 3 (7), 4427–4435. doi:10.1021/acsabm.0c00411

- Pan, K., Li, X., Shi, H., Dai, M., Yang, Z., Chen, M., et al. (2022). Preparation of photo-crosslinked aliphatic polycarbonate coatings with predictable degradation behavior on magnesium-alloy stents by electrophoretic deposition. *Chem. Eng. J.* 427, 131596. doi:10.1016/j.cej.2021.131596
- Pauli, E. M., Schomisch, S. J., Furlan, J. P., Marks, A. S., Chak, A., Lash, R. H., et al. (2012). Biodegradable esophageal stent placement does not prevent high-grade stricture formation after circumferential mucosal resection in a porcine model. *Surg. Endosc.* 26, 3500–3508. doi:10.1007/s00464-012-2373-6
- Peng, L., Wan, R., Chen, S., Wu, J., Yang, J., Wang, X., et al. (2023). Efficacy of endoscopic anterior fundoplication with a novel ultrasonic surgical endostapler for gastroesophageal reflux disease: six-month results from a multicenter prospective trial. *Endosc. ultrasound* 12 (1), 128. doi:10.4103/eus-d-21-00244
- Perkins, J., Xu, Z., Smith, C., Roy, A., Kumta, P. N., Waterman, J., et al. (2015). Direct writing of polymeric coatings on magnesium alloy for tracheal stent applications. *Ann. Biomed. Eng.* 43, 1158–1165. doi:10.1007/s10439-014-1169-3
- Pruksawan, S., Chee, H. L., Wang, Z., Luo, P., Chong, Y. T., Thitsartarn, W., et al. (2022). Toughened hydrogels for 3D printing of soft auxetic structures. *Chemistry—An Asian J.* 17 (19), e202200677. doi:10.1002/asia.202200677
- Rabenstein, T. (2015). Palliative endoscopic therapy of esophageal cancer. *Visc. Med.* 31 (5), 354–359. doi:10.1159/000441175
- Ragunath, K. (2008). Refractory benign esophageal strictures: extending the role of expandable stents. *Official J. Am. Coll. Gastroenterology* 12, 2995–2996. doi:10.1111/j.1572-0241.2008.02178.x
- Rai, A., Senapati, S., Saraf, S. K., and Maiti, P. (2016). Biodegradable poly (ϵ -caprolactone) as a controlled drug delivery vehicle of vancomycin for the treatment of MRSA infection. *J. Mater. Chem. B* 4 (30), 5151–5160. doi:10.1039/c6tb01623e
- Raman, R., Hua, T., Gwynne, D., Collins, J., Tamang, S., Zhou, J., et al. (2020). Light-degradable hydrogels as dynamic triggers for gastrointestinal applications. *Sci. Adv.* 6 (3), eaay0065. doi:10.1126/sciadv.aay0065
- Rejchrt, S., Kopacova, M., Brozik, J., and Bures, J. (2011). Biodegradable stents for the treatment of benign stenoses of the small and large intestines. *Endoscopy* 43, 911–917. doi:10.1055/s-0030-1256405
- Repici, A., Vleggaar, F. P., Hassan, C., van Boeckel, P. G., Romeo, F., Pagano, N., et al. (2010). Efficacy and safety of biodegradable stents for refractory benign esophageal strictures: the BEST (Biodegradable Esophageal Stent) study. *Gastrointest. Endosc.* 72 (5), 927–934. doi:10.1016/j.gie.2010.07.031
- Rozanes, I., Poyanlı, A., and Acunaş, B. (2002). Palliative treatment of inoperable malignant esophageal strictures with metal stents: one center's experience with four different stents. *Eur. J. radiology* 43 (3), 196–203. doi:10.1016/s0720-048x(02)00154-7
- Saito, Y., Minami, K.-i., Kaneda, H., Okada, T., Maniwa, T., Araki, Y., et al. (2004). New tubular bioabsorbable knitted airway stent: feasibility assessment for delivery and deployment in a dog model. *Ann. Thorac. Surg.* 78 (4), 1438–1440. doi:10.1016/s0003-4975(03)01408-5
- Saito, Y., Tanaka, T., Andoh, A., Minematsu, H., Hata, K., Tsujikawa, T., et al. (2007). Usefulness of biodegradable stents constructed of poly-L-lactic acid monofilaments in patients with benign esophageal stenosis. *World J. Gastroenterology WJG* 13 (29), 3977. doi:10.3748/wjg.v13.i29.3977
- Saito, Y., Tanaka, T., Andoh, A., Minematsu, H., Hata, K., Tsujikawa, T., et al. (2008). Novel biodegradable stents for benign esophageal strictures following endoscopic submucosal dissection. *Dig. Dis. Sci.* 53, 330–333. doi:10.1007/s10620-007-9873-6
- Saska, S., Pilatti, L., Silva, E. S. d. S., Nagasawa, M. A., Câmara, D., Lizier, N., et al. (2021). Polydioxanone-based membranes for bone regeneration. *Polymers* 13 (11), 1685. doi:10.3390/polym13111685
- Sehgal, V., and Sami, S. (2021). Management of chronic refractory oesophageal strictures. *Curr. Treat. Options Gastroenterology* 19 (3), 443–458. doi:10.1007/s11938-021-00352-z
- Shaikh, M., Choudhury, N. R., Knott, R., and Garg, S. (2015). Engineering stent based delivery system for esophageal cancer using docetaxel. *Mol. Pharm.* 12 (7), 2305–2317. doi:10.1021/mp500851u
- Shakya, A. K., Al-Sulaibi, M., Naik, R. R., Nsairat, H., Suboh, S., and Abulaila, A. (2023). Review on PLGA polymer based nanoparticles with antimicrobial properties and their application in various medical conditions or infections. *Polymers* 15 (17), 3597. doi:10.3390/polym15173597
- Shuai, C., Yang, W., Feng, P., Peng, S., and Pan, H. (2021). Accelerated degradation of HAP/PLLA bone scaffold by PGA blending facilitates bioactivity and osteoconductivity. *Bioact. Mater.* 6 (2), 490–502. doi:10.1016/j.bioactmat.2020.09.001
- Shuai, C., Zan, J., Qi, F., Wang, G., Liu, Z., Yang, Y., et al. (2019). nMgO-incorporated PLLA bone scaffolds: enhanced crystallinity and neutralized acidic products. *Mater. Des.* 174, 107801. doi:10.1016/j.matdes.2019.107801
- Siersema, P. D. (2008). Treatment options for esophageal strictures. *Nat. Clin. Pract. Gastroenterology Hepatology* 5 (3), 142–152. doi:10.1038/ncpgasthep1053
- Siersema, P. D. (2019). How to approach a patient with refractory or recurrent benign esophageal stricture. *Gastroenterology* 156 (1), 7–10. doi:10.1053/j.gastro.2018.11.040
- Siiki, A., Rinta-Kiikka, I., Sand, J., and Laukkarinen, J. (2017). Endoscopic biodegradable biliary stents in the treatment of benign biliary strictures: first report of clinical use in patients. *Dig. Endosc.* 29 (1), 118–121. doi:10.1111/den.12709
- Sinha, V., Bansal, K., Kaushik, R., Kumria, R., and Trehan, A. (2004). Poly- ϵ -caprolactone microspheres and nanospheres: an overview. *Int. J. Pharm.* 278 (1), 1–23. doi:10.1016/j.ijpharm.2004.01.044
- Smyth, E. C., Lagergren, J., Fitzgerald, R. C., Lordick, F., Shah, M. A., Lagergren, P., et al. (2017). Oesophageal cancer. *Nat. Rev. Dis. Prim.* 3 (1), 17048–17121. doi:10.1038/nrdp.2017.48
- Song, G., Zhao, H. Q., Liu, Q., and Fan, Z. (2022). A review on biodegradable biliary stents: materials and future trends. *Bioact. Mater.* 17, 488–495. doi:10.1016/j.bioactmat.2022.01.017
- Song, H.-Y., Park, S.-I., Do, Y.-S., Yoon, H. K., Sung, K.-B., Sohn, K.-H., et al. (1997). Expandable metallic stent placement in patients with benign esophageal strictures: results of long-term follow-up. *Radiology* 203 (1), 131–136. doi:10.1148/radiology.203.1.9122381
- Stevanović, M., Maksin, T., Petković, J., Filipić, M., and Uskoković, D. (2009). An innovative, quick and convenient labeling method for the investigation of pharmacological behavior and the metabolism of poly (DL-lactide-co-glycolide) nanospheres. *Nanotechnology* 20 (33), 335102. doi:10.1088/0957-4484/20/33/335102
- Stivaros, S., Williams, L., Senger, C., Wilbraham, L., and Laasch, H.-U. (2010). Woven polydioxanone biodegradable stents: a new treatment option for benign and malignant oesophageal strictures. *Eur. Radiol.* 20, 1069–1072. doi:10.1007/s00330-009-1662-5
- Tamai, H., Igaki, K., Kyo, E., Kosuga, K., Kawashima, A., Matsui, S., et al. (2000). Initial and 6-month results of biodegradable poly-L-lactic acid coronary stents in humans. *Circulation* 102 (4), 399–404. doi:10.1161/01.cir.102.4.399
- Tanaka, T., Takahashi, M., Nitta, N., Furukawa, A., Andoh, A., Saito, Y., et al. (2007). Newly developed biodegradable stents for benign gastrointestinal tract stenoses: a preliminary clinical trial. *Digestion* 74 (3–4), 199–205. doi:10.1159/000100504
- Tang, H., Li, S., Zhao, Y., Liu, C., Gu, X., and Fan, Y. (2022). A surface-eroding poly (1, 3-trimethylene carbonate) coating for magnesium based cardiovascular stents with stable drug release and improved corrosion resistance. *Bioact. Mater.* 7, 144–153. doi:10.1016/j.bioactmat.2021.05.045
- Thakur, M., Majid, I., Hussain, S., and Nanda, V. (2021). Poly (ϵ -caprolactone): a potential polymer for biodegradable food packaging applications. *Packag. Technol. Sci.* 34 (8), 449–461. doi:10.1002/pts.2572
- Unal, A. Z., and West, J. L. (2020). Synthetic ECM: bioactive synthetic hydrogels for 3D tissue engineering. *Bioconjugate Chem.* 31 (10), 2253–2271. doi:10.1021/acs.bioconjugchem.0c00270
- Ustürk, S., Altundag, E. M., and Yilmaz, E. (2022). Pullulan/polyHEMA cryogels: synthesis, physicochemical properties, and cell viability. *J. Appl. Polym. Sci.* 139 (12), 51822. doi:10.1002/app.51822
- van Boeckel, P. G., Vleggaar, F. P., and Siersema, P. D. (2011). A comparison of temporary self-expanding plastic and biodegradable stents for refractory benign esophageal strictures. *Clin. Gastroenterology Hepatology* 9 (8), 653–659. doi:10.1016/j.cgh.2011.04.006
- van den Berg, M. W., Walter, D., de Vries, E. M., Vleggaar, F. P., van Berge Henegouwen, M. I., van Hillegersberg, R., et al. (2014). Biodegradable stent placement before neoadjuvant chemoradiotherapy as a bridge to surgery in patients with locally advanced esophageal cancer. *Gastrointest. Endosc.* 80 (5), 908–913. doi:10.1016/j.gie.2014.06.004
- Vandenplas, Y., Hauser, B., Devreker, T., Urbain, D., and Reynaert, H. (2009). A biodegradable esophageal stent in the treatment of a corrosive esophageal stenosis in a child. *J. Pediatr. gastroenterology Nutr.* 49 (2), 254–257. doi:10.1097/mpg.0b013e31819de871
- van Hooft, J. E., van Berge Henegouwen, M. I., Rauws, E. A., Bergman, J. J., Busch, O. R., and Fockens, P. (2011). Endoscopic treatment of benign anastomotic esophagogastric strictures with a biodegradable stent. *Gastrointest. Endosc.* 73 (5), 1043–1047. doi:10.1016/j.gie.2011.01.001
- Verschuur, E. M., Repici, A., Kuipers, E. J., Steyerberg, E. W., and Siersema, P. D. (2008). New design esophageal stents for the palliation of dysphagia from esophageal or gastric cardia cancer: a randomized trial. *Official J. Am. Coll. Gastroenterology ACG* 103 (2), 304–312. doi:10.1111/j.1572-0241.2007.01542.x
- Walter, D., Van Den Berg, M. W., Hirdes, M. M., Vleggaar, F. P., Repici, A., Deprez, P. H., et al. (2018). Dilation or biodegradable stent placement for recurrent benign esophageal strictures: a randomized controlled trial. *Endoscopy* 50 (12), 1146–1155. doi:10.1055/a-0602-4169
- Wang, J., He, Y., Maitz, M. F., Collins, B., Xiong, K., Guo, L., et al. (2013). A surface-eroding poly (1, 3-trimethylene carbonate) coating for fully biodegradable magnesium-based stent applications: toward better biofunction, biodegradation and biocompatibility. *Acta biomater.* 9 (10), 8678–8689. doi:10.1016/j.actbio.2013.02.041
- Wang, L., Jiao, L., Pang, S., Yan, P., Wang, X., and Qiu, T. (2021a). The development of design and manufacture techniques for bioresorbable coronary artery stents. *Micromachines* 12 (8), 990. doi:10.3390/mi12080990
- Wang, S., Zhang, X., Li, J., Liu, C., and Guan, S. (2020). Investigation of Mg–Zn–Y–Nd alloy for potential application of biodegradable esophageal stent material. *Bioact. Mater.* 5 (1), 1–8. doi:10.1016/j.bioactmat.2020.01.002
- Wang, S., Zhu, S.-J., Zhang, X.-Q., Li, J.-A., and Guan, S.-K. (2019). Effects of degradation products of biomedical magnesium alloys on nitric oxide release from vascular endothelial cells. *Med. Gas Res.* 9 (3), 153. doi:10.4103/2045-9912.266991

- Wang, T., Cui, H., Shao, Y., Jiang, H., Dong, Y., and Guo, R. (2021b). Esophageal stent types and clinical applications. *Int. J. Clin. Exp. Med.* 14 (7), 2054–2066.
- Wang, X., Venkatraman, S. S., Boey, F. Y., Loo, J. S., and Tan, L. P. (2006). Controlled release of sirolimus from a multilayered PLGA stent matrix. *Biomaterials* 27 (32), 5588–5595. doi:10.1016/j.biomaterials.2006.07.016
- Wang, Z., Liu, J., Wu, K., Shen, Y., Mao, A., Li, J., et al. (2015). Nitinol stents loaded with a high dose of antitumor 5-fluorouracil or paclitaxel: esophageal tissue responses in a porcine model. *Gastrointest. Endosc.* 82 (1), 153–160. doi:10.1016/j.gie.2015.02.034
- Washington, K. E., Kularatne, R. N., Karmegam, V., Biewer, M. C., and Stefan, M. C. (2017). Recent advances in aliphatic polyesters for drug delivery applications. *Wiley Interdiscip. Rev. Nanomedicine Nanobiotechnology* 9 (4), e1446. doi:10.1002/wnan.1446
- Wong, H. M., Yeung, K. W., Lam, K. O., Tam, V., Chu, P. K., Luk, K. D., et al. (2010). A biodegradable polymer-based coating to control the performance of magnesium alloy orthopaedic implants. *Biomaterials* 31 (8), 2084–2096. doi:10.1016/j.biomaterials.2009.11.111
- Woodruff, M. A., and Hutmacher, D. W. (2010). The return of a forgotten polymer—polycaprolactone in the 21st century. *Prog. Polym. Sci.* 35 (10), 1217–1256. doi:10.1016/j.progpolymsci.2010.04.002
- Wu, Q., Zhu, S., Wang, L., Liu, Q., Yue, G., Wang, J., et al. (2012). The microstructure and properties of cyclic extrusion compression treated Mg–Zn–Y–Nd alloy for vascular stent application. *J. Mech. Behav. Biomed. Mater.* 8, 1–7. doi:10.1016/j.jmbbm.2011.12.011
- Wu, Y., Gao, X., Wu, J., Zhou, T., Nguyen, T. T., and Wang, Y. (2023). Biodegradable polylactic acid and its composites: characteristics, processing, and sustainable applications in sports. *Polymers* 15 (14), 3096. doi:10.3390/polym15143096
- Xu, L., Yu, G., Zhang, E., Pan, F., and Yang, K. (2007). *In vivo* corrosion behavior of Mg–Mn–Zn alloy for bone implant application. *J. Biomed. Mater. Res.* 83 (3), 703–711. doi:10.1002/jbm.a.31273
- Yang, K., Cao, J., Yuan, T.-W., Zhu, Y.-Q., Zhou, B., and Cheng, Y.-S. (2019). Silicone-covered biodegradable magnesium stent for treating benign esophageal stricture in a rabbit model. *World J. Gastroenterology* 25 (25), 3207–3217. doi:10.3748/wjg.v25.i25.3207
- Yang, K., Ling, C., Yuan, T., Zhu, Y., Cheng, Y., and Cui, W. (2016). Polymeric biodegradable stent insertion in the esophagus. *Polymers* 8 (5), 158. doi:10.3390/polym8050158
- Yang, L., Li, J., Meng, S., Jin, Y., Zhang, J., Li, M., et al. (2014). The *in vitro* and *in vivo* degradation behavior of poly (trimethylene carbonate-co-ε-caprolactone) implants. *Polymer* 55 (20), 5111–5124. doi:10.1016/j.polymer.2014.08.027
- Yang, L., Li, J., Zhang, W., Jin, Y., Zhang, J., Liu, Y., et al. (2015). The degradation of poly (trimethylene carbonate) implants: the role of molecular weight and enzymes. *Polym. Degrad. Stab.* 122, 77–87. doi:10.1016/j.polymdegradstab.2015.10.016
- Yano, T., Yoda, Y., Nomura, S., Toyosaki, K., Hasegawa, H., Ono, H., et al. (2017). Prospective trial of biodegradable stents for refractory benign esophageal strictures after curative treatment of esophageal cancer. *Gastrointest. Endosc.* 86 (3), 492–499. doi:10.1016/j.gie.2017.01.011
- Yano, T., Yoda, Y., Nonaka, S., Abe, S., Kawata, N., Yoshio, T., et al. (2022). Pivotal trial of a biodegradable stent for patients with refractory benign esophageal stricture. *Esophagus* 19 (3), 516–524. doi:10.1007/s10388-022-00909-6
- Yin, T., Du, R., Wang, Y., Huang, J., Ge, S., Huang, Y., et al. (2022). Two-stage degradation and novel functional endothelium characteristics of a 3-D printed bioresorbable scaffold. *Bioact. Mater.* 10, 378–396. doi:10.1016/j.bioactmat.2021.08.020
- Yuan, T., Yu, J., Cao, J., Gao, F., Zhu, Y., Cheng, Y., et al. (2016). Fabrication of a delaying biodegradable magnesium alloy-based esophageal stent via coating elastic polymer. *Materials* 9 (5), 384. doi:10.3390/ma9050384
- Yue, Y., Wang, L., Yang, N., Huang, J., Lei, L., Ye, H., et al. (2015). Effectiveness of biodegradable magnesium alloy stents in coronary artery and femoral artery. *J. Interventional Cardiol.* 28 (4), 358–364. doi:10.1111/joic.12217
- Yusoff, N. H., Pal, K., Narayanan, T., and de Souza, F. G. (2021). Recent trends on bioplastics synthesis and characterizations: polylactic acid (PLA) incorporated with tapioca starch for packaging applications. *J. Mol. Struct.* 1232, 129954. doi:10.1016/j.molstruc.2021.129954
- Zein, N. N., Greseth, J. M., and Perrault, J. (1995). Endoscopic intralesional steroid injections in the management of refractory esophageal strictures. *Gastrointest. Endosc.* 41 (6), 596–598. doi:10.1016/s0016-5107(95)70198-2
- Zhang, E., Yang, L., Xu, J., and Chen, H. (2010). Microstructure, mechanical properties and bio-corrosion properties of Mg–Si (–Ca, Zn) alloy for biomedical application. *Acta biomater.* 6 (5), 1756–1762. doi:10.1016/j.actbio.2009.11.024
- Zhang, L., Zuo, X., Li, S., Sun, M., Xie, H., Zhang, K., et al. (2019). Synergistic therapy of magnetism-responsive hydrogel for soft tissue injuries. *Bioact. Mater.* 4, 160–166. doi:10.1016/j.bioactmat.2019.03.002
- Zhang, W., Chen, Y., Chen, M., Zhao, S., Mao, J., Qu, A., et al. (2016). Strengthened corrosion control of poly (lactic acid)(PLA) and poly (ε-caprolactone)(PCL) polymer-coated magnesium by imbedded hydrophobic stearic acid (SA) thin layer. *Corros. Sci.* 112, 327–337. doi:10.1016/j.corsci.2016.07.027
- Zhang, Y. S., and Khademhosseini, A. (2017). Advances in engineering hydrogels. *Science* 356 (6337), eaaf3627. doi:10.1126/science.aaf3627
- Zhang, Z.-Q., Yang, Y.-X., Li, J.-A., Zeng, R.-C., and Guan, S.-K. (2021). Advances in coatings on magnesium alloys for cardiovascular stents—a review. *Bioact. Mater.* 6 (12), 4729–4757. doi:10.1016/j.bioactmat.2021.04.044
- Zhao, J., Mo, Z., Guo, F., Shi, D., Han, Q. Q., and Liu, Q. (2018). Drug loaded nanoparticle coating on totally bioresorbable PLLA stents to prevent in-stent restenosis. *J. Biomed. Mater. Res. Part B Appl. Biomaterials* 106 (1), 88–95. doi:10.1002/jbm.b.33794
- Zhou, L., Ke, K., Yang, M.-B., and Yang, W. (2021). Recent progress on chemical modification of cellulose for high mechanical-performance Poly (lactic acid)/Cellulose composite: a review. *Compos. Commun.* 23, 100548. doi:10.1016/j.coco.2020.100548
- Zhu, X., and Braatz, R. D. (2015). A mechanistic model for drug release in PLGA biodegradable stent coatings coupled with polymer degradation and erosion. *J. Biomed. Mater. Res. Part A* 103 (7), 2269–2279. doi:10.1002/jbm.a.35357
- Zhu, Y., Cui, W., Cheng, Y., Chang, J., Chen, N., and Yan, L. (2013a). Evaluation of biodegradable paclitaxel-eluting nanofibre-covered metal stents for the treatment of benign cardia stricture in an experimental model. *J. Br. Surg.* 100 (6), 784–793. doi:10.1002/bjs.9106
- Zhu, Y., Hu, C., Li, B., Yang, H., Cheng, Y., and Cui, W. (2013b). A highly flexible paclitaxel-loaded poly (ε-caprolactone) electrospun fibrous-membrane-covered stent for benign cardia stricture. *Acta biomater.* 9 (9), 8328–8336. doi:10.1016/j.actbio.2013.06.004
- Zhu, Y.-Q., Edmonds, L., Wei, L.-M., Zheng, R.-L., Cheng, R.-Y., Cui, W.-G., et al. (2017). Technical feasibility and tissue reaction after silicone-covered biodegradable magnesium stent insertion in the oesophagus: a primary study *in vitro* and *in vivo*. *Eur. Radiol.* 27, 2546–2553. doi:10.1007/s00330-016-4602-1



OPEN ACCESS

EDITED BY

Yang Yao,
ETH Zürich, Switzerland

REVIEWED BY

Qiang Ao,
China Medical University, China
Yixiu Liu,
Central Hospital Affiliated to Shenyang
Medical College, China
Xing Zhang,
Chinese Academy of Sciences (CAS),
China

*CORRESPONDENCE

Xin-an Zhang,
✉ zhangxa2725@163.com
Mingjie Hu,
✉ hmj811119@163.com

RECEIVED 08 September 2023

ACCEPTED 28 November 2023

PUBLISHED 07 December 2023

CITATION

Wang G, Zhang X-a, Kapilevich L and
Hu M (2023), Recent advances in
polymeric microparticle-based drug
delivery systems for knee
osteoarthritis treatment.
Front. Bioeng. Biotechnol. 11:1290870.
doi: 10.3389/fbioe.2023.1290870

COPYRIGHT

© 2023 Wang, Zhang, Kapilevich and Hu.
This is an open-access article distributed
under the terms of the [Creative
Commons Attribution License \(CC BY\)](#).
The use, distribution or reproduction in
other forums is permitted, provided the
original author(s) and the copyright
owner(s) are credited and that the original
publication in this journal is cited, in
accordance with accepted academic
practice. No use, distribution or
reproduction is permitted which does not
comply with these terms.

Recent advances in polymeric microparticle-based drug delivery systems for knee osteoarthritis treatment

Guangxin Wang¹, Xin-an Zhang^{2*}, Leonid Kapilevich³ and
Mingjie Hu^{2*}

¹Department of Orthopedics, The Fourth People's Hospital of Shenyang, Shenyang, China, ²College of Exercise and Health, Shenyang Sport University, Shenyang, China, ³Faculty of Physical Education, National Research Tomsk State University, Tomsk, Russia

Due to the poor bioavailability and high joint clearance of drugs, sustained delivery of therapeutic agents has proven difficult in the treatment of osteoarthritis (OA). Intra-articular (IA) drug delivery strategy is an attractive option for enhancing OA patients' prognosis, for which various polymer materials have been used as drug carriers due to their attractive delivery properties, to slow or even reverse the progress of OA by prolonging the duration of therapeutic agent residence in the joint. This article focuses on the recent developments in natural and synthetic polymer-based microsphere drug delivery systems for treating knee osteoarthritis. It evaluates the translational potential of some novel formulations for clinical application.

KEYWORDS

knee osteoarthritis, drug delivery systems, intra-articular, microparticles, biodegradable polymers

1 Introduction

Osteoarthritis (OA) is the most common degenerative disease of the joints and is characterized by cartilage degeneration and bone hyperplasia, and is emerging as a major cause of chronic disability (He et al., 2017; Cucchiari and Madry, 2019), influencing over 300 million individuals globally (Boer et al., 2021). Although OA may be genetic, there are many risk factors associated with its development; among them, aging, gender, and obesity are the direct influences (Ondresik et al., 2017), and aging is a major risk factor for the OA progression, which impacts both the mechanical and biochemical changes within tissue's structure (Bellamy et al., 1997; Bas et al., 2018; Berenbaum et al., 2018; Peters et al., 2018); and female cartilage is thinner, leading to greater cartilage wear and tear, and there are larger differences in the mechanical alignment (Blanco and Rego-Pérez, 2018), they are more susceptible to OA than men; Obesity can limit physical activity and lead to muscle weakness, which can also greatly increase the prevalence of OA; in addition, excessive mechanical load, strenuous physical activity, and insufficient nutritional supply are also several important factors that lead to joint degeneration (Bajpayee and Grodzinsky, 2017; Abbas et al., 2018; Ahmad et al., 2019; Jain & Ravikumar, 2020).

Knee osteoarthritis (KOA) is a chronic joint disease involving the entire knee joint (Johnson and Hunter, 2014; Glyn-Jones et al., 2015; Park et al., 2021), and is common in middle-aged and elderly adults (Jamshidi et al., 2019; Sharma, 2021). The prevalence of KOA has more than doubled in the last decade (Palazzo et al., 2016; Kyu et al., 2018), accounting

for about 85% of all OA cases worldwide (Vos et al., 2016; James et al., 2018), making it an increasingly important public health challenge in the coming decades.

KOA is characterised by dysfunction of the knee joint and persistent pain. It is caused by joint deformation and destruction (Eitner et al., 2017). Gradual cartilage erosion stimulates chondrocytes to enhance anabolism via compensatory hypertrophy (Goldring and Goldring, 2016), which generates both degradation products and pro-inflammatory factors to expedite KOA development (Hunter and Bierma-Zeinstra, 2019). Therefore, early treatment after the disease is advocated to reduce the inflammatory response and delay the joints degeneration (Fan et al., 2018; Törmälehto et al., 2018). The articular cartilage of KOA patients usually degenerates gradually. The degenerated cartilage becomes worn and rough (Lane and Corr, 2017), resulting in symptoms like muscle weakness, pain and stiffness in the knee joint, which in the long run can lead to reduced physical activity, decreased physical function, sleep disturbance, fatigue, depression, and even disability.

Currently, the diagnosis of OA is usually made by X-ray imaging, MRI, or joint fluid analysis after the patient's medical history and physical examination (Braun and Gold, 2012; Demehri et al., 2016). Osteoarthritis cannot be cured entirely at present, and most treatment options rely solely on symptomatic interventions, with a particular focus on relieving pain and enhancing physical function. The treatment depends largely on the severity of OA and the patient's degree of pain, and there are no disease-relieving therapies to stabilize or reverse the progression of OA. The first choice is the treatment of symptomatic pain, with analgesics, specific cyclooxygenase-2 (COX-2) inhibitors, non-steroidal anti-inflammatory drugs (NSAIDs), and opioids commonly used for systemic treatment (Block et al., 2010; Bowman et al., 2018; da Costa et al., 2017; Lane, 1997; Leopoldino et al., 1996). However, many traditional medicines have significant risk profiles. They may cause gut, heart, or brain side-effects. As OA treatments evolve, intra-articular (IA) injections have become an option alongside oral and local treatments (Nelson et al., 2014). In contrast, IA can effectively avoid systemic toxicities (Nguyen and Rannou, 2017) and improve the drug bioavailability, thus reducing the cost of treatment. Also, IA is the last option before hip or knee replacement surgery.

Nevertheless, intra-articular injection remains an invasive therapy, and the quick elimination of small-molecule drugs in the joint is one of the main limitations of the current clinical methods for the treatment of osteoarthritis. This means that most drugs remain in the joint for only several hours after injection before being rapidly eliminated because of the joint's unique physiological environment (Owen et al., 1994; Schumacher, 2003; Gerwin et al., 2006; Chevalier et al., 2009; Vugmeyster et al., 2012). As a result, repeated intra-articular injections are necessary, which will greatly reduce patient adherence and increase the risk of infection (Lin et al., 2004). In addition, IA only relieves inflammatory symptoms to slow the disease's advancement, but reversing the disease course to successfully treat OA is difficult.

Therefore, ensuring continuous and effective drug delivery to joint targets remains a major challenge (Evans et al., 2014), and advanced drug delivery strategies hold promise for improving OA patient outcomes by prolonging the release cycle of medicinal substances in the knee joint. The encapsulation of drugs in polymeric drug delivery systems (DDSs) for controlled release is the fundamental principle of this strategy. The goal is the direct

delivery of the therapeutic agent to the targeted tissue to increase the drug concentration in the affected area, thereby reducing the dosage necessary to produce the desired therapeutic result. To prolong drug residence time in joints, reduce dosing frequency and side effects, researchers have worked to develop DDSs with sustained release effects (Zhang et al., 2018; Kou et al., 2019; Xue et al., 2021).

Among them, the microsphere delivery systems may provide a potential way to improve the co-retention of small molecule drugs. Polymeric microspheres range in size from approximately 1–100 μm (Bhaskar et al., 2010; He and Park, 2016). Microspheres can generally be prepared from natural or synthetic polymers acting as matrices. In this review, we outline current developments in knee intra-articular drug delivery systems in recent years and evaluate the application prospects of microscale DDSs based on different carrier matrices for KOA therapy.

2 Application of polymeric microparticles (MPs) in knee osteoarthritis treatment

2.1 Natural polymeric microparticle-based drug delivery systems

Chitosan (CS) is a natural polymer material with biodegradability, biocompatibility, and mucoadhesion. It can be used as an excellent drug carrier material. Microspheres prepared from chitosan can improve drug stability, enhance efficacy, and minimize systemic adverse effects. Zhu et al. (2015) explored the Rac1's function and mechanistic pathways in OA chondrocyte pathology and OA development. They developed a potential OA therapeutic strategy using polymers to encapsulate and release Rac1 inhibitors to modulate its activity. Specifically, the anterior cruciate ligament transection was used to create a mice OA model, and CS microspheres encapsulated with the Rac1 inhibitor NSC23766 were encapsulated within hyaluronic acid (HA). Then, the OA knee joint received an injection of the mixed system. The results demonstrated that the drug-loaded microsphere system was able to release the inhibitor continuously while lubricating the joints (Figure 1). To reduce the side effects associated with long-term oral administration of lornoxicam in KOA patients, Abd-Allah group prepared CS microspheres coated with clonoxicam based on ionotropic-gelation technique with tripolyphosphate acting as a crosslinker. Compared with lornoxicam solution, drug-loaded microspheres showed long-term *in vivo* anti-inflammatory effects in the monosodium iodoacetate (MIA)-induced rat osteoarthritis model, significantly reducing the histology, inflammation, and biochemical parameters (Abd-Allah et al., 2016). Subsequently, Zhang et al. (2020) found that YAP (Yes-associated protein), a co-transcriptional factor, may be a mechanistic mediator of extracellular matrix stiffness and a therapeutic target of osteoarthritis. The results demonstrated that chitosan microspheres loaded with a selective inhibitor of YAP can target activity of subcellular YAP and slow down OA progression. These findings may provide additional information regarding their application in the future OA transformation (Figure 2).

A class of injectable and hydrolytically degradable heparin-based delivery systems has also been prepared for the delivery of

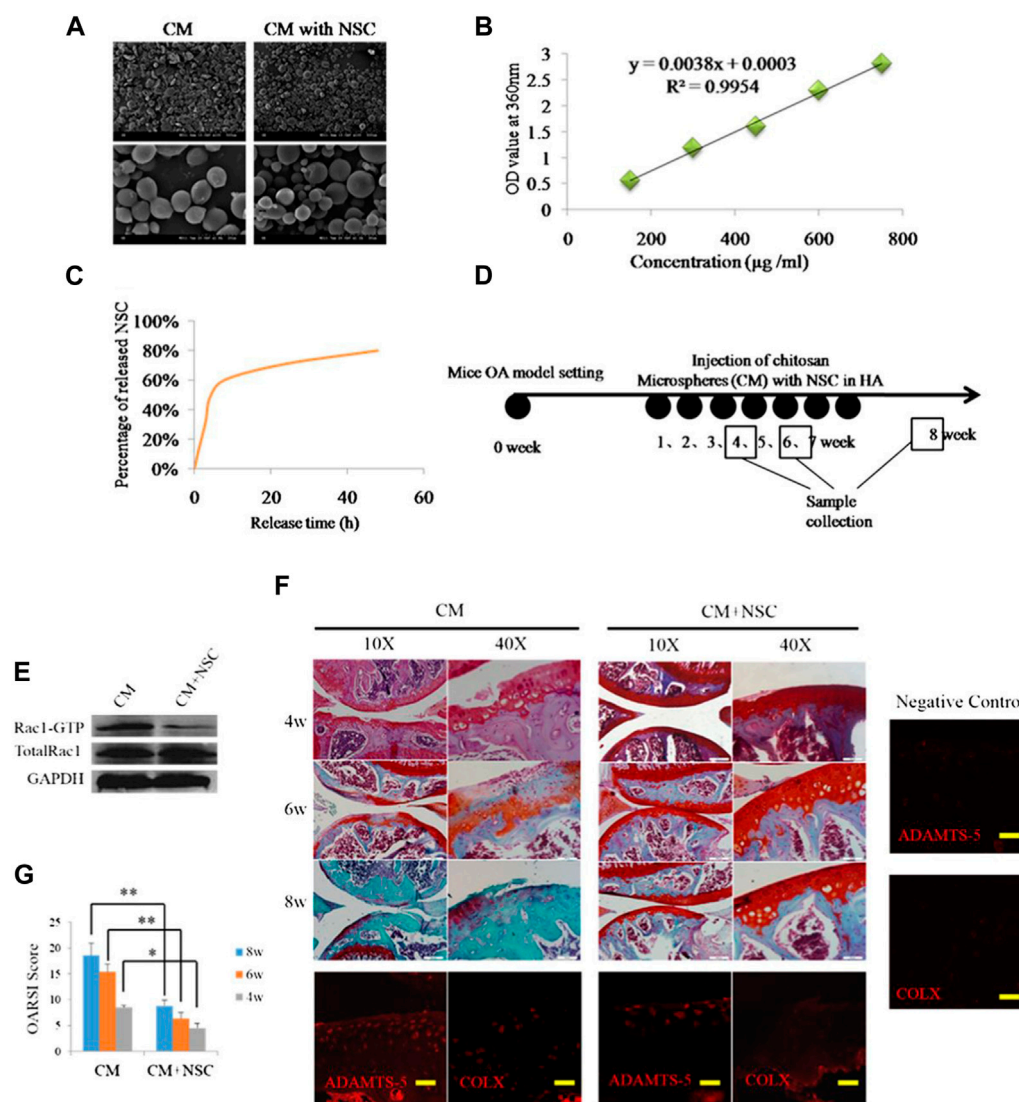


FIGURE 1

(A) SEM images of CS microspheres. (B) Standard curve of NSC23766. (C) Release curve of CS microspheres. (D) Animal study schedule. (E) The inhibitory effect of release of NSC23766 on Rac1 activity in chondrocytes. (F) Results of safranin staining and gene expression. (G) OARSI scoring of OA severity following treatment with HA containing NSC23766 loaded CS microspheres. Reproduced with permission from ref (Zhu et al., 2015). CC BY-NC 3.0. Copyright 2015 The Author(s).

tumor necrosis factor- α -stimulated gene 6 (TSG-6) to slow the progression of OA. Heparin is a highly-sulphated natural polysaccharide. It can be used as a biomaterial carrier to bind to various positively charged proteins. TSG-6 is a protein known as an inhibitor of plasmin, and plasmin degrades the extracellular matrix in OA joints. Moreover, research has demonstrated that heparin sulfation is a crucial regulator of the antiplasmin bioactivity of TSG-6. Animal experiments also verified that the MPs prepared in this study are expected to be effective for TSG-6 delivery in OA treatment. Analysis after 21 days shows that MPs loaded with TSG-6 reduce the damage to the cartilage after medial meniscal transection (MMT) (Tellier et al., 2018).

Gelatin is widely used in drug delivery systems because it has high biocompatibility, biodegradability, does not produce other by-products after degradation in the body, is non-immunogenic, and has the same components and biological properties as collagen.

Park's group has loaded anti-inflammatory cytokines in gelatin microspheres through ion complexation and chelation. Since proteolytic enzymes expressed in arthritis attacks can specifically degrade gelatin, the as-prepared bioactive gelatin microspheres can achieve targeted release of anti-inflammatory cytokines in joints with OA. The experimental results showed that gelatin microspheres could significantly reduce chondrocyte inflammation (up to 80%). Thus, this catabolic response-synchronized on-demand delivery system is universally applicable for wound healing applications, especially in preventing OA inflammation-mediated cartilage damage (Park et al., 2020). Ratanavaraporn et al. combined gelatin with silk fibroin to develop composite drug-loaded microspheres loaded with curcumin, also induced by MIA, to create a rat OA injury model. After 8 weeks of minimally invasive injection treatment of drug-loaded microspheres, the cell destruction in the joint and synovial tissues was effectively delayed,

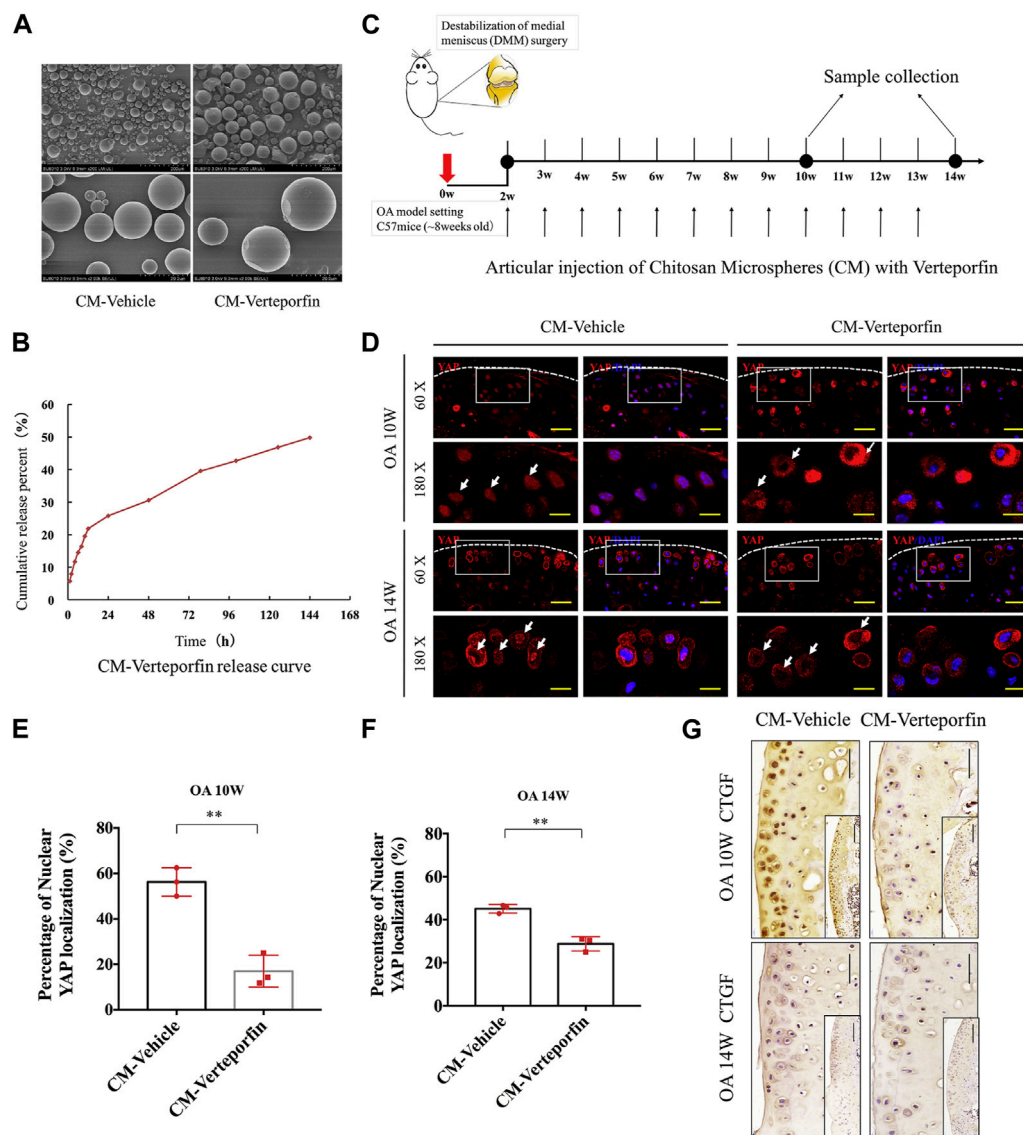


FIGURE 2

(A) Microscopic morphology of chitosan microspheres (CM) and verteporfin-loaded CM. (B) *In vitro* release results of CMs loaded with verteporfin. (C) Schematic of DDS used to treat OA model of mice. (D) Immunofluorescence images of articular cartilage sections of OA mice in each experimental group. (E, F) Percentage of nuclear YAP localization in the treated groups at various times following surgery. (G) Immunohistochemical results in cartilage sections of OA mice at various times following surgery. Reproduced with permission from ref (Zhang et al., 2020). Copyright 2020 Elsevier Ltd.

and the radiological and histological grading of articular cartilage damage and synovial tissue alterations in experimental animals were similar to those in normal rats. The incorporation of silk fibroin effectively reduced the degradation rate of the microsphere matrix, and curcumin was able to achieve a longer sustained release in the joints and showed a prolonged anti-inflammatory effect (Ratanavaraporn et al., 2017).

2.2 Synthetic polymeric microparticle-based drug delivery systems

Poly(lactic-co-glycolic acid) (PLGA), as the most commonly utilized synthetic polymer for developing drug-delivery

microsystems, is biocompatibility, biodegradability, non-toxicity, and non-immunogenicity, and most importantly, the material has adjustable mechanical and degradation properties and has FDA approval for human use. Many researchers have prepared various PLGA drug-loaded microparticles for OA treatment, and some microparticle formulations have entered the stage of clinical studies.

Gómez-Gaete's group prepared MPs loaded with rhein with anti-inflammatory properties by emulsion-solvent evaporation technique to improve the bioavailability of rhein and its utility in OA therapy. The morphology, encapsulation efficiency, and release behavior of drug-loaded MPs were investigated in a preliminary study, in addition to the evaluation of the *in vitro* cytotoxicity of the formulation (Gómez-Gaete et al., 2017). More recently, the safety of sterilization procedures for microparticle formulations before use

has been systematically investigated. The results showed that the sterilization process did not have any major impact on the relevant properties of the microspheres loaded with drugs and no change in the *in vitro* release curve. In conclusion, gamma radiation is a suitable sterilization method, and intra-articular delivery of microparticle formulations also offers a promising therapeutic option for patients suffering from chronic joint disease (Avendaño-Godoy et al., 2023). Dhanabalan et al. (Dhanabalan et al., 2020; Dhanabalan et al., 2023) also developed MPs encapsulating rapamycin using PLGA as a carrier. The microsphere preparation is non-toxic and biocompatible and can achieve the sustained-release of rapamycin over several weeks. The MPs can effectively induce autophagy, prevent cellular senescence in human chondrocytes, and reduce inflammatory markers. Moreover, rapamycin MPs treatment maintained sulphated glycosaminoglycan (sGAG) production in 3D cultures under genotoxicity and oxidative stress conditions. This biomaterial-based rapamycin delivery system is expected to be further clinically translated as a therapeutic approach that meets patient requirements and provides new insight into aging prevention and autophagy activation therapies for treating trauma-induced OA via sustained-release formulations (Figure 3).

OA can also be managed with IA injections of steroid drugs examples include triamcinolone acetonide and dexamethasone for short-term pain relief. Bodick's group (Bodick et al., 2018) developed a PLGA microsphere preparation coated with triamcinolone acetonide (TA), and IA injection of microspheres in experimental dogs can significantly prolong the release period of TA and cause mild foreign body reaction (FBR). Stefani et al. (2020) prepared a class of PLGA microsphere-agarose implants embedded with dexamethasone (DEX), which can continuously deliver low doses of DEX into the joint for at least 99 days. Chondroprotection observed *in vitro* in the context of IL-1-induced degradation and enhanced functional outcomes *in vivo*, and be able to optimize the IA delivery strategy of DEX to improve cartilage graft survival and functionality. Francesco's research group (Di Francesco et al., 2021) developed a microscale PLGA plate loaded with dexamethasone. Microplates (μ PLs) have tunable geometry and mechanical properties and can be deposited in joints for sustained release of DEX. Anti-inflammatory molecules were continuously released over 1 month in a biologically relevant confined volume and were detected to reduce the expression of inflammatory gene. Following administration of drug-laden μ PLs to a mice model of knee overload injury (posttraumatic osteoarthritis, PTOA), a significant reduction in load-induced histological changes was observed. This innovative study also provides the proof-of-concept for the role of Shape-Defined μ PLs in preventing joint degeneration associated with PTOA (Figure 4). Liang et al. (2021) also developed a novel PLGA-based microsphere formulation by oil-in-water emulsion and solvent evaporation method, which was loaded with mometasone furoate and was capable of stable, sustained release for more than 1 month. The release of the preparation in PBS was affected by the erosion of PLGA and proceeded by a non-Fick diffusion mechanism. The relevant research results demonstrated the long-term effectiveness and good biosecurity of the preparation. Hence, the delivery system has considerable application potential in the field of treatment of knee arthritis.

Flavopiridol is capable of making progress in the treatment of PTOA by inhibiting cyclin-dependent kinase 9 (CDK9). For prolongation of Flavopiridol retention time in joints, Sangsuwan et al. (2022) prepared corresponding microsphere preparations by encapsulating Flavopiridol with PLGA microparticles as a strategy to reduce PTOA-related inflammation by inhibiting CDK9. The characterization results of drug-loaded microparticles showed that the microspheres had good injectability, low phagocytic potential, and cytotoxic potential and could maintain drug activity in a high-temperature environment. Flavopiridol microparticles subsequently exhibited the expected slow-release behavior in the PTOA rat knee injury model. The joint inflammation index (matrix metalloproteinase, MMP) was significantly reduced after 3 days of injection, and the drug-loaded microparticles could reduce the severity of PTOA after 28 days of injury. Thus, the drug-loaded microparticle formulation developed in this study was verified as a promising biomaterial platform as a potential therapeutic option for PTOA (Figure 5). Platelet lysate is a bioactive substance released from platelets and has a variety of biological functions. It contains various cell growth factors, cytokines, and many proteins required for cell proliferation. Li et al. (2021) as well prepared chitosan/gelatin/PLGA three-phase hybrid microspheres loaded with superactive platelet lysate (sPL) for the prevention and treatment of OA. The sPL-loaded microparticle formulation markedly increased proliferation of chondrocyte, reduced cell necrosis, and resulted in a smooth cartilage surface when administered to animal models while increasing cartilage integrity. This biofactor delivery platform has the potential for efficient and non-invasive repair of articular cartilage in OA (Figure 6).

Further, Bodick's group conducted a series of preclinical studies on the PLGA microsphere preparation (FX006) loaded with TA based on previous studies to evaluate its clinical transformation potential. First, the team recruited 81 KOA patients intending to compare the pharmacokinetics of IA injections of TA sustained-release microsphere formulation (FX006) with that of crystalline suspension (TAcS) at the diseased joints of the patients. The results of the clinical research showed that a single FX006 injection significantly prolonged TA retention time in the joint and reduced peak plasma levels, thereby attenuating the systemic toxic effects of TA in humans (Kraus et al., 2018). This was followed by a preclinical study of the analgesic effects of different doses of FX006, which showed that FX006 provided long-term symptomatic relief, that 32 mg FX006 provided a higher therapeutic benefit, and that the preparation's good safety profile was initially confirmed (Conaghan et al., 2018a). The symptom benefit and biosafety of FX006 were subsequently evaluated compared with saline placebo and TAcS. Compared to saline placebo, FX006 afforded significant and clinically meaningful pain relief in the primary endpoint. However, the improvement in osteoarthritis pain was insignificant with FX006 compared with TAcS (Conaghan et al., 2018b). About 30% of patients with type II diabetes suffer from KOA. Because of the glucose-raising effect of steroids, Bodick's team recently carried out another clinical randomized, double-blind study to investigate the changes in blood glucose levels of patients after IA injection of FX006 and TAcS. The trial results indicated that IA injection of FX006 could be administered with minimal interference with glycemic control in patients with OA and type II diabetes (Russell et al., 2018). The above-mentioned series of preclinical research results also show that the FX006 preparation has good potential for clinical application in treating KOA.

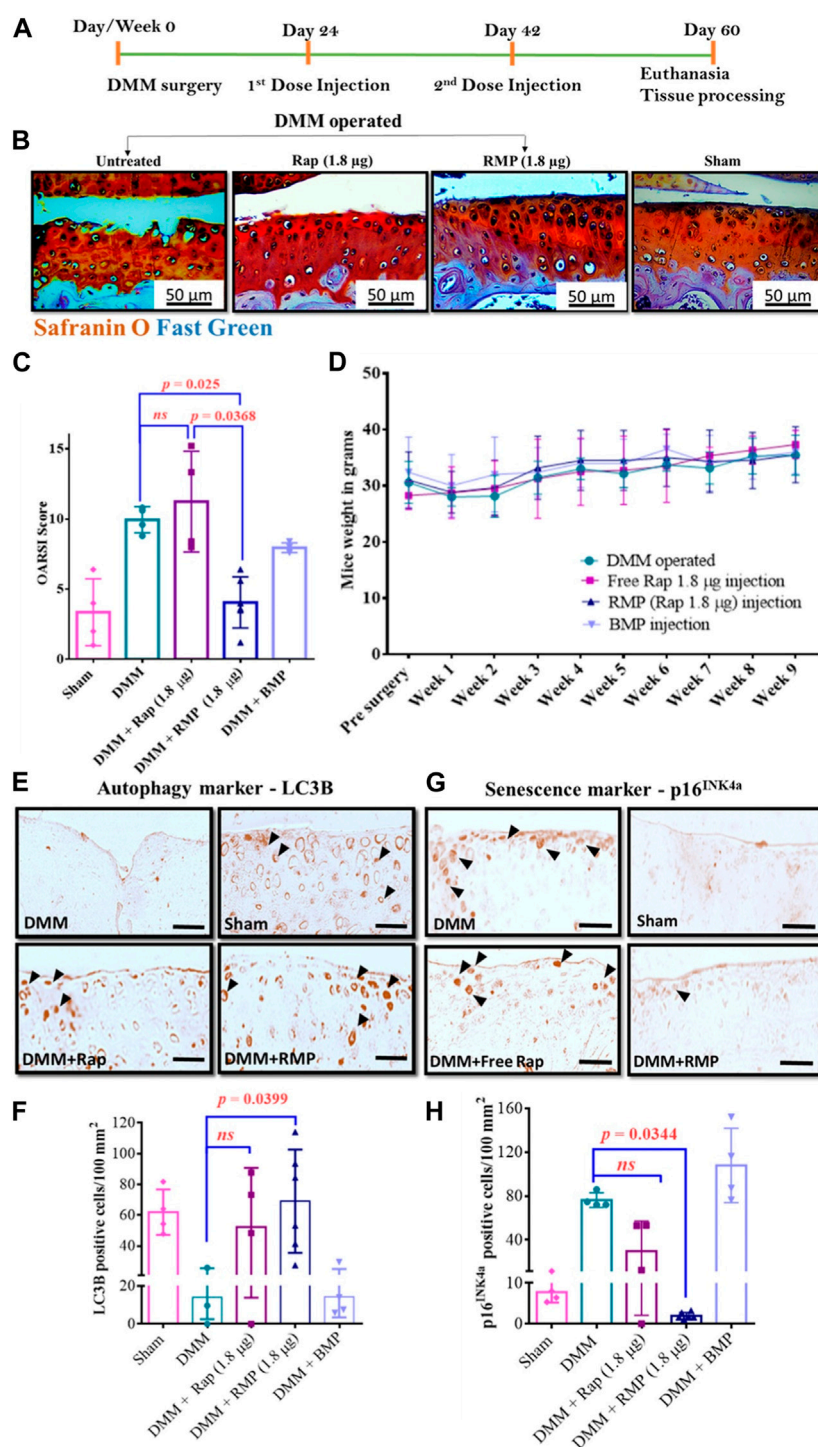


FIGURE 3

(A) Diagram illustrating the course of treatment. (B) Representative images of the mice knee joints' medial tibial plateau (MTP) from various groups. (C) Results of OARSI scoring in mouse. (D) Changes in mice body weight over time following different treatments. Representative LC3B IHC-staining images (E) and number of LC3B-positive cells per unit area (F). Representative p16^{INK4a} IHC-staining images (G) and number of p16^{INK4a}-positive cells per unit area (H). Reproduced with permission from ref (Dhanabalan et al., 2023). CC BY 4.0. Copyright 2023 The Author(s).

In addition, a number of researchers have selected other types of synthetic polymers as delivery matrix platforms. Ho et al. (2019) used spray-drying technology to incorporate triamcinolone acetonide microcrystals into PLGA/PLA polymer microspheres (MSs). The proposed drug-loaded MSs can extend the period of

drug retention in the rat joints while loading the systemic exposure of TA is significantly reduced (<50%). MSs also have excellent physicochemical stability, and the drug crystallinity and release profile do not change within 1 year. Similarly, polymeric particles coated with ketorolac were recently developed by Wongrakpanich

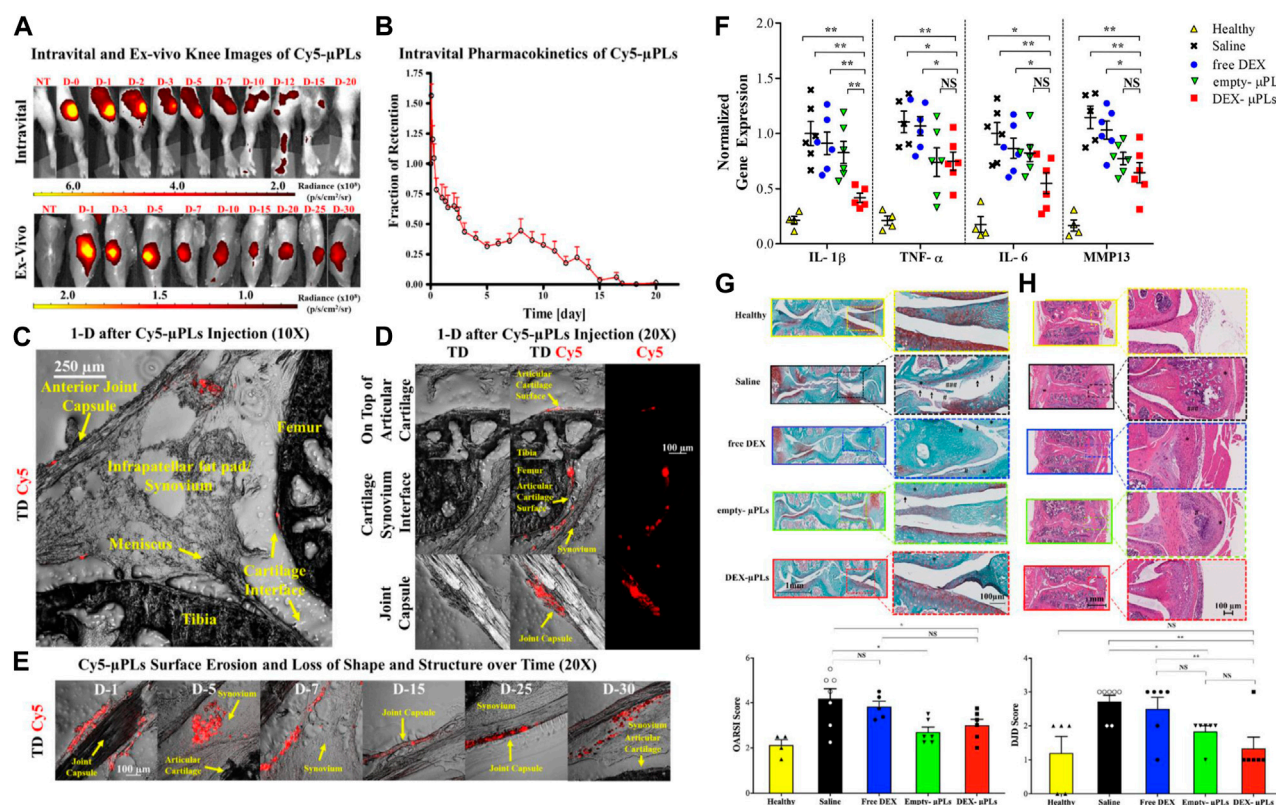


FIGURE 4

(A) Representative intravital images and ex vivo images of the knee joints of PTOA mouse injected with Cy5-μPLs. (B) *In vivo* retention fraction of Cy5-μPLs. (C) Anatomically labeled sagittal sections of mouse knee joint. (D) Distribution of Cy5-μPLs. (E) Imaging of Cy5-μPLs distribution after injection into the knee joint at various times. (F) Expression results of related cytokines. (G) Representative safranin-O stained images of tibial and femoral articular surfaces. (H) Representative H&E staining images of PTOA joints. Reproduced with permission from ref (Di Francesco et al., 2021). CC BY 4.0. Copyright 2021 The Author(s).

et al. (2023) for treating OA using PLGA/PLA and their mixtures as carrier materials. A matrix composed of two homopolymers is more convenient to provide tailored drug release kinetics and improved physicochemical properties. As an alternative for OA patients, the drug-loaded microparticles can improve patient compliance and reduce treatment costs. Another research team prepared PLGA/PCL microspheres by solvent emulsification and evaporation method for prolonging the release of aceclofenac through parenteral administration. *In vivo* research findings demonstrated that the microspheres showed significant anti-inflammatory activity and were also promising in OA treatment (Kaur et al., 2017).

Abou-ElNour et al. (2019) copolymerized polyδ-decalactone (PDL) with methoxy poly(ethylene glycol) (mPEG) to form PEG-PDL with different molecular weights and subsequently co-blended with poly(propylene glycol) (PLA) to prepare novel composite particles loaded with triamcinolone acetonide. Afterward, the drug-loaded microparticles were administered to the rat knee osteoarthritis model. Compared with the drug suspension, the retention time of triamcinolone acetonide in the joint was longer, resulting in a more pronounced inhibition of inflammation. Sandker's team developed a biodegradable microsphere formulation that can continuously deliver the anti-inflammatory drug tacrolimus into the joint based on the P(DLLA-PEG)-b-PLA multi-block copolymer. It is easy to adjust the release kinetics of the

formulation by changing the ratio of hydrophilic and hydrophobic blocks. The drug can be released in the joint continuously for more than 1 month without causing systemic effects, and the excellent biocompatibility and local anti-inflammatory effect of the microsphere formulation were confirmed (Sandker et al., 2018).

Polyester amide (PEA) is a polymer based on aliphatic dicarboxylic acids, α-amino acids, and aliphatic α-ω diols (Castaldo et al., 1992). The presence of amino acid components in the structure makes it easy to be enzymatically broken down by proteolytic enzymes. Serine proteases exist in synovial fluid and are key components of the inflammatory response, which makes it possible for PEA-based DDSs to complete the bioreactive release of drugs along with the process of tissue inflammation (Nakano et al., 1999; Sharony et al., 2010). In recent years, Woike's research group has developed a PEA-based polymer microsphere platform to load various therapeutic agents to expand the therapeutic options for KOA. In one of the studies, the group loaded celecoxib inside PEA microspheres to develop a safe DDS with self-regulating behavior. It has been verified that the degradation rate of PEA microspheres is higher in the inflammatory environment, while the celecoxib-loaded microspheres can significantly reduce the degradation rate of PEA, which indicates that the DDS does have autoregulatory behavior (Janssen et al., 2016). Subsequently, the effect of celecoxib polyester amide microspheres on disease relief and the optimal dose was further investigated in the rat OA model. No

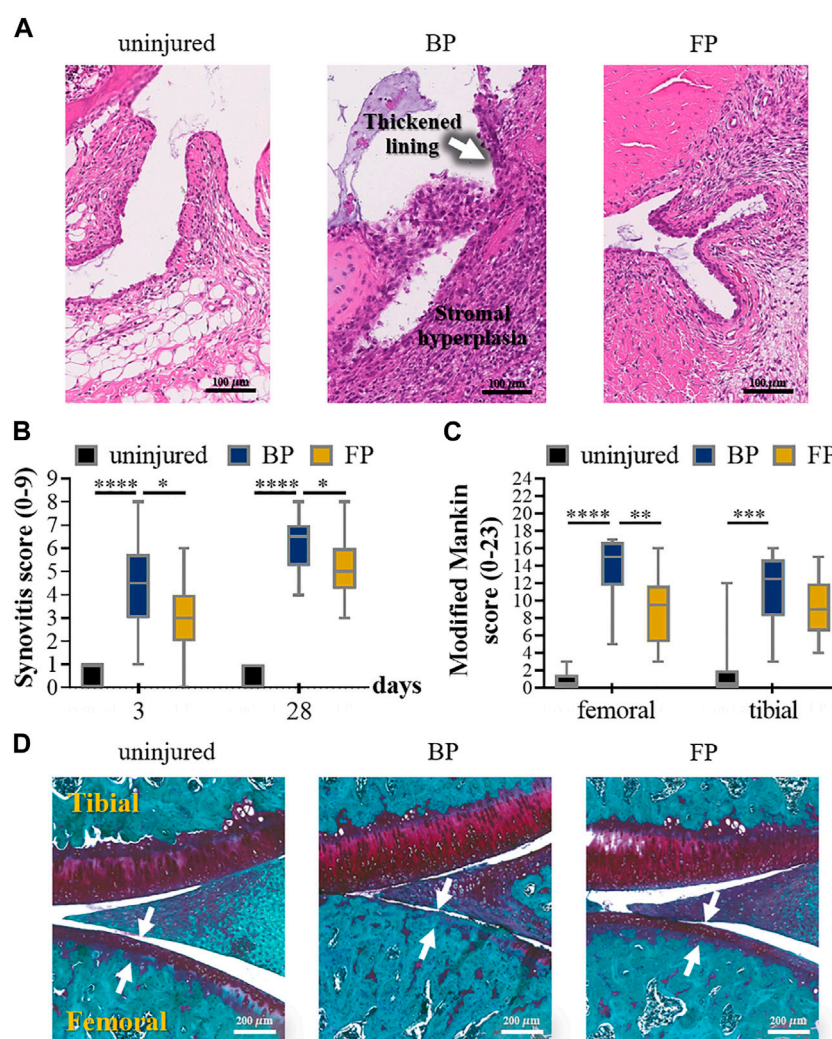


FIGURE 5

(A) Representative images of HE-stained synovial tissue on the third day after the injury to anterior cruciate ligament (ACL). (B) 2 blinded observers evaluated the individual synovitis score results according to the experimental procedures. (C) Results of the semi-quantitative assessment of the severity of osteoarthritis by modified Mankin score. (D) The individual osteoarthritis scores using S.E. 4 weeks after injury. Reproduced with permission from ref (Sangsuwan et al., 2022). Copyright 2022 Acta Materialia Inc.

systemic and local adverse reactions were observed in the experimental group of rats. At the same time, cartilage histology was not affected (Tellegen et al., 2018). Thus, celecoxib PEA microspheres are expected to be a promising strategy for alleviating inflammation and pain in OA. In another study, TA was loaded into the PEA microsphere platform. TA microspheres can achieve sustained release over 60 days in PBS. Drug-loaded microspheres were retained for up to 70 days after intra-articular injection in OA, and synovial inflammation in diseased joints was significantly reduced with no effect on cartilage integrity. Longer pain relief and greater reduction in claudication were achieved than with TA-coated PLGA microspheres. In sum, the PEA microsphere platform demonstrated safety and efficacy when injected intra-articularly, making it an attractive potential OA treatment (Rudnik-Jansen et al., 2017; Rudnik-Jansen et al., 2019).

Yang et al. (2020) prepared a type of polyampholyte modified methacrylate microspheres by using microfluidic technology. Among

them, the grafting of poly(sulfobetaine methacrylate) provided the microspheres with stronger lubricity, lower degradation rate and sustained drug release properties. Subsequently, super-lubricating microspheres with excellent biocompatibility loaded with diclofenac sodium (DS) were further developed, which showed great potential in the osteoarthritis treatment by providing excellent hydrated lubrication and sustained drug release while protecting chondrocytes from inflammatory factor-induced degeneration *in vitro*. In a subsequent study, the research team selected 2-methacryloyloxyethyl phosphorylcholine (MPC) grafted methacrylate gelatin to prepare injectable hydrogel drug-loaded microspheres (GelMA@DMA-MPC@DS) with enhanced lubricity by photo-cross-linking, which confirmed that biocompatible functionalized microspheres provide significant therapeutic effects on OA development and represent a simple and promising technology for OA treatment (Han et al., 2021) (Figure 7).

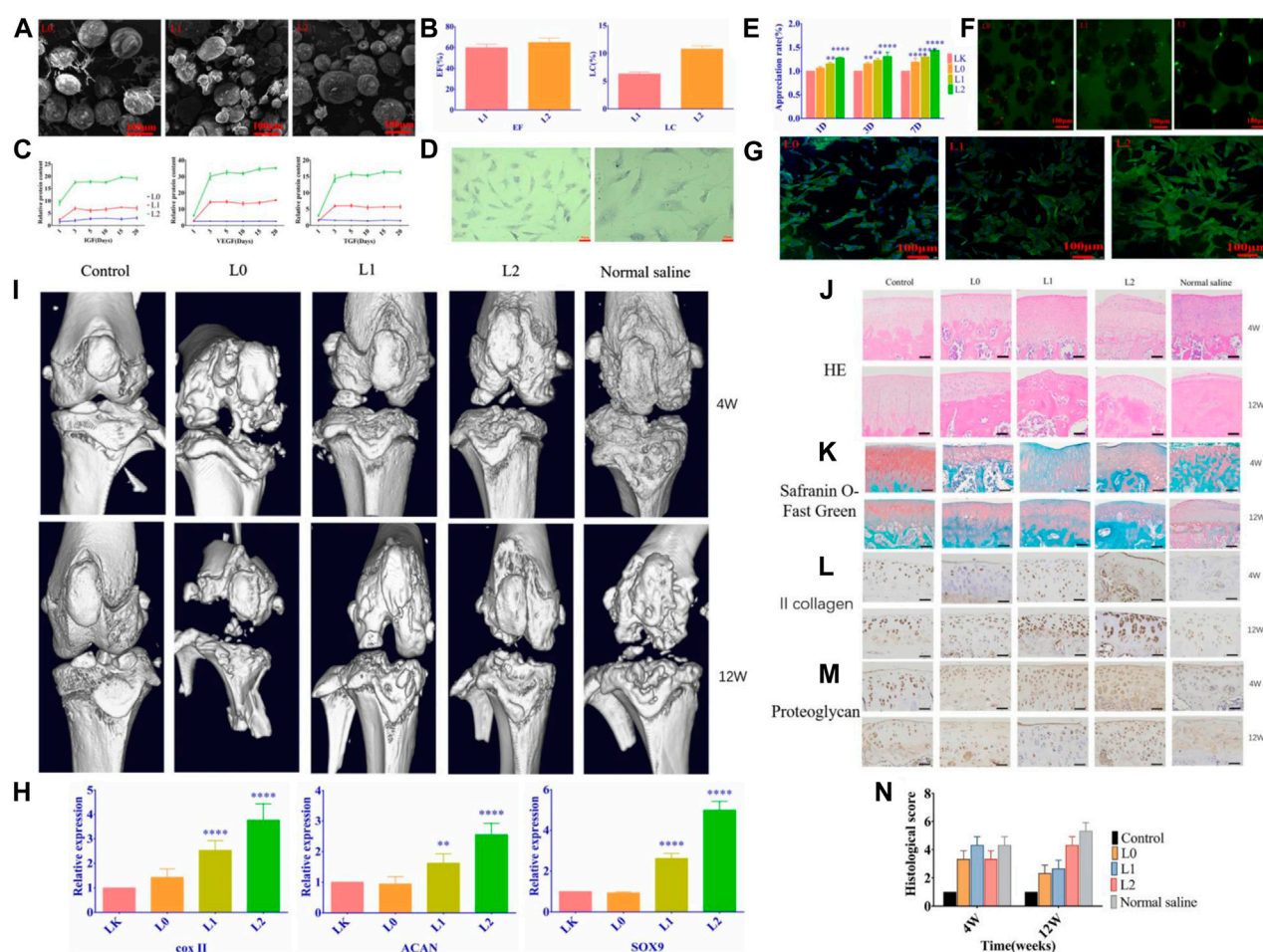


FIGURE 6

(A) SEM images of the microspheres. (B) Loading rate and encapsulation rate of the microspheres. (C) The release curve of related growth factors. (D) Optical micrograph of chondrocytes. (E) Proliferation of chondrocytes co-cultured with microspheres. (F) The percentage of viable cells after having treated with different groups of microspheres. (G) Cellular changes in microsphere-cultured cells. (H) Each group's relative expression of chondrogenic genes. (I) Micro-CT scan images of the effect of microspheres on bone and articular cartilage damage. HE staining. (J) and Safranin-O fast green staining (K) results images. (L) Type II collagen staining results (M) Chondrocyte proteoglycan staining results. (N) Histological scoring of the cartilage according to OARSI. Reproduced with permission from ref (Li et al., 2021). CC BY 4.0. Copyright 2021 The Author(s).

2.3 Composite matrix microparticle-based drug delivery systems

Moreover, composite carriers between nanoparticles, liposomes, hydrogels, and microspheres can incorporate the advantages of various material forms, showing stronger plasticity and functionality than traditional single carriers, and the composite carrier platform is often loaded with two or more therapeutic agents to achieve more significant therapeutic effects. Thus, it is anticipated to be a promising novel topical drug delivery systems.

Yu et al. (2022) developed reactive oxygen species (ROS)-responsive hydrogel microspheres with cartilage-targeting. Specifically, ROS-responsive drug-loaded nanoparticles and type II collagen-targeting peptides were anchored in the hydrogel matrix by microfluidic technology, thereafter a polymerization process is implemented via UV light. The introduction of targeting peptides can achieve real targeted therapy, and the ROS-responsive nanoparticles react with the ROS in the cells and induce the drug to achieve a responsive and steady release, which can further reduce the inflammation and facilitate cartilage

differentiation for achieving local and long-term therapeutic benefits after injection. Thus, it has important application prospects in OA treatment. Fang et al. (2022) developed a new microsphere-microcrystal-gel delivery system in which DEX-loaded microspheres were prepared from sodium alginate and hyaluronic acid. Moreover, another drug called celecoxib (CLX) microcrystals (CM) were fabricated using ultrasonication to enhance solubility and bioavailability. Finally, an injectable gel was prepared by cross-linking method to encapsulate both therapeutic agents. *In vitro*, the synergistic drug delivery system enabled sustained drug release and showed good biocompatibility and anti-inflammatory characteristics. *In vivo*, the release of inflammatory cytokines was downregulated, and cartilage matrix erosion and chondrocyte loss were significantly ameliorated. Therefore, this composite delivery platform offers a promising treatment to revolutionize traditional therapies for chronic joint diseases. Injectable degradable hydrogel microspheres with drug-loaded liposomes as a secondary structure have also been developed. The liposomes loaded with liquiritin (LQ) have a good effect on scavenging ROS in chondrocytes, and the chondroitin sulfate obtained from ChsMA gel degraded by

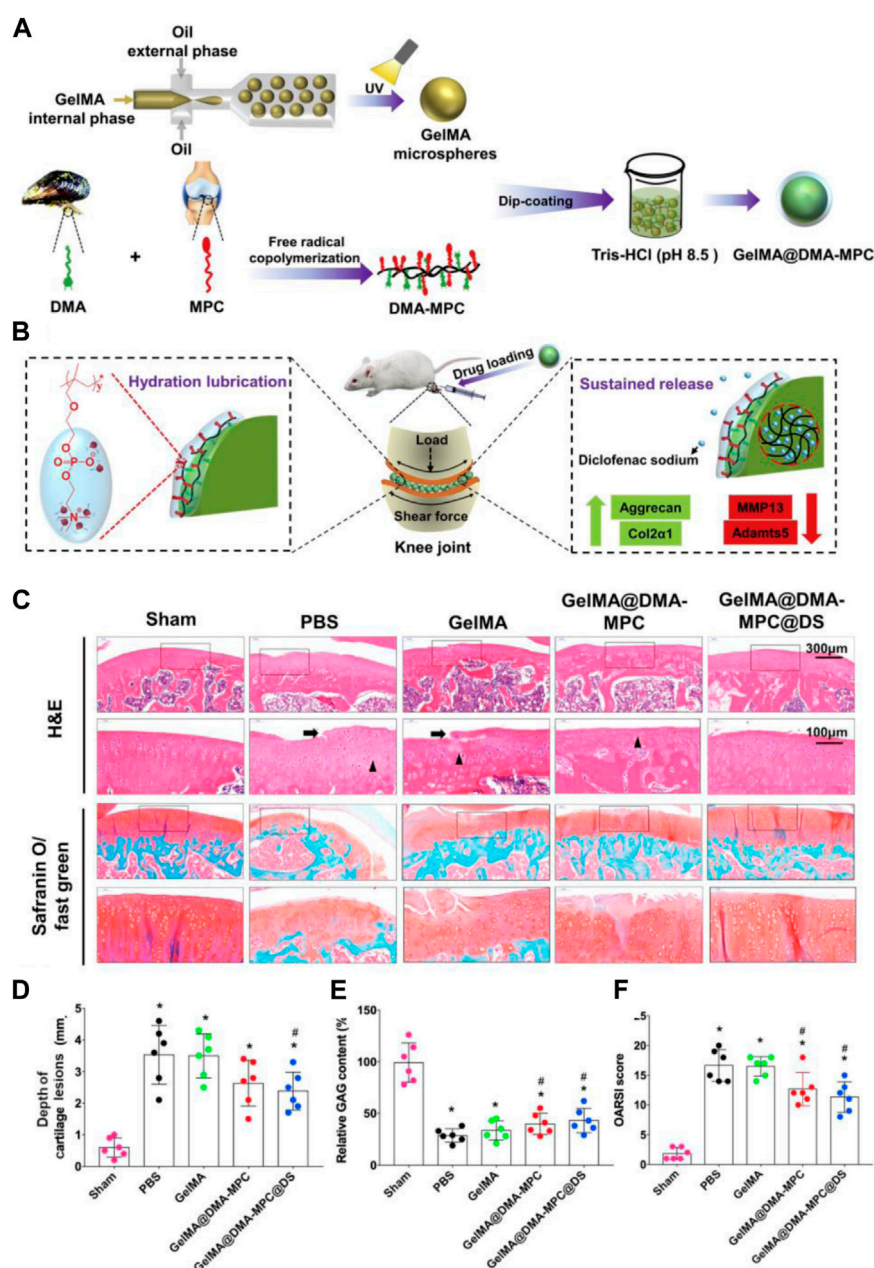


FIGURE 7

(A) Schematic illustration of GelMA@DMA-MPC microspheres preparation. (B) Delaying the OA progression using GelMA@DMA-MPC drug-loaded microspheres injected intra-articularly. (C) Representative images of rat cartilage sections with H&E and Safranin O-Fast Green staining (Arrows point to eroded fissures, triangles represent cloned tissue cellular structures). (D) The corresponding cartilage lesions depth, (E) relative GAG content and (F) OARSI score of rats' articular cartilage. Reproduced with permission from ref (Han et al., 2021). CC BY-NC-ND 4.0 Copyright 2021 The Author(s).

hyaluronidase can also effectively fulfil its antioxidant activity. Thus, the composite delivery platform can provide dual antioxidant effects to eliminate ROS for OA therapy, and this novel delivery system also becomes a prospective option for treating osteoarthritis (He et al., 2022).

3 Conclusion and outlook

In the field of medicine, polymeric materials provide novel platforms for delivering drugs to target tissues. Novel formulations using polymers

as drug delivery matrix have advantages over conventional formulations regarding prolonged drug residence time, improved curative effect, and enhanced patient compliance. There is currently a lack of effective and convenient treatments for OA, so developing new drug delivery systems is required for safe treatment. Intra-articular drug delivery strategies play an essential role in treating KOA, and different intra-articular drug delivery systems (IA DDSs) are being developed rapidly and have made notable progress. Desirable properties of IA DDSs for KOA treatment include excellent sustained and/or controlled release drug delivery, lubricating properties, and disease targeting. In this review, we

TABLE 1 Drug-loaded microspheres DDSs with different polymer carriers for OA treatment.

| Natural polymers | | | | |
|-----------------------------------|--|--|---|---|
| Polymer carriers | Drug | Animal model | Outcome | Refs |
| Chitosan/Hyaluronic acid | Rac1 inhibitor NSC23766 | OA model in mice | The preparation has a lubricating effect, can achieve sustained release of inhibitors, and can protect cartilage from damage and delay OA development | Zhu et al. (2015) |
| Chitosan | Lornoxicam | OA model in rat | It reduces inflammatory conditions and has long-lasting pharmacological effects | Abd-Allah et al. (2016) |
| Chitosan | Verteporfin | OA model in mice | The continuous release of Verteporfin can dramatically lower YAP activity in chondrocytes, effectively maintain cartilage homeostasis, and delay OA development | Zhang et al. (2020) |
| Heparin | Tumor necrosis factor- α -stimulated gene 6 (TSG-6) | Medial meniscal transection model in rat | Sulfated heparin can increase the biological activity of TSG-6, and IA injection of drug-loaded microspheres can lessen cartilage damage | Tellier et al. (2018) |
| Gelatin | IL-4; IL-10; IL-13 | N/A | Drug-loaded microspheres are biologically responsive, prolong the residence time of anti-inflammatory cytokines, and significantly reduce inflammation | Park et al. (2020) |
| Gelatin/silk fibroin | Curcumin | OA model in rats | It delays cell destruction in joint and synovial tissues and exhibits long-lasting anti-inflammatory effects | Ratanavaraporn et al. (2017) |
| Synthetic polymers | | | | |
| Poly (lactide-co-glycolide)(PLGA) | Rhein | N/A | Suitable for intra-articular administration in the treatment of OA after sterilization by gamma irradiation | Gómez-Gaete et al. (2017) , Avendaño-Godoy et al. (2023) |
| PLGA | Rapamycin | OA model in mice | It can induce autophagy and prevent the aging of human chondrocytes, reducing cartilage damage and inflammation | Dhanabalan et al. (2020) , Dhanabalan et al. (2023) |
| PLGA | Triamcinolone acetonide | Normal knee joint of the beagle | Extend drug retention time and reduce dosing frequency | Bodick et al. (2018) |
| PLGA | Triamcinolone acetonide | KOA patients | Extend the residence time of drugs in joints and lessen systemic side effects of patients. It has good biosafety and clinically provides long-term symptom relief | Conaghan et al. (2018a) , Conaghan et al. (2018b) , Kraus et al. (2018) |
| PLGA/Agarose | Dexamethasone | Adult mongrel dogs | It provides cartilage protection <i>in vitro</i> and improves function <i>in vivo</i> | Stefani et al. (2020) |
| PLGA | Dexamethasone | Posttraumatic osteoarthritis model in mice | Reduces the expression of inflammatory genes and comprehensively protects articular cartilage and broader joint structures | Di Francesco et al. (2021) |
| PLGA | Mometasone Furoate | Male Sprague Dawley rats | Stable and long-acting sustained release, good efficacy, and high safety <i>in vivo</i> | Liang et al. (2021) |

(Continued on following page)

TABLE 1 (Continued) Drug-loaded microspheres DDSs with different polymer carriers for OA treatment.

| Natural polymers | | | | |
|--|-----------------------------------|---|---|--|
| Polymer carriers | Drug | Animal model | Outcome | Refs |
| PLGA | Flavopiridol | Posttraumatic osteoarthritis model in rat | Reduce inflammation and PTOA damage | Sangsuwan et al. (2022) |
| PLGA/Chitosan/Gelatin | superactive platelet lysate (sPL) | OA model in SD male rats | It increases chondrocyte proliferation, smoothes the cartilage surface, and increases cartilage integrity | Li et al. (2021) |
| PLGA/PLA | Triamcinolone acetonide | N/A | Extend drug retention time and reduce systemic exposure and dosing frequency | Ho et al. (2019) |
| PLGA/PLA | Ketorolac | N/A | Sustained and stable drug release | Wongrakpanich et al. (2023) |
| PLGA/PCL | Aceclofenac | Paw oedema model in female Sprague Dawley (SD) rats | Significant anti-inflammatory activity <i>in vivo</i> | Kaur et al. (2017) |
| PLA/PEG/poly- δ -decalactone (PDL) | Triamcinolone acetonide | KOA model in rats | Exhibits sustained anti-inflammatory effects | Abou-ElNour et al. (2019) |
| P(DLLA-PEG)-b-PLA | Tacrolimus | Horse joints | Excellent local anti-inflammatory ability and no systemic side effects | Sandker et al. (2018) |
| Polyester amide (PEA) | Celecoxib | OA model in rats | Reduce OA inflammation and pain | Janssen et al. (2016), Tellegen et al. (2018) |
| PEA | Triamcinolone acetonide | KOA model in rats | Synovial inflammation in diseased joints is significantly reduced | Rudnik-Jansen et al. (2017), Rudnik-Jansen et al. (2019) |
| Poly (dopamine methacrylamide-to-sulfbobetaine methacrylate)/Gelatin | Diclofenac sodium | OA model in rats | It reduces osteophyte load and cartilage degradation and has therapeutic effects on osteoarthritis | Yang et al. (2020) |

searched, collected, and analyzed studies on applying different microsphere-based IA DDSs in preclinical/clinical trials (Table 1). Microsphere formulations are widely in use for the controlled delivery of therapeutic agents to enhance efficacy and reduce systemic drug toxicity. However, stability and scale-up of microsphere preparation are still issues to be resolved. In addition, the duration of efficacy, targeting properties, and the safety of the formulations still have major challenges.

Multifunctional drug delivery systems with good biosafety and drug targeting are a prospective trend for the further development of IA DDSs. It is gaining attraction to combine different strategies to prepare DDSs for treating KOA. Nevertheless, synergistic effects between different strategies need to be taken into account as the strategies for DDSs become more complex. Generally, it is still necessary to further expand the research and application of polymers in KOA drug delivery systems to provide guidance for future clinical trials and enhance the long-term retention of drugs in the joints and diffusion to targeted tissues. At the same time, the benefits of novel therapies are meticulously balanced against their costs and potential risks.

Author contributions

GW: Writing—original draft. X-aZ: Writing—review and editing. LK: Writing—original draft. MH: Writing—review and editing.

Funding

The author(s) declare financial support was received for the research, authorship, and/or publication of this article. This work was supported by the National Natural Science Foundation of China (32371184), Liaoning Province Applied Basic Research Program (2023JH2/101300072) and the Science and Technology Innovation Program of the General Administration of Sport of China (22KJCX040).

Conflict of interest

The authors declare that the research was conducted in the absence of any commercial or financial relationships that could be construed as a potential conflict of interest.

Publisher's note

All claims expressed in this article are solely those of the authors and do not necessarily represent those of their affiliated organizations, or those of the publisher, the editors and the reviewers. Any product that may be evaluated in this article, or claim that may be made by its manufacturer, is not guaranteed or endorsed by the publisher.

References

- Abbas, M., Alkaff, M., Jilani, A., Alsehl, H., Damiati, L., Kotb, M., et al. (2018). Combination of mesenchymal stem cells, cartilage pellet and bioscaffold supported cartilage regeneration of a full thickness articular surface defect in rabbits. *Tissue Eng. Regen. Med.* 15, 661–671. doi:10.1007/s13770-018-0131-0
- Abd-Allah, H., Kamel, A. O., and Sammour, O. A. (2016). Injectable long acting chitosan/tripolyphosphate microspheres for the intra-articular delivery of lornoxicam: optimization and *in vivo* evaluation. *Carbohydr. Polym.* 149, 263–273. doi:10.1016/j.carbpol.2016.04.096
- Abou-ElNour, M., Ishak, R. A., Tiboni, M., Bonacucina, G., Cespi, M., Casettari, L., et al. (2019). Triamcinolone acetate-loaded PLA/PEG-PDL microparticles for effective intra-articular delivery: synthesis, optimization, *in vitro* and *in vivo* evaluation. *J. Control. Release* 309, 125–144. doi:10.1016/j.jconrel.2019.07.030
- Ahmad, M., Manzoor, K., and Ikram, S. (2019). “Chitosan nanocomposites for bone and cartilage regeneration,” in *Applications of nanocomposite materials in dentistry*, 307–317.
- Avenidaño-Godoy, J., Poblete, M. G., Ramos, R. G., and Gómez-Gaete, C. (2023). Evaluation of the effects of gamma radiation sterilization on rhin-loaded biodegradable microparticles for the treatment of osteoarthritis. *J. Pharm. Sci.* 112 (3), 837–843. doi:10.1016/j.xphs.2022.11.003
- Bajpayee, A. G., and Grodzinsky, A. J. (2017). Cartilage-targeting drug delivery: can electrostatic interactions help? *Nat. Rev. Rheumatol.* 13 (3), 183–193. doi:10.1038/nrrheum.2016.210
- Bas, O., Lucarotti, S., Angella, D. D., Castro, N. J., Meinert, C., Wunner, F. M., et al. (2018). Rational design and fabrication of multiphasic soft network composites for tissue engineering articular cartilage: a numerical model-based approach. *Chem. Eng. J.* 340, 15–23. doi:10.1016/j.cej.2018.01.020
- Bellamy, N., Bachmeier, C., Brooks, P., Browne, C., Cohen, M., March, L., et al. (1997). Osteoarthritis antirheumatic drug trials: effects of a standardized instructional videotape on the reliability of observer-dependent dependent outcome measures. *Inflammopharmacology* 5, 285–295. doi:10.1007/s10787-997-0006-9
- Berenbaum, F., Wallace, I. J., Lieberman, D. E., and Felson, D. T. (2018). Modern-day environmental factors in the pathogenesis of osteoarthritis. *Nat. Rev. Rheumatol.* 14 (11), 674–681. doi:10.1038/s41584-018-0073-x
- Bhaskar, S., Pollock, K. M., Yoshida, M., and Lahann, J. (2010). Towards designer microparticles: simultaneous control of anisotropy, shape, and size. *Small* 6 (3), 404–411. doi:10.1002/sml.200901306
- Blanco, F. J., and Rego-Pérez, I. (2018). Mitochondria and mitophagy: biosensors for cartilage degradation and osteoarthritis. *Osteoarthr. Cartil.* 26 (8), 989–991. doi:10.1016/j.joca.2018.05.018
- Block, J., Oegema, T., Sandy, J., and Plaas, A. (2010). The effects of oral glucosamine on joint health: is a change in research approach needed? *Osteoarthr. Cartil.* 18 (1), 5–11. doi:10.1016/j.joca.2009.07.005
- Bodick, N., Williamson, T., Strand, V., Senter, B., Kelley, S., Boyce, R., et al. (2018). Local effects following single and repeat intra-articular injections of triamcinolone acetate extended-release: results from three nonclinical toxicity studies in dogs. *Rheumatology Ther.* 5, 475–498. doi:10.1007/s40744-018-0125-3
- Boer, C. G., Hatzikotoulas, K., Southam, L., Stefánssdóttir, L., Zhang, Y., de Almeida, R. C., et al. (2021). Deciphering osteoarthritis genetics across 826,690 individuals from 9 populations. *Cell* 184 (18), 4784–4818. e17. doi:10.1016/j.cell.2021.07.038
- Bowman, S., Awad, M. E., Hamrick, M. W., Hunter, M., and Fulzele, S. (2018). Recent advances in hyaluronic acid based therapy for osteoarthritis. *Clin. Transl. Med.* 7 (1), 6–11. doi:10.1186/s40169-017-0180-3
- Braun, H. J., and Gold, G. E. (2012). Diagnosis of osteoarthritis: imaging. *Bone* 51 (2), 278–288. doi:10.1016/j.bone.2011.11.019
- Castaldo, L., Corbo, P., Maglio, G., and Palumbo, R. (1992). Synthesis and preliminary characterization of polyesteramides containing enzymatically degradable amide bonds. *Polym. Bull.* 28, 301–307. doi:10.1007/bf00294826
- Chevalier, X., Goupille, P., Beaulieu, A., Burch, F., Bensen, W., Conrozier, T., et al. (2009). Intraarticular injection of anakinra in osteoarthritis of the knee: a multicenter, randomized, double-blind, placebo-controlled study. *Arthritis Care & Res.* 61 (3), 344–352. doi:10.1002/art.24096
- Conaghan, P. G., Cohen, S. B., Berenbaum, F., Lufkin, J., Johnson, J. R., and Bodick, N. (2018a). Brief report: a phase II b trial of a novel extended-release microsphere formulation of triamcinolone acetate for intraarticular injection in knee osteoarthritis. *Arthritis & Rheumatology* 70 (2), 204–211. doi:10.1002/art.40364
- Conaghan, P. G., Hunter, D. J., Cohen, S. B., Kraus, V. B., Berenbaum, F., Lieberman, J. R., et al. (2018b). Effects of a single intra-articular injection of a microsphere formulation of triamcinolone acetate on knee osteoarthritis pain: a double-blind, randomized, placebo-controlled, multinational study. *J. Bone Jt. Surg. Am. Volume* 100 (8), 666–677. doi:10.2106/jbjs.17.00154
- Cucchiari, M., and Madry, H. (2019). Biomaterial-guided delivery of gene vectors for targeted articular cartilage repair. *Nat. Rev. Rheumatol.* 15 (1), 18–29. doi:10.1038/s41584-018-0125-2
- da Costa, B. R., Reichenbach, S., Keller, N., Nartey, L., Wandel, S., Jüni, P., et al. (2017). Effectiveness of non-steroidal anti-inflammatory drugs for the treatment of pain in knee and hip osteoarthritis: a network meta-analysis. *Lancet* 390 (10090), e21–e33. doi:10.1016/s0140-6736(17)31744-0
- Demehri, S., Guermazi, A., and Kwoh, C. K. (2016). Diagnosis and longitudinal assessment of osteoarthritis: review of available imaging techniques. *Rheum. Dis. Clin.* 42 (4), 607–620. doi:10.1016/j.rdc.2016.07.004
- Dhanabalan, K. M., Dravid, A. A., Agarwal, S., Sharath, R. K., Padmanabhan, A. K., and Agarwal, R. (2023). Intra-articular injection of rapamycin microparticles prevent senescence and effectively treat osteoarthritis. *Bioeng. Transl. Med.* 8 (1), e10298. doi:10.1002/btm2.10298
- Dhanabalan, K. M., Gupta, V. K., and Agarwal, R. (2020). Rapamycin-PLGA microparticles prevent senescence, sustain cartilage matrix production under stress and exhibit prolonged retention in mouse joints. *Biomaterials Sci.* 8 (15), 4308–4321. doi:10.1039/d0bm00596g
- Di Francesco, M., Bedingfield, S. K., Di Francesco, V., Colazo, J. M., Yu, F., Ceseracci, L., et al. (2021). Shape-defined microplates for the sustained intra-articular release of dexamethasone in the management of overload-induced osteoarthritis. *ACS Appl. Mater. Interfaces* 13 (27), 31379–31392. doi:10.1021/acsami.1c02082
- Eitner, A., Hofmann, G. O., and Schaible, H.-G. (2017). Mechanisms of osteoarthritic pain. Studies in humans and experimental models. *Front. Mol. Neurosci.* 10, 349. doi:10.3389/fnmol.2017.00349
- Evans, C. H., Kraus, V. B., and Setton, L. A. (2014). Progress in intra-articular therapy. *Nat. Rev. Rheumatol.* 10 (1), 11–22. doi:10.1038/nrrheum.2013.159
- Fan, W., Li, J., Yuan, L., Chen, J., Wang, Z., Wang, Y., et al. (2018). Intra-articular injection of kartogenin-conjugated polyurethane nanoparticles attenuates the progression of osteoarthritis. *Drug Deliv.* 25 (1), 1004–1012. doi:10.1080/10717544.2018.1461279
- Fang, W., Yang, F., Li, W., Hu, Q., Chen, W., Yang, M., et al. (2022). Dexamethasone microspheres and celecoxib microcrystals loaded into injectable gels for enhanced knee osteoarthritis therapy. *Int. J. Pharm.* 622, 121802. doi:10.1016/j.ijpharm.2022.121802
- Gerwin, N., Hops, C., and Lucke, A. (2006). Intraarticular drug delivery in osteoarthritis. *Adv. Drug Deliv. Rev.* 58 (2), 226–242. doi:10.1016/j.addr.2006.01.018
- Glyn-Jones, S., Palmer, A. J. R., Agricola, R., Price, A. J., Vincent, T. L., Weinans, H., et al. (2015). Osteoarthritis. *Lancet* 386 (9991), 376–387. doi:10.1016/s0140-6736(14)60802-3
- Goldring, S. R., and Goldring, M. B. (2016). Changes in the osteochondral unit during osteoarthritis: structure, function and cartilage–bone crosstalk. *Nat. Rev. Rheumatol.* 12 (11), 632–644. doi:10.1038/nrrheum.2016.148
- Gómez-Gaete, C., Retamal, M., Chávez, C., Bustos, P., Godoy, R., and Torres-Vergara, P. (2017). Development, characterization and *in vitro* evaluation of biodegradable rhin-loaded microparticles for treatment of osteoarthritis. *Eur. J. Pharm. Sci.* 96, 390–397. doi:10.1016/j.ejps.2016.10.010
- Han, Y., Yang, J., Zhao, W., Wang, H., Sun, Y., Chen, Y., et al. (2021). Biomimetic injectable hydrogel microspheres with enhanced lubrication and controllable drug release for the treatment of osteoarthritis. *Bioact. Mater.* 6 (10), 3596–3607. doi:10.1016/j.bioactmat.2021.03.022
- He, Y., and Park, K. (2016). Effects of the microparticle shape on cellular uptake. *Mol. Pharm.* 13 (7), 2164–2171. doi:10.1021/acs.molpharmaceut.5b00992
- He, Y., Sun, M., Wang, J., Yang, X., Lin, C., Ge, L., et al. (2022). Chondroitin sulfate microspheres anchored with drug-loaded liposomes play a dual antioxidant role in the treatment of osteoarthritis. *Acta Biomater.* 151, 512–527. doi:10.1016/j.actbio.2022.07.052
- He, Z., Wang, B., Hu, C., and Zhao, J. (2017). An overview of hydrogel-based intra-articular drug delivery for the treatment of osteoarthritis. *Colloids Surfaces B Biointerfaces* 154, 33–39. doi:10.1016/j.colsurfb.2017.03.003
- Ho, M. J., Jeong, H. T., Im, S. H., Kim, H. T., Lee, J. E., Park, J. S., et al. (2019). Design and *in vivo* pharmacokinetic evaluation of triamcinolone acetate microcrystals-loaded PLGA microsphere for increased drug retention in knees after intra-articular injection. *Pharmaceutics* 11 (8), 419. doi:10.3390/pharmaceutics11080419
- Hunter, B., and Bierma-Zeinstra, S. (2019). Osteoarthritis. *Lancet* 393 (10182), 1745–1759. doi:10.1016/s0140-6736(19)30417-9
- Jain, K., and Ravikumar, P. (2020). Recent advances in treatments of cartilage regeneration for knee osteoarthritis. *J. Drug Deliv. Sci. Technol.* 60, 102014. doi:10.1016/j.jddst.2020.102014
- James, S. L., Abate, D., Abate, K. H., Abay, S. M., Abbafati, C., Abbasi, N., et al. (2018). Global, regional, and national incidence, prevalence, and years lived with disability for 354 diseases and injuries for 195 countries and territories, 1990–2017: a systematic analysis for the Global Burden of Disease Study 2017. *The Lancet* 392 (10159), 1789–1858. doi:10.1016/S0140-6736(18)32279-7
- Jamshidi, A., Pelletier, J.-P., and Martel-Pelletier, J. (2019). Machine-learning-based patient-specific prediction models for knee osteoarthritis. *Nat. Rev. Rheumatol.* 15 (1), 49–60. doi:10.1038/s41584-018-0130-5
- Janssen, M., Timur, U. T., Woike, N., Welting, T. J., Draaisma, G., Gijbels, M., et al. (2016). Celecoxib-loaded PEA microspheres as an auto regulatory drug-delivery system after intra-articular injection. *J. Control. Release* 244, 30–40. doi:10.1016/j.jconrel.2016.11.003

- Johnson, V. L., and Hunter, D. J. (2014). The epidemiology of osteoarthritis. *Best Pract. Res. Clin. Rheumatology* 28 (1), 5–15. doi:10.1016/j.berh.2014.01.004
- Kaur, M., Sharma, S., and Sinha, V. (2017). Polymer based microspheres of aceclofenac as sustained release parenterals for prolonged anti-inflammatory effect. *Mater. Sci. Eng. C* 72, 492–500. doi:10.1016/j.msec.2016.11.092
- Kou, L., Xiao, S., Sun, R., Bao, S., Yao, Q., and Chen, R. (2019). Biomaterial-engineered intra-articular drug delivery systems for osteoarthritis therapy. *Drug Deliv.* 26 (1), 870–885. doi:10.1080/10717544.2019.1660434
- Kraus, V., Conaghan, P. G., Aazami, H., Mehra, P., Kivitz, A., Lufkin, J., et al. (2018). Synovial and systemic pharmacokinetics (PK) of triamcinolone acetonide (TA) following intra-articular (IA) injection of an extended-release microsphere-based formulation (FX006) or standard crystalline suspension in patients with knee osteoarthritis (OA). *Osteoarthr. Cartil.* 26 (1), 34–42. doi:10.1016/j.joca.2017.10.003
- Kyu, H., Abate, D., Abate, K., Abay, S., Abbafati, C., Abbasi, N., et al. (2018). Global, regional, and national disability-adjusted life-years (DALYs) for 359 diseases and injuries and healthy life expectancy (HALE) for 195 countries and territories, 1990–2017: a systematic analysis for the Global Burden of Disease Study 2017. *Lancet* 392 (10159), 1859–1922. doi:10.1016/s0140-6736(18)32335-3
- Lane, N. (1997). Pain management in osteoarthritis: the role of COX-2 inhibitors. *J. Rheumatology* 49, 20–24. Supplement.
- Lane, N. E., and Corr, M. (2017). Anti-NGF treatments for pain-two steps forward, one step back? *Nat. Rev. Rheumatol.* 13 (2), 76–78. doi:10.1038/nrrheum.2016.224
- Leopoldino, A. O., Machado, G. C., Ferreira, P. H., Pinheiro, M. B., Day, R., McLachlan, A. J., et al. (1996). Paracetamol versus placebo for knee and hip osteoarthritis. *Cochrane Database Syst. Rev.* 2019 (8), CD013273. doi:10.1002/14651858.cd013273
- Li, J., Liu, N., Huang, Z., Wang, W., Hou, D., and Wang, W. (2021). Intra-articular injection of loaded sPL sustained-release microspheres inhibits osteoarthritis and promotes cartilaginous repairs. *J. Orthop. Surg. Res.* 16, 646–649. doi:10.1186/s13018-021-02777-9
- Liang, Y., Zhang, J., Zhao, X., Wang, M., Ding, S., Wang, Y., et al. (2021). Study on the slow-release mometasone furoate injection of PLGA for the treatment of knee arthritis. *Curr. Drug Deliv.* 18 (3), 357–368. doi:10.2174/1567201817666200917124759
- Lin, J., Zhang, W., Jones, A., and Doherty, M. (2004). Efficacy of topical non-steroidal anti-inflammatory drugs in the treatment of osteoarthritis: meta-analysis of randomised controlled trials. *BMJ* 329 (7461), 324. doi:10.1136/bmj.38159.639028.7c
- Nakano, S., Ikata, T., Kinoshita, I., Kanematsu, J., and Yasuoka, S. (1999). Characteristics of the protease activity in synovial fluid from patients with rheumatoid arthritis and osteoarthritis. *Clin. Exp. Rheumatology* 17 (2), 161–170.
- Nelson, A. E., Allen, K. D., Golightly, Y. M., Goode, A. P., and Jordan, J. M. (2014). A systematic review of recommendations and guidelines for the management of osteoarthritis: the chronic osteoarthritis management initiative of the US bone and joint initiative. *Seminars Arthritis Rheumatism* 43 (6), 701–712. doi:10.1016/j.semarthrit.2013.11.012
- Nguyen, C., and Rannou, F. (2017). The safety of intra-articular injections for the treatment of knee osteoarthritis: a critical narrative review. *Expert Opin. Drug Saf.* 16 (8), 897–902. doi:10.1080/14740338.2017.1344211
- Ondresik, M., Azevedo Maia, F. R., da Silva Morais, A., Gertrudes, A. C., Dias Bacelar, A. H., Correia, C., et al. (2017). Management of knee osteoarthritis. Current status and future trends. *Biotechnol. Bioeng.* 114 (4), 717–739. doi:10.1002/bit.26182
- Owen, S. G., Francis, H. W., and Roberts, M. S. (1994). Disappearance kinetics of solutes from synovial fluid after intra-articular injection. *Br. J. Clin. Pharmacol.* 38 (4), 349–355. doi:10.1111/j.1365-2125.1994.tb04365.x
- Palazzo, C., Nguyen, C., Lefevre-Colau, M. M., Rannou, F., and Poiraudou, S. (2016). Risk factors and burden of osteoarthritis. *Ann. Phys. Rehabilitation Med.* 59 (3), 134–138. doi:10.1016/j.rehab.2016.01.006
- Park, E., Hart, M. L., Rolauffs, B., Stegmann, J. P., and Annamalai, R. (2020). Bioresponsive microspheres for on-demand delivery of anti-inflammatory cytokines for articular cartilage repair. *J. Biomed. Mater. Res. Part A* 108 (3), 722–733. doi:10.1002/jbm.a.36852
- Park, J. H., Lee, H., Cho, J.-s., Kim, I., Lee, J., and Jang, S. H. (2021). Effects of knee osteoarthritis severity on inter-joint coordination and gait variability as measured by hip-knee cyclograms. *Sci. Rep.* 11 (1), 1789. doi:10.1038/s41598-020-80237-w
- Peters, A. E., Akhtar, R., Comerford, E. J., and Bates, K. T. (2018). The effect of ageing and osteoarthritis on the mechanical properties of cartilage and bone in the human knee joint. *Sci. Rep.* 8 (1), 5931. doi:10.1038/s41598-018-24258-6
- Ratanavaraporn, J., Soontornvipart, K., Shuangshoti, S., Shuangshoti, S., and Damrongsakkul, S. (2017). Localized delivery of curcumin from injectable gelatin/Thai silk fibroin microspheres for anti-inflammatory treatment of osteoarthritis in a rat model. *Inflammopharmacology* 25, 211–221. doi:10.1007/s10787-017-0318-3
- Rudnik-Jansen, I., Colen, S., Berard, J., Plomp, S., Que, I., van Rijen, M., et al. (2017). Prolonged inhibition of inflammation in osteoarthritis by triamcinolone acetonide released from a polyester amide microsphere platform. *J. Control. Release* 253, 64–72. doi:10.1016/j.jconrel.2017.03.014
- Rudnik-Jansen, I., Schrijver, K., Woike, N., Tellegen, A., Versteeg, S., Emans, P., et al. (2019). Intra-articular injection of triamcinolone acetonide releasing biomaterial microspheres inhibits pain and inflammation in an acute arthritis model. *Drug Deliv.* 26 (1), 226–236. doi:10.1080/10717544.2019.1568625
- Russell, S. J., Sala, R., Conaghan, P. G., Habib, G., Vo, Q., Manning, R., et al. (2018). Triamcinolone acetonide extended-release in patients with osteoarthritis and type 2 diabetes: a randomized, phase 2 study. *Rheumatology* 57 (12), 2235–2241. doi:10.1093/rheumatology/key265
- Sandker, M. J., Duque, L. F., Redout, E. M., Klijnstra, E. C., Steendam, R., Kops, N., et al. (2018). Degradation, intra-articular biocompatibility, drug release, and bioactivity of tacrolimus-loaded poly (dl-lactide-PEG)-b-poly (l-lactide) multiblock copolymer-based monospheres. *ACS Biomaterials Sci. Eng.* 4 (7), 2390–2403. doi:10.1021/acsbiomaterials.8b00116
- Sangsuwan, R., Yik, J. H., Owen, M., Liu, G.-Y., Haudenschild, D. R., and Lewis, J. S. (2022). Intra-articular injection of flavopiridol-loaded microparticles for treatment of post-traumatic osteoarthritis. *Acta Biomater.* 149, 347–358. doi:10.1016/j.actbio.2022.06.042
- Schumacher, H. R. (2003). Aspiration and injection therapies for joints. *Arthritis & Rheumatism* 49 (3), 413–420. doi:10.1002/art.11056
- Sharma, L. (2021). Osteoarthritis of the knee. *N. Engl. J. Med.* 384 (1), 51–59. doi:10.1056/nejmc1903768
- Sharony, R., Yu, P.-J., Park, J., Galloway, A. C., Mignatti, P., and Pintucci, G. (2010). Protein targets of inflammatory serine proteases and cardiovascular disease. *J. Inflamm.* 7 (1), 45–17. doi:10.1186/1476-9255-7-45
- Stefani, R. M., Lee, A. J., Tan, A. R., Halder, S. S., Hu, Y., Guo, X. E., et al. (2020). Sustained low-dose dexamethasone delivery via a PLGA microsphere-embedded agarose implant for enhanced osteochondral repair. *Acta Biomater.* 102, 326–340. doi:10.1016/j.actbio.2019.11.052
- Tellegen, A., Rudnik-Jansen, I., Pouran, B., De Visser, H., Weinans, H., Thomas, R., et al. (2018). Controlled release of celecoxib inhibits inflammation, bone cysts and osteophyte formation in a preclinical model of osteoarthritis. *Drug Deliv.* 25 (1), 1438–1447. doi:10.1080/10717544.2018.1482971
- Telleg, L. E., Treviño, E. A., Brimeyer, A. L., Reece, D. S., Willett, N. J., Gulberg, R. E., et al. (2018). Intra-articular TSG-6 delivery from heparin-based microparticles reduces cartilage damage in a rat model of osteoarthritis. *Biomaterials Sci.* 6 (5), 1159–1167. doi:10.1039/c8bm00010g
- Törmälä, S., Mononen, M. E., Aarnio, E., Arokoski, J., Korhonen, R. K., and Martikainen, J. (2018). Health-related quality of life in relation to symptomatic and radiographic definitions of knee osteoarthritis: data from Osteoarthritis Initiative (OAI) 4-year follow-up study. *Health Qual. Life Outcomes* 16 (1), 1–12. doi:10.1186/s12955-018-0979-7
- Vos, T., Allen, C., Arora, M., Barber, R. M., Bhutta, Z. A., Brown, A., et al. (2016). Global, regional, and national incidence, prevalence, and years lived with disability for 310 diseases and injuries, 1990–2015: a systematic analysis for the Global Burden of Disease Study 2015. *Lancet* 388 (10053), 1545–1602. doi:10.1016/s0140-6736(16)31678-6
- Vugmeyster, Y., Wang, Q., Xu, X., Harrold, J., Daugusta, D., Li, J., et al. (2012). Disposition of human recombinant lubricin in naive rats and in a rat model of post-traumatic arthritis after intra-articular or intravenous administration. *AAPS J.* 14, 97–104. doi:10.1208/s12248-011-9315-4
- Wongrakpanich, A., Khunkitchai, N., Achayawat, Y., and Suksiriworapong, J. (2023). Ketorolac-loaded PLGA-/PLA-Based microparticles stabilized by hyaluronic acid: effects of formulation composition and emulsification technique on particle characteristics and drug release behaviors. *Polymers* 15 (2), 266. doi:10.3390/polym15020266
- Xue, S., Zhou, X., Sang, W., Wang, C., Lu, H., Xu, Y., et al. (2021). Cartilage-targeting peptide-modified dual-drug delivery nanoplateform with NIR laser response for osteoarthritis therapy. *Bioact. Mater.* 6 (8), 2372–2389. doi:10.1016/j.bioactmat.2021.01.017
- Yang, J., Han, Y., Lin, J., Zhu, Y., Wang, F., Deng, L., et al. (2020). Ball-bearing-inspired polyampholyte-modified microspheres as bio-lubricants attenuate osteoarthritis. *Small* 16 (44), 2004519. doi:10.1002/sml.202004519
- Yu, H., Huang, C., Kong, X., Ma, J., Ren, P., Chen, J., et al. (2022). Nanoarchitectonics of cartilage-targeting hydrogel microspheres with reactive oxygen species responsiveness for the repair of osteoarthritis. *ACS Appl. Mater. Interfaces* 14 (36), 40711–40723. doi:10.1021/acsami.2c12703
- Zhang, H.-f., Wang, C.-g., Li, H., Huang, Y.-t., and Li, Z.-j. (2018). Intra-articular platelet-rich plasma versus hyaluronic acid in the treatment of knee osteoarthritis: a meta-analysis. *Drug Des. Dev. Ther.* 12, 445–453. doi:10.2147/dddt.s156724
- Zhang, X., Cai, D., Zhou, F., Yu, J., Wu, X., Yu, D., et al. (2020). Targeting downstream subcellular YAP activity as a function of matrix stiffness with Verteporfin-encapsulated chitosan microsphere attenuates osteoarthritis. *Biomaterials* 232, 119724. doi:10.1016/j.biomaterials.2019.119724
- Zhu, S., Lu, P., Liu, H., Chen, P., Wu, Y., Wang, Y., et al. (2015). Inhibition of Rac1 activity by controlled release of NSC23766 from chitosan microspheres effectively ameliorates osteoarthritis development in vivo. *Ann. Rheumatic Dis.* 74 (1), 285–293. doi:10.1136/annrheumdis-2013-203901



OPEN ACCESS

EDITED BY

Liqun Yang,
Shengjing Hospital of China Medical
University, China

REVIEWED BY

Bhupendra Gopalbhai Prajapati,
Ganpat University, Gujarat, India
Xuefang Hao,
Inner Mongolia University for
Nationalities, China

*CORRESPONDENCE

Guiyun Jin,
✉ 13976609625@163.com
Xueying Ji,
✉ jixueying@163.com

†These authors have contributed equally
to this work

RECEIVED 29 October 2023

ACCEPTED 11 December 2023

PUBLISHED 08 January 2024

CITATION

Wei S, Deng T, Wu C, Shi J, Liao Y,
Huang L, Liu Y, Zhong S, Ji X and Jin G
(2024), Application of modified sodium
alginate hydrogel for interventional
embolization of hemorrhagic diseases.
Front. Mater. 10:1329667.
doi: 10.3389/fmats.2023.1329667

COPYRIGHT

© 2024 Wei, Deng, Wu, Shi, Liao, Huang,
Liu, Zhong, Ji and Jin. This is an
open-access article distributed under
the terms of the [Creative Commons
Attribution License \(CC BY\)](https://creativecommons.org/licenses/by/4.0/). The use,
distribution or reproduction in other
forums is permitted, provided the
original author(s) and the copyright
owner(s) are credited and that the
original publication in this journal is
cited, in accordance with accepted
academic practice. No use, distribution
or reproduction is permitted which does
not comply with these terms.

Application of modified sodium alginate hydrogel for interventional embolization of hemorrhagic diseases

Shengchao Wei^{1,2,3†}, Tang Deng^{4†}, Caixia Wu^{3,5†}, Jianshan Shi¹,
Yong Liao¹, Lin Huang⁴, Yongjie Liu^{3,5}, Shijie Zhong¹,
Xueying Ji^{5*} and Guiyun Jin^{1,2,3*}

¹Department of Interventional Radiology and Vascular Surgery, The First Affiliated Hospital of Hainan Medical University, Hainan Medical University, Haikou, China, ²Department of Emergency, The First Affiliated Hospital of Hainan Medical University, Hainan Medical University, Haikou, China, ³Key Laboratory of Emergency and Trauma of Hainan Medical University, Ministry of Education, Key Laboratory of Hainan Trauma and Disaster Rescue, Hainan Medical University, Haikou, China, ⁴Division of Vascular Surgery, The First Affiliated Hospital, Sun Yat-sen University, Guangzhou, China, ⁵Hainan Medical University, Haikou, China

Traditional particulate embolic agents are small in diameter, but can easily embolize the ends of blood vessels, resulting in ischemia and necrosis of normal tissues and organs. The metal spring embolic agent has a larger diameter, but it cannot be degraded and can easily cause permanent damage to blood vessels. Ideally, a bleeding embolism should achieve rapid hemostasis without causing long-term necrosis of organs and tissues. In this study, a modified sodium alginate hydrogel (MSAH) was prepared by mixing an oxidized sodium alginate (OSA) aqueous solution with a carboxymethyl chitosan (CMC) aqueous solution at a ratio of 1:6 in a 38°C bath for 8 min. The feasibility of this modified hydrogel was then tested in an internal iliac artery hemorrhage model using New Zealand rabbits. The MSAH had good adhesion. The hydrogel was injected through a single curved 4F catheter without obvious effects on uterine smooth muscle cell proliferation and apoptosis. The blood flow of the internal iliac artery was restored by long-term degradation of the sodium alginate hydrogel, and no ischemia and necrosis were observed by histopathology. The MSAH prepared using a mixture of OSA and CMC had good adhesion, biocompatibility, and injectability and could be used for target-vessel embolization in an internal iliac artery hemorrhage model. The MSAH can achieve main artery embolization without affecting the peripheral artery blood supply, resulting in both short-term rapid hemostasis and long-term degradation, with no target organ necrosis.

KEYWORDS

modified sodium alginate hydrogel, embolic agent, animal model of hemorrhage, interventional embolization, biomaterial

Introduction

Hemorrhagic diseases, including pelvic fracture bleeding, postpartum hemorrhage (PPH), and acute upper gastrointestinal bleeding (AUGIB), are commonly seen in emergency departments, accounting for approximately 15%–20% of emergent visits every year (Majeed et al., 2016). Pelvic fractures account for about 3% of all fractures

(Chen et al., 2017) and are the main cause of death within 24 h after injury due to massive bleeding, with a fatality rate of as high as 40% (Cothren et al., 2007). In addition, the proportion of pregnant and lying-in women aged over 35 years was as high as 17.13% nationwide, and 53.9% of maternal deaths were directly due to obstetric causes, with PPH being the number one cause of maternal death (Butwick et al., 2020; Liu and Lei, 2020; Zaidi et al., 2020). Furthermore, in the United States, more than 400,000 patients have been hospitalized every year because of AUGIB, with an annual death toll of more than 30,000 people (Cappell and Friedel, 2008).

Early and rapid hemostasis, including drug hemostasis, surgery, and interventional therapy, is critical for the treatment of hemorrhagic diseases. Interventional hemostatic therapy achieves the goal of hemostasis by identifying the bleeding vessel using digital subtraction angiography (DSA) and blocking the blood flow using embolic materials. Interventional therapy has become the first choice for the treatment of fatal bleeding diseases due to several advantages such as accuracy, rapidity, minimal invasion, no absolute contraindication, and repeatability. Ideally, a bleeding embolism should achieve rapid hemostasis without long-term necrosis of the tissues and organs. At present, the commonly used endovascular embolic materials include gelatin sponge particles (Alicon), alginate microspheres (SHENGYIYAO), polyvinyl alcohol (Merit), and metal coils (COOK, Boston). Traditional particulate embolic agents have a diameter of 100–2,000 μm , but these can block the vascular ends and cause ischemia and necrosis of normal tissues and organs. Although metal coils have a relatively large diameter and can block the vascular trunks, they cannot be degraded, and thus can easily cause permanent damage to blood vessels.

Oxidized sodium alginate (OSA) has been widely prepared as a biomedical material due to its swelling, extensibility, biocompatibility, adhesion, and biodegradability. Chen et al. planted rabbit bone marrow mesenchymal stem cells on SA hydrogel scaffolds, and the mesenchymal stem cells demonstrated survival after 1, 3, 5, and 7 days of culture on the scaffolds. On day 7, the cells proliferated rapidly on the scaffolds, and the cells exhibited a spindle shape, indicating that the mesenchymal stem cells not only survived on the scaffolds but could proliferate and differentiate normally. Thus, the alginate hydrogel scaffolds showed good biocompatibility. Mineralized alginate microspheres (M-ALG) have good biocompatibility and osteogenic properties (Chen et al., 2018). To verify the degradability of OSA, Park et al. conducted two cartilage regeneration studies on alginate and OSA. They preferentially mixed unoxidized SA with hyaluronic acid and injected this mixture with calcium to form a physical hydrogel for cartilage regeneration. They found that the non-oxidized alginate hydrogel remained in the animal model after cartilage regeneration, but under the same conditions, the oxidized alginate hydrogel treated with alginate completely degraded within 60 days (Park and Lee, 2014). Zhao et al. loaded SA hydrogel microspheres onto chondrocytes of New Zealand rabbits to study the degradation of the SA hydrogel microspheres. They found that the degradation time of the SA hydrogel *in vivo* and *in vitro* was 1 week and 4 weeks, respectively, and the complete degradation time was 4 and 6 weeks, respectively (Yu et al., 2016). In addition, Wu et al. subcutaneously implanted the SA hydrogel scaffold seeded with Schwann cells in the backs of rats, and showed that some of the alginate

hydrogel scaffolds were degraded 4 weeks later (Wu et al., 2020). Devi et al. prepared calcium ion crosslinked alginate composite microspheres as bone graft substitutes (Yashaswini et al., 2021; Liu et al., 2023).

OSA is often used to prepare SA microspheres. The alginate microsphere is commonly used in embolization treatment of benign and malignant tumors and achieves the therapeutic goal of causing tumor necrosis. However, when used for the treatment of hemorrhagic diseases, due to its small diameter, it can embolize the ends of blood vessels and cause ischemia and necrosis of normal tissues and organs (Tada et al., 2007). In this study, we prepared a modified SA hydrogel by mixing an OSA aqueous solution with a carboxymethyl chitosan (CMC) aqueous solution. The modified hydrogel retains the advantages of SA, such as biocompatibility, non-toxicity, and degradability, but also possesses new characteristics such as high strength and strong viscosity. Because the hydrogel does not embolize the terminal branch of the bleeding artery and can be degraded, it cannot cause long-term ischemia and necrosis of organs and is expected to become a new and safe embolic material for clinical application.

Materials and methods

Instruments and materials

The instruments and materials used in this study include biomicroscope (Laika, Germany), analytical balance (Seidolis), collector magnetic agitator (Jintan Medical Instrument Factory), digital subtraction angiography (GE), SA (Shenyang Bramble), CMC (Shanghai Macklin), sodium periodate (Zhejiang Haichuan), ethanol (Xilong Science and Technology), 21 G needle (Cook, United States), V18 Guide Wire (Boston Scientific, United States), microcatheter micro guide wires (Boston Scientific, United States), iohexol injection (GE, United States), Semisynne II (Dunhua Santa), Choutet 50 (Vicker, France), GELFOAM particles (ALICON), and embolized coil (COOK, United States).

Laboratory animals

New Zealand female rabbits (6 months old, weighing 8–10 kg) were purchased from Tian Qin, Changsha, China (permit no. SCXK (Hunan) 2019-0015). The animals were bred and treated according to the requirements for the management of experimental animals.

Preparation of MSAH

A dispersion of SA in ethanol was prepared by dissolving 10 g of SA in 50 g of ethanol using an analytical balance and stirring for 2 h using a magnetic agitator heated by a collector. NAI04 was dissolved in 50 mL of pure water, and the sodium periodate was dissolved in 50 mL of pure water. The mixture was mixed at room temperature in the ratio of N (NAIO4/SA) = 1 and then left to react in the dark for 4 h. After the oxidation reaction was completed, ethylene glycol with the same mass fraction as NAI04

was added, and the reaction was stopped for 30 min. SA was precipitated using ethanol with a volume ratio of 1:5, and the powder was obtained. After vacuum drying, the residual iodate and ethanol were removed using dialysis with distilled water for 3 days, and the OSA powder was obtained using lyophilization of the purified product.

OSA and CMC were mixed in a flask at ratios of 1:1, 1:2, 1:4, 1:6, 1:8, and 1:10, and shaken for 1 min. The mixture was placed in a 38°C bath for 1–9 min. The time for formation of the OSA aqueous solution and CMC aqueous solution was observed to obtain the fastest gelatinous ratio of the solution with the fastest gel formation time. To obtain the best gel formation time, the modified sodium alginate hydrogel (MSAH) was placed in the bath for 1–9 min and then injected onto glass slides with a 5-mL syringe to observe gel formation.

Biocompatibility of the injectable MSAH

Uterine smooth muscle cells (USMCs) were cultured in a high glucose medium (Control group) and high glucose medium with the MSAH (MSAH group). The growth of the USMCs was observed at 3, 6, 12, 24, 48, and 72 h. After culturing for 72 h, the cell proliferation rate was detected using the CCK8 kit, and apoptosis rates were detected using flow cytometry.

Injectability and adhesion of the MSAH

The MSAH was extracted with a 1-mL syringe and injected through a 4F single-curved catheter and a microcatheter, respectively. The injectability of the MSAH was evaluated by observing whether the MSAH was successfully injected on the glass slides through a 4F single curved catheter and microcatheter. The MSAH was injected into food-grade silica gel tubes with inner diameters of 16, 12, and 5 mm, respectively, and the adhesion to the tube wall was observed.

Evaluating the effects of the MSAH in the animal hemorrhage model

Twenty New Zealand female rabbits (3 months old, weighing 8–10 kg) were randomly divided into four groups ($n = 5$ for each group): Control group; MSAH group, embolized with MSAH; Gelfoam group, embolized with gelfoam particles; and Coil group, embolized with coil. The internal iliac artery (IIA) hemorrhage model was successfully established in the MSAH group, Gelfoam group, and Coil group, and the internal iliac arteries were embolized by injecting the MSAH, gelfoam particles, and coils via a microcatheter, respectively. Embolization was evaluated using angiography immediately after embolization. The puncture point of the left CCA was pressed with a gelatin sponge for 30 min until no blood overflow from the CAA was observed. The operation area was sterilized, and the skin was sutured and bandaged with sterile gauze. After waking from anesthesia, the rabbits were placed back in the experimental center, and penicillin (500,000 u/d) was administered

1 week after the operation to prevent infection. DSA was performed 1 month after the operation to check the recanalization of the bilateral internal iliac arteries.

Assessment of plasma inflammatory factors

Blood (2 mL) was collected from the ear vein into a sterile centrifuge tube containing sodium citrate after the first angiography in the Control group, and 3 days after IIA embolization in the MSAH group, Gelfoam group, and Coil group. After centrifugation, the plasma was collected with a pipette and the precipitate was discarded. Plasma levels of tumor necrosis factor- α (TNF- α) and interleukin (IL)-1 β were determined using ELISA kits.

Histopathology

The rabbits were euthanized by air embolism after the first angiography (Control group) or after bilateral IIA embolization (MSAH group, Gelfoam group, and Coil group). The uterus was removed to observe pathological changes in the uterine smooth muscle using hematoxylin and eosin (HE) staining.

ELISA

The uterus was cut with scissors, and the tissue was homogenized in a glass homogenizer. After centrifugation at 4°C, the supernatant was obtained. The levels of tumor growth factor (TGF- β) and IL-1 β in the tissue homogenates were detected using ELISA kits.

Statistical analysis

SPSS25.0 statistical software was used to analyze the data. Data with normal distribution are expressed as mean and standard deviation and were analyzed using the independent sample *t*-test. $p < 0.05$ was considered statistically significant.

Results

Preparation and performance evaluation of MSAH

The OSA aqueous solution and CMC aqueous solution at a ratio of 1:1 was largely ungelatinized. The mixtures at ratios of 1:2, 1:4, 1:6, 1:8, and 1:10 were gelatinized at 4 min and complete gelatinization was achieved at 15 min in a 38°C water bath (Figure 1A). The mixture at the ratio of 1:6 had the fastest gelatinization time, which exhibited gelatinization at 4 min and stabilized at 8 min (Figure 1B). A stable MSAH was prepared by placing the OSA aqueous solution and CMC aqueous solution at a ratio of 1:6 into a 38°C water bath for 8 min and was injected on the slide using a syringe, a glue-head

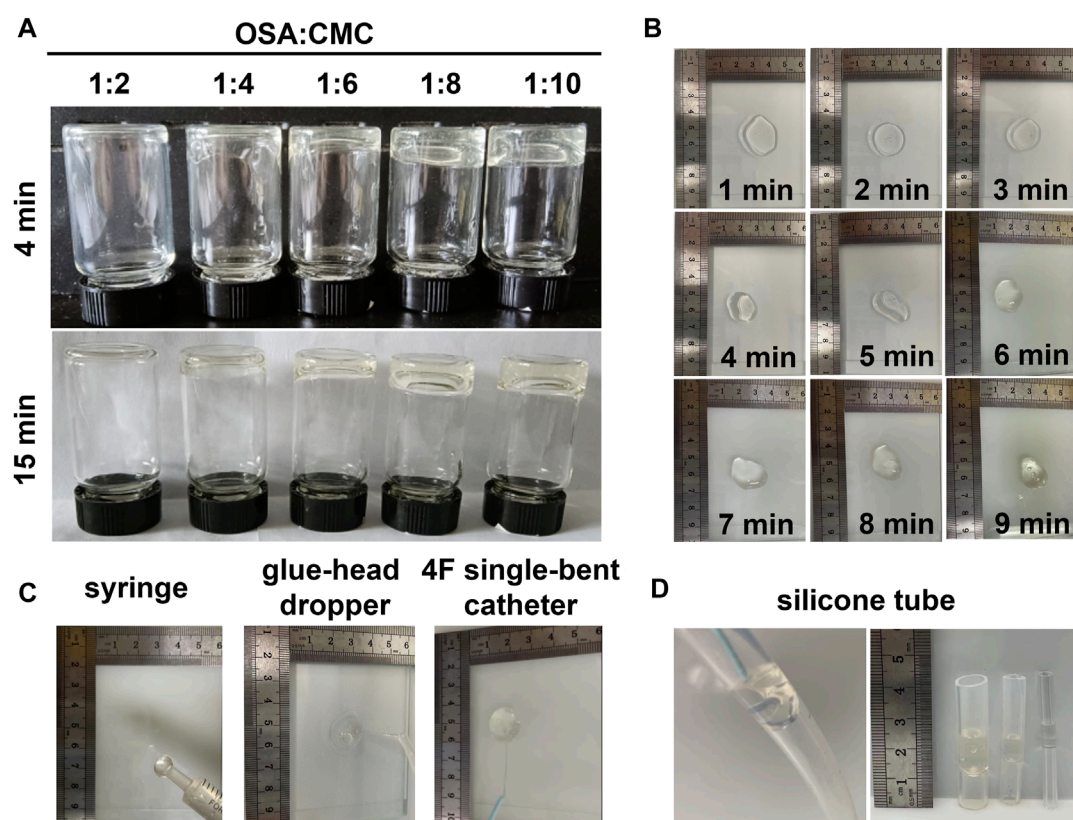


FIGURE 1

Preparation and evaluation of MSAH. (A) OSA aqueous solution: Gelling of CMC aqueous solution at different proportions; (B) gel formation of MSAH at different times in the water bath; (C) injectability of the MSAH was verified by using 1 mL syringe, 4F single curved catheter and microcatheter; (D) The MSAH was injected into food-grade silica gel tubes with inner diameters of 16mm, 12mm and 5 mm to verify its adhesion.

dropper, and a 4F single-bent catheter (Figure 1C). The hydrogel was injected into silicone tubes using a syringe through a 4F single-bent catheter and adhered to different diameters of silicone tube walls (Figure 1D).

USMCS WERE treated with MSAH for 72 h in the MSAH group (Figure 2A). There was no significant difference in the proliferation rate between the MSAH group and the Control group ($p > 0.05$; Figure 2B), and there was no significant difference in the apoptosis rate between the MSAH group and the control group (Figures 2C–E).

Establishment of the hemorrhage model

New Zealand female rabbits were fasted for 12 h before the operation. Anesthesia was induced by xylazine hydrochloride injection II (2 mg/kg) and maintained by intravenous injection of Zoletil (7.5 mg/kg). The left common carotid artery (CCA) was passively separated using elbow hemostatic forceps (12.5 cm) (Figure 3). After placement of 2–0 Mousse thread at the proximal and distal segments, the left CCA was punctured with a 21 g micropipette, and a V18-wire exchange microcatheter was inserted. Heparin saline (0.5 mg/kg) was infused into the artery according to the weight of rabbits.

Under the road map, the microcatheter was super-selected into the left internal iliac artery. After the microcatheter was fixed, the microcatheter was removed, and the hard end of the V18 guide wire was entered into the microcatheter to quickly puncture the left internal iliac artery. The leakage of contrast media in the left IIA was confirmed using angiography. Before and 10 min after the establishment of the IIA hemorrhage model, 5 mL of whole blood was taken from the ear vein and placed into the blood collection tube containing EDTA-k2 anticoagulants. Red blood cell (RBC) count, hemoglobin (HGB) content, and hematocrit (HCT) were measured using a hematology analyzer. No infection, death, hematuria, bloody stool, hemiplegia, lip deviation, or any other complications of cerebral infarction were found in any of the rabbits. In the first 3 days after modeling, the appetite and mental state of the rabbits decreased.

DSA of the rabbit model

According to the angiographic findings, the vascular anatomy of the rabbit was similar to that of the human body. Angiographic results via subclavian artery catheterization showed that the brachiocephalic trunk (BCT), left CCA, left subclavian artery (LSA), and right subclavian artery (RSA) originated from the aortic arch.

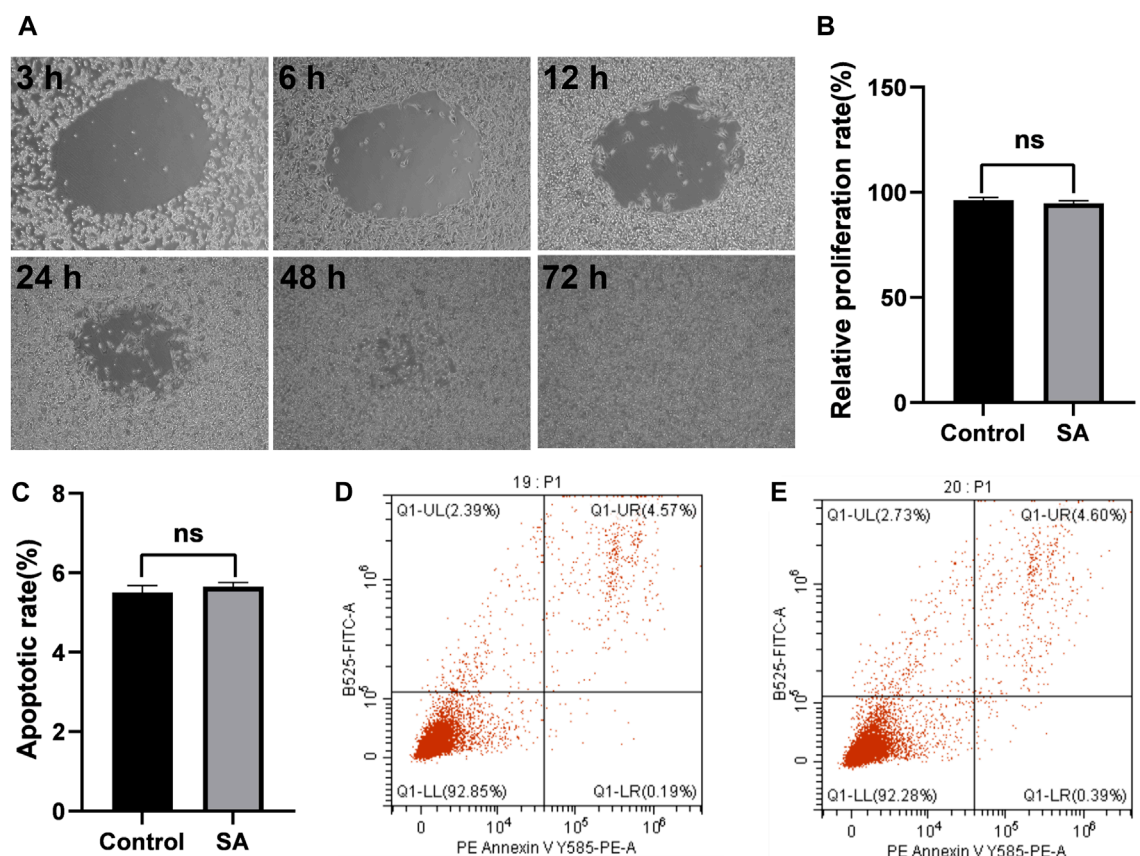


FIGURE 2

Cell compatibility of the MASH. (A) Proliferation of USMCs in the SA group at different times, (B) proliferation rate of USMCs in the MSAH group and Control group, (C) apoptosis rate of USMCs in the MSAH group and Control group, (D) apoptosis rate of USMCs in the Control group, and (E) apoptosis rate of USMCs in the MSAH group.

The celiac axis (CA), splenic artery (SA), superior mesenteric artery (SMA), left renal artery (LRA), and right renal artery (RRA) were visualized on the upper segment of the abdominal aorta, and the common iliac artery (CIA) was visualized on the lower segment of the abdominal aorta. The IIA was the first branch of the CIA, followed by the external iliac artery (EIA), common femoral artery (CFA), and deep femoral artery (DFA). The left IIA showed the superior gluteal artery (SGA), inferior gluteal artery (IGA), uterine artery (UA), vesical arteries (VA), and internal pudendal artery internal iliac artery (IPA) (Figure 4A).

DSA images before and after establishing the hemorrhage model

Before establishing the hemorrhage model, the bilateral IIA showed normal deformation without abnormal stenosis and tumor-like dilatation. After the microcatheter was placed on the left IIA, the left IIA was punctured by the hard end of the V18 guide wire, and signs of hemorrhage were observed, evidenced by the spilling of the contrast medium. After the bilateral IIA was super-selected

separately via the microcatheter and embolized with a self-made gelatin sponge strip, DSA showed that the bilateral IIA was blocked, and bleeding signs disappeared (Figure 4B).

Erythrocyte count, hemoglobin and hematocrit

Before establishing the hemorrhage model, total RBC was $4.4 \times 10^{12}/L$, HGB content was 93 G/L, and HCT was 32%. After model establishment, the total RBC was $3.6 \times 10^{12}/L$, HGB content was 75 G/L, and HCT was 25%. The levels of RBC (Figure 4C), HGB (Figure 4D), and HCT (Figure 4E) after model establishment were significantly lower than before model establishment ($p < 0.01$).

Effects of different embolic materials in the hemorrhage model

DSA images before establishing the hemorrhage model showed that the bilateral IIA and its branches were visualized in the MSAH

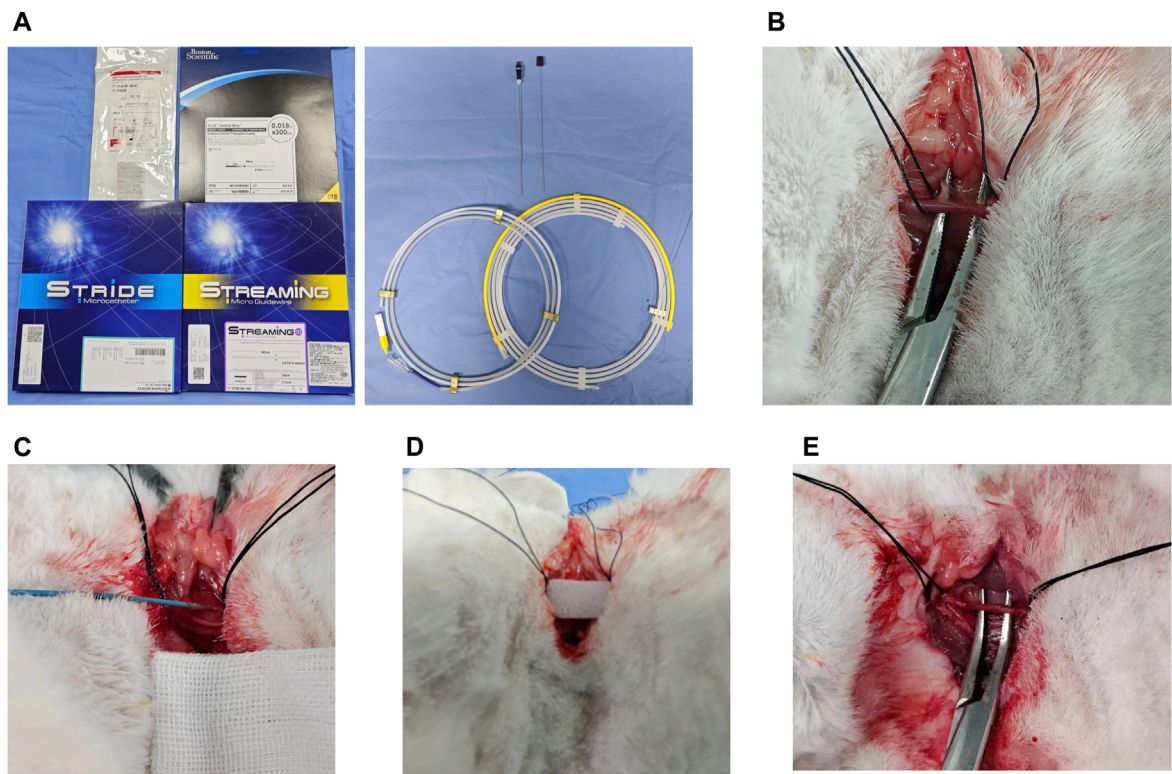


FIGURE 3
Hemorrhagic rabbit model established using interventional therapy. (A) Surgical instrument; (B) leaky carotid artery; (C) microcatheter placement in the carotid artery; (D) postoperative gelfoam tablet compression puncture point; and (E) carotid artery healed postoperatively.

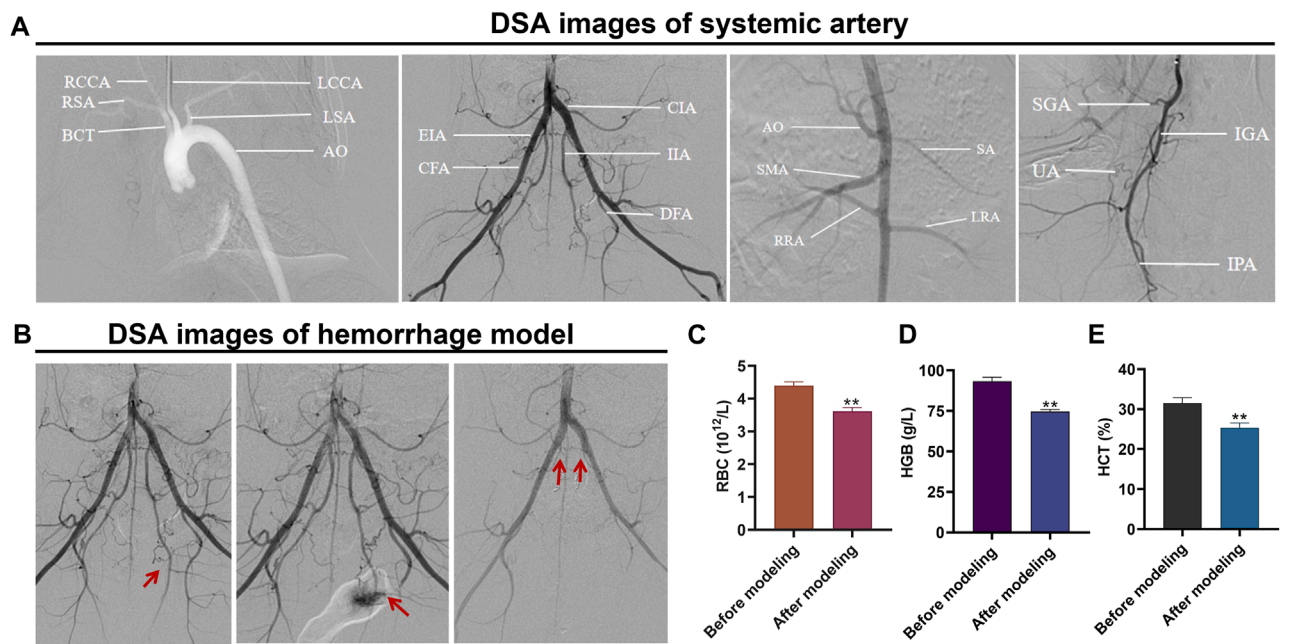
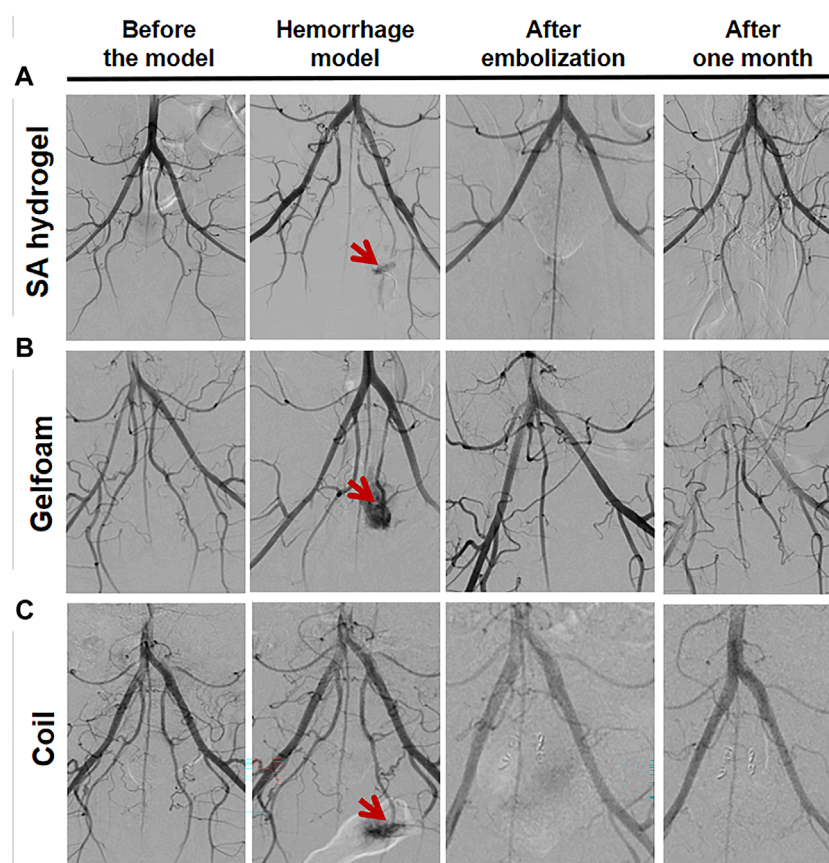


FIGURE 4
Hemorrhagic rabbit model established using interventional therapy. (A) DSA image of the systemic artery; (B) DSA images of the hemorrhage model before and after establishment and embolization; (C) changes in RBC, HGB, and HCT levels before and after establishment of the hemorrhage model; (D) changes in HGB levels before and after establishment of the hemorrhage model; and (E) changes in HCT levels before and after establishment of the hemorrhage model.

**FIGURE 5**

DSA images of IIA bleeding following embolization with different embolic materials. **(A)** DSA images of the MSAH group, **(B)** DSA images of the Gelfoam group, and **(C)** DSA images of the Coil group.

group, Gelfoam group, and Coil group, but the left IIA showed contrast agent overflow on DSA after the hemorrhage model was constructed. The bilateral IIA and its branches were not shown on DSA after embolization with the MSAH, and DSA taken 1 month later showed clear visualization of the bilateral IIA and its branches (Figure 5A). The bilateral IIA and its branches were not developed on DSA after embolization with the gelfoam particles, and DSA taken 1 month later showed no evidence of the bilateral IIA and its peripheral branches (Figure 5B). The bilateral IIA and its branches were not developed on DSA after embolization with the coil, and DSA taken 1 month later showed no evidence of the bilateral IIA and its peripheral branches (Figure 5C).

Effects of different embolic materials on plasma inflammatory factors in the hemorrhage model

Blood was withdrawn from the ear vein 3 days after the operation. Plasma levels of TNF- α and IL-1 β were detected using ELISA kits. The TNF- α levels were significantly higher in the MSAH group ($p < 0.05$), in the GELFOAM group ($p < 0.01$), and in the Coil group ($p < 0.01$) compared to the Control group. Compared

with the MSAH group, the TGF- α levels were significantly higher in the Gelfoam group ($p < 0.01$) and in the Coil group ($p < 0.01$) (Figure 6A). Compared with the Control group, the plasma levels of IL-1 β were significantly higher in the Gelfoam group ($p < 0.01$) and in the Coil group ($p < 0.01$), but not in the MSAH group ($p > 0.05$). The plasma levels of IL-1 β were significantly increased in the Gelfoam group ($p < 0.01$) and the Coil group ($p < 0.01$) compared to the MSAH group (Figure 6B).

Changes in inflammatory factors in the uterine tissues after embolization in the hemorrhage model

The uterine homogenate supernatant was obtained 3 days after the second operation in the Control group and after bilateral IIA embolization in the MSAH group, Gelfoam group, and Coil group. Compared with the Control group, the TGF- α levels in the MSAH group ($p < 0.01$) and the Gelfoam group ($p < 0.01$) were significantly increased. Compared with the Control group, the TGF- α level in the Coil group was significantly increased ($p < 0.01$). The TGF- α levels in the Gelfoam group were significantly increased compared with the MSAH group ($p < 0.01$). The TGF- α levels were significantly

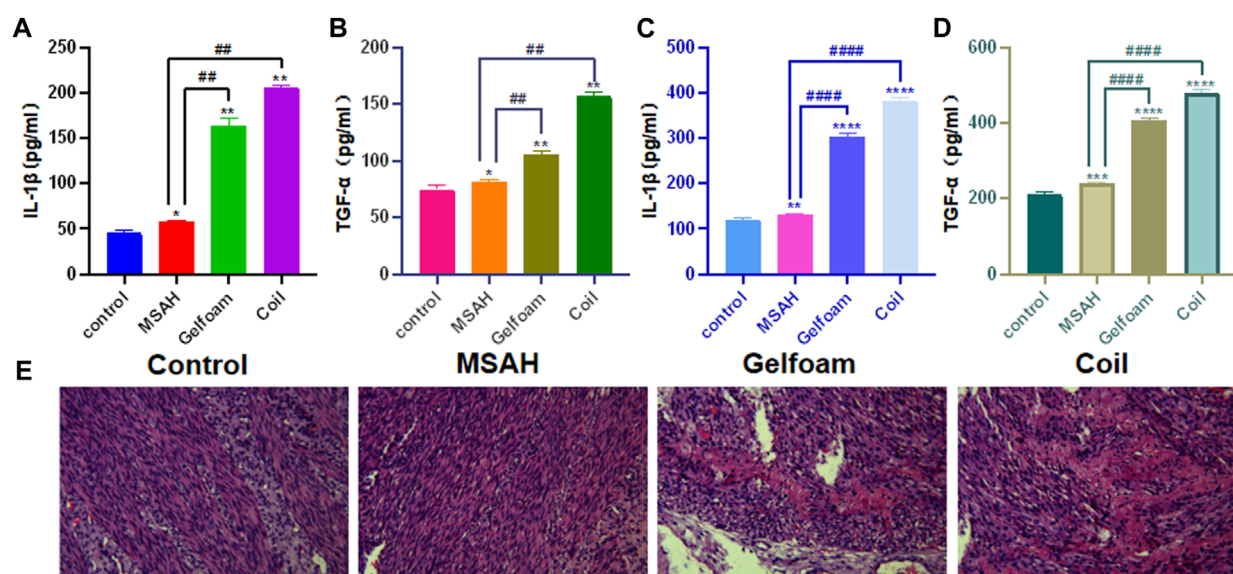


FIGURE 6

Evaluation of IIA hemorrhage after embolization with different embolic materials (A) ELISA for plasma IL-1 β , (B) ELISA for plasma TGF- α , (C) ELISA for homogenate IL-1 β , (D) ELISA for homogenate TGF- α ; and (E) histopathology analyses.

higher in the Coil group compared to the MSAH group ($p < 0.01$) (Figure 6C). Compared with the blank control group, the IL-1 β levels were significantly higher in the MSAH group ($p < 0.01$), in the Gelfoam group ($p < 0.01$), and in the Coil group ($p < 0.01$). The IL-1 β levels in the Gelfoam group were significantly higher than that in the MSAH group ($p < 0.01$), and the IL-1 β levels in the coil group were significantly higher than that in the MSAH group ($p < 0.01$) (Figure 6D).

Effect of different embolic materials on myometrium histopathology in a model of bleeding

Uterine pathology showed no lytic necrotic smooth muscle cells in the myometrium in the Control group. There were no necrotic smooth muscle cells in the myometrium in the MSAH group. There were moderate amounts of necrotic smooth muscle cells in the myometrium in the Gelfoam group. There was a large number of lytic and necrotic smooth muscle cells in the myometrium in the Coil group (Figure 6E).

Discussion

In this study, SA was dissolved in ethanol, dispersed by magnetic stirring, and then mixed with NAO4 in different proportions for oxidation. Using this method, the oxidation effect was relatively satisfactory when the ratio of NAO4/SA was 1. The alginate was oxidized by NAO4 twice during the oxidation process, and the carbon-carbon bond of the alginate chain was destroyed after each oxidation, resulting in two aldehydes. The aldehydes increase the number of active functional groups of alginates, which makes

alginate biodegradable. This study provides a theoretical basis for the application of MSAH as a degradable vascular embolic material. In addition, the swelling rate and degradation rate of alginate can be adjusted by changing the oxidation degree (OD) of OSA. It has been reported that OSA, which has higher OD values, has a higher water absorption rate and higher degradation rate (Cai K et al., 2007). The biodegradable properties of alginate provide a new choice for biological tissue materials.

OSA powder was dissolved in purified water to prepare the OSA aqueous solution at 100 mg/mL, and CMC was dissolved in purified water to prepare the CMC aqueous solution at 30 mg/mL. The Schiff base reaction between the aldehyde group of OSA and the amino group of CMC is a mild chemical covalent cross-linking reaction, which does not require special and difficult reaction conditions. The Schiff base reaction is also a rapid reaction to ensure the speed of gelation. The rapid gelation of the MSAH provides a theoretical basis for its function as a vascular embolization material. In addition, when kept at 38°C for a longer time, the MSAH is more stable, adhesive, and hard, but the injectability worsens. Therefore, it is necessary to find an optimal water bath time to ensure the injectability of the modified alginate hydrogel with certain adhesion and hardness. Here, we found that the MSAH not only adhered to the wall of the silica gel tube but also had a certain hardness when the hydrogel was incubated in the water bath for 8 min. In addition, the hydrogel was successfully injected into the silica gel tube using a 1-mL syringe through a microcatheter.

It has been reported that Cynomolgus monkeys, pigs, dogs, rabbits, and mice can be used to establish a hemorrhage model. Although pigs, monkeys, and dogs have advantages, including large body size, thick blood vessels, and relatively easy intravascular intervention, they also have some disadvantages such as high cost and high demand for feeding site and conditions. Mice are

less costly and the feeding condition is simple, but the size of the mouse is too small and the blood vessels are thin, resulting in extreme difficulty of intravascular interventional procedures. The rabbit model of pelvic hemorrhage established in this study has been used in basic research to investigate the efficacy of interventional embolic materials. New Zealand rabbits are medium in size, and the vessel diameter is suitable for intravascular interventional procedures. In addition, the rabbits are not too costly and the feeding conditions are not demanding (Gao et al., 2008; Zhu et al., 2009; Chi Keung et al., 2014; Chang et al., 2018; Yu and Yi, 2019; Huang et al., 2021). Furthermore, the CIA of New Zealand rabbits is divided into the bilateral IIA and EIA, and the UA originates from the IIA, which is similar in humans (Liu et al., 2020). In this study, we found that the shape and anatomy of the arteries in the New Zealand rabbits nicely paralleled human anatomy.

Ideal bleeding embolism should achieve rapid hemostasis, without long-term necrosis of organs and tissues. At present, the commonly used materials for intravascular embolization are gelatin sponge particles, polyvinyl alcohol microspheres, and metal coils. Traditional particulate embolic agents are small in diameter, but can easily embolize the ends of blood vessels, resulting in ischemia and necrosis of normal tissues and organs. The metal spring embolic agent has a larger diameter but cannot be degraded and can easily cause permanent damage to blood vessels. Some studies have found that SA has the properties of swelling, biocompatibility, adhesion, and biodegradability. However, there are some disadvantages of using alginate alone as the embolic material, including weak mechanical properties of the gel, fragile gel structure in physiological saline, poor adhesion of the gel, and ease of embolizing vascular terminals due to its small particle diameter. In this study, the MSAH was prepared by oxidizing SA and then mixing it with a CMC aqueous solution at a certain proportion. This modification not only has the advantages of SA, such as biocompatibility, non-toxicity, and degradability, but also has new characteristics of high strength, strong viscosity, and embolization of the main arteries of bleeding vessels without influence on the vascular ends.

In this study, the MSAH was used to embolize the bilateral IIA in a New Zealand rabbit hemorrhage model. The modified alginate hydrogel resulted in the development of both sides of IIA and peripheral arteries, suggesting the long-term degradability of the modified alginate hydrogel. One month after embolization, the myometrium had almost no lysis and necrosis of myometrial smooth muscle cells, suggesting that the MSAH did not affect the blood flow of peripheral blood vessels and did not cause tissue ischemia and necrosis. It has been reported (Prieto-Moure et al., 2017; Xu et al., 2017) that tissue cells produce and release TNF- α after tissue ischemia to activate T cells, promote the production and secretion of IL-1 β , and induce inflammation. In this study, we found that the levels of TNF- α and IL-1 β both in the plasma and uterine tissue were significantly lower in the MSAH group than in the Gelfoam group and the Coil group, suggesting that MSAH can induce a slight inflammatory reaction and does not cause the peripheral tissue necrosis.

Altun et al. combined platelet rich fibrin fraction, nanoclay, and ethiodized oil to prepare a novel embolic biomaterial, blood-derived embolic materials (BEM). However, the disadvantages of

BEM are that it is a permanent embolism, which can easily lead to ischemic necrosis of organs and tissues (Altun et al., 2020). Rong et al. prepared a new biodegradable macromolecule material (thrombin-loaded alginate-calcium microspheres (TACMs), which is capable of hemostasis in a rabbit model of renal hemorrhage. TACMs are biodegradable, but due to their small diameter, they can easily embolize the peripheral blood vessels and cause tissue necrosis (Rong et al., 2015).

Through this study, we found that, on the one hand, MSAH can quickly embolize bleeding vessels with its strong viscosity and high intensity, but on the other hand, MSAH is characterized by good biocompatibility and degradability. After embolization of the bleeding vessels, we observed a mild inflammatory reaction and no necrosis of the peripheral tissues. Thus, MSAH could potentially be used in the treatment of varying bleeding diseases, such as postpartum hemorrhage, acute gastrointestinal bleeding, traumatic rupture of parenchymal organs, bronchial artery hemorrhage, and tumor hemorrhage.

Conclusion

In summary, MSAH not only has the same advantages of an alginate hydrogel such as biocompatibility, non-toxicity, and degradability, but also possesses new characteristics such as high strength and strong viscosity. In addition, the material can quickly embolize the main artery to stop bleeding in the early stage but does not embolize the peripheral branches of the bleeding artery to cause organ necrosis. Furthermore, the material can be degraded in the medium- and long-term without affecting the blood supply to the organs. This MSAH could be a new embolic material for clinical application.

Data availability statement

The original contributions presented in the study are included in the article/supplementary material, further inquiries can be directed to the corresponding authors.

Ethics statement

The animal study was approved by Animal Experimental Ethics Committee of Hainan Medical University. The study was conducted in accordance with the local legislation and institutional requirements.

Author contributions

SW: Conceptualization, Data curation, Methodology, Writing—original draft. TD: Conceptualization, Methodology, Writing—review and editing. CW: Data curation, Writing—original draft. JS: Conceptualization, Writing—original draft. YL: Data curation, Writing—original draft. LH: Conceptualization, Writing—original draft. YL: Data curation, Writing—original draft. SZ: Conceptualization, Data curation, Writing—original draft. XJ: Conceptualization, Methodology, Writing—review and editing. GJ:

Conceptualization, Funding acquisition, Methodology, Resources, Validation, Writing–review and editing.

Funding

The author(s) declare financial support was received for the research, authorship, and/or publication of this article. Natural Science Foundation of Hainan Province (820RC764, 823MS146), 2023 Provincial College Student Innovation and Entrepreneurship Training Program (S202311810051), Hainan Provincial Health Commission Scientific Research Project (22A200032), National College Students Innovation and Entrepreneurship Training Program (202211810017), Hainan Key Research and Development Social Development Project (ZDYF2022SHFZ293), and Hainan Province Clinical Medical Center (2021).

References

- Altun, I., Hu, J., Albadawi, H., Zhang, Z., Salomao, M. A., Mayer, J. L., et al. (2020). Blood-derived biomaterial for catheter-directed arterial embolization. *Adv. Mater.* 32 (52), e2005603. doi:10.1002/adma.202005603
- Butwick, A., Lyell, D., and Goodnough, L. (2020). How do I manage severe postpartum hemorrhage? *Transfusion* 60 (5), 897–907. doi:10.1111/trf.15794
- Cai, K., Zhang, J., Deng, L., Yang, L., Hu, Y., Chen, C., et al. (2007). Physical and biological properties of a novel hydrogel composite based on oxidized alginate, gelatin and tricalcium phosphate for bone tissue engineering. *Adv. Eng. Mater.* 9 (12), 1082–1088. doi:10.1002/adem.200700222
- Cappell, M. S., and Friedel, D. (2008). Initial management of acute upper gastrointestinal bleeding: from initial evaluation up to gastrointestinal endoscopy. *Med. Clin. North Am.* 92 (3), 491–509. doi:10.1016/j.mcna.2008.01.005
- Chang, P., Cui, Y., and Xuemei, J. (2018). Application of ultrasound guidance in the establishment of rabbit model of knee joint hemorrhage. *Chin. J. Integr. Traditional West. Med.* 16 (5), 465–467.
- Chen, P., Xia, C., Mo, J., Mei, S., Lin, X., and Fan, S. (2018). Interpenetrating polymer network scaffold of sodium hyaluronate and sodium alginate combined with berberine for osteochondral defect regeneration. *Mater. Sci. Eng. C Mater. Biol. Appl.* 91, 190–200. doi:10.1016/j.msec.2018.05.034
- Chen, W., Lv, H., Liu, S., Liu, B., Zhu, Y., Chen, X., et al. (2017). National incidence of traumatic fractures in China: a retrospective survey of 512 187 individuals. *Lancet Glob. Health* 5 (8), e807–e817. doi:10.1016/s2214-109x(17)30222-x
- Chi Keung, T., Leung, M., and Ryoo, R. (2014). Application of minimally invasive balloon occlusion combined with surgical suture in the treatment of hemorrhagic renal injury in dogs. *PLA Med. J.* 26 (1), 10–12.
- Cothren, C. C., Osborn, P. M., Moore, E. E., Morgan, S. J., Johnson, J. L., and Smith, W. R. (2007). Preperitoneal pelvic packing for hemodynamically unstable pelvic fractures: a paradigm shift. *J. Trauma* 62 (4), 834–842. doi:10.1097/TA.0b013e31803c7632
- Gao, C., Chen, H., and Xiangzhen, L. (2008). Rat subarachnoid hemorrhage model was made by three methods. *Chin. J. Minim. Invasive Neurosurg.* 13 (9), 409–411.
- Huang, Y., Wu, S., and Xianghui, C. (2021). Establishment of a model of iliac artery rupture and bleeding under ultrasound guidance. *Chin. J. Ultrasound* 18 (4), 407–411.
- Liu, X., and Lei, H. (2020). Prevention and management of postpartum hemorrhage. *Chin. J. Pract. Gynecol. Obstet.* 36 (02), 123–126. doi:10.19538/j.fk2020020109
- Liu, X., Wang, Y., Liang, Z., Lian, X., Huang, D., Hu, Y., et al. (2023). Progress in preparation and application of sodium alginate microspheres. *Sheng Wu Yi Xue Gong Cheng Xue Za Zhi* 40 (4), 792–798. doi:10.7507/1001-5515.202211048
- Liu, Y., Zhang, Y., Ding, Y., Li, J., Tang, Q., Zhang, X., et al. (2020). Successful orthotopic uterine allotransplantation in a rabbit model using aorta and cava anastomoses: a short-term viability study. *Arch. Gynecol. Obstet.* 301 (2), 533–544. doi:10.1007/s00404-019-05381-9
- Majeed, A., Hwang, H. G., Eikelboom, J. W., Connolly, S., Wallentin, L., Feuring, M., et al. (2016). Effectiveness and outcome of management strategies for dabigatran- or warfarin-related major bleeding events. *Thromb. Res.* 140, 81–88. doi:10.1016/j.thromres.2016.02.005
- Park, H., and Lee, K. Y. (2014). Cartilage regeneration using biodegradable oxidized alginate/hyaluronate hydrogels. *J. Biomed. Mater. Res. A* 102 (12), 4519–4525. doi:10.1002/jbm.a.35126
- Prieto-Moure, B., Lloris-Carsí, J. M., Belda-Antolí, M., Toledo-Pereyra, L. H., and Cejalo-Lapeña, D. (2017). Allopurinol protective effect of renal ischemia by downregulating TNF- α , IL-1 β , and IL-6 response. *J. Invest. Surg.* 30 (3), 143–151. doi:10.1080/08941939.2016.1230658
- Rong, J. J., Liang, M., Xuan, F. Q., Sun, J. Y., Zhao, L. J., Zhen, H. Z., et al. (2015). Alginate-calcium microsphere loaded with thrombin: a new composite biomaterial for hemostatic embolization. *Int. J. Biol. Macromol.* 75, 479–488. doi:10.1016/j.ijbiomac.2014.12.043
- Tada, D., Tanabe, T., Tachibana, A., and Yamauchi, K. (2007). Recognition of four structurally resembled benzoic acid derivatives by albumin-crosslinked poly(acrylamide) hydrogel. *Mater. Sci. Eng. C, Biomim. Supramol. Syst.* C27 (4), 895–897. doi:10.1016/j.msec.2006.10.009
- Wu, Z., Li, Q., Xie, S., Shan, X., and Cai, Z. (2020). *In vitro* and *in vivo* biocompatibility evaluation of a 3D bioprinted gelatin-sodium alginate/rat Schwann-cell scaffold. *Mater. Sci. Eng. C Mater. Biol. Appl.* 109 (12), 110530. doi:10.1016/j.msec.2019.110530
- Xu, B., Hu, Q. H., Zhao, B., and Zhou, Z. K. (2017). Variation and significance of serum leptin, blood lipid level, adiponectin, NO and TNF- α for patients with non-traumatic ischemic necrosis of the femoral head. *Saudi J. Biol. Sci.* 24 (8), 1763–1766. doi:10.1016/j.sjbs.2017.11.008
- Yashaswini, D. G. V., Prabhu, A., Anil, S., and Venkatesan, J. (2021). Preparation and characterization of dexamethasone loaded sodium alginate-graphene oxide microspheres for bone tissue engineering. *J. Drug Deliv. Sci. Technol.* 64, 102624. doi:10.1016/j.jddst.2021.102624
- Yu, J., and Yi, Z. (2019). Outline of traumatic hemorrhage model in swine. *J. Northwest Def. Med.* 40 (3), 144–148.
- Yu, Z., Wang-Ping, D., Jian-Gong, L. U., and Orthopedics, D. O. (2016). *In vivo* and *in vitro* degradation of calcium alginate beads combined with chondrocytes. *Orthop. J. China* 24 (12), 1101–1106.
- Zaidi, A., Kohli, R., Daru, J., Estcourt, L., Khan, K. S., Thangaratinam, S., et al. (2020). Early use of fibrinogen replacement therapy in postpartum hemorrhage-A systematic review. *Transfus. Med. Rev.* 34 (2), 101–107. doi:10.1016/j.tmr.2019.12.002
- Zhu, H., Qin, L., and Minghua, F. (2009). Establishment and evaluation of Cynomolgus monkey cerebral hemorrhage model. *Chin. J. Comp. Med.* 19 (7), 29–32.

Conflict of interest

The authors declare that the research was conducted in the absence of any commercial or financial relationships that could be construed as a potential conflict of interest.

Publisher's note

All claims expressed in this article are solely those of the authors and do not necessarily represent those of their affiliated organizations, or those of the publisher, the editors and the reviewers. Any product that may be evaluated in this article, or claim that may be made by its manufacturer, is not guaranteed or endorsed by the publisher.



OPEN ACCESS

EDITED BY

Liqun Yang,
Shengjing Hospital of China Medical
University, China

REVIEWED BY

Soodabeh Davaran,
Tabriz University of Medical Sciences, Iran
Guangqi Yan,
China Medical University, China

*CORRESPONDENCE

Yuanjun Xia,
✉ yuanjunxia@aliyun.com
Ying Zhang,
✉ zhangying_doc@aliyun.com

[†]These authors have contributed equally to
this work

RECEIVED 22 January 2024

ACCEPTED 11 April 2024

PUBLISHED 17 May 2024

CITATION

Zhao L, Zhao X, Deng F, Ye X, Shen Z, Xia Y
and Zhang Y (2024), Integration of
BMP-2/PLGA microspheres with the 3D
printed PLGA/CaSO₄ scaffold enhances bone
regeneration.
Front. Mater. 11:1374409.
doi: 10.3389/fmats.2024.1374409

COPYRIGHT

© 2024 Zhao, Zhao, Deng, Ye, Shen, Xia and
Zhang. This is an open-access article
distributed under the terms of the [Creative
Commons Attribution License \(CC BY\)](#). The
use, distribution or reproduction in other
forums is permitted, provided the original
author(s) and the copyright owner(s) are
credited and that the original publication in
this journal is cited, in accordance with
accepted academic practice. No use,
distribution or reproduction is permitted
which does not comply with these terms.

Integration of BMP-2/PLGA microspheres with the 3D printed PLGA/CaSO₄ scaffold enhances bone regeneration

Li Zhao^{1†}, Xiaoliang Zhao^{1†}, Fengpiao Deng^{1†}, Xiangling Ye^{2,3},
Zhen Shen⁴, Yuanjun Xia^{1,5*} and Ying Zhang^{1,5*}

¹Department of Orthopedics, General Hospital of Southern Command Theater of PLA, Guangzhou, Guangdong, China, ²Dongguan Hospital, Guangzhou University of Chinese Medicine, Dongguan, Guangdong, China, ³The Second Clinical College of Guangzhou University of Chinese Medicine, Guangzhou, Guangdong, China, ⁴Department of Rehabilitation, Kunming Municipal Hospital of Traditional Chinese Medicine, The Third Affiliated Hospital of Yunnan University of Chinese Medicine, Kunming, Yunnan, China, ⁵The First School of Clinical Medicine, Southern Medical University, Guangzhou, Guangdong, China

Treatment of large and complex irregular bone defects is a major clinical challenge in orthopedic surgery. The current treatment includes bone transportation using the Ilizarov technique and bone cement repair using the Masquelet technique, but they require long-term manual intervention or secondary operation. To improve this situation, we compared the different implanting materials in the literature published in the past 10 years, finding that glycolic acid copolymer (PLGA) and Calcium sulfate (CaSO₄) are appropriated to be used as synthetic bone materials due to their advantages of easy-availability, nontoxicity, osteogenic properties and rapid degradation. Meanwhile, the development of 3D printing technique and devices makes it relatively easier to synthesize customized bio-mimetic porous scaffolds, thus facilitating the release of modified protein. In this study, we compounded BMP-2/PLGA microspheres with polylactic glycolic acid copolymer/CaSO₄ (PC) 3D printed scaffold to improve the osteogenic properties of the scaffold. The result of our *in vitro* experiment demonstrated that the prepared PCB scaffold not only had satisfactory bio-compatibility, but also promoted osteogenic differentiation. This 3D printed scaffold is capable to accelerate the repair of complex bone defects by promoting new bone formation, suggesting that it may prove to be a potential bone tissue engineering substitute.

KEYWORDS

bone defect, 3D printed, PLGA microspheres, calcium sulfate, BMP-2

1 Introduction

Bone defects are one of the most common clinical conditions and can be caused by trauma, tumors and skeletal abnormalities (Giannoudis et al., 2011). With the development and prevalence of transportation, the incidence of open fractures caused by high-energy injuries is increasing and becoming a serious health problem worldwide. Such injuries often cause complex bone defects, which pose a great challenge for clinical management (Myeroff and Archdeacon, 2011). Allogeneic bone transplantation, and artificial bone transplantation are among the other methods for the treatment of bone defects. However, the

shortcomings of bone transplantation limit its wider application; for instance, the current relatively single and fixed clinical bone graft substitutes are far from adequate for filling and repairing complex and variable bone defects (Dimitriou et al., 2011). Compared with simple internal fixation, bone transplantation usually takes months to complete numerous surgeries including installing and removing the bone material, or using an external fixator for the large bone defect, which often requires a relatively long rehab process, while the recovery of limb function may not be fully satisfied. As the currently available materials and techniques cannot meet all clinical requirements for large bone defects, there is an urgent need to search for a biomaterial that can meet the needs of various types of bone defects.

In recent years, three-dimensional (3D)-printed technology has received increasing attention in bone tissue engineering, knowing that it can obtain porous scaffolds with certain mechanical properties through precise parameter design (Kumar et al., 2011). Such scaffolds can not only meet a variety of bone defect filling requirements at the macroscopic level but also provide a good microenvironment for bone tissue regeneration and promote bone healing by simulating the natural human bone through precise parameter design (Lutzweiler et al., 2020). A variety of materials have been developed and used for 3D-printed scaffolds, including natural polymers (Liu et al., 2019; Farris et al., 2022), metals (Zadpoor, 2019; Ghorai et al., 2022), and ceramics (Ma et al., 2018; Eugen et al., 2023). However, limited by the materials themselves, the disadvantages of single-material scaffolds are also very obvious, such as the slow degradation of metal scaffolds or inadequate osteogenic induction (Helaehil et al., 2021). Therefore, researchers have focused on composite materials, hoping to solve the disadvantages of single materials through complementary advantages (Turnbull et al., 2018). PLGA is a biodegradable biopolymer approved by the US Food and Drug Administration (FDA) due to its good biocompatibility (Kumari et al., 2010), excellent processing properties (Lee et al., 2016), degradability and suitable mechanical strength. In addition, PLGA scaffolds can be loaded with various nanomaterials and a variety of bioactive factors to promote the regeneration of bone defects (Han et al., 2019). So, it is considered as one of the most promising materials for bone defect repair. In our previous study (Liu et al., 2022), we synthesized the PLGA/CaSO₄ scaffolds 3D-printed scaffolds (PC) with different ratios, and found that the incorporation of CaSO₄ with 20% wt in PLGA not only improved the mechanical properties of the scaffold but also enhanced its *in vitro* osteogenic effect (Liu et al., 2022), demonstrating that it is a promising material for bone repair. However, it is difficult to achieve sufficient bone defect repair with a single functional scaffold. Bone morphogenetic protein-2 (BMP-2) is a potent bone-inducing cytokine from the transforming growth factor- β (TGF- β) family and has currently been commonly used as a protein bone graft alternative (Chen et al., 2004). It is the most important and widely used bone growth factor because it promotes the early enrichment of osteogenic precursor cells at the site of bone injury, and their differentiation and mineralization into mature osteoblasts, thereby facilitating osteogenic repair (Zanotti et al., 2008; Kimura et al., 2010). However, it has the disadvantages of a short half-life, high price, and easy inactivation *in vivo* (Xu et al., 2019). Studies have shown that PLGA microspheres, as microcarriers for drugs or proteins, can protect the activity of

proteins and achieve a slow release of proteins (Wei et al., 2006; Park et al., 2008).

In this study, we wrapped the BMP-2 into the PLGA to obtain microspheres and then composited them on the surface of PC scaffolds to prepare PCB scaffolds. Our experiment showed that the osteogenic ability of the PCB scaffolds was superior to that of the PC scaffolds *in vitro* (Figure 1). Therefore, PCB scaffolds may provide a new idea for the treatment of bone defects, especially large and complex defects.

2 Materials and methods

2.1 Scaffold preparation

2.1.1 Synthesis of 3D polylactic glycolic acid Copolymer/CaSO₄ scaffolds (PC)

The PLGA/CaSO₄ scaffolds were synthesized by using a biological 3D printer (Livprint® N series, Medprin, Guangzhou, China). PLGA and CaSO₄ (20 wt% of the quality of PLGA) powder were added into the beaker and then stirred evenly at 200°C. The mixture was then injected into the 3D printer and the scaffold was printed according to the set parameters of the previous study (Liu et al., 2022). The nozzle temperature was 180 °C, and the temperature of supporting substrates during FDM printing was 120 °C.

2.1.2 Synthesis of BMP-2/PLGA microspheres

BMP-2/PLGA microspheres were prepared using a double emulsion method (Li et al., 2022). 100 mg PLGA was dissolved in 2.5 mL dichloromethane (DCM, Macklin, China) and 0.2 mL BMP-2 solution (20 mg/mL) was added to the PLGA solution. The primary emulsion (W/O) was obtained after 30-se swirling, slowly dripped into 20 mL polyvinyl alcohol (PVA) solution (1% w/v), and swirled again for 2 min to form a double emulsion (W/O/W). The double emulsion solution was stirred at room temperature for 12 h in a fume cabinet to evaporate DCM. BMP-2/PLGA microspheres were collected by centrifugation (4,000 rpm, 5 min), washed with deionized water 3 times, and freeze-dried.

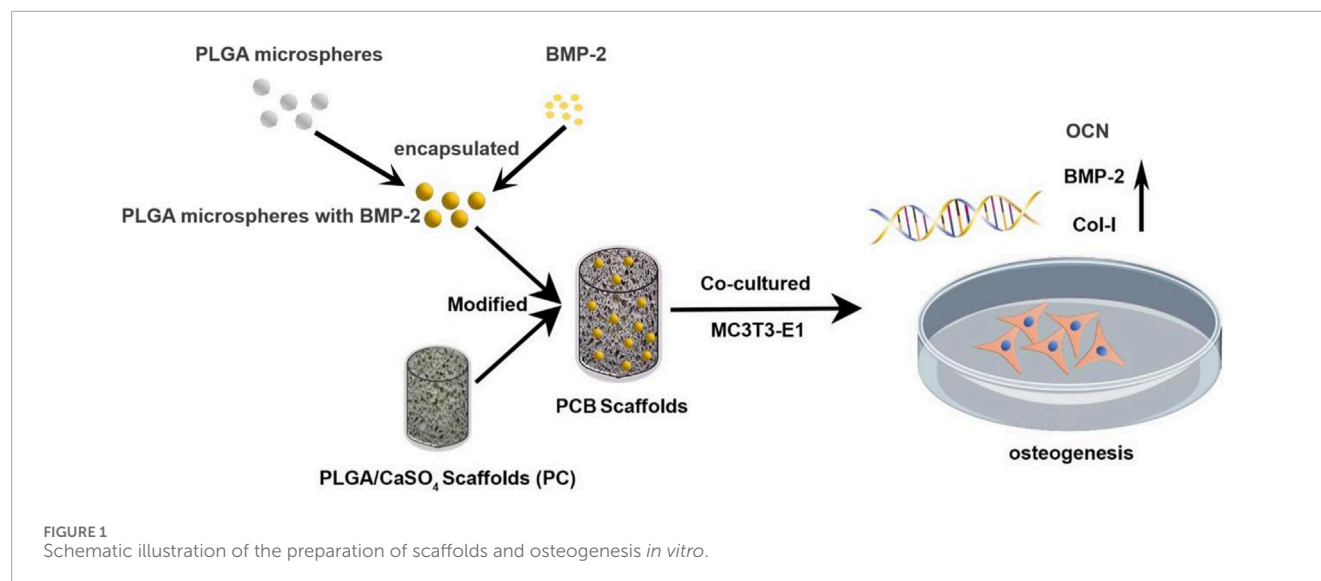
2.1.3 Synthesis of BMP-2/PLGA microspheres modified PLGA/CaSO₄ scaffolds (PCB)

Dopamine hydrochloride (2 mg/mL) and the PB scaffolds were added to the Tris buffer solution (pH = 8.5). After being stirred for 48 h, they were taken out and placed in a dehumidifier to dry. Then, these scaffolds were placed into PLGA microspheres solution (4 mg/mL) and mixed in a decolorization shaker for 4 h. Finally, the scaffolds were dried in a dehumidifier and PCB scaffolds.

2.2 Characterization of scaffolds

2.2.1 Scanning electron microscopy (SEM) analysis

The surface morphology and pore size of the scaffolds were evaluated by SEM. All samples were dried under vacuum, coated with gold, and then the sample placed on the sample stage of



SEM, using SEM (EM-30, COXEM, South Korea) to observe the structure, surface, and compression fracture morphology of the samples.

2.2.2 X-ray diffractometer (XRD) analysis

X-ray diffraction (DMX-220, Rigaku, Tokyo, Japan) was performed to investigate the scaffolds using Cu K α X-rays generated at 40 kV and 30 mA at a diffraction angle (2θ) from 10° to 60° with a step size of $0.05^\circ/\text{step}$ and an interval of $0.2 \text{ s}/\text{step}$.

2.2.3 Contact angle

The hydrophilicity of each scaffold was measured using a contact angle measurement system (ASUMI GIKEN Limited, Tokyo, Japan). A droplet of deionized water was deposited on the scaffold. Then, the image of the static liquid deposition was obtained within a few seconds and the contact angles were measured. Three samples were assessed for each group to ensure reproducibility and the average value.

2.2.4 Encapsulation efficiency of BMP-2/PLGA microspheres and *in vitro* release kinetics of PCB scaffolds

10 mg BMP-2/PLGA microspheres were added to a mixture of 0.9 mL NaOH (1 mol/L) and 0.1 mL PBS, shaken at room temperature for 2 h, and neutralized by addition of 1 mL 0.9 mol/L HCl. The BMP-2 concentration in the solution was detected using a human BMP-2 ELISA kit (Abcam) according to the manufacturer's instructions. The encapsulation efficiency was calculated using the following formula (1):

$$\text{Encapsulation efficiency} = \frac{\text{Actual protein loading}}{\text{theoretical protein loading}} \times 100\% \quad (1)$$

Subsequently, the sustained release of BMP-2 was measured as follows: 10 mg BMP-2/PLGA microspheres coated on the PCB scaffold were soaked in 2 mL PBS and incubated at 37°C and 100 rpm. At the set time intervals, 1 mL supernatant was

collected by centrifugation and the BMP-2 content in the supernatant was determined using the human BMP-2 ELISA kit. 1 mL fresh PBS was added every time after the supernatant was collected.

2.2.5 Degradation of scaffolds

The degradation and pH values of the scaffolds were investigated over 6 weeks in simulated body fluid (SBF). Initially, the scaffolds were weighed (m_1) and subsequently immersed in centrifuge tubes containing 10 mL SBF at 37°C . After rinsing the scaffolds with distilled water, they were dried until reaching a stable weight and then re-weighed (m_2) over 6 weeks. The degradation rate was calculated using the formula: $(m_1 - m_2)/m_1 \times 100\%$. The pH of the degradation medium was measured using a pH meter from Mettler Toledo.

2.3 *In vitro* study

2.3.1 Cell proliferation and biocompatibility

Cell Counting Kit-8 (CCK-8) was used to assess the proliferation of MC3T3-E1 cells co-culture with the sterile scaffolds. 1 mL suspension of cells ($1 \times 10^4/\text{mL}$) was seeded in 24-well plates in different scaffolds and incubated. After co-culture for 1, 3, and 5 days, 500 μL CCK-8 solution (10%) was added to each well for continuous incubation for 1 h. Then, optical density (OD) was measured at 450 nm using a microplate reader (Multiskan GO, Thermo Scientific, USA).

2.3.2 Live/dead staining

The cytotoxicity of scaffolds was also determined by live/dead staining classically. MC3T3-E1 cells were co-cultured with scaffolds as described above. On days 1, 3, and 5, each well was washed with PBS gently after removing the medium, and stained with 1 μM calcein-AM (Beyotime Biotechnology, China) and 2 μM propidium iodide (PI) for 30 min. The stained samples were then analyzed using a fluorescence microscope (Leica, Germany).

2.3.3 Hemolysis test

Healthy human blood was collected in anti-coagulant tubes and then 8 mL of blood was taken and diluted with around 10 mL of PBS. Then 0.2 mL of this diluted blood was added to 5 mL of PBS and further scaffolds were added. PBS and deionized (DI) water added of 0.2 mL were set as the negative and positive control. Then these test samples along with controls were incubated at 37°C for 30 min and centrifuged at 3,000 rpm for 10 min. The supernatant was collected and its optical density (OD) was measured at 545 nm. The hemolysis ratio (HR) was calculated as follows:

$$HR(\%) = \frac{(OD_{\text{sample}} - OD_{\text{negative control}})}{(OD_{\text{positive control}} - OD_{\text{negative control}})} \times 100$$

2.3.4 Alkaline phosphatase (ALP) staining

For ALP staining, MC3T3-E1 cells were seeded in a 6-well plate at a density of 1×10^4 cells per well and incubated with different scaffolds for 7 days. ALP activity was assayed using the BCIP/NBT alkaline phosphatase color development kit (Beyotime, China) according to the manufacturer's instructions. After removing the ALP stain working solution and washing with PBS, the stained MC3T3-E1 cells were visualized with an inverted research microscope (Leica, Germany).

2.3.5 Alizarin red S staining (ARS)

After 14 days culture as described above, the medium was removed and the cells were washed with PBS 3 times, fixed with 4% paraformaldehyde for 30 min, washed twice with double-distilled water (ddH₂O), and stained with ARS solution (Solarbio, China) for 2 h. After removing the dye solution and washed with ddH₂O three times, cells were observed under a microscope (KEYENCE, VK-X1,100, Tokyo, Japan). To quantitatively evaluate the coloration, 10% cetylpyridinium chloride solution was added to each scaffold and incubated for 2 h. The solution was transferred to an Eppendorf tube and centrifuged at 13,000 rpm for 15 min. From each group, 100 μ L solution was collected, placed in a 96-well plate, and measured using a microplate reader at 620 nm.

2.3.6 Expression of osteogenic genes

The osteogenic gene expression level of MC3T3-E1 was evaluated by real-time quantitative polymerase chain reaction (RT-qPCR). After 7 and 14 days of culture, total RNA was extracted using TRIzol reagent (AG, China), and then reverse transcribed into cDNA using a reverse transcription kit (AG, China). The gene expression of osteogenesis-related factors BMP-2, COL-1, and OCN was quantitatively detected using SYBR Green qPCR kit (AG, China), using the housekeeper gene GAPDH as a control. The primer sequences for all genes are listed in [Supplementary Table S1](#).

2.3.7 Immunofluorescence (IF) staining

The expression of BMP-2 was further evaluated by IF staining. Briefly, after 14 days of culture, MC3T3-E1 was fixed with 4% paraformaldehyde, washed with PBS 5 times, and blocked with 5 wt% BSA in PBS at 37°C for 30 min. After adding 200 μ L rabbit anti-Rat BMP-2 IgG antibody (Abcam, UK, diluted 1:200 in PBS), samples were incubated at 37°C for 12h, washed with PBS again

5 times, added with 200 μ L goat anti-rabbit IgG antibody (Abcam, UK, diluted 1:500 in PBS), and incubated at 37°C for 1 h. After five washes with PBS, the nucleus was stained with 4,6-diamino-2-phenyl indole (DAPI) for 5 min at room temperature. Finally, the stained cells on the samples were observed using an inverted fluorescence microscope (Nikon, Japan).

2.4 Statistical analysis

The analysis was performed by SPSS (V20, IBM Corp). The experimental results are expressed as the mean \pm standard deviation (SD). The significance level was determined by an analysis of variance. Statistical significance was set at $p < 0.05$.

3 Results and discussion

3.1 Synthesis and characterization of scaffolds

PLGA microspheres are often used as microcarriers for drugs or proteins to protect the activity of proteins and achieve slow release of proteins (Wei et al., 2006; Park et al., 2008). In this study, we used a strategy of PLGA microspheres encapsulating BMP-2 to achieve a long-lasting slow release of bone morphogenetic protein (BMP-2) to better promote bone defect repair. It was found that the BMP-2/PLGA microspheres were spherically shaped with a smooth and rounded surface and a mean particle size of approximately 182 ± 54.68 nm, with 72.18% of the microspheres ranging from 150–220 μ m in size (Figure 2A). The encapsulation rate of the BMP-2 microspheres was $48.55\% \pm 5.67\%$. Subsequently, we used the classical method to synthesize the PC 3D-printed scaffolds (Ye et al., 2022). As reported in our preliminary study (Liu et al., 2022), the PC scaffold was a typical plastic material, and its stress-strain was improved markedly compared with the pure PLGA material. When the content of CaSO₄ was 20%wt, it is breaking strength and yield strength reached the maximum, with the best compressive strength and shore hardness, close to the natural cancellous bone, which is a more ideal scaffold material for bone tissue engineering. To further improve the osteogenic effect of the scaffolds, we compounded BMP-2/PLGA microspheres on the PC scaffolds. The electron micrographs of PC and PCB scaffolds are shown in Figure 2B. It could be found that all scaffolds had a regular 3D porous structure, which facilitates the growth of osteoblasts and blood vessels (Swanson et al., 2021). In particular, when the BMP-2/PLGA microspheres were compounded with PC scaffolds, the scaffold surface became rougher, which was more favorable to the adhesion of osteoblasts (Chen et al., 2018; Rahmati et al., 2020).

The XRD patterns (Figure 2C) of the PC scaffolds showed characteristic crystalline peaks at 15, 25, 30, 31, and 48° corresponding to (200), (020), (102), and (302) planes of CaSO₄ (Sindhura Reddy et al., 2014; Zhu et al., 2022), indicating the successful doping of the CaSO₄ into the PC scaffolds. However, when the BMP-2/PLGA microspheres were compounded with the scaffolds, all the characteristic absorption peaks of CaSO₄ disappeared, indicating that the microspheres were successfully

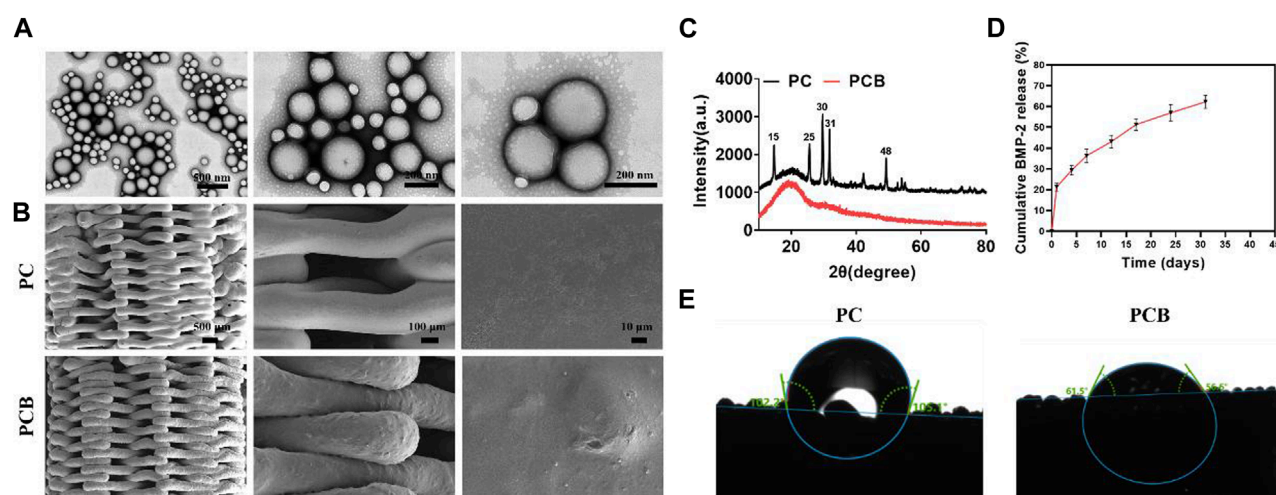


FIGURE 2
Characterization of scaffolds. **(A)** SEM images of the BMP-2/PLGA microspheres. **(B)** SEM images of the scaffolds. **(C)** XRD analysis of the scaffolds. **(D)** Release kinetics of the PCB scaffolds *in vitro*. **(E)** Contact angle measurement of the scaffolds.

coated on the printed filament surface of the PC scaffolds, resulting in a weakened signal for detection. The surface hydrophilicity of the scaffolds was evaluated by the water contact angle test. The encapsulation rate of the BMP-2 microspheres prepared in this study was tested as $67.13\% \pm 9.43\%$. The release profile of BMP-2 from the PCB scaffolds *in vitro* is shown in Figure 2D. The release of BMP-2 on the first day was approximately 21.36% and the subsequent release rate gradually slowed down to approximately $58.92\% \pm 3.14\%$ by day 30. It was found that with the degradation of PLGA, BMP-2 was still slowly released after more than 30 days, thus effectively and continuously promoting osteogenic differentiation. The contact angle images of the scaffolds are shown in Figure 2E. It was found that the addition of BMP-2/PLGA microspheres reduced the contact angle of the scaffold and therefore the PCB scaffold was more hydrophilic, knowing that hydrophilicity plays an important role in protein uptake and cell proliferation (Liu et al., 2018).

The degradation performance of materials holds significant importance in bone tissue engineering. The degradation products of materials should be non-toxic to surrounding tissues and not induce allergic reactions or rejection. Excellent degradation performance ensures that the material can harmoniously coexist with biological tissues in the body. The degradation rate of materials should match the rate of new tissue formation. If the degradation rate is too slow, the implant may persist for an extended period, affecting the development of new tissues. Conversely, if the degradation rate is too fast, the material may lose its function before new tissue formation occurs. We found that the scaffolds degraded slowly in the first 2 weeks (Figure 3A). The early and slow degradation of the scaffold can provide long-term stable support after implantation, which is crucial for initial bone tissue formation. The existence of the scaffold can simulate the structure of natural bone and provide support during the process of bone cell adhesion, proliferation, and differentiation. In addition, the slow early degradation of the scaffold can also allow new bone tissue to grow on its surface, while the

mechanical properties of the scaffold gradually weakened. This smooth transition helps avoid stress concentrations and promotes adaptive growth of the new bone tissue. After 2 weeks, the degradation rate of the scaffold accelerated and was degraded at 6 weeks. As shown in Figure 3B, after 6 weeks of soaking in SBF solution, the pH value of the scaffold showed a slowly decreasing trend, and there was no significant difference in the change of culture medium pH during degradation.

3.2 *In vitro* biocompatibility of the scaffolds

Biocompatibility is one of the most important functions of biomaterials, which requires that the materials have no damage to cells and tissues (Wang et al., 2020). In our previous study, we used the CCK-8 assay to test the cytotoxicity and proliferation of the scaffolds, finding that PC scaffolds had good biocompatibility *in vitro* (Liu et al., 2022). First, we verified the biocompatibility of the scaffolds again using live/dead cell staining (Figure 4A). The number and proportion of live cells (green) and dead cells (red) were similar in both PC and PCB scaffold groups compared with the control group. Then, we further explored the effect of the scaffolds on cell proliferation in the two groups (Figures 4B, C) and found that after co-culturing the MC3TE-E1 cells with scaffolds for 1, 3 and 5 days, cell proliferation was the same in each group, indicating that none scaffold had significant adverse effects on cell proliferation, which is consistent with the results of live/dead cell staining experiment. These results show that our scaffolds have good biocompatibility *in vitro* and can meet the basic requirements for bone tissue engineering scaffolds. The hemolysis test is another essential parameter to assess the safety of biological materials, reflecting the rejection of the implant by the blood in the body (Wang et al., 2019). As shown in Figure 4D, the supernatant of the positive control group was red due to the rupture of erythrocytes in response to hemolysis. In contrast, the supernatant of the other two groups of stents and the negative control group was

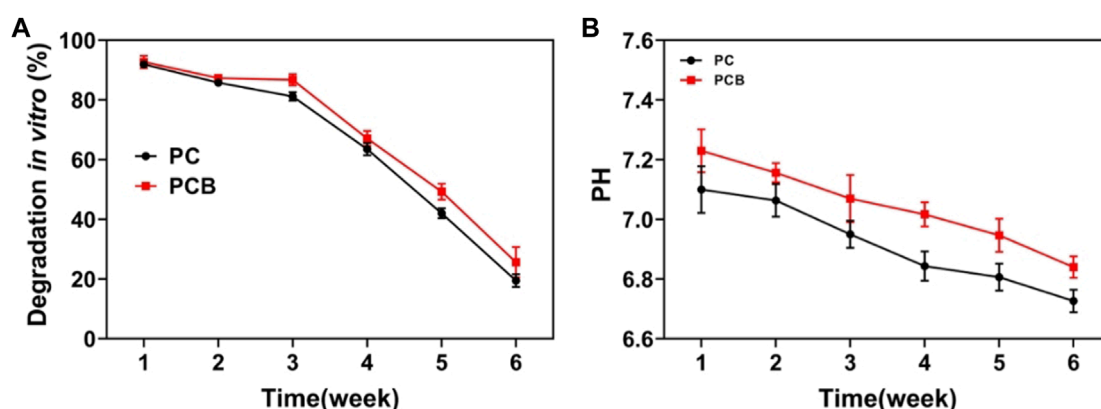


FIGURE 3 Degradation of the scaffold. (A) Weight of scaffolds after degradation *in vitro*. (B) pH value in the simulated body fluid.

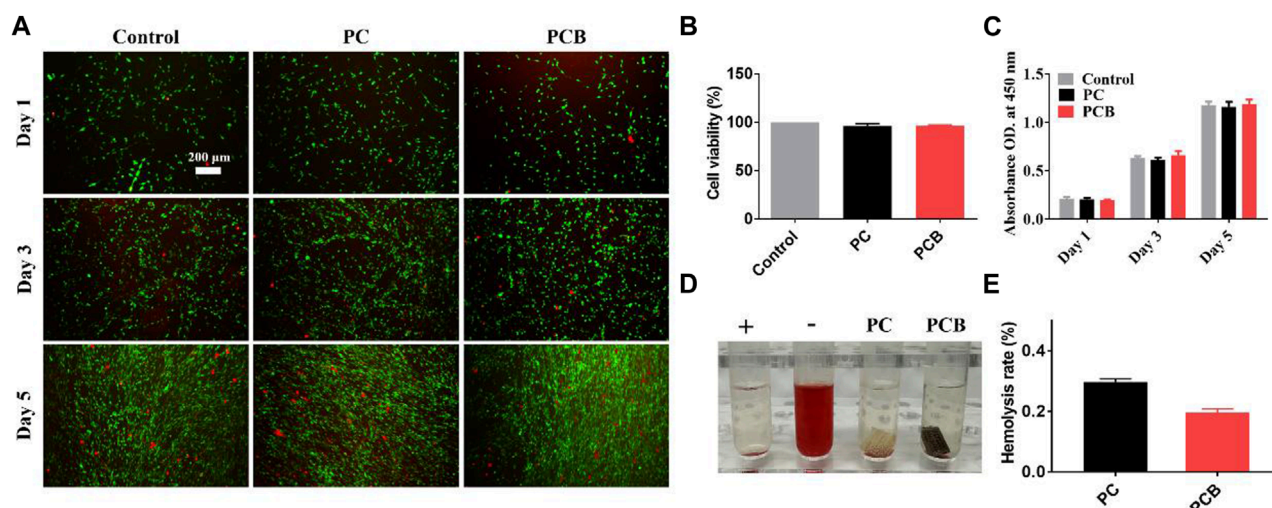


FIGURE 4 Biocompatibility of the scaffolds *in vitro*. (A) Live/dead staining of preosteoblasts after incubation with the scaffolds. Scale bar = 200 μm. (B) Cell viability of preosteoblasts after incubation with scaffolds. (C) The proliferation of preosteoblasts after 1, 3, and 5 days of incubation with the scaffolds (determined by a CCK-8 assay). (D) Hemocompatibility test and hemolysis rate of the scaffolds. (E) The hemolysis ratio was measured at 545 nm. Data are presented as the mean ± SD (* $p < 0.05$, ** $p < 0.01$, *** $p < 0.001$; $n = 3$).

a clarified solution, and the hemolysis rate was less than 0.5% (Figure 4E), proving that all stents had a negligible effect on erythrocytes.

3.3 *In vitro* osteoinductivity of the scaffolds

Bone tissue engineering scaffolds should have good osteoconductivity and osteoinductivity to facilitate the repair of bone defects (Tang et al., 2016). Among them, osteoinductivity refers to its ability to contribute to osteogenic differentiation and is an important index for the performance evaluation of bone repair materials (Meijer et al., 2007). In this study, we used ALP staining, alizarin red staining, cellular IF analysis,

and osteogenesis-related gene expression levels to detect the *in vitro* osteoinductivity of the scaffolds. ALP is an exonuclease of osteoblasts, and its expression activity is an important marker of osteogenic differentiation (Sun et al., 2018). Figure 5A shows ALP staining of MC3T3-E1 cells after 7-day co-culture, demonstrating that ALP staining in the PC scaffold group was not significantly deeper than that in the control group, both were lavender in color, and a small number of calcium crystals are visible in the field of view. However, the staining of the PCB scaffold group was significantly deeper, with a dark purple color, and a large distribution of calcium crystals could be seen microscopically. This result suggests that the released BMP-2 protein significantly promoted the osteogenic differentiation of MC3T3-E1 as the microspheres were compounded.

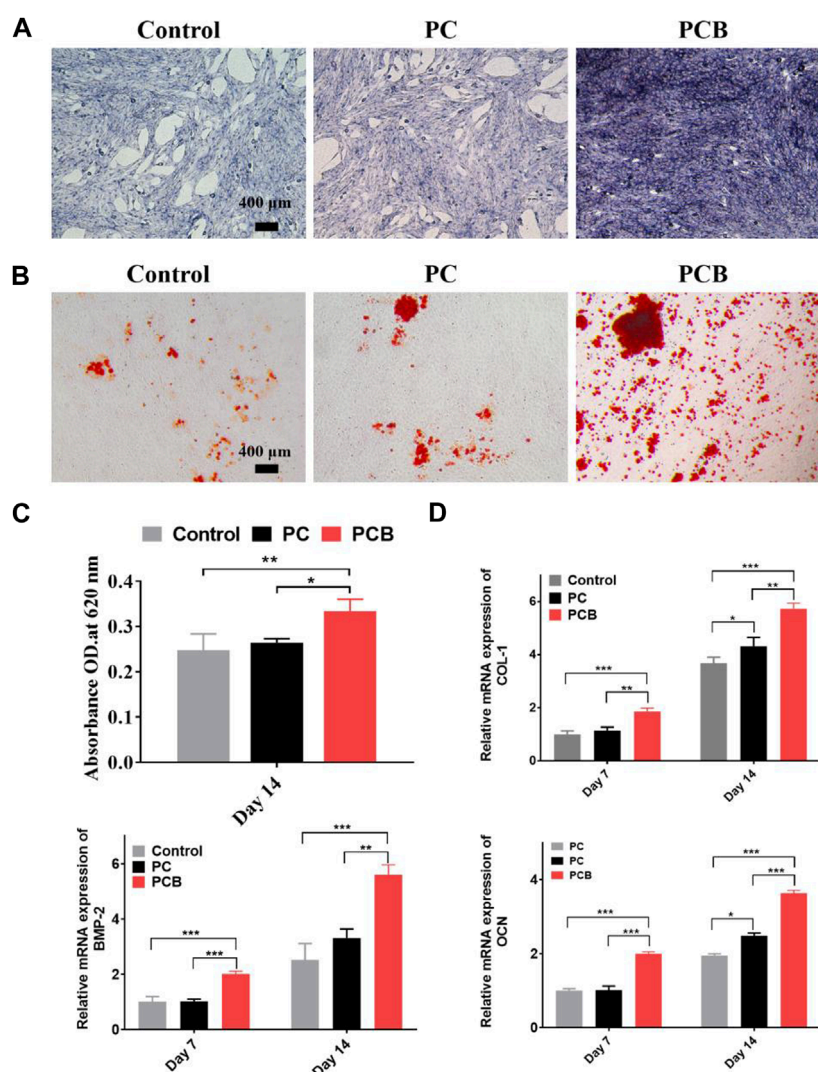


FIGURE 5

In vitro osteogenesis of the scaffolds. (A) ALP staining of preosteoblasts after 7-day culture with the scaffolds. Scale bar = 400 μ m. (B) Alizarin red S staining of the extracellular calcium nodules in preosteoblasts cultured with the scaffolds for 14 days. Scale bar = 400 μ m. (C) Semi-quantitative analysis of alizarin red S staining. Cetylpyridinium chloride solution. The stained extracellular calcium nodules were dissolved in a cetylpyridinium chloride solution. (D) The relative expression of osteogenic genes of preosteoblasts cultured with different scaffolds. (E) Representative images of IF staining of BMP-2. Data are presented as the mean \pm SD (* p < 0.05, ** p < 0.01, *** p < 0.001; n = 3).

Calcium nodules are a product of late osteogenic differentiation, which can be detected by binding specifically to an alizarin red stain to form a dark red substance (Lee et al., 2020). The result of alizarin red staining of each scaffold group showed that the number of calcium nodules in the PCB scaffold groups was significantly increased compared with the scattered calcium nodules in the control group and PC group (Figure 5B). Microscopically, MC3T3-E1 cells produced a large number of calcium crystals after the addition of BMP-2/PLGA microspheres, which gradually fused into clusters and were deeply stained by the staining solution, indicating that the osteogenic differentiation of cells in the PCB group was more advanced. Semi-quantitative analysis showed that OD in both PC and PCB groups was higher than that in the control group, being the highest in the PCB group (Figure 5C). These data demonstrate that PT/CA/Cu scaffolds possess excellent osteoinductivity.

The expression levels of osteogenic-related genes also directly reflect the level of osteogenic differentiation of cells. We examined the expression levels of BMP-2, COL-1, and OCN genes using qPCR, and the results are shown in Figure 5D. The mRNA expression levels of all three genes showed similar trends, with the highest expression in the PCB group, followed by the PC group, and the lowest expression in the control group. Gene expression levels in the PC group were only upregulated at day 14 except for the BMP-2 gene, which might be related to the release of more calcium from scaffold degradation. In contrast, the expression of the remaining PCB groups was significantly higher at both 7 and 14 days compared with the control group, demonstrating a stronger osteogenic effect. It is interesting to find that the BMP-2 gene was most upregulated in the PCB group at day 14 compared with COL-1. COL-1 expresses the type I collagen, which is a major component of the extracellular

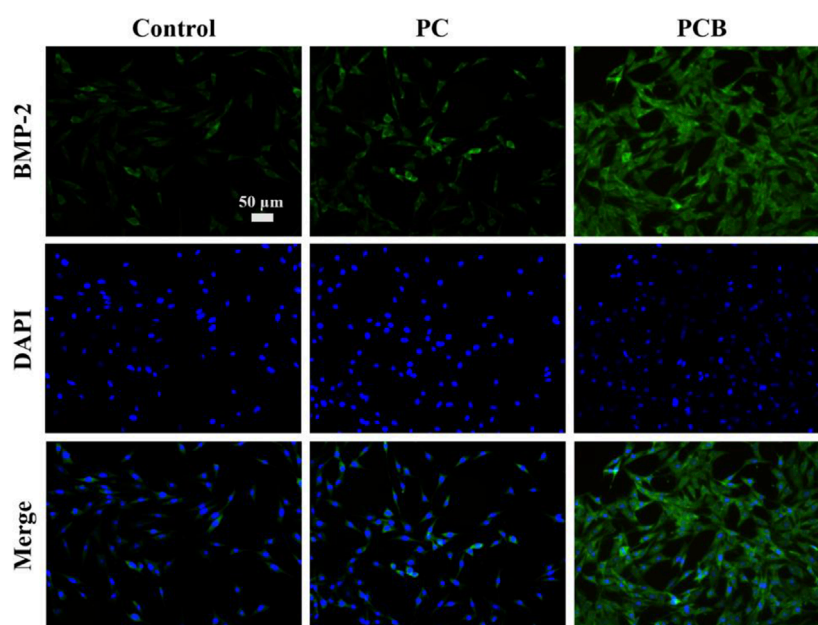


FIGURE 6
Representative images of immunofluorescence staining of BMP-2. Scale bar = 50 μ m.

matrix and could direct calcium salt deposition and mineralization, thus promoting new bone formation (Park et al., 2014). This would also explain why the difference in our ALP staining was significantly higher than the result of the alizarin red staining.

Based on the above results, we used cellular IF to further detect the protein expression level of the BMP-2 gene, and the results are shown in Figure 6. After 14-day co-culture, the expression level of BMP-2 was generally low and the fluorescence signal was weak in the control groups. However, we found that the fluorescence signal was enhanced in the other two groups, and the PCB group had the highest fluorescence intensity, which was significantly different from the rest of the scaffolds. This indicates that the osteogenic differentiation of the cells gradually deepened as the osteogenic induction proceeded, and the effect was more obvious with the addition of BMP-2/PLGA microspheres, which is consistent with the previous findings. In summary, our study shows that PCB scaffolds can effectively promote the osteogenic differentiation of cells and are expected to accelerate the repair of bone defects.

Repairing bone defects by using artificial bone material has been widely researched in recent years, and its most essential property is its osteogenic ability. With the development of nanometer materials and 3D printing, many innovative materials were designed and proved their effectiveness. Some researchers have summarized the application of nanofiber scaffolds in hyaline cartilage tissue repair (Ahmadian et al., 2023). Due to the natural association between bone cells and highly nano-rough surfaces, the adhesion ability and biocompatibility of nano-modified scaffolds are effectively improved. Besides, by using internal and external triggers, the release of growth factors and cells could be more precisely and individually controlled (Khalilov, 2023). Therefore, we can also expect the application of nanometer materials in the research

about complex bone defects/infections by precisely and individually designing the modified growth factor or antibiotics.

4 Conclusion

A PCB 3D printed scaffold was successfully prepared in this study. Our *in vitro* experiments demonstrated that the scaffold had good biocompatibility, and the addition of BMP-2/PLGA microspheres could markedly improve its *in vitro* bone-enabling ability. These findings provide a new idea for the treatment of long bone shaft and metaphysis defects. So we can also expect that the PCB scaffold will have a broad prospect in the treatment of long bone shaft and metaphysis defects due to its excellent characteristics of easy availability, good biocompatibility, osteogenic properties, and rapid degradation.

Data availability statement

The original contributions presented in the study are included in the article/Supplementary Material, further inquiries can be directed to the corresponding authors.

Ethics statement

Ethical approval was not required for the studies involving humans because the human blood samples were obtained from another researcher (Tao Liu) of our group, whose research has been published on frontier in 2022. The studies were conducted in accordance with the local legislation and institutional requirements.

The human samples used in this study were acquired from primarily isolated as part of your previous study for which ethical approval was obtained. Written informed consent to participate in this study was not required from the participants or the participants' legal guardians/next of kin in accordance with the national legislation and the institutional requirements.

Author contributions

LZ: Writing—original draft, Writing—review and editing, Conceptualization, Data curation, Formal Analysis, Funding acquisition, Investigation, Methodology, Project administration, Resources, Software, Supervision, Validation, Visualization. XZ: Conceptualization, Data curation, Formal Analysis, Funding acquisition, Investigation, Methodology, Project administration, Resources, Software, Supervision, Validation, Visualization, Writing—original draft, Writing—review and editing. FD: Investigation, Software, Conceptualization, Data curation, Formal Analysis, Funding acquisition, Methodology, Project administration, Resources, Supervision, Validation, Visualization, Writing—original draft, Writing—review and editing. XY: Writing—review and editing. YZ: Writing—original draft, Writing—review and editing.

Funding

The author(s) declare that financial support was received for the research, authorship, and/or publication of this article. This work was financially supported by the Guangzhou Science

and Technology Program (N0. 201804010136), National Natural Science Foundations of China (grant no. 82360943), the Basic Research Project of Science and Technology Department of Yunnan Province (grant nos 202101AZ070001123, 202201AU070120), Guangdong Basic and Applied Basic Research Foundation (No. 2023A1515110833), China Postdoctoral Science Foundation (No. 2023M740862).

Conflict of interest

The authors declare that the research was conducted in the absence of any commercial or financial relationships that could be construed as a potential conflict of interest.

Publisher's note

All claims expressed in this article are solely those of the authors and do not necessarily represent those of their affiliated organizations, or those of the publisher, the editors and the reviewers. Any product that may be evaluated in this article, or claim that may be made by its manufacturer, is not guaranteed or endorsed by the publisher.

Supplementary material

The Supplementary Material for this article can be found online at: <https://www.frontiersin.org/articles/10.3389/fmats.2024.1374409/full#supplementary-material>

References

- Ahmadian, E., Eftekhari, A., Janas, D., and Vahedi, P. (2023). Nanofiber scaffolds based on extracellular matrix for articular cartilage engineering: a perspective. *Nanotheranostics* 7 (1), 61–69. PMID: 36593799; PMCID: PMC9760364. doi:10.7150/ntno.78611
- Chen, D., Zhao, M., and Mundy, G. R. (2004). Bone morphogenetic proteins. *Growth factors* 22, 233–241. doi:10.1080/08977190412331279890
- Chen, S. C., Guo, Y. L., Liu, R. H., Wu, S. Y., Fang, J. H., Huang, B. X., et al. (2018). Tuning surface properties of bone biomaterials to manipulate osteoblastic cell adhesion and the signaling pathways for the enhancement of early osseointegration. *Colloids surfaces. B, Biointerfaces* 164, 58–69. doi:10.1016/j.colsurfb.2018.01.022
- Dimitriou, R., Jones, E., McGonagle, D., and Giannoudis, P. V. (2011). Bone regeneration: current concepts and future directions. *BMC Med.* 9, 66. doi:10.1186/1741-7015-9-66
- Eugen, G., Claus, M., Anna-Maria, S., Niklas, D., Philipp, S., Andrea, E., et al. (2023). Degradation of 3D-printed magnesium phosphate ceramics *in vitro* and a prognosis on their bone regeneration potential. *Bioact. Mater.* 19, 376–391. doi:10.1016/j.bioactmat.2022.04.015
- Farris, A. L., Lambrechts, D., Zhou, Y., Zhang, N. Y., Sarkar, N., Moorer, M. C., et al. (2022). 3D-printed oxygen-releasing scaffolds improve bone regeneration in mice. *Biomaterials* 280, 121318. doi:10.1016/j.biomaterials.2021.121318
- Ghorai, S. K., Dutta, A., Roy, T., Guha Ray, P., Ganguly, D., Ashokkumar, M., et al. (2022). Metal ion augmented mussel inspired polydopamine immobilized 3D printed osteoconductive scaffolds for accelerated bone tissue regeneration. *ACS Appl. Mat. Inter.* 14, 28455–28475. doi:10.1021/acsami.2c01657
- Giannoudis, P. V., Jones, E., and Einhorn, T. A. (2011). Fracture healing and bone repair. *Injury* 42, 549–550. doi:10.1016/j.injury.2011.03.037
- Han, Y., Li, X., Zhang, Y., Han, Y., Chang, F., and Ding, J. (2019). Mesenchymal stem cells for regenerative medicine. *Cells* 8, 886. doi:10.3390/cells8080886
- Helaehil, J. V., Lourenco, C. B., Huang, B., Helaehil, L. V., de Camargo, I. X., Chiarotto, G. B., et al. (2021). *In vivo* investigation of polymer-ceramic PCL/HA and PCL/ β -TCP 3D composite scaffolds and electrical stimulation for bone regeneration. *Polymers* 14, 65. doi:10.3390/polym14010065
- Khalilov, R. (2023). A comprehensive review of advanced nano-biomaterials in regenerative medicine and drug delivery. *Adv. Biol. Ear Sci.* 8 (No.1), 5–18.
- Kimura, Y., Miyazaki, N., Hayashi, N., Otsuru, S., Tamai, K., Kaneda, Y., et al. (2010). Controlled release of bone morphogenetic protein-2 enhances recruitment of osteogenic progenitor cells for *de novo* generation of bone tissue. *Part A* 16, 1263–1270. doi:10.1089/ten.TEA.2009.0322
- Kumar, G., Tison, C. K., Chatterjee, K., Pine, P. S., McDaniel, J. H., Salit, M. L., et al. (2011). The determination of stem cell fate by 3D scaffold structures through the control of cell shape. *Biomaterials* 32, 9188–9196. doi:10.1016/j.biomaterials.2011.08.054
- Kumari, A., Yadav, S. K., and Yadav, S. C. (2010). Biodegradable polymeric nanoparticles based drug delivery systems. *Colloids Surf. B. Biointerfaces* 75, 1–18. doi:10.1016/j.colsurfb.2009.09.001
- Lee, H., Yoo, J. J., Kang, H. W., and Cho, D. W. (2016). Investigation of thermal degradation with extrusion-based dispensing modules for 3D bioprinting technology. *Biofabrication* 8, 015011. doi:10.1088/1758-5090/8/1/015011
- Lee, S. S., Kim, J. H., Jeong, J., Kim, S. H. L., Koh, R. H., Kim, I., et al. (2020). Sequential growth factor releasing double cryogel system for enhanced bone regeneration. *Biomaterials* 257, 120223. doi:10.1016/j.biomaterials.2020.120223
- Li, W., Li, S., Zhang, J., Zhong, H., Liang, J., Huang, S., et al. (2022). Fabrication and evaluation of bone morphogenetic protein-2 microspheres coated black phosphorus nanosheets@poly(lactic-glycolic acid) copolymers scaffold: a multifunctional antibacterial photothermal scaffold for bone regeneration. *Int. J. Biol. Macromol.* 210, 350–364. doi:10.1016/j.ijbiomac.2022.05.028

- Liu, J., Sun, L. S., Xu, W. Y., Wang, Q. Q., Yu, S. J., and Sun, J. Z. (2019). Current advances and future perspectives of 3D printing natural-derived biopolymers. *Carbohydr. Polym.* 207, 297–316. doi:10.1016/j.carbpol.2018.11.077
- Liu, P., Sun, L., Liu, P., Yu, W., Zhang, Q., Zhang, W., et al. (2018). Surface modification of porous PLGA scaffolds with plasma for preventing dimensional shrinkage and promoting scaffold-cell/tissue interactions. *J. Mater. Chem.* 6, 7605–7613. doi:10.1039/c8tb02374c
- Liu, T., Li, Z., Zhao, L., Chen, Z., Lin, Z., Li, B., et al. (2022). Customized design 3D printed PLGA/calcium sulfate scaffold enhances mechanical and biological properties for bone regeneration. *Front. Bioeng. Biotechnol.* 10, 874931. doi:10.3389/fbioe.2022.874931
- Lutzweiler, G., Ndreu Halili, A., and Engin Vrana, N. (2020). The overview of porous, bioactive scaffolds as instructive biomaterials for tissue regeneration and their clinical translation. *Pharmaceutics* 12, 602. doi:10.3390/pharmaceutics12070602
- Ma, H. S., Feng, C., Chang, J., and Wu, C. T. (2018). 3D-printed bioceramic scaffolds: from bone tissue engineering to tumor therapy. *Acta Biomater.* 79, 37–59. doi:10.1016/j.actbio.2018.08.026
- Meijer, G. J., de Bruijn, J. D., Koole, R., and van Blitterswijk, C. A. (2007). Cell-based bone tissue engineering. *PLoS Med.* 4, e9. doi:10.1371/journal.pmed.0040009
- Myeroff, C., and Archdeacon, M. (2011). Autogenous bone graft: donor sites and techniques. *J. Bone Jt. Surg. Am.* 93, 2227–2236. doi:10.2106/JBJS.J.01513
- Park, J. S., Park, K., Woo, D. G., Yang, H. N., Chung, H. M., and Park, K. H. (2008). PLGA microsphere construct coated with TGF- β 3 loaded nanoparticles for neocartilage formation. *Biomacromolecules* 9, 2162–2169. doi:10.1021/bm800251x
- Park, J. Y., Choi, J. C., Shim, J. H., Lee, J. S., Park, H., Kim, S. W., et al. (2014). A comparative study on collagen type I and hyaluronic acid dependent cell behavior for osteochondral tissue bioprinting. *Biofabrication* 6, 035004. doi:10.1088/1758-5082/6/3/035004
- Rahmati, M., Silva, E. A., Reseland, J. E., and Haugen, H. J. (2020). Biological responses to physicochemical properties of biomaterial surface. *Chem. Soc. Rev.* 49, 5178–5224. doi:10.1039/d0cs00103a
- Sindhura Reddy, N., Sowmya, S., Bumgardner, J. D., Chennazhi, K. P., Biswas, R., and Jayakumar, R. (2014). Tetracycline nanoparticles loaded calcium sulfate composite beads for periodontal management. *Biochim. Biophys. Acta* 1840, 2080–2090. doi:10.1016/j.bbagen.2014.02.007
- Sun, J., Zhao, J. H., Bao, X. F., Wang, Q. F., and Yang, X. R. (2018). Alkaline phosphatase assay based on the chromogenic interaction of diethanolamine with 4-aminophenol. *Anal. Chem.* 90, 6339–6345. doi:10.1021/acs.analchem.8b01371
- Swanson, W. B., Omi, M., Zhang, Z., Nam, H. K., Jung, Y., Wang, G., et al. (2021). Macropore design of tissue engineering scaffolds regulates mesenchymal stem cell differentiation fate. *Biomaterials* 272, 120769. doi:10.1016/j.biomaterials.2021.120769
- Tang, D., Tare, R. S., Yang, L. Y., Williams, D. F., Ou, K. L., and Oreffo, R. O. (2016). Biofabrication of bone tissue: approaches, challenges and translation for bone regeneration. *Biomaterials* 83, 363–382. doi:10.1016/j.biomaterials.2016.01.024
- Turnbull, G., Clarke, J., Picard, F., Riches, P., Jia, L. L., Han, F. X., et al. (2018). 3D bioactive composite scaffolds for bone tissue engineering. *Bioact. Mater.* 3, 278–314. doi:10.1016/j.bioactmat.2017.10.001
- Wang, C., Huang, W., Zhou, Y., He, L. B., He, Z., Chen, Z. L., et al. (2020). 3D printing of bone tissue engineering scaffolds. *Bioact. Mater.* 5, 82–91. doi:10.1016/j.bioactmat.2020.01.004
- Wang, W. S., Cheng, X. H., Liao, J. W., Lin, Z. F., Chen, L. L., Liu, D. D., et al. (2019). Synergistic photothermal and photodynamic therapy for effective implant-related bacterial infection elimination and biofilm disruption using Cu₉S₈ nanoparticles. *ACS Biomater. Sci. Eng.* 5, 6243–6253. doi:10.1021/acsbomaterials.9b01280
- Wei, G., Jin, Q., Giannobile, W. V., and Ma, P. X. (2006). Nano-fibrous scaffold for controlled delivery of recombinant human PDGF-BB. *J. Control. Release* 112, 103–110. doi:10.1016/j.jconrel.2006.01.011
- Xu, X., Sun, M., Wang, D., Bu, W., Wang, Z., Shen, Y., et al. (2019). Bone formation promoted by bone morphogenetic protein-2 plasmid-loaded porous silica nanoparticles with the involvement of autophagy. *Nanoscale* 11, 21953–21963. doi:10.1039/c9nr07017f
- Ye, X. L., Zhang, Y. Q., Liu, T., Chen, Z. H., Chen, W. J., Wu, Z. G., et al. (2022). Beta-tricalcium phosphate enhanced mechanical and biological properties of 3D-printed polyhydroxyalkanoates scaffold for bone tissue engineering. *Int. J. Biol. Macromol.* 209, 1553–1561. doi:10.1016/j.ijbiomac.2022.04.056
- Zadpoor, A. A. (2019). Meta-biomaterials. *Biomaterials Sci.* 8, 18–38. doi:10.1039/c9bm01247h
- Zanotti, S., Smerdel-Ramoya, A., Stadmeier, L., and Canalis, E. (2008). Activation of the ERK pathway in osteoblastic cells, role of gremlin and BMP-2. *J. Cell. Biochem.* 104, 1421–1426. doi:10.1002/jcb.21715
- Zhu, T., Jiang, M., Zhang, M., Cui, L., Yang, X., Wang, X., et al. (2022). Biofunctionalized composite scaffold to potentiate osteoconduction, angiogenesis, and favorable metabolic microenvironment for osteonecrosis therapy. *Bioact. Mater.* 9, 446–460. doi:10.1016/j.bioactmat.2021.08.005



OPEN ACCESS

EDITED BY

Jianshe Hu,
Northeastern University, China

REVIEWED BY

Goutam Thakur,
Manipal Institute of Technology, India
Jun Liu,
Yangzhou University, China

*CORRESPONDENCE

Behrooz Dousti,
✉ doostybehrooz@gmail.com
Mahdi Karami-Khorramabadi,
✉ m.k.khorramabadi@gmail.com
Hamed Afkhami,
✉ hamedafkhami70@gmail.com

RECEIVED 08 March 2024

ACCEPTED 04 July 2024

PUBLISHED 02 August 2024

CITATION

Yarahmadi A, Dousti B, Karami-Khorramabadi M and Afkhami H (2024), Materials based on biodegradable polymers chitosan/gelatin: a review of potential applications. *Front. Bioeng. Biotechnol.* 12:1397668. doi: 10.3389/fbioe.2024.1397668

COPYRIGHT

© 2024 Yarahmadi, Dousti, Karami-Khorramabadi and Afkhami. This is an open-access article distributed under the terms of the [Creative Commons Attribution License \(CC BY\)](https://creativecommons.org/licenses/by/4.0/). The use, distribution or reproduction in other forums is permitted, provided the original author(s) and the copyright owner(s) are credited and that the original publication in this journal is cited, in accordance with accepted academic practice. No use, distribution or reproduction is permitted which does not comply with these terms.

Materials based on biodegradable polymers chitosan/gelatin: a review of potential applications

Aref Yarahmadi¹, Behrooz Dousti^{1*},
Mahdi Karami-Khorramabadi^{2*} and Hamed Afkhami^{3,4,5*}

¹Department of Biology, Khorramabad Branch, Islamic Azad University, Khorramabad, Iran, ²Department of Mechanical Engineering, Khorramabad Branch, Islamic Azad University, Khorramabad, Iran, ³Cellular and Molecular Research Centre, Qom University of Medical Sciences, Qom, Iran, ⁴Nervous System Stem Cells Research Center, Semnan University of Medical Sciences, Semnan, Iran, ⁵Department of Medical Microbiology, Faculty of Medicine, Shahed University, Tehran, Alborz, Iran

Increased mass manufacturing and the pervasive use of plastics in many facets of daily life have had detrimental effects on the environment. As a result, these worries heighten the possibility of climate change due to the carbon dioxide emissions from burning conventional, non-biodegradable polymers. Accordingly, biodegradable gelatin and chitosan polymers are being created as a sustainable substitute for non-biodegradable polymeric materials in various applications. Chitosan is the only naturally occurring cationic alkaline polysaccharide, a well-known edible polymer derived from chitin. The biological activities of chitosan, such as its antioxidant, anticancer, and antimicrobial qualities, have recently piqued the interest of researchers. Similarly, gelatin is a naturally occurring polymer derived from the hydrolytic breakdown of collagen protein and offers various medicinal advantages owing to its unique amino acid composition. In this review, we present an overview of recent studies focusing on applying chitosan and gelatin polymers in various fields. These include using gelatin and chitosan as food packaging, antioxidants and antimicrobial properties, properties encapsulating biologically active substances, tissue engineering, microencapsulation technology, water treatment, and drug delivery. This review emphasizes the significance of investigating sustainable options for non-biodegradable plastics. It showcases the diverse uses of gelatin and chitosan polymers in tackling environmental issues and driving progress across different industries.

KEYWORDS

chitosan, gelatin, antimicrobial, antioxidant, biodegradable polymers

1 Introduction

The management of plastic waste presents a significant environmental challenge in contemporary society. The widespread utilization of plastics in various aspects of daily life, coupled with the escalation of mass production, has led to significant environmental consequences (Moharir and Kumar, 2019; PanSu et al., 2020). As a result, these concerns contribute to the increasing risk of climate change caused by releasing carbon dioxide from the incineration of non-biodegradable traditional polymers like polyethylene, polyvinylchloride, and polypropylene. It is also essential to consider the environmental impacts associated with the production processes of biodegradable alternatives (Amulya et al., 2021). Biodegradable polymers are developing as a sustainable substitute for non-biodegradable polymer materials

across various applications (Ahmed et al., 2023). The most effective approach for addressing non-biodegradable plastic waste involves substituting economically inefficient materials with biodegradable polymers for recycling or reutilization, given their environmentally sustainable properties (Flury and Narayan, 2021). A biodegradable polymer is a substance that can be broken down by microorganisms, as well as environmental factors like temperature and oxygen, into less complex components that do not pose harm to the ecosystem (Yin and Yang, 2020; Wu et al., 2021). Moreover, biodegradable polymers are utilized in various industries based on their price, ability to absorb moisture, accessibility, mechanical properties, antibacterial characteristics, thermal resistance, and compatibility with living organisms (Christian, 2020; Vieira et al., 2022). Chitosan, a polysaccharide, and gelatin, a protein, are two biodegradable polymers that have demonstrated diverse utility in various fields such as packaging, agriculture, wastewater treatment, drug delivery, orthopedics, wound dressings, tissue engineering, and other applications (Wang et al., 2021; Ebhodaghe, 2022; Sethi and Kaith, 2022). Chitosan, specifically, possesses antimicrobial characteristics that can prolong the storage duration of food items by suppressing the proliferation of bacteria and fungi. In contrast, gelatin is an effective barrier material that protects against oxygen, moisture, and various contaminants, rendering it a viable choice for food packaging applications (Flórez et al., 2022; Lu et al., 2022). Also, they have demonstrated potential in a range of medical applications within the healthcare sector, including but not limited to wound dressings, drug delivery mechanisms, and tissue engineering. For instance, chitosan has been employed in wound dressings because of its hemostatic and antimicrobial characteristics. In contrast, gelatin has been applied in tissue engineering as a support structure for promoting cell proliferation (Bello et al., 2020; Moeini et al., 2020; Ding et al., 2021; Lukin et al., 2022). Numerous studies have shown that combining chitosan and gelatin produces a high-quality and uniform film (Xu D. et al., 2021a; Roy and Rhim, 2021). Chitosan and gelatin possess additional advantageous characteristics, including the ability to minimize harm to non-targeted cells or tissues and inhibit the enzymatic breakdown of medications (Liu Y. et al., 2022a; Battogtokh et al., 2022; Zhu et al., 2022). Because of these qualities, gelatin and chitosan are excellent materials for biological imaging and diagnostics, medication delivery systems, and cancer therapy (Węgrzynowska-Drzymalska et al., 2022; Zhou et al., 2022). Moreover, previous studies have indicated that the gradual decomposition of gelatin and chitosan nanoparticles (NPs) contributes to a regulated and sustained release of drugs. This is attributed to the solid positive surface charges of these NPs, which serve as stable vehicles for delivering substances to specific locations within the human body (Nagpal et al., 2010; Sahoo et al., 2015; Garg et al., 2019). Nevertheless, chitosan and gelatin possess constraints related to their physicochemical stability. Scholars persist in investigating strategies to address these obstacles by implementing modifications and incorporating other materials to enhance their efficacy (Rodríguez-Rodríguez et al., 2020; Ebhodaghe, 2022).

The objective of this review is to provide an overview of the biopolymers chitosan and gelatin, as well as to outline the latest advancements in their utilization as animal-derived products in food, pharmaceuticals, and medicine.

1.1 Chitosan

Chitosan is the only naturally occurring cationic alkaline polysaccharide. Its scientific composition is 2-amino-2-deoxy-D-glucose. Chitosan can be synthesized through the deacetylation of chitin using NaOH, as illustrated in Figure 1, and through fermentation processes involving certain microbial cultures. Shrimp, crab, and bug shells are the primary sources of chitin (Mohan et al., 2020; Mulyani et al., 2020; Tan et al., 2020). Chitosan is a readily accessible and cost-effective polysaccharide with semi-crystalline properties, primarily soluble in mild organic acids, including lactic, acetic, citric, tartaric, formic, and malic acids (Cazón et al., 2021; Bhowmik et al., 2022). Chitosan, derived from various sustainable sources, is a bio-resource known for its exceptional antibacterial and antioxidant properties, as well as its ability to inhibit enzymes. It is considered safe for consumption, environmentally friendly, and biodegradable. Consequently, extensive research is being conducted on chitosan across various sectors, such as food science, pharmaceuticals, environmental conservation, chemical engineering, cosmetics, agriculture, and textiles (Wang et al., 2020; Kou et al., 2021). Chitosan has been the subject of extensive research across various applications and sectors owing to its antibacterial, antioxidant, biodegradable, enzyme-inhibitory, and biocompatible properties (Jiménez-Gómez and Cecilia, 2020; Ahghari et al., 2022; Bashir et al., 2022; Liu T. et al., 2022b). Chitosan is a biopolymer that shows promise for food packaging applications due to its capacity to suppress the growth of Gram-negative and Gram-positive bacteria, yeasts, and food-borne filamentous fungi. Furthermore, it functions as an antimicrobial substance, a vehicle for delivering antimicrobial agents and prebiotics that can improve the body's ability to resist colonization by harmful pathogens (Jiang et al., 2023). The fascination with the structure and utilization of chitosan can be traced back to the 19th century. In 1859, Rouget was the first to explore the deacetylated variations of chitin, the parent natural polymer found abundantly in nature. Presently, chitosan has obtained Generally Recognized as Safe status from the U.S. Food and Drug Administration (Oleksy et al., 2023). Chitosan is recognized for its diverse advantageous characteristics, such as its capacity to adhere to fats and cholesterol within the gastrointestinal (GI) system, potentially leading to a decrease in cholesterol levels and facilitating weight management (Huang et al., 2020). Nevertheless, its drawbacks encompass a diminished capacity for dissolving in water, resulting in the formation of a firm crystal structure. Furthermore, its elevated water vapor permeability proves unsuitable for environments with high humidity levels (Elsabee, 2013; Candir et al., 2018; Chaudhary et al., 2020). Table 1 shows that chitosan can be used in many industries.

Depending on the degree of deacetylation and the chitin source, the molar mass of commercially available chitosan products varies greatly, usually ranging from 50 kDa to over 1,000 kDa. Chitosan exhibits solubility in acidic to neutral solutions due to its pKa value of around 6.5 (Kumar et al., 2004; Ogawa et al., 2004; de Alvarenga, 2011). Since chitosan is mainly derived from the shells of crustaceans, nations with sizable seafood industries dominate chitosan manufacturing. China, India, and Japan are the top manufacturers; these countries have set up extensive production plants to fulfill the demand

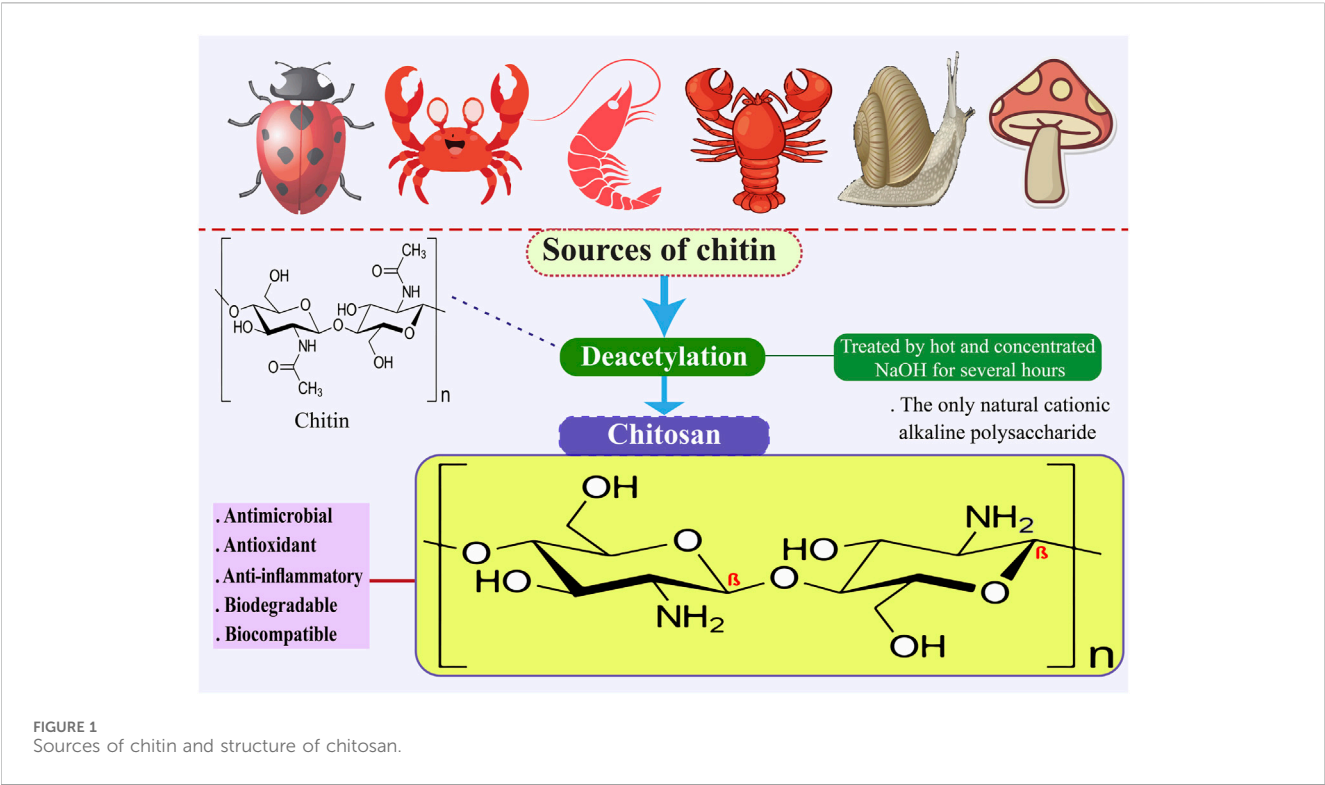


TABLE 1 Various applications of chitosan.

| Applications | Examples | References |
|---|---|---|
| Tissue engineering | Repair of scaffolds, regeneration of bones and tissues, regeneration of sulphate sponges in bone, diabetes treatment, development of artificial pancreas, cartilage regeneration, skin tissue regeneration, cardiac tissue regeneration | Islam et al. (2020), Kołodziejska et al. (2021), Kim et al. (2023) |
| Pharmaceutical and biomedical materials | Drug delivery systems, treating burns, surgical structures, dental repair and treatment, lenses for eyes, artificial skin, dialysis of blood, accelerated wound healing, antitumor and antibiotic uses, and synthetic blood vessels | Iacob et al. (2021), Khalaf et al. (2023), Almajidi et al. (2024) |
| Cosmetics | Skin and hair care products | Guzmán et al. (2022), Kulka and Sionkowska (2023) |
| Food and feed additives | Extension of natural flavor, color stabilization in foods, lipid absorption reduction, food and beverage de-acidification, antioxidant and food preservation, stabilizing agent, thickening agent, controlling agent, additives in livestock and fish food, manufacture of dietary fibers | Muzzarelli and De Vincenzi (2020), Anggraeni et al. (2022) |
| Water engineering | Treatment of waste water, dye removal from water, removal of pesticides and ions from water, removal of heavy metals from water, removal of petroleum products from water, color removal from textile waste waters, removal of dyes from effluents | Ahmed et al. (2020), Bhatt et al. (2023) |
| Food packaging | Covering various fruits and vegetables, spraying chitosan on food, preparing a film, controlling food contaminating microbes, covering meat, fish, chicken, increasing the shelf life of food | Kumar et al. (2020a), Priyadarshi and Rhim (2020), Flórez et al. (2022) |
| Gene therapy | It delivers numerous genes employed in gene therapy, siRNA, and cancer therapy technologies | Wu et al. (2020), Reshad et al. (2021) |
| Agriculture | Seed coating, excellent film coating with antimicrobial activities, removal of pesticides and herbicides from soil and water, preservation of post harvested foods, enhancing soil quality, enhancing plant growth | Faqir et al. (2021), Zhang et al. (2022a), Hidangmayum and Dwivedi (2022) |

from throughout the world (de Alvarenga, 2011; Yadav et al., 2019; Santos et al., 2020; Huq et al., 2022). Hydrogen bonding between the polymer chains of chitosan plays a crucial role in its structural stability and contributes to its distinct physical features (Ogawa et al., 2004; Chen et al., 2018). Furthermore, lysozyme—an enzyme in human tears, saliva, and other physiological fluids—acts as the primary biodegradation agent for chitosan. Chitosan is an advantageous material for biomedical applications because of its enzymatic breakdown, which produces non-toxic byproducts (Lončarević et al., 2017; Desai et al., 2023).

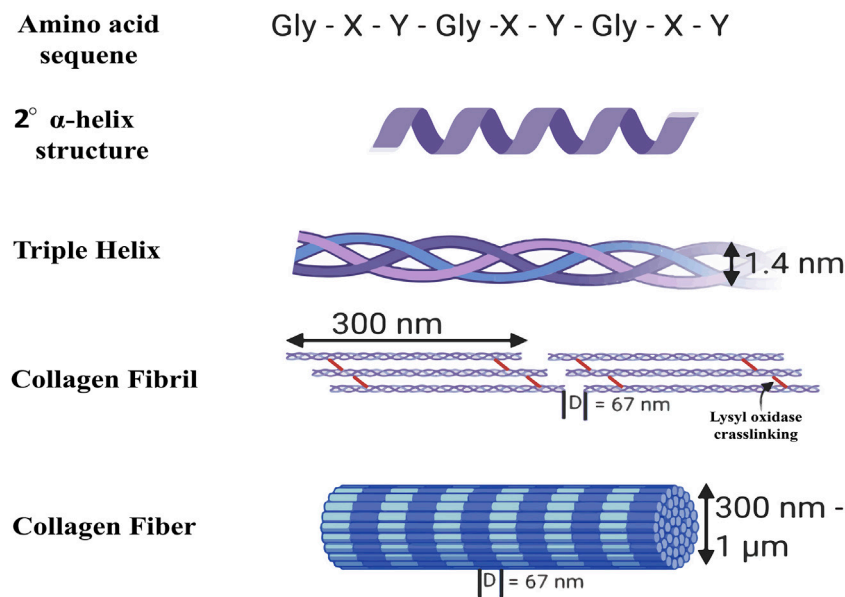


FIGURE 2
Structure of collagen (Walimbe and Panitch, 2020).

1.2 Gelatin

Gelatin is a naturally occurring polymer derived from the hydrolytic breakdown of collagen protein. Its unique amino acid composition imparts various medicinal advantages (Figure 2) (Kumosa et al., 2018). The substance is a transparent gel that exhibits fissures upon desiccation due to the degradation of collagen within tissues and skeletal structures (Alipal et al., 2021). Following collagen isolation, gelatin can be obtained through two methods: acid hydrolysis or alkaline hydrolysis (Bello et al., 2020; Echave et al., 2017; Tabata and Ikada, 1998). Collagen, the predominant protein in mammals, is distinguished by its distinctive triple-helix configuration, offering exceptional tensile strength and stability (Brodsky et al., 1997; Di Lullo et al., 2002). Collagen's isoelectric point varies according to its kind and source; however, it typically ranges from pH five to 6. There are several uses for collagen in the culinary, cosmetic, and pharmaceutical sectors (Thomas and Kelly, 1922; Lee et al., 2001; Avila Rodríguez et al., 2018). In addition to covalent cross-links that boost collagen's mechanical strength, intra- and intermolecular hydrogen bonds preserve the protein's three-dimensional structure. Collagen has a wide range of molar masses; Type I collagen has a molecular weight of about 300 kDa (Ramachandran et al., 1955; Bella et al., 1996; Gores et al., 2021). The growing demand for collagen and collagen-derived products in medical, cosmetic, and nutraceutical uses has resulted in a considerable global industry (Avila Rodríguez et al., 2018; Vieira et al., 2023).

Typically, gelatin is available in tablet, granule, or powder form and may require dissolution in water before utilization (Yang et al., 2016). The favorable attributes of this material, such as its ability to biodegrade, biocompatibility, and low toxicity, promote enhanced cell adhesion, differentiation, and proliferation. Simultaneously, it undergoes degradation by endogenous enzymes metalloproteinases within the body without eliciting an immunogenic reaction (C

Echave et al., 2017; Echave et al., 2017; Echave et al., 2019). Gelatin is extensively utilized in various industries such as pharmaceuticals, food, cosmetics, and photography due to its unique functional properties. Gelatin is a food ingredient employed in the dairy, bread, beverage, and confectionery sectors to offer gelling, texturization, stability, and emulsification properties (Hanani et al., 2014). Gelatin is protein-rich and can be a viable alternative to fats and carbohydrates in some nutritionally balanced food products (Lv et al., 2019). Collagen, the predominant protein in both humans and animals, serves as the protein matrix for gelatin, providing a source of protein. Collagen is present in various body parts, with the highest concentrations found in bones, skin, tendons, and ligaments (Alipal et al., 2021). Gelatin is free of fat and cholesterol, making it a low-energy option. Additionally, it contains protective colloids that offer potential health benefits (Alipal et al., 2021). Pang and colleagues (Pang et al., 2014) suggest that gelatin exhibits significant emulsifying properties and has the potential to inhibit the coagulation of proteins from milk, soybean milk, and other sources in the presence of gastric acid within the stomach, thereby facilitating the process of food digestion (Pang et al., 2014).

2 Chitosan and gelatin processing techniques

Chitosan and gelatin can undergo diverse processing methods for various applications (Kou et al., 2021; Rigueto et al., 2022). Chitosan and gelatin are versatile materials that may be included in many products, including tablets, capsules, nano- and microparticles, beads, gels, and films. It can also be precipitated, blended, spray-dried, emulsified, and crosslinked (Bansal et al., 2011). Utilizing the solvent evaporation technique, membranes and films suitable for use in water and air filtering procedures

may be produced. In the straightforward three-step solvent evaporation method, nano- or micron-sized biopolymer fillers are combined with polymer resin; occasionally, fibers are added to improve the mechanical qualities. The evaporation process is then started by pouring the combined solution into a glass container and heating it. The cast membrane or film can be removed from the container once it has evaporated (Alipal et al., 2021; Ilyas et al., 2022). The electrospun fibers are smaller in diameter and have a greater surface area. The potential differences produced between the spinneret and collector are applied to the polymer solution. The pendant-like droplets become jets due to the electric filling. At a critical point, the tension provided by the solution on the surface is exceeded by the electricity's repulsion. This process causes fast whipping of the extruded polymer solution, which is unstable and causes nanofibers to develop on the collector due to evaporation (Sajkiewicz et al., 2014; Qasim et al., 2018; Green-Warren et al., 2022). During this procedure, biopolymer particles are blended with a polymer solution and maintained within a dispersion needle. The solution in the needle receives a high voltage. The droplets resist one another because of their equal charges. As a result of instability at the needle tip, the droplets begin to disperse into micron-sized particles and land on surfaces that are oppositely charged, all the while the solvent quickly evaporates (Choktaweasap et al., 2007; Islam et al., 2011; Sahoo et al., 2015; Garg et al., 2019; Hathout and Metwally, 2019). The best substitutes for chemically made wax coatings are biopolymers (Shyu et al., 2019; Shiekh et al., 2021). These coverings shield fruits from oxidation, reducing the amount of microorganisms present. To preserve their quality, fruits and vegetables are coated with gelatin and chitosan after harvest (Poverenov et al., 2014; Shyu et al., 2019).

3 Chitosan and gelatin as antimicrobial

The antimicrobial efficacy of chitosan is influenced by various fundamental factors, including the specific type of microorganism, the concentration and source of chitosan, its structural characteristics such as molecular weight and degree of acetylation, pH levels, environmental conditions, temperature, incorporation into composite materials, and the use of chitosan derivatives (Li and Zhuang, 2020; Yan et al., 2020). Chitosan with a lower molecular weight typically demonstrates greater antimicrobial efficacy due to its enhanced solubility, facilitating improved penetration of bacterial cell membranes (Gopi et al., 2020). Chitosan and chitooligosaccharide were incorporated into the cellulose matrix to enhance its antibacterial properties, with assessments conducted on both Gram-positive and Gram-negative bacterial strains. The findings demonstrated that Bacterial cellulose–chitosan and Bacterial cellulose–chitooligosaccharide composites displayed advantageous antibacterial properties compared to pure bacterial cellulose matrix. Additionally, these composites were characterized by reduced porosity and a compact structure. The composite material of bacterial cellulose/chitooligosaccharide demonstrates exceptional compatibility in food and medicinal contexts (Yin et al., 2020). Through the process of synthesis and testing, the antibacterial activity of chitosan NPs against tomato phytopathogens was

evaluated. Pathogens include *Colletotrichum gelosporidies*, *Phytophthora capsici*, *Gibberella fugikuri*, *Sclerotinia sclerotiorum*, and *Fusarium oxysporum* are used in the testing procedure (Oh et al., 2019). Elwakil et al. (2020) prepared chitosan NPs and liposomes incorporating ethanolic cinnamon extract. They examined their chemical and physical characteristics before assessing their ability to heal wounds. Using chitosan and liposomes containing ethanolic cinnamon extract, they made a gel and tested it on diabetic mice. They discovered that the liposome/cinnamon gel was required for more effective treatment of bacterial infections and enzyme inhibition. Previous research has shown that chitosan exhibits greater efficacy in combating Gram-positive bacteria compared to Gram-negative bacteria. Additionally, chitosan has been found to possess inhibitory properties against various bacteria and fungi (Yan et al., 2021). The incorporation of chitosan and essential oil formulation in chitosan-derived edible packaging films enhanced the antimicrobial efficacy against a range of Gram-negative bacteria, notably *Escherichia coli*, *Pseudomonas aeruginosa*, *Klebsiella pneumoniae*, *Pseudomonas fluorescens*, *Shewanella baltica*, *Shewanella putrefaciens*, *Serratia* spp., as well as Gram-positive bacteria like *Staphylococcus saprophyticus* and *Staphylococcus aureus* (Altiok et al., 2010; Wang et al., 2011; Hafsa et al., 2016; Sani et al., 2019; Amor et al., 2021; Punia Bangar et al., 2021). Nevertheless, the growth of yeast, fungus, and mold is also suppressed (Pavlátková et al., 2023). Chitosan sheets were evaluated for their effectiveness against *Penicillium italicum* when combined with bergamot essential oil, demonstrating significant inhibitory properties. However, the inhibitory efficacy of the composite sheets was observed to diminish throughout the storage duration (Sánchez-González et al., 2010). The essential oils derived from cinnamon were found to have inhibitory effects on the growth of various fungi such as *Botrytis cinerea*, *Aspergillus oryzae*, *Penicillium digitatum*, *Aspergillus niger*, and *Rhizopus stolonifera* when applied to chitosan films (Mutlu-Ingok et al., 2020; El-araby et al., 2022). Li Z. et al. (2019a) noted that incorporating turmeric essential oil into chitosan led to notable anti-aflatoxigenic effects due to its demonstrated antifungal properties against *Aspergillus flavus*. Kavooosi et al. (2013) found that gelatin films containing thymol exhibited significant antibacterial efficacy, indicating their potential utility as antibacterial nano wound dressings for combating pathogens responsible for wound burns. This characteristic renders them appropriate for application as nano wound dressings with antibacterial properties for treating burns caused by pathogenic microorganisms (Ndlovu et al., 2021). They absorb wound exudates, maintain a moist wound environment, mimic the structure of the extracellular matrix (ECM), and exhibit antibacterial properties (Deng et al., 2022).

In the research conducted by Roy and Rhim (2021), it was observed that composite films comprising gelatin and chitosan exhibited effective antibacterial characteristics against pathogenic bacteria such as *E. coli* and *L. monocytogenes*. This antimicrobial efficacy was attributed to the inherent antimicrobial properties of chitosan. Furthermore, the study revealed that the antibacterial properties of the composite films were enhanced by the addition of functional fillers, cinnamon, and rutin (Roy and Rhim, 2021). Kurczewska (2022) states that gelatin and chitosan, along with their derivatives, are biodegradable polysaccharides characterized by

biocompatibility, non-toxicity, and possessing antimicrobial and antifungal attributes (Kurczewska, 2022). The antibacterial efficacy of a chitosan-polyphenol extract was examined on Gram-negative bacterial strains including *Proteus mirabilis*, *P. aeruginosa*, *E. coli*, *Salmonella enterica*, *Salmonella typhimurium*, and *Proteus vulgaris*, demonstrating notable antimicrobial effects (Balti et al., 2017; Pires et al., 2022). Also, chitosan-polyphenol extracts exhibited notable antibacterial efficacy against Gram-positive bacterial strains including *Bacillus subtilis*, *Listeria innocua*, *Bacillus cereus*, *Streptococcus mutans*, *Listeria monocytogenes*, *S. aureus*, *Lactobacillus plantarum*, *Lactobacillus sakei*, and *Bacillus thuringiensis* (Balti et al., 2017; Zhang et al., 2019; Amankwaah et al., 2020; Zarandona et al., 2020). A hybrid hydrogel composed of chitosan and gelatin, supplemented with berberine hydrochloride (BBR) and gallic acid, demonstrated improved antibiofilm properties against *E. coli* and *S. aureus*. This formulation shows promise for potential use in biomedical settings (Liu et al., 2023). In addition, in a study, composite films made of chitosan, gelatin, and polyvinyl alcohol (PVA), which include antimicrobial agents such as *Duchesnea indica* extract, have demonstrated the ability to inhibit pathogens like *S. aureus*. This indicates the promising application of these films in food packaging (Choi et al., 2022).

4 Chitosan and gelatin as antioxidants

It is acknowledged that oxidation poses a significant challenge to the quality of food items. Additionally, the high-temperature processing of protein-based foods leads to the formation of heterocyclic amines, which are identified as carcinogenic compounds (Flores Llovera et al., 2019). Various elements, including processing parameters, culinary techniques, the existence of antioxidants, duration, and heat levels, can impact the generation of heterocyclic amines. Consequently, the mitigation or prevention of the creation of these carcinogenic compounds has emerged as a significant concern (Nadeem et al., 2021). A component that can postpone or prevent the oxidation of the molecules present in the medium is an antioxidant compound (Shahidi and Zhong, 2015). Gelatin and chitosan are both excellent options for creating antioxidant formulations and products since they both have antioxidant qualities (Jridi et al., 2014). The strong propensity of chitosan biopolymer to act as a hydrogen atom donor enhances its antioxidant capacity (Negm et al., 2020). Chitosan, when incorporated into food products as a food additive, can function as an antioxidant agent. This stops foods from forming heterocyclic amines (Liu T. et al., 2022b). Oz et al. (2017) investigated the effects of utilizing chitosan at varying concentrations of 0.25%, 0.50%, 0.75%, and 1% w/w on the quality of meatballs and the production of heterocyclic aromatic amines. The meatballs underwent preparation at different temperature levels (150°C, 200°C, and 250°C). Findings indicated that elevating the temperature from 150°C to 250°C resulted in a rise in the concentration of heterocyclic amine within the meatballs. However, upgrading the concentration of chitosan resulted in a notable reduction in the levels of the heterocyclic amine. Frozen meat's 2-thiobarbituric acid reactive substance (TBARS) levels decreased by 70% when 1% chitosan was added. It has been observed that adding chitosan causes the free iron in beef heme

proteins that are liberated during processing to be chelated (Tharanathan and Kittur, 2003). The antioxidant properties of chitosan have been found to correlate positively with its molecular weight, concentration, and viscosity. Chitosan derived from discarded crab shells was evaluated on herring tissue, and chitosan samples of varying viscosities were similarly assessed on fish specimens. The highest activity was observed with low-viscosity chitosan, and its action was similar to that of butylated hydroxytoluene (BHT), butylated hydroxy-anisole (BHA), and tert-butylhydroquinone (TBHQ). TBHQ, BHT, and BHA are synthetic antioxidants. Chitosan is believed to inhibit lipid oxidation in fish by sequestering ferrous ions (No et al., 2007; Muthu et al., 2021). Mirsadeghi et al. (2019) demonstrated that the incorporation of acid-soluble chitosan at a concentration of 1% into Huso filets during the cooking process resulted in a significant decrease in the formation of heterocyclic amines, with an observed inhibitory effect of 68.09%. Adiletta and colleagues (Adiletta et al., 2019) assessed the functionality of enzymes including polyphenol oxidase, peroxidase, ascorbate peroxidase, and catalase to investigate the effects of chitosan-based coatings on preserving fig freshness. The findings indicated that applying a chitosan coating led to a notable enhancement in the levels of anthocyanins, flavonoids, and total polyphenols, as well as increased antioxidant activity in the preserved figs. This treatment also resulted in a decrease in oxidative stress and inhibited browning reactions when compared to the control group that did not receive the coating (Adiletta et al., 2019). The gelatin obtained from by-products of skipjack tuna (*Katsuwonus pelamis*) canning was refined to yield nineteen peptides exhibiting significant antioxidant properties. The gel's exceptional clarity and strength are attributed to its elevated concentration of amino acids. These findings suggest that the antioxidant peptides derived from this gelatin could serve as potential supplements in health-promoting products to prevent ultraviolet-A damage (Zhang Y. et al., 2022b). In a study conducted by Sul et al., they found that adding carbon dots (CDs) from banana peel to chitosan/gelatin-based films improved the antioxidant properties of the films (Sul et al., 2023). Similarly, Roy and Rhim (2021) antioxidant activity of chitosan/gelatin-based films was evaluated using ABTS and DPPH methods. They have found that by adding cinnamon and rutin to chitosan/gelatin films, the antioxidant properties of the films increase. Furthermore, it has been shown various naturally derived bioactive compounds, including volatile oils, extracts from black or green tea, apple extract, purple and black eggplant, as well as purple and black rice, have been found to enhance the antioxidant properties of chitosan (Riaz et al., 2018; Yong et al., 2019a; Yong et al., 2019b; Asli et al., 2020). This occurrence has been linked to the ability of the polyphenols present in the extract to eliminate free radicals through the release of phenolic hydrogen atoms (Pattnaik et al., 2022).

5 Chitosan and gelatin in food packaging

Over two hundred human illnesses, spanning from GI issues to cancer, are attributed to the consumption of food contaminated with pathogenic microorganisms, parasites, viruses, or toxic substances, resulting in approximately 600 million new cases and

420,000 fatalities annually (Suvana et al., 2022). Food items derived from agricultural sources, such as fruits, are significantly tainted by harmful microorganisms due to inadequate safety measures (Paramithiotis et al., 2017). Similarly, the heightened levels of global trade have amplified the potential for disease transmission via contaminated food products, leading to an increased incidence of foodborne illnesses. Therefore, there is a necessity for intensified and targeted endeavors aimed at enhancing food packaging systems to mitigate the potential for foodborne illnesses (Bahrami et al., 2020). Food packaging systems provide a range of advantages, including improved handling, extended shelf life, and safeguarding against physicochemical harm during storage and transportation. As such, they play a vital function within the worldwide food sector. Additionally, individuals are seeking food packaging materials that are innovative, cost-efficient, environmentally sustainable, and effective in ensuring the safety, nutritional value, and quality of products (Omerović et al., 2021). Novel packaging techniques incorporating antioxidant and antibacterial properties are currently under development to enhance food safety measures (Roy and Rhim, 2021). Biopolymers, including proteins and carbohydrates, offer numerous advantages over traditional synthetic polymers when utilized as a stable matrix in active packaging films (Atarés and Chiralt, 2016). Using petroleum-based materials has negative environmental implications since they are neither renewable, recyclable, reused, or obtained responsibly (Cruz et al., 2022; Zhao et al., 2022). In a study, Sul et al. (2023) prepared active films with an equal mixture of chitosan and gelatin and added CDs from banana peel to be used for food packaging. They discovered that adding CD to chitosan/gelatin functional films has a wide range of applications in food packaging, particularly in extending the shelf life of meat and preserving its visual quality. Hamann et al. (2022) prepared active films consisting of 15% gelatin, 1% green tea extract, and 30% glycerol. These films were incorporated into the outer layer of the newly prepared sausages. The results of their study indicated that the application of an active gelatin film on sausages led to a decrease in TBARS levels during refrigerated storage. Ultimately, they determined that gelatin films incorporating green tea extract show potential as a viable alternative for prolonging the shelf life of sausages (Hamann et al., 2022). Wu et al. (2019) developed chitosan films by incorporating curcumin-loaded mesoporous silica nanoparticles (CMSNP) through the solvent-casting technique. The film's dimensions, mechanical properties, and water vapor permeability were determined to be 0.0931 ± 0.0021 mm in thickness, 19.87 ± 1.02 MPa in tensile strength, $25.46\% \pm 2.16\%$ in elongation at break, and 15.21 ± 1.83 g 10^{-11} /s m^2 Pa in water vapor permeability. The CMSNP film and the plain Chitosan/Curcumin blend film demonstrated zones of inhibitions (ZOI) measuring approximately 7.5 and 8 mm against *E. coli* and 8 mm and 10 mm against *S. aureus*, respectively (Wu et al., 2019). Siripatrawan and Kaewklin (2018) created active packaging using chitosan and Titanium dioxide (TiO₂) NPs at varying concentrations (0%, 0.25%, 0.5%, 1%, and 2% w/w). The chitosan film with a 1% concentration of TiO₂ NPs exhibited antibacterial effects against various strains of bacteria, including *S. aureus*, *E. coli*, *P. aeruginosa*, and *S. typhimurium*, as well as fungi such as *Penicillium* and *Aspergillus*. Therefore, the findings indicated that chitosan-TiO₂ nanocomposite films have the potential to serve as effective active packaging materials (Siripatrawan and Kaewklin,

2018). Dehghani et al. (2022) developed coating dispersions using combinations of fish gelatin, conjugates, and bitter almond gum in varying ratios of 1:2, 2:1, and 1:1. The researchers examined the impact of coating suspensions on the physicochemical and qualitative characteristics of tomatoes during a 28-day storage period at a temperature of 20°C. The researchers discovered that combining fish gelatin with a greater proportion of bitter almond gum has the potential to be an effective method for creating coating dispersion and preserving the quality of fruits over time (Dehghani et al., 2022). Wang et al. (2018) utilized a blend of chitosan and gold NPs to demonstrate the frozen state and temperature profile of food by observing the color variation resulting from the aggregation of gold NPs due to their localized surface plasmon resonance. Moreover, due to the alterations in the physical and chemical properties of food, chitosan-derived materials developed for tracking pH fluctuations in food products can also detect bacterial presence and oxidative degradation of food. Singh et al. (2021) incorporated gallic acid and sodium carbonate into the chitosan film to create an oxygen-absorbing substance. The findings indicated a reduction in the mechanical properties of the chitosan films with escalating levels of sodium carbonate and gallic acid additives. This phenomenon could be attributed to the significant quantity of sodium carbonate disrupting the internal structure of the chitosan film. El-Gioushy et al. (2022) conducted research on the utilization of nano-chitosan as a functional edible coating film at varying concentrations (1, 2, and 3 cm³/L) to improve the shelf life and quality attributes of Barhi cultivar date palm fruits during refrigerated storage at $\pm 2^\circ\text{C}$ for 70 days. Their findings indicated that applying three cm³/L of nano-chitosan as a spray on Barhi date fruits yielded optimal outcomes after the storage period (El-Gioushy et al., 2022). In an investigation involving gelatin-chitosan and pectin-chitosan, films and coatings were produced. The researchers integrated lemongrass essential oil, Zn, or ZnO as active components into the films. The thermal analysis indicated a notable level of stability. Regarding mechanical properties, the gelatin-chitosan films exhibited favorable attributes suitable for practical utilization. Furthermore, the antibacterial efficacy was evaluated, revealing a synergistic interaction among the active components integrated within the films. The unique aspect of this research lies in the experimentation conducted on the protective coating applied to containers holding raspberries. The most favorable microbiological performance was observed in containers treated with a gelatin-chitosan emulsion containing ZnO. The longevity of the fruit was extended by all formulations examined, ranging from four to 8 days (Jovanović et al., 2021). Table 2 Summary of recent studies on the use of chitosan/gelatin composites reinforced for food packaging.

The capacity of food packaging materials to regulate the transfer of water vapor is one of the most critical factors. This characteristic, which stops moisture loss and oxidation, is essential for preserving the quality and lengthening the shelf life of perishable foods. It has been discovered that chitosan films have a low water vapor transmission rate, which helps to keep food items wet. Because chitosan is hydrophilic, it may create strong hydrogen bonds that aid in forming a barrier against water vapor (Cazón et al., 2019; Long et al., 2023). Gelatin exhibits notable gas barrier characteristics and swelling behavior in aqueous environments, yet it is hindered by limited mechanical strength and susceptibility to water vapor

TABLE 2 Recent studies on the use of chitosan/gelatin for food packaging.

| Biodegradable matrix | Reinforcement | Conclusion | Reference |
|----------------------|---|---|-------------------------|
| Gelatin/chitosan | Curcumin | Based on the results, protein-rich animal goods like meat and seafood are protected, and their freshness is tracked using gelatin, chitosan, and curcumin nanofiber packing, which has a lot of promise | Duan et al. (2023) |
| Chitosan | Nanocellulose | While maintaining water vapor permeability, adding nanocellulose increased the material's thermal stability and oxygen barrier. The chitosan/nanocellulose films' increased tensile strength and Young's modulus indicated improved mechanical characteristics. These films showed fungicidal action against <i>Candida albicans</i> as well as bactericidal impact against both Gram-positive and Gram-negative bacteria | Costa et al. (2021) |
| Chitosan/gelatin | Green synthesized zinc oxide (ZnO) | -The hybrid films reinforced with ZnO NPs had better compactness, elongation-at-break, and thermal stability -The produced hybrid nanocomposite films can be used as a biodegradable substitute for fresh fruit and vegetable postharvest packaging | Kumar et al. (2020b) |
| Chitosan | Peppermint essential oil and berberis extract | The turkey breast meat treated with a chitosan solution containing berberis extract and peppermint essential oil showed significantly reduced bacterial counts and oxidation levels under refrigeration | Yuceer and Caner (2014) |
| Chitosan/gelatin | AgNPs | The produced composite films were considered a biodegradable and biocompatible food packaging material and a substitute for petroleum-based plastics since they had all the necessary qualities for packaging material, including mechanical strength, flexibility, barrier properties, and antimicrobial activity, according to the results | Ediyilyam et al. (2021) |
| Chitosan/gelatin | Apple Peel NPs | The outcomes showed that the films made of chitosan/gelatin and apple peel extract had strong antioxidant qualities, suggesting they could be developed as a bio-nanocomposite food packaging material for the food sector | Riaz et al. (2020) |

permeation (Sobral et al., 2001; Zhang et al., 2010). Pellá et al. (2020) developed a thin film with low solubility and exceptionally low water vapor permeability by physically mixing cassava starch, gelatin, casein, and sorbitol. The fruit with coating saw less quality loss and had a higher concentration of soluble solid and vitamin C due to the delayed rate of chlorophyll breakdown. In addition, the guava fruit covered with this film had a 2-day shelf life increase. After 9 days of storage, fruit with a coating remained green, but fruit without a coating had turned brown after 3 days. It is evident that gelatin-based mixtures efficiently postpone the ripening and rotting of fruit (Pellá et al., 2020). A combination coating consisting of chitosan, gelatin, gallic acid, and clove oil was created by Xiong et al. (2021) to study the fresh-keeping properties of fresh salmon fillet that was kept in a refrigerator for 15 days at 4°C. It was found that the combination coating may successfully stop the salmon fillet's brightness from decreasing. This may be because the film has an antioxidant effect that protects and isolates the fish from the environment. Adding chitosan/gelatin and clove oil significantly enhanced the antioxidant and antibacterial effects, resulting in a shelf-life extension of at least 5 days. Additionally, the gas and water vapor permeability of the gelatin coating and the PH value of all the coated fillet samples decreased (Xiong et al., 2021).

The studies summarized in Table 2 collectively highlight the potential of chitosan/gelatin composites reinforced with various nanomaterials for food packaging applications (Yuceer and Caner, 2014; Kumar et al., 2020b; Riaz et al., 2020; Costa et al., 2021; Ediyilyam et al., 2021; Duan et al., 2023). The reinforcement materials consistently increase the mechanical strength, barrier characteristics, and antimicrobial activity of the composites. However, the environmental impact and cost-effectiveness of large-scale production of these composites

need to be investigated further. Future research should focus on addressing these gaps and developing standardized testing protocols.

5.1 The process of producing food packaging films

5.1.1 Casting method

The casting method, solvent casting, is the predominant technique utilized for film formation in laboratory and pilot-scale settings. The procedure for preparing biopolymer films includes dissolving the biopolymer in an appropriate solvent, pouring the solution into a mold, and subsequently drying the casted solution. The initial stage involves choosing the polymer or combination of polymers to form the fundamental film. The selected polymer is dissolved in an appropriate solvent, a critical step as the film-forming capability primarily hinges on the solubility of the polymer rather than its melting characteristics. During the casting process, the solution obtained is poured into a preselected mold or a Petri dish coated with Teflon. During the drying phase, the solvent undergoes evaporation, leading to the formation of a polymer film that attaches to the mold. Various types of air dryers, including hot air ovens, microwaves, tray dryers, and vacuum driers, are employed to efficiently eliminate solvents and facilitate the successful peeling of formed films (Jensen et al., 2015; Suhag et al., 2020). To increase chitosan's solubility, dissolves in an acidic solution like acetic acid. Water is used to dissolve gelatin, and heat is frequently used to promote total dissolving (Park et al., 2002; Chuaynukul et al., 2018). Usually, the casting procedure is carried out at ambient

temperature (20°C–25°C). To preserve their fluidity, gelatin solutions can be cast at somewhat higher temperatures (30°C–40°C) (Acerno et al., 1999; Aniunoh et al., 2006; Biscarat et al., 2015). It might be necessary to wash chitosan films with distilled water or a neutralizing solution such as sodium hydroxide to eliminate any remaining solvent and balance the pH (Kim et al., 2006; Chang et al., 2019).

5.1.2 Extrusion method

The extrusion technique is commonly employed in polymer processing for producing polymeric films. This procedure modifies the composition of the substances and enhances the physical and chemical properties of the extruded material. The extrusion process typically consists of three main stages: (i) feeding, (ii) kneading, and (iii) heating as the exits the machine. Initially, the film-forming mixture is introduced into the feeding zone and compacted with air assistance. This procedure is commonly called a dry process due to its limited use of water or solvents. Plasticizers like sorbitol or polyethylene glycol are employed in concentrations ranging from 10% to 60% by weight to enhance the flexibility of the film. During the kneading process, there is an elevation in the strain, temperature, and density of the mixture. Ultimately, during the heating phase, the thermal energy fluctuates within the temperature range of 120°C–170°C. This procedure relies on the thermoplastic nature of polymers, which occurs when plasticization and heating occur above the glass transition temperature under low moisture conditions (Fitch-Vargas et al., 2016; Suhag et al., 2020). The extrusion method is indeed utilized for producing films of chitosan and gelatin. This method offers advantages such as continuous production, uniform film thickness, and scalability for industrial applications. However, specific considerations must be made due to the thermal sensitivity and properties of chitosan and gelatin. High temperatures have the potential to degrade both gelatin and chitosan. For these biopolymers, the 120°C–170°C temperature range usually employed for polymer extrusion may be too high (Aider, 2010; Pelissari et al., 2011; Hanani et al., 2012; Krishna et al., 2012).

5.1.3 Electrospinning method

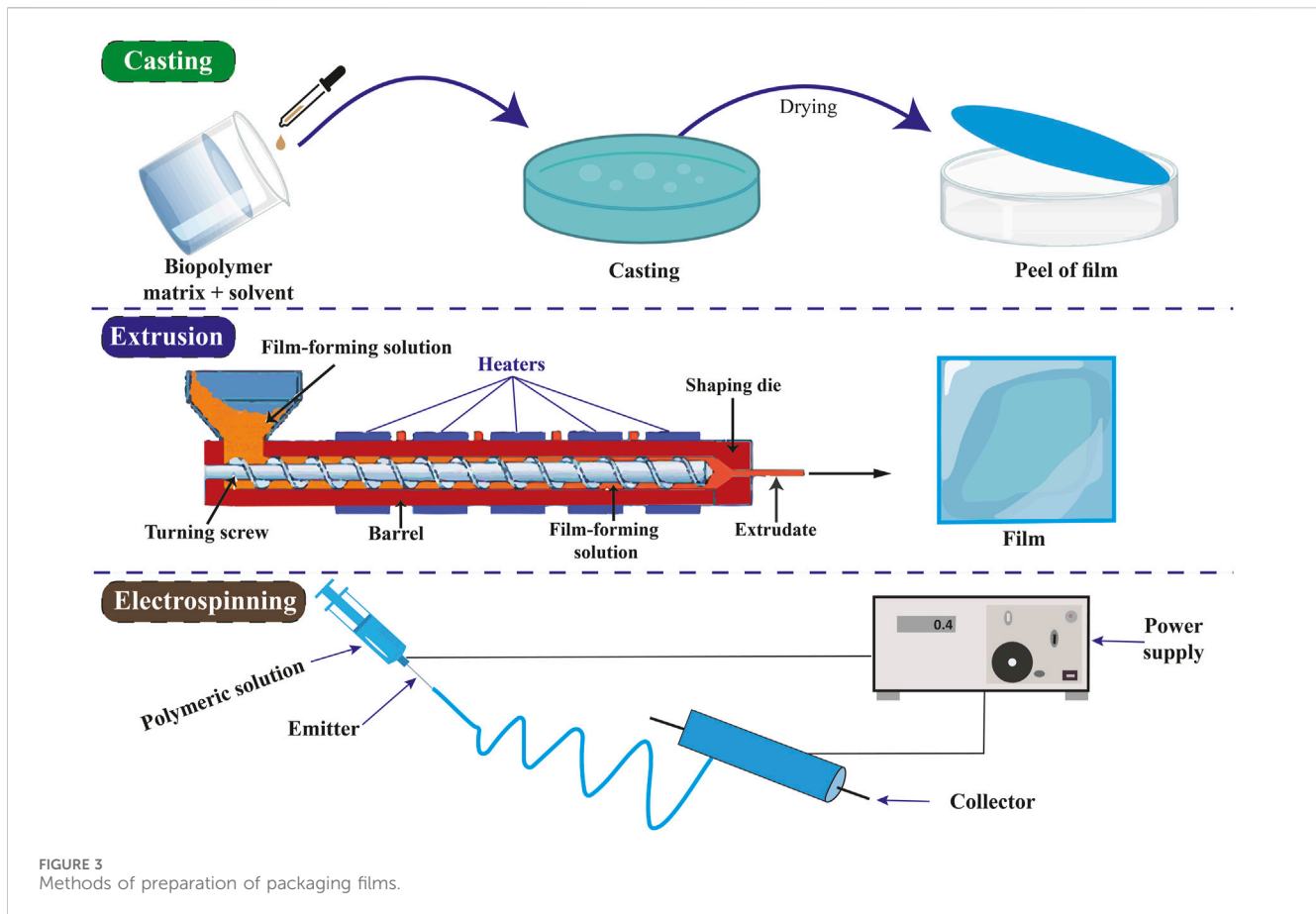
The electrospinning technique produces a nonwoven mesh composed of micro- or nanofibers. This method involves the application of high-voltage electricity to a liquid solution and a collector, resulting in the extrusion of the solution from a nozzle to form a jet. During the drying phase, the fibers generated by the jet are accumulated on the collector. Electrospinning represents a rapid and efficient method for producing micro- or nanoscale polymer fibers. The presence of polymers in the electrospinning solution results in modifications to its viscosity, molecular weight, surface tension, conductivity, concentration, solvent, and various other characteristics, all of which play a crucial role in influencing the electrospinning process. During the electrospinning process, the dispersed fibers undergo self-assembly due to electric charges, which are controlled by mechanical forces and geometric conditions. Electrospinning was employed to fabricate nanofiber polymers, including chitosan, collagen, alginate, cellulose, polyesters, and polyurethanes (Nayak et al., 2012; Yang et al.,

2020). The methods of preparing packaging films are shown in Figure 3.

To get the required viscosity for electrospinning, gelatin is usually dissolved in acetic acid-containing aqueous solutions or in a mixture of water and ethanol. Concentrations typically vary from 10% to 20% w/v, contingent upon the gelatin's molecular weight. Typically, chitosan is dissolved in 1%–2% v/v diluted acetic acid solutions to get the necessary electrospinnable viscosity (Ohkawa et al., 2004; Choktaweasap et al., 2007; Habibi and Hajinasrollah, 2018).

6 Chitosan and gelatin in microencapsulation technology

Microencapsulation is a novel technological advancement that involves safeguarding diverse food components or functional constituents from different processing conditions by encapsulating them within a polymeric or nonpolymeric substance. This encapsulation method enables the controlled release of these components under specific circumstances. Furthermore, it improves the sensory attributes of food products by concealing undesirable tastes, aromas, and flavors while bolstering food safety by suppressing microbial growth (Choudhury et al., 2021). The effectiveness of the capsule is contingent upon the characteristics of both the wall and base materials. Significant outcomes can be achieved by utilizing a blend of the wall material to formulate the microcapsules. The primary active constituents in Turkish oregano extract, carvacrol and rosmarinic acid, have demonstrated enhanced release in laboratory settings when encapsulated with gelatin, Tween 20, gum arabic, and cyclodextrin as coating agents (Baranauskaitė et al., 2019). Chitosan possesses characteristics that render it a suitable material for encapsulating a diverse range of bioactive compounds. This characteristic renders it valuable across various sectors, including food, biomedical, pharmaceutical, agricultural, environmental, and industrial (Ho et al., 2021). This polymer is utilized to encapsulate multiple substances such as food ingredients, medications, vitamins, lipids, essential oils, vaccines, hemoglobin, and microbial metabolites (Raza et al., 2020). Chitosan and its encapsulated derivatives are extensively employed in agriculture with various environmentally friendly products, including biopesticides, organic fertilizers, seed treatments, soil conditioners, and growth-promoting agents (Ambaye et al., 2022). Chitosan has been employed as a co-encapsulation agent for curcumin and resveratrol in various studies (Chen et al., 2020). Chitosan is used in the creation of nanocomposite active substances incorporated into films to suppress the proliferation of fungi like *A. niger*, *Aspergillus parasiticus*, *A. flavus*, and *Penicillium chrysogenum*, thereby facilitating the management and suppression of these harmful microorganisms (Hossain et al., 2019). Non-toxic chitosan has been extensively employed for the encapsulation of anthocyanins. Anthocyanin-chitosan NPs are created through the establishment of non-covalent interactions, such as weak ionic bonding and hydrogen bonding (Sreerekha et al., 2021). According to the findings, applying a dual coating comprising chitosan and a polyanionic polysaccharide to stabilize



anthocyanins resulted in a notable increase in encapsulation efficiency. This approach also conferred resistance against auto-oxidation, ascorbic acid degradation, exposure to heat, and neutral environmental conditions (Tan et al., 2021). The covalent bonds established between proteins and polysaccharides play a crucial role in increasing stability and preventing the release of anthocyanins in challenging conditions (Gonçalves et al., 2018). Overall, gelatin and chitosan show promise as polymeric matrices for microencapsulation.

The following specific techniques are commonly used for producing gelatin and chitosan particles.

6.1 Emulsification-solvent evaporation method

Using this procedure, a polymer solution is created by dissolving biopolymers in an organic solvent (such as dichloromethane or ethyl acetate). This solution is used to disperse or dissolve the active component, creating an emulsion (water-in-oil or oil-in-water). After that, the emulsion is agitated to allow the solvent to evaporate and solid particles containing the active component to form (Watts et al., 1990; Yang et al., 2001; Essa et al., 2020).

6.1.1 Ionic gelation method

Chitosan is well-suited for this approach because of its polycationic properties. The process entails the interaction of

chitosan with an anionic polymer or cross-linker (such as sodium tripolyphosphate or alginate) to create NPs or microspheres (Fan et al., 2012; Desai, 2016).

6.1.2 Coacervation method

This procedure, which includes phase separation, frequently uses gelatin. Warm water dissolves the gelatin, and the active component is then mixed into the mixture. To cause phase separation, an appropriate coacervating agent (such as gum arabic or gelatinized starch) is applied (Veis and Aranyi, 1960; Burgess and Carless, 1985).

6.1.3 Spray drying

Using this method, the active component and a solution or suspension of gelatin or chitosan are atomized and placed into a heated chamber to dry quickly. Microcapsules of the encapsulated item are left behind as the solvent swiftly evaporates (Bruschi et al., 2003; Estevinho et al., 2013).

7 Chitosan and gelatin in water treatment

Water serves as the fundamental cornerstone for supporting and sustaining life on the planet Earth. Access to clean drinking water is considered a basic human right; however, the issue of water scarcity has become a significant global challenge in contemporary times. This is primarily attributed to the swift expansion of industries, agriculture,

and technology, driven by the increasing world population. This phenomenon has resulted in the excessive utilization and pollution of current freshwater reservoirs (Kumar et al., 2014; Zhang et al., 2016a). According to a report published by the World Health Organization, the implementation of fundamental water hygiene and sanitation practices has the potential to reduce waterborne illnesses such as diarrhea by 35% (Pendergast et al., 2011; Sen Gupta et al., 2023). Inadequate sanitation can result in the introduction of new pathogens like the Ebola virus and the more recent SARS-CoV-2 into water systems, thereby presenting potential health risks for individuals (Quilliam et al., 2020; Lahrich et al., 2021). Two-thirds of the world's population is predicted to live in water-stressed areas with intermittent or persistent freshwater shortages by 2050, according to another analysis (Lee et al., 2016; Samantaray et al., 2018). In almost every facet of human existence, including sanitation, industry, agriculture, power production, building, and transportation, freshwater is required (Chelu et al., 2023). Even in minute concentrations, heavy metals including lead, nickel, copper, cadmium, zinc, mercury, arsenic, chromium, bismuth, cobalt, and iron are detrimental to the environment and public health (Engwa et al., 2019). It is crucial to remove numerous dangerous pollutants from wastewater, including paints, heavy metals, medicines, healthcare products, detergents, derivatives, and industrial by-products, since they not only contaminate water but also pose a toxic risk to the ecosystem (Ethaib and Zubaidi, 2022; Chelu et al., 2023). The GelYst biosorbent, used to enhance the extraction and biosorption of Cr (VI) from water, is made of yeast and gelatin. The use of this biosorbent in the treatment of water has proven effective (Mahmoud, 2015). Because of their numerous natural qualities, hydrogels based on natural polysaccharides are now employed as coagulants and adsorbents in the filtration of drinking water (Chelu et al., 2023). Chitosan-based hydrogels are promising matrices for treating contaminated waters because of their low cost, excellent chemical stability, mechanical solid and heat resistance, and ease of recovery—reusing the hydrogel and the contaminants (Chelu et al., 2023). Moreover, the mechanical strength of hydrogels based on chitosan can be increased by crosslinking with synthetic or biopolymers or by incorporating NPs. Through hydrogen bonding and electrostatic interactions, chitosan may readily adsorb various contaminants (such as heavy metals and dyes) because of its abundance of hydroxyl and amino groups (Luo et al., 2022). Chitosan has drawn a lot of interest in water treatment applications because of its unique qualities, which include cationic, high adsorption capacity, macromolecular structure, low cost, and abundance as compared to other commercial adsorbents (Ahmed et al., 2020). It has been claimed that chitosan or different variations of this biopolymer may successfully remove various metals and other contaminants (Russo et al., 2021). Furthermore, a gelatin/chitosan composite has been created and applied to pesticide wastewater samples, demonstrating a high level of atrazine and fenitrothion removal effectiveness (Attallah et al., 2021).

8 Chitosan and gelatin in drug delivery

Since drug distribution affects a therapeutic agent's safety and effectiveness, it is a crucial component of modern medicine. Targeted medication distribution is a challenging process that has

to get past several obstacles, such as the liver and kidneys' capacity to eliminate drugs, the bloodstream's quick breakdown, and biological membranes' limited permeability. A suitable carrier or vehicle is required to protect the drug from degradation, prolong its circulation, and improve its localization at the target site. The optimum drug delivery vehicle should have numerous critical traits, such as biodegradability, biocompatibility, and controlled release properties (Homayun et al., 2019). Biocompatibility assures that the delivery vehicle has no adverse effects on the body. In contrast, biodegradability ensures that it may be safely metabolized and eliminated from the body once its job is complete. Drugs with controlled release qualities release the medication in a regulated way over a predetermined time, maintaining therapeutic levels and minimizing dose frequency (Kantak and Bharate, 2022). The distinct attributes of gelatin and chitosan make them popular choices for medication delivery applications (Sethi and Kaith, 2022). Chitosan is authorized for use in tissue engineering and medication delivery applications by the FDA and is categorized as "Generally Recognized as Safe" (GRAS) (Kantak and Bharate, 2022). According to the results of several acute toxicity tests, chitosan has an LD50 of more than 16 g/kg when given orally to mice, and it is safe to use throughout the body (Kean and Thanou, 2010). One of chitosan's main advantages is its adaptability; it can be made into various dosage forms, each with unique qualities and uses (Desai et al., 2023). According to research on rabbit eyes by Zhang et al. (2016b), chitosan does not irritate the eyes. Santhi et al. (2017) employed spontaneous emulsification and a cross-linking strategy to generate fluconazole-loaded chitosan NPs. Using the cup-plate approach, they evaluated these NPs' antifungal properties in comparison to those of conventional eye drops. The average size of these particles was 152.85 ± 13.7 nm. It was found that every drug-loaded NP had an ideal (50%) drug-loading capacity. After their investigation, they concluded that the fluconazole-formulated chitosan NPs were a functional drug loading, antifungal efficacious, and delayed release delivery method for fluconazole (Santhi et al., 2017). Gelatin capsules can regulate medicine dosage, effectively increase drug use, and improve drug consumption and storage convenience (Gullapalli et al., 2017). Gelatin readily binds to medication molecules due to its high water solubility (Yildirim et al., 2023). Ramanathan et al. (2022) released 5-fluorouracil (5-FU), which is very hydrophilic, and methotrexate (MT), which is less hydrophilic, using polyhydroxy butyric acid/gelatin nanofibers. When the release of two distinct drug classes with varying hydrophilic characteristics was evaluated, the highly hydrophilic 5-FU was released first and at a faster pace than MT. MT and 5-FU showed a steady release rate after 24–96 h, which may efficiently satisfy the requirements of various medications in the postoperative management of cancer (Ramanathan et al., 2022). Furthermore, by increasing hydrophilicity, gelatin may alter other anticancer drug delivery vehicles, improving the stability *in vivo*. Li et al. (2022) created a gelatin, chitosan, and doxorubicin NP by loading doxorubicin (DOX) into chitosan and utilizing gelatin to crosslink it. When compared to chitosan/DOX NPs, gelatin, which functions as the nanoshell of the NPs, efficiently enhances the loading of DOX and exhibits high stability *in vivo*. It can also speed up how cancer cells absorb drugs (Li et al., 2022). Similarly, by hydrophobic interactions on the graphene surface, gelatin may also be employed to improve the durability of graphene structures *in vivo* (Hasanin et al., 2022). Many

TABLE 3 Chitosan/gelatin-based systems for biomedical and pharmaceutical applications.

| Type of system | Overview | Method of preparation | Key attributes/Features | Reference |
|----------------------|---|---|---|--|
| Tablets | To regulate medication release, enhance stability and shelf life, and improve the mechanical qualities of tablets, they are utilized as a matrix material during tablet manufacture | <ul style="list-style-type: none"> - Wet granulation - Direct compression | <ul style="list-style-type: none"> - Ability to produce oral mucoadhesive pills - Extends the profile of medication release <ul style="list-style-type: none"> - increases the gastric stability of medications taken orally - A smooth, appealing coating that made swallowing the pills easy and appealing to the user | Badwan et al. (2015), Al-Nimry et al. (2021) |
| Microspheres | The particles are round and range in diameter from 10 μm to 1,000 μm . Variants that enable modification of the release profile include hollow, core-shell, and fibrous microspheres | <ul style="list-style-type: none"> - Spray drying - Coacervation/precipitation - Ionotropic gelation - Emulsion or thermal cross-linking | <ul style="list-style-type: none"> - High effectiveness of trapping and drug loading - Sustained drug release - Adaptability in the administration's path - Stabilizes trapped biomolecules physically | Esposito et al. (1996), Saranya et al. (2018) |
| NPs | Because of their variable size (1–100 nm) and capacity for surface modification, these particulate systems are used as flexible platforms for the targeted administration of medications, DNA, and proteins | <ul style="list-style-type: none"> - Cross-linking and emulsification - Desolvation technique - Polyelectrolyte complexation - Modified ionic gelation - Reverse micellization - Emulsion-Solvent Evaporation | <ul style="list-style-type: none"> - High site-specific medication localization (in cancer) by improved permeability and retention effect or by using targeting ligands - Adaptable to produce stimuli-triggered medication release (pH, redox, temperature) - Enables the co-delivery of pharmaceutical compounds | Sahoo et al. (2015), Garg et al. (2019) |
| Nanofibers | They are a unique platform in which the medication is linked to or enclosed in fibers that have nanometer-sized dimensions. Nanofibers' high surface area to volume ratio qualifies them for regenerative medicine and controlled drug release applications | <ul style="list-style-type: none"> - Templating - Melt/solution blowing - Electrospinning | <ul style="list-style-type: none"> - Their large surface area about their volume enables effective release and substantial drug loading - By changing the concentration and composition of polymeric materials, drug release may be modified - Bilayered or trilayered nanofibers can be manufactured to combine several medicines | Al-Jbour et al. (2019), Arun et al. (2021) |
| Hydrogels | These are chains of cross-linked polymers that come together to form a 3D network that can hold a lot of water. Hydrogels with specific physicochemical qualities for various biomedical applications can be made more accessible by the molecular control of the gelation chemistry involved | <ul style="list-style-type: none"> - Physical and chemical crosslinking - Enzymatic crosslinking - Photo-crosslinking | <ul style="list-style-type: none"> - Excellent biocompatibility, biodegradability, and injectability - It is possible to regulate the degradation of the platform better and, therefore, the rates of drug release by making molecular-level alterations - It is possible to include <i>in situ</i> forming qualities - Has a hydrating effect when used in tropical climates | Peers et al. (2020), Akın Şahbaz (2023) |
| Membranes | They are pliable, thin sheets that may be formed to precise measurements and serve as a dose form. They also make it easier for medications to be released directly into biological settings | <ul style="list-style-type: none"> - Hot pressing - Solvent casting - co-electrospinning | <ul style="list-style-type: none"> - Chitosan enhances the way polar medications are transported across epithelial surfaces - Chitosan is a polymer that has the potential to bind cells and attract negatively charged cell surfaces because of its cationic polyelectrolyte structure | Al-Baadani et al. (2021), Trombino et al. (2021) |
| Microgranules/powder | These are subclasses of solid dosage forms made of gelatin and polymeric chitosan combined with non-uniform micron-sized drug particles | <ul style="list-style-type: none"> - Salt-/Organic solvent-induced precipitation - Gelation - Spray drying | <ul style="list-style-type: none"> - Simplicity of usage, management, and preparation - Enhances the chemical stability of integrated medications - Powders and granules with small particle sizes dissolve quickly in the body, improving their bioavailability - Useful for large-dose, bulky medications | Singh et al. (2012) |

pharmaceuticals have been found to work better when chitosan is added. Using chitosan as the polymer, rifampicin, an antitubercular medication, was developed as a powdered dry NP inhalation. This structure showed that the medication may be released continuously for up to 24 h without endangering any cells or organs (Rawal et al., 2017). Debnath et al. (2018) administered prothionamide, an antitubercular drug, via the lungs as chitosan-coated NPs. The drug's inhalation half-life in the lungs was extended by this

modification. The antifungal medicine itraconazole has limited oral solubility; hence, Jafarnejad et al. (2012) created chitosan NPs for the antifungal agent's pulmonary administration in a dry powder format. By including chitosan NPs, lactose, mannitol, and leucine in the formulation, they improved the drug's aerosolization properties. There was a consequent rise in the pulmonary deposition of itraconazole. Table 3 provides an overview of many popular chitosan/gelatin-based delivery methods.

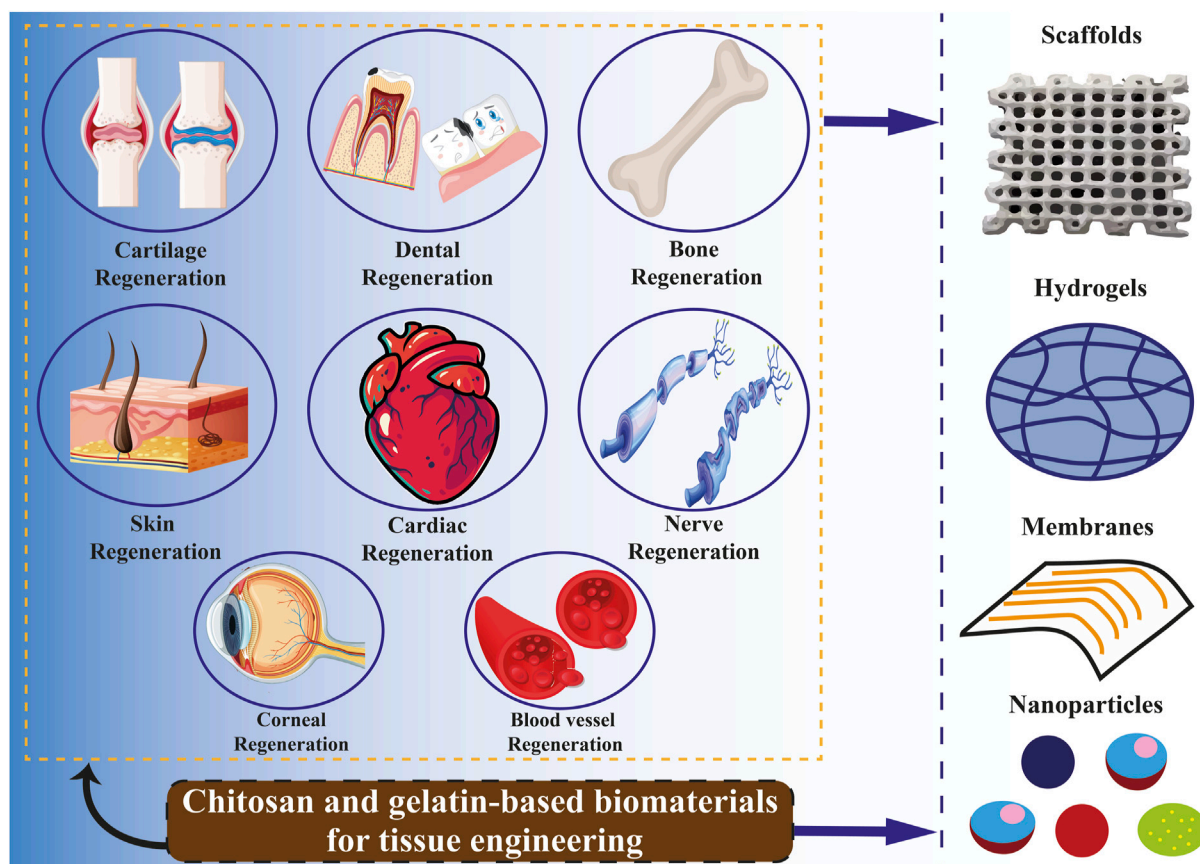


FIGURE 4
Use of chitosan and gelatin biomaterials for tissue regeneration.

9 Chitosan and gelatin in tissue engineering

Tissue engineering is an emerging field of study that integrates technologies from various research disciplines, such as biology, engineering, medicine, chemistry, material science, and pharmacy (Biswal, 2021). In light of the present health concern of organ and tissue failure, this interdisciplinary field may offer a medicinal substitute. According to recent reports from the United States (US) government, 107,000 individuals are waiting for organ transplants, and up to 17 people on these lists pass away every day. In Europe, six new patients are added to the waiting list every hour, with an estimated 18 individuals succumbing daily while awaiting medical care (Lukin et al., 2022). In this line, tissue engineering is to advance the utilization of biomaterials, such as scaffolds, in facilitating effective tissue regeneration and restoration. These are formations characterized by pores of diverse sizes and shapes, which may be interconnected or isolated. These attributes are determined based on the specific cell type of the tissue or organ in which a scaffold is intended to be utilized (Naghieh et al., 2018; Rahmani Del Bakhshayesh et al., 2018; Rider et al., 2018). Natural polymers such as gelatin, collagen, and chitosan are favored in tissue engineering due to their low antigenicity, ability to degrade naturally, compatibility with biological systems, and resemblance to the standard ECM Figure 4 (Khalilimofrad et al., 2023). Utilizing a

blend of polysaccharide and protein, exemplified by chitosan and gelatin, has demonstrated efficacy as a viable approach in emulating the characteristics of the native ECM. Consequently, this combination is a promising alternative for fabricating scaffolds intended for tissue engineering applications (Cheng et al., 2014; Rosellini et al., 2018; Ghaee et al., 2019). The limited mechanical strength of biomaterials derived from pure chitosan restricts their potential applications. Hence, chitosan has been frequently combined with other polymers to leverage their synergistic properties. Chitosan can readily be integrated into a hybrid composite material with various natural polymers like gelatin, silk, DNA, cellulose, proteins, and wool, owing to the presence of hydroxyl and amino groups, which facilitate compatibility and interaction between the components (Khalilimofrad et al., 2023). Combining chitosan with gelatin is a successful approach due to an Arg-Gly-Asp (RGD)-like sequence in the protein, which enhances cell adhesion and migration. This interaction results in the formation of a polyelectrolyte complex with the polysaccharide (Huang et al., 2005; Thein-Han et al., 2009; Kumar et al., 2017; Rajasree et al., 2020). Xu et al. (2021b) created scaffolds utilizing gelatin, chitosan. They decellularized ECM through freeze-drying, demonstrating notable biocompatibility, effective antibacterial properties, and suitable mechanical characteristics conducive to applications in skin tissue engineering. Zhang et al. (2020) constructed sandwich-like scaffolds using polycaprolactone,

gelatin, and chitosan through electrospinning and lyophilization techniques. The resultant scaffold exhibited favorable biocompatibility and demonstrated the ability to enhance blood clotting, thereby facilitating guided periodontal tissue regeneration. Chitosan-derived biomaterials have been shown to exhibit various beneficial impacts on the regeneration of the heart and blood vessels. In particular, hydrogels containing chitosan demonstrated efficacy in mitigating adverse cardiac remodeling and enhancing cardiac performance in experimental models of cardiomyopathy and myocardial infarction (Domengé et al., 2021; Beleño Acosta et al., 2023). Additionally, specific composite chitosan formulations effectively facilitate electrical conduction, a critical factor in the regeneration of myocardial tissue (Jiang et al., 2019). Chitosan exhibits significant promise in skin regeneration and wound healing due to its antimicrobial and hemostatic characteristics (Ahmed et al., 2018; Abourehab et al., 2022). Gelatin methacryloyl (GelMA) hydrogels containing cell-responsive arginyl-glycyl-aspartic acid (RGD) and matrix metalloproteinases peptide sequences are commonly utilized in tissue engineering due to their flexible mechanical properties, excellent processing capabilities, and exceptional biocompatibility characteristics. Hydrogel microstructures derived from GelMA can be accurately manipulated through contemporary manufacturing methods like 3D printing and electrospinning. Various GelMA hydrogels with diverse microarchitectures have been developed and investigated to replicate the characteristics of the native ECM and regulate the growth, movement, and specialization of different cell populations (Zhang et al., 2022c).

Spinal cord injuries are treated with chitosan-based scaffolds with neural stem cells (NSC). The formation of neurofilament between the scaffold and host tissue was seen by the researcher, which bodes well for further research in the long run (Parvizifard et al., 2020). Thanks to its characteristics, chitosan is frequently employed in products like garakani as an extender or to enhance mechanical and rheological qualities. By combining chitosan, agarose, and cartilage ECM, Garakani created a unique system with sufficient qualities for the tissue engineering of nasal cartilage (Wang et al., 2008).

Zhang et al. (2021) created a thermosensitive hydrogel for skin wound healing by combining oyster peptide microspheres (OPM), β -sodium glycerophosphate (β -GP), and catechol-functionalized chitosan. As per the findings, the hydrogel that has been described quickens the migration of fibroblasts and also speeds up the development of collagen and new blood vessels surrounding the lesion. Additionally, the scientists observed increased total protein (TP) synthesis, suggesting a quicker regeneration process.

An injectable hydrogel with a gelatin foundation that heals itself was created by Vahedi et al. (2020). In particular, combining amylopectin aldehyde groups with gelatin amino groups produced hydrogels that could regain their structure and rheological characteristics. Furthermore, they verified their suitability for scaffolds with osteoinductive qualities in the regeneration of bone tissue (Vahedi et al., 2020).

Tavares et al. (2020) created chitosan/zein composite films with ellagic acid to treat skin infections and speed skin healing. The films that were made had a sufficient thickness that ranged from 133 ± 51 to $283 \pm 75 \mu\text{m}$. They also demonstrated a sustained drug release of up to 6% after 48 h and a high percentage of water absorption between 114.44 ± 8.07 and $227.94 \pm 25.88\%$. Additionally, films showed

antibacterial properties against *P. aeruginosa* and *S. aureus* *in vitro* (Tavares et al., 2020). To promote wound healing, Maged et al. (2019) created crosslinked-chitosan scaffolds that contained rosuvastatin and were then filled with mesenchymal stem cells (MSCs). Scaffolds demonstrated improved human fibroblast cell proliferation, excellent porosity, and prolonged drug release for 60 hours. An *in vivo* study on Albino rats showed the superiority of MSC-laden scaffolds over plain ones in encouraging wound closure and cell proliferation. Additionally, a histological investigation indicated that scaffolds loaded with stem cells promoted proper collagen distribution in the epidermal layer (Maged et al., 2019).

Miranda et al. (2011) utilized a chitosan-gelatin composite as a framework for cultivating 3D bone marrow mesenchymal stem cells (BMMSCs). The glutaraldehyde crosslinking technique created the porous biocomposite, which enhanced cell adherence, spreading, and vitality. The scaffold exhibited favorable biocompatibility and gradual degradation *in vivo* following its implantation in the tooth sockets of the rat model. The implant remained *in situ* for the full 35 days that the bone healing process took. The chitosan-gelatin composites that are crosslinked exhibit interconnected pores, leading to a reduction in pore size when compared to the gel composites that are not crosslinked. The maximum amount of gelatin needed to achieve 90% cell viability was around 25%; at concentrations more significant than this, such as 50% and 100%, cell viability dropped to less than 40%. Crucially, the crosslinking process boosted the mechanical strength, improved chemical stability, and delayed degradation of the composite scaffolds, all of which improved cell survival (Miranda et al., 2011).

Bio-ink is a substance utilized in 3D printing, comprising living cells and biomaterials designed to replicate the ECM environment. This bio-ink facilitates cell adhesion, proliferation, and differentiation post-printing (Li et al., 2019b; Shen et al., 2020). The extensive usage of chitosan bio-ink in the bioprinting process is demonstrated by the use of the material in the bioprinting of artificial human organs and structures, such as liver or heart valves (Lee et al., 2018; Pisani et al., 2020; Ghahremanzadeh et al., 2021), neural connections (Maturavongsadit et al., 2021), cartilage tissue (Zhao et al., 2020), and bone tissue (Ramirez Caballero et al., 2019).

10 Related patents review

Many patents in the field of chitosan and gelatin have been registered in the world. For instance, Patent CN115007114 Chitosan/gelatin composite microsphere is an innovation for water pollution treatment. This innovation highlights the potential of removing heavy metals from water by chitosan/gelatin composite. Patent EP4285737, using chitosan as a food preservative has shown that chitosan inhibits pathogenic and food-spoiling microbes protects food, and increases the life of food products. Another invention, CN116725941, is a chitosan/gelatin/citric acid gel, which belongs to the technical field of drug carriers. This invention uses chitosan and gelatin as cross-linking monomers and citric acid as a cross-linking agent in conditions where the acid content Citric is more than or equal to 0.4% and has good swelling properties, bioavailability, biocompatibility, biodegradability, safety, effective delivery and slow release of hydrophobic drug molecules. This invention realizes a massive potential in the aspect of providing hydrophobic drugs. In patent EP3226923, they made a

cartilage gel for cartilage repair, comprising chitosan and chondrocytes. This invention relates to a process for obtaining an implantable cartilage gel for hyaline cartilage tissue repair, consisting of particles from the hydrogel of chitosan and cells capable of forming hyaline cartilage; said process comprises a step of amplification of primary cells in a three-dimensional structure consisting of particles from the physical hydrogel chitosan or chitosan derivative, then a step of redifferentiation and induction of extracellular matrix synthesis by said amplified cells, within the same three-dimensional structure, wherein said cells are primary articular chondrocytes and, or primary mesenchymal stem cells differentiated into chondrocytes. The invention also relates to the resulting cartilage gel and the various uses thereof for cartilage repair following a traumatic impact or an osteoarticular disease such as osteoarthritis. In another patent, US20240165291, they designed a superabsorbent wound dressing using chitosan. This invention provides a superabsorbent dressing comprising non-woven protonated chitosan fabric/sheet with superior fluid absorption and retention capacity, enhanced tensile strength, and coherency. Patent US20230346726 innovation of soft gelatin capsule that contains ibuprofen drug. This invention relates to a composition for encapsulation in a soft gelatin shell that comprises ibuprofen, one or more polyvinyl pyrrolidone, and one or more polyethylene glycols.

11 Conclusion

The knowledge that has lately become accessible about gelatin and chitosan and its uses in tissue engineering, biomedical, food, medicine, water treatment, microencapsulation technology and pharmaceutical management is highlighted in this study. These biomaterials hold great potential for product development owing to their exceptional biodegradability, biocompatibility, antimicrobial, and antioxidant characteristics. Chitosan is a biopolymer that shows promise for food packaging applications due to its capacity to suppress the growth of Gram-negative and Gram-positive bacteria, yeasts, and food-borne filamentous fungi. The favorable attributes of gelatin, such as its ability to biodegrade, biocompatibility, and low toxicity, promote enhanced cell adhesion, differentiation, and proliferation. The distinct qualities of gelatin and chitosan make them popular choices for medication delivery applications. It has been shown that the removal of heavy metals from water by using these bioabsorbents has been effective in water treatment. Consequently, the use of chitosan and gelatin, owing to their distinct attributes, has an extensive range of potential applications across several domains and can significantly contribute to environmental conservation and sustainable growth.

12 Future perspectives

Investigating biodegradable polymers, specifically chitosan, and gelatin, shows significant potential for diverse applications in multiple disciplines. Further investigation into chitosan-gelatin composites may result in the creation of sophisticated biomedical products, such as wound dressings, medication delivery systems, and scaffolds for tissue engineering (Huang et al., 2005; Fan et al., 2016; Wang et al., 2016). To satisfy the expanding needs of the healthcare

sector, future research may concentrate on improving biocompatibility, optimizing material qualities, and investigating cutting-edge production methods (Bosworth et al., 2019). Using chitosan in packaging applications can potentially reduce environmental pollution on a global scale, notwithstanding various limitations related to thermal stability, barrier properties, mechanical attributes, and manufacturing expenses. Chitosan, when combined with popular cosmetic ingredients like algae extracts, fruit extracts, and essential oils in gel formulations, presents an appealing option for cosmetic products. Chitosan and its derivatives are recommended for incorporation into pharmaceutical formulations intended for slimming products, body weight management, and cosmetics to enhance the efficacy of skin care products and other applications (Morin-Crini et al., 2019). An exciting direction for future study is the creation of biodegradable packaging materials, given the growing emphasis on sustainability and environmental consciousness. Additional research on the characteristics and efficacy of chitosan-gelatin films may open the door to creative packaging options that combine environmental friendliness with practicality (Kan et al., 2019; Wang et al., 2021). Research cooperation amongst scientists from several fields, including biology, materials science, engineering, and food science, will be critical to developing biodegradable polymer-based products. Multidisciplinary research initiatives have the potential to stimulate creativity, promote the sharing of information, and quicken the creation of significant solutions with practical applications (Yin and Yang, 2020). By utilizing their unique qualities and investigating new uses, researchers may help solve urgent social issues, advance sustainability, and enhance human health and wellbeing (Rai et al., 2021; Mukherjee et al., 2023).

Author contributions

AY: Data curation, Writing—original draft. BD: Methodology, Project administration, Supervision, Writing—review and editing. MK-K: Writing—review and editing. HA: Project administration, Supervision, Writing—review and editing.

Funding

The author(s) declare that no financial support was received for the research, authorship, and/or publication of this article.

Conflict of interest

The authors declare that the research was conducted in the absence of any commercial or financial relationships that could be construed as a potential conflict of interest.

Publisher's note

All claims expressed in this article are solely those of the authors and do not necessarily represent those of their affiliated organizations, or those of the publisher, the editors and the reviewers. Any product that may be evaluated in this article, or claim that may be made by its manufacturer, is not guaranteed or endorsed by the publisher.

References

- Abourehab, M. A., Sheersha, P., Abualsoud, B. M., Kadi, A., Ansari, M. J., Deepak, A., et al. (2022). Recent advances of chitosan formulations in biomedical applications. *Int. J. Mol. Sci.* 23 (18), 10975. doi:10.3390/ijms231810975
- Acierno, D., Di Maio, L., and Cuccurullo, G. (1999). Analysis of temperature fields in film casting. *J. Polym. Eng.* 19 (2), 75–94. doi:10.1515/polyeng-1999-0202
- Adiletta, G., Zampella, L., Coletta, C., Petriccione, M., et al. (2019). Chitosan coating to preserve the qualitative traits and improve antioxidant system in fresh figs (*Ficus carica* L.). *Agriculture* 9 (4), 84. doi:10.3390/agriculture9040084
- Ahghari, M. A., Ahghari, M. R., Maryam, K., Maleki, A., et al. (2022). Design, synthesis, and characterization of novel eco-friendly chitosan-AgIO₃ bionanocomposite and study its antibacterial activity. *Sci. Rep.* 12 (1), 10491. doi:10.1038/s41598-022-14501-6
- Ahmed, A. S., Negm, A. N. R. M., Mohammed, M., Abd El-Majeed, M., Ali, A. K., Abdelmotalieb, M., et al. (2023). Biodegradable polymers for industrial applications. *Biodegradable polymers for industrial applications*. 451–476. doi:10.1007/978-3-031-09710-2_37
- Ahmed, M., Hameed, B., and Hummadi, E. (2020). Review on recent progress in chitosan/chitin-carbonaceous material composites for the adsorption of water pollutants. *Carbohydr. Polym.* 247, 116690. doi:10.1016/j.carbpol.2020.116690
- Ahmed, S., Ali, A., and Sheikh, J. (2018). A review on chitosan centred scaffolds and their applications in tissue engineering. *Int. J. Biol. Macromol.* 116, 849–862. doi:10.1016/j.jbiomac.2018.04.176
- Aider, M. (2010). Chitosan application for active bio-based films production and potential in the food industry: review. *LWT - Food Sci. Technol.* 43 (6), 837–842. doi:10.1016/j.lwt.2010.01.021
- Akın Şahbaz, D. J. P. B. (2023). Gelatin-based hydrogels and ferrogels as smart drug delivery systems: synthesis, characterization and drug release kinetics. *Polym. Bull. Berl.* 81, 5215–5235. doi:10.1007/s00289-023-04963-7
- Al-Baadani, M. A., Hii Ru Yie, K., Al-Bishari, A. M., Alshobi, B. A., Zhou, Z., Fang, K., et al. (2021). Co-electrospinning polycaprolactone/gelatin membrane as a tunable drug delivery system for bone tissue regeneration. *Mater. Des.* 209, 109962. doi:10.1016/j.matdes.2021.109962
- Alipal, J., Nayan, N., Sahari, N., Basri, H., et al. (2021). A review of gelatin: properties, sources, process, applications, and commercialisation. *A Rev. gelatin Prop. sources, process, Appl. Commer.* 42, 240–250. doi:10.1016/j.matpr.2020.12.922
- Al-Jbour, N. D., Beg, M. D., Gimbut, J., Alam, A. M., et al. (2019). An overview of chitosan nanofibers and their applications in the drug delivery process. *Curr. Drug Deliv.* 16 (4), 272–294. doi:10.2174/1567201816666190123121425
- Almajidi, Y. Q., Marisetti, A. L., Hsu, C. Y., Dhiaa, A. M., et al. (2024). Chitosan-based nanofibrous scaffolds for biomedical and pharmaceutical applications: a comprehensive review. *Int. J. Biol. Macromol.* 264, 130683. doi:10.1016/j.jbiomac.2024.130683
- Al-Nimry, S., Dayah, A. A., Inas, H., Rawand, D., et al. (2021). Cosmetic, biomedical and pharmaceutical applications of fish gelatin/hydrolysates. *Mar. Drugs* 19 (3), 145. doi:10.3390/md19030145
- Altiock, D., Altiock, S., and Tihminlioglu, F. (2010). Physical, antibacterial and antioxidant properties of chitosan films incorporated with thyme oil for potential wound healing applications. *J. Mat. Sci. Mat. Med.* 21, 2227–2236. doi:10.1007/s10856-010-4065-x
- Amankwaah, C., Li, J., Lee, J., and Pascall, M. A. (2020). Antimicrobial activity of chitosan-based films enriched with green tea extracts on murine norovirus, *Escherichia coli*, and *Listeria innocua*. *Int. J. Food Sci.* 2020, 1–9. doi:10.1155/2020/3941924
- Ambaye, T. G., van Hullebusch, E. D., Rtimi, S., et al. (2022). Preparation and applications of chitosan and cellulose composite materials. *J. Environ. Manage.* 301, 113850. doi:10.1016/j.jenvman.2021.113850
- Amor, G., Idbella, M., De Feo, V., Porta, R., et al. (2021). Basil essential oil: composition, antimicrobial properties, and microencapsulation to produce active chitosan films for food packaging. *Foods* 10 (1), 121. doi:10.3390/foods10010121
- Amulya, K., Ramakrishna, S., Ranapathap, K., Venkata Mohan, S., et al. (2021). c. *Composites-part-c-open-access* 4, 100111. doi:10.1016/j.jcomc.2021.100111
- Anggraeni, A. S., Anuraga, J., Laconi, E. B., Kumalasari, N. R., Sofyan, A., et al. (2022). Marine by-products and insects as a potential chitosan source for ruminant feed additives. *CZECH J. Anim. Sci.* 67 (8), 295–317. doi:10.17221/42/2022-cjas
- Aniunoh, K. K., and Harrisony, G. (2006). Experimental investigation of film formation: film casting. *J. Plastic Film Sheeting* 22 (3), 177–192. doi:10.1177/8756087906067323
- Arun, A., Malraut, P., Laha, A., Seeram, R., et al. (2021). Gelatin nanofibers in drug delivery systems and tissue engineering. *Eng. Sci.* 16, 71–81. doi:10.30919/es8d527
- Ashl, C., Vural, N., and Şarer, E. (2020). Determination of volatile compounds in green tea and black tea from Turkey by using HS-SPME and GC-MS. *Istanbul J. Pharm.* 50 (2), 111–115. doi:10.26650/istanbuljpharm.2019.0075
- Atarés, L., and Chiralt, A. (2016). Essential oils as additives in biodegradable films and coatings for active food packaging. *Trends-In-Food-Science-And-Technology* 48, 51–62. doi:10.1016/j.tifs.2015.12.001
- Attallah, O., Wafa, M. M. A., Ai-Ghobashy, M. A., Nebsen, M., Monir, H. H., et al. (2021). Adsorptive removal of pesticides from aqueous solutions using chitosan/gelatin polymeric composite Process monitoring and optimization. *Int. J. Environ. Sci. Technol.* 19, 8183–8194. doi:10.1007/s13762-021-03694-4
- Avila Rodríguez, M. I., Rodríguez Barroso, L. G., and Sánchez, M. (2018). Collagen: a review on its sources and potential cosmetic applications. *J. Cosmet. Dermatol.* 17 (1), 20–26. doi:10.1111/jocd.12450
- Badwan, A. A., Iyad, R., Omari, M., Darras, F., et al. (2015). Chitin and chitosan as direct compression excipients in pharmaceutical applications. *Mar. Drugs* 13 (3), 1519–1547. doi:10.3390/md13031519
- Bahrami, A., Jafari, S. M., Williams, L., et al. (2020). Antimicrobial-loaded nanocarriers for food packaging applications. *Adv. Colloid Interface Sci.* 278, 102140. doi:10.1016/j.cis.2020.102140
- Balti, R., Yacoubi, L., Rabauoi, L., Brodu, N., et al. (2017). Development and characterization of bioactive edible films from spider crab (*Maja crispata*) chitosan incorporated with *Spirulina* extract. *Int. J. Biol. Macromol.* 105, 1464–1472. doi:10.1016/j.jbiomac.2017.07.046
- Bansal, V., Pramod, K. S., Nitin, S., Om Prakash, R., Rishabha, M., et al. (2011). Applications of chitosan and chitosan derivatives in drug delivery. *Int. J. Biol. Chem. Sci.* 5 (1), 28–37.
- Baranauskaitė, J., Kopustinskiene, D. M., and Bernatoniene, J. J. M. (2019). Impact of gelatin supplemented with gum Arabic, tween 20, and β -cyclodextrin on the microencapsulation of Turkish oregano extract. *Molecules* 24 (1), 176. doi:10.3390/molecules24010176
- Bashir, S. M., Gulzar, A. R., Ana, P., Haq, Z., Saqib, H., Fonte, P., et al. (2022). Chitosan nanoparticles: a versatile platform for biomedical applications. *Materials* 15 (19), 6521. doi:10.3390/ma15196521
- Battogtokh, G., Park, H., Hwang, S. J., et al. (2022). Gelatin coating for the improvement of stability and cell uptake of hydrophobic drug-containing liposomes. *Molecules* 27 (3), 1041. doi:10.3390/molecules27031041
- Beleño Acosta, B., Advincula, R. C., and Grande-Tovar, C. D. J. M. (2023). Chitosan-based scaffolds for the treatment of myocardial infarction: a systematic review. *Molecules* 28 (4), 1920. doi:10.3390/molecules28041920
- Bella, J., and Berman, H. (1996). Crystallographic evidence for Ca-H \cdots O=C hydrogen bonds in a collagen triple helix. *J. Mol. Biol.* 264 (4), 734–742. doi:10.1006/jmbi.1996.0673
- Bello, A. B., Park, H., Lee, S. H., et al. (2020). Engineering and functionalization of gelatin biomaterials: from cell culture to medical applications. *Tissue Eng. Part B Rev.* 26 (2), 164–180. doi:10.1089/ten.teb.2019.0256
- Bhatt, P., Khati, P., Gulsum, M. U. B., Joshi, S., Simsek, H., et al. (2023). Developments and application of chitosan-based adsorbents for wastewater treatments. *Environ. Res.* 226, 115530. doi:10.1016/j.envres.2023.115530
- Bhowmik, S., Agyei, D., Azam, A., et al. (2022). Bioactive chitosan and essential oils in sustainable active food packaging Recent trends, mechanisms, and applications. *Food Packag. Shelf Life* 34, 100962. doi:10.1016/j.fpsl.2022.100962
- Biscarat, J., Charmette, C., Sanchez, J., and Pochat-Bohatier, C. (2015). Preparation of dense gelatin membranes by combining temperature induced gelation and dry-casting. *J. Membr. Sci.* 473, 45–53. doi:10.1016/j.memsci.2014.09.004
- Biswal, T. J. M. T. P. (2021). Biopolymers for tissue engineering applications: a review. *Mater. Proc.* 41, 397–402. doi:10.1016/j.matpr.2020.09.628
- Bosworth, L. A., Hu, W., Shi, Y., and Cartmell, S. H. (2019). Enhancing biocompatibility without compromising material properties: an optimised NaOH treatment for electrospun polycaprolactone fibres. *J. Nanomater.* 2019, 1–11. doi:10.1155/2019/4605092
- Brodsky, B., and Ramshaw, J. (1997). The collagen triple-helix structure. *Matrix Biol.* 15 (8–9), 545–554. doi:10.1016/s0945-053x(97)90030-5
- Bruschi, M., Cardoso, M. L. C., Lucchesi, M. B., Gremião, M., et al. (2003). Gelatin microparticles containing propolis obtained by spray-drying technique: preparation and characterization. *Int. J. Pharm.* X. 264 (1–2), 45–55. doi:10.1016/s0378-5173(03)00386-7
- Burgess, D., and Carless, J. (1985). Manufacture of gelatin/gelatin coacervate microcapsules. *Int. J. Pharm.* X. 27 (1), 61–70. doi:10.1016/0378-5173(85)90185-1
- Candir, E., Ozdemir, A. E., and Aksoy, M. C. (2018). Effects of chitosan coating and modified atmosphere packaging on postharvest quality and bioactive compounds of pomegranate fruit cv. 'Hicaznar'. *Sci. Hortic.* 235, 235–243. doi:10.1016/j.scienta.2018.03.017
- Cazón, P., Agata, A., Jaroslawa, A., Vázquez, M., et al. (2021). Evaluation of easy-removing antioxidant films of chitosan with *Melaleuca alternifolia* essential oil. *Int. J. Biol. Macromol.* 186, 365–376. doi:10.1016/j.jbiomac.2021.07.035
- Cazón, P., et al. (2019). *Applications of chitosan as food packaging materials*, 81–123.
- C Echave, M., Laura, S. D. B., Jose, L. P., Orive, G., et al. (2017). Gelatin as biomaterial for tissue engineering. *Curr. Pharm. Des.* 23 (24), 3567–3584. doi:10.2174/0929867324666170511123101

- Chang, W., Liu, F., Sharif, H. R., Huang, Z., Goff, H., and Zhong, F. (2019). Preparation of chitosan films by neutralization for improving their preservation effects on chilled meat. *Food Hydrocoll.* 90, 50–61. doi:10.1016/j.foodhyd.2018.09.026
- Chaudhary, S., Satish, K., Vikas, K., Rakesh, K., et al. (2020). Chitosan nanoemulsions as advanced edible coatings for fruits and vegetables: composition, fabrication and developments in last decade. *Int. J. Biol. Macromol.* 152, 154–170. doi:10.1016/j.jbiomac.2020.02.276
- Chelu, M., Musuc, A. M., Popa, M., Calderon Moreno, J. M., et al. (2023). Chitosan hydrogels for water purification applications. *Gels* 9 (8), 664. doi:10.3390/gels9080664
- Chen, M., Li, R., Feng, J., Shu, X. L., et al. (2018). Hydrogen bonding impact on chitosan plasticization. *Carbohydr. Polym.* 200, 115–121. doi:10.1016/j.carbpol.2018.07.062
- Chen, S., Liao, W., Zhang, Y., Gao, Y., et al. (2020). Fabrication, characterization, physicochemical stability of zein-chitosan nanocomplex for co-encapsulating curcumin and resveratrol. *Carbohydr. Polym.* 236, 116090. doi:10.1016/j.carbpol.2020.116090
- Cheng, Y.-H., Lee, C. J., Ku, R. Y., Chiu, A. W. H., et al. (2014). Sustained delivery of latanoprost by thermosensitive chitosan-gelatin-based hydrogel for controlling ocular hypertension. *Acta Biomater.* 10 (10), 4360–4366. doi:10.1016/j.actbio.2014.05.031
- Choi, H.-J., Sung-Wook, C., Nari, L., Chang, H. J., et al. (2022). Antimicrobial activity of chitosan/gelatin/poly (vinyl alcohol) ternary blend film incorporated with duchesnea indica extract in strawberry applications. *Foods* 11 (24), 3963. doi:10.3390/foods11243963
- Choktaweesap, N., Meechai, C., Supaphol, P., et al. (2007). Electrospun gelatin fibers: effect of solvent system on morphology and fiber diameters. *Polym. J.* 39 (6), 622–631. doi:10.1295/polymj.pj2006190
- Choudhury, N., Meghwal, M., and Das, K. J. F. F. (2021). Microencapsulation: an overview on concepts, methods, properties and applications in foods. *Food Front.* 2 (4), 426–442. doi:10.1002/fft2.94
- Christian, S. J. (2020). “Natural fibre-reinforced noncementitious composites (biocomposites),” in *Nonconventional and vernacular construction materials*. Elsevier, 169–187.
- Chuaynukul, K., Nagarajan, M., Prodpran, T., Benjakul, S., Songtipya, P., and Songtipya, L. (2018). Comparative characterization of bovine and fish gelatin films fabricated by compression molding and solution casting methods. *J. Polym. Environ.* 26, 1239–1252. doi:10.1007/s10924-017-1030-5
- Costa, S. M., Ballesteros, L. F., Teixeira, J. A., Fanguero, R., et al. (2021). Active natural-based films for food packaging applications: the combined effect of chitosan and nanocellulose. *Int. J. Biol. Macromol.* 177, 241–251. doi:10.1016/j.jbiomac.2021.02.105
- Cruz, R. M., Agriopoulou, S., Weinrich, R., Herbes, C., et al. (2022). Bioplastics for food packaging: environmental impact, trends and regulatory aspects. *Foods* 11 (19), 3087. doi:10.3390/foods11193087
- de Alvarenga, E. S. (2011). Characterization and properties of chitosan. *Biotechnology of Biopolymers* 91, 48–53. doi:10.5772/17020
- Debnath, S. K., Omri, A., et al. (2018). Development and evaluation of Chitosan nanoparticles based dry powder inhalation formulations of Prothionamide. *PLoS ONE* 13 (1), e0190976. doi:10.1371/journal.pone.0190976
- Dehghani, S., Hosseini, E., and Rousta, E. (2022). Shelf-life extension of tomato (*Solanum lycopersicum* L.) using an edible coating of bitter almond gum-fish gelatin conjugates. *Prog. Org. Coat.* 170, 106980. doi:10.1016/j.porgcoat.2022.106980
- Deng, P., Liang, X., Chen, F., Chen, Y., and Zhou, J. (2022). Novel multifunctional dual-dynamic-bonds crosslinked hydrogels for multi-strategy therapy of MRSA-infected wounds. *Appl. Mat. Today* 26, 101362. doi:10.1016/j.apmt.2022.101362
- Desai, K. (2016). Chitosan nanoparticles prepared by ionotropic gelation: an overview of recent advances. *Crit. Rev. Ther. Drug Carr. Syst.* 33 (2), 107–158. doi:10.1615/critrevtherdrugcarriersyst.2016014850
- Desai, N., Gupta, R., Patel, P., Karunakaran, B., et al. (2023). Chitosan: a potential biopolymer in drug delivery and biomedical applications. *Pharmaceutics* 15 (4), 1313. doi:10.3390/pharmaceutics15041313
- Di Lullo, G. A., Ala-Kokko, L., San Antonio, J. D., et al. (2002). Mapping the ligand-binding sites and disease-associated mutations on the most abundant protein in the human, type I collagen. *J. Biol. Chem.* 277 (6), 4223–4231. doi:10.1074/jbc.m110709200
- Ding, S., Wang, Y., Li, J., and Chen, S. (2021). Progress and prospects in chitosan derivatives: modification strategies and medical applications. *J. Mater. Sci. Technol.* 89, 209–224. doi:10.1016/j.jmst.2020.12.008
- Doméngé, O., Crépet, A., Revet, G., Boitard, S. E., et al. (2021). Efficacy of epicardial implantation of acellular chitosan hydrogels in ischemic and nonischemic heart failure: impact of the acetylation degree of chitosan. *Acta Biomater.* 119, 125–139. doi:10.1016/j.actbio.2020.10.045
- Duan, M., Jiang, H., Hu, Y., Pang, J., et al. (2023). Electrospun gelatin/chitosan nanofibers containing curcumin for multifunctional food packaging. *Food Sci. Hum. Wellness* 12 (2), 614–621. doi:10.1016/j.fshw.2022.07.064
- Ebhodaghe, S. O. (2022). A short review on chitosan and gelatin-based hydrogel composite polymers for wound healing. *J. Biomater. Sci. Polym. Ed.* 33 (12), 1595–1622. doi:10.1080/09205063.2022.2068941
- Echave, M., Sánchez, P., Pedraz, J., and Orive, G. (2017). Progress of gelatin-based 3D approaches for bone regeneration. *J. Drug Deliv. Sci. Technol.* 42, 63–74. doi:10.1016/j.jddst.2017.04.012
- Echave, M. C., Pedraz, J. L., Lakshminarayanan, R., Dolatshahi-Pirouz, A., et al. (2019). Recent advances in gelatin-based therapeutics. *Expert Opin. Biol. Ther.* 19 (8), 773–779. doi:10.1080/14712598.2019.1610383
- Ediyilam, S., Dennis, T. T., Wacławek, S., Černík, M., et al. (2021). Chitosan/gelatin/silver nanoparticles composites films for biodegradable food packaging applications. *Polym. (Basel).* 13 (11), 1680. doi:10.3390/polym13111680
- El-araby, A., El Ghadraoui, L., and Errachidi, F. (2022). Usage of biological chitosan against the contamination of post-harvest treatment of strawberries by aspergillus Niger. *Front. Sustain. Food Syst.* 6, 881434. doi:10.3389/fsufs.2022.881434
- El-Gioushy, S. F., El-Kholy, M. F., Shaban, A. E., Sami, R., et al. (2022). Utilization of active edible films (Chitosan, chitosan nanoparticle, and CACL2) for enhancing the quality properties and the shelf life of Date palm fruits (Barhi cultivar) during Cold storage. *Coatings (Basel).* 12 (2), 255. doi:10.3390/coatings12020255
- Elisabee, M. Z. (2013). Chitosan based edible films and coatings: a review. *Mater. Sci. Eng. C Mater. Biol. Appl.* 33 (4), 1819–1841. doi:10.1016/j.msec.2013.01.010
- Elwakil, B. H., Doaa, A., Ahmed, A. H., Reem, A. H., Yousry, M. G., et al. (2020). Chitosan and liposomes nanoparticles encapsulated cinnamon extract: antiproteolytic activity and wound healing efficiency of diabetic rats running head: chitosan vs liposomes nanoparticles as drug delivery carriers. *CMU J. Nat. S. C.* 19, 595. doi:10.12982/CMUJNS.2020.0039
- Engwa, G. A., Ferdinand, P. U., Friday, N. N., Marian, N., et al. (2019). Mechanism and health effects of heavy metal toxicity in humans. *Poisoning in the Modern World - New Tricks for an Old Dog?* 10, 70–90. doi:10.5772/intechopen.82511
- Esposito, E., Cortesi, R., and Nastruzzi, C. J. B. (1996). Gelatin microspheres: influence of preparation parameters and thermal treatment on chemico-physical and biopharmaceutical properties. *Biomaterials* 17 (20), 2009–2020. doi:10.1016/0142-9612(95)00325-8
- Essa, D., Yahya, E. C., Pierre, P. D. K., Pillay, V., et al. (2020). Comparative nanofabrication of PLGA-chitosan-PEG systems employing microfluidics and emulsification solvent evaporation techniques. *Polym. (Basel).* 12 (9), 1882. doi:10.3390/polym12091882
- Estevinho, B. N., Rocha, F., Santos, L., Alves, A., et al. (2013). Microencapsulation with chitosan by spray drying for industry applications—A review. *Trends Food Sci. Technol.* 31 (2), 138–155. doi:10.1016/j.tifs.2013.04.001
- Ethaib, S., and Zubaidi, S. L. (2022). Function of nanomaterials in removing heavy metals for water and wastewater remediation: a review. *Funct. Nanomater. removing heavy metals wastewater Remediat. A Rev.* 9 (10), 123. doi:10.3390/environments9100123
- Fan, L., Peng, M., Hu, J., et al. (2016). Preparation and characterization of chitosan/gelatin/PVA hydrogel for wound dressings. *Carbohydr. Polym.* 146, 427–434. doi:10.1016/j.carbpol.2016.03.002
- Fan, W., Yan, W., Xu, Z., Ni, H., et al. (2012). Formation mechanism of monodisperse, low molecular weight chitosan nanoparticles by ionic gelation technique. *Colloids Surf. B Biointerfaces* 90, 21–27. doi:10.1016/j.colsurf.2011.09.042
- Faqir, Y., Ma, J., Chai, Y., et al. (2021). Chitosan in modern agriculture production. *Plant, Soil Environ.* 67 (12), 679–699. doi:10.17221/332/2021-pse
- Fitch-Vargas, P. R., Vega-García, M. O., Valdez-Morales, J. E., Martínez-Bustos, F., et al. (2016). Physicochemical and microstructural characterization of corn starch edible films obtained by a combination of extrusion technology and casting technique. *J. Food Sci.* 81 (9), E2224–E2232. doi:10.1111/1750-3841.13416
- Flores Llovera, M., Mora, L., Reig, M., and Toldrá, F. (2019). Risk assessment of chemical substances of safety concern generated in processed meats. *Food Sci. Hum. Wellness* 8, 244–251. doi:10.1016/j.fshw.2019.07.003
- Flórez, M., Guerra-Rodríguez, E., Cazón, P., and Vázquez, M. (2022). Chitosan for food packaging: recent advances in active and intelligent films. *Food Hydrocoll.* 124, 107328. doi:10.1016/j.foodhyd.2021.107328
- Flury, M., and Narayan, R. (2021). Biodegradable plastic as an integral part of the solution to plastic waste pollution of the environment. *Curr. Opin. Green Sustain. Chem.* 30, 100490. doi:10.1016/j.cogsc.2021.100490
- Garg, U., Swati, C., Upendra, N., Jain, N., et al. (2019). Current advances in chitosan nanoparticles based drug delivery and targeting. *Adv. Pharm. Bull.* 9 (2), 195–204. doi:10.1517/apb.2019.023
- Ghaee, A., Bagheri-Khoulanjani, S., Amir Afshar, H., and Bogheiri, H. (2019). Biomimetic nanocomposite scaffolds based on surface modified PCL-nanofibers containing curcumin embedded in chitosan/gelatin for skin regeneration. *Compos. Part B Eng.* 177, 107339. doi:10.1016/j.compositesb.2019.107339
- Ghahremanzadeh, F., Alihosseini, F., and Semnani, D. J. (2021). Investigation and comparison of new galactosylation methods on PCL/chitosan scaffolds for enhanced liver tissue engineering. *Int. J. Biol. Macromol.* 174, 278–288. doi:10.1016/j.jbiomac.2021.01.158
- Gonçalves, F. J., Cardoso, S. M., Rocha, S. M., Coimbra, M. A., et al. (2018). Interaction of wine mannoproteins and arabinogalactans with anthocyanins. *Food Chem.* 243, 1–10. doi:10.1016/j.foodchem.2017.09.097
- Gopi, S., Thomas, S., and Pius, A. (2020). *Handbook of chitin and chitosan*. Elsevier.
- Gores, F., Radke, W., and Held, D. (2021). *Molar mass determination of collagen peptides*.

- Green-Warren, R. A., Kovacevich, D. A., Shaikh, A., Kuznetsova, C., et al. (2022). Determining the self-limiting electrospray deposition compositional limits for mechanically tunable polymer composites. *ACS Appl. Polym. Mat.* 4 (5), 3511–3519. doi:10.1021/acsp.2c00106
- Gullapalli, R. P., and Mazzitelli, C. L. J. (2017). Gelatin and non-gelatin capsule dosage forms. *J. Pharm. Sci.* 106 (6), 1453–1465. doi:10.1016/j.xphs.2017.02.006
- Guzmán, E., Ortega, F., and Rubio, R. G. J. C. (2022). Chitosan: a promising multifunctional cosmetic ingredient for skin and hair care. *Cosmetics* 9 (5), 99. doi:10.3390/cosmetics9050099
- Habibi, S., and Hajinasrollah, K. (2018). Electrospinning of nanofibers based on chitosan/gelatin blend for antibacterial uses. *Russ. J. Appl. Chem.* 91, 877–881. doi:10.1134/s1070427218050191
- Hafsa, J., Smach, M. a., Ben Khedher, M. R., Charfeddine, B., Limem, K., Majdoub, H., et al. (2016). Physical, antioxidant and antimicrobial properties of chitosan films containing Eucalyptus globulus essential oil. *LWT - Food Sci. Technol.* 68, 356–364. doi:10.1016/j.lwt.2015.12.050
- Hamann, D., Colet, R., Valduga, E., Zeni, J., et al. (2022). Active edible films based on green tea extract and gelatin for coating of fresh sausage. *Meat Sci.* 194, 108966. doi:10.1016/j.meatsci.2022.108966
- Hanani, Z. N., Morris, M., Kerry, J., et al. (2012). Manufacture and characterization of gelatin films derived from beef, pork and fish sources using twin screw extrusion. *J. Food Eng.* 113 (4), 606–614. doi:10.1016/j.jfoodeng.2012.07.002
- Hanani, Z. N., Roos, Y. H., and Kerry, J. (2014). Use and application of gelatin as potential biodegradable packaging materials for food products. *Int. J. Biol. Macromol.* 71, 94–102. doi:10.1016/j.ijbiomac.2014.04.027
- Hasanin, M., Emara, L. H., et al. (2022). Green decoration of graphene oxide Nano sheets with gelatin and gum Arabic for targeted delivery of doxorubicin. *Biotechnol. Rep. (Amst)*. 34, e00722. doi:10.1016/j.btre.2022.e00722
- Hathout, R. M., and Metwally, A. (2019). Gelatin nanoparticles. *Pharm. Nanotechnol.* 2000, 71–78. doi:10.1007/978-1-4939-9516-5_6
- Hidangmayum, A., and Dwivedi, P. J. (2022). Chitosan based nanoformulation for sustainable agriculture with special reference to abiotic stress: a review. *Chitosan based nanoformulation Sustain. Agric. special reference abiotic stress a Rev.* 30 (4), 1264–1283. doi:10.1007/s10924-021-02296-y
- Ho, T. M., Yoshii, H., Terao, K., Bhandari, B. R., et al. (2021). *Functionality of cyclodextrins in encapsulation for food applications*. Springer.
- Homayun, B., Lin, X., and Choi, H.-J. J. P. (2019). Challenges and recent progress in oral drug delivery systems for biopharmaceuticals. *Pharmaceutics* 11 (3), 129. doi:10.3390/pharmaceutics11030129
- Hossain, F., Vu, K. D., Frascini, C., Lacroix, M., et al. (2019). Antifungal activities of combined treatments of irradiation and essential oils (EOs) encapsulated chitosan nanocomposite films in *in vitro* and *in situ* conditions. *Int. J. Food Microbiol.* 295, 33–40. doi:10.1016/j.jfoodmicro.2019.02.009
- Huang, H., Dan, L., Ying, Z., Chi, H., et al. (2020). The effects of chitosan supplementation on body weight and body composition: a systematic review and meta-analysis of randomized controlled trials. *Crit. Rev. Food Sci. Nutr.* 60 (11), 1815–1825. doi:10.1080/10408398.2019.1602822
- Huang, Y., Stella, O., Siewe, M., Aliakbar, M., Madihally, S. V., et al. (2005). *In vitro* characterization of chitosan–gelatin scaffolds for tissue engineering. *Biomaterials* 26 (36), 7616–7627. doi:10.1016/j.biomaterials.2005.05.036
- Huq, T., Dhayagude, N., He, Z., Ni, Y., et al. (2022). Sources, production and commercial applications of fungal chitosan: a review. *J. Bioresour. Bioprod.* 7 (2), 85–98. doi:10.1016/j.jobab.2022.01.002
- Iacob, A. T., Vasincu, I. M., Tauser, R. G., Lupascu, D., et al. (2021). Recent biomedical approaches for chitosan based materials as drug delivery nanocarriers. *Pharmaceutics* 13 (4), 587. doi:10.3390/pharmaceutics13040587
- Ilyas, R. A., Ngadi, N., Zuhri, M., Asyraf, M., et al. (2022). Natural-fiber-reinforced chitosan, chitosan blends and their nanocomposites for various advanced applications. *Polym. (Basel)*. 14 (5), 874. doi:10.3390/polym14050874
- Islam, M. M., Nurus Sakib, M., Shanta, B., Rashid, T. U., et al. (2020). Chitosan based bioactive materials in tissue engineering applications-A review. *Bioact. Mat.* 5 (1), 164–183. doi:10.1016/j.bioactmat.2020.01.012
- Islam, S., Jadhav, A., Fang, J., Arnold, L., Wang, L. J., Padhye, R. J., et al. (2011). Surface deposition of chitosan on wool substrate by electrospraying. *Adv. Mat. Res.* 331, 165–170. doi:10.4028/scientific.net/amr.331.165
- Jafarinejad, S., Ghazi-Khansari, M., Najafabadi, A. R., Mohajel, N., et al. (2012). Development of chitosan-based nanoparticles for pulmonary delivery of itraconazole as dry powder formulation. *Powder Technol.* 222, 65–70. doi:10.1016/j.powtec.2012.01.045
- Jensen, A., Lim, L. T., Barbut, S., Marcone, M., et al. (2015). Development and characterization of soy protein films incorporated with cellulose fibers using a hot surface casting technique. *LWT - Food Sci. Technol.* 60 (1), 162–170. doi:10.1016/j.lwt.2014.09.027
- Jiang, A., Palimkar, S., Galgali, P., Adhikari, A., et al. (2023). Chitosan based biodegradable composite for antibacterial food packaging application. *Polym. (Basel)*. 15 (10), 2235. doi:10.3390/polym15102235
- Jiang, L., Zhang, Z., Xia, Y., Xue, H., et al. (2019). Preparation of an electrically conductive graphene oxide/chitosan scaffold for cardiac tissue engineering. *Appl. Biochem. Biotechnol.* 188, 952–964. doi:10.1007/s12010-019-02967-6
- Jiménez-Gómez, C. P., and Cecilia, J. A. (2020). Chitosan: a natural biopolymer with a wide and varied range of applications. *Molecules* 25 (17), 3981. doi:10.3390/molecules25173981
- Jovanović, J., Mutavdžić, D., Tanasijević, G., Joksimović, K., et al. (2021). Chitosan and pectin-based films and coatings with active components for application in antimicrobial food packaging. *Prog. Org. Coat.* 158, 106349. doi:10.1016/j.porgcoat.2021.106349
- Jridi, M., Lassoued, I., Mbarek, A., Kammoun, M., et al. (2014). Physical, structural, antioxidant and antimicrobial properties of gelatin–chitosan composite edible films. *Int. J. Biol. Macromol.* 67, 373–379. doi:10.1016/j.ijbiomac.2014.03.054
- Kan, J., Liu, Y., Qin, Y., Liu, J., et al. (2019). Development of active packaging based on chitosan-gelatin blend films functionalized with Chinese Hawthorn (*Crataegus pinnatifida*) fruit extract. *Int. J. Biol. Macromol.* 140, 384–392. doi:10.1016/j.ijbiomac.2019.08.155
- Kantak, M. N., and Bharate, S. S. J. C. p. (2022). Analysis of clinical trials on biomaterial and therapeutic applications of chitosan: a review. *Carbohydr. Polym.* 278, 118999. doi:10.1016/j.carbpol.2021.118999
- Kavoosi, G., Dadfar, S. M. M., and Purfard, A. (2013). Mechanical, physical, antioxidant, and antimicrobial properties of gelatin films incorporated with thymol for potential use as nano wound dressing. *J. Food Sci.* 78 (2), E244–E250. doi:10.1111/1750-3841.12015
- Kean, T., and Thanou, M. J. A. d.d.r. (2010). Biodegradation, biodistribution and toxicity of chitosan. *Biodegradation* 62 (1), 3–11. doi:10.1016/j.addr.2009.09.004
- Khalaf, E. M., Ramírez-Coronel, A. A., Alazragi, R., Parra, R. M. R., et al. (2023). Recent progressions in biomedical and pharmaceutical applications of chitosan nanoparticles: a comprehensive review. *Int. J. Biol. Macromol.* 231, 123354. doi:10.1016/j.ijbiomac.2023.123354
- Khalilimofrad, Z., Baharifar, H., Asefnejad, A., and Khoshnevisan, K. (2023). Collagen type I cross-linked to gelatin/chitosan electrospun mats: application for skin tissue engineering. *Mat. Today Commun.* 35, 105889. doi:10.1016/j.mtcomm.2023.105889
- Kim, K. M., Weller, C. L., Hanna, M. A., et al. (2006). Properties of chitosan films as a function of pH and solvent type. *J. Food Sci.* 71 (3), E119–E124. doi:10.1111/j.1365-2621.2006.tb15624.x
- Kim, Y., Tabyldiyeva, L., Berikova, K., Zhmagul, D., et al. (2023). Chitosan-based biomaterials for tissue regeneration. *Pharmaceutics* 15 (3), 807. doi:10.3390/pharmaceutics15030807
- Kołodziejka, M., Wszola, M., et al. (2021). Chitosan as an underrated polymer in modern tissue engineering. *Nanomater. (Basel)*. 11 (11), 3019. doi:10.3390/nano11113019
- Kou, S. G., Peters, L. M., and Mucalo, M. R. (2021). Chitosan: a review of sources and preparation methods. *Int. J. Biol. Macromol.* 169, 85–94. doi:10.1016/j.ijbiomac.2020.12.005
- Krishna, M., Nindo, C. I., and Min, S. (2012). Development of fish gelatin edible films using extrusion and compression molding. *J. Food Eng.* 108 (2), 337–344. doi:10.1016/j.jfoodeng.2011.08.002
- Kulka, K., and Sionkowska, A. J. M. (2023). Chitosan based materials in cosmetic applications: a review. *Molecules* 28 (4), 1817. doi:10.3390/molecules28041817
- Kumar, M. R., Muzzarelli, R. A. A., Muzzarelli, C., Domb, A. J., et al. (2004). Chitosan chemistry and pharmaceutical perspectives. *Chem. Rev.* 104 (12), 6017–6084. doi:10.1021/cr030441b
- Kumar, P., Dehiya, B. S., and Sindhu, A. (2017). Comparative study of chitosan and chitosan–gelatin scaffold for tissue engineering. *Int. Nano Lett.* 7, 285–290. doi:10.1007/s40089-017-0222-2
- Kumar, S., Avik, M., Dutta, J., et al. (2020a). Chitosan based nanocomposite films and coatings: emerging antimicrobial food packaging alternatives. *Trends Food Sci. Technol.* 97, 196–209. doi:10.1016/j.tifs.2020.01.002
- Kumar, S., Basumatary, I. B., Mukherjee, A., Dutta, J., et al. (2020b). Biodegradable hybrid nanocomposite of chitosan/gelatin and green synthesized zinc oxide nanoparticles for food packaging. *Foods* 9 (9), 1143. doi:10.3390/foods9091143
- Kumar, S., Heydarifard, S., Nazhad, M. M., Dilbaghi, N., et al. (2014). Nanotechnology-based water treatment strategies. *J. Nanosci. Nanotechnol.* 14 (2), 1838–1858. doi:10.1166/jnn.2014.9050
- Kumosa, L. S., Zetterberg, V., and Schouenborg, J. J. A. B. (2018). Gelatin promotes rapid restoration of the blood brain barrier after acute brain injury. *Acta Biomater.* 65, 137–149. doi:10.1016/j.actbio.2017.10.020
- Kurczewska, J. J. P. (2022). Recent reports on polysaccharide-based materials for drug delivery. *Polym. (Basel)*. 14 (19), 4189. doi:10.3390/polym14194189
- Lahrich, S., Bakasse, M., Saqrane, S., El Mhammedi, M. A., et al. (2021). Review on the contamination of wastewater by COVID-19 virus: impact and treatment. *Sci. Total Environ.* 751, 142325. doi:10.1016/j.scitotenv.2020.142325
- Lee, A., Elam, J. W., Darling, S. B., et al. (2016). Membrane materials for water purification: design, development, and application. *Environ. Sci. Water Res. Technol.* 2 (1), 17–42. doi:10.1039/c5ew00159e

- Lee, C. H., Singla, A., and Lee, Y. (2001). Biomedical applications of collagen. *Int. J. Pharm. X* 221 (1–2), 1–22. doi:10.1016/s0378-5173(01)00691-3
- Lee, D., Koh, M. Y., Kim, P., Lee, J., Shin, M., et al. (2018). Chitosan-catechol: a writable bioink under serum culture media. *Biomater. Sci.* 6 (5), 1040–1047. doi:10.1039/c8bm00174j
- Li, C., Li, T., Xu, Y., Qiang, L., et al. (2019b). Controllable fabrication of hydroxybutyl chitosan/oxidized chondroitin sulfate hydrogels by 3D bioprinting technique for cartilage tissue engineering. *Biomed. Mat.* 14 (2), 025006. doi:10.1088/1748-605x/aaf8ed
- Li, J., and Zhuang, S. J. E. P. J. (2020). Antibacterial activity of chitosan and its derivatives and their interaction mechanism with bacteria: current state and perspectives. *Eur. Polym. J.* 138, 109984. doi:10.1016/j.eurpolymj.2020.109984
- Li, K., Mo, G., Liu, Y., Zheng, K., et al. (2022). Size-transformable gelatin/nanochitosan/doxorubicin nanoparticles with sequentially triggered drug release for anticancer therapy. *Colloids Surf. B Biointerfaces* 220, 112927. doi:10.1016/j.colsurfb.2022.112927
- Li, Z., Liu, L., Hu, Y., Wan, L., et al. (2019a). Preparation, characterization and anti-aflatoxigenic activity of chitosan packaging films incorporated with turmeric essential oil. *Int. J. Biol. Macromol.* 131, 420–434. doi:10.1016/j.ijbiomac.2019.02.169
- Liu, C., Du, W., Jiang, L., Li, Y., Jian, X., et al. (2023). Enhanced antibacterial and adhesive properties of chitosan/gelatin hydrogel containing berberine hydrochloride and prepolymerized gallic acid exhibiting aggregation-induced emission. *Polym. Eng. Sci.* 63 (8), 2596–2612. doi:10.1002/pen.26398
- Liu, T., Qiu, P., Gou, D., Zhao, J., et al. (2022b). Chitosan-based materials: an overview of potential applications in food packaging. *Foods* 11 (10), 1490. doi:10.3390/foods11101490
- Liu, Y., Yao, H., Lin, L., Cui, H., et al. (2022a). Emerging theranostic nanomaterials in diabetes and its complications. *Adv. Sci. (Weinh.)* 9 (3), 2102466. doi:10.1002/adv.202102466
- Lončarević, A., Marica, I., Anamarija, R., et al. (2017). Lysozyme-induced degradation of chitosan: the characterisation of degraded chitosan scaffolds. *J. Tissue Repair Regen.* 1 (1), 12–22. doi:10.14302/issn.2640-6403.jtrr-17-1840
- Long, J., Zhang, W., Zhao, M., Ruan, C. Q., et al. (2023). The reduce of water vapor permeability of polysaccharide-based films in food packaging: a comprehensive review. *reduce water Vap. permeability polysaccharide-based films food Packag. A Compr. Rev.* 321, 121267. doi:10.1016/j.carbpol.2023.121267
- Lu, Y., Tao, N., Deng, S., Wang, L., et al. (2022). Application of gelatin in food packaging: a review. *Appl. gelatin food Packag. A Rev.* 14 (3), 436. doi:10.3390/polym14030436
- Lukin, I., Maeso, L., Zarate, J., Desimone, M. F., Al-Tel, T. H., et al. (2022). Progress in gelatin as biomaterial for tissue engineering. *Pharmaceutics* 14 (6), 1177. doi:10.3390/pharmaceutics14061177
- Luo, Q., Ren, T., Lei, Z., Huang, Y., Xu, D., et al. (2022). Non-toxic chitosan-based hydrogel with strong adsorption and sensitive detection abilities for tetracycline. *Chem. Eng. J.* 427, 131738. doi:10.1016/j.cej.2021.131738
- Lv, L.-C., Huang, Q. Y., Ding, W., Xiao, X. H., Zhang, H. Y., and Xiong, L. X. (2019). Fish gelatin: the novel potential applications. *J. Funct. Foods* 63, 103581. doi:10.1016/j.jff.2019.103581
- Maged, A., Salah, S., Ammar, M. M., Ghorab, M. M., et al. (2019). Mesenchymal stem cells associated with chitosan scaffolds loaded with rosuvastatin to improve wound healing. *Eur. J. Pharm. Sci.* 127, 185–198. doi:10.1016/j.ejps.2018.11.002
- Mahmoud, M. (2015). Water treatment of hexavalent chromium by gelatin-impregnated-yeast (Gel-Yst) biosorbent. *J. Environ. Manage.* 147, 264–270. doi:10.1016/j.jenvman.2014.08.022
- Maturavongsadit, P., Shirwaiker, R., Benhabbour, S. R., et al. (2021). Cell-laden nanocellulose/chitosan-based bioinks for 3D bioprinting and enhanced osteogenic cell differentiation. *ACS Appl. Bio Mat.* 4 (3), 2342–2353. doi:10.1021/acsabm.0c01108
- Miranda, S. C., Alves, J. B., Goes, A. M., et al. (2011). Three-dimensional culture of rat BMMSCs in a porous chitosan-gelatin scaffold: a promising association for bone tissue engineering in oral reconstruction. *Arch. Oral Biol.* 56 (1), 1–15. doi:10.1016/j.archoralbio.2010.08.018
- Mirsadeghi, H., Alireza, V., Hasan, N., Pourashouri, P., et al. (2019). The effect of different kinds of chitosans and cooking methods on the formation of heterocyclic aromatic amines in huso (*Huso huso*) fillet. *J. Food Process. Preserv.* 43 (12), e14253. doi:10.1111/jfpp.14253
- Moeini, A., Malinconico, M., Gomez d'Ayala, G., and Makvandi, P. (2020). Wound healing and antimicrobial effect of active secondary metabolites in chitosan-based wound dressings: a review. *Wound Heal. Antimicrob. Eff. Act. Second. metabolites chitosan-based wound dressings A Rev.* 233, 115839. doi:10.1016/j.carbpol.2020.115839
- Mohan, K., Jayakumar, R., Sathishkumar, P., Uthayakumar, V., et al. (2020). Recent insights into the extraction, characterization, and bioactivities of chitin and chitosan from insects. *Trends Food Sci. Technol.* 105, 17–42. doi:10.1016/j.tifs.2020.08.016
- Moharir, R. V., and Kumar, S. (2019). Challenges associated with plastic waste disposal and allied microbial routes for its effective degradation: a comprehensive review. *J. Clean. Prod.* 208, 65–76. doi:10.1016/j.jclepro.2018.10.059
- Morin-Crini, N., Lichtfouse, E., Torri, G., and Crini, G. (2019). Fundamentals and applications of chitosan. *Sustain. Agric. Rev.* 49–123. doi:10.1007/978-3-030-16538-3_2
- Mukherjee, C., Dissa, V., Krishna, J. S., Boominathan, T., Rakeshkumar, R., Dineshkumar, S., et al. (2023). Recent advances in biodegradable polymers—Properties, applications and future prospects. *Eur. Polym. J.* 192, 112068. doi:10.1016/j.eurpolymj.2023.112068
- Mulyani, R., Mulyadi, D., and Yusuf, N. (2020). Chitosan membrane from shrimp shells (*panaeus modonon*) as an antibacterial food. *Journal of physics: conference series* 1477, 072006. doi:10.1088/1742-6596/1477/7/072006
- Muthu, M., Devadoss, A. J. P., Hasan, N., Sivanesan, I., et al. (2021). Crustacean waste-derived chitosan: antioxidant properties and future perspective. *Antioxidants (Basel)* 10 (2), 228. doi:10.3390/antiox10020228
- Mutlu-Ingok, A., Dilara, D., Dilara, N. D., Karbancioglu-Guler, F., Capanoglu, E., et al. (2020). Antibacterial, antifungal, antimycotoxigenic, and antioxidant activities of essential oils: an updated review. *Molecules* 25 (20), 4711. doi:10.3390/molecules25204711
- Muzzarelli, R. A., and De Vincenzi, M. (2020). “Chitosans as dietary food additives,” in *Applications of chitan and chitosan* (CRC Press), 115–127.
- Nadeem, H. R., Sestili, P., Lorenzo, J. M., Ranjha, M. M. A. N., et al. (2021). Heterocyclic aromatic amines in meat: formation, isolation, risk assessment, and inhibitory effect of plant extracts. *Heterocycl. aromatic amines meat Form. Isol. risk Assess. inhibitory Eff. plant Extr.* 10 (7), 1466. doi:10.3390/foods10071466
- Naghieh, S., Chen, X., et al. (2018). Dispensing-based bioprinting of mechanically-functional hybrid scaffolds with vessel-like channels for tissue engineering applications - a brief review. *J. Mech. Behav. Biomed. Mat.* 78, 298–314. doi:10.1016/j.jmbbm.2017.11.037
- Nagpal, K., Shailendra, K. S., Dina, N. M., et al. (2010). Chitosan nanoparticles: a promising system in novel drug delivery. *Chem. Pharm. Bull. (Tokyo)* 58 (11), 1423–1430. doi:10.1248/cpb.58.1423
- Nayak, R., Truong, Y. B., Arnold, L., et al. (2012). Recent advances in nanofibre fabrication techniques. *Text. Res. J.* 82 (2), 129–147. doi:10.1177/0040517511424524
- Ndlovu, S. P., Ngece, L., Alven, S., Aderibigbe, B. A., et al. (2021). Gelatin-based hybrid scaffolds: promising wound dressings. *Polym. (Basel)* 13 (17), 2959. doi:10.3390/polym13172959
- Negm, N. A., Kana, M. T. H. A., Samar, A. A., Betiha, M. A., et al. (2020). Effectuality of chitosan biopolymer and its derivatives during antioxidant applications. *Int. J. Biol. Macromol.* 164, 1342–1369. doi:10.1016/j.ijbiomac.2020.07.197
- No, H., Meyers, S. P., Prinyawiwatkul, W., Xu, Z., et al. (2007). Applications of chitosan for improvement of quality and shelf life of foods: a review. *J. Food Sci.* 72 (5), R87–R100. doi:10.1111/j.1750-3841.2007.00383.x
- Ogawa, K., Yui, T., and Okuyama, K. (2004). Three D structures of chitosan. *Int. J. Biol. Macromol.* 34 (1–2), 1–8. doi:10.1016/j.ijbiomac.2003.11.002
- Oh, J.-W., Chun, S. C., and Chandrasekaran, M. J. A. (2019). Preparation and *in vitro* characterization of chitosan nanoparticles and their broad-spectrum antifungal action compared to antibacterial activities against phytopathogens of tomato. *Agron. (Basel)* 9 (1), 21. doi:10.3390/agronomy9010021
- Ohkawa, K., Nishida, A., Yamamoto, H., et al. (2004). Electrospinning of chitosan. *Macromol. Rapid Commun.* 25 (18), 1600–1605. doi:10.1002/marc.200400253
- Oleksy, M., Dynarowicz, K., and Aebischer, D. J. M. (2023). Advances in biodegradable polymers and biomaterials for medical applications—a review. *Molecules* 28 (17), 6213. doi:10.3390/molecules28176213
- Omerović, N., Mladenović, M., Vunduk, J., Milenković, I., et al. (2021). Antimicrobial nanoparticles and biodegradable polymer composites for active food packaging applications. *Compr. Rev. Food Sci. Food Saf.* 20 (3), 2428–2454. doi:10.1111/1541-4337.12727
- Oz, F., Ali, Z., Kaya, M., et al. (2017). Effect of chitosan on the formation of heterocyclic aromatic amines and some quality properties of meatball. *J. Food Process. Preserv.* 41 (4), e13065. doi:10.1111/jfpp.13065
- Pang, Z., Hilton, D., Peter, S., Sharma, R., Bansal, N., et al. (2014). Rheology, texture and microstructure of gelatin gels with and without milk proteins. *Food Hydrocoll.* 35, 484–493. doi:10.1016/j.foodhyd.2013.07.007
- PanSu, D. F., Liu, C., and Guo, Z. (2020). Research progress for plastic waste management and manufacture of value-added products. *Adv. Compos. Hybrid. Mat.* 3, 443–461. doi:10.1007/s42114-020-00190-0
- Paramithiotis, S., Drosinos, E. H., and Skandamis, P. (2017). Food recalls and warnings due to the presence of foodborne pathogens—a focus on fresh fruits, vegetables, dairy and eggs. *Curr. Opin. Food Sci.* 18, 71–75. doi:10.1016/j.cofs.2017.11.007
- Park, S., Marsh, K., and Rhim, J. J. J. o.F. S. (2002). Characteristics of different molecular weight chitosan films affected by the type of organic solvents. *J. Food Sci.* 67 (1), 194–197. doi:10.1111/j.1365-2621.2002.tb11382.x
- Parvizifard, M., and Karbasi, S. (2020). Physical, mechanical and biological performance of PHB-Chitosan/MWCNTs nanocomposite coating deposited on bioglass based scaffold: potential application in bone tissue engineering. *Int. J. Biol. Macromol.* 152, 645–662. doi:10.1016/j.ijbiomac.2020.02.266
- Pattanaik, A., Pati, S., and Samal, S. K. J. L. (2022). Chitosan-polyphenol conjugates for human health. *Life* 12 (11), 1768. doi:10.3390/life12111768

- Pavlíková, L., Peer, P., Uysal-Unalan, I., Janalíková, M., et al. (2023). Bioactive zein/chitosan systems loaded with essential oils for food-packaging applications. *J. Sci. Food Agric.* 103 (3), 1097–1104. doi:10.1002/jsfa.11978
- Peers, S., Montebault, A., and Ladavière, C. (2020). Chitosan hydrogels for sustained drug delivery. *J. Control. Release* 326, 150–163. doi:10.1016/j.jconrel.2020.06.012
- Pelissari, F. M., Fabio, Y., Maria, V., Grossmann, E., et al. (2011). Extrusion parameters related to starch/chitosan active films properties. *Int. J. Food Sci. Tech.* 46 (4), 702–710. doi:10.1111/j.1365-2621.2010.02533.x
- Pellá, M. C., Beneton, A. G., Caetano, J., Simões, M. R., et al. (2020). Effect of gelatin and casein additions on starch edible biodegradable films for fruit surface coating. *Food Chem.* 309, 125764. doi:10.1016/j.foodchem.2019.125764
- Pendergast, M. M., Hoek, E. M. J. E., and Science, E. (2011). A review of water treatment membrane nanotechnologies. *Energy Environ. Sci.* 4 (6), 1946–1971. doi:10.1039/c0ee00541j
- Pires, J. R. A., Vieira, Ê. T., Fernando, A. L., Souza, V. G. L., et al. (2022). Application of biocomposite films of chitosan/natural active compounds for shelf life extension of fresh poultry meat. *J. Compos. Sci.* 6 (11), 342. doi:10.3390/jcs6110342
- Pisani, S., Scocozza, F., Mariotti, C., Chiesa, E., Bruni, G., et al. (2020). Preliminary investigation on a new natural based poly(gamma-glutamic acid)/Chitosan bioink. *J. Biomed. Mat. Res.* 108 (7), 2718–2732. doi:10.1002/jbm.b.34602
- Poverenov, E., Zaitsev, Y., Arnon, H., Granit, R., Alkalai-Tuvia, S., Perzelan, Y., et al. (2014). Effects of a composite chitosan–gelatin edible coating on postharvest quality and storability of red bell peppers. *Postharvest Biol. Technol.* 96, 106–109. doi:10.1016/j.postharvbio.2014.05.015
- Priyadarshi, R., and Rhim, J.-W. (2020). Chitosan-based biodegradable functional films for food packaging applications. *Innovative Food Sci. Emerg. Technol.* 62, 102346. doi:10.1016/j.ifset.2020.102346
- Punia Bangar, S., Kajla, P., Kumar, M., Trif, M., et al. (2021). Natural antimicrobials as additives for edible food packaging applications: a review. *Nat. Antimicrob. as Addit. edible food Packag. Appl. A Rev.* 10 (10), 2282. doi:10.3390/foods10102282
- Qasim, S. B., Khurshid, Z., Shah, A., Husain, S., et al. (2018). Electrospinning of chitosan-based solutions for tissue engineering and regenerative medicine. *Int. J. Mol. Sci.* 19 (2), 407. doi:10.3390/ijms19020407
- Quilliam, R. S., Purshouse, H., O'Hara, Z., Oliver, D. M., et al. (2020). COVID-19: the environmental implications of shedding SARS-CoV-2 in human faeces. *Environ. Int.* 140, 105790. doi:10.1016/j.envint.2020.105790
- Rahmani Del Bakhshayesh, A., Akbarzadeh, A., Samiei, M., Alizadeh, E., et al. (2018). Recent advances on biomedical applications of scaffolds in wound healing and dermal tissue engineering. *Artif. Cells Nanomed. Biotechnol.* 46 (4), 691–705. doi:10.1080/21691401.2017.1349778
- Rai, P., Gnansounou, E., Sharma, S. K., et al. (2021). Recent advances in the sustainable design and applications of biodegradable polymers. *Bioresour. Technol.* 325, 124739. doi:10.1016/j.biortech.2021.124739
- Rajasree, S. R., Gopalakrishnan, M., Aranganathan, L., and Karthih, M. (2020). Fabrication and characterization of chitosan based collagen/gelatin composite scaffolds from big eye snapper *Priacanthus hamrur* skin for antimicrobial and anti oxidant applications. *Mater. Sci. Eng. C* 107, 110270. doi:10.1016/j.msec.2019.110270
- Ramachandran, G., and Kartha, G. J. N. (1955). Structure of collagen. *Nature* 176, 593–595. doi:10.1038/176593a0
- Ramanathan, G., Thangavelu, M., Jeyakumar Grace Felciya, S., and Tiruchirapalli Sivagnanam, U. (2022). Dual drug loaded polyhydroxy butyric acid/gelatin nanofibrous scaffold for possible post-surgery cancer treatment. *Mat. Lett.* 323, 132597. doi:10.1016/j.matlet.2022.132597
- Ramirez Caballero, S. S., Montebault, A., Tadier, S., Maire, E., David, L., et al. (2019). 3-D printing of chitosan-calcium phosphate inks: rheology, interactions and characterization. *J. Mat. Sci. Mat. Med.* 30, 6–15. doi:10.1007/s10856-018-6201-y
- Rawal, T., Butani, S., et al. (2017). Rifampicin loaded chitosan nanoparticle dry powder presents an improved therapeutic approach for alveolar tuberculosis. *Colloids Surf. B Biointerfaces* 154, 321–330. doi:10.1016/j.colsurfb.2017.03.044
- Raza, Z. A., Khalil, S., Asif, A., Banat, I. M., et al. (2020). Recent developments in chitosan encapsulation of various active ingredients for multifunctional applications. *Carbohydr. Res.* 492, 108004. doi:10.1016/j.carres.2020.108004
- Reshad, R. A. I., Jishan, T. A., and Chowdhury, N. N. (2021). Chitosan and its broad applications: a brief review. *J. Clin. Exp. INVESTIGATIONS* 12, em00779. doi:10.29333/jcei/11268
- Riaz, A., Lagnika, C., Abidin, M., Hashim, M. M., and Ahmed, W. (2020). Preparation and characterization of chitosan/gelatin-based active food packaging films containing apple peel nanoparticles. *J. Polym. Environ.* 28, 411–420. doi:10.1007/s10924-019-01619-4
- Riaz, A., Wan, P., Chen, D., Jabbar, S., et al. (2018). Preparation and characterization of chitosan-based antimicrobial active food packaging film incorporated with apple peel polyphenols. *Int. J. Biol. Macromol.* 114, 547–555. doi:10.1016/j.jbiomac.2018.03.126
- Rider, P., Retnasingh, S., Barbeck, M., et al. (2018). Bioprinting of tissue engineering scaffolds. *J. Tissue Eng.* 9, 2041731418802090. doi:10.1177/2041731418802090
- Rigueto, C. V. T., de Oliveira, R., Wohlmuth, D. A. R., Ferreira Menezes, J., et al. (2022). Gelatin films from wastes: a review of production, characterization, and application trends in food preservation and agriculture. *Food Res. Int.* 162, 112114. doi:10.1016/j.foodres.2022.112114
- Rodríguez-Rodríguez, R., García-Carvajal, Z. Y., et al. (2020). Composite hydrogels based on gelatin, chitosan and polyvinyl alcohol to biomedical applications: a review. *Compos. hydrogels based gelatin, chitosan polyvinyl alcohol Biomed. Appl. A Rev.* 69 (1), 1–20. doi:10.1080/00914037.2019.1581780
- Rosellini, E., Barbani, N., Lazzeri, L., Shin, S. R., et al. (2018). Protein/polysaccharide-based scaffolds mimicking native extracellular matrix for cardiac tissue engineering applications. *J. Biomed. Mat. Res. A* 106 (3), 769–781. doi:10.1002/jbm.a.36272
- Roy, S., and Rhim, J.-W. (2021). Fabrication of bioactive binary composite film based on gelatin/chitosan incorporated with cinnamon essential oil and rutin. *Colloids Surf. B Biointerfaces* 204, 111830. doi:10.1016/j.colsurfb.2021.111830
- Russo, T., Fucile, P., Rosa, G., Sannino, F., et al. (2021). Sustainable removal of contaminants by biopolymers: a novel approach for wastewater treatment. Current state and future perspectives. *Sustain. Remov. Contam. by biopolymers a Nov. approach wastewater Treat. Curr. state future Perspect.* 9 (4), 719. doi:10.3390/pr9040719
- Sahoo, N., Guha, A., Kuotsu, K., et al. (2015). Recent advancement of gelatin nanoparticles in drug and vaccine delivery. *Int. J. Biol. Macromol.* 81, 317–331. doi:10.1016/j.jbiomac.2015.08.006
- Sajkiewicz, P., and Kolbuk, D. (2014). Polymer Edition, Electrospinning of gelatin for tissue engineering—molecular conformation as one of the overlooked problems. *J. Biomaterials Sci.* 25 (18), 2009–2022. doi:10.1080/09205063.2014.975392
- Samantaray, P. K., Baloda, S., Madras, G., Bose, S., et al. (2018). A designer membrane tool-box with a mixed metal organic framework and RAFT-synthesized antibacterial polymer perform in tandem towards desalination, antifouling and heavy metal exclusion. *J. Mat. Chem. A Mat.* 6 (34), 16664–16679. doi:10.1039/c8ta05052j
- Sánchez-González, L., Maite, C., Amparo, C., González-Martínez, C., et al. (2010). Physical properties of edible chitosan films containing bergamot essential oil and their inhibitory action on *Penicillium italicum*. *Carbohydr. Polym.* 82 (2), 277–283. doi:10.1016/j.carbpol.2010.04.047
- Sani, I. K., Pirsia, S., and Tağı, Ş. J. P. T. (2019). Preparation of chitosan/zinc oxide/Melissa officinalis essential oil nano-composite film and evaluation of physical, mechanical and antimicrobial properties by response surface method. *Polym. Test.* 79, 106004. doi:10.1016/j.polymertesting.2019.106004
- Santhi, K., Min, F. M., Ting, C. Z., Devi, D., et al. (2017). In-vitro characterization of chitosan nanoparticles of fluconazole as a carrier for sustained ocular delivery. *Nanosci. Nanotechnology-Asia* 7 (1), 41–50. doi:10.2174/2210681206666160402003316
- Santos, V. P., Lima, M. A. B. d., Franco, L. d. O., Campos-Takaki, G. M. d., et al. (2020). Seaford waste as attractive source of chitin and chitosan production and their applications. *Int. J. Mol. Sci.* 21 (12), 4290. doi:10.3390/ijms21124290
- Saranya, T., Rajan, V. K., Raja, B., Jayakumar, R., Sathianarayanan, S., et al. (2018). Synthesis, characterisation and biomedical applications of curcumin conjugated chitosan microspheres. *Int. J. Biol. Macromol.* 110, 227–233. doi:10.1016/j.jbiomac.2017.12.044
- Sen Gupta, R., Samantaray, P. K., and Bose, S. (2023). Going beyond cellulose and chitosan: synthetic biodegradable membranes for drinking water, wastewater, and oil–water remediation. *Going beyond Cellul. Chitosan Synthetic Biodegrad. Membr. Drink. Water, Wastewater, Oil–Water Remediat.* 8 (28), 24695–24717. doi:10.1021/acsomega.3c01699
- Sethi, S., and Kaith, B. S. (2022). A review on chitosan-gelatin nanocomposites: Synthesis, characterization and biomedical applications. *Reactive-and-Functional-Polymers* 179, 105362. doi:10.1016/j.reactfunctpolym.2022.105362
- Shahidi, F., and Zhong, Y. (2015). Measurement of antioxidant activity. *Food Chem.* 18, 757–781. doi:10.1016/j.jff.2015.01.047
- Shen, Y., Hang, R., Zhang, X., Wang, Y., et al. (2020). DLP printing photocurable chitosan to build bio-constructs for tissue engineering. *Carbohydr. Polym.* 235, 115970. doi:10.1016/j.carbpol.2020.115970
- Shiekh, K. A., Ngwngam, K., and Tongdeesoonorn, W. J. C. (2021). Polysaccharide-based active coatings incorporated with bioactive compounds for reducing postharvest losses of fresh fruits. *Coatings (Basel)* 12 (1), 8. doi:10.3390/coatings12010008
- Shyu, Y.-S., Chen, G.-W., Chiang, S.-C., Sung, W. C., et al. (2019). Effect of chitosan and fish gelatin coatings on preventing the deterioration and preserving the quality of fresh-cut apples. *Molecules* 24 (10), 2008. doi:10.3390/molecules24102008
- Singh, D., Parmar, J., Hegde, D., Soni, P., et al. (2012). Development of chitosan-based dry powder inhalation system of cisplatin for lung cancer. *Indian J. Pharm. Sci.* 74 (6), 521. doi:10.4103/0250-474x.110584
- Singh, G., Singh, S., Kumar, B., and Gaikwad, K. K. (2021). Active barrier chitosan films containing gallic acid based oxygen scavenger. *Food Meas.* 15, 585–593. doi:10.1007/s11694-020-00669-w
- Siripatrawan, U., and Kaewklin, P. J. F. H. (2018). Fabrication and characterization of chitosan-titanium dioxide nanocomposite film as ethylene scavenging and antimicrobial active food packaging. *Food Hydrocoll.* 84, 125–134. doi:10.1016/j.foodhyd.2018.04.049

- Sobral, P., Menegalli, F. C., Hubinger, M. D., Roques, M., et al. (2001). Mechanical, water vapor barrier and thermal properties of gelatin based edible films. *Food Hydrocoll.* 15 (4-6), 423–432. doi:10.1016/s0268-005x(01)00061-3
- Sreerekha, P., Chatterjee, N. S., Raghavankutty, M., Mathew, S., et al. (2021). Dietary supplementation of encapsulated anthocyanin loaded-chitosan nanoparticles attenuates hyperlipidemic aberrations in male Wistar rats. *Carbohydr. Polym. Technol. Appl.* 2, 100051. doi:10.1016/j.carpta.2021.100051
- Suhag, R., Upadhyay, A., et al. (2020). Film formation and deposition methods of edible coating on food products: a review. *Film Form. deposition methods edible Coat. food Prod. A Rev.* 136, 109582. doi:10.1016/j.foodres.2020.109582
- Sul, Y., Ezati, P., and Rhim, J. (2023). Preparation of chitosan/gelatin-based functional films integrated with carbon dots from banana peel for active packaging application. *Int. J. Biol. Macromol.* 246, 125600. doi:10.1016/j.ijbiomac.2023.125600
- Suvarna, V., Khan, T., Omri, A., et al. (2022). Antimicrobial nanomaterials for food packaging. *Antibiot. (Basel)*. 11 (6), 729. doi:10.3390/antibiotics11060729
- Tabata, Y., and Ikada, Y. (1998). Protein release from gelatin matrices. *Adv. Drug Deliv. Rev.* 31 (3), 287–301. doi:10.1016/s0169-409x(97)00125-7
- Tan, C., Wang, J., and Sun, B. J. F. C. (2021). Polysaccharide dual coating of yeast capsules for stabilization of anthocyanins. *Food Chem.* 357, 129652. doi:10.1016/j.foodchem.2021.129652
- Tan, Y. N., Lee, P. P., and Chen, W. N. (2020). Dual extraction of crustacean and fungal chitosan from a single *Mucor circinelloides* fermentation. *Ferment. (Basel)*. 6 (2), 40. doi:10.3390/fermentation6020040
- Tavares, W. S., Tavares-Júnior, A. G., Otero-Espinar, F. J., Martín-Pastor, M., and Sousa, F. F. (2020). Design of ellagic acid-loaded chitosan/zein films for wound bandaging. *J. Drug Deliv. Sci. Technol.* 59, 101903. doi:10.1016/j.jddst.2020.101903
- Tharanathan, R. N., and Kittur, F. S. (2003). Chitin—the undisputed biomolecule of great potential. *Crit. Rev. Food Sci. Nutr.* 43 (1), 61–87. doi:10.1080/10408690390826455
- Thein-Han, W., Saikhun, J., Pholpramoo, C., Misra, R., Kitiyanant, Y., et al. (2009). Chitosan–gelatin scaffolds for tissue engineering: physico-chemical properties and biological response of buffalo embryonic stem cells and transfectant of GFP–buffalo embryonic stem cells. *Acta Biomater.* 5 (9), 3453–3466. doi:10.1016/j.actbio.2009.05.012
- Thomas, A. W., and Kelly, M. (1922). THE ISO-ELECTRIC POINT OF COLLAGEN. *J. Am. Chem. Soc.* 44 (1), 195–201. doi:10.1021/ja01422a025
- Trombino, S., Pellegrino, M., Russo, R., Cassano, R., et al. (2021). Chitosan membranes filled with cyclosporine a as possible devices for local administration of drugs in the treatment of breast cancer. *Molecules* 26 (7), 1889. doi:10.3390/molecules26071889
- Vahedi, M., Barzin, J., Shokrollahi, P., Taghiyar, L., and Ashtiani, M. K. (2020). Amylopectin multiple aldehyde crosslinked hydrogel as an injectable and self-healing cell carrier for bone tissue engineering. *Macromol. Mat. Eng.* 305 (4), 2000045. doi:10.1002/mame.202070008
- Veis, A., and Aranyi, C. (1960). *Phase Sep. polyelectrolyte Syst. I. Complex coacervates gelatin*. 64 (9), 1203–1210. doi:10.1021/j100838a022
- Vieira, H., Cabral, A. E., Botelho, A., Helbig, C., et al. (2023). Current and expected trends for the marine chitin/chitosan and collagen value chains. *Mar. Drugs* 21 (12), 605. doi:10.3390/md21120605
- Vieira, I. R. S., Anna, P. A. D. D. C., Carlos, A. C. J., et al. (2022). Recent advances in biobased and biodegradable polymer nanocomposites, nanoparticles, and natural antioxidants for antibacterial and antioxidant food packaging applications. *Compr. Rev. Food Sci. Food Saf.* 21 (4), 3673–3716. doi:10.1111/1541-4337.12990
- Walimbe, T., and Panitch, A. J. B. (2020). Best of both hydrogel worlds: harnessing bioactivity and tunability by incorporating glycosaminoglycans in collagen hydrogels. *Bioeng. (Basel)*. 7 (4), 156. doi:10.3390/bioengineering7040156
- Wang, H., Ding, F., Liang, M., Zhang, Y., et al. (2021). Edible films from chitosan-gelatin: physical properties and food packaging application. *Food Biosci.* 40, 100871. doi:10.1016/j.fbio.2020.100871
- Wang, K., Lin, S., Nune, K. C., Misra, R. D. K., et al. (2016). Chitosan-gelatin-based microgel for sustained drug delivery. *J. Biomater. Sci. Polym. Ed.* 27 (5), 441–453. doi:10.1080/09205063.2016.1143673
- Wang, L., Chai, Z., Li, P., Cheng, Y., et al. (2011). Synergistic antimicrobial activities of natural essential oils with chitosan films. *J. Agric. Food Chem.* 59 (23), 12411–12419. doi:10.1021/jf203165k
- Wang, W., Xue, C., and Mao, X. (2020). Chitosan: structural modification, biological activity and application. *Int. J. Biol. Macromol.* 164, 4532–4546. doi:10.1016/j.ijbiomac.2020.09.042
- Wang, X., Yu, X., Yan, Y., Zhang, R., et al. (2008). Liver tissue responses to gelatin and gelatin/chitosan gels. *J. Biomed. Mat. Res. A* 87 (1), 62–68. doi:10.1002/jbm.a.31712
- Wang, Y.-C., Ravishanker, C., Gunasekaran, S., et al. (2018). Chitosan and gold nanoparticles-based thermal history indicators and frozen indicators for perishable and temperature-sensitive products. *Food control*. 85, 186–193. doi:10.1016/j.foodcont.2017.09.031
- Watts, P., Davies, M., and Melia, C. (1990). Microencapsulation using emulsification/solvent evaporation: an overview of techniques and applications. *Crit. Rev. Ther. Drug. Carrier Syst.* 7 (3), 235–259.
- Wegrzynowska-Drzymalska, K., Kaczmarek, H., Goslinski, T., Ziegler-Borowska, M., et al. (2022). Chitosan-gelatin films cross-linked with dialdehyde cellulose nanocrystals as potential materials for wound dressings. *Int. J. Mol. Sci.* 23 (17), 9700. doi:10.3390/ijms23179700
- Wu, C., Wang, L., Yuan, Y., Chen, J., et al. (2019). Enhanced functional properties of biopolymer film incorporated with curcumin-loaded mesoporous silica nanoparticles for food packaging. *Food Chem.* 288, 139–145. doi:10.1016/j.foodchem.2019.03.010
- Wu, F., Misra, M., and Mohanty, A. K. (2021). Challenges and new opportunities on barrier performance of biodegradable polymers for sustainable packaging. *Prog. Polym. Sci.* 117, 101395. doi:10.1016/j.progpolymsci.2021.101395
- Wu, Y., Ania, R., Maria, P. A., Metón, I., et al. (2020). Chitosan-based drug delivery system: applications in fish biotechnology. *Polym. (Basel)*. 12 (5), 1177. doi:10.3390/polym12051177
- Xiong, Y., Fang, Z., et al. (2021). Incorporation of salmon bone gelatine with chitosan, gallic acid and clove oil as edible coating for the cold storage of fresh salmon fillet. *Food control*. 125, 107994. doi:10.1016/j.foodcont.2021.107994
- Xu, D., Chen, T., and Liu, Y. (2021a). The physical properties, antioxidant and antimicrobial activity of chitosan–gelatin edible films incorporated with the extract from hop plant. *Polym. Bull. Berl.* 78, 3607–3624. doi:10.1007/s00289-020-03294-1
- Xu, J., Li, L., Jiao, Z., Wang, H., et al. (2021b). A biological functional hybrid scaffold based on decellularized extracellular matrix/gelatin/chitosan with high biocompatibility and antibacterial activity for skin tissue engineering. *Int. J. Biol. Macromol.* 187, 840–849. doi:10.1016/j.ijbiomac.2021.07.162
- Yadav, M., Goswami, P., Paritosh, K., Kumar, M., Pareek, N., and Vivekanand, V. (2019). Seafood waste: a source for preparation of commercially employable chitin/chitosan materials. *Bioresour. Bioprocess.* 6 (1), 8–20. doi:10.1186/s40643-019-0243-y
- Yan, C., Zhang, C., Cao, X., Feng, B., Li, X., et al. (2020). Intestinal population in host with metabolic syndrome during administration of chitosan and its derivatives. *Molecules* 25 (24), 5857. doi:10.3390/molecules25245857
- Yan, D., Li, Y., Liu, Y., Li, N., Yan, C., et al. (2021). Antimicrobial properties of chitosan and chitosan derivatives in the treatment of enteric infections. *Molecules* 26 (23), 7136. doi:10.3390/molecules26237136
- Yang, C.-Y., Tsay, S.-Y., and Chen, B.-K. J. C. E. C. (2001). Application of gelatin for encapsulating aspirin into ethyl cellulose microcapsule in an O/W emulsion. *Chem. Eng. Commun.* 186 (1), 241–255. doi:10.1080/00986440108912876
- Yang, T., Zhan, L., and Huang, C. (2020). Recent insights into functionalized electrospun nanofibrous films for chemo-/bio-sensors. *TrAC Trends Anal. Chem.* 124, 115813. doi:10.1016/j.trac.2020.115813
- Yang, Z., Gilbert, E. P., McGillivray, D. J., Williams, M. A. K., et al. (2016). Nonlinear behavior of gelatin networks reveals a hierarchical structure. *Biomacromolecules* 17 (2), 590–600. doi:10.1021/acs.biomac.5b01538
- Yildirim, M., Weiss, A.-V., and Schneider, M. J. P. (2023). The effect of elasticity of gelatin nanoparticles on the interaction with macrophages. *Pharmaceutics* 15 (1), 199. doi:10.3390/pharmaceutics15010199
- Yin, G.-Z., and Yang, X.-M. (2020). Biodegradable polymers: a cure for the planet, but a long way to go. *J. Polym. Res.* 27 (2), 38. doi:10.1007/s10965-020-2004-1
- Yin, N., Du, R., Zhao, F., Han, Y., Zhou, Z., et al. (2020). Characterization of antibacterial bacterial cellulose composite membranes modified with chitosan or chito oligosaccharide. *Carbohydr. Polym.* 229, 115520. doi:10.1016/j.carbpol.2019.115520
- Yong, H., Bai, R., Zhang, X., Liu, J., et al. (2019b). Antioxidant and pH-sensitive films developed by incorporating purple and black rice extracts into chitosan matrix. *Int. J. Biol. Macromol.* 137, 307–316. doi:10.1016/j.ijbiomac.2019.07.009
- Yong, H., Liu, Y., Qin, Y., Liu, J., et al. (2019a). Effects of anthocyanin-rich purple and black eggplant extracts on the physical, antioxidant and pH-sensitive properties of chitosan film. *Eff. anthocyanin-rich purple black eggplant Extr. Phys. Antioxid. pH-sensitive Prop. chitosan film* 94, 93–104. doi:10.1016/j.foodhyd.2019.03.012
- Yuceer, M., and Caner, C. (2014). Antimicrobial lysozyme–chitosan coatings affect functional properties and shelf life of chicken eggs during storage. *Antimicrob. lysozyme-chitosan coatings affect Funct. Prop. shelf life Chick. eggs Dur. storage* 94 (1), 153–162. doi:10.1002/jsfa.6322
- Zarandona, I., Puertas, A., Dueñas, M., Guerrero, P., and de la Caba, K. (2020). Assessment of active chitosan films incorporated with gallic acid. *Food Hydrocoll.* 101, 105486. doi:10.1016/j.foodhyd.2019.105486
- Zhang, D., Lu, S., Quan, W., Li, P., et al. (2021). Catechol functionalized chitosan/active peptide microsphere hydrogel for skin wound healing. *Int. J. Biol. Macromol.* 173, 591–606. doi:10.1016/j.ijbiomac.2021.01.157
- Zhang, L., Shi, J., Zhang, X., Qi, C., et al. (2020). Potentials of sandwich-like chitosan/polycaprolactone/gelatin scaffolds for guided tissue regeneration membrane. *Mat. Sci. Eng. C Mat. Biol. Appl.* 109, 110618. doi:10.1016/j.msec.2019.110618
- Zhang, M., Wan, T., Zhang, P., et al. (2022a). Application of chitosan and its derivative polymers in clinical medicine and agriculture. *Polym. (Basel)*. 14 (5), 958. doi:10.3390/polym14050958

- Zhang, P., Bai, Y., and Zhang, L. (2016b). Preparation and evaluation of naringenin-loaded sulfobutylether- β -cyclodextrin/chitosan nanoparticles for ocular drug delivery. *Carbohydr. Polym.* 149, 224–230. doi:10.1016/j.carbpol.2016.04.115
- Zhang, R., Su, Y., Zhao, X., Elimelech, M., et al. (2016a). Antifouling membranes for sustainable water purification: strategies and mechanisms. *Chem. Soc. Rev.* 45 (21), 5888–5924. doi:10.1039/c5cs00579e
- Zhang, S.-Y., Yang, X. R., Chi, C. F., Wang, B., et al. (2022c). Gelatins and antioxidant peptides from Skipjack tuna (*Katsuwonus pelamis*) skins: purification, characterization, and cytoprotection on ultraviolet-A injured human skin fibroblasts. *Food Biosci.* 50, 102138. doi:10.1016/j.fbio.2022.102138
- Zhang, X., Qin, Y., Liu, J., Liu, J., et al. (2019). Development of multifunctional food packaging films based on chitosan, TiO₂ nanoparticles and anthocyanin-rich black plum peel extract. *Food Hydrocoll.* 94, 80–92. doi:10.1016/j.foodhyd.2019.03.009
- Zhang, X., Sulistio, A., Qiao, G. G., Lundin, L., et al. (2010). Chemical modification of gelatin by a natural phenolic cross-linker, tannic acid. *J. Agric. Food Chem.* 58 (11), 6809–6815. doi:10.1021/jf1004226
- Zhang, Y., Chen, H., and Li, J. (2022b). Recent advances on gelatin methacrylate hydrogels with controlled microstructures for tissue engineering. *Int. J. Biol. Macromol.* 221, 91–107. doi:10.1016/j.ijbiomac.2022.08.171
- Zhao, C., Li, J. G., Huang, T. T., Lu, Y. J., et al. (2020). Chitosan ducts fabricated by extrusion-based 3D printing for soft-tissue engineering. *Carbohydr. Polym.* 236, 116058. doi:10.1016/j.carbpol.2020.116058
- Zhao, Z., Li, Y., and Du, Z. J. S. (2022). Seafood waste-based materials for sustainable food packing: from waste to wealth. *Sustainability* 14 (24), 16579. doi:10.3390/su142416579
- Zhou, M., Ye, W., Zheng, Z., Huang, K., et al. (2022). Chitosan-gelatin-EGCG nanoparticle-mediated LncRNA TMEM44-AS1 silencing to activate the P53 signaling pathway for the synergistic reversal of 5-FU resistance in gastric cancer. *Adv. Sci. (Weinh.)* 9 (22), 2105077. doi:10.1002/advs.202105077
- Zhu, J., Chen, W., Sun, Y., Huang, X., Chu, R., Wang, R., et al. (2022). Recent advances on drug delivery nanoplatfoms for the treatment of autoimmune inflammatory diseases. *Mat. Adv.* 3, 7687–7708. doi:10.1039/d2ma00814a



OPEN ACCESS

EDITED BY

Jianshe Hu,
Northeastern University, China

REVIEWED BY

Yiming Zhang,
Xinqiao Hospital, China
Vincenza De Gregorio,
University of Naples Federico II, Italy

*CORRESPONDENCE

Lili Cao,
✉ caoll215@163.com

RECEIVED 04 June 2024

ACCEPTED 17 September 2024

PUBLISHED 30 September 2024

CITATION

Cao L, Qian X, Min J, Zhang Z, Yu M and
Yuan D (2024) Cutting-edge developments in
the application of hydrogels for treating skin
photoaging.
Front. Mater. 11:1443514.
doi: 10.3389/fmats.2024.1443514

COPYRIGHT

© 2024 Cao, Qian, Min, Zhang, Yu and Yuan.
This is an open-access article distributed
under the terms of the [Creative Commons
Attribution License \(CC BY\)](https://creativecommons.org/licenses/by/4.0/). The use,
distribution or reproduction in other forums is
permitted, provided the original author(s) and
the copyright owner(s) are credited and that
the original publication in this journal is cited,
in accordance with accepted academic
practice. No use, distribution or reproduction
is permitted which does not comply with
these terms.

Cutting-edge developments in the application of hydrogels for treating skin photoaging

Lili Cao^{1*}, Xiaoying Qian², Jie Min³, Zhongfeng Zhang¹,
Meiping Yu¹ and Dan Yuan¹

¹Department of Plastic Surgery, Zhejiang Rongjun Hospital, Jiaxing, Zhejiang, China, ²Department of Dermatology, Zhejiang Rongjun Hospital, Jiaxing, Zhejiang, China, ³General Surgery Department, Jiaxing No. 1 Hospital, Jiaxing, Zhejiang, China

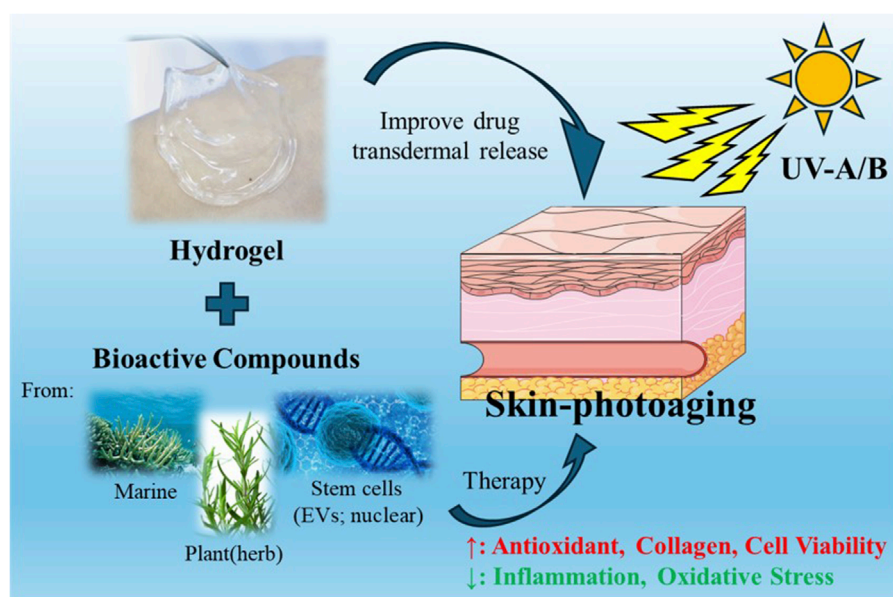
Skin photoaging, caused by prolonged exposure to ultraviolet (UV) radiation, manifests as intricate biological transformations, encompassing oxidative damage and structural alterations. Despite a growing need for effective interventions, the existing therapeutic repertoire for treating skin photoaging remains constrained. Recent investigations have shifted focus towards the application of hydrogels as a novel avenue for addressing this concern. Various active substances can be combined with hydrogels for transdermal delivery, including compounds from the ocean, plants, cell active substances, which can promote skin UV damage repair mainly through antioxidant, anti-inflammatory and promote collagen production. This review seeks to offer a thorough summary of recent progress in employing hydrogels for addressing skin photoaging. Topics covered include the mechanism of skin photoaging, and emerging trends in hydrogel-based therapies for skin rejuvenation. The discussion also explores challenges and outlines potential future directions in leveraging hydrogels as therapeutic agents to address skin photoaging.

KEYWORDS

hydrogel, stem cells, photoaging, collagen, rejuvenation

1 Introduction

The skin, our body's largest protective organ, is prone to injuries from genetic factors, lifestyle choices, diet, sunlight, and the environment (Hubbard et al., 2014; Belkaid and Segre, 2014). The consequences of skin aging and diseases go beyond physical implications, impacting individuals, families, and society at large in terms of mental, social, and financial aspects (Rittié and Fisher, 2015; Gu et al., 2020; Sreedhar et al., 2020). Notably, skin photoaging, a prominent sign of skin aging, mainly results from prolonged UV radiation exposure (Fisher et al., 2002; Battie et al., 2014). This type of aging is marked by fine lines, wrinkles, uneven pigmentation, and decreased skin elasticity (Cao et al., 2020; Zhang and Duan, 2018; Letsiou, 2021). Structural changes in photoaged skin involve collagen fiber breakdown, abnormal elastic fiber buildup, and disruption of the epidermal barrier (Papaccio et al., 2022; Schuch et al., 2017; Nakanishi et al., 2009). Skin photoaging, characterized by the premature aging of the skin due to chronic exposure to UV radiation, is a significant dermatological concern. Unlike intrinsic aging, which occurs naturally over time, photoaging is primarily induced by external environmental factors, particularly UV radiation from the sun. This process



GRAPHICAL ABSTRACT

involves a complex interplay of molecular and cellular mechanisms, leading to visible changes such as wrinkles, loss of elasticity, and hyperpigmentation (Chaudhary et al., 2020; Zhao Y. et al., 2021a; Sales et al., 2022). The pathophysiology of skin photoaging is primarily driven by DNA damage and collagen degradation. UV radiation penetrates the skin and generates reactive oxygen species (ROS), which in turn cause oxidative stress (Kim et al., 2022). This oxidative stress results in direct damage to cellular DNA, leading to mutations and impaired cellular functions (Schuch et al., 2017; Poon et al., 2015). Moreover, UV radiation disrupts the extracellular matrix by accelerating the degradation of collagen, the protein responsible for maintaining skin structure and elasticity (Battie et al., 2014). The combination of these effects results in the characteristic signs of photoaged skin.

Current treatment methods for skin photoaging include topical antioxidants, laser therapy, and chemical peels (Poon et al., 2015). Topical antioxidants, such as vitamins C and E, aim to neutralize ROS and reduce oxidative stress (Tran et al., 2023). However, their efficacy is often limited by poor skin penetration and stability issues. Laser therapy and chemical peels, while effective in promoting skin renewal and collagen production, can be associated with side effects such as redness, swelling, and risk of infection (Hamilton and Kao, 2020; Sharad, 2013). Additionally, these treatments often require multiple sessions and maintenance, posing a challenge for long-term management of photoaging. Given these limitations, there is an urgent need for innovative and effective approaches to prevent and treat skin photoaging. Current research aims to address these gaps by exploring novel therapeutic strategies that target the underlying mechanisms of photoaging. By focusing on enhancing skin repair and protection at the molecular level, we hope to develop treatments that offer more sustained and comprehensive benefits for aging skin.

Recently, hydrogel materials, renowned for their exceptional water retention capabilities and biocompatibility, have emerged

as versatile substances with vast applications (Cao H. et al., 2021a; Ho et al., 2022; Zhao et al., 2020). Their unique properties make them well-suited for creating conducive environments that promote various biological processes, particularly in the realms of wound healing and skin injury repair (Kim et al., 2023; Xiong et al., 2022; Wang et al., 2021). In the context of wound healing, hydrogel materials play a pivotal role in maintaining a moist and supportive milieu at the wound site (Cortes et al., 2020; Wang Y. et al., 2024a). This environment accelerates the healing process by facilitating cell migration, proliferation, and tissue regeneration (Mast et al., 1991). The inherent softness and permeability of hydrogels distinguish them from traditional dressings, providing a more favorable substrate for wound recovery (Francesco et al., 2018). The synergy of hydrogel materials with stem cells has garnered significant attention in advancing wound healing and skin injury repair (Fu et al., 2023). The combination capitalizes on the regenerative potential of stem cells, further enhancing tissue repair mechanisms. Studies have demonstrated promising outcomes in burn injuries, ulcers, and various skin lesions, showcasing the considerable potential of hydrogel-stem cell combinations as innovative therapeutic strategies (Li et al., 2021; Khayambashi et al., 2021). Skin photoaging is essentially a form of skin damage. Hydrogels can also serve as a drug delivery tool for treating skin photoaging damage, facilitating the administration of drugs to rejuvenate the skin, promoting a more youthful appearance (Zhao X. et al., 2021b; Li et al., 2023). Additionally, hydrogels can be combined with manufacturing technologies such as 3D printing to create more efficient transdermal drug delivery systems, including innovations like microneedle patch (Vijayavenkataraman et al., 2018; Huang et al., 2023; Cassano et al., 2023).

This review offers a detailed look at the recent advancements in using hydrogels as carriers for therapeutic agents or bioactive molecules to treat skin aging. Hydrogels, primarily composed of diverse polymeric materials, are employed to deliver a variety

of substances, including natural products, stem cell extracts, extracellular vesicles, and growth factors, to address skin damage caused by UVA/UVB and facilitate skin rejuvenation. Additionally, we explore how hydrogels can enhance the loading efficiency of these bioactive substances and facilitate effective transdermal delivery for therapeutic interventions. In conclusion, we address the challenges and outline future directions for utilizing hydrogels in the treatment of skin photoaging.

2 Attributes of skin photoaging

Skin photoaging is a complex biological process marked by premature aging and damage due to extended exposure to sunlight's ultraviolet (UV) radiation (Wang et al., 2019). This issue has worldwide ramifications for individuals' looks, health, and general welfare. This section offers a thorough overview of the mechanisms behind skin photoaging, encompassing molecular and cellular changes induced by UV exposure (Battie et al., 2014). The exploration expands to cover the clinical signs of photoaged skin, including wrinkles, pigmentation changes, and decreased elasticity (Pourang et al., 2022; Fitsiou et al., 2021). Many studies have shown that skin photoaging mainly involves epidermal fibroblasts, keratinocytes and mesenchymal dermal cells.

UV radiation initiates a sequence of molecular and cellular processes that contribute to accelerated skin aging as depicted in Figure 1 (Kim et al., 2022). These processes result in the production of reactive oxygen species (ROS), leading to oxidative stress and DNA damage (Tan et al., 2022). Ferritin is an important marker of antioxidant activity, and its elevation proves that UV radiation induces oxidative stress. Activation of inflammatory pathways, such as NF- κ B signaling, they increased expression of matrix metalloproteinases (MMPs), heme oxygenase-1, superoxide dismutase-2 and interference with collagen and elastin synthesis contribute to skin degradation and reduced elasticity (Kim et al., 2022). Additionally, UVA radiation also induced a significant increase in the expression of tenascin, a protein closely associated with skin cancer lesions, and UVA radiation induced significant lysozyme deposition. In the skin, lysozyme deposits are seen on elastic fibers in sunburned areas, and the number of lysozyme-containing elastin fibers appears to correlate with the degree of sunburn (Lim et al., 2008; Ortonne, 1990).

A variety of therapeutic strategies are employed to prevent and treat skin aging. Key preventive measures include the use of broad-spectrum sunscreens and other photoprotective practices such as minimizing sun exposure and wearing protective clothing (Poon et al., 2015). Topical antioxidants like vitamins C and E have shown potential in mitigating oxidative stress and protecting against UV-induced damage (Greul et al., 2002; Gaspar and Campos, 2007; Steenvoorden and Beijersbergen van Henegouwen, 1999). Retinoids, which are vitamin A derivatives, have been proven effective in enhancing skin texture, boosting collagen production, and reducing pigmentation (Mukherjee et al., 2006; Riahi et al., 2016). The TGF signaling pathway is the most common therapeutic target for skin photoaging because it is closely related to collagen degradation caused by metalloproteinases and skin inflammation caused by UV (Li et al., 2024). Advanced technologies, such as laser therapy, intense pulsed light (IPL), and photodynamic

therapy (PDT) provide targeted methods to address specific signs of photoaging (Sales et al., 2022; Wang Y. et al., 2023a). Furthermore, new approaches such as regenerative medicine, which use stem cells, growth factors, and tissue engineering, offer potential for skin rejuvenation and repair (Yan et al., 2023; Zhang et al., 2022; Zhang et al., 2020). Hydrogels can be formulated for antioxidant properties or as carriers for drugs or cytokines with photoaging repair effects.

3 Hydrogel for skin photoaging damage repair

Hydrogels, composed of natural or synthetic polymers like proteins and polysaccharides, form three-dimensional networks with high water content (Ho et al., 2022; Francesko et al., 2018). Notably, these hydrogels find significant application in tissue damage repair, creating a conducive environment for cell proliferation and migration, preventing infections, and allowing controlled release of bioactive compounds (Hu et al., 2022; Chawla et al., 2011; Xia et al., 2022). Looking ahead, their versatile and customizable nature positions bio-based hydrogels for promising roles in drug delivery, tissue engineering, and various medical innovations, including wearable sensors (Du et al., 2023; Luo et al., 2023; Rahmani and Shojaei, 2021) and regenerative medicine (Brown and Anseth, 2017; Chyzy and Plonska-Brzezinska, 2020), marking a dynamic trajectory in biomedical research with implications for personalized medicine and diverse clinical applications (Xu et al., 2021; Burdick and Prestwich, 2011; Chen et al., 2023). Here we would like to introduce some of the latest research on the application of hydrogels to skin photoaging damage.

3.1 Hydrogels derived from marine organisms resist photoaging

The use of marine resources can reduce the reliance on chemically synthesized materials in medical applications. Currently, many marine-derived biomaterials, such as sodium alginate, fish collagen, and chitosan, are commonly found in everyday life. In recent years, these materials have been extensively researched and applied in the field of hydrogels (Lewicka et al., 2024; Amnuaykan et al., 2024; Rahman et al., 2024; Guo et al., 2024). Their unique biocompatibility, degradability, and processability make them ideal choices not only for biomedical and tissue engineering applications but also for anti-aging skincare products. This is due to their ability to provide moisturizing, anti-inflammatory, and antioxidant benefits. Additionally, through certain modifications, they can become solutions for drug delivery and tissue regeneration. Recently, A team utilized marine algae extract, including sulfated galactofucan polysaccharides and alginate oligosaccharides as active ingredients, with modified polyacrylonitrile κ -carrageenan serving as the substrate, to develop a multifunctional composite hydrogel (FACP5) (Wu et al., 2023). Animal experiments assessing anti-photoaging properties showed that after FACP5 treatment, there was an increase in skin water content, a reduction in epidermal and dermal thickness, an increase in the activities of catalase and superoxide dismutase, among other

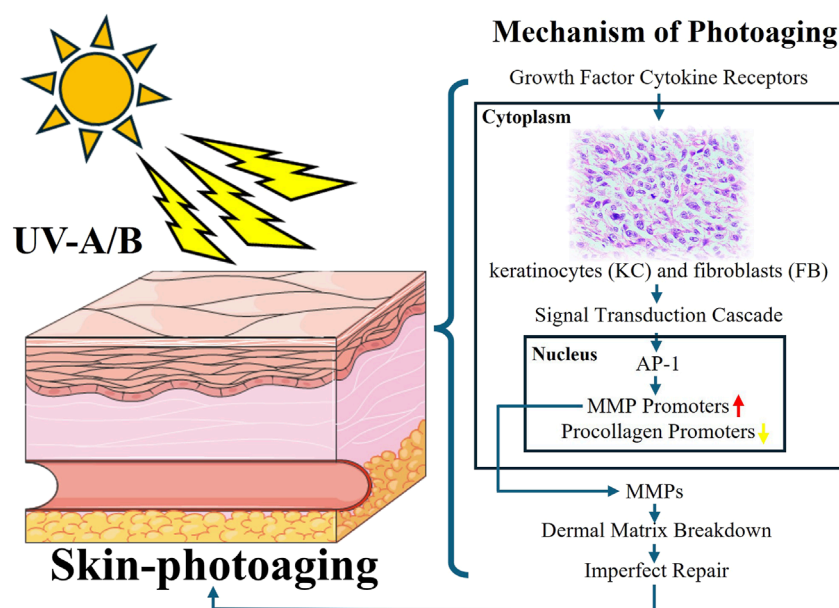


FIGURE 1
Schematic illustration of the mechanism of photoaging.

effects (Wu et al., 2023). These results suggest that FACP5 has skin barrier repair, antioxidant, anti-inflammatory, and collagen degradation inhibition activities, positioning it as a skincare product for protecting against photoaging (Wu et al., 2023). And extract from fish scales of marine fish was also used to prepare a natural composite hydrogel known as SE-gel (Figure 2B) (Liu et al., 2023). This hydrogel, rich in glycine and proline, exhibits excellent ultraviolet absorption, water absorption, moisturizing, and free radical scavenging abilities (Liu et al., 2023). SE glue can effectively increase the ability of antioxidant and reduce ROS damage in L929 cells under UV irradiation (Liu et al., 2023). Some materials like chitosan can also be processed into drug delivery carriers to enhance the transdermal delivery efficiency of certain anti-photoaging drugs. For instance, carboxymethyl-modified chitosan/hyaluronic acid (CMC/HA, CMH) thermosensitive hydrogel can be used for the sustained transdermal delivery of exosomes (Figures 2A–C) (Wu et al., 2024). Its thermosensitive property allows it to quickly gel on the skin surface, delaying the release of liposomes. The release rate of ascorbyl glucoside (AA2G) over 24 h ranges from 33.92% to 49.35% (Wu et al., 2024). This system achieves the long-term release of bioactive ingredients and promotes the anti-photoaging effects of AA2G on the skin, reducing epidermal thickness, melanin deposition, and lipid oxidative damage while increasing collagen density (Figure 2D) (Wu et al., 2024).

In addition to directly using marine extracts for the preparation of related hydrogels, some scholars have also engaged in biomimetic design, drawing inspiration from sea anemones. From the 1,262 adhesive-related proteins found in sea anemones, they identified the cysteine-rich thrombospondin-1 type I repeat-like (TSRL) protein, which is a biocompatible protein with excellent antioxidative properties (Wang et al., 2022). They prepared TSRL recombinant protein based on this protein sequence, and the produced TSRL recombinant protein can self-assemble into a gel (Figure 2C),

exhibiting antioxidant effects in L929 cells, a kind of mouse fibroblast (Wang et al., 2022). Animal experiments have demonstrated that this hydrogel can effectively prevent photoaging of the skin (Wang et al., 2022). The above research demonstrates that the ocean is a rich resource treasure trove with many substances suitable for clinical therapeutic applications, addressing challenges in treating skin photoaging (Table 1). In practical life, these marine-derived biomaterials already have a wide range of applications, including clinical settings and skincare products. Therefore, some of their new application forms should also be quickly utilized in actual treatments. This is also due to the fact that their processing methods and side effects have been thoroughly explored and understood. However, within the plant kingdom on land, there are also numerous medicinal components worthy of exploration.

3.2 Hydrogels derived from plants resist photoaging

There are numerous natural active substances in plants, many of which possess antioxidant properties and even medicinal value. For instance, certain traditional Chinese medicinal herbs contain these properties. Due to the antioxidant effects found in plants, many plant-based ingredients are now incorporated into anti-aging skincare products. And there are plant extracts such as dried fruits of European blueberry (*Vaccinium myrtillus*) or blueberry (*Vaccinium corymbosum*). Extracts from these fruits, along with chitosan, are jointly used to prepare antioxidant hydrogels (Studzinska-Sroka et al., 2024). These hydrogels are employed for protecting the skin against UV damage and have been proven to exhibit excellent biocompatibility through relevant HaCaT cell experiments (Studzinska-Sroka et al., 2024). Additionally, other tests have confirmed their antioxidant, anti-hyaluronidase, and

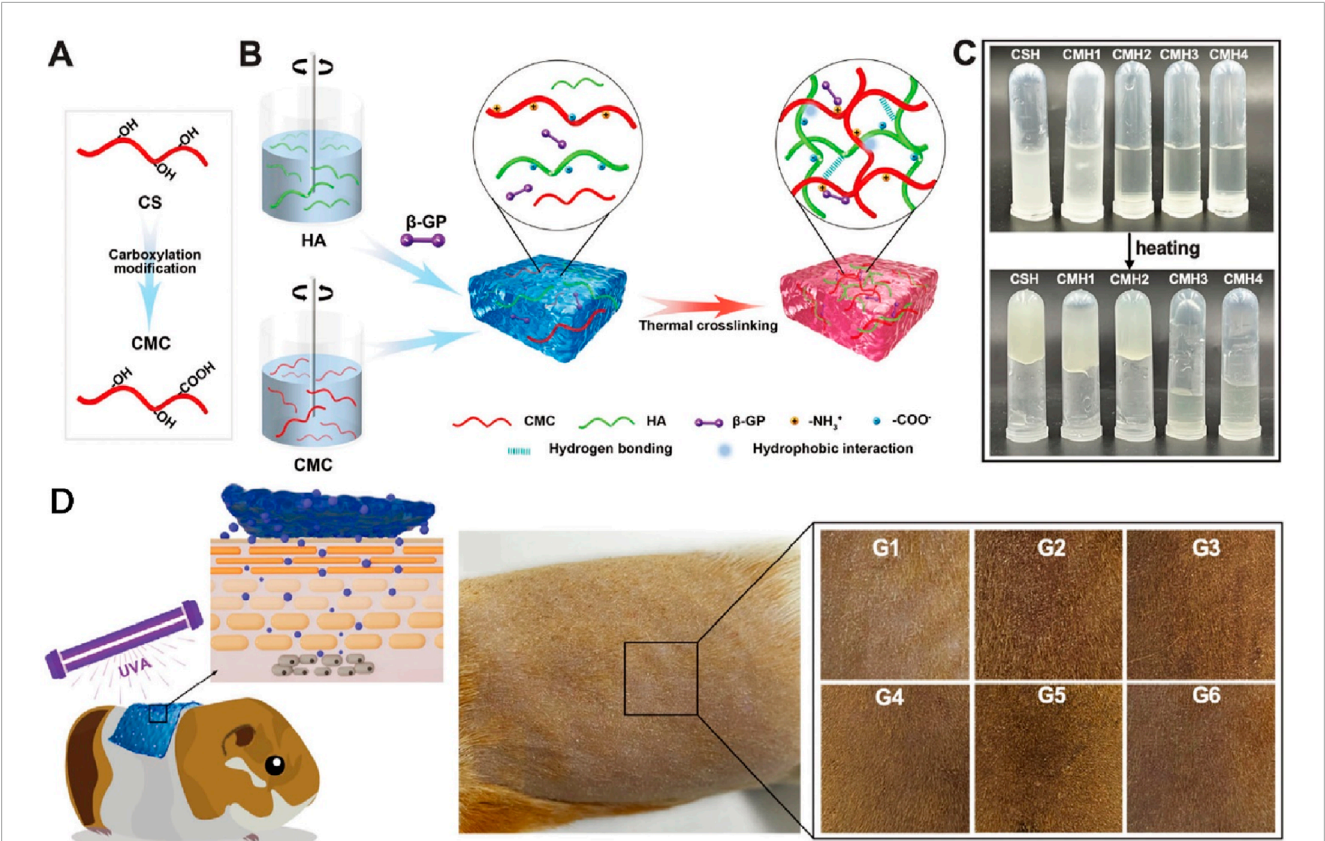


FIGURE 2 The preparation and skin photoaging therapy of thermosensitive hydrogels. (A) Chitosan carboxylation modification. (B) Schematic diagram of hydrogel synthesis. (C) Observation of the hydrogel. (D) Skin photoaging treatment experiment on Guinea pig. Reproduced with permission of Wu et al. (2024).

TABLE 1 Hydrogels prepared from ingredients of marine origin.

| Hydrogel | Agent | Effect | Ref. |
|-------------|---|--|--------------------|
| EACP5 | Marine algae extract (sulfated galactofucan polysaccharides and alginate oligosaccharides); polyacrylonitrile κ -carrageenan | Antioxidant and anti-tyrosinase activities | Wu et al. (2023) |
| SE-gel | Fish scales of marine fish extract | Ultraviolet absorption; water absorption; moisturizing and free radical scavenging abilities | Liu et al. (2023) |
| CMC/HA, CMH | Carboxymethyl-modified chitosan and hyaluronic acid | Long-term release of AA2G and promote its anti-photoaging effects | Wu et al. (2024) |
| TSRL-gel | Thrombospondin-1 type I repeat-like (TSRL) recombinant protein | Antioxidant effects | Wang et al. (2022) |

anti-tyrosinase activities (Studzińska-Sroka et al., 2024). Scientists have also achieved controlled release of anti-photoaging agents by preparing specialized hydrogels to enhance their efficacy against photodamage. They utilized hyaluronic acid to create a novel hydrogel crosslinked with boronate esters (de Oliveira et al., 2020). The release of the anti-photoaging agent dihydrocaffeic acid (DHCA) from this dynamic covalent hydrogel (HG) is controlled through the dynamic properties of complexes between

phenylboronic acid and diol-containing molecules, as well as the pH dependence (de Oliveira et al., 2020). The hydrogel, formed through reversible drug complexation/decomplexation, extends the release of DHCA at pH 7.4, with the fastest release rate observed under acidic (skin) conditions (de Oliveira et al., 2020). Interestingly, incorporating DHCA into the network enhances its protective effect against UVB-induced L929 fibroblast death. Unlike extracting natural compounds from plants, experts have directly

extracted exosome-like nanovesicles from *Olea europaea* leaves (OLELVs) and enhanced them into a potent core biomaterial with high-dose effects that are skin-friendly and non-cytotoxic, inhibiting cell aging (Wang Z. et al., 2024b). These nanovesicles were incorporated into a cross-linked hyaluronic acid (HA) and tannic acid (TA) hydrogel with strong UV-absorbing properties, creating the OLELVs@HA/TA hydrogel system as shown in Figure 3A. *In vitro* and *in vivo* experiments demonstrated that the OLELVs@HA/TA hydrogel can effectively reduce UV-induced skin damage and promote skin repair and regeneration (Figure 3B) (Wang Z. et al., 2024b). Additionally, RNA-seq and clustering analysis of miR168a-5p predicted targets revealed significant downregulation of the NF- κ B signaling pathway, mediating inflammatory aging responses (Wang Z. et al., 2024b). Overall, the OLELVs@HA/TA hydrogel represents a novel dual-strategy approach for clinical application in treating photoaging.

In addition, there are other special plant extracts used in the preparation research of hydrogels for anti-photoaging, such as *Lycium barbarum* fruit polysaccharides, olive leaf extracts, and hesperetin. Researchers prepared a hydrogel named LBP from polysaccharides extracted from *Lycium barbarum* fruits (Neves et al., 2020). Their study revealed that this hydrogel, in combination with red light laser treatment, could inhibit UVR-induced skin thickening, decreasing the expression of c-Fos, c-Jun, MMP-1, -2, and -9, while simultaneously increasing the levels of collagen I, III, and FGF2. The combined treatment of PBM (Photobiomodulation) and LBP holds potential clinical applications in skin rejuvenation (Neves et al., 2020). Giglio et al. utilized olive leaf extracts (OLEs) combined with gellan gum and sodium alginate to prepare a hydrogel crosslinked with tartaric acid (Busto et al., 2023). This hydrogel demonstrated excellent antioxidant properties and effectively protected human dermal fibroblasts under UVA exposure (Busto et al., 2023). Furthermore, some researchers incorporated hesperetin into an AAMVPC hydrogel, achieving significant anti-UV effects by visibly reducing redness and skin aging caused by UV irradiation (de Araújo Andrade et al., 2022). The above hydrogels exhibit excellent anti-photoaging effects. However, directly incorporating relevant components into hydrogels may still face challenges such as uncontrolled release and poor transdermal efficacy.

Therefore, scientists have further explored combining other technologies, such as nanoparticles and liposomes, to enhance the controlled release of active ingredients within hydrogels and even improve the transdermal drug delivery effects. As early as 2015, a team undertook the nanocapsulation of rice bran oil, loading it into hydrogels to enhance its UV protective properties and more effectively reduce skin photoaging damage (Rigo et al., 2015). In this study, researchers initially prepared lipid-core nanocapsules containing rice bran oil with an average particle size of approximately 200 nm (Rigo et al., 2015). These nanocapsules were then incorporated into hydrogels made from acrylic acid polymers (Rigo et al., 2015). In animal experiments aimed at combating photoaging, the hydrogel containing nanocapsulated rice bran oil demonstrated a significant reduction in protein carbonylation levels (a biomarker of oxidative stress) and decrease in NF- κ B nuclear translocation (a biomarker of pro-inflammatory and carcinogenic response). These *in vivo* experimental results substantiate the beneficial effects of nanocapsulation in enhancing

the protective properties of rice bran oil against skin damage induced by UVB exposure (Rigo et al., 2015). As shown in Figure 4, another study discussed the preparation and evaluation of ligustrazine hydrochloride (TMPZ)-loaded liposome-hydrogel (TMPZ-LG) for its antioxidant properties and potential application in the treatment and prevention of ultraviolet (UV) radiation-induced skin damage (Liu et al., 2022). TMPZ-LG was prepared by the membrane dispersion method and natural swelling method using sodium carboxymethyl cellulose (2%, CMC-Na), achieving a transdermal release rate of 40% *in vitro*. The feasibility of TMPZ-LG in preventing and treating UV radiation-induced skin oxidation was demonstrated through DPPH and hydrogen peroxide (H₂O₂) scavenging experiments as well as malondialdehyde (MDA) and low-density lipoprotein (LDL) oxidation experiments (Liu et al., 2022). This indicates its potential as a novel antioxidant drug for transdermal delivery systems.

Oroxylin A (OA) is a flavonoid compound with excellent antioxidant activity and protective effects against photoaging induced by UV radiation. To enhance the transdermal delivery of OA, Nan Li and colleagues utilized nanostructured lipid carriers (NLC) to load OA, encapsulated it in a hydrogel composed of carbomer 940 as a gel matrix and hydroxypropyl methyl cellulose (HPMC) as a thickener (Zhu et al., 2022). *In vitro* studies revealed that OA-NLC exhibited superior therapeutic effects in a UVB radiation cell model compared to OA solution (OA-Sol) (Zhu et al., 2022). OA-Sol and OA-NLC were immobilized in a hydrogel matrix for topical application to the dorsal skin of mice. The results demonstrated that OA-NLC-gel, in comparison to OA-Sol-gel, exhibited significant antioxidant and anti-apoptotic activities, effectively protecting the skin from damage after UV radiation in mice (Zhu et al., 2022). The research findings indicate that OA-BLC-gel is a promising nanocarrier system for treating UV-induced skin oxidative stress damage (Zhu et al., 2022). However, further in-depth investigation is needed to study its long-term effects and potential side effects. To enhance the transdermal absorption of poorly soluble drugs for local use, researchers prepared nanocrystals of 18- β -glycyrrhetic acid (NGAs) using high-pressure homogenization (Quan et al., 2023). These NGAs were combined with amphiphilic chitosan (ACS) to form ANGA composites through electrostatic adsorption (Quan et al., 2023). By incorporating glycerol, they prepared ANGA hydrogel. The ANGA hydrogel significantly improved the characteristics of photoaging in mouse skin under UV irradiation (Quan et al., 2023). It achieved this by inhibiting the abnormal expression of matrix metalloproteinase (MMP)-1 and MMP-3, thereby mitigating the damage caused by UV radiation to the collagen fiber structure (Quan et al., 2023). Therefore, with the advancement of nanotechnology, the transdermal delivery efficiency of certain ingredients has been enhanced, further promoting innovation in skincare product ingredients and the development of the industry.

From the above studies (Table 2), we can see that many plant ingredients have antioxidant and anti-inflammatory effects, which also makes them effective in treating skin damage caused by UV. And with the progress of nanotechnology, the transdermal effect of related drugs can also be further improved, the progress of these studies can also improve the progress of related skin care industry. Most plant-derived natural products are generally considered to

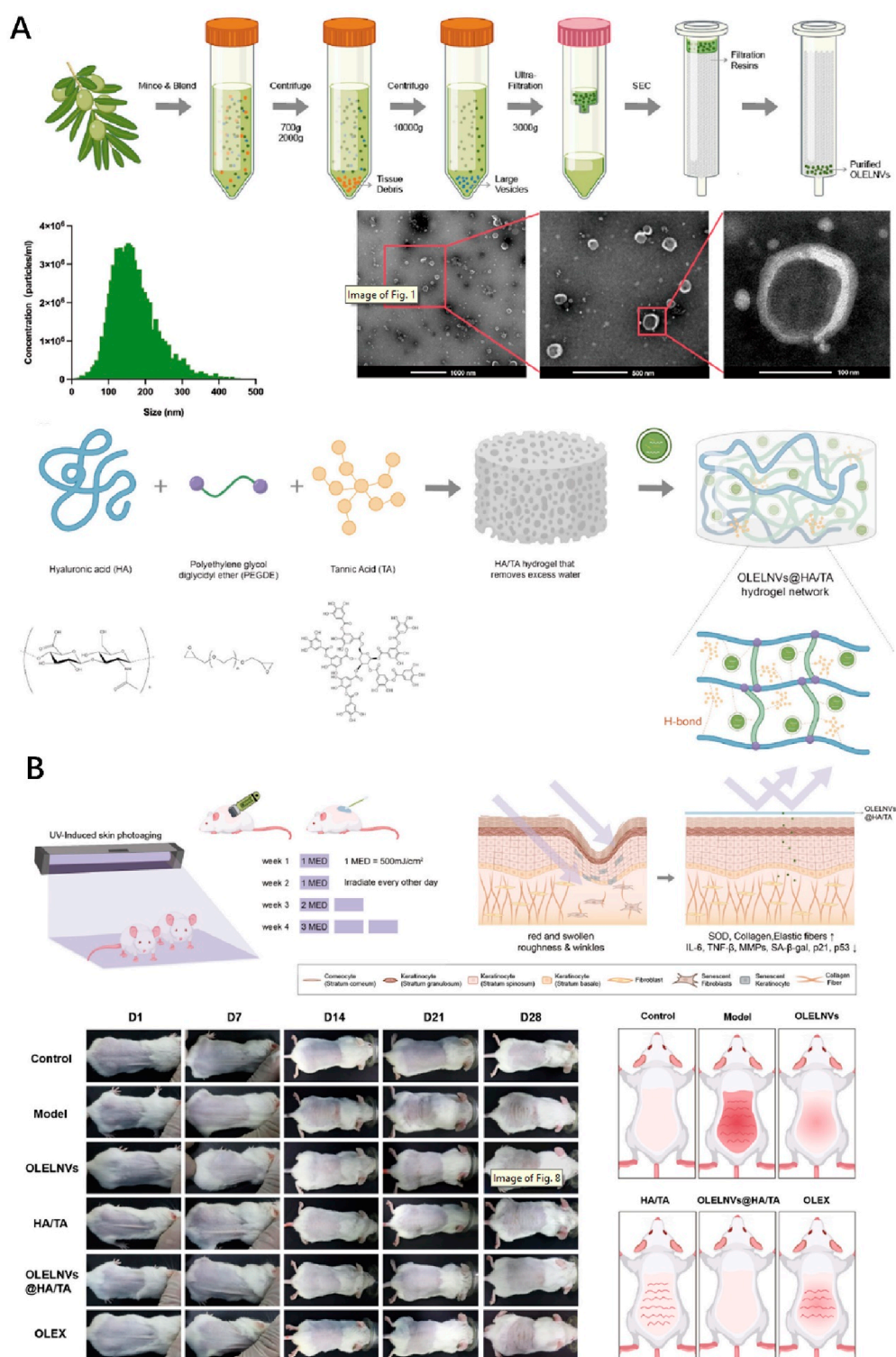


FIGURE 3

The preparation and skin photoaging therapy of OLELVs@HA/TA hydrogel system. **(A)** Schematic diagram of exosome-like nanovesicles extraction and hydrogel synthesis. **(B)** Animal experiment on skin photoaging treatment using the OLELVs@HA/TA hydrogel system. Reproduced with permission of Wang Z. et al. (2024).

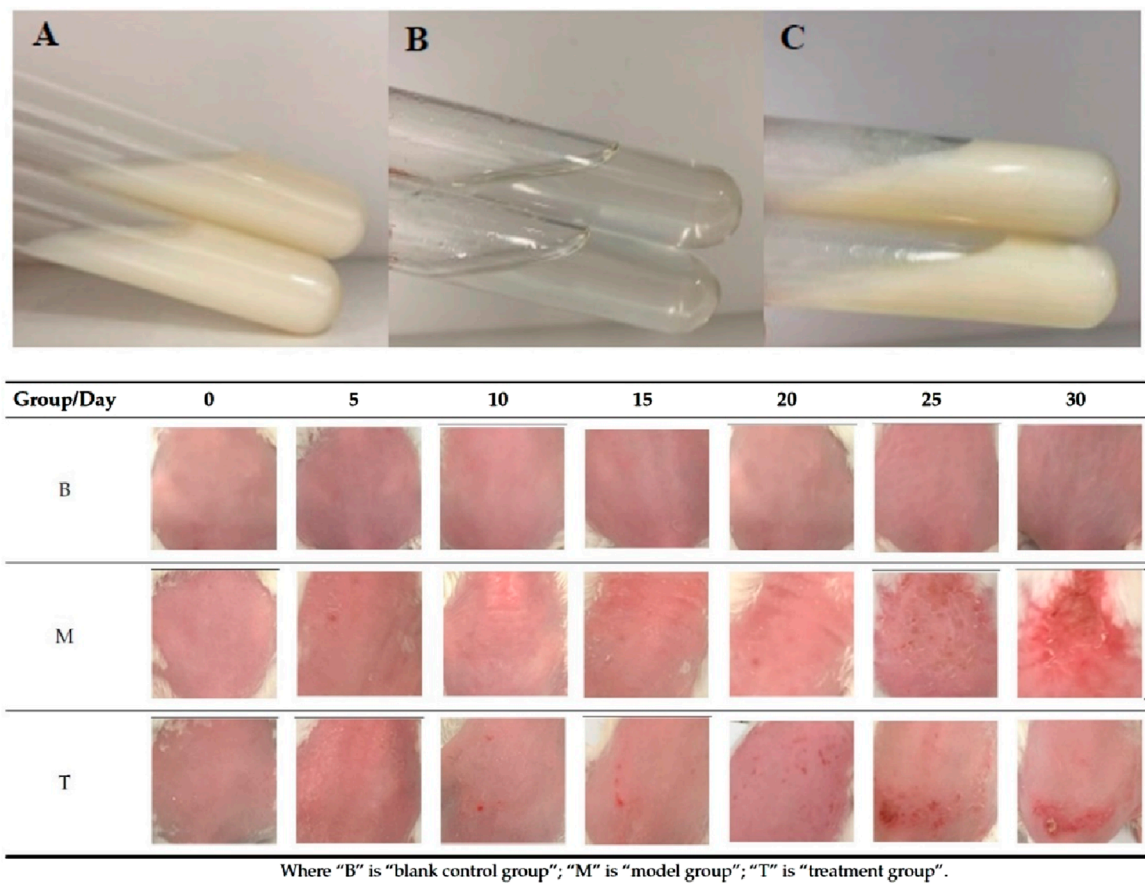


FIGURE 4 Hydrogel preparations (A) TMPZ-L; (B) TMPZ-G; (C) TMPZ-LG and the skin status of mice in each group after treatment 30 days. Reproduced with permission of Liu et al. (2022).

have low physiological toxicity or side effects, making them relatively safe for use. However, extensive human trials are necessary to thoroughly investigate and validate their safety and efficacy for specific applications.

3.3 A hydrogel composed of a special natural product

A team from China conducted a study on skin photoaging therapy using the natural compound selenomethionine (Se-Met), which presents an innovative approach to address the challenges of skin aging by targeting epidermal stem cells (EpiSCs) and their role in wound healing (Sun et al., 2024). By integrating transcriptomics and untargeted metabolomics, the research identifies age-dependent changes in the Gpx gene family and arachidonic acid (AA) metabolic pathways, which contribute to increased susceptibility to ferroptosis—a form of cell death driven by lipid peroxidation. The study proposes Se-Met as a potential therapeutic agent to counteract these effects. Se-Met is shown to enhance the expression of GPX4, a key enzyme involved in

protecting cells from lipid peroxidation and ferroptosis (Sun et al., 2024). Furthermore, Se-Met exhibits antioxidative properties and effective absorption of ultraviolet (UV) radiation, making it suitable for addressing multiple aspects of skin aging, including oxidative stress and UV damage.

To facilitate controlled release of Se-Met, the researchers develop a novel delivery system by covalently grafting Se-Met onto UV-responsive GelMA hydrogels using AC-PEG-NHS tethers. This Se-Met@GelMA hydrogel is demonstrated to accelerate wound healing in aging mice models by inhibiting lipid peroxidation and ferroptosis while enhancing GPX4 expression. Additionally, in a photoaging model, the hydrogel reduces inflammatory responses, promotes extracellular matrix remodeling, and mitigates ferroptosis induced by UV exposure (Sun et al., 2024).

The findings suggest that Se-Met@GelMA hydrogel holds promise for practical clinical applications in addressing various aspects of skin aging, including wound healing and protection against UV-induced damage (Sun et al., 2024). The controlled release mechanism provided by the hydrogel system ensures sustained and localized delivery of Se-Met, enhancing its therapeutic efficacy.

TABLE 2 Hydrogels prepared from plant extracts and natural product.

| Source | Hydrogel | Agent | Effect | Ref. |
|--------------------------------|----------------------------------|---|--|---|
| Plants | Blueberry fruit extract hydrogel | Chitosan (CS); Bilberry Fruit Extract | Anti-hyaluronidase and anti-tyrosinase, antioxidant | Studzińska-Sroka et al. (2024) |
| | HG + DHCA | Hyaluronic acid (HA) modified with saccharide (GLU) residues; HA functionalized with 3-aminophenylboronic acid (APBA); Dihydrocaffeic acid (DHCA) | Protecting against UVB-induced L929 fibroblast death | de Oliveira et al. (2020) |
| | OLELVs@HA/TA hydrogel | Exosome-like nanovesicles from <i>Olea europaea</i> leaves (OLELVs) hyaluronic acid (HA) and tannic acid (TA) | UV-absorbing Down regulation of the NF-κB signaling pathway and mediating inflammatory | Wang et al. (2024b) |
| | LBP | Polysaccharides extracted from <i>Lycium barbarum</i> fruits | Decreasing the expression of c-Fos, c-Jun, MM-P-1, -2, and -9, while simultaneously increasing the levels of collagen I, III, and FGF2 | Neves et al. (2020) |
| | GG-NaALG-OLE film | Gellan gum and sodium alginate; Olive leaf extracts (OLEs) | Antioxidant | Busto et al. (2023) |
| | Hesperetin-Based Hydrogels | AAMVPC gel; Hesperetin | Antioxidant and anti-inflammatory | de Araújo Andrade et al. (2022) |
| Nanocarriers of Plants extract | LNC hydrogel | Acrylic acid polymers rice bran oil | Antioxidant and anti-inflammatory | Rigo et al. (2015) |
| | TMPZ-LG | CMC-Na; Ligustrazine hydrochloride (TMPZ) | Antioxidant | Liu et al. (2022) |
| | OA-NLC-gel | Carbomer 940; Hydroxypropyl methyl cellulose (HPMC) Oroxylin A (OA) | Antioxidant and anti-apoptotic | Zhu et al. (2022) |
| | ANGA hydrogel | Amphiphilic chitosan (ACS); Nanocrystals of 18-β-glycyrrhetic acid (NGAs) | inhibiting (MMP)-1 and MMP-3 | Quan et al. (2023) |

4 Hydrogels based on microneedle patches promote skin photoaging damage repair

Drug delivery systems have become a major focus of research in the biomedical field. Liposomes are a prominent area of study in drug delivery, and integrating liposomes into hydrogels enhances the development of more powerful multifunctional systems for achieving more efficient and sustained local drug delivery. Like the above-mentioned hydrogel system CMC/HA, CMH for the purpose of sustained transdermal delivery of AAG2 loaded liposomes (Wu et al., 2024), they serves as a multifunctional delivery system for sustained transdermal delivery. However, to achieve better delivery outcomes, some researchers

have started using hydrogels to prepare more advanced delivery system—microneedle patches.

The research team led by Xiuli Wang investigated the utilization of roller microneedles (MN) to deliver adipose-derived stem cell-derived extracellular vesicles (ADSC-EVs) to the skin. ADSCs-EVs have been demonstrated to have immunomodulatory and anti-photoaging effects (Cao Z. et al., 2021b). The MN + EVs group exhibited the least wrinkles, the highest collagen density, and the most organized collagen fibers. Extensive research has confirmed the reparative effects of extracellular vesicles from adipose-derived stem cells (ADSCs-EVs) on skin photoaging. Some laboratories have focused on studying the extracellular matrix components of adipose tissue, such as purifying adipose collagen fragments (ACF) (Jin et al., 2022). In order to facilitate its clinical applications, researchers have

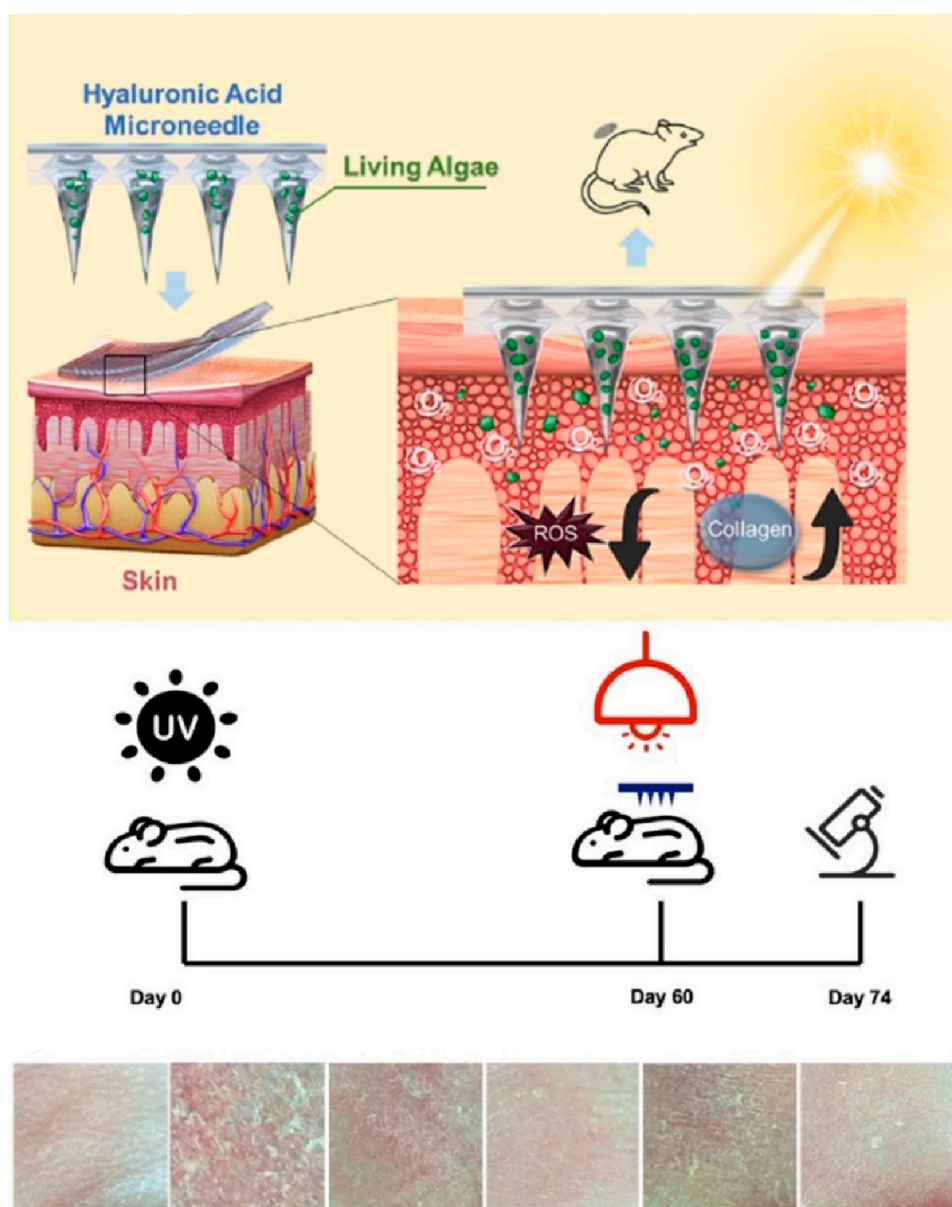


FIGURE 5

Living algae loading HA microneedle treat skin photoaging. Reproduced with permission of Wang Z. et al. (2023).

designed a detachable ACF microneedle (ACF-MN) patch, where the needle tip and the patch backing can be separated (Jin et al., 2022). The research results indicate that ACF-MN exhibits excellent skin puncture performance and can release ACF components slowly. Moreover, this microneedle device carrying ACF shows therapeutic effects on skin photoaging in a mouse model (Jin et al., 2022). Its main anti-photoaging effect on the skin is that it prevents ROS accumulation and induces antioxidase production and induces neovascularization and reduction apoptosis (Jin et al., 2022).

Supplementing collagen in the skin is a reliable anti-aging method, but the effectiveness of some transdermal deliveries is hindered by the large molecular weight of collagen. Some researchers have attempted to address this issue through gene regulation, similar to the success of mRNA therapy, which largely

depends on the safe, effective, and stable transformation of genetic material into functional proteins. Lee et al. combined extracellular vesicles (EVs) encapsulating mRNA encoding extracellular matrix $\alpha 1$ type-I collagen (COL1A1) with microneedle patches (You et al., 2023). Their EVs were primarily produced through cellular nanoporation of human dermal fibroblasts (You et al., 2023). Their results demonstrated that the microneedle patches could induce the formation of collagen-protein grafts and reduce wrinkle formation in the collagen-depleted dermal tissue of mice with photoaged skin (You et al., 2023). Injecting COL1A1 mRNA enclosed in extracellular vesicles (EVs) into the skin shows potential as a protein replacement therapy for treating photoaged skin (You et al., 2023). Currently, researchers are also incorporating certain cytokines into microneedle patch systems. For instance, Ke

TABLE 3 Hydrogels prepared from bioactive ingredients such as cytokines and nucleic acids.

| Hydrogel | Agent | Effect | Ref. |
|-----------------|--|---|---------------------|
| ADSC-EVs MN | Adipose-derived stem cell-derived extracellular vesicles (ADSC-EVs) | Improving epidermal structure and function of photoaging skin. (improving the content of collagen) | Cao et al. (2021b) |
| ACF-MN | Adipose collagen fragments (ACF); gelatin | Preventing ROS accumulation and inducing antioxidase production; inducing neovascularization and reduce apoptosis | Jin et al. (2022) |
| COL1A1-EVs-MN | mRNA encoding for extracellular-matrix α 1 type-I collagen (COL1A1); hyaluronic acid (HA) | Collagen protein-replacement therapy | You et al. (2023) |
| FGF-2/FGF-21 MN | FGF-2 and FGF-21; hyaluronic acid (HA) | Reversing the UVB-induced cell senescence | Yang et al. (2023) |
| Microalgae-MN | Chlorella (GY-H60); hyaluronic acid (HA) | Antioxidant and anti-inflammatory, enhancing collagen regeneration | Wang et al. (2023b) |

Cheng et al. loaded FGF-2 and FGF-21 into microneedle patches made from hyaluronic acid (HA) hydrogel for the treatment of skin photoaging. Significant improvement was observed after 4 weeks of treatment (Yang et al., 2023).

Microneedle patches, in addition to delivering common bioactive substances, can also be used to administer microalgae for treating skin photoaging (Wang Z. et al., 2023b). This is based on the principle previously demonstrated that dissolved oxygen could reverse photoaged skin (Shin et al., 2019). Researchers have developed microneedle patch systems carrying active microalgae (Figure 5), the patch use microalgae to generate reactive oxygen species under light, which helps reverse skin damage by reducing inflammation, promoting collagen regeneration, and diminishing wrinkles. This approach offers a novel method for skin oxygenation and photoaging reversal, laying a theoretical foundation for future clinical applications (Wang Z. et al., 2023b).

We have made a summary of the microneedle system that will be applied in skin photoaging treatment, as shown in Table 3. In addition to the different substances contained in each microneedle, their main solutions to the problems of skin photoaging are mainly aimed at solving the skin inflammation, oxidative stress and cell aging caused by UV. Moreover, HA is the most used polymer hydrogel material for MN production, which has been widely used in medical and cosmetic fields. Its biocompatibility has been extensively validated in clinical settings, proving to be very safe. Therefore, when considering the application of such microneedle patches, the primary focus should be on the safety and efficacy evaluation of the incorporated drugs.

5 TiO2-based materials for UV resistance

TiO2 serves as an inorganic sunscreen and photocatalyst to protect the human body from environmental pollutants. Researchers, led by Jia-You Fang, incorporated TiO2 into

mesoporous silica, where this material effectively filters environmental pollutants, shielding the skin from environmental harm (Lin et al., 2021). Additionally, the material exhibits excellent UV-blocking properties, and the inclusion of avobenzone further enhances its UV-blocking effectiveness (Lin et al., 2021). The combination of avobenzone and TiO2 in SBA-15 (TiO2/SBA) significantly alleviated skin cell death and neutrophil recruitment in photoaged mouse skin compared to the application of SBA-15 alone (Lin et al., 2021). The researchers also formulated avobenzone-loaded TiO2/SBA into a Carbopol 940 hydrogel, creating a sunscreen gel applicable to the skin. avobenzone-loaded TiO2/SBA-S hydrogel demonstrated greater improvement in skin barrier recovery and proinflammatory mediator mitigation compared to SBA-S hydrogel (without TiO2) (Alalaiwe et al., 2023). After avobenzone-loaded TiO2/SBA-S treatment, cytokines/chemokines in photoaged skin were reduced by two to three times compared to the untreated control group (Alalaiwe et al., 2023). The data suggests that mesoporous formulations with low porosity and specific surface area exhibit effective adsorption of environmental pollutants and UVA protective properties (Alalaiwe et al., 2023). This study provides valuable insights into the development of versatile mesoporous silica for safeguarding the skin from environmental stress.

6 Discussion and the future perspectives

As the quality of life in developed regions continues to improve year by year, people's expectations for their own lives are also increasing, especially among some young women who place great emphasis on anti-aging. Ultraviolet radiation is a major factor causing skin aging, and beauty-conscious women always take measures to protect themselves from UV exposure during the summer. Therefore, there is an urgent need for the development of an effective, skin-applicable anti-aging gel product. In addition to providing basic protection against ultraviolet rays, it is preferable

for these products to have a certain effect in promoting skin regeneration and repair, aiming to reduce the occurrence of wrinkles and signs of aging.

We discussed various hydrogels for the treatment of skin photoaging, including those containing components derived from Marine organisms, including components derived from plants, and cytokines and nucleic acids derived from some human stem cells. These studies have shown that they can repair the damage caused by photoaging of the skin, but these effects need to be further demonstrated through clinical trials. When hydrogels are used for treating photoaged skin, biocompatibility and non-toxicity are crucial considerations. Although non-toxicity is a key requirement, it alone is not sufficient to ensure the safety and efficacy of hydrogels. It is also necessary to consider degradability, mechanical properties, absorption and release performance, and moisturizing effects. If the hydrogel is degradable, its degradation products must also be non-toxic and capable of being safely metabolized or excreted by the body. The hydrogel should have appropriate mechanical properties to ensure it remains on the skin surface for a sufficient period. Additionally, hydrogels should have good drug loading and release characteristics to ensure that their active ingredients can be continuously and stably released into the skin. Furthermore, hydrogels usually should have moisturizing effects to help maintain the skin's moisture balance. However, most of the current research on hydrogels primarily demonstrates their efficacy in treating photoaged skin, while other aspects have been less frequently tested, with only a few studies addressing them. Among these hydrogels, individuals prefer hydrogels from bioactive substances containing human self-cells, which do not have to worry about xenograft rejection and should have better effects, and other sources of hydrogels can play a greater role in the field of cosmetics.

From the current research progress, the application of natural product extracts is extensive, encompassing substances from natural sources such as the ocean and plants. On one hand, they serve as high-quality bioactive substances with specific anti-photoaging effects; on the other hand, during the development and industrialization of related products, they can be rapidly deployed for practical applications, providing consumers with efficient anti-photoaging products. Therefore, efforts should be intensified in the development of relevant components, allocating more resources to related research, and driving the development of associated industries. In addition, the functional effectiveness and side effects

of some new ingredients must undergo clinical trials. As for research outcomes involving stem cells, extracellular vesicles, or even genetic engineering approaches in anti-photoaging, there are currently challenges in industrialization due to ethical and technological maturity issues. Nevertheless, in the near future, they still hold significant market prospects, as related research continues to mature, leading to more outstanding anti-photoaging effects. In summary, in the field of combating skin photoaging, it is anticipated that numerous innovations will emerge, further transforming skincare approaches and market dynamics.

Author contributions

LC: Conceptualization, Writing—original draft, Writing—review and editing. XQ: Writing—review and editing. JM: Writing—review and editing. ZZ: Writing—review and editing. MY: Writing—review and editing. DY: Writing—review and editing.

Funding

The author(s) declare that no financial support was received for the research, authorship, and/or publication of this article.

Conflict of interest

The authors declare that the research was conducted in the absence of any commercial or financial relationships that could be construed as a potential conflict of interest.

Publisher's note

All claims expressed in this article are solely those of the authors and do not necessarily represent those of their affiliated organizations, or those of the publisher, the editors and the reviewers. Any product that may be evaluated in this article, or claim that may be made by its manufacturer, is not guaranteed or endorsed by the publisher.

References

- Alalaiwe, A., Lin, Y. C., Lin, C. F., Huang, C. C., Wang, P. W., and Fang, J. Y. (2023). TiO₂-embedded mesoporous silica with lower porosity is beneficial to adsorb the pollutants and retard UV filter absorption: a possible application for outdoor skin protection. *Eur. J. Pharm. Sci.* 180, 106344. doi:10.1016/j.ejps.2022.106344
- Amnuaykan, P., Juntapirom, S., Kanjanakawinkul, W., and Chaiyana, W. (2024). Enhanced antioxidant, anti-aging, anti-tyrosinase, and anti-inflammatory properties of vanda coerulea griff. Ex lindl. Protocorm through elicitations with chitosan. *Plants (Basel)* 13 (13), 1770. doi:10.3390/plants13131770
- Battie, C., Jitsukawa, S., Bernerd, F., Del Bino, S., Marionnet, C., and Verschoore, M. (2014). New insights in photoaging, UVA induced damage and skin types. *Exp. Dermatol* 23 (Suppl. 1), 7–12. doi:10.1111/exd.12388
- Belkaid, Y., and Segre, J. A. (2014). Dialogue between skin microbiota and immunity. *Science* 346 (6212), 954–959. doi:10.1126/science.1260144
- Brown, T. E., and Anseth, K. S. (2017). Spatiotemporal hydrogel biomaterials for regenerative medicine. *Chem. Soc. Rev.* 46 (21), 6532–6552. doi:10.1039/c7cs00445a
- Burdick, J. A., and Prestwich, G. D. (2011). Hyaluronic acid hydrogels for biomedical applications. *Adv. Mater* 23 (12), H41–H56. doi:10.1002/adma.201003963
- Busto, F., Licini, C., Luccarini, A., Damiani, E., Mattioli-Belmonte, M., Cometa, S., et al. (2023). Oleuropein-rich gellan gum/alginate films as innovative treatments against photo-induced skin aging. *Molecules* 28 (11), 4352. doi:10.3390/molecules28114352
- Cao, C., Xiao, Z., Wu, Y., and Ge, C. (2020). Diet and skin aging—from the perspective of food nutrition. *Nutrients* 12 (3), 870. doi:10.3390/nu12030870
- Cao, H., Duan, L., Zhang, Y., Cao, J., and Zhang, K. (2021a). Current hydrogel advances in physicochemical and biological response-driven biomedical application diversity. *Signal Transduct. Target Ther.* 6 (1), 426. doi:10.1038/s41392-021-00830-x
- Cao, Z., Jin, S., Wang, P., He, Q., Yang, Y., Gao, Z., et al. (2021b). Microneedle based adipose derived stem cells-derived extracellular vesicles therapy ameliorates UV-induced photoaging in SKH-1 mice. *J. Biomed. Mater. Res. A* 109 (10), 1849–1857. doi:10.1002/jbm.a.37177

- Cassano, R., Curcio, F., Sole, R., and Trombino, S. (2023). Transdermal delivery of phloretin by gallic acid microparticles. *Gels* 9 (3), 226. doi:10.3390/gels9030226
- Chaudhary, M., Khan, A., and Gupta, M. (2020). Skin ageing: pathophysiology and current market treatment approaches. *Curr. Aging Sci.* 13 (1), 22–30. doi:10.2174/1567205016666190809161115
- Chawla, K., Yu, T., Liao, S. W., and Guan, Z. (2011). Biodegradable and biocompatible synthetic saccharide-Peptide hydrogels for three-dimensional stem cell culture. *Biomacromolecules* 12 (3), 560–567. doi:10.1021/bm100980w
- Chen, Y., Wang, X., Tao, S., Wang, Q., Ma, P. Q., Li, Z. B., et al. (2023). Research advances in smart responsive-hydrogel dressings with potential clinical diabetic wound healing properties. *Mil. Med. Res.* 10 (1), 37. doi:10.1186/s40779-023-00473-9
- Chyzy, A., and Plonska-Brzezinska, M. E. (2020). Hydrogel properties and their impact on regenerative medicine and tissue engineering. *Molecules* 25 (24), 5795. doi:10.3390/molecules25245795
- Cortes, H., Caballero-Florán, I. H., Mendoza-Muñoz, N., Córdova-Villanueva, E. N., Escutia-Guadarrama, L., Figueroa-González, G., et al. (2022). Hyaluronic acid in wound dressings. *Cell. Mol. Biol. (Noisy-le-grand)* 66 (4), 191–198. doi:10.14715/cmb/2020.66.4.23
- de Araújo Andrade, T., Heimfarth, L., dos Santos, D. M., dos Santos, M. R. V., de Albuquerque-Júnior, R. L. C., dos Santos-Neto, A. G., et al. (2022). Hesperetin-based hydrogels protect the skin against UV radiation-induced damage. *AAPS PharmSciTech* 23 (6), 170. doi:10.1208/s12249-022-02323-8
- de Oliveira, M. M., Nakamura, C. V., and Auzély-Velty, R. (2020). Boronate-ester crosslinked hyaluronic acid hydrogels for dihydrocaffeic acid delivery and fibroblasts protection against UVB irradiation. *Carbohydr. Polym.* 247, 116845. doi:10.1016/j.carbpol.2020.116845
- Du, J., Ma, Q., Wang, B., Sun, L., and Liu, L. (2023). Hydrogel fibers for wearable sensors and soft actuators. *iScience* 26 (6), 106796. doi:10.1016/j.isci.2023.106796
- Fisher, G. J., Kang, S., Varani, J., Bata-Csorgo, Z., Wan, Y., Datta, S., et al. (2002). Mechanisms of photoaging and chronological skin aging. *Arch. Dermatol.* 138 (11), 1462–1470. doi:10.1001/archderm.138.11.1462
- Fitsiou, E., Pulido, T., Campisi, J., Alimirah, F., and Demaria, M. (2021). Cellular senescence and the senescence-associated secretory phenotype as drivers of skin photoaging. *J. Invest. Dermatol.* 141 (4s), 1119–1126. doi:10.1016/j.jid.2020.09.031
- Francesco, A., Petkova, P., and Tzanov, T. (2018). Hydrogel dressings for advanced wound management. *Curr. Med. Chem.* 25 (41), 5782–5797. doi:10.2174/0929867324666170920161246
- Fu, H., Zhang, D., Zeng, J., Fu, Q., Chen, Z., Sun, X., et al. (2023). Application of 3D-printed tissue-engineered skin substitute using innovative biomaterial loaded with human adipose-derived stem cells in wound healing. *Int. J. Bioprint* 9 (2), 674. doi:10.18063/ijb.v9i2.674
- Gaspar, L. R., and Campos, P. M. (2007). Photostability and efficacy studies of topical formulations containing UV-filters combination and vitamins A, C and E. *Int. J. Pharm.* 343 (1–2), 181–189. doi:10.1016/j.jipharm.2007.05.048
- Greul, A. K., Grundmann, J. U., Heinrich, F., Pfltzner, I., Bernhardt, J., Ambach, A., et al. (2002). Photoprotection of UV-irradiated human skin: an antioxidative combination of vitamins E and C, carotenoids, selenium and proanthocyanidins. *Skin. Pharmacol. Appl. Skin. Physiol.* 15 (5), 307–315. doi:10.1159/000064534
- Gu, Y., Han, J., Jiang, C., and Zhang, Y. (2020). Biomarkers, oxidative stress and autophagy in skin aging. *Ageing Res. Rev.* 59, 101036. doi:10.1016/j.arr.2020.101036
- Guo, K., Zheng, L., Zeng, X., Huang, G., Meng, L., and Yin, Y. (2024). Compound collagen peptide powder improves skin photoaging by reducing oxidative stress and activating TGF- β 1/Smad pathway. *Photochem Photobiol.* doi:10.1111/php.13940
- Hamilton, M. M., and Kao, R. (2020). Recognizing and managing complications in laser resurfacing, chemical peels, and dermabrasion. *Facial Plast. Surg. Clin. North Am.* 28 (4), 493–501. doi:10.1016/j.fsc.2020.06.008
- Ho, T. C., Chang, C. C., Chan, H. P., Chung, T. W., Shu, C. W., Chuang, K. P., et al. (2022). Hydrogels: properties and applications in biomedicine. *Molecules* 27 (9), 2902. doi:10.3390/molecules27092902
- Hu, X., Xia, Z., and Cai, K. (2022). Recent advances in 3D hydrogel culture systems for mesenchymal stem cell-based therapy and cell behavior regulation. *J. Mater. Chem. B* 10 (10), 1486–1507. doi:10.1039/d1tb02537f
- Huang, X., Chang, Q., Gao, J. h., and Lu, F. (2023). Sustained release microneedles: materials and applications in facial rejuvenation. *Tissue Eng. Part B Rev.* 29 (3), 190–202. doi:10.1089/ten.teb.2022.0131
- Hubbard, B. A., Unger, J. G., and Rohrich, R. J. (2014). Reversal of skin aging with topical retinoids. *Plast. Reconstr. Surg.* 133 (4), 481e–490e. doi:10.1097/prs.0000000000000043
- Jin, X., Zhang, X., Li, Y., Xu, M., Yao, Y., Wu, Z., et al. (2022). Long-acting microneedle patch loaded with adipose collagen fragment for preventing the skin photoaging in mice. *Biomater. Adv.* 135, 212744. doi:10.1016/j.bioadv.2022.212744
- Khayambashi, P., Iyer, J., Pillai, S., Upadhyay, A., Zhang, Y., and Tran, S. (2021). Hydrogel encapsulation of mesenchymal stem cells and their derived exosomes for tissue engineering. *Int. J. Mol. Sci.* 22 (2), 684. doi:10.3390/ijms22020684
- Kim, D. J., Iwasaki, A., Chien, A. L., and Kang, S. (2022). UVB-mediated DNA damage induces matrix metalloproteinases to promote photoaging in an AhR- and SP1-dependent manner. *JCI Insight* 7 (9). doi:10.1172/jci.insight.156344
- Kim, N., Lee, H., Han, G., Kang, M., Park, S., Kim, D. E., et al. (2023). 3D-Printed functional hydrogel by DNA-induced biomineralization for accelerated diabetic wound healing. *Adv. Sci. (Weinh)* 10 (17), e2300816. doi:10.1002/adv.202300816
- Letsiou, S. (2021). Tracing skin aging process: a mini-review of *in vitro* approaches. *Biogerontology* 22 (3), 261–272. doi:10.1007/s10522-021-09916-z
- Lewicka, K., Smola-Dmochowska, A., Dobrzyński, P., Śmigiel-Gac, N., Jelonek, K., Musiał-Kulik, M., et al. (2024). Microspheres based on blends of chitosan derivatives with carrageenan as vitamin carriers in cosmeceuticals. *Polym. (Basel)* 16 (13), 1815. doi:10.3390/polym16131815
- Li, P., Fu, L., Liao, Z., Peng, Y., Ning, C., Gao, C., et al. (2021). Chitosan hydrogel/3D-printed poly(ϵ -caprolactone) hybrid scaffold containing synovial mesenchymal stem cells for cartilage regeneration based on tetrahedral framework nucleic acid recruitment. *Biomaterials* 278, 121131. doi:10.1016/j.biomaterials.2021.121131
- Li, S., Sun, J., Yang, J., Yang, Y., Ding, H., Yu, B., et al. (2023). Gelatin methacryloyl (GelMA) loaded with concentrated hypoxic pretreated adipose-derived mesenchymal stem cells (ADSCs) conditioned medium promotes wound healing and vascular regeneration in aged skin. *Biomater. Res.* 27 (1), 11. doi:10.1186/s40824-023-00352-3
- Li, Y., Zhao, L., Li, S., Ruan, D., Xiong, L., Tang, J., et al. (2024). Skin-derived precursor conditioned medium alleviated photoaging via early activation of TGF- β /Smad signaling pathway by thrombospondin1: *in vitro* and *in vivo* studies. *J. Photochem Photobiol. B* 253, 112873. doi:10.1016/j.jphotobiol.2024.112873
- Lim, S. H., Kim, S. M., Lee, Y. W., Ahn, K. J., and Choe, Y. B. (2008). Change of biophysical properties of the skin caused by ultraviolet radiation-induced photodamage in Koreans. *Skin. Res. Technol.* 14 (1), 93–102. doi:10.1111/j.1600-0846.2007.00272.x
- Lin, Y. C., Fang, Y. P., Hung, C. F., Yu, H. P., Alalawi, A., Wu, Z. Y., et al. (2021). Multifunctional TiO₂(2)/SBA-15 mesoporous silica hybrids loaded with organic sunscreens for skin application: the role in photoprotection and pollutant adsorption with reduced sunscreen permeation. *Colloids Surf. B Biointerfaces* 202, 111658. doi:10.1016/j.colsurfb.2021.111658
- Liu, C., Xia, Y., Li, Y., Cheng, Y., Xia, H., Wang, Y., et al. (2022). Ligustrazine as an extract from medicinal and edible plant chuanxiong encapsulated in liposome-hydrogel exerting antioxidant effect on preventing skin photoaging. *Polym. (Basel)* 14 (21), 4778. doi:10.3390/polym14214778
- Liu, Y., Qin, D., Wang, H., Zhu, Y., Bi, S., et al. (2023). Effect and mechanism of fish scale extract natural hydrogel on skin protection and cell damage repair after UV irradiation. *Colloids Surf. B Biointerfaces* 225, 113281. doi:10.1016/j.colsurfb.2023.113281
- Luo, Y., Li, J., Ding, Q., Wang, H., Liu, C., and Wu, J. (2023). Functionalized hydrogel-based wearable gas and humidity sensors. *Nanomicro Lett.* 15 (1), 136. doi:10.1007/s40820-023-01109-2
- Mast, B. A., Flood, L. C., Haynes, J. H., Depalma, R. L., Cohen, I. K., Diegelmann, R. F., et al. (1991). Hyaluronic acid is a major component of the matrix of fetal rabbit skin and wounds: implications for healing by regeneration. *Matrix* 11 (1), 63–68. doi:10.1016/s0934-8832(11)80228-3
- Mukherjee, S., Date, A., Patravale, V., Korting, H. C., Roeder, A., and Weindl, G. (2006). Retinoids in the treatment of skin aging: an overview of clinical efficacy and safety. *Clin. Interv. Aging* 1 (4), 327–348. doi:10.2147/cia.2006.1.4.327
- Nakanishi, M., Niida, H., Murakami, H., and Shimada, M. (2009). DNA damage responses in skin biology—implications in tumor prevention and aging acceleration. *J. Dermatol. Sci.* 56 (2), 76–81. doi:10.1016/j.jdermsci.2009.09.001
- Neves, L. M. G., Parizotto, N. A., Tim, C. R., Floriano, E. M., Lopez, R. F. V., Venâncio, T., et al. (2020). Polysaccharide-rich hydrogel formulation combined with photobiomodulation repairs UV-induced photodamage in mice skin. *Wound Repair Regen.* 28 (5), 645–655. doi:10.1111/wrr.12826
- Ortonne, J. P. (1990). The effects of ultraviolet exposure on skin melanin pigmentation. *J. Int. Med. Res.* 18 (Suppl. 3), 8C–17C.
- Papaccio, F., D'Arino, A., Caputo, S., and Bellei, B. (2022). Focus on the contribution of oxidative stress in skin aging. *Antioxidants (Basel)* 11 (6), 1121. doi:10.3390/antiox11061121
- Poon, F., Kang, S., and Chien, A. L. (2015). Mechanisms and treatments of photoaging. *Photodermatol. Photoimmunol. Photomed.* 31 (2), 65–74. doi:10.1111/php.12145
- Pourang, A., Tisack, A., Ezekwe, N., Torres, A. E., Kohli, I., Hamzavi, I. H., et al. (2022). Effects of visible light on mechanisms of skin photoaging. *Photodermatol. Photoimmunol. Photomed.* 38 (3), 191–196. doi:10.1111/php.12736
- Quan, W., Kong, S., Li, S., Ouyang, Q., Lu, S., Guo, J., et al. (2023). Anti-photoaging effects of nanocomposites of amphiphilic chitosan/18 β -glycyrrhetic acid. *Molecules* 28 (11), 4362. doi:10.3390/molecules28114362
- Rahman, A., Rehmani, R., Pirvu, D. G., Huang, S. M., Puri, S., and Arcos, M. (2024). Unlocking the therapeutic potential of marine collagen: a scientific exploration for delaying skin aging. *Mar. Drugs* 22 (4), 159. doi:10.3390/md22040159

- Rahmani, P., and Shojaei, A. (2021). A review on the features, performance and potential applications of hydrogel-based wearable strain/pressure sensors. *Adv. Colloid Interface Sci.* 298, 102553. doi:10.1016/j.cis.2021.102553
- Riahi, R. R., Bush, A. E., and Cohen, P. R. (2016). Topical retinoids: therapeutic mechanisms in the treatment of photodamaged skin. *Am. J. Clin. Dermatol.* 17 (3), 265–276. doi:10.1007/s40257-016-0185-5
- Rigo, L. A., da Silva, C. R., de Oliveira, S. M., Cabreira, T. N., de Bona da Silva, C., Ferreira, J., et al. (2015). Nanoencapsulation of rice bran oil increases its protective effects against UVB radiation-induced skin injury in mice. *Eur. J. Pharm. Biopharm.* 93, 11–17. doi:10.1016/j.ejpb.2015.03.020
- Rittié, L., and Fisher, G. J. (2015). Natural and sun-induced aging of human skin. *Cold Spring Harb. Perspect. Med.* 5 (1), a015370. doi:10.1101/cshperspect.a015370
- Sales, A. F. S., Pandolfo, I. L., de Almeida Cruz, M., Parisi, J. R., Garcia, L. A., Martignago, C. C. S., et al. (2022). Intense Pulsed Light on skin rejuvenation: a systematic review. *Arch. Dermatol. Res.* 314 (9), 823–838. doi:10.1007/s00403-021-02283-2
- Schuch, A. P., Moreno, N. C., Schuch, N. J., Menck, C. F. M., and Garcia, C. C. M. (2017). Sunlight damage to cellular DNA: focus on oxidatively generated lesions. *Free Radic. Biol. Med.* 107, 110–124. doi:10.1016/j.freeradbiomed.2017.01.029
- Sharad, J. (2013). Glycolic acid peel therapy - a current review. *Clin. Cosmet. Investig. Dermatol.* 6, 281–288. doi:10.2147/ccid.s34029
- Shin, J. W., Kwon, S. H., Choi, J. Y., Na, J. I., Huh, C. H., Choi, H. R., et al. (2019). Molecular mechanisms of dermal aging and antiaging approaches. *Int. J. Mol. Sci.* 20 (9), 2126. doi:10.3390/ijms20092126
- Sreedhar, A., Aguilera-Aguirre, L., and Singh, K. K. (2020). Mitochondria in skin health, aging, and disease. *Cell. Death Dis.* 11 (6), 444. doi:10.1038/s41419-020-2649-z
- Steenvoorden, D. P., and Beijersbergen van Henegouwen, G. (1999). Protection against UV-induced systemic immunosuppression in mice by a single topical application of the antioxidant vitamins C and E. *Int. J. Radiat. Biol.* 75 (6), 747–755. doi:10.1080/095530099140096
- Studzinska-Sroka, E., Paczkowska-Walendowska, M., Erdem, C., Paluszczak, J., Kleszcz, R., Hoszman-Kulisz, M., et al. (2024). Anti-aging properties of chitosan-based hydrogels rich in bilberry fruit extract. *Antioxidants (Basel)* 13 (1), 105. doi:10.3390/antiox13010105
- Sun, J., Xie, X., Song, Y., Sun, T., Liu, X., Yuan, H., et al. (2024). Selenomethionine in gelatin methacryloyl hydrogels: modulating ferroptosis to attenuate skin aging. *Bioact. Mater.* 35, 495–516. doi:10.1016/j.bioactmat.2024.02.013
- Tan, C. Y. R., Chin, T., Morenc, M., Ho, C. Y., Rovito, H. A., et al. (2022). Nicotinamide prevents UVB- and oxidative stress-induced photoaging in human primary keratinocytes. *J. Investig. Dermatol.* 142 (6), 1670–1681.e12. doi:10.1016/j.jid.2021.10.021
- Tran, J. T., Diaz, M. J., Rodriguez, D., Kleinberg, G., Aflatooni, S., Palreddy, S., et al. (2023). Evidence-based utility of adjunct antioxidant supplementation for the prevention and treatment of dermatologic diseases: a comprehensive systematic review. *Antioxidants (Basel)* 12 (8), 1503. doi:10.3390/antiox12081503
- Vijayavenkataraman, S., Yan, W. C., Lu, W. F., Wang, C. H., and Fuh, J. Y. H. (2018). 3D bioprinting of tissues and organs for regenerative medicine. *Adv. Drug Deliv. Rev.* 132, 296–332. doi:10.1016/j.addr.2018.07.004
- Wang, L., Zhang, X., Xu, P., Yan, J., Zhang, Y., Su, H., et al. (2022). Exploration of sea anemone-inspired high-performance biomaterials with enhanced antioxidant activity. *Bioact. Mater.* 10, 504–514. doi:10.1016/j.bioactmat.2021.08.021
- Wang, M., Charareh, P., Lei, X., and Zhong, J. L. (2019). Autophagy: multiple mechanisms to protect skin from ultraviolet radiation-driven photoaging. *Oxid. Med. Cell. Longev.* 2019, 1–14. doi:10.1155/2019/8135985
- Wang, X., Song, R., Johnson, M., He, Z., Milne, C., et al. (2021). An injectable chitosan-based self-healable hydrogel system as an antibacterial wound dressing. *Mater. (Basel)* 14 (20), 5956. doi:10.3390/ma14205956
- Wang, Y., Lu, Z., Huang, Y., Jia, W., Wang, W., Zhang, X., et al. (2023a). Smart nanostructures for targeted oxygen-producing photodynamic therapy of skin photoaging and potential mechanism. *Nanomedicine (Lond)* 18 (3), 217–231. doi:10.2217/nnm-2022-0170
- Wang, Y., Zhang, Y., Yang, Y. P., Jin, M. Y., Huang, S., Zhuang, Z. M., et al. (2024a). Versatile dopamine-functionalized hyaluronic acid-recombinant human collagen hydrogel promoting diabetic wound healing via inflammation control and vascularization tissue regeneration. *Bioact. Mater.* 35, 330–345. doi:10.1016/j.bioactmat.2024.02.010
- Wang, Z., Kwong, C. H. T., Zhao, H., Ding, Y. F., Gao, C., Zhang, D., et al. (2023b). Microalgae microneedle supplies oxygen for antiphotaging treatment. *ACS Appl. Bio Mater.* 6 (9), 3463–3471. doi:10.1021/acsabm.3c00192
- Wang, Z., Yuan, J., Xu, Y., Shi, N., Lin, L., Wang, R., et al. (2024b). Olea europaea leaf exosome-like nanovesicles encapsulated in a hyaluronic acid/tannic acid hydrogel dressing with dual “defense-repair” effects for treating skin photoaging. *Mater Today Bio* 26, 101103. doi:10.1016/j.mtbio.2024.101103
- Wu, S., Liu, G., Shao, P., Lin, X., Yu, J., Chen, H., et al. (2024). Transdermal sustained release properties and anti-photoaging efficacy of liposome-thermosensitive hydrogel system. *Adv. Healthc. Mater.* 13 (2), e2301933. doi:10.1002/adhm.202301933
- Wu, Y., Geng, L., Zhang, J., Wu, N., Yang, Y., Zhang, Q., et al. (2023). Preparation of multifunctional seaweed polysaccharides derivatives composite hydrogel to protect ultraviolet B-induced photoaging *in vitro* and *in vivo*. *Macromol. Biosci.* 24, e2300292. doi:10.1002/mabi.202300292
- Xia, J., Liu, Z. Y., Han, Z. Y., Yuan, Y., Shao, Y., Feng, X. Q., et al. (2022). Regulation of cell attachment, spreading, and migration by hydrogel substrates with independently tunable mesh size. *Acta Biomater.* 141, 178–189. doi:10.1016/j.actbio.2022.01.025
- Xiong, Y., Chen, L., Liu, P., Yu, T., Lin, C., Yan, C., et al. (2022). All-in-One: multifunctional hydrogel accelerates oxidative diabetic wound healing through timed-release of exosome and fibroblast growth factor. *Small* 18 (1), e2104229. doi:10.1002/sml.202104229
- Xu, Q., et al. (2021). Collagen- and hyaluronic acid-based hydrogels and their biomedical applications. *Mater Sci. Eng. R. Rep.*, 146.
- Yan, T., Huang, L., Yan, Y., Zhong, Y., Xie, H., and Wang, X. (2023). Bone marrow mesenchymal stem cell-derived exosome miR-29b-3p alleviates UV irradiation-induced photoaging in skin fibroblast. *Photodermatol. Photoimmunol. Photomed.* 39 (3), 235–245. doi:10.1111/phpp.12827
- Yang, G., Hu, S., Jiang, H., and Cheng, K. (2023). Peelable microneedle patches deliver fibroblast growth factors to repair skin photoaging damage. *Nanotheranostics* 7 (4), 380–392. doi:10.7150/ntno.79187
- You, Y., Tian, Y., Yang, Z., Shi, J., Kwak, K. J., Tong, Y., et al. (2023). Intradermally delivered mRNA-encapsulating extracellular vesicles for collagen-replacement therapy. *Nat. Biomed. Eng.* 7, 887–900. doi:10.1038/s41551-022-00989-w
- Zhang, K., Yu, L., Li, F. R., Li, X., Wang, Z., Zou, X., et al. (2020). Topical application of exosomes derived from human umbilical cord mesenchymal stem cells in combination with sponge spicules for treatment of photoaging. *Int. J. Nanomedicine* 15, 2859–2872. doi:10.2147/ijn.s249751
- Zhang, S., and Duan, E. (2018). Fighting against skin aging: the way from bench to bedside. *Cell. Transpl.* 27 (5), 729–738. doi:10.1177/0963689717725755
- Zhang, Y., Zhang, M., Yao, A., Xie, Y., Lin, J., Sharifullah, F., et al. (2022). Circ_0011129 encapsulated by the small extracellular vesicles derived from human stem cells ameliorate skin photoaging. *Int. J. Mol. Sci.* 23 (23), 15390. doi:10.3390/ijms232315390
- Zhao, C., Zhou, L., Chiao, M., and Yang, W. (2020). Antibacterial hydrogel coating: strategies in surface chemistry. *Adv. Colloid Interface Sci.* 285, 102280. doi:10.1016/j.cis.2020.102280
- Zhao, X., Liu, Y., Jia, P., Cheng, H., Wang, C., Chen, S., et al. (2021b). Chitosan hydrogel-loaded MSC-derived extracellular vesicles promote skin rejuvenation by ameliorating the senescence of dermal fibroblasts. *Stem Cell. Res. Ther.* 12 (1), 196. doi:10.1186/s13287-021-02262-4
- Zhao, Y., Dai, Q., and Xiao, R. (2021a). Photoaged skin therapy with adipose-derived stem cells. *Plast. Reconstr. Surg.* 148 (3), 494e. doi:10.1097/prs.00000000000008242
- Zhu, S., Zhao, Z., Qin, W., Liu, T., Yang, Y., Wang, Z., et al. (2022). The Nanostructured lipid carrier gel of Oroxylin A reduced UV-induced skin oxidative stress damage. *Colloids Surf. B Biointerfaces* 216, 112578. doi:10.1016/j.colsurfb.2022.112578

Frontiers in Bioengineering and Biotechnology

Accelerates the development of therapies,
devices, and technologies to improve our lives

A multidisciplinary journal that accelerates the
development of biological therapies, devices,
processes and technologies to improve our lives
by bridging the gap between discoveries and their
application.

Discover the latest Research Topics

[See more →](#)

Frontiers

Avenue du Tribunal-Fédéral 34
1005 Lausanne, Switzerland
frontiersin.org

Contact us

+41 (0)21 510 17 00
frontiersin.org/about/contact



Frontiers in
Bioengineering
and Biotechnology

